Disease Markers

Stroke Biomarkers: Diagnosis, Prognosis, and Treatment

Lead Guest Editor: Xianwei Zeng
Guest Editors: Mark Slevin and Liangqun Rong

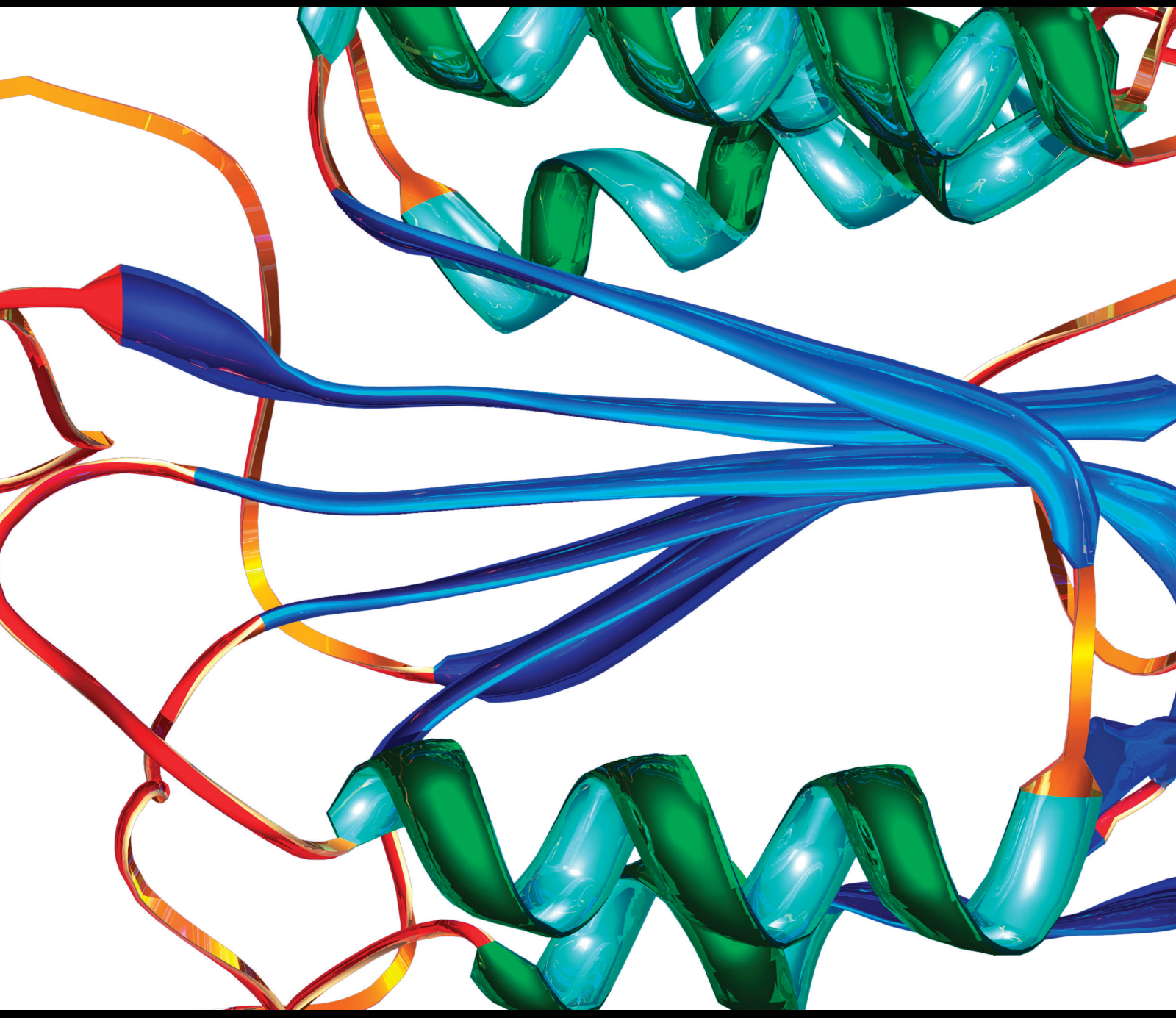

Stroke Biomarkers: Diagnosis, Prognosis, and Treatment

Disease Markers

Stroke Biomarkers: Diagnosis, Prognosis, and Treatment

Lead Guest Editor: Xianwei Zeng
Guest Editors: Mark Slevin and Liangqun Rong

Chief Editor

Paola Gazzaniga, Italy

Associate Editors

Donald H. Chace, USA
Mariann Harangi, Hungary
Hubertus Himmerich, United Kingdom
Yi-Chia Huang, Taiwan
Giuseppe Murdaca, Italy
Irene Rebelo, Portugal

Academic Editors

Muhammad Abdel Ghafar, Egypt
George Agrogiannis, Greece
Mojgan Alaeddini, Iran
Atif Ali Hashmi, Pakistan
Cornelia Amalinei, Romania
Pasquale Ambrosino, Italy
Paul Ashwood, USA
Faryal Mehwish Awan, Pakistan
Atif Baig, Malaysia
Valeria Barresi, Italy
Lalit Batra, USA
Francesca Belardinilli, Italy
Elisa Belluzzi, Italy
Laura Bergantini, Italy
Sourav Bhattacharya, USA
Anna Birková, Slovakia
Giulia Bivona, Italy
Luisella Bocchio-Chiavetto, Italy
Francesco Paolo Busardó, Italy
Andrea Cabrera-Pastor, Spain
Paolo Cameli, Italy
Chiara Caselli, Italy
Jin Chai, China
Qixing Chen, China
Shaoqiu Chen, USA
Xiangmei Chen, China
Carlo Chiarla, Italy
Marcello Ciaccio, Italy
Luciano Colangelo, Italy
Alexandru Corlateanu, Moldova
Miriana D'Alessandro, Saint Vincent and the Grenadines
Waaqo B. Daddacha, USA
Xi-jian Dai, China
Maria Dalamaga, Greece
Serena Del Turco, Italy
Jiang Du, USA
Xing Du, China
Benoit Dugue, France
Paulina Dumnicka, Poland
Nashwa El-Khazragy, Egypt
Zhe Fan, China
Rudy Foddis, Italy
Serena Fragiotta, Italy
Helge Frieling, Germany
Alain J. Gelibter, Italy
Matteo Giulietti, Italy
Damjan Glavač, Slovenia
Alvaro González, Spain
Rohit Gundamaraju, USA
Emilia Hadziyannis, Greece
Michael Hawkes, Canada
Shih-Ping Hsu, Taiwan
Menghao Huang, USA
Shu-Hong Huang, China
Xuan Huang, China
Ding-Sheng Jiang, China
Esteban Jorge Galarza, Mexico
Mohamed Gomaa Kamel, Japan
Michalis V. Karamouzis, Greece
Muhammad Babar Khawar, Pakistan
Young-Kug Kim, Republic of Korea
Mallikarjuna Korivi, China
Arun Kumar, India
Jinan Li, USA
Peng-fei Li, China
Yiping Li, China
Michael Lichtenauer, Austria
Daniela Ligi, Italy
Hui Liu, China
Jin-Hui Liu, China
Ying Liu, USA
Zhengwen Liu, China
César López-Camarillo, Mexico
Xin Luo, USA
Zhiwen Luo, China
Valentina Magri, Italy
Michele Malaguarnera, Italy
Erminia Manfrin, Italy
Upender Manne, USA

Contents

Contents

Hindawi
Disease Markers
Volume 2023, Article ID 9867801, 1 page
https://doi.org/10.1155/2023/9867801

Retraction

Retracted: Long Noncoding RNA TFAP2A-AS1 Suppressed Hepatitis B Virus Replication by Modulating miR-933/HDAC11

Disease Markers

Received 20 June 2023; Accepted 20 June 2023; Published 21 June 2023

This article has been retracted by Hindawi following an investigation undertaken by the publisher [1]. This investigation has uncovered evidence of one or more of the following indicators of systematic manipulation of the publication process:

(1) Discrepancies in scope

(2) Discrepancies in the description of the research reported

(3) Discrepancies between the availability of data and the research described

(4) Inappropriate citations

(5) Incoherent, meaningless and/or irrelevant content included in the article

(6) Peer-review manipulation

The presence of these indicators undermines our confidence in the integrity of the article's content and we cannot, therefore, vouch for its reliability. Please note that this notice is intended solely to alert readers that the content of this article is unreliable. We have not investigated whether authors were aware of or involved in the systematic manipulation of the publication process.

In addition, our investigation has also shown that one or more of the following human-subject reporting requirements has not been met in this article: ethical approval by an Institutional Review Board (IRB) committee or equivalent, patient/participant consent to participate, and/or agreement to publish patient/participant details (where relevant).

Wiley and Hindawi regrets that the usual quality checks did not identify these issues before publication and have since put additional measures in place to safeguard research integrity.

We wish to credit our own Research Integrity and Research Publishing teams and anonymous and named external researchers and research integrity experts for contributing to this investigation.

The corresponding author, as the representative of all authors, has been given the opportunity to register their agreement or disagreement to this retraction. We have kept a record of any response received.

References

[1] Y. Cheng, W. Shi, X. Cui et al., "Long Noncoding RNA TFAP2A-AS1 Suppressed Hepatitis B Virus Replication by Modulating miR-933/HDAC11," *Disease Markers*, vol. 2022, Article ID 7733390, 11 pages, 2022.

Hindawi
Disease Markers
Volume 2023, Article ID 9861260, 1 page
https://doi.org/10.1155/2023/9861260

Retraction

Retracted: Multiomics Immune-Related lncRNA Analysis of Oral Squamous Cell Carcinoma and Its Correlation with Prognosis

Disease Markers

Received 20 June 2023; Accepted 20 June 2023; Published 21 June 2023

This article has been retracted by Hindawi following an investigation undertaken by the publisher [1]. This investigation has uncovered evidence of one or more of the following indicators of systematic manipulation of the publication process:

(1) Discrepancies in scope

(2) Discrepancies in the description of the research reported

(3) Discrepancies between the availability of data and the research described

(4) Inappropriate citations

(5) Incoherent, meaningless and/or irrelevant content included in the article

(6) Peer-review manipulation

The presence of these indicators undermines our confidence in the integrity of the article's content and we cannot, therefore, vouch for its reliability. Please note that this notice is intended solely to alert readers that the content of this article is unreliable. We have not investigated whether authors were aware of or involved in the systematic manipulation of the publication process.

Wiley and Hindawi regrets that the usual quality checks did not identify these issues before publication and have since put additional measures in place to safeguard research integrity.

We wish to credit our own Research Integrity and Research Publishing teams and anonymous and named external researchers and research integrity experts for contributing to this investigation.

The corresponding author, as the representative of all authors, has been given the opportunity to register their agreement or disagreement to this retraction. We have kept a record of any response received.

References

[1] Z. Liu, Q. Liu, X. Wang, L. Liu, L. Shi, and H. Li, "Multiomics Immune-Related lncRNA Analysis of Oral Squamous Cell Carcinoma and Its Correlation with Prognosis," *Disease Markers*, vol. 2022, Article ID 6106503, 15 pages, 2022.

Hindawi
Disease Markers
Volume 2023, Article ID 9823853, 1 page
https://doi.org/10.1155/2023/9823853

Retraction

Retracted: Correlation of Clinicopathological Factors with Brain Tumor-Related Epilepsy in Glioma

Disease Markers

Received 20 June 2023; Accepted 20 June 2023; Published 21 June 2023

This article has been retracted by Hindawi following an investigation undertaken by the publisher [1]. This investigation has uncovered evidence of one or more of the following indicators of systematic manipulation of the publication process:

(1) Discrepancies in scope

(2) Discrepancies in the description of the research reported

(3) Discrepancies between the availability of data and the research described

(4) Inappropriate citations

(5) Incoherent, meaningless and/or irrelevant content included in the article

(6) Peer-review manipulation

The presence of these indicators undermines our confidence in the integrity of the article's content and we cannot, therefore, vouch for its reliability. Please note that this notice is intended solely to alert readers that the content of this article is unreliable. We have not investigated whether authors were aware of or involved in the systematic manipulation of the publication process.

Wiley and Hindawi regrets that the usual quality checks did not identify these issues before publication and have since put additional measures in place to safeguard research integrity.

We wish to credit our own Research Integrity and Research Publishing teams and anonymous and named external researchers and research integrity experts for contributing to this investigation.

The corresponding author, as the representative of all authors, has been given the opportunity to register their agreement or disagreement to this retraction. We have kept a record of any response received.

References

[1] Z. Wang, W. Yang, Y. Wang et al., "Correlation of Clinicopathological Factors with Brain Tumor-Related Epilepsy in Glioma," *Disease Markers*, vol. 2022, Article ID 4918294, 13 pages, 2022.

Hindawi
Disease Markers
Volume 2023, Article ID 9813418, 1 page
https://doi.org/10.1155/2023/9813418

Retraction

Retracted: Association between Mutation in SMARCAD1 and Basan Syndrome with Cutaneous Squamous Cell Carcinoma

Disease Markers

Received 20 June 2023; Accepted 20 June 2023; Published 21 June 2023

This article has been retracted by Hindawi following an investigation undertaken by the publisher [1]. This investigation has uncovered evidence of one or more of the following indicators of systematic manipulation of the publication process:

(1) Discrepancies in scope

(2) Discrepancies in the description of the research reported

(3) Discrepancies between the availability of data and the research described

(4) Inappropriate citations

(5) Incoherent, meaningless and/or irrelevant content included in the article

(6) Peer-review manipulation

The presence of these indicators undermines our confidence in the integrity of the article's content and we cannot, therefore, vouch for its reliability. Please note that this notice is intended solely to alert readers that the content of this article is unreliable. We have not investigated whether authors were aware of or involved in the systematic manipulation of the publication process.

In addition, our investigation has also shown that one or more of the following human-subject reporting requirements has not been met in this article: ethical approval by an Institutional Review Board (IRB) committee or equivalent, patient/participant consent to participate, and/or agreement to publish patient/participant details (where relevant).

Wiley and Hindawi regrets that the usual quality checks did not identify these issues before publication and have since put additional measures in place to safeguard research integrity.

We wish to credit our own Research Integrity and Research Publishing teams and anonymous and named external researchers and research integrity experts for contributing to this investigation.

The corresponding author, as the representative of all authors, has been given the opportunity to register their agreement or disagreement to this retraction. We have kept a record of any response received.

References

[1] Y. Xiong, T. Chen, J. Yu et al., "Association between Mutation in SMARCAD1 and Basan Syndrome with Cutaneous Squamous Cell Carcinoma," *Disease Markers*, vol. 2022, Article ID 7840710, 9 pages, 2022.

Hindawi
Disease Markers
Volume 2023, Article ID 9754281, 1 page
https://doi.org/10.1155/2023/9754281

Retraction

Retracted: Activated Hepatic Stellate Cells Promote the M1 to M2 Macrophage Transformation and Liver Fibrosis by Elevating the Histone Acetylation Level

Disease Markers

Received 20 June 2023; Accepted 20 June 2023; Published 21 June 2023

This article has been retracted by Hindawi following an investigation undertaken by the publisher [1]. This investigation has uncovered evidence of one or more of the following indicators of systematic manipulation of the publication process:

(1) Discrepancies in scope

(2) Discrepancies in the description of the research reported

(3) Discrepancies between the availability of data and the research described

(4) Inappropriate citations

(5) Incoherent, meaningless and/or irrelevant content included in the article

(6) Peer-review manipulation

The presence of these indicators undermines our confidence in the integrity of the article's content and we cannot, therefore, vouch for its reliability. Please note that this notice is intended solely to alert readers that the content of this article is unreliable. We have not investigated whether authors were aware of or involved in the systematic manipulation of the publication process.

Wiley and Hindawi regrets that the usual quality checks did not identify these issues before publication and have since put additional measures in place to safeguard research integrity.

We wish to credit our own Research Integrity and Research Publishing teams and anonymous and named external researchers and research integrity experts for contributing to this investigation.

The corresponding author, as the representative of all authors, has been given the opportunity to register their agreement or disagreement to this retraction. We have kept a record of any response received.

References

[1] J. Chen, X. Huang, Z. Huang, and Y. Cao, "Activated Hepatic Stellate Cells Promote the M1 to M2 Macrophage Transformation and Liver Fibrosis by Elevating the Histone Acetylation Level," *Disease Markers*, vol. 2022, Article ID 9883831, 8 pages, 2022.

Hindawi
Disease Markers
Volume 2023, Article ID 9823853, 1 page
https://doi.org/10.1155/2023/9823853

Retraction

Retracted: Correlation of Clinicopathological Factors with Brain Tumor-Related Epilepsy in Glioma

Disease Markers

Received 20 June 2023; Accepted 20 June 2023; Published 21 June 2023

This article has been retracted by Hindawi following an investigation undertaken by the publisher [1]. This investigation has uncovered evidence of one or more of the following indicators of systematic manipulation of the publication process:

(1) Discrepancies in scope

(2) Discrepancies in the description of the research reported

(3) Discrepancies between the availability of data and the research described

(4) Inappropriate citations

(5) Incoherent, meaningless and/or irrelevant content included in the article

(6) Peer-review manipulation

The presence of these indicators undermines our confidence in the integrity of the article's content and we cannot, therefore, vouch for its reliability. Please note that this notice is intended solely to alert readers that the content of this article is unreliable. We have not investigated whether authors were aware of or involved in the systematic manipulation of the publication process.

Wiley and Hindawi regrets that the usual quality checks did not identify these issues before publication and have since put additional measures in place to safeguard research integrity.

We wish to credit our own Research Integrity and Research Publishing teams and anonymous and named external researchers and research integrity experts for contributing to this investigation.

The corresponding author, as the representative of all authors, has been given the opportunity to register their agreement or disagreement to this retraction. We have kept a record of any response received.

References

[1] Z. Wang, W. Yang, Y. Wang et al., "Correlation of Clinicopathological Factors with Brain Tumor-Related Epilepsy in Glioma," *Disease Markers*, vol. 2022, Article ID 4918294, 13 pages, 2022.

Hindawi
Disease Markers
Volume 2022, Article ID 4918294, 13 pages
https://doi.org/10.1155/2022/4918294

Research Article

Correlation of Clinicopathological Factors with Brain Tumor-Related Epilepsy in Glioma

Zengliang Wang,[1,2] **Wensheng Yang**,[3] **Yongxin Wang**,[1] **Yirizhati Aili**,[1] **Zhitao Wang**,[1] **Quanyi Wang**,[4] **Shunli Jiang**,[5] **Guangning Zhang**,[6] **Junchen Zhang**,[6] **and Bo Li**[6]

[1]*Department of Neurosurgery, First Affiliated Hospital of Xinjiang Medical University, Urumqi, Xinjiang, China*
[2]*Department of Neurosurgery, Xinjiang Bazhou People's Hospital, Xinjiang, China*
[3]*Department of Pathology, The Affiliated Chenggong Hospital of Xiamen University, Fujian, China*
[4]*Department of Pathology, Affiliated Hospital of Jining Medical University, Jining, Shandong, China*
[5]*Key Laboratory of Occupational Health and Environmental Medicine, Department of Public Health, Jining Medical University, Jining, Shandong, China*
[6]*Department of Neurosurgery, Affiliated Hospital of Jining Medical University, Jining, Shandong, China*

Correspondence should be addressed to Junchen Zhang; 11junchzh@163.com and Bo Li; libo5479937@126.com

Received 3 July 2022; Revised 3 August 2022; Accepted 9 September 2022; Published 30 September 2022

Academic Editor: Xianwei Zeng

Objectives. Glioma patients with brain tumor-related epilepsy (BTRE) have a complex profile due to the simultaneous presence of two pathologies, glioma and epilepsy; however, they have not traditionally received as much attention as those with more malignant brain tumors. The underlying pathophysiology of brain tumor-related epilepsy remains poorly understood. The purpose of this study was to investigate the possible correlation between molecular neuropathology and glioma with BTRE and a wide range of BTRE-associated molecular markers of glioma patients. *Methods*. A retrospective cohort study of 186 glioma patients was evaluated at our hospital, of which 64 had BTRE. The chi-square test, Spearman rank correlation, and multivariate logistic analyses were used to identify clinicopathological factors associated with BTRE in glioma patients. *Results*. Of the 186 patients examined in this study, 64 (34.4%) had BTRE. Based on the analysis of the characteristics of these patients, the results showed that patient age (over 40 years; $P = 0.007$), low WHO grade (grade I, II; $P = 0.001$), IDH-1 positive mutation ($P = 0.027$), low ATR-X expression level (OR = 0.44; 95% CI: 0.21, 0.92), and low Ki-67 PI (OR = 0.25; 95% CI: 0.10, 0.68) were associated with the occurrence of BTRE. In our cohort, BTRE patients did not differ by sex, tumor location, or expression of olig-2 and CD34. The results of the matching study showed that low Ki-67 PI and negative ATR-X expression levels were independent factors for a higher incidence of preoperative seizures in glioma patients. *Conclusion*. The current study updates existing information on genetic markers in gliomas with BTRE and explores the correlation of a wide range of clinicopathological factors and glioma patients with BTRE and suggests three putative biomarkers for BTRE: positive IDH1 mutation, low Ki-67 PI, and negative ATR-X expression. These factors may provide insights for developing a more thorough understanding of the pathogenesis of epilepsy and effective treatment strategies aimed at seizure control.

1. Introduction

Epilepsy associated with brain tumors is called brain tumor-related epilepsy (BTRE), and the International Union of Antiepileptics (ILAE) defines tumor-related epilepsy as a persistent tumor lesion in the brain that causes more than one seizure [1, 2]. As the main symptom of brain tumors, epilepsy seriously affects the quality of life of patients. As a common brain tumor, most gliomas are caused by epilepsy, especially in patients with low-grade gliomas [3]. The frequency of epilepsy in patients with brain tumors ranges from 30 to 100% depending on the tumor type [1, 3–5],

and the proportion of patients with epilepsy as the first symptom of gliomas can be as high as 50%-80% [6, 7], some studies in China showed that the incidence of glioma-related epilepsy before surgery was 34.1%, and the incidence of glioma-related epilepsy after surgery was 19.4%, the incidence of both preoperative and postoperative glioma-associated epilepsy was highest in anaplastic oligodendroglioma (AO) and lowest in IDH wild-type glioblastoma (GBM), and, patients less than 45 years old, with normal neurological function and lower WHO grade were more likely to have glioma-related epilepsy [8–10]. Although surgical resection of the tumor can improve the prognosis of epilepsy, there are still a small number of patients after surgical treatment who will still require drugs that have difficulty controlling epilepsy, known as refractory epilepsy [11, 12]. As the most common presentation of glioma and one of the main clinical symptoms in the early stage of glioma, epileptic seizures are also one of the most common reasons that many glioma patients visit the clinic for the first time, and most patients are diagnosed with gliomas due to seizures, which are often considered an early warning sign for glioma patients [13–16]. Both epileptic seizures and the use of antiepileptic drugs can lead to cognitive impairment in patients, and more than 10% of glioma patients will develop epileptic persistence. Despite various antitumor treatments, one-half of the patients had a seizure within 1 month and two-thirds within 3 months before the last evaluation, which affects their long-term quality of life and the therapeutic effect of glioma [7]. Also, numerous studies had shown that epilepsy was significantly associated with survival in patients with glioma, some studies found that postoperative glioma-associated epilepsy – but not preoperative glioma-associated epilepsy, predicted longer overall survival [8–10]. Therefore, a better understanding of BTRE's associated risks and production mechanisms can help to better predict, prevent, and control the occurrence of epilepsy, which is also of great significance for the comprehensive intervention of glioma patients.

The mechanism of brain tumor-related epilepsy is currently believed to be related to the tumor mass effect [17], formation of intracranial hypersensitized areas [18], local microenvironment changes in surrounding tumor tissues [19], and activation of the glutamate NMDA receptor [3]. Some studies have found that patients have extremely excited epileptogenic foci in the brain, including tumor cells and surrounding adjacent tissues caused by tumor compression or stimulation, and they can disrupt the brain's balance between excitement and inhibition by altering the expression of neuropeptides, neurotransmitters, and their receptors [3, 19]. In addition, the regional destruction of nerve cells in tumor cells and adjacent tissues leads to the blocking of afferent nerves in some cortical areas, which promotes the formation of an epileptogenic environment and the gradual development of a highly sensitized area for epileptic seizures [16]. Other studies have shown that local microenvironmental changes in brain tumor surrounding tissues can also induce seizures, such as swelling, ischemia, hypoxia, and acidosis. The depolarization and repolarization of ion channels on the cell membrane are unbalanced, which destroys the equilibrium of the local microenvironment of Na^+, Ca^{2+}, and Cl^- plasma; increases the excitability of neurons, making them more vulnerable to external stimulation, and produces sudden, temporary abnormal discharge of neurons, leading to seizures. Studies have also shown that the NMDA receptor (N-methyl-d-aspartic acid receptor, or N-methyl-D-aspartate receptor) of glutamate can activate intracellular mTOR, AKT, MAPK, and other signaling pathways, leading to an increase in the frequency of epileptic seizures and a faster growth rate of tumor cells [3, 20, 21].

Previous studies have shown that the risk of seizures decreases with age, and that men are at higher risk than women. Additionally, tumor location (frontal, temporal, cap, pillow, island) and WHO classification (grades I ~ IV) are associated with brain tumor-related epilepsy [22, 23]. The incidence of brain tumor-related epilepsy in the frontal lobe, temporal lobe, insular lobe, and parietal lobe was higher than that in deep tumor tissues [24]. In summary, the pathophysiological mechanisms of brain tumor-related epilepsy are numerous and very complex, and there is no consensus on the effect of histopathological types and biomarkers on epilepsy risk. The correlation between IDH1 mutation, WHO pathological grade, and glioma tumor-related epilepsy has become a research hot spot; however, most of these studies have looked at prognostic relevance and drug therapy. Our study retrospectively analyzed the clinical and molecular pathologic data of all glioma patients surgically resected and routinely pathologically confirmed in our hospital over a 3-year period to study the relationship between gender, age, location of occurrence, and different molecular pathological markers in the occurrence of brain tumor-related epilepsy in glioma patients. We hope to have a more systematic and comprehensive understanding of epilepsy in glioma patients and provide theoretical support for better improving the quality of life of glioma patients.

2. Patients and Methods

2.1. Patients and Examination. This was a retrospective cohort study. The study was approved by the institutional review board (approval number: 2022C210) and was conducted according to the guidelines in the Helsinki Declaration and its later amendments. The informed consent was waived owing to the retrospective nature of this study. All the patients in this study were selected as following: a total of 256 human glioma specimens were collected from the Affiliated Hospital of Jining Medical University from January 2017 to December 2019, which were resected by neurosurgery and preserved completely and were diagnosed as glioma by pathology. All cases had complete clinical, imaging, and pathological data. MRI was performed in all patients after hospitalization to determine the location, size, and proximity of the tumor and to determine the tumor involvement in the lobe. Histological classification was carried out according to the 2016 WHO standards for grading tumors of the central nervous system. There were a total of I ~ IV levels, and the histological types mainly included astrocytoma, oligodendroglioma, and glioblastoma. The diagnosis of epileptic seizures was based on the criteria established by the 2017 International League Against Epilepsy (ILAE), and semiological seizure classification was

performed by preoperative evaluation. The exclusion criteria were as follows: (1) craniocerebral trauma; (2) congenital cerebral vascular malformation, such as arteriovenous malformation and cavernous hemangioma; (3) other intracranial tumors, such as meningiomas and brain metastases; (4) infectious diseases of the central nervous system; (5) primary epilepsy caused by congenital neurological diseases, such as cortical dysplasia; (6) febrile epilepsy, drug-induced epilepsy, and other epilepsy unrelated to intracranial tumors; (7) nonfirst operation, chemoradiotherapy, and other treatments. And, the research flow chart of this study was shown in Figure 1. There is a department in our hospital that specializes in the follow-up of discharged patients, however, it is inevitable that some patients will be lost to follow-up, because some patients are involved in China and they are reluctant to disclose the condition of patients after discharge, especially the patients who died after discharge.

2.2. Clinical Variables. Information was collected, including age, gender, epileptic seizure, lesion location, IDH-1 mutation, WHO classification, Ki-67 proliferation index, CD34 expression, GFAP expression, olig-2 expression, and ATRX expression (Tables 1 and 2 for details). The diagnosis of epileptic seizures was evaluated and guided jointly by certified neurologists and neurosurgeons. MRI was performed for all patients, and the lesion site was evaluated by a certified radiologist.

2.3. Laboratory Testing. All glioma specimens were immunostained, including CD34, oligo-specific nuclear transcription factor (OLIg-2), ATRX, P53, proliferation index (KI-67), and glial fibrillary acidic protein (GFAP), and all of the above monoclonal antibodies were purchased from Beijing Zhongshan Jinqiao Biological Co. Ltd. Sanger sequencing was used to detect the IDH1 R132H mutation. Immunohistochemistry (SP) used the following method: paraffin sections were placed in the oven at 60°C for 1 hour to prevent defoliation. Samples were dewaxed and rinsed 3 times with double steaming water for 5 minutes; the slices were put into citric acid buffer solution with pH 6.0, put into a pressure cooker and heated to boiling in a water bath. After 2 minutes in the water bath, the slices were naturally cooled at room temperature for 30 minutes and rinsed 3 times with PBS for 5 minutes. Next, 3% hydrogen peroxide was added to inactivate endogenous peroxidase; the samples were left at room temperature for 5-10 minutes and rinsed 3 times with distilled water for 5 minutes. Normal goat serum blocking solution was added, and the samples were incubated at room temperature for 20 minutes, added to 1 : 150 diluted primary antibody, and refrigerated overnight at 4°C. The cells were rinsed 3 times with PBS for 5 min, dripped with biotin-labeled secondary antibody, left at room temperature for 20 minutes, and rinsed 3 times with PBS for 5 minutes. Streptomycin antibiotic protein-horseradish catalase complex working solution was added, and the samples were incubated at 37°C for 10-15 minutes and rinsed 4 times with PBS for 5 minutes. DAB color developing agent was added to control the color developing under the microscope. The samples were fully rinsed with tap water, hematlignin was redyed for 25 seconds, and 1% alcohol was differentiated for 50 seconds. Ammonia returned the samples to blue, the samples were fully rinsed with tap water, hematlignin was slightly redyed, and the final samples were dehydrated and transparent. Neutral gum was used as the seal tablet, and PBS was used as the negative control instead of primary antibody. All operations were carried out in strict accordance with the kit instructions.

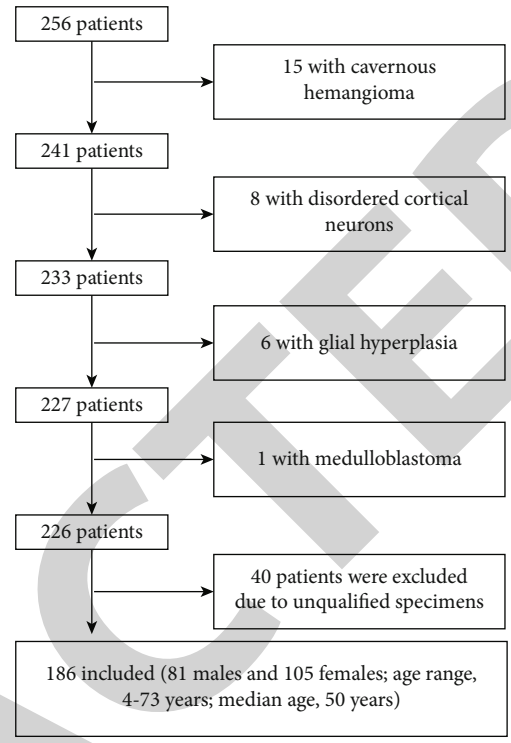

Figure 1: Research flow chart.

The YCTY2050 pathological image analysis system was used for quantitative determination. Specimens subjected to immunohistochemistry were assigned a grade for the staining intensity based on qualitative observations by two independent observers. GFAP was brownish yellow and stained in the cytoplasm and cell membrane. ATRX, Ki-67, and P53 were brownish yellow or brown particles, and the staining sites were the nuclei. The staining sites of CD34-positive cells were mainly in the cell boundary and cytoplasm, and uniform yellow staining was observed in vascular endothelial cells. Olig-2 was brownish yellow, with nuclei and cytoplasm as the staining sites, mainly nuclei.

The immunostained sections were observed with microscopes under low and high magnification, and 5 visual fields were randomly selected under high magnification (400X) to count 1,000 tumor cells and calculate the percentage of positive cells. The determination criteria for the results were as follows: negative (−): the tumor tissues were not stained at all or the number of positive cells was less than 5%; weak positive (+): the number of positive cells in tumor tissues was 6%-25%; positive (++): the number of positive cells in tumor tissues was 25%-50%; strong positive (+++): the positive number of tumor tissues was more than 50%. For the convenience of statistics, weak positive and negative were

Table 1: Basic characteristics and immunohistochemical indices of the study population. Of the 186 glioma patients, 56.5% were women and 75.8% were aged 40 or older. In terms of immunohistochemical indices, the positive rate of IDH-1 in the epileptic group was significantly higher than that in the nonepileptic group, but the positive rates of ATR-X and Ki-67 proliferation were significantly lower than those in the nonepileptic group (all $P < 0.05$).

Characteristics	Total cases ($N = 186$)	Cases with epilepsy ($N = 64$)	Cases without epilepsy ($N = 122$)	P value
Sex, N (%)				0.056
(i) Male	81 (43.5)	34 (53.1)	47 (38.5)	
(ii) Female	105 (56.5)	30 (46.9)	75 (61.5)	
Age, years, N (%)				**0.007**
(i) < 40	45 (24.2)	23 (35.9)	22 (18.0)	
(ii) ≥ 40	141 (75.8)	41 (64.1)	100 (82.0)	
Immunohistochemical indexes				
GFAP, N (%)				0.530
(i) (-)	2 (1.1)	0 (0.0)	2 (1.6)	
(ii) (+)	182 (97.8)	63 (98.4)	119 (97.5)	
Missing	2 (1.1)	1 (1.6)	1 (0.8)	
Olig-2, N (%)				0.942
(i) (-)	7 (3.8)	2 (3.1)	5 (4.1)	
(ii) (+)	167 (89.8)	58 (90.6)	109 (89.3)	
Missing	12 (6.5)	4 (6.3)	8 (6.6)	
IDH-1, N (%)				**0.027**
(i) (-)	133 (71.5)	38 (59.4)	95 (77.9)	
(ii) (+)	32 (17.2)	15 (23.4)	17 (13.9)	
Missing	21 (11.3)	11 (17.2)	10 (8.2)	
ATR-X, N (%)				**0.041**
(i) (-)	70 (37.6)	29 (45.3)	41 (33.6)	
(ii) (+)	93 (50.0)	24 (37.5)	69 (56.6)	
Missing	23 (12.4)	11 (17.2)	12 (9.8)	
Ki-67, N (%)				**0.001**
(i) Low	41 (22.0)	22 (34.4)	19 (15.6)	
(ii) Medium	73 (39.2)	28 (43.8)	45 (36.9)	
(iii) High	72 (38.7)	14 (21.9)	58 (47.5)	
CD34, N (%)				
(i) (-)	30 (16.1)	9 (14.1)	21 (17.2)	0.731
(ii) (+)	123 (66.1)	42 (65.6)	81 (66.4)	
Missing	33 (17.7)	13 (20.3)	20 (16.4)	

classified as negative, while positive and strong positive were classified as positive. The Ki-67 proliferation index (PI) was defined as the percentage of immunoreactive tumor cell nuclei among the total number of cells. PI was evaluated as follows: the number of positive cells ≤ 5% was considered low PI; the number of positive cells 6-20% was considered medium PI; and the number of positive cells > 20% was considered high PI.

2.4. Statistical Analyses. The results were analyzed with SPSS, version 22.0 (SPSS Inc., Chicago, IL, USA). Descriptive statistical methods were used to analyze the demographic characteristics, tumor location distribution, and immunohistochemical indices of the subjects. The frequency and percentage were used to describe the categorical variables statistically, and the chi-square test was used to analyze whether the difference between the two groups was statistically significant. The Spearman rank correlation was used to analyze the correlation between the immunohistochemical index and glioma with epilepsy. Multiple logistic regression was used to analyze the association between immunohistochemical indices and the risk of glioma with epilepsy, and the OR value and 95% CI were used as effect estimates. $P < 0.05$ was considered to be significant.

3. Results

3.1. Descriptive Characteristics of Glioma Patients. A total of 256 patients with glioma were included. And, none of the patients died during hospitalization. A total of 226 patients were recorded after excluding 15 patients with cavernous hemangioma, 8 with disordered cortical neurons, 6 with glial

Table 2: Pathological grade, tumor location, and histopathological type of the study population. There was no significant difference in tumor location between the epileptic group and the nonepileptic group ($P = 0.594$). IDH wild-type glioblastoma and IDH wild-type anaplastic astrocytoma were lower in the epileptic group, while IDH wild-type diffuse astrocytoma was higher in the epileptic group, and the difference in tumor histological type between the two groups was statistically significant ($P < 0.001$). The WHO pathological grade of the epileptic group was mainly low grade, while that of the nonepileptic group was mainly high grade, and the difference was statistically significant ($P < 0.001$).

Characteristics	Total cases ($N = 186$)	Cases with epilepsy ($N = 64$)	Cases without epilepsy ($N = 122$)	P value
Pathological grade, N (%)				**0.001**
(i) Grade 1	12 (6.5)	5 (7.8)	7 (5.7)	
(ii) Grade 2	67 (36.0)	35 (54.7)	32 (26.2)	
(iii) Grade 3	54 (29.0)	14 (21.9)	40 (32.8)	
(iv) Grade 4	53 (28.5)	10 (15.6)	43 (35.2)	
Tumor location, N (%)				0.594
(i) Frontal	55 (29.6)	23 (35.9)	32 (26.2)	
(ii) Temporal	44 (23.7)	15 (23.4)	29 (23.8)	
(iii) Parietal	6 (3.2)	2 (3.1)	4 (3.3)	
(iv) Occipital	2 (1.1)	0 (0.0)	2 (1.6)	
(v) Insula	1 (0.5)	0 (0.0)	1 (0.8)	
(vi) Thalamus	2 (1.1)	1 (1.6)	1 (0.8)	
(vii) Cerebellar hemisphere	7 (3.8)	0 (0.0)	7 (5.7)	
(viii) Ventricle	1 (0.5)	0 (0.0)	1 (0.8)	
(ix) Basal ganglia	3 (1.6)	1 (1.6)	2 (1.6)	
(x) Multiple lobes	65 (34.9)	22 (34.4)	43 (35.2)	
Histopathological type, N (%)				<0.001
(i) Glioblastoma, IDH-wild type	38 (20.4)	7 (10.9)	31 (25.4)	
(ii) Diffuse astrocytoma, IDH-wild type	33 (17.7)	15 (23.4)	18 (14.8)	
(iii) Anaplastic astrocytoma, IDH-wild type	25 (13.4)	4 (6.3)	21 (17.2)	
(iv) Diffuse astrocytoma, IDH-mutant	11 (5.9)	6 (9.4)	5 (4.1)	
(v) Anaplastic oligodendroglioma, NOS	9 (4.8)	1 (1.6)	8 (6.6)	
(vi) Oligodendrocytoma, NOS	9 (4.8)	7 (10.9)	2 (1.6)	
(vii) Astrocytoma, NOS	8 (4.3)	4 (6.3)	4 (3.3)	
(viii) Oligodendroglioma, NOS	8 (4.3)	4 (6.3)	4 (3.3)	
(ix) Anaplastic astrocytoma, NOS	6 (3.2)	3 (4.7)	53 (2.5)	
(x) Glioblastoma, NOS	6 (3.2)	1 (1.6)	5 (4.1)	
(xi) Diffuse astrocytoma, NOS	6 (3.2)	4 (6.3)	2 (1.6)	
(xii) Pilocytic astrocytoma	5 (2.7)	0 (0.0)	5 (4.1)	
(xiii) Gliosarcoma	4 (2.2)	0 (0.0)	4 (3.3)	
(xiv) Anaplastic astrocytoma, NOS	3 (1.6)	1 (1.6)	2 (1.6)	
(xv) Glioblastoma, IDH-mutant	3 (1.6)	2 (3.1)	1 (0.8)	
(xvi) Pilomyxoid astrocytoma	2 (1.1)	1 (1.6)	1 (0.8)	
(xvii) Gemistocytic astrocytoma, IDH-wild type	1 (0.5)	1 (1.6)	0 (0.0)	
(xviii) Gemistocytic astrocytoma, IDH-mutant	1 (0.5)	0 (0.0)	1 (0.8)	
(xix) Anaplastic glioma, NOS	1 (0.5)	0 (0.0)	1 (0.8)	
(xx) Anaplastic pleomorphic xanthoastrocytoma	1 (0.5)	0 (0.0)	1 (0.8)	
(xxi) Anaplastic astrocytoma, IDH-mutant	1 (0.5)	0 (0.0)	1 (0.8)	
(xxii) Glial hyperplasia	1 (0.5)	1 (1.6)	0 (0.0)	
(xxiii) Ganglioglioma	1 (0.5)	1 (1.6)	0 (0.0)	
(xxiv) Diffuse glioma, NOS	1 (0.5)	0 (0.0)	1 (0.8)	
(xxv) Gangliocytoma	1 (0.5)	0 (0.0)	1 (0.8)	
(xxvi) Pilocytic astrocytoma	1 (0.5)	1 (1.6)	0 (0.0)	

Table 3: Spearman correlation coefficients among basic characteristics and tumor-related epilepsy. The Spearman correlation coefficient between the IDH-1 positive rate and tumor-related epilepsy was 0.16, with a significant positive correlation ($P < 0.05$). The Spearman correlation coefficients between the positive rate of ATR-X expression and the Ki-67 proliferation index and tumor-related epilepsy were −0.17 and −0.28, respectively, and they were significantly negatively correlated with tumor-related epilepsy ($P < 0.05$).

Variables	GFAP	Olig-2	IDH-1	ATR-X	Ki-67	CD34	Epilepsy
GFAP	1.00	0.25**	0.05	−0.10	−0.12	0.16*	0.08
Olig-2		1.00	0.01	−0.03	−0.07	0.13	0.03
IDH-1			1.00	−0.03	−0.19*	−0.09	0.16*
ATR-X				1.00	−0.004	0.04	−0.17*
Ki-67					1.00	−0.07	−0.28**
CD34						1.00	0.03
Epilepsy							1.00

*$P < 0.05$; **$P < 0.001$.

hyperplasia and 1 with medulloblastoma. In addition, 40 patients were excluded due to unqualified specimens (insufficient tissue, damaged wax blocks). Finally, 186 patients were included (81 males and 105 females; age range, 4–73 years; median age, 50 years) (Figure 1). We divided all patients into two groups based on preoperative seizure status: the BTRE (brain tumor-related epilepsy) group and the NO BTRE group. In the BTRE group, there were 64 patients, including 34 males and 30 females, 23 (35.9%) under the age of 40 years and 41 (64.1%) over the age of 40 years. In the NO BTRE group, there were 122 patients, including 47 males and 75 females, 22 (18.0%) under the age of 40 years and 100 (82.0%) over the age of 40 years. Tumor location was analyzed using MRI characteristics, and the tumor side was not considered in this study to better define the correlation between molecular indicators and tumors related to epilepsy. The most commonly involved location was multiple lobes ($N = 65$, 34.9%), followed by the frontal lobe ($N = 55$, 29.6%), the temporal lobe ($N = 44$, 23.7%), the cerebellum ($N = 7$, 3.8%), the parietal lobe ($N = 6$, 3.2%), the basal ganglia region ($N = 3$, 1.6%), the thalamus and occipital lobe ($N = 2$, 1.1%), and the insula, and intraventricular regions ($N = 1$, 0.5%) (for details, see Tables 1 and 2). Since the focus of this study was on the correlation of clinicopathological factors with brain tumor-related epilepsy in glioma of the patients, the survival rate of patients was not counted, so patients who died or were lost to follow-up after discharge were not counted.

The pathological results showed that the BTRE group included 5 grade I, 35 grade II, 14 grade III, and 10 grade IV patients; the NO BTRE group included 7 grade I, 32 grade II, 40 grade III, and 43 grade IV patients. The baseline information of all patients is summarized in Table 2. All 186 patients were successfully collected and analyzed for the expression levels of GFAP, olig-2, ATR-X, CD34, and p53. IDH mutation and Ki-67 PI were also recorded and analyzed (Table 1). The histopathological type of all the patients was also collected and analyzed (2016 World Health Organization (WHO) Classification of Tumors of the Central Nervous System); see Table 2.

3.2. Main Results. To identify factors that might be associated with tumor-related epilepsy, demographic and tumor information was compared between patients with and without seizures (see Table 1 for a complete list). Demographic statistics showed that there were significantly more female (56.5%) glioma patients than male (43.5%) patients; however, males (53.1%) had a higher incidence of BTRE than females (46.9%). The chi-square test showed no statistical significance ($P = 0.056$). The statistical results showed that there were significantly more glioma patients older than 40 years than younger than 40 years, and the incidence of TRE in patients older than 40 years was significantly higher than that in patients younger than 40 years ($P < 0.05$). The statistical results of the correlation between tumor location and epilepsy showed that glioma tended to occur in multiple lobes (34.9%), followed by the frontal (29.6%) and temporal lobes (23.7%), while BTRE tended to occur in the frontal lobe (35.9%), followed by multiple (34.4%) and temporal lobes (23.4%), and the difference was not statistically significant ($P = 0.594$). The WHO classification results showed that TRE occurred mainly in patients with low-grade glioma (WHO grade II (54.7%)), followed by patients with high-grade glioma (WHO grade III (32.8%), WHO grade IV (35.2%)), and the difference was statistically significant ($P < 0.05$). Histopathological results showed that glioblastoma IDH wild-type (20.4%) and anaplastic astrocytoma IDH wild-type (17.7%) were lower in the NO BTRE group, diffuse astrocytoma IDH wild-type (23.4%) was higher in the TRE group, and the difference in tumor histological type between the two groups was statistically significant ($P < 0.001$); for details, see Table 2. Analysis of immunohistochemical indices and IDH1 mutation results showed that three variables were significantly associated with the presence of epilepsy: IDH-1 mutation ($P = 0.027$), low ATR-X expression level ($P = 0.041$), and low Ki-67 PI ($P = 0.001$) (Table 2). The Spearman rank correlation analysis showed that the correlation coefficient between IDH-1 mutation and BTRE was 0.16, with a significant positive correlation ($P < 0.05$). The correlation coefficients between ATR-X-positive expression and Ki-67 PI and BTRE were −0.17 and −0.28, respectively, and they were significantly negatively correlated with TRE ($P < 0.05$) (Table 3). Representative immunohistochemical staining for Ki-67 labeled from low to high (low, ≤5%; medium, 6-20%; high, >20%), ATR-X positive or negative expression and analysis of IDH1 mutation with negative and positive results are shown in Figures 2,

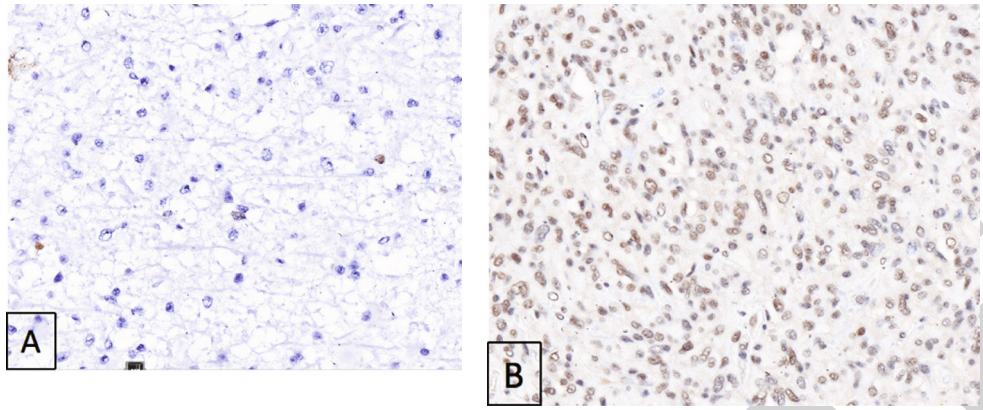

(a) (b)

Figure 2: Photomicrographs of tumor tissue stained for ATR-X: (a) negative expression, (b) positive expression, original magnification: x400.

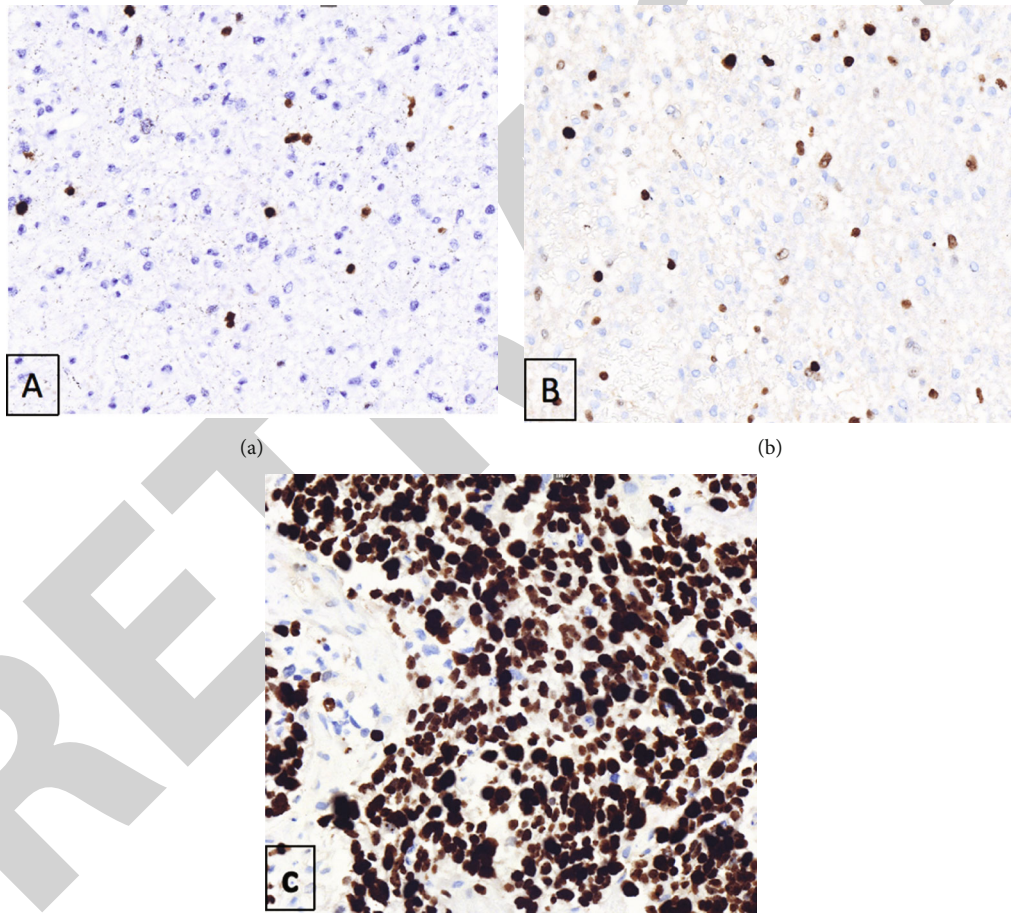

(a) (b)

(c)

Figure 3: Photomicrographs of tumor tissue stained for Ki-67 PI: (a) low Ki-67 PI (≤5%), (b) medium Ki-67 PI (6-20%), (c) high Ki-67 PI (>20%), original magnification: x400.

3, and 4, respectively. No other clinical or pathological variables were found to be associated with an increased risk for preoperative seizures in this group of patients. In the multinomial logistic regression analysis, after adjusting for gender, age, and WHO grade, the incidence of epilepsy in glioma patients with ATR-X-positive expression was significantly reduced ($P = 0.029$), and the risk was 56% lower than that in the ATR-X-negative expression group (OR = 0.44; 95% CI: 0.21, 0.92). Compared with that in the low-proliferation Ki-67 group, the incidence of epilepsy in glioma patients in the

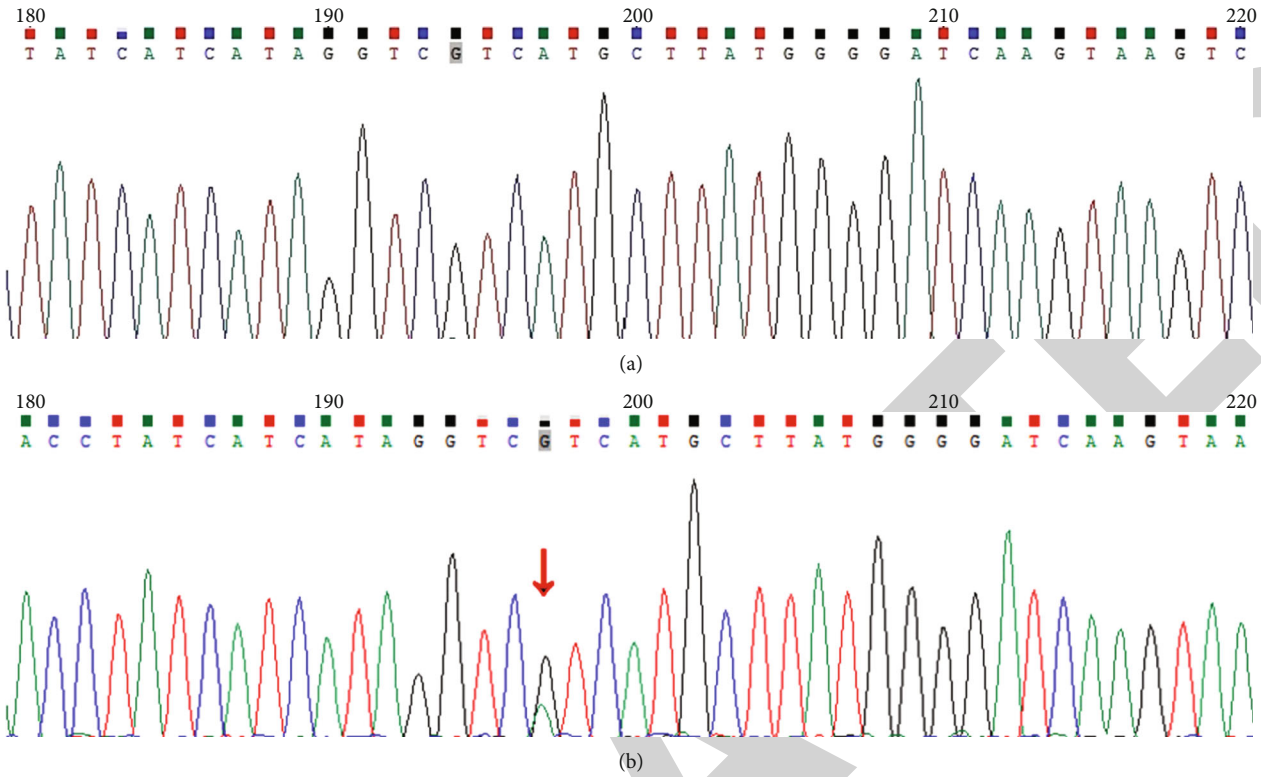

Figure 4: Sanger sequencing analysis of IDH1 R132H mutation with negative (a) and positive (b) (the red arrow) results.

high-proliferation Ki-67 group was significantly reduced ($P = 0.006$), and the risk was reduced by 75% (OR = 0.25; 95% CI: 0.10, 0.68). That is, low Ki-67 PI and low ATR-X expression levels were found to have a strong association with preoperative seizures, which were independent factors for a higher incidence of preoperative seizures (Table 4).

4. Discussion

Brain tumor-related epilepsy (BTRE) is a type of epilepsy induced by the abnormal discharge of the intracranial tumor itself or its mass effect caused by the abnormal discharge of nerve cells around the lesion[1]. Seizures are one of the clinical symptoms of brain tumors, so patients can also present with disorders of consciousness, limb movement, and sensory and autonomic nervous function [25–27]. Seizures are often seen in patients with brain tumors and occur at different rates. However, there is no clear conclusion on the pathogenesis and pathophysiology of BTRE, and there is no single theory that can explain the cause of BTRE, which is a relatively complex and multifactor seizure [28–31].

Seizures and the use of antiepileptic drugs can lead to cognitive impairment, affect the long-term quality of life of patients, and have curative effects on brain tumors, which can also affect patients' family harmony, poor working conditions, and low moods [29]. Patients with brain tumor-related epilepsy (BTRE) present a complex therapeutic profile and require a unique and multidisciplinary approach. They, in fact, must face two different pathologies at the same time, brain tumor and epilepsy. In brain tumor patients, the presence of epilepsy is considered the most important risk factor for long-term disability [32, 33]. The problem of the proper administration of medications and their potential side effects is of great importance because good seizure control also has a significant impact on the patient's psychological and relational sphere [33]. Therefore, it is necessary to understand the mechanism of BTRE to better predict, prevent, and control the occurrence of epilepsy. With the progress of research methods and technologies, BTRE has been deeply explored, especially in terms of its pathogenesis and the corresponding brain neural network. However, there is still a lack of sufficient attention and systematic research on the pathogenesis, clinical diagnosis, and treatment of BTRE. At present, few studies have focused on the molecular neuropathologic correlation of glioma with tumor-related epilepsy [11], except for several studies on the association between WHO classification and IDH1 mutation in brain tumor-related epilepsy of patients with low-grade glioma [25, 34, 35]. Therefore, to better define the etiology of tumor-related epilepsy in glioma patients, our study focused on the correlation between molecular neuropathic indicators and BTRE in low and high glioma patients, which was expected to clarify the pathogenesis of glioma patients with BTRE and benefit glioma patients. This large cohort of glioma patients was treated at a single institute in China over a period of 3 years.

To our knowledge, this is the first systematic retrospective study to investigate the correlation between molecular neuropathology and different grades of glioma in patients with BTRE. In the 186 glioma patients, the results showed

Table 4: Associations of immunohistochemical indices with the risk of having tumor-related epilepsy[a]. Multiple logistic regression was used to analyze the association between immunohistochemical indices and the risk of glioma complicated with epilepsy, and the results are shown in Table 4. After adjusting for gender, age, and WHO pathological grade, the incidence of epilepsy in patients with ATR-X-positive glioma was significantly reduced ($P = 0.029$), and the risk was 56% lower (OR = 0.44) than that in the ATR-X-negative group. 95% CI: 0.21, 0.92). Compared with the low-proliferation Ki-67 group, the incidence of epilepsy in glioma patients in the high-proliferation Ki-67 group was significantly reduced ($P = 0.006$), and the risk was reduced by 75% (OR = 0.25; 95% CI: 0.10, 0.68).

Variables		ORs (95% CIs)	*P* value
GPAF	(-)	1.00 (reference)	—
	(+)	0.31 (0.02, 5.09)	0.409
Oli-2	(-)	1.00 (reference)	—
	(+)	1.14 (0.32, 4.07)	0.840
IDH-1	(-)	1.00 (reference)	—
	(+)	2.30 (0.94, 5.63)	0.068
ATR-X	(-)	1.00 (reference)	—
	(+)	**0.44 (0.21, 0.92)**	**0.029**
Ki-67	Low	1.00 (reference)	—
	Medium	0.67 (0.27, 1.68)	0.394
	High	**0.25 (0.10, 0.68)**	**0.006**
CD34	(-)	1.00 (reference)	—
	(+)	0.86 (0.38, 1.96)	0.718

[a]Sex and age were adjusted in the model.

that patients aged over 40 years old and with a low WHO grade were significantly correlated with BTRE. Additionally, we identified one histopathological type and three molecular pathological characteristics that were specifically associated with BTRE: diffuse astrocytoma, IDH wild type, low Ki-67 PI, negative ATR-X expression, and IDH-1 positive mutation status. In addition, Ki-67 PI and ATR-X expression were independent factors correlated with a higher incidence of preoperative seizures. Future research should focus on identifying susceptibility candidate genes for BTRE in larger multicenter studies, including low- and high-grade gliomas with and without symptomatic seizures.

Previous studies have shown that age, sex, tumor location, histopathological type, and WHO grade were the influencing factors of glioma with BTRE, although the results of various reports were inconsistent [25, 36, 37]. At present, there is no agreement on the influence of age, sex, and histopathological type on the occurrence of epilepsy. One study showed that the risk was higher in men than in women, and the risk of seizure decreased with age; however, the results varied among different histopathological types [38]. Previous studies have shown that the most common gliomas associated with epilepsy are diffuse astrocytoma, oligodendroglioma, and pleomorphic xanthoastrocytoma [39]. According to the World Health Organization Classification, 2016 edition [40], gliomas are classified as diffuse gliomas (astrocytoma, oligodendroglioma, and glioblastoma) and circumscribed and low-grade gliomas (angiocentric glioma, pilocytic astrocytoma, subependymal giant cell astrocytoma, pleomorphic xanthoastrocytoma, pilomyxoid astrocytoma, ependymoma, myxopapillary ependymoma, and subependymoma). Some research results showed that most patients with angiocentric glioma were children and young people, with no significant gender difference, and epilepsy was the main clinical manifestation [22]; diffuse astrocytoma and oligodendroglial tumors were common in the cerebral hemisphere of young patients (frontal and temporal lobes were common), and epilepsy was one of the most common clinical symptoms [41]. These results showed that low-grade gliomas were more common in young adults and were more common in the supratentorial frontal and temporal lobes, with no gender difference, and epilepsy was one of the main clinical symptoms. However, the previous studies were not entirely consistent with our findings. Our statistical results showed that BTRE was higher in male glioma patients than in female patients, but the results were not statistically significant. The incidence of BTRE in glioma patients older than 40 years was higher than that in glioma patients younger than 40 years, and the results were statistically significant. In addition, the most common histological types of BTRE in our study were diffuse astrocytoma, IDH wildtype, followed by oligodendrogastrocytoma, NOS; glioblastoma, IDH wildtype; and diffuse astrocytoma, IDH mutant. The relationship between the location of the glioma and BTRE risk has been controversial. Gliomas can occur in any part of the brain; however, frontal, temporal, and parietal gliomas are the most likely to be associated with BTRE, while occipital and supratentinal gliomas are less likely to have BTRE [39]. Our results showed that BTRE was most likely to occur in gliomas involving the frontal lobe and multiple lobes (see Table 2). The frontal lobe, temporal lobe, and parietal lobe are closely related to human language, consciousness, and motor functions. Lesions in these areas could cause abnormal discharge of these brain functional areas, leading to epilepsy. If the glioma invades the cortical functional area, the incidence of epilepsy will be higher. However, statistical

results showed that the occurrence of BTRE was not statistically significant in relation to the location of the tumor, which was different from previous studies [36]. The reasons for the different statistical results may be related to differences in study design and populations or the complex mechanism of BTRE, and the results of individual research centers could be different.

Previous studies have shown that seizures are more common in low-grade gliomas than in high-grade gliomas [1, 3]. The results were similar to those in our study, which showed that BTRE was present in lower grade gliomas at 62.5% and in higher grade gliomas at 37.5%. This may be related to the faster growth rate of high-grade glioma, which will cause severe ischemic and hypoxic damage to the surrounding tissues and tumor tissues themselves, making them less likely to form epileptogenic foci. Other studies have suggested that high-grade gliomas release excessive amounts of the neuroexcitatory transmitter glutamate, which is neurotoxic and can lead to neuronal death in large quantities, so high-grade gliomas are less likely to have seizures [42]. Some studies have also suggested that the rapid growth of high-grade gliomas destroys the brain's electrical transmission network; however, low-grade glioma has a slow growth rate and little influence on the surrounding tissues, presenting with gradual degeneration, causing partial cortical afferent nerve block, leading to high sensitivity of demulsification, and promoting the formation of epileptogenic foci [17, 43]. At present, the correlation and mechanism of BTRE in different WHO grade gliomas mainly focus on the destruction of the blood–brain barrier, gene mutations, changes in neurotransmitters, and receptors, and changes in ion concentration. Additionally, studies have shown that cellular inflammatory factors are involved in the occurrence and development of BTRE in glioma [44, 45]. Despite numerous studies, the mechanism of BTRE in different grades of gliomas is still unclear and needs further research.

Isocitrate dehydrogenase (IDH) is a member of the α-hydroxy acid oxidative decarboxylase family. IDH mainly acts on the tricarboxylic acid cycle to convert isocitrate into α-ketoglutaric acid, while the IDH mutation could convert isocitrate into 2-hydroxyglutaric acid (2-HG); the altered reaction is known as the weakening of alpha-ketoglutaric acid, which increases the level of 2-HG [46]. The IDH mutation was first identified in low-grade glioma patients, which was an early event in gliomagenesis and has significant implications for glioma progression and tumor behavior [47]. A previous study showed that mutation of the IDH gene occurred in ~80% of lower-grade (WHO grade II and grade III) gliomas [48]. Mutant IDH produces (R)-2-hydroxyglutarate, which induces DNA hypermethylation and presumably drives tumorigenesis, which also suggests that 2-HG plays an important role in the occurrence and development of epilepsy. Due to 2-HG being structurally similar to glutamate, IDH1 mutant glioma cells release a large amount of 2-HG that will combine multiple neurons and activate receptors, such as NMDARs and AMPARs, causing the influx of sodium ions, potassium ions, and calcium ions, increasing the action potential triggered by neurons, and damaging the balance between the inhibition and excitation of neurons, thus causing abnormal excitation of neurons and promoting the occurrence of epilepsy [49]. Therefore, the incidence of BTRE in IDH1 mutant glioma patients is much higher than that in IDH1 wild-type patients. Our study showed that the IDH1 positive mutation incidence in glioma patients with epilepsy was 23.4%, which was different from IDH1 negative mutation incidence in the NO BTRE group (13.9%), and the difference was statistically significant, which suggested that IDH1 positive mutation was closely related to BTRE in glioma patients. Our study also showed that IDH1 mutation was more likely to occur in diffuse astrocytoma patients.

In our study, we identified two important molecular pathological characteristics associated with BTRE in glioma patients: Ki-67 PI and ATR-X expression. Tumor-correlated biomarkers in glioma patients with BTRE have been a popular research topic for decades; however, they have not traditionally enjoyed as much attention as more malignant brain tumors. In recent years, a number of developments have been achieved toward further understanding the molecular and developmental backgrounds of glioma patients with BTRE, which helps to clarify the mechanism of glioma leading to epileptic seizures. Several studies have shown that a number of candidate genes cause seizures in glioma patients, such as interleukin-1β (IL-1β) [50], CD34 [51], and tuberous sclerosis complex (TSC) [52]. Molecular genetic effects may alter the balance between intracortical inhibitory and excitatory mechanisms, therefore inducing epileptogenic activity. However, the molecular mechanism underlying BTRE remains largely unknown, and there is still an issue of whether BTRE in glioma patients results from localized epileptic foci that lead to abnormal circuits or from molecular defects. Ki-67 is a protein found in the nucleus of a cell. Ki was discovered in the 1980s in Kiel, Germany, and the number 67 comes from the experiment number. Researchers have found a strong link between the amount of this protein and the cell division cycle; the higher the positive rate of Ki-67 is, the higher the proportion of cells in the proliferative cycle and the faster the tumor growth [53]. At present, Ki-67 has become a very important indicator to judge the activity level of tumor cells. The association between Ki-67 and BTRE in glioma patients has rarely been studied, and the results have been inconsistent [54]. One study showed that the Ki-67 proliferation index was not associated with the risk of epileptic seizures in glioma patients [55]. However, some studies have also suggested that Ki-67 significantly affects seizure prognosis [56] and is related to BTRE in glioma by increasing proliferation [56]. These results indicated that Ki-67 may play a role in epilepsy in glioma patients. Low Ki-67 PI is usually associated with benign tumors or low-grade glioma (WHO grade I, II), and our study already showed that WHO grade I or II was associated with BTRE in glioma patients (Table 2), which supports our hypothesis that it could increase the incidence of preoperative seizures in glioma patients. In our study, a low Ki-67 PI was clearly associated with BTRE in glioma, with statistical significance. Of course, the results of this study cannot be taken as the final result, and the correlation between Ki-67 PI and epilepsy in glioma patients need

further study. The ATR-X gene is a pathogenic gene of X-linked α thalassemia/mental retardation syndrome located on the X chromosome and plays an important role in chromatin remodeling, genome, and maintenance of telomere stability [57]. Mutations in ATR-X have been identified in multiple tumor types; in 2011, Heaphy et al. found that ATR-X gene mutation existed in tumors of the central nervous system, and a series of subsequent studies confirmed that ATR-X gene mutation mainly occurred in diffuse astrocytoma [58]; in 2014, the consensus of the International Society of Neuropathology considered the deletion of the ATR-X gene as a characteristic molecular marker of diffuse astrocytoma [59]; in 2016, the World Health Organization (WHO) integrated IDH, TERT, 1P19Q, and other molecular markers into the histopathological diagnosis of glioma, promoting the accurate diagnosis of glioma [37]. Under the guidance of molecular typing, the accurate treatment of glioma has been a popular research topic in recent years. The ATR-X gene mutation can be used as a prognostic indicator for glioma patients. However, the association between ATR-X and epilepsy in glioma patients has not been described. Our study showed that compared with the epilepsy group, glioma patients with ATRX gene-positive mutations in the nonepileptic group were less likely to develop epilepsy, which was statistically significant (see Tables 3 and 4). In this study, positive expression of the ATR-X gene in glioma patients was significantly negatively correlated with concurrent tumor epilepsy ($P < 0.05$), which was shown to be an independent predictor for preoperative seizures in glioma patients. This finding has not been previously reported, and the mechanism needs to be confirmed by further research. Therefore, we expect and speculate that Ki-67 and ATR-X may become novel diagnostic or therapeutic targets for tumor-related epilepsy in glioma in the future.

In our study, we did not find that glioma patients with tumors of different lobes and positive or negative expression of olig-2 and CD34 were significantly likely to present with epilepsy. These results differ from previous studies and may be due to differences in the number of cases, methods, and mechanisms involved [51]. In addition, some limitations should be presented as follows. First, the project design of a small sample ($N = 186$) and single center cannot produce effective results. Second, only 64 glioma patients had epilepsy, leading to a relatively limited statistical power. Thus, the adjustment in logistic regression may be too extensive. Third, there were no data for other molecules, such as p53, EGFR amplification, and 1p/19q deletion, which should clarify their correlation with BTRE in glioma patients. Thus, further studies are needed to provide more evidence to identify molecular markers related to glioma with BTRE.

5. Conclusion

In summary, this retrospective study investigated new molecular pathologic indicators in glioma patients with BTRE. Low WHO grade, age over 40 years old, IDH1 positive mutation, and low Ki-67 PI and ATR-X negative expression were predictive of the likelihood of epilepsy occurring in glioma patients. Thus, some of these factors will be worthy of further research as possible therapeutic targets, which may provide insights into developing a more thorough understanding of the pathogenesis of epilepsy and aim to improve the long-term remission rate of epilepsy before and after surgery.

Data Availability

The data used to support the findings of this study are included within the article.

Ethical Approval

The study was approved by the Institute's Ethics Committee of the Affiliated Hospital of Jining Medical University, Jining, China (approval number: 2022C210), and before the patient was enrolled, the ethics had been approved. Also, we have signed the Application Form for Waiving Consent Form.

Consent

The patients in this study agreed to the publication of this manuscript (One of the admission instructions of our hospital stipulates that, for medical research needs, tissue samples or information of patients during hospitalization (excluding personal information) can be used by physicians or research institutions affiliated with the hospital, and each patient admitted has signed an informed consent form. These rules have been unanimously approved by the Institute's Ethics Committee of Affiliated Hospital of Jining Medical University).

Conflicts of Interest

The authors declare that they have no competing interests.

Authors' Contributions

Bo Li and Junchen Zhang were assigned to the conception and design. Bo Li, Shunli Jiang, Guangning Zhang, and Junchen Zhang worked on the collection and assembly of data. Bo Li, Shunli Jiang, Guangning Zhang, and Junchen Zhang contributed on data analysis and interpretation. Bo Li and Junchen Zhang worked on the manuscript writing. Zengliang Wang, Wensheng Yang, Yongxin Wang, Yirizhati Aili, Zhitao Wang, and Quanyi Wang were assigned on the innovative discussion of the full text and recommendation of journals. All authors read and approved the final manuscript. Zengliang Wang and Wensheng Yang are co-first authors. Zengliang Wang, Wensheng Yang, Junchen Zhang, and Bo Li have contributed equally to this work.

Acknowledgments

This study was supported by Natural Science Foundation of Xinjiang Uygur Autonomous Region (NO.2021D01A02), PhD Research Foundation of Affiliated Hospital of Jining Medical University (Grant No. 2021-BS-006), and Research Fund for Lin He's Academician Workstation of New Medicine and Clinical Translation in Jining Medical University (JYHL2019FMS21). Thanks so much to my teachers Shuo

Wang, Shugan Zhu, and Andrew Kaye for encouraging me to finish the work. A preprint has previously been published by Research Square [60]; however, it has not been accepted by any journal.

References

[1] J. Pallud and G. M. McKhann, "Diffuse low-grade glioma-related epilepsy," *Neurosurgery Clinics of North America*, vol. 30, no. 1, pp. 43–54, 2019.

[2] C. Wessling, S. Bartels, R. Sassen, J. C. Schoene-Bake, and M. von Lehe, "Brain tumors in children with refractory seizures—a long-term follow-up study after epilepsy surgery," *Child's Nervous System*, vol. 31, no. 9, pp. 1471–1477, 2015.

[3] M. S. van Breemen, E. B. Wilms, and C. J. Vecht, "Epilepsy in patients with brain tumours: epidemiology, mechanisms, and management," *Lancet Neurology*, vol. 6, no. 5, pp. 421–430, 2007.

[4] C. Brogna, S. Gil Robles, and H. Duffau, "Brain tumors and epilepsy," *Expert Review of Neurotherapeutics*, vol. 8, no. 6, pp. 941–955, 2008.

[5] E. K. Avila, M. Chamberlain, D. Schiff et al., "Seizure control as a new metric in assessing efficacy of tumor treatment in low-grade glioma trials," *Neuro-Oncology*, vol. 19, no. 1, pp. 12–21, 2017.

[6] M. Kerkhof and C. J. Vecht, "Seizure characteristics and prognostic factors of gliomas," *Epilepsia*, vol. 54, Supplement 9, pp. 12–17, 2013.

[7] J. Hildebrand, C. Lecaille, J. Perennes, and J. Y. Delattre, "Epileptic seizures during follow-up of patients treated for primary brain tumors," *Neurology*, vol. 65, no. 2, pp. 212–215, 2005.

[8] S. Liang, X. Fan, M. Zhao et al., "Clinical practice guidelines for the diagnosis and treatment of adult diffuse glioma-related epilepsy," *Cancer Medicine*, vol. 8, no. 10, pp. 4527–4535, 2019.

[9] L. Li, S. Fang, G. Li et al., "Glioma-related epilepsy in patients with diffuse high-grade glioma after the 2016 WHO update: seizure characteristics, risk factors, and clinical outcomes," *Journal of Neurosurgery*, vol. 136, no. 1, pp. 67–75, 2022.

[10] CAAE, *Chinese Guideline of Diagnosis and Treatment for Epilepsy*, People's Medical Publishing House, Beijing, 2015.

[11] G. You, Z. Sha, and T. Jiang, "The pathogenesis of tumor-related epilepsy and its implications for clinical treatment," *Seizure*, vol. 21, no. 3, pp. 153–159, 2012.

[12] S. G. Berntsson, B. Malmer, M. L. Bondy, M. Qu, and A. Smits, "Tumor-associated epilepsy and glioma: are there common genetic pathways?," *Acta Oncologica*, vol. 48, no. 7, pp. 955–963, 2009.

[13] F. Santos-Pinheiro, M. Park, D. Liu et al., "Seizure burden pre- and postresection of low-grade gliomas as a predictor of tumor progression in low-grade gliomas," *Neuro-oncology practice*, vol. 6, no. 3, pp. 209–217, 2019.

[14] A. Wasilewski, J. Serventi, C. Ibegbu, T. Wychowski, J. Burke, and N. Mohile, "Epilepsy education in gliomas: engaging patients and caregivers to improve care," *Supportive Care in Cancer*, vol. 28, no. 3, pp. 1405–1409, 2020.

[15] G. You, W. Yan, W. Zhang et al., "Significance of miR-196b in tumor-related epilepsy of patients with gliomas," *PLoS One*, vol. 7, no. 9, article e46218, 2012.

[16] P. Gallagher, J. P. Leach, and R. Grant, "Time to focus on brain tumor-related epilepsy trials," *Neuro-Oncology Practice*, vol. 1, no. 3, pp. 123–133, 2014.

[17] H. K. Wolf, D. Roos, I. Blümcke, T. Pietsch, and O. D. Wiestler, "Perilesional neurochemical changes in focal epilepsies," *Acta Neuropathologica*, vol. 91, no. 4, pp. 376–384, 1996.

[18] G. Terrone, A. Salamone, and A. Vezzani, "Inflammation and epilepsy: preclinical findings and potential clinical translation," *Current Pharmaceutical Design*, vol. 23, no. 37, pp. 5569–5576, 2017.

[19] M. F. Shamji, E. C. Fric-Shamji, and B. G. Benoit, "Brain tumors and epilepsy: pathophysiology of peritumoral changes," *Neurosurgical Review*, vol. 32, no. 3, pp. 275–285, 2009.

[20] M. C. Lai, R. C. Tzeng, C. W. Huang, and S. N. Wu, "The novel direct modulatory effects of perampanel, an antagonist of AMPA receptors, on voltage-gated sodium and M-type potassium currents," *Biomolecules*, vol. 9, no. 10, p. 638, 2019.

[21] Y. Yuan, W. Xiang, L. Yanhui et al., "Activation of the mTOR signaling pathway in peritumoral tissues can cause glioma-associated seizures," *Neurological Sciences*, vol. 38, no. 1, pp. 61–66, 2017.

[22] D. Adamek, G. P. Siwek, A. A. Chrobak et al., "Angiocentric glioma from a perspective of A-B-C classification of epilepsy associated tumors," *Folia Neuropathologica*, vol. 54, no. 1, pp. 40–49, 2016.

[23] D. J. Englot, M. S. Berger, E. F. Chang, and P. A. Garcia, "Characteristics and treatment of seizures in patients with high-grade glioma: a review," *Neurosurgery Clinics of North America*, vol. 23, no. 2, pp. 227–235, 2012.

[24] Z. Yu, N. Zhang, N. U. F. Hameed et al., "The analysis of risk factors and survival outcome for Chinese patients with epilepsy with high-grade glioma," *World Neurosurgery*, vol. 125, pp. e947–e957, 2019.

[25] E. D. Goldstein and A. M. Feyissa, "Brain tumor related-epilepsy," *Neurologia i Neurochirurgia Polska*, vol. 52, no. 4, pp. 436–447, 2018.

[26] M. Maschio, A. Zarabla, A. Maialetti et al., "Quality of life, mood and seizure control in patients with brain tumor related epilepsy treated with lacosamide as add-on therapy: a prospective explorative study with a historical control group," *Epilepsy & Behavior*, vol. 73, pp. 83–89, 2017.

[27] D. J. Englot, E. F. Chang, and C. J. Vecht, "Epilepsy and brain tumors," *Handbook of Clinical Neurology*, vol. 134, pp. 267–285, 2016.

[28] L. Vercueil, "Épilepsie et tumeurs cerebrales : une mise au point et six questions encore en debat," *Revue Neurologique (Paris)*, vol. 167, no. 10, pp. 751–761, 2011.

[29] T. S. Armstrong, R. Grant, M. R. Gilbert, J. W. Lee, and A. D. Norden, "Epilepsy in glioma patients: mechanisms, management, and impact of anticonvulsant therapy," *Neuro-Oncology*, vol. 18, no. 6, pp. 779–789, 2016.

[30] C. Vecht, L. Royer-Perron, C. Houillier, and G. Huberfeld, "Seizures and anticonvulsants in brain tumours: frequency, mechanisms and anti-epileptic management," *Current Pharmaceutical Design*, vol. 23, no. 42, pp. 6464–6487, 2017.

[31] M. Roberts, T. Northmore, J. Shires, P. Taylor, and C. Hayhurst, "Diffuse low grade glioma after the 2016 WHO update, seizure characteristics, imaging correlates and outcomes," *Clinical Neurology and Neurosurgery*, vol. 175, pp. 9–15, 2018.

Hindawi
Disease Markers
Volume 2022, Article ID 5382100, 10 pages
https://doi.org/10.1155/2022/5382100

Research Article

Long-Term Elevated Siglec-10 in Cerebral Spinal Fluid Heralds Better Prognosis for Patients with Aneurysmal Subarachnoid Hemorrhage

Sen Gao,[1,2] **Xun-Zhi Liu**,[1] **Ling-Yun Wu**,[1] **Zheng Peng**,[1] **Xiang-Xin Chen**,[1] **Han Wang**,[1] **Yue Lu**,[1] **Zong Zhuang**,[1] **Qian Tan**,[2] **Chun-Hua Hang**,[1] **and Wei Li**[1]

[1]*Department of Neurosurgery, Nanjing Drum Tower Hospital, The Affiliated Hospital of Nanjing University Medical School, Nanjing, China*
[2]*Department of Burns and Plastic Surgery, Nanjing Drum Tower Hospital, The Affiliated Hospital of Nanjing University Medical School, Nanjing, China*

Correspondence should be addressed to Qian Tan; smmutanqian@sina.com, Chun-Hua Hang; hang_neurosurgery@163.com, and Wei Li; wei.li@nju.edu.cn

Received 28 July 2022; Revised 18 August 2022; Accepted 25 August 2022; Published 21 September 2022

Academic Editor: Xianwei Zeng

The presence of aneurysmal subarachnoid hemorrhage (aSAH) is usually accompanied by excessive inflammatory response leading to damage of the central nervous system, and the sialic acid-binding Ig-like lectin 10 (Siglec-10) is a recognized factor being able to modify the inflammatory reaction. To investigate the potential role of Siglec-10 in aSAH, we collected the cerebrospinal fluid (CSF) of control ($n = 11$) and aSAH ($n = 14$) patients at separate times and measured the Siglec-10 concentration utilizing the enzyme-linked immunosorbent assay (ELISA) and evaluated the alterations of GOS and GCS during the disease process. In accordance with the STROBE statement, results showed that Siglec-10 in CSF rose quickly in response aSAH attack and then fell back to a slightly higher range above baseline, while it remained at relative high concentration and last longer in several severely injured patients. In general, higher Siglec-10 expression over a longer period usually indicated a better clinical prognosis. This prospective cohort study suggested that Siglec-10 could possibly be used as a biomarker for predicting prognosis of aSAH due to its ability to balance aSAH-induced nonsterile inflammation. Additionally, these findings might provide novel therapeutic perspectives for aSAH and other inflammation-related diseases.

1. Introduction

Aneurysmal subarachnoid hemorrhage (aSAH) refers to extravasation of blood into the subarachnoid space caused by the aneurysm rupture, which is the most common cause for SAH [1, 2]. After aSAH attack, a cascade of pathophysiological changes including inflammation, ionic disbalance, oxidative stress, ischemia, and hypoxia would sabotage central nervous system [3]. Unfortunately, despite advanced progress in surgical technique and intensive caring capacity, SAH-related mortality rate still remained around 8% to 67% with high morbidity [4–7]. Therefore, there is an urgent demand to make clear the pathological mechanism of and find beneficial factors promoting better clinical prognosis for aSAH.

The sialic acid-binding Ig-like lectins (Siglecs) are members of the immunoglobulin superfamily expressed on the cell surface and were recognized as negative regulator in modulating innate and adaptive immune functions [8, 9], which depends on so-called immunoreceptor tyrosine-based inhibitory motifs (ITIMs) [10, 11]. Siglec-10 is a member of the Siglec family working upstream of ITIMs. It is widely expressed on human leucocytes, including B cells, eosinophils, monocytes, dendritic cells, T cells, and NK cells [12–16]. Studies have shown that Siglec-10 is embed with an important role in regulating the immune balance. For example, the interaction of Siglec-10 and CD24 could reduce the damage-associated molecular patterns- (DAMPs-) induced inflammatory response via inhibiting the activation of high

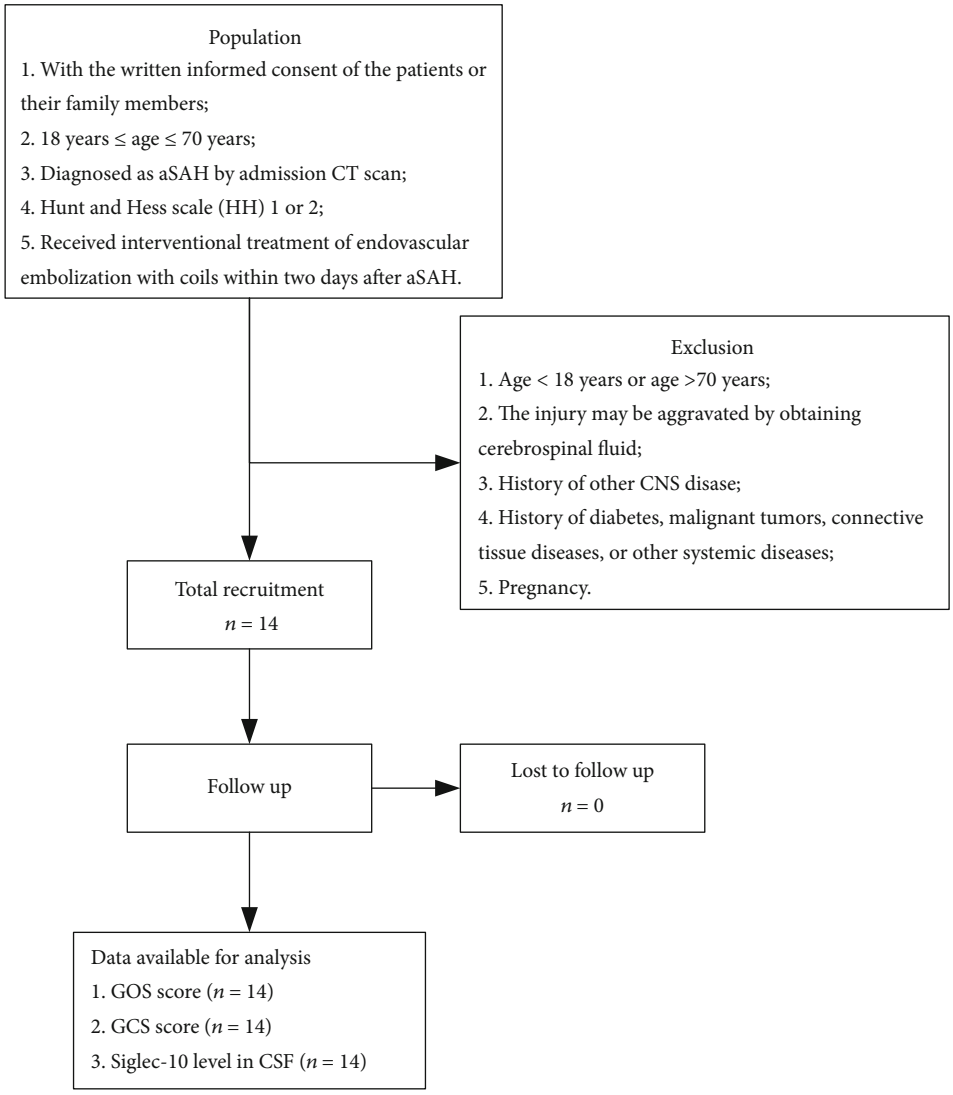

Figure 1: Flow diagram of patient selection.

Table 1: Injury status of aSAH patients.

Case	Gender	Age	Aneurysm location	Hunt-Hess	GCS on admission	GOS on admission
1	Male	42	V4 segment of left vertebral artery	II	13	3
2	Female	57	Anterior communicating artery	II	15	3
3	Female	57	Right posterior communicating artery	II	13	3
4	Male	49	The bifurcation of right middle cerebral artery	I	15	4
5	Female	51	Anterior communicating artery	II	12	3
6	Female	76	Anterior communicating artery	I	15	4
7	Female	46	Posterior communicating artery	II	12	3
8	Female	48	Apex of basilar artery	II	15	3
9	Female	65	Left anterior choroidal artery	I	15	4
10	Male	52	The bifurcation of middle cerebral artery	I	15	4
11	Female	65	Left posterior communicating artery	I	15	5
12	Female	49	Right posterior communicating artery	I	13	4
13	Male	68	Right anterior choroidal artery	II	13	3
14	Female	45	Apex of basilar artery	I	15	4

Table 2: GOS of aSAH patients at different time points.

Case	Admission	Day 3	Day 7	Day 9	Discharge
1	3	3	3	4	5
2	3	3	4	4	5
3	3	3	3	4	5
4	4	3	4	4	5
5	3	3	4	4	5
6	4	3	4	4	5
7	3	3	4	4	5
8	3	3	4	4	5
9	4	3	4	4	5
10	4	4	4	5	5
11	5	5	5	5	5
12	4	4	4	4	5
13	3	3	4	4	5
14	4	5	5	5	5

Table 3: GCS of aSAH patients at different time points.

Case	Admission	Day 3	Day 7	Day 9	Discharge
1	13	13	15	15	15
2	15	15	15	15	15
3	13	15	15	15	15
4	15	15	15	15	15
5	12	12	15	15	15
6	15	15	15	15	15
7	12	14	15	15	15
8	15	15	15	15	15
9	15	15	15	15	15
10	15	15	15	15	15
11	15	15	15	15	15
12	13	15	15	15	15
13	13	15	15	15	15
14	15	15	15	15	15

mobility group box 1 (HMGB1) and NF-κB [17–20]. The interaction between Siglec-10 expressed on human DCs and pseudaminic acid can promote the expression of IL-10 through MyD88 and p38/MAPK signaling pathway to boost anti-inflammatory function [21]. Several other reports have also validated its immune-modulating influence on the inflammatory microenvironment [22–25]. Research on oncology indicates that tumors could evade immunological surveillance through inhibiting NK cells and T cells and repressing tumour-killing capacity of macrophages with high Siglec-10 expression [26, 27]. In contrast, blocking macrophage Siglec-10 can increase macrophage-mediated phagocytosis [28]. Additionally, Siglec-10 also plays a role in the establishment of immune tolerance [29].

Given that inflammatory response is an important pathological process of aSAH, excessive unresolved inflammation could cause considerable damage to central nervous system [20], thus Siglec-10, as an anti-inflammatory factor,

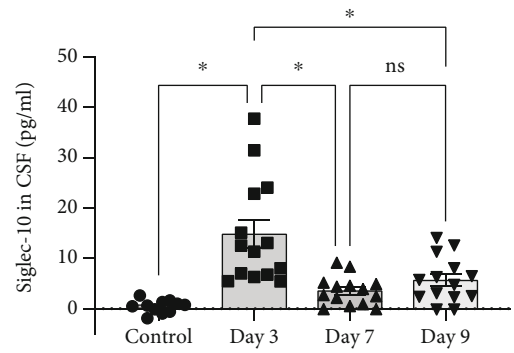

Figure 2: Siglec-10 in CSF measured by ELISA. The protein levels of Siglec-10 in CSF of patients on the 3rd, 7th, and 9th days after the occurrence of aSAH and the control group. The Siglec-10 levels on day 3 show a significant difference with other days ($P < 0.05$ versus indicated groups). All data were expressed as the mean ± SEM.

may affect the recovery of aSAH patients by via balancing proper inflammation, while this has yet not been validated in vivo or in vitro. To test this hypothesis, we conducted this clinical experiment to figure out if Siglec-10 is involved in the pathophysiological process after aSAH and the potential relationship between cerebrospinal Siglec-10 content and the prognosis of patients.

2. Materials and Methods

All the methods used for human trials were made in line with the Helsinki Declaration and approved by the medical institutional review board (no. 2020-041-01) at Nanjing Drum Tower Hospital. All clinical samples were obtained with the written informed consent of the patients or their families.

2.1. Patient Selection. The selection criteria of the experimental group were described as below: (1) diagnosed as aSAH by admission CT scan; (2) Hunt and Hess scale (HH) 1 or 2, while more severely injured patients were not enrolled to avoid iatrogenic damage; (3) no other CNS disease; (4) the experimental group received interventional treatment of endovascular embolization with coils within two days after aSAH; (5) no diabetes, malignant tumors, connective tissue diseases, or other systemic diseases. A flow diagram for the inclusion of aSAH patients in this study is presented in Figure 1. The patients' condition evaluation of the experimental group was shown in Table 1. The control group was obtained from patients who undergone surgeries with lumbar subdural anaesthesia with no SAH or any other CNS disease.

2.2. Sample Collection and Detections. The cerebrospinal fluid (CSF) samples (5 mL per sample) in the experiment was obtained from the experimental group ($n = 14$) and the control group ($n = 11$) by lumbar puncture or external ventricular drainage. CSF of the experimental group was extracted from patients on day 3, day 7, and day 9 after aSAH. And CSF from control group patients was set as control. All clinical samples were centrifuged (3000 g, 5 min) in

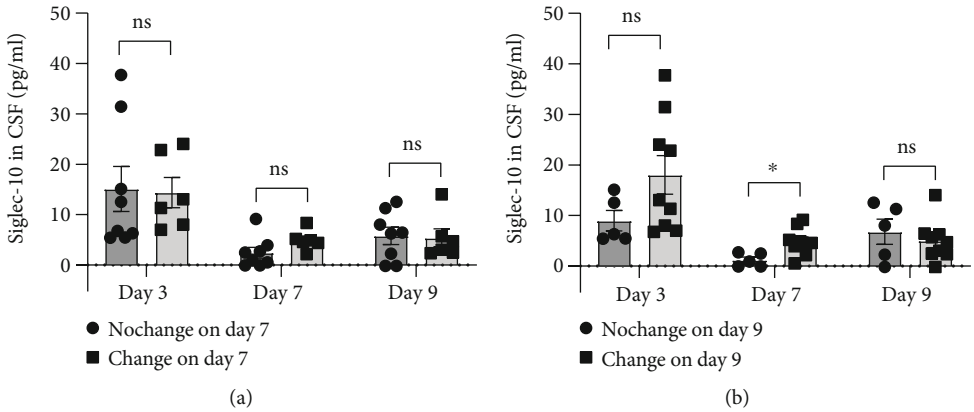

Figure 3: Differences in Siglec-10 levels between GOS-elevated and unchanged groups. (a) Grouped according to whether GOS was higher than admission on day 7, there was no significant difference in Siglec-10 content at each time point. (b) Grouped according to whether GOS was higher than admission on day 9, the Siglec-10 levels in CSF on day 7 showed a difference ($P < 0.05$ versus indicated groups). All data were expressed as the mean ± SEM.

Table 4: Differences in age between GOS-elevated and unchanged groups.

Way to group	Average age of GOS-elevated group	Average age of unchanged group	P
By day 7	56.88	52.50	0.4425
By day 9	51.78	60.80	0.1097

a sterile tube, and the supernatant was taken and stored at -80°C before test.

The enzyme-linked immunosorbent assay (ELISA) was then conducted to determine the protein levels of Siglec-10 in CSF after enough samples were collected. We used the commercial human ELISA kit (cat# MBS2509371, MyBioSource) in this study according to the manual.

2.3. Assessment of Recovery Status and Grouping. We evaluated the Glasgow Outcome Scale (GOS) and Glasgow Coma Scale (GCS) of patients on admission, day 3, day 7, day 9, and at discharge. All patients were admitted and received interventional therapy within two days after aSAH.

To explore the correlation between Siglec-10 and the prognosis of patients, a feasible method was to allocate patients on the basis of GOS score alteration-patients with better GOS amelioration were assigned to one group and the others to another. Then, the Siglec-10 levels variance between different groups were compared. As shown in Table 2, only one patient's GOS deteriorated on day 3 and all patients' GOS increased to 5 points at discharge, making data not suitable for being grouped by GOS score alterations day 3 or at discharge. Still, we can make reasonable groupings based on GOS score changes on day 7 and day 9. In this way, patients were divided into GOS-elevated and unchanged groups. Another way to investigate their correlation was to analyze whether the GOS at admission was related to Siglec-10 levels in the following days.

The GCS of the patients is shown in Table 3. It was difficult to group by score changes to make qualitative analysis because only one patient among the patients had no full GCS score on admission and had no GCS change on day 3. Meanwhile, all patients got full 15 points since day 7. Considering the potential protective effects of Siglec-10, we directly analyzed the relationship between Siglec-10 levels and GCS changes, including the correlation between Siglec-10 levels on day 3 and GCS changes on day 3 or day 7 and the correlation between Siglec-10 levels on day 7 and GCS changes on day 7. Besides, the correlation between GOS at admission and Siglec-10 levels on the following days was also examined.

2.4. Data Analysis. We used GraphPad Prism7.0 to analyze the data. One-way analysis of variance with Dunnett's T3 and Tukey's post hoc tests was used when comparing three or more groups. Unpaired Student's t-test was used when comparing two groups. Pearson correlation coefficient was used to evaluate the simple correlation between continuous variables. $P < 0.05$ was considered to be statistically significant. Data were expressed as mean ± SEM.

3. Results

3.1. Siglec-10 Levels in CSF Increased Rapidly after aSAH. We observed that patients in different groups and at different time points had different Siglec-10 levels (Figure 2). The Siglec-10 expression in the control group was at a low level. Meanwhile, Siglec-10 of aSAH patients quickly peaked on day 3 ($P < 0.05$) and then plateaued since day 7, though not as high as day 3 but still higher than that of the control group ($P < 0.05$).

3.2. Longer Maintenance of High-Level Siglec-10 Indicated Better GOS Improvements. Whether Siglec-10 played a role in the process of aSAH can be clarified by group comparison. When groups were divided according to GOS alteration on day 7, there was no significant difference in Siglec-10 levels at any given time point (Figure 3(a)). While on day 9, different groups showed a significant difference of Siglec-10 levels on day 7 (Figure 3(b), $P < 0.05$), but not on day 3 or day 9. This meant that the interblock difference could not be observed by the time of Siglec-10 expression

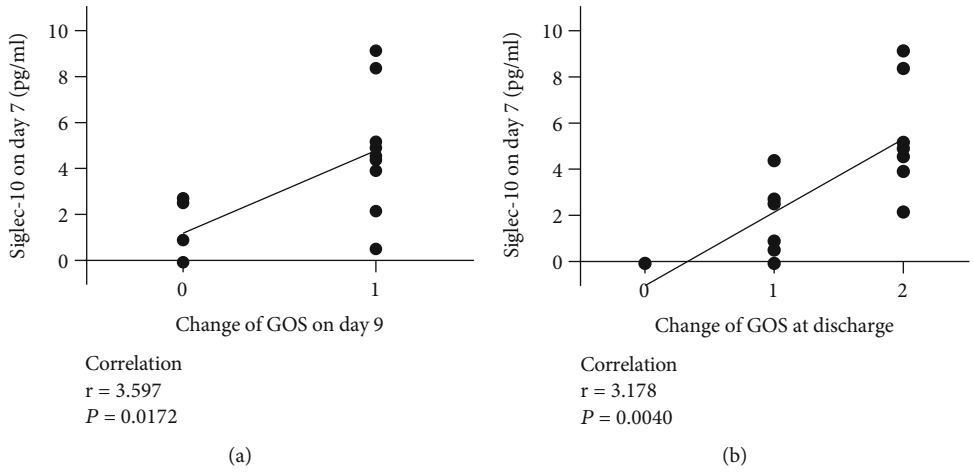

Figure 4: Relationship between Siglec-10 levels on day 7 and changes of GOS on the following days. The relationship between the Siglec-10 levels on day 7 and the changes of GOS on day 9 (a) and at discharge (b) was significantly correlated.

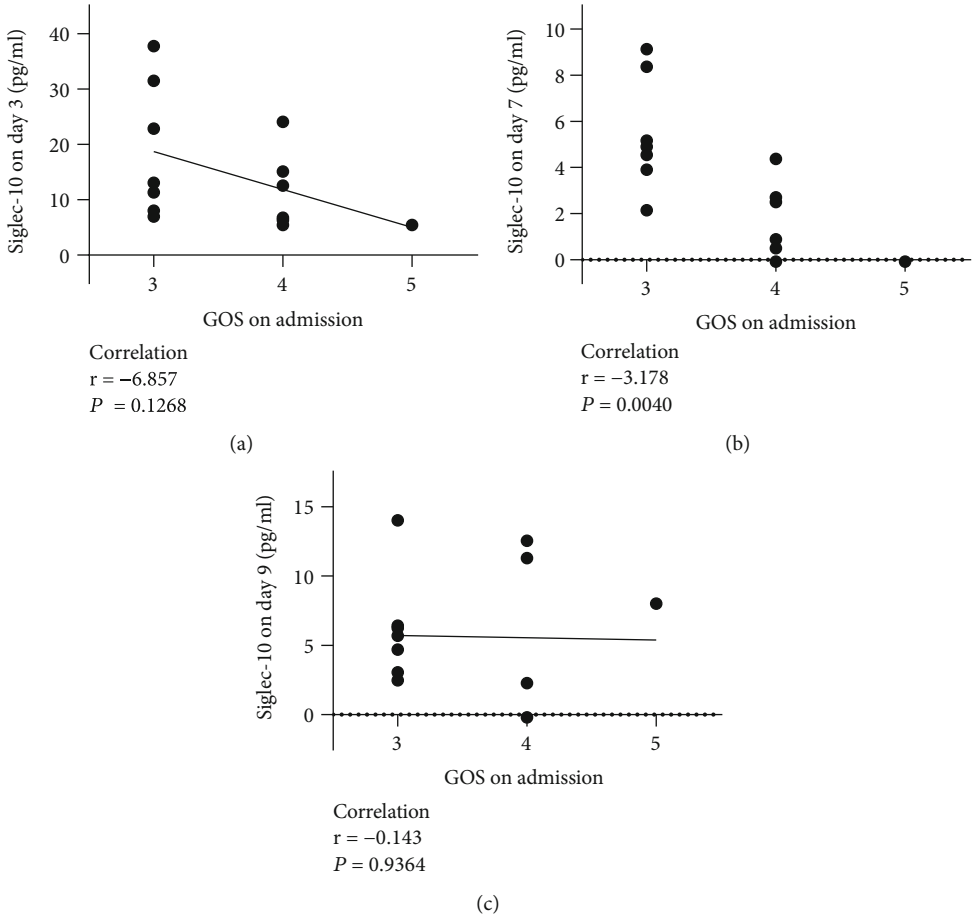

Figure 5: Relationship between GOS at admission and Siglec-10 levels at various time points. The Siglec-10 levels on day 7 was significantly correlated with GOS at admission (b). There was no significant correlation between GOS at admission and Siglec-10 levels on day 3 (a) or day 9 (c).

peak until day 7, indicating that the difference observed on day 7 was more likely a result of different Siglec-10 expression fluctuations. In addition, regardless of the grouping, there is no difference in age between groups (Table 4).

There was not only a qualitative but also a quantitative relationship between Siglec-10 expression level and GOS changes. Our results showed that the GOS score alterations from admission to day 9 was positively correlated with the

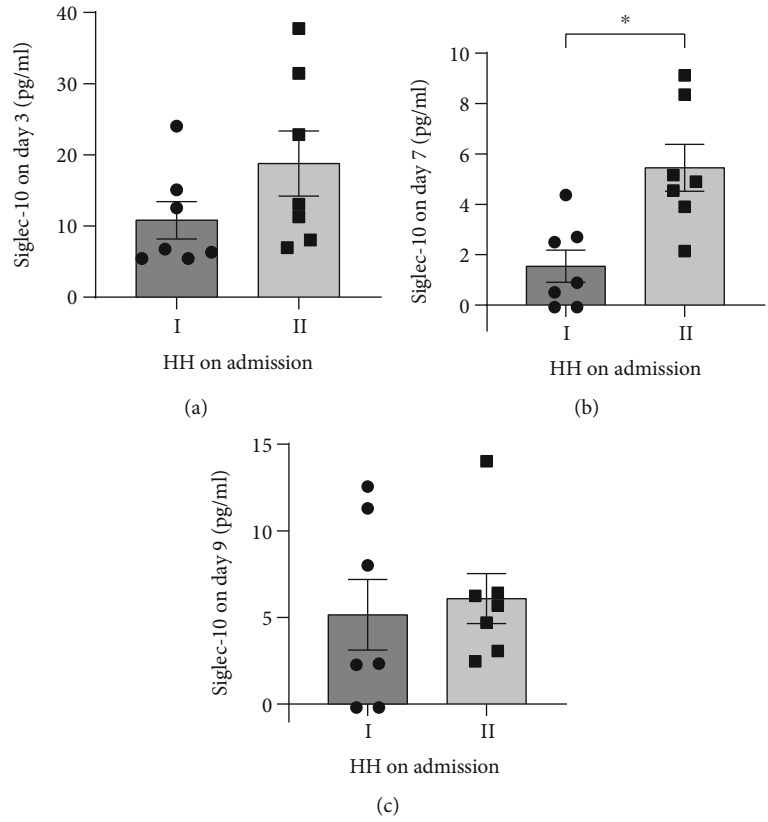

Figure 6: Differences in Siglec-10 levels of patients with different HH. The Siglec-10 levels on day 7 between HH1 and HH2 patients show a difference ($P < 0.05$ versus indicated groups). All data were expressed as the mean ± SEM.

Siglec-10 expression on day 7 (Figure 4(a), $r = 3.597$, $P < 0.05$). The GOS score variation between admission and discharge conformed to the same pattern (Figure 4(b), $r = 3.178$, $P < 0.05$). As the level on day 7 reflected whether Siglec-10 maintained high concentration for a longer time, it can be summarized that the longer the Siglec-10 can be maintained at a high level, the better the prognosis seemed to be in the following days.

3.3. The High-Level Siglec-10 Lasted Longer in Patients with Relatively Severe Injuries. Further, we analyzed the relationship between Siglec-10 levels and the severity of patients on admission, which is reflected by GOS and HH. The results showed that Siglec-10 levels on day 7 was significantly correlated with the GOS on admission. Patients with lower GOS on admission had higher Siglec-10 levels on day 7 (Figure 5(b), $r = -3.178$, $P < 0.05$). No such phenomenon was observed on day 3 (Figure 5(a)) or day 9 (Figure 5(c)).

There were similar results in HH. Compared to HH1, HH2 patients had even higher levels of Siglec-10 on day 7 (Figure 6(b), $P < 0.05$).

3.4. Siglec-10 Was Not Significantly Related to the Changes of GCS. The association between GCS and Siglec-10 could not be clearly observed. On the one hand, there was no significant correlation between the GCS at admission and Siglec-10 levels, whether on day 3 (Figure 7(a)), day 7 (Figure 7(b)), or day 9 (Figure 7(c)). On the other hand, there was no correlation between the changes of GCS on day 3 and Siglec-10 levels on day 3 (Figure 7(d)), or the changes of GCS on day 7 and Siglec-10 levels on day 3 (Figure 7(e)) or day 7 (Figure 7(f)).

4. Discussion

After binding to its ligand, the tyrosine residing in the ITIM domain of Siglec-10 will be phosphorylated and serves as a binding site for proteins containing the SH2 domain (SHP phosphatase for instance). Which would then lead to the dephosphorylation of cytoplasmic proteins and therefore downregulate the downstream signaling pathways [30]. By negatively regulating the resultant inhibition of NF-κB, Siglec-10 can retain the damage of DAMP-related inflammatory response [17]. Through MyD88 and p38 MAPK signaling pathways, Siglec-10 can increase the expression of IL-10 to promote anti-inflammatory function [21]. Siglec-10 can also inhibit the function of NK cells and T cells or interact with HSP70, HSP90, and VAP1 to repress inflammation [17, 22]. There are many consistent researches in the field of aSAH, such as MyD88/NF-κB pathway, HMGB1 and DAMPs [31–34]. Our results showed that Siglec-10 rose instantly and soon peaked after aSAH and remained at a high concentration afterwards, indicating that Siglec-10 did participate in the pathophysiological process after aSAH. Still, these results alone cannot characterize the comprehensive role of Siglec-10 due to the complex pathological

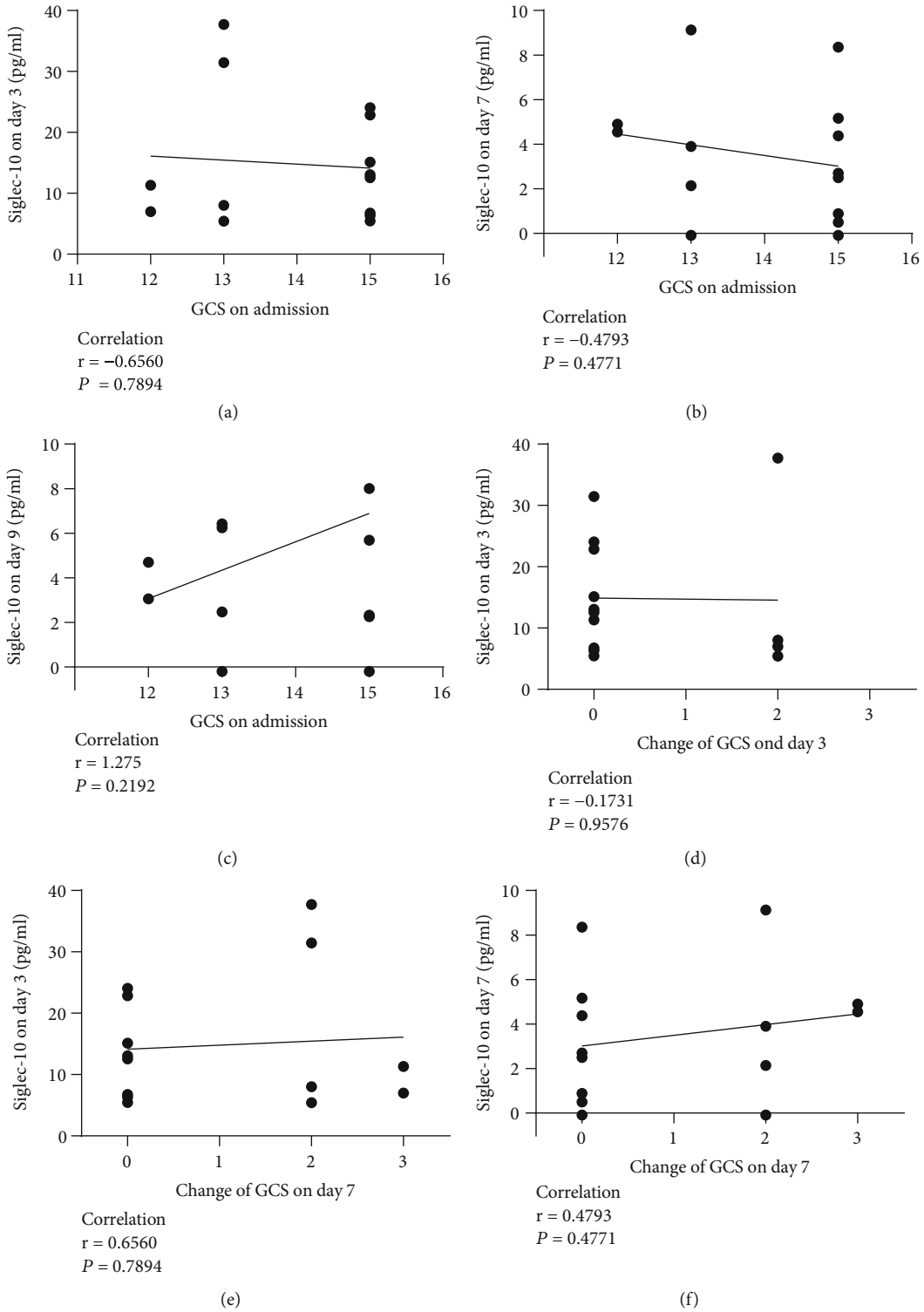

Figure 7: Relationship between Siglec-10 levels at different time points and the GCS levels and changes. (a) Relationship between GCS at admission and Siglec-10 levels on day 3. (b) Relationship between GCS at admission and Siglec-10 levels on day 7. (c) Relationship between GCS at admission and Siglec-10 levels on day 9. (d) Relationship between the changes of GCS on day 3 and Siglec-10 levels on day 3. (e) Relationship between the changes in GCS on day 7 and Siglec-10 levels on day 3. (f) Relationship between the changes in GCS on day 7 and Siglec-10 levels on day 7.

process as well as numerous cytokines or inflammatory mediators released during this process, so we conducted the analysis below.

In our experiment, patients with Siglec-10 maintained at high levels for a longer period seemed to have better prognosis, which was approved by both qualitative and quantitative analysis. This finding confirmed that high-level and long-term Siglec-10 in CSF was associated with better outcomes for aSAH patients. Another potential role of Siglec-10 was that expression and duration of CSF Siglec-10 expression seemed to be related with severity on admission. Upon exposing to damage, the host initiates defensive mechanisms in react to such stress. Naturally, the heavier the host was injured, the prompter protective reactions would be provoked. This phenomenon is consistent with the performance of Siglec-10 in our experiment. Another noteworthy point is that why Siglec-10, generally regarded as a membrane-tethered receptor, appeared in CSF. We suspect that it might be the result of blood-brain barrier breaking down and the subsequent infiltration of inflammatory cells expressing Siglec-10 into the CSF. This also explains why the Siglec-10 levels of the control group were relatively low.

Interestingly, we could find that Figures 4(b) and 5(b) have the symmetrical correlation coefficients. The reason is that the GOS of patients all reached a perfect score of 5 at discharge. Presume that if not all patients had a full score when they get discharged, then Figure 5(b) would remain the same, but Figure 4(b) would show a different correlation coefficient. Furthermore, if there were data of more time points such as day 8, day 10, and day 11, new results would support our argumentation more strongly.

As for the analysis of GCS, regrettably, no correlation was found, and the explanation was quite complex. For example, though both scales were used to assess aSAH patients, GCS tends to characterize the degree of consciousness, while GOS is the more accurate descriptor of prognosis. Besides, patients in our experiment were mildly injured with almost all GCS above 12 points, which might result in less significant comparisons; most patients had recovered to the full score on day 3, causing difficulties in the grouping. These biases could be possibly reduced by recruiting more severely injured patients, increasing the frequency of evaluating GCS, and expanding the sample size. Speaking of the limits, future research should be carried out more complicated experiments combined with other factors that may affect the prognosis, such as vasospasm, hydrocephalus, location, and size of the ruptured aneurysm, so that the results will be more accurate and more likely to reflect the characteristics of Siglec-10. Whether upregulating Siglec-10 exogenously could promote recovery also can be included in our future research.

5. Conclusions

Altogether, the present study suggested that the Siglec-10 expression level in CSF boosted in response to aSAH quickly peaked and then fall back to a stable range slightly higher above normal limit. Patients who were relatively severely injured are more likely to maintain high-level Siglec-10 for a longer period compensatorily. In general, having high-level and long-term Siglec-10 expression usually indicates superior prognosis, which is probably due to the anti-inflammatory effects avoiding the host's excessive inflammatory response to damage. The potential explanation might be that the anti-inflammatory function of Siglec-10 could avoid excessive host defense and ameliorating secondary damages. The exploration of the role of Siglec-10 in aSAH may provide a new predictive biomarker or new treatment alternatives for aSAH and other inflammation-related diseases.

Data Availability

Data of this study is available on request.

Ethical Approval

The conducted research was preregistered in Nanjing Drum Tower Hospital as no. 2020-041-01 by the medical institutional review board.

Disclosure

The manuscript was published as a preprint in "Long-term Elevated Siglec-10 in Cerebral Spinal Fluid Heralds Better Prognosis for Patients with Aneurysmal Subarachnoid Hemorrhage" [35], and the content has been improved. The funder of which had no role in study design, data collection and analysis, decision to publish, or preparation of the manuscript

Conflicts of Interest

The authors declare that there is no conflicts of interest regarding the publication of this paper.

Authors' Contributions

Sen Gao, Xun-Zhi Liu, and Ling-Yun Wu contributed equally to this study.

Acknowledgments

This work was supported by grants from the National Natural Science Foundation of China (no. 81971122 and no. 81771291 for C.H. Hang), Natural Science Foundation of Jiangsu Province, China (BK20201113 for W. Li), and Key Project supported by Medical Science and Technology Development Foundation, Nanjing Department of Health (no. JQX18001 for W. Li). These funders were the corresponding authors of this article. This study was partially supported by the National Natural Science Foundation of China (no. 81801166 for L.Y. Wu).

References

[1] M. K. Abraham and W. T. W. Chang, "Subarachnoid hemorrhage," *Emergency Medicine Clinics of North America*, vol. 34, no. 4, pp. 901–916, 2016.

[2] R. L. Macdonald and T. A. Schweizer, "Spontaneous subarachnoid haemorrhage," *Lancet*, vol. 389, no. 10069, pp. 655–666, 2017.

[3] J. H. van Lieshout, M. Dibue-Adjei, J. F. Cornelius et al., "An introduction to the pathophysiology of aneurysmal subarachnoid hemorrhage," *Neurosurgical Review*, vol. 41, no. 4, pp. 917–930, 2018.

[4] D. J. Nieuwkamp, L. E. Setz, A. Algra, F. H. H. Linn, N. K. de Rooij, and G. E. Rinkel, "Changes in case fatality of aneurysmal subarachnoid haemorrhage over time, according to age, sex, and region: a meta-analysis," *Lancet Neurology*, vol. 8, no. 7, pp. 635–642, 2009.

[5] D. Rivero Rodriguez, C. Scherle Matamoros, L. F. Cue, J. L. Miranda Hernandez, Y. Pernas Sanchez, and J. Perez Nellar, "Predictor's of mortality in patients with aneurysmal subarachnoid haemorrhage and reebleding," *Neurology Research International*, vol. 2015, Article ID 545407, 6 pages, 2015.

[6] W. J. Tu, B. H. Chao, L. Ma et al., "Case-fatality, disability and recurrence rates after first-ever stroke: a study from bigdata observatory platform for stroke of China," *Brain Research Bulletin*, vol. 175, pp. 130–135, 2021.

[7] W. J. Tu, Y. Hua, F. Yan et al., "Prevalence of Stroke in China, 2013–2019: A Population-Based Study," *The Lancet Regional Health - Western Pacific*, p. 100550, 2022.

[8] P. R. Crocker, J. C. Paulson, and A. Varki, "Siglecs and their roles in the immune system," *Nature Reviews Immunology*, vol. 7, no. 4, pp. 255–266, 2007.

[9] M. S. Macauley, P. R. Crocker, and J. C. Paulson, "Siglec-mediated regulation of immune cell function in disease," *Nature Reviews Immunology*, vol. 14, no. 10, pp. 653–666, 2014.

[10] G. Whitney, S. L. Wang, H. Chang et al., "A new siglec family member, siglec-10, is expressed in cells of the immune system and has signaling properties similar to cd33," *European Journal of Biochemistry*, vol. 268, no. 23, pp. 6083–6096, 2001.

[11] T. Tsubata, "Role of inhibitory bcr co-receptors in immunity," *Infectious Disorders Drug Targets*, vol. 12, no. 3, pp. 181–190, 2012.

[12] N. Li, W. P. Zhang, T. Wan et al., "Cloning and characterization of siglec-10, a novel sialic acid binding member of the Ig superfamily, from human dendritic cells," *Journal of Biological Chemistry*, vol. 276, no. 30, pp. 28106–28112, 2001.

[13] J. Munday, S. Kerr, J. Ni et al., "Identification, characterization and leucocyte expression of siglec-10, a novel human sialic acid-binding receptor," *Biochemical Journal*, vol. 355, no. 2, pp. 489–497, 2001.

[14] B. H. Toh, T. Kyaw, P. Tipping, and A. Bobik, "Immune regulation by cd52-expressing cd4 t cells," *Cellular & Molecular Immunology*, vol. 10, no. 5, pp. 379–382, 2013.

[15] Z. Escalona, B. Alvarez, H. Uenishi et al., "Molecular characterization of porcine siglec-10 and analysis of its expression in blood and tissues," *Developmental and Comparative Immunology*, vol. 48, no. 1, pp. 116–123, 2015.

[16] T. Tsubata, "Inhibitory b cell co-receptors and autoimmune diseases," *Immunological Medicine*, vol. 42, no. 3, pp. 108–116, 2019.

[17] G. Y. Chen, J. Tang, P. Zheng, and Y. Liu, "Cd24 and siglec-10 selectively repress tissue damage-induced immune responses," *Science*, vol. 323, no. 5922, pp. 1722–1725, 2009.

[18] E. Bandala-Sanchez, Y. X. Zhang, S. Reinwald et al., "T cell regulation mediated by interaction of soluble cd52 with the inhibitory receptor siglec-10," *Nature Immunology*, vol. 14, no. 7, pp. 741–748, 2013.

[19] Y. Zhao, H. T. Su, X. F. Shen, J. F. Du, X. D. Zhang, and Y. Zhao, "The immunological function of cd52 and its targeting in organ transplantation," *Inflammation Research*, vol. 66, no. 7, pp. 571–578, 2017.

[20] E. Bandala-Sanchez, N. G. Bediaga, E. D. Goddard-Borger et al., "Cd52 glycan binds the proinflammatory b box of hmgb1 to engage the siglec-10 receptor and suppress human t cell function," *Proceedings of the National Academy of Sciences of the United States of America*, vol. 115, no. 30, pp. 7783–7788, 2018.

[21] H. N. Stephenson, D. C. Mills, H. Jones et al., "Pseudaminic acid on campylobacter jejuni flagella modulates dendritic cell il-10 expression via siglec-10 receptor: a novel flagellin-host interaction," *Journal of Infectious Diseases*, vol. 210, no. 9, pp. 1487–1498, 2014.

[22] E. Kivi, K. Elima, K. Aalto et al., "Human siglec-10 can bind to vascular adhesion protein-1 and serves as its substrate," *Blood*, vol. 114, no. 26, pp. 5385–5392, 2009.

[23] Y. C. Liu, M. M. Yu, Y. F. Chai, and S. T. Shou, "Sialic acids in the immune response during sepsis," *Frontiers in Immunology*, vol. 8, p. 1601, 2017.

[24] S. I. Thornhill, A. Mak, B. Lee et al., "Monocyte siglec-14 expression is upregulated in patients with systemic lupus erythematosus and correlates with lupus disease activity," *Rheumatology*, vol. 56, no. 6, pp. 1025–1030, 2017.

[25] J. Jellusova, S. Duber, E. Guckel et al., "Siglec-g regulates b1 cell survival and selection," *Journal of Immunology*, vol. 185, no. 6, pp. 3277–3284, 2010.

[26] P. Zhang, X. M. Lu, K. X. Tao et al., "Siglec-10 is associated with survival and natural killer cell dysfunction in hepatocellular carcinoma," *Journal of Surgical Research*, vol. 194, no. 1, pp. 107–113, 2015.

[27] Y. J. Li, J. Zhou, Q. Zhuo et al., "Malignant ascite-derived extracellular vesicles inhibit t cell activity by upregulating siglec-10 expression," *Cancer Management and Research*, vol. 11, pp. 7123–7134, 2019.

[28] A. A. Barkal, R. E. Brewer, M. Markovic et al., "Cd24 signalling through macrophage siglec-10 is a target for cancer immunotherapy," *Nature*, vol. 572, no. 7769, pp. 392–396, 2019.

[29] M. Sammar, M. Siwetz, H. Meiri, V. Fleming, P. Altevogt, and B. Huppertz, "Expression of cd24 and siglec-10 in first trimester placenta: implications for immune tolerance at the fetal-maternal interface," *Histochemistry and Cell Biology*, vol. 147, no. 5, pp. 565–574, 2017.

[30] S. Pillai, I. A. Netravali, A. Cariappa, and H. Mattoo, "Siglecs and immune regulation," *Annual Review of Immunology*, vol. 30, no. 1, pp. 357–392, 2012.

[31] X. D. Zhu, J. S. Chen, F. Zhou, Q. C. Liu, G. Chen, and J. M. Zhang, "Japanese encephalitis virus induces matrix metalloproteinase-9 expression via a ROS/c-Src/PDGFR/PI3K/Akt/MAPKs-dependent AP-1 pathway in rat brain astrocytes," *Journal of Neuroinflammation*, vol. 9, no. 1, p. 12, 2012.

[32] H. Y. Yan, D. D. Zhang, Y. X. Wei et al., "Inhibition of myeloid differentiation primary response protein 88 provides neuroprotection in early brain injury following experimental subarachnoid hemorrhage," *Scientific Reports*, vol. 7, no. 1, p. 11, 2017.

[33] S. R. Chaudhry, A. Hafez, B. R. Jahromi et al., "Role of damage associated molecular pattern molecules (damps) in aneurysmal

subarachnoid hemorrhage (asah)," *International Journal of Molecular Sciences*, vol. 19, pp. 7–2035, 2018.

[34] L. Y. Wu, Z. N. Ye, Z. Zhuang et al., "Biochanin a reduces inflammatory injury and neuronal apoptosis following subarachnoid hemorrhage via suppression of the lrs/tirap/myd88/nf-kappa b pathway," *Behavioural Neurology*, vol. 2018, Article ID 1960106, 10 pages, 2018.

[35] S. Gao, Z. Peng, X.-X. Chen et al., *Long-term elevated siglec-10 in cerebral spinal fluid heralds better prognosis for patients with aneurysmal subarachnoid hemorrhage*, Research Square, 2020.

Hindawi
Disease Markers
Volume 2023, Article ID 9754281, 1 page
https://doi.org/10.1155/2023/9754281

Retraction

Retracted: Activated Hepatic Stellate Cells Promote the M1 to M2 Macrophage Transformation and Liver Fibrosis by Elevating the Histone Acetylation Level

Disease Markers

Received 20 June 2023; Accepted 20 June 2023; Published 21 June 2023

This article has been retracted by Hindawi following an investigation undertaken by the publisher [1]. This investigation has uncovered evidence of one or more of the following indicators of systematic manipulation of the publication process:

(1) Discrepancies in scope

(2) Discrepancies in the description of the research reported

(3) Discrepancies between the availability of data and the research described

(4) Inappropriate citations

(5) Incoherent, meaningless and/or irrelevant content included in the article

(6) Peer-review manipulation

The presence of these indicators undermines our confidence in the integrity of the article's content and we cannot, therefore, vouch for its reliability. Please note that this notice is intended solely to alert readers that the content of this article is unreliable. We have not investigated whether authors were aware of or involved in the systematic manipulation of the publication process.

Wiley and Hindawi regrets that the usual quality checks did not identify these issues before publication and have since put additional measures in place to safeguard research integrity.

We wish to credit our own Research Integrity and Research Publishing teams and anonymous and named external researchers and research integrity experts for contributing to this investigation.

The corresponding author, as the representative of all authors, has been given the opportunity to register their agreement or disagreement to this retraction. We have kept a record of any response received.

References

[1] J. Chen, X. Huang, Z. Huang, and Y. Cao, "Activated Hepatic Stellate Cells Promote the M1 to M2 Macrophage Transformation and Liver Fibrosis by Elevating the Histone Acetylation Level," *Disease Markers*, vol. 2022, Article ID 9883831, 8 pages, 2022.

Hindawi
Disease Markers
Volume 2022, Article ID 9883831, 8 pages
https://doi.org/10.1155/2022/9883831

Research Article

Activated Hepatic Stellate Cells Promote the M1 to M2 Macrophage Transformation and Liver Fibrosis by Elevating the Histone Acetylation Level

Junru Chen,[1,2] **Xueqing Huang**,[3] **Zhi Huang**,[3] **and Yu Cao**[1,4]

[1]*Department of Dermatology and Venereology, College of Clinical Medicine, Guizhou Medical University, Guiyang 550025, China*
[2]*The Maternal and Child Health Care Hospital of Guizhou Medical University, Guiyang 550003, China*
[3]*Department of Intervention, The Affiliated Hospital of Guizhou Medical University, Guiyang 550002, China*
[4]*College of Greater Health, Guizhou Medical University, Guiyang 550025, China*

Correspondence should be addressed to Zhi Huang; gydoctor@gmc.edu.cn and Yu Cao; 2692327139@qq.com

Received 18 June 2022; Revised 9 August 2022; Accepted 13 August 2022; Published 12 September 2022

Academic Editor: Xianwei Zeng

Liver fibrosis results from the formation of fibrous scars of hepatic stellate cells by various chronic liver diseases. Considering that the liver is the most important metabolic organ in the human body, exploring the metabolic characteristics of liver fibrosis is expected to discover new markers and therapeutic targets. In this study, we first used mouse model to verify that both lactate content and histone acetylation levels were significantly increased in hepatic fibrosis mice. At the same time, it was confirmed that activated hepatic stellate cells (HSCs) cocultured with M1 macrophages can promote their transformation into M2 macrophages in hepatic stellate cell line and primary hepatic stellate cells. In addition, the addition of lactic acid to the medium in which M1 cells are cultured can promote their transformation into M2 macrophages. Therefore, we concluded that activated HSCs can promote the transformation of M1 to M2 macrophages through lactate accumulation, thereby causing liver fibrosis.

1. Introduction

Hepatic fibrosis is characterized by the formation of fibrous scar by the accumulation of extracellular matrix components after liver injury caused by various chronic liver diseases [1]. If not effectively controlled, liver fibrosis can develop into liver cirrhosis and even liver cancer [2]. In fact, cirrhosis is reversible, and effective antifibrotic therapy can significantly change the treatment and prognosis of patients with liver disease [3, 4]. So, it is very important to explore the mechanism of liver fibrosis and find effective methods to inhibit it.

It is generally believed that the activation of hepatic stellate cells (HSCs) is the key cause of the occurrence and development of hepatic fibrosis [5]. In physiological state, HSCs are quiescent [6]. When the liver is injured, quiescent HSCs become activated HSCs by downregulating the expressions of vitamin A and peroxisome proliferator-activated receptor γ (PPARγ) [7, 8]. Subsequently, activated HSCs migrate to the liver injury site, secrete extracellular matrix, and form a fibrous scar [9]. Interestingly, recent studies have shown that activated hepatic stellate cells can increase the enrichment of hepatic M2 macrophages, and the number of hepatic M2 macrophages is positively correlated with the severity of liver fibrosis [10]. In fact, as the first line of defense against pathogens, hepatic macrophages are involved in all stages of liver fibrosis, from initiation of inflammation and progression of fibrosis to degradation of fibrous collagen and regression of scarring [11, 12]. M1 and M2 macrophages, the two most typical phenotypes of hepatic macrophages, mediate hepatic inflammation and tissue remodeling, respectively [13]. Interestingly, phenotypic switching between M1 and M2 can occur under specific stimuli in vivo and in vitro [14]. Therefore, it is of great significance to study how M1 and M2 are transformed and their relationship with HSCs for the treatment of liver fibrosis.

The liver is a key metabolic organ that controls energy metabolism in the body, and its life activities produce thousands of metabolic small molecules [15]. These small molecules are not only the products catalyzed by enzymes but also can affect the function of proteins through covalent modification [16]. Recent studies have found that lactate accumulated during metabolism can act as a precursor to lactate modification of histone lysine and participate in the homeostatic regulation of bacterial-infected M1 macrophages [17, 18]. Interestingly, elevated levels of glycolysis are a hallmark of HSC activation [19], and glycolysis can generate large amounts of lactate, which can as a substrate to catalyze lactate modification of histones. Importantly, elevated levels of acetylation in M1 macrophages promote their transformation into M2 macrophages [20]. So, we speculate that activated HSCs can increase the level of histone lactate modification in M1 macrophages by secreting a large amount of lactate, thereby promoting the transformation of hepatic macrophages from M1 type to M2 type and promoting the progression of liver fibrosis. Moreover, histone deacetylase inhibitors (HDAC inhibitors) have also been used as a class of clinical drugs [21]. It is a great pity that there is no effective treatment for liver fibrosis other than liver transplantation. Therefore, revealing the regulatory mechanism of lactate, a metabolite of HSCs, has important scientific significance for understanding the occurrence, diagnosis, and treatment of liver fibrosis.

In our study, we first constructed liver fibrosis mice and examined the changes in lactate and histone acetylation levels in the model mice. Then, we clarified the relationship between HSC activation and macrophage transformation by coculture of HSCs with M1 macrophages. Furthermore, we revealed whether activated HSCs could cause liver fibrosis through lactate accumulation with macrophage transformation. Therefore, the current study may provide a theoretical basis for the therapy of liver fibrosis.

2. Materials and Methods

2.1. Mouse Treatment and Tissue Section. All the mice used in this study were purchased from Shanghai SLAC Laboratory Animal Co., Ltd. All animal experiments were approved by the institutional animal care and use committee (IACUC) of Guizhou Medical University (approval no. 2101003). 8-week-old female mice were intraperitoneally injected with 1 ml/kg carbon tetrachloride (CCl4; Sigma, in peanut oil) twice a week for 8 weeks before ultrasound imaging was performed to assess liver cirrhosis. Each group contained 12 mice. Animals were sacrificed when the mice were moribund and livers were used for subsequent analysis.

2.2. Pathological Examination. The livers were weighed, fixed in 3.7% formaldehyde solution, embedded in paraffin, then sectioned (4 μm) with a paraffin microtome. Paraffin sections were then roasted at 60°C for 2 h, dewaxed in xylene, gradient alcohol rehydrated, and routinely stained by applying hematoxylin and eosin (H&E) staining. And the results were observed and photographed under a light microscopy. The pathologic structure was analyzed by 2 pathologists independently to observe the degree of inflammation and fibrosis of liver tissue. Based on the studies [22, 23], paraffin sections were also routinely processed before performing Masson and Sirius red staining. And the data were observed and photographed under the light microscope.

2.3. Cell Culture and Activation. LX-2 cells were cultured in Dulbecco's modified Eagle medium (DMEM; Gibco, Rockville, MD, USA, 21068028) supplemented with 10% fetal bovine serum (FBS; Gibco, 10099141C), 50 U/ml penicillin and 50 μg/ml streptomycin (Gibco) at 37°C in humid incubator containing 5% CO_2. According to You et al. [24], for activation, LX-2 cells were cultured in DMEM containing 2% FBS and 10 ng/ml transforming growth factor-β (TGF-β; Cell Signaling Technology, Inc., Danvers, MA, USA, cat. no. 2519) for 48 h. Primary HSCs were isolated from C57BL/6 mice according to the study [25], and TGF-β was used for activation of HSCs. M1 macrophage was transformed form THP-1 cell by treating with 100 ng/ml lipopolysaccharide (LPS; Sigma-Aldrich, St Louis, MO, USA) for 12 h. To detect the specific mechanism of transformation from M1 to M2 macrophage, M1 macrophage was treated with 20 mM lactate for 24 h.

2.4. Isolation of Primary Mouse HSCs. After the circular perfusion using 0.05% Type IV collagenase (Sigma) and 0.01% Pronase E (Sigma) to remove liver collagen tissue, the HSCs were isolated by density gradient centrifugation. All the cells after digestion were centrifuged in 18% Nycodenz (Sigma) at 3200 rpm for 15 min. Then, HSCs were distributed at the middle layer. Primary HSCs were cultured in DMEM (Gibco) supplemented with 20% FBS at 37°C 5% CO_2.

2.5. Western Blot. Protein extracts were prepared from equal number of cultured cells or equal weight of liver tissue using 1× SDS loading buffer. Equal volumes of protein liquid were separated by SDS-PAGE gel electrophoresis, transferred to polyvinylidene fluoride (PVDF; Millipore, IPVH20200 membranes), and incubated with the anti-Kla (PTM bio), anti-histone H3 (Cell signaling technology, CST4499s), anti-αSMA (Abcam, ab32575), or anti-GAPDH (Proteintech, 60004-1-Ig) overnight at 4°C. Blots were visualized with HRP-conjugated secondary antibodies (Jackson, 115-035-003). And the signal was analyzed using the enhanced chemiluminescence reagent (Beyotime, China, P0018FM).

2.6. Chromatin Immunoprecipitation (ChIP) Assay. ChIP assay was carried out as the method of Lan et al. [26]. M1 macrophages were crosslinked with 1% formaldehyde for 10 mins and then stopped by 125 mM glycine. After lysis and sonication, 3 μg of Kla (PTM bio) antibody was incubated with chromatin sample overnight at 4°C, and 20 μl protein A/G beads (Smart lifesciences SA032005) were used for immunoprecipitation. Finally, DNA were purified with PCR recovery kit (QIAGEN #28006) and used for qPCR analysis. And the protein sample was analyzed by western blot to detect the histone acetylation level.

Table 1: Real-time PCR primer sequences.

Gene	Sense (5′-3′)	Antisense (5′-3′)
CD163	TCAGCTGATTTCAGTGCTGCT	TCACGTAACTGTGAGGCTCTT
Arg1	TGACTGAAGTAGACAAGCTGGGGAT	CGACATCAAAGCTCAGGTGAATCGG
IL-10	GAAAGGAAGCCAGCTACCCC	ACAGAATCTCCCCGTTAGCC
TGF-β1	GGCAATCTACAAGTTCATTGGGC	AAGGAACCGCAGCACTCATA

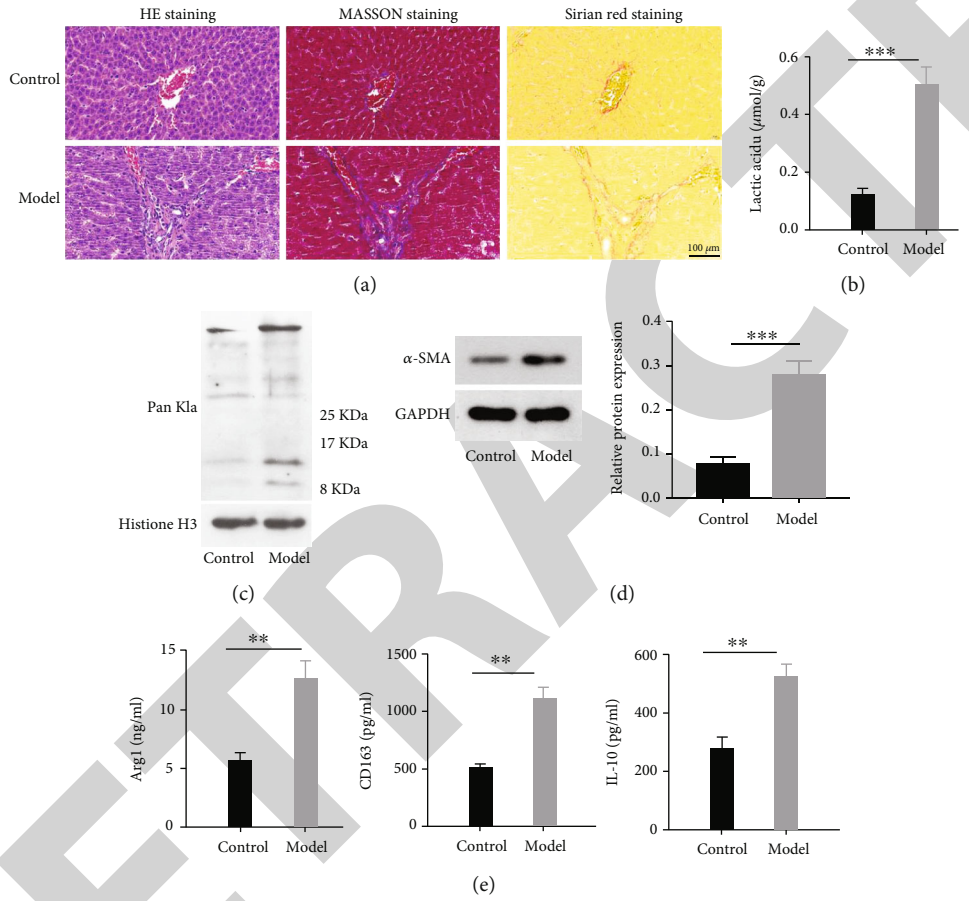

Figure 1: Lactate levels are elevated in mice with liver fibrosis. (a) The 8-week-old mice were treated with CCl4 for 6 weeks, and the fibrosis was assessed by H&E, Masson, and Sirius red staining. Scale bars are 100 μm. (b) Kit to detect lactate level in the liver tissue. At least 3 liver sections were analyzed per mouse (number of mice: $n = 12$). (c, d) Western blot showing expression of acetylation and α-SMA in the livers of mice treated with CCl4. (e) Detection of the expression levels of M2 macrophage surface markers CD163, Arg1, and IL-10 in the liver by ELISA. $^{**}P < 0.01$, $^{***}P < 0.001$.

2.7. Reverse Transcription Quantitative Polymerase Chain Reaction (RT-qPCR). The total RNA was extracted with TRIzol reagent (Invitrogen), and cDNA was synthesized by PrimeScript™ RT reagent Kit with gDNA Eraser (TaKaRa #RR047A). SYBR® Premix Ex Taq™ GC (TaKaRa #RR071A) was used for RT-qPCR analysis. The primer sequences are listed in Table 1.

2.8. Lactate Assay and ELISA Assay. The assay medium for glycolytic capacity consisted of 2 mM glutamine in hippocampal XF basal medium [15]. The intracellular and extracellular concentrations of lactate were determined using the Lactate Colorimetric/Fluorometric Assay Kit (K607–100; BioVision) according to the manufacturer's instructions. The surface markers of M1 and M2 macrophages were determined by enzyme-linked immunosorbent assay kits, and the specific product numbers are as follows: TGF-β 1 (Abcam, ab119557), TNF alpha (Abcam, ab285327), CD163 (Abcam, ab272204), IL-1β (Beyotime, PI301), IL-10 (Beyotime PI522), IL-6 (Beyotime PI326), Arg1 (sangon biotech D721046), and iNOS (ab253219).

2.9. Statistical Analysis. Statistical analysis was performed using SPSS version 22.0 (IBM Corporation, New York, USA). Statistical significance was calculated by a two-tailed test. GraphPad Prism 8.0 (GraphPad Software, La Jolla,

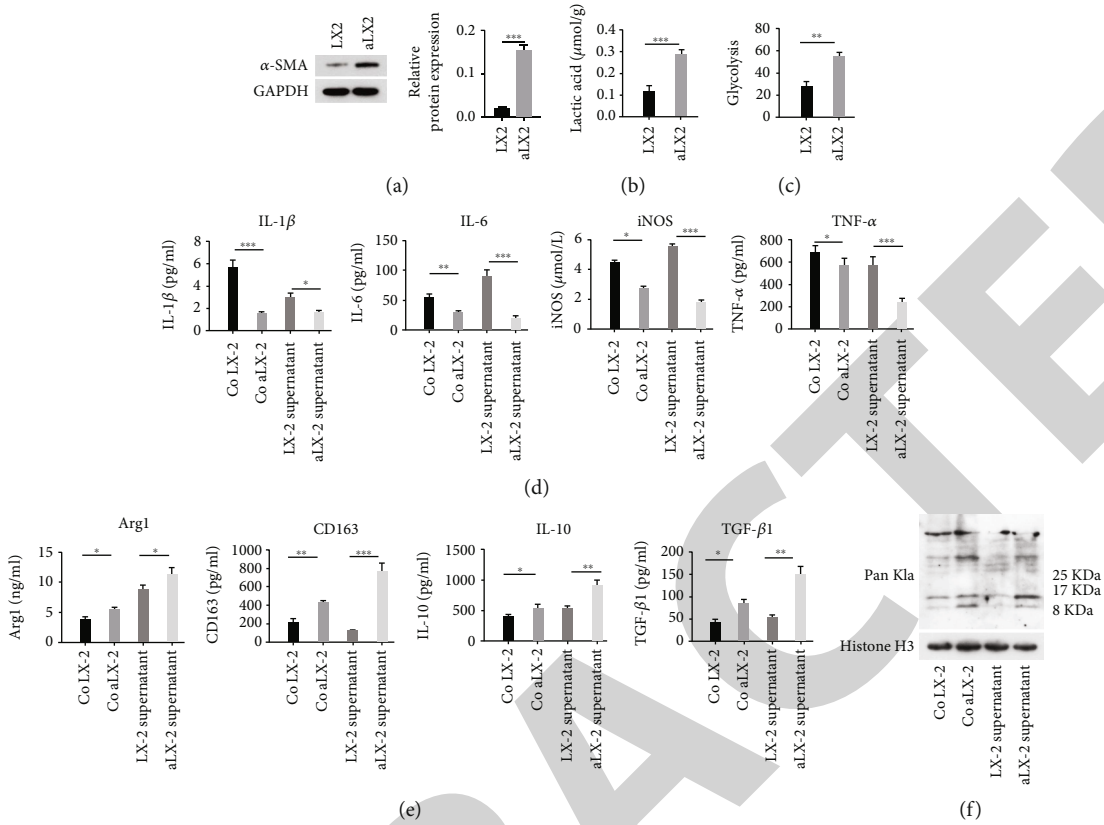

Figure 2: HSCs regulate the transformation of M1/M2 macrophages. (a) Western blot showing expression of α-SMA in the aLX-2. Activated HSCs (aLX-2) were obtained by treating LX-2 cells with TGF-β. (b) Lactate level in aLX-2. (c) The level of glycolysis in aLX-2. (d) Detection of the expression levels of M1 macrophage surface markers IL-1β, IL-6, iNOS, and TNF-α in transformed THP-1 cells cultured with aLX or its supernatant and their supernatants by ELISA. (e) Detection of the expression levels of M2 macrophage surface markers Arg1, CD163, IL-10, and TGFβ in co-aLX-2 co-LX-a cells and their supernatants by ELISA. (f) Western blot showing expression of acetylation n co-aLX-2 co-LX-a cells and their supernatants. $^{*}P < 0.05$, $^{**}P < 0.01$, and $^{***}P < 0.001$.

CA, USA) was applied to generate statistical analysis. Significance values are $^{*}P < 0.05$, $^{**}P < 0.01$, and $^{***}P < 0.001$.

3. Results

3.1. Lactate Levels Are Elevated in Mice with Liver Fibrosis. To study the function of lactate in liver fibrosis, we first treated 8-week-old mice with a well-studied fibrosis inducer (CCl4) for 6 weeks. Then, liver fibrosis and liver morphology was assessed by hematoxylin and eosin (H&E) staining, Masson staining, and Sirius Red staining. H&E staining in the model group showed degeneration and necrosis of liver cells belonging to postnecrotic cirrhosis. Masson staining showed a large amount of blue collagen fiber deposition. The fiber cords were thick and stained deeply, indicating that there were many collagen fibers and had formed false lobules. Sirius Red staining showed that the collagen fibers of various types expanded outwards (Figure 1(a)). It turns out that the level of lactate is significantly higher in mice with liver fibrosis than in control mice (Figure 1(b)). As in previous study [17], we found that in fibrotic mice with elevated lactate, histone lactate levels were also significantly increased (Figure 1(c)). Alpha smooth muscle actin (α-SMA) is an indicator of HSC activation and a valuable marker of fibrosis progression and an early indicator of fibrosis development [27]. We detected the protein level of α-SMA by western blot and found that the protein level of α-SMA was indeed significantly increased in mice with liver fibrosis (Figure 1(d)). Importantly, elevated levels of acetylation in M1 macrophages promote their transformation into M2 macrophages [20]. So, we also used ELISA kit to detect the protein levels of M2 macrophage markers Arg1, CD163, and IL-10 and found that M2 macrophages in liver fibrosis mice were significantly higher than those in the control group, as in the previous study (Figure 1(e)) [10]. In conclusion, the levels of lactate, histone acetylation, and the number of M2 macrophages were significantly increased in liver fibrotic mice.

3.2. Activated HSC Cell Line LX-2 Can Stimulate the Transformation of M1 to M2 Macrophages. To explore the regulation of activated HSCs on the M1/M2 transformation of macrophages, we cultured LX-2 cells and treated them with TGF-β to obtain activated HSCs (aLX2). First, the increased level of α-SAM identified by western blot indicates that LX-2 is indeed activated (Figure 2(a)). In fact, consistent with previous findings, both glycolysis levels and lactate content were significantly increased in activated HSCs aLX-2

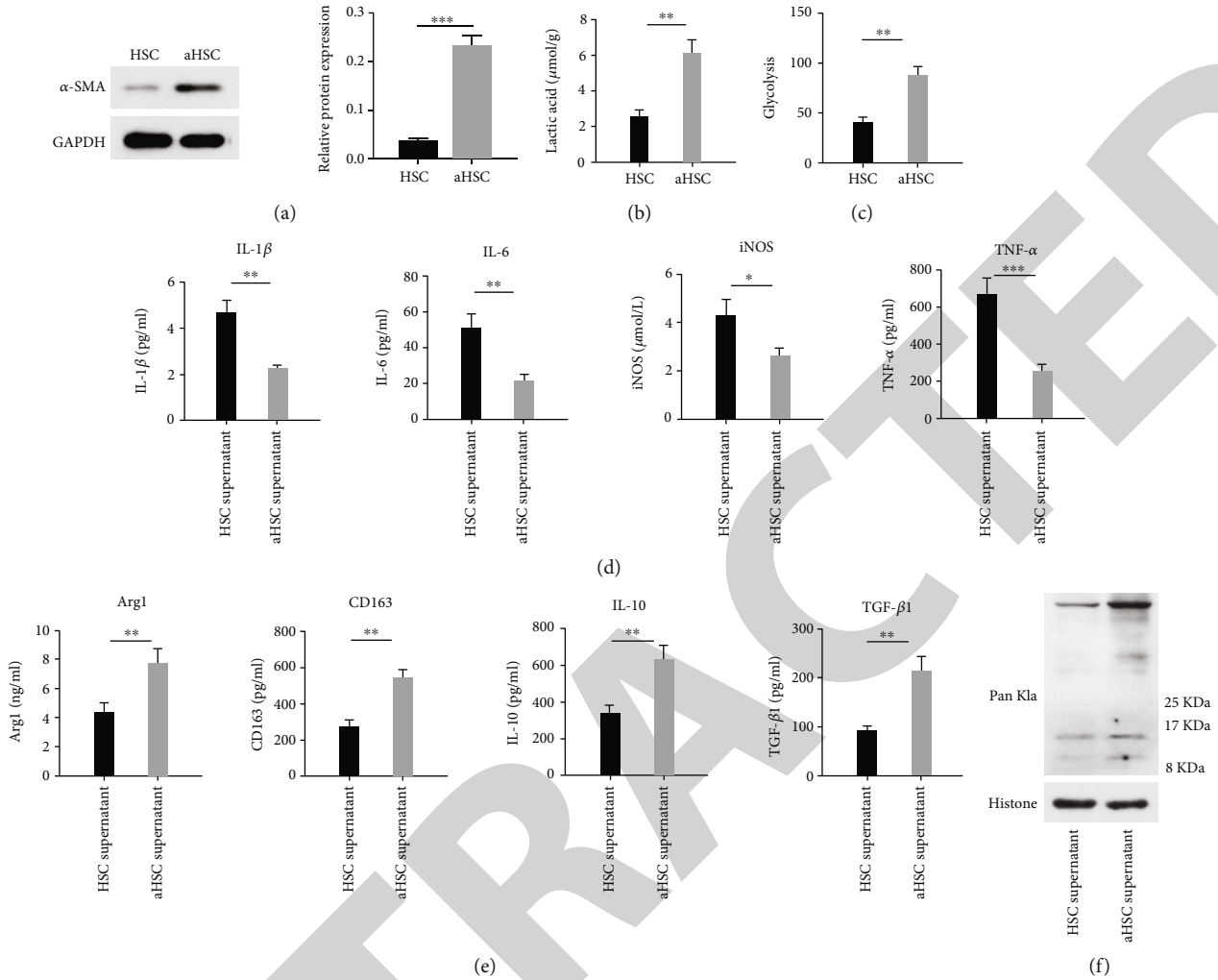

Figure 3: Regulation of primary activated HSCs on the M1/M2 phenotypic transition of macrophages. (a) Western blot showing expression of α-SMA in the HSC and a-HSC (activated HSCs). (b) Lactate level in HSCs and a-HSCs. (c) The level of glycolysis in HSCs and a-HSCs. (d) Detection of the expression levels of M1 macrophage surface markers IL-1β, IL-6, iNOS, and TNF-α in co-aLX-2 co-LX-a cells and their supernatants by ELISA. (e) Detection of the expression levels of M2 macrophage surface markers Arg1, CD163, IL-10, and TGFβ in the supernatants of HSCs and a-HSCs by ELISA. (f) Western blot shows the expression of histone acetylation in the supernatants of HSCs and a-HSCs. $^{*}P < 0.05$, $^{**}P < 0.01$, and $^{***}P < 0.001$.

cells (Figures 2(b) and 2(c)). Then, the aLX-2 were cocultured with M1-type macrophages to observe whether M1 could transform into M2. We detected the following indicators by ELISA and found that the expression levels of M1 macrophage surface markers IL-1β, IL-6, iNOS, and TNF-α in co-aLX-2 cells and supernatants were markedly decreased, but the expression levels of M2 macrophage surface markers Arg1, CD163, IL-10, and TGFβ were significantly increased (Figures 2(d) and 2(e)). Importantly, the level of histone acetylation was also significantly increased in co-LX-2 cells and their supernatants (Figure 2(f)). This suggests that activated HSCs aLX-2 can stimulate the transformation of M1 to M2 macrophages, which may be related to the accumulation of lactate and the promotion of histone acetylation.

3.3. Activated HSCs Can Stimulate the Transformation of M1 to M2 Macrophages. We previously demonstrated that activated LX-2 can stimulate the transformation of M1 to M2 macrophages in hepatic stellate cell lines, but it is unknown whether primary cell lines have the same function. So, we isolated and cultured HSCs from mice and used TGF-β1 to activate them. As shown in Figure 3(a), the protein level of α-SAM was significantly increased in activated HSCs compared with unactivated HSCs. Similarly, consistent with previous findings, both glycolysis levels and lactate content were significantly increased in activated HSCs (Figures 3(b) and 3(c)). Next, we examined the expression of M1 and M2 macrophage markers in the cell supernatants of cultured HSCs and activated HSCs and found that the expression levels of M1 macrophage surface markers IL-1β, IL-6, iNOS, and TNF-α in a-HSC supernatants were markedly decreased, but the expression levels of M2 macrophage surface markers Arg1, CD163, IL-10, and TGFβ were significantly increased (Figures 3(d) and 3(e)). Importantly, the level of histone acetylation was also

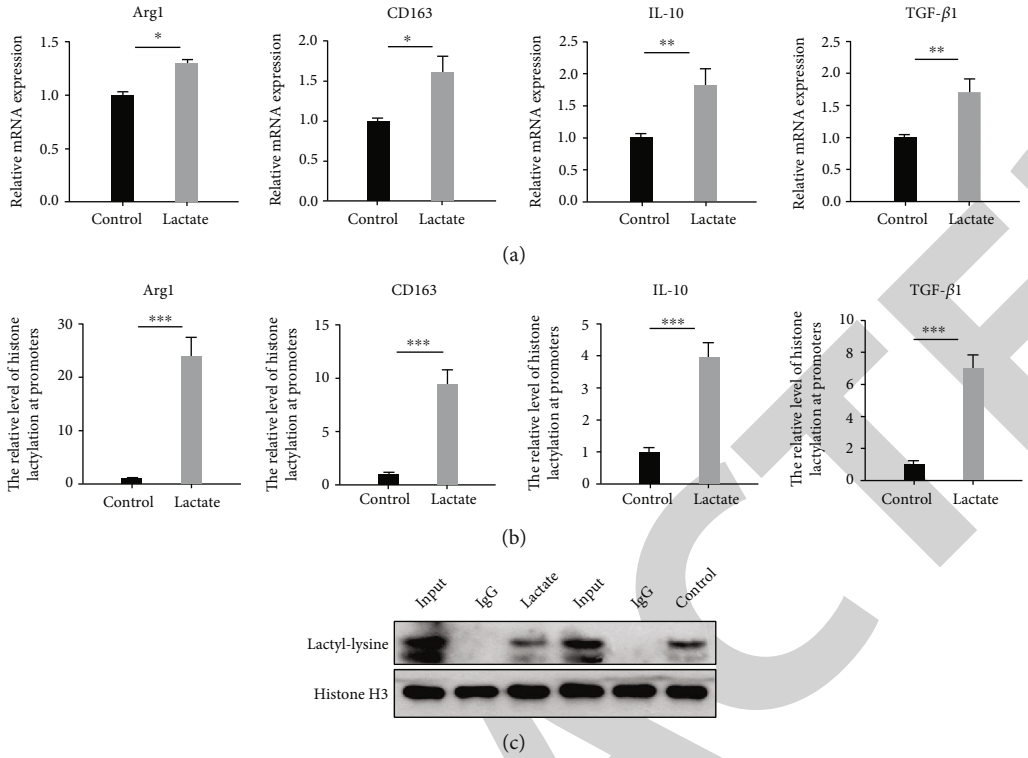

Figure 4: Lactic acid stimulates the conversion of M1 to M2 macrophages. (a) The mRNA expression levels of Arg-1, CD163, IL-10, and TGF-β1 in M1 macrophages cultured with and without lactate by qPCR. (b) The levels of histone acetylation modifications at the promoter regions of genes (Arg-1, CD163, IL-10, and TGF-β1) were examined by ChIP-qPCR. (c) IP-western blot detected the level of histone acetylation inM1 macrophages after treated with 20 mM lactate or vehicle for 24H. $^{*}P < 0.05$, $^{**}P < 0.01$, and $^{***}P < 0.001$.

significantly increased in the supernatants of a-HSCs (Figure 3(f)). This suggests that activated primary HSCs can stimulate the transformation of M1 to M2 macrophages, which may be related to the accumulation of lactate and the promotion of histone acetylation.

3.4. Lactate Promotes the Transformation of M1 into M2 Macrophages by Promoting Histone Acetylation at the Promoters of Genes CD163, Arg-1, IL-10, and TGF-β1. To determine whether lactate can promote the conversion of M1 into M2 macrophages, we supplemented lactate in the medium in which M1 macrophages were cultured, and the results demonstrated that lactate indeed promoted the conversion of M1 into M2 macrophages (Figure 4(a)). To further analyze the mechanism of M1 into M2 macrophage transformation, we performed ChIP experiment with histone acetylation antibody. Since the level of histone acetylation in the promoter region of the M2 marker cannot be directly detected, we used histone acetylation antibody for ChIP experiment, and qPCR detected the expression of related genes. The higher the expression level of the genes, the higher the level of their histone acetylation. This also indicates that the higher level of histone acetylation bound to the promoter region of the M2 marker genes. Therefore, the levels of histone acetylation modifications at the promoter regions of genes (*Arg-1*, *CD*163, *IL*-10, and *TGF-β*1) were then examined by ChIP-qPCR. As shown in Figure 4(b), the levels of acetylation modification at the promoters of these genes were all significantly increased in M1 cells cultured with lactate. And immunoprecipitation assay showed that the acetylation of histone was mildly elevated in M2 macrophage transformed from M1 macrophage after treating with 20 mM lactate for 24 h (Figure 4(c)).

4. Discussion

Hepatic fibrosis is a major cause of morbidity and mortality worldwide because it ultimately leads to cirrhosis. Following liver injury, quiescent HSCs enter the cell cycle, differentiate, and maintain a chronic inflammatory response that accompanies fibrosis [28]. There is increasing evidence that hepatic fibrosis results in alterations in carbohydrate metabolism [12]. Glycolytic levels in both activated hepatic stellate cells and the entire fibrotic liver were significantly increased [29]. As the final product of the glycolytic pathway, whether lactate is important in hepatic fibrosis is particularly worth investigating. In our study, we first established a mouse model of liver fibrosis using CCl4 based on the previous research [30]. Considering that the cellular response to liver injury is highly dependent on sex [31], only female mice were used in our study. So, it was first demonstrated that both glycolysis levels and lactate were significantly increased in hepatic fibrotic mice (Figure 1). When liver injury occurs, HSCs are activated and generate an extracellular matrix network, resulting in the appearance of fibrotic scars [32]. Importantly, it was also shown that the level of lactate was

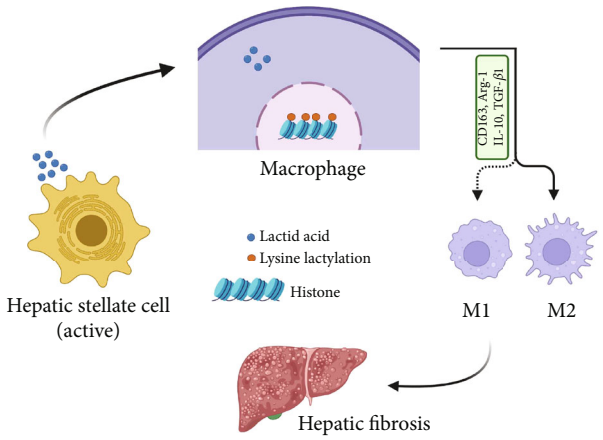

FIGURE 5: Schematic representation of the process that activated HSCs promoted M1 to M2 macrophage transformation and liver fibrosis by elevating the histone acetylation level.

significantly increased in both activated HSC cell line and activated primary HSCs in this study (Figures 2 and 3).

The mechanisms linking M1/M2 macrophage transformation to the development of hepatic fibrosis remain a subject of intensive research, highlighting the necessity to better understand the complex functional interactions that occur between the two macrophage types in the liver [33]. Extracellular signals from activated HSCs, macrophages, and hepatocytes are thought to be essential mediators of the fibrotic cascade in hepatic fibrosis [34, 35]. A previous research shows that phenotypic switching between M1 and M2 can occur under specific stimuli in vivo and in vitro [14]. Interestingly, the number of hepatic M2 macrophages is positively correlated with the severity of liver fibrosis [10]. Considering that the elevated level of lactate modification in M1 macrophages can promote the transformation of macrophages into M2 macrophages [20], we detected the surface markers (Arg-1, CD163, IL-10, and TGF-β1) of M2 macrophages after adding lactate to the culture medium when culturing M1 macrophages. The results demonstrated that lactate indeed promoted the conversion of M1 into M2 macrophages (Figure 4). With ChIP-qPCR assay, we found that the levels of acetylation modification at the promoters of these genes were all significantly increased in M1 cells cultured with lactate. However, this study only describes the phenomenon of M1 and M2 conversion and the effect of lactate and histone acetylation on the conversion of M1 to M2, and the molecular mechanism has not been elucidated, which needs to be further studied.

In conclusion, we demonstrate that activated HSCs can promote the progression of liver fibrosis by secreting a large amount of lactate, increasing the level of histone lactate modification in hepatic M1 macrophages, and promoting the transformation of M1 into M2 macrophages (Figure 5). This fact provides us with new insights into the generation of liver fibrosis and provides an optimistic view that lactate inhibitors or acetylation inhibitors may be used in the treatment of liver fibrosis and reducing the incidence of liver cancer. Overall, modulation of HSCs can prevent and treat liver fibrosis by inhibiting the activation of HSCs, promoting the phenotypic transformation of HSCs, promoting apoptosis of HSCs, and inducing senescence of HSCs. Currently, one of the main focuses of fibrosis research is the development of targeted therapies with high liver specificity. Therefore, further investigation of the mechanisms involved in HSC activation may provide new therapeutic targets for the treatment of liver fibrosis.

Data Availability

The data used to support the findings of this study are included within the manuscript.

Conflicts of Interest

The authors declare that they have no conflicts of interest.

Authors' Contributions

Junru Chen and Xueqing Huang are regarded as co-first author.

Acknowledgments

This work was funded by the Special grant for central government supporting local science and technology development, Science and Technology Department of Guizhou Province (Guizhou specific grant (2019) 4008).

References

[1] T. Kisseleva and D. Brenner, "Molecular and cellular mechanisms of liver fibrosis and its regression," *Nature Reviews Gastroenterology & Hepatology*, vol. 18, no. 3, pp. 151–166, 2021.

[2] D. Dhar, J. Baglieri, T. Kisseleva, and D. A. Brenner, "Mechanisms of liver fibrosis and its role in liver cancer," *Experimental Biology and Medicine*, vol. 245, no. 2, pp. 96–108, 2020.

[3] S. L. Friedman, "Liver fibrosis – from bench to bedside," *Journal of Hepatology*, vol. 38, Supplement 1, pp. 38–S53, 2003.

[4] R. C. Lo and H. Kim, "Histopathological evaluation of liver fibrosis and cirrhosis regression," *Clinical and Molecular Hepatology*, vol. 23, no. 4, pp. 302–307, 2017.

[5] O. Khomich, A. V. Ivanov, and B. Bartosch, "Metabolic hallmarks of hepatic stellate cells in liver fibrosis," *Cells*, vol. 9, no. 1, p. 24, 2020.

[6] A. Geerts, "History, heterogeneity, developmental biology, and functions of quiescent hepatic stellate cells," *Seminars in Liver Disease*, vol. 21, no. 3, pp. 311–336, 2001.

[7] H. Senoo, N. Kojima, and M. Sato, "Vitamin A-storing cells (stellate cells)," *Vitamin A*, vol. 75, pp. 131–159, 2007.

[8] S. Hazra, S. Xiong, J. Wang et al., "Peroxisome proliferator-activated receptor γ induces a phenotypic switch from activated to quiescent hepatic stellate cells," vol. 279, no. 12, pp. 11392–11401, 2004.

[9] Y. Koyama, P. Wang, S. Liang et al., "Mesothelin/mucin 16 signaling in activated portal fibroblasts regulates cholestatic liver fibrosis," *Journal of Clinical Investigation*, vol. 127, no. 4, pp. 1254–1270, 2017.

Hindawi
Disease Markers
Volume 2023, Article ID 9861260, 1 page
https://doi.org/10.1155/2023/9861260

Retraction

Retracted: Multiomics Immune-Related lncRNA Analysis of Oral Squamous Cell Carcinoma and Its Correlation with Prognosis

Disease Markers

Received 20 June 2023; Accepted 20 June 2023; Published 21 June 2023

This article has been retracted by Hindawi following an investigation undertaken by the publisher [1]. This investigation has uncovered evidence of one or more of the following indicators of systematic manipulation of the publication process:

(1) Discrepancies in scope

(2) Discrepancies in the description of the research reported

(3) Discrepancies between the availability of data and the research described

(4) Inappropriate citations

(5) Incoherent, meaningless and/or irrelevant content included in the article

(6) Peer-review manipulation

The presence of these indicators undermines our confidence in the integrity of the article's content and we cannot, therefore, vouch for its reliability. Please note that this notice is intended solely to alert readers that the content of this article is unreliable. We have not investigated whether authors were aware of or involved in the systematic manipulation of the publication process.

Wiley and Hindawi regrets that the usual quality checks did not identify these issues before publication and have since put additional measures in place to safeguard research integrity.

We wish to credit our own Research Integrity and Research Publishing teams and anonymous and named external researchers and research integrity experts for contributing to this investigation.

The corresponding author, as the representative of all authors, has been given the opportunity to register their agreement or disagreement to this retraction. We have kept a record of any response received.

References

[1] Z. Liu, Q. Liu, X. Wang, L. Liu, L. Shi, and H. Li, "Multiomics Immune-Related lncRNA Analysis of Oral Squamous Cell Carcinoma and Its Correlation with Prognosis," *Disease Markers*, vol. 2022, Article ID 6106503, 15 pages, 2022.

Hindawi
Disease Markers
Volume 2022, Article ID 6106503, 15 pages
https://doi.org/10.1155/2022/6106503

Research Article

Multiomics Immune-Related lncRNA Analysis of Oral Squamous Cell Carcinoma and Its Correlation with Prognosis

Zhen Liu,[1] **Qian Liu**,[2] **Xiaoyu Wang**,[2] **Lin Liu**,[2] **Lianrui Shi**,[3] **and Hongbo Li**[2]

[1]*Department of Stomatology, The Eighth Medical Center, Chinese PLA General Hospital, China*
[2]*Department of Stomatology, The First Medical Center, Chinese PLA General Hospital, China*
[3]*Department of Stomatology, The Sixth Medical Center, Chinese PLA General Hospital, China*

Correspondence should be addressed to Hongbo Li; lihongbo@301hospital.com.cn

Received 12 June 2022; Revised 21 July 2022; Accepted 19 August 2022; Published 8 September 2022

Academic Editor: Xianwei Zeng

Objective. To investigate the multiomics immune-related lncRNA analysis of oral squamous cell carcinoma and its correlation with prognosis. *Methods*. Through the bioinformatics database, a total of 346 oral squamous cell carcinoma (OSCC) related samples were retrieved. Bioinformatics analysis screened out the difference lncRNAs in the sample tissue and normal tissue, combined with literature research to clarify the target. The biological functions of differentially expressed lncRNAs were predicted. The differential expression network of differentially expressed lncRNAs and mRNAs was established. The correlation analysis software was used to analyze the correlation between oral squamous cell carcinoma multiomics immune-related lncRNA and prognosis. *Results*. 3054 lncRNAs in OSCC tissues are highly correlated with immune genes. 76 immune-related lncRNAs were different in tumor and adjacent tissues. Cancer Hallmark, Phenotype, and Subcellular Location analysis were completed. The results showed that lncRNAs can participate in tumor cell invasion, metastasis, proliferation, and apoptosis. Select the 15 most important lncRNAs above, draw Kaplan-Meier curve to complete the survival curve analysis, and complete the analysis and arrangement of the relevant data. LINC00460, CASC9, and HCG22 were screened for subsequent analysis. Complete the GO and KEGG enrichment analysis. LINC00460, CASC9, and macrophages M0 are positively correlated; CASC9 is negatively correlated with macrophages M1; LINC00460 is positively correlated with macrophages M1; HCG22 is associated with mast cells resting positive correlation; LINC00460 was negatively correlated with mast cell resting. CASC9 and HCG22 were significantly correlated with the age and stage of OSCC patients; 2 key lncRNA and 79 miRNAs were extracted from the database, to complete 86 pairs of interactions; the target mRNAs were predicted based on the above miRNAs. A total of 631 pairs of interactions were predicted (including 21 miRNAs and 562 mRNAs), and the regulatory mechanism of key gene ceRNA network was constructed. *Conclusion*. The differential expression of multiple lncRNAs and mRNAs was screened, and the downregulated lncRNAs were more than the upregulated lncRNAs. The lncRNA LINC00460, CASC9, and HCG22 had a strong correlation with prognosis.

1. Introduction

Characterized by different degrees of keratinization, oral squamous cell carcinoma (OSCC) is a malignant tumor that occurs in epidermal or appendage cells, mostly observed in regions covered by squamous epithelium, such as skin, oral cavity, and esophagus [1]. Previous studies have shown [2] that the pathogenesis of OSCC is complex, which is related to factors of race and immunosuppression, etc., and involves multistep variation of multiple genetic mutations [3]. Genomic sequencing shows that among human genomic sequences, only 1.5% are used for protein coding, while 98.5% are noncoding sequences [4, 5]. Previous studies have shown [6] that noncoding sequences can be divided into two types according to the length of transcripts: short noncoding RNA and long noncoding RNA. The former RNA is relatively well studied; has a high degree of sequence conservation, temporal expression, and tissue specificity; and plays an important role in various processes of life. The latter directly participates in tumor pathogenesis, invasion, and

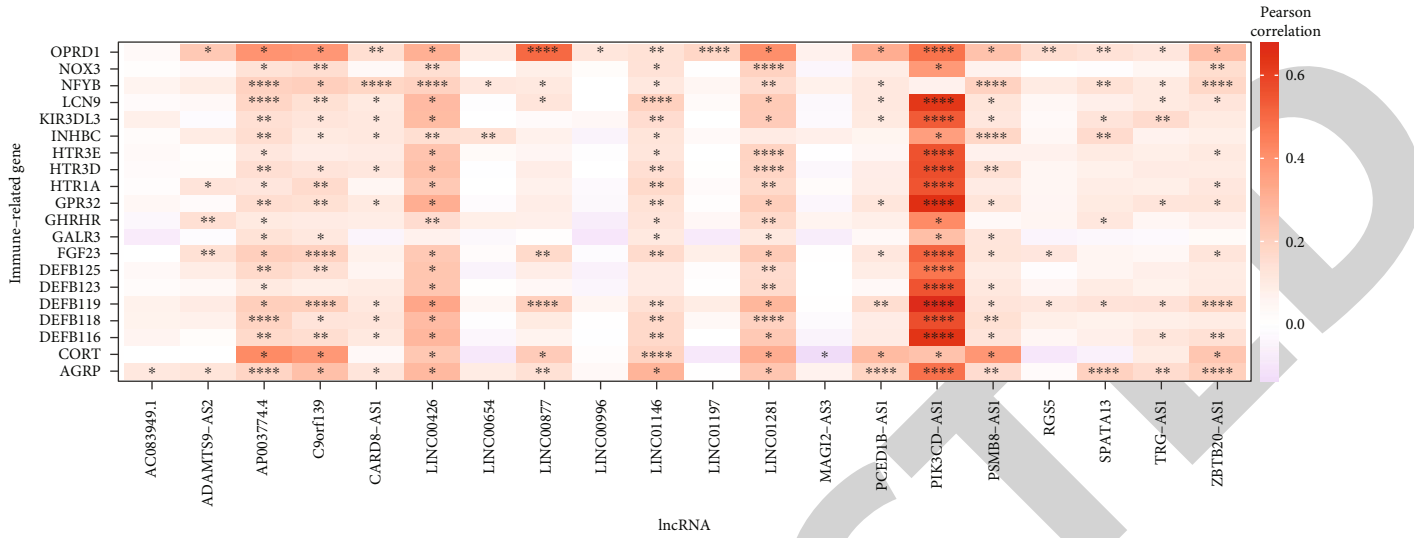

Figure 1: Some lncRNA differentially expressed in OSCC tissues and highly associated with immunogenes.

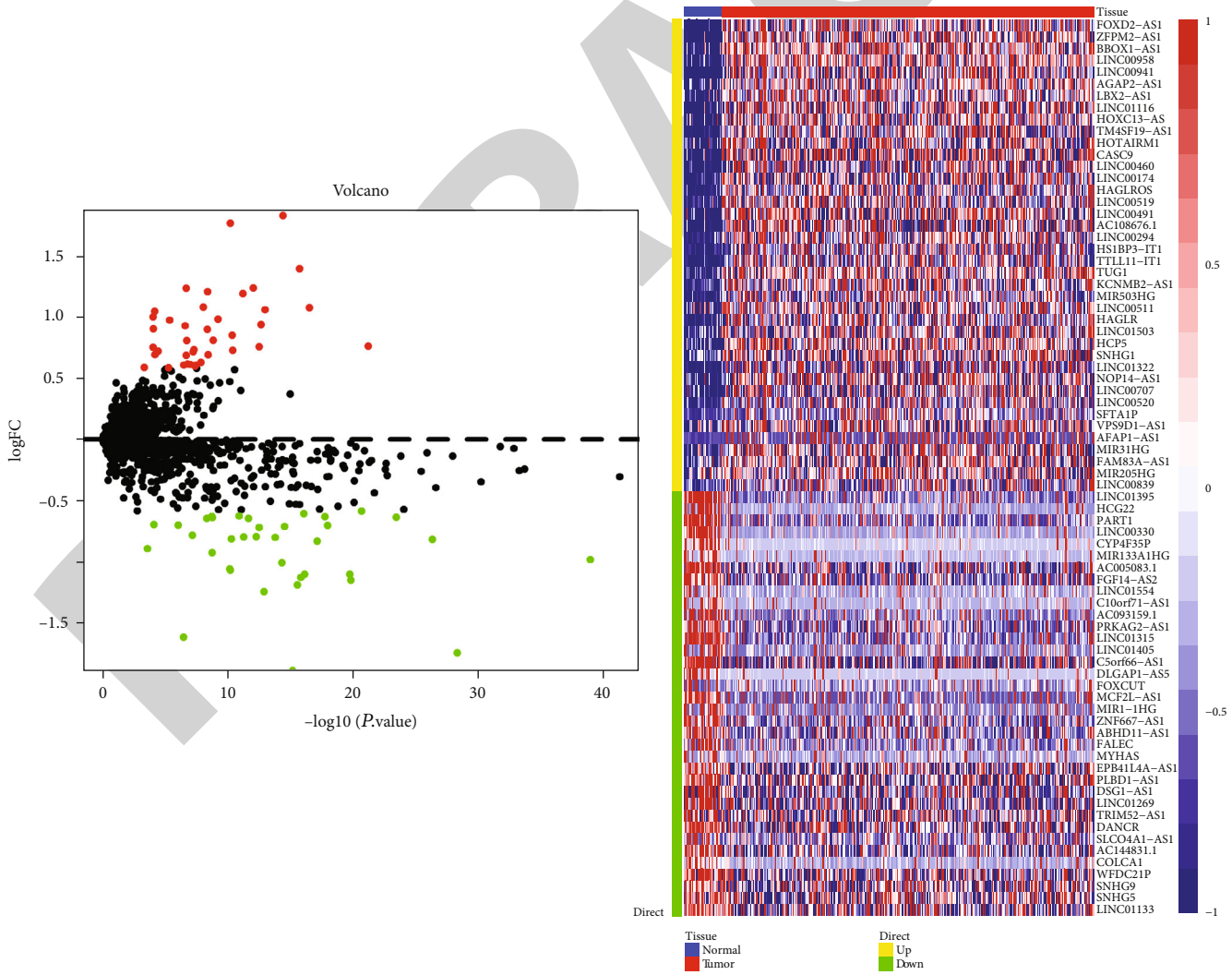

Figure 2: Immune-related lncRNA with significant differences from normal tissues.

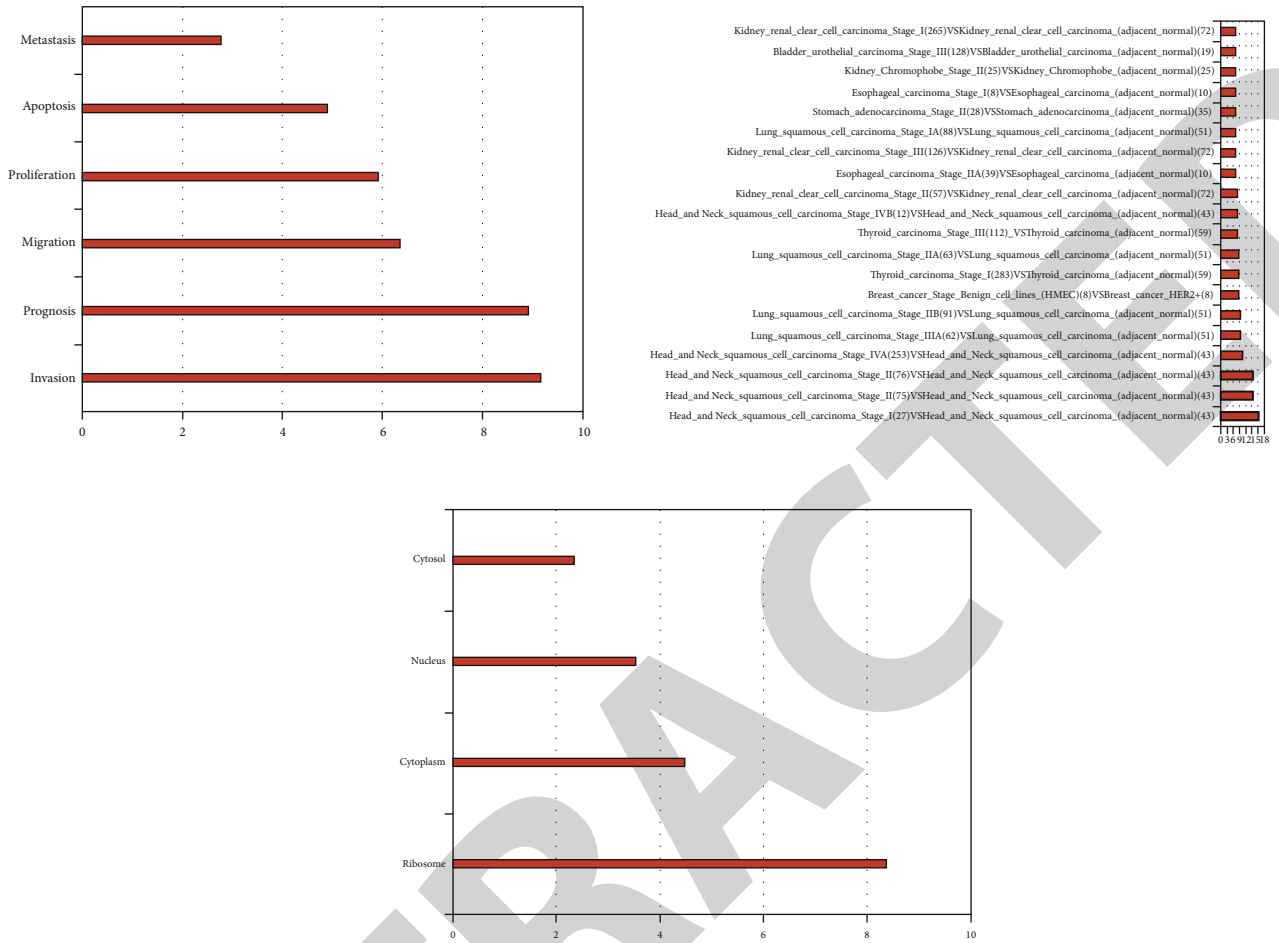

Figure 3: Cancer characteristics, phenotype, and subcellular localization of differentially expressed lncRNA.

metastasis. As a type of RNA with the transcript longer than 200 nucleotides but lacking a functional open reading frame, lncRNA completes the regulation of related proteins before and after transcription and participates in many different types of biological processes, becoming a new choice of drug targeting therapy for cancer [7, 8]. Previous studies have identified many different lncRNA expression profiles from OSCC and normal human tissues, and some are closely related to the occurrence and development of OSCC. Meanwhile, some of the lncRNA function as oncogenes that can participate in the proliferation, differentiation, tumor invasion, and metastasis of different cells. In the present study, using patients with OSCC as subjects, we performed the multiomics immune-related lncRNA analysis, investigated correlation with prognosis of OSCC patients, and reported as follows.

2. Materials and Methods

2.1. General Information. Main bioinformatics databases, including GEO database, HGNC database, cBioPortal database, TCGA database, GEPIA database, and UALCAN database, were considered.

2.2. Bioinformatics Analysis

2.2.1. Acquisition of Data. Based on the advantages and disadvantages of the databases mentioned above, we gave priority to the TCGA database which is the largest cancer gene information database at present, searched this database, and saved the following data: gene expression data, miRNA expression data, copy number variation, DNA methylation, and SNP. Based on the characteristics of OSCC, a total of 346 OSCC related sample expression profile data were extracted from the TCGA database, including 32 cases in the normal group and 314 cases in the tumor group, and used for the immunogene set (a total of 1811 immune-related genes were included) which was obtained through the ImmPort database [9, 10].

2.2.2. Automated Machine Screening of Key lncRNAs. The immune-related genes obtained above were automatically screened by the machine. Meanwhile, random forest (which is an integrated learning algorithm using decision trees as the learner) was introduced to the screening process. Adopting the method of sampling and recursion, this method selects multiple samples from the sample set, considers them as a training set, obtains the sample set through sampling

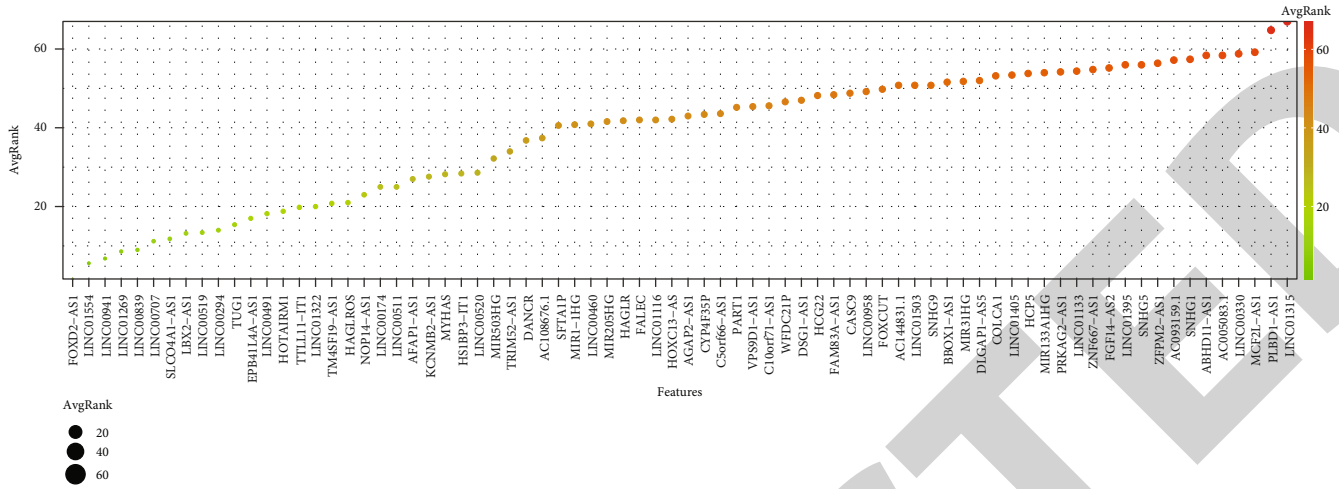

Figure 4: Feature selection by SVM regression.

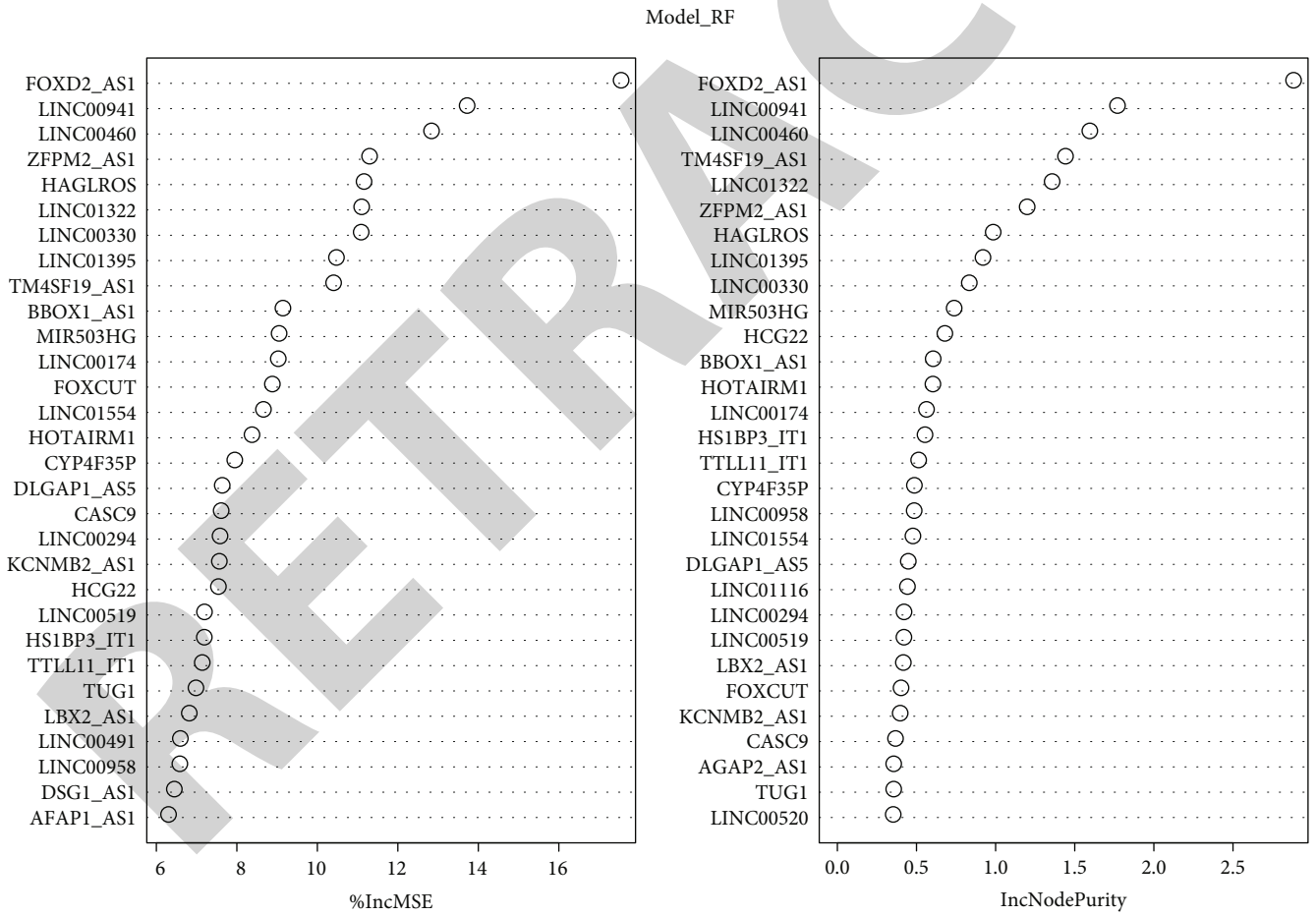

Figure 5: Feature selection by random forest regression.

and generates a decision tree, selects features randomly without repetition at each node generated, and completes the classification of the sample set with the help of the above-mentioned features. Thus, the best classification feature is found, and the prediction result is decided. Therefore, in this study, one thousand classification trees were constructed in the random forest algorithm and mixed 50 times, and the importance of the features was evaluated according to

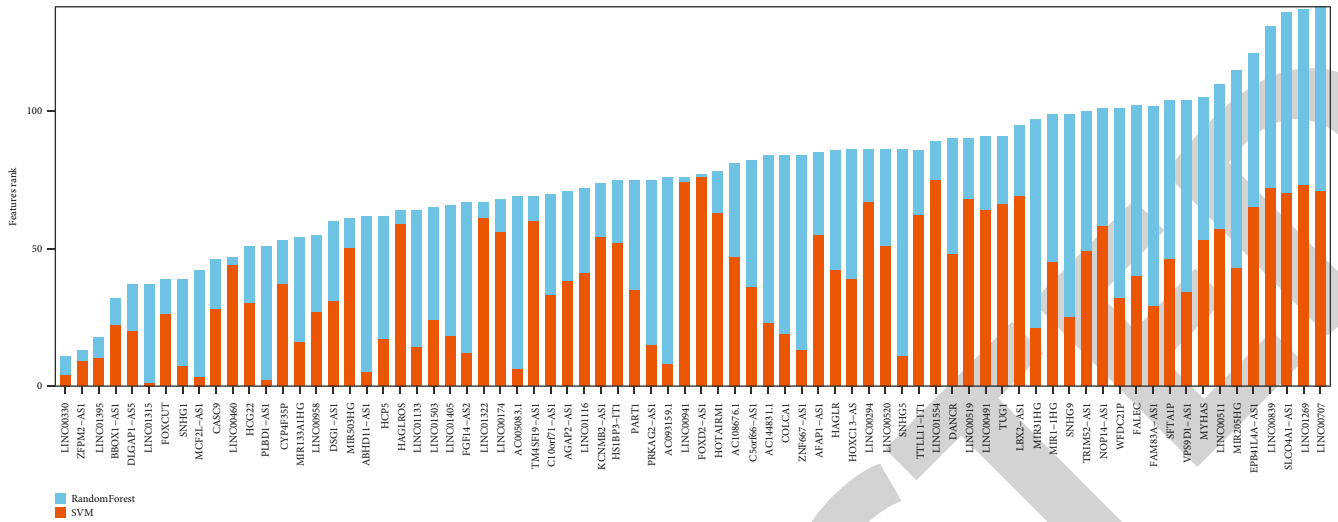

Figure 6: Feature selection by SVM and random forest regression.

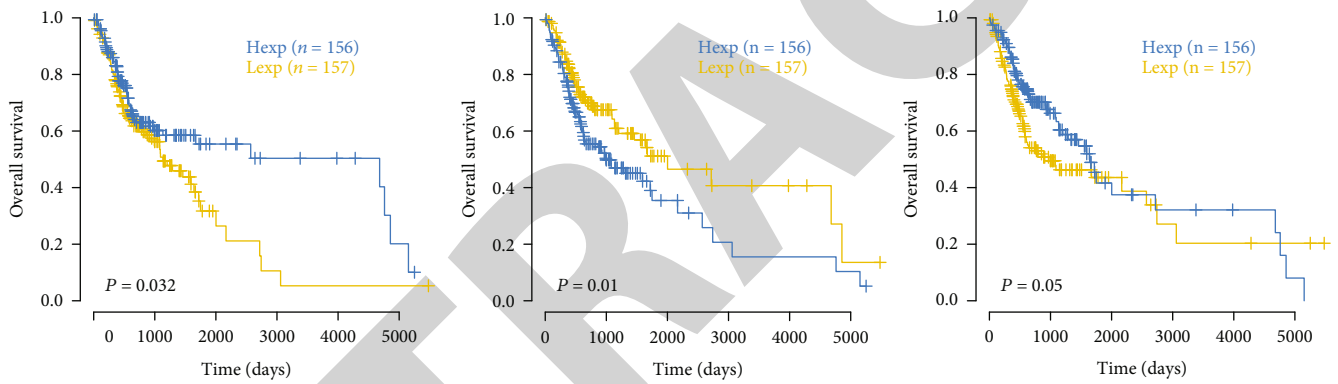

Figure 7: Survival curve analysis on CASC9, HCG22, and LINC00460. Note: (a)–(c) correspond to CASC9, HCG22, and LINC00460.

%IncMSE. Previous studies indicate that SVM-RFE is a machine learning method based on the support vector machine (SVM), which removes the feature vectors generated by SVM, finds the best variables, and establishes a SVM model with the help of e1071 software package to further identify the above biomarkers for disease diagnosis [11, 12].

2.2.3. LncSEA Enrichment Analysis. The lncRNA enrichment analysis is essential for investigating biological information of abnormally expressed lncRNA, supporting more than 40,000 reference lncRNA sets, often involving different categories of miRNAs, diseases, drugs, methylation patterns, lncRNA-binding proteins, cellular markers, subcellular localization, cancer markers, accessible chromatin, exosomal protection, and smORF. Meanwhile, during lncRNA enrichment analysis, annotation and enrichment analysis for lncRNA sets associated with upstream regulators and downstream targets are provided [13]. Therefore, to further determine the biological information of lncRNA abnormally expressed in OSCC tissues, we set the *P* value, BH, and Bonferroni threshold to 0.01, 0.05, and 0.05, respectively, and completed the enrichment for abnormally expressed lncRNA using lncRNAs of GENCODE as the dataset.

2.2.4. Multiomics Immune-Related lncRNA Analysis and Correlation with Prognosis

(1) Drug Sensitivity Analysis. Based on the Genomics of Drug Sensitivity in Cancer (GDSC, https://www.cancerrxgene.org/) database, the largest pharmacogenomic database, we used the R software package "pRRophetic" to predict the chemosensitivity of each tumor sample, obtained the IC50 estimate of each specific chemotherapeutic drug treatment using regression, and performed 10 cross-validations with the GDSC training set to test the regression and prediction accuracy. Default values were chosen for all parameters, including "combats" to remove batching effects and averaging of duplicate gene expression.

(2) Immune Cell Infiltration Analysis. RNA-seq data from different subgroups of OSCC patients were analyzed using the "CIBERPORT" package in R language and used to infer the relative proportions of 22 immune infiltrating cells, and

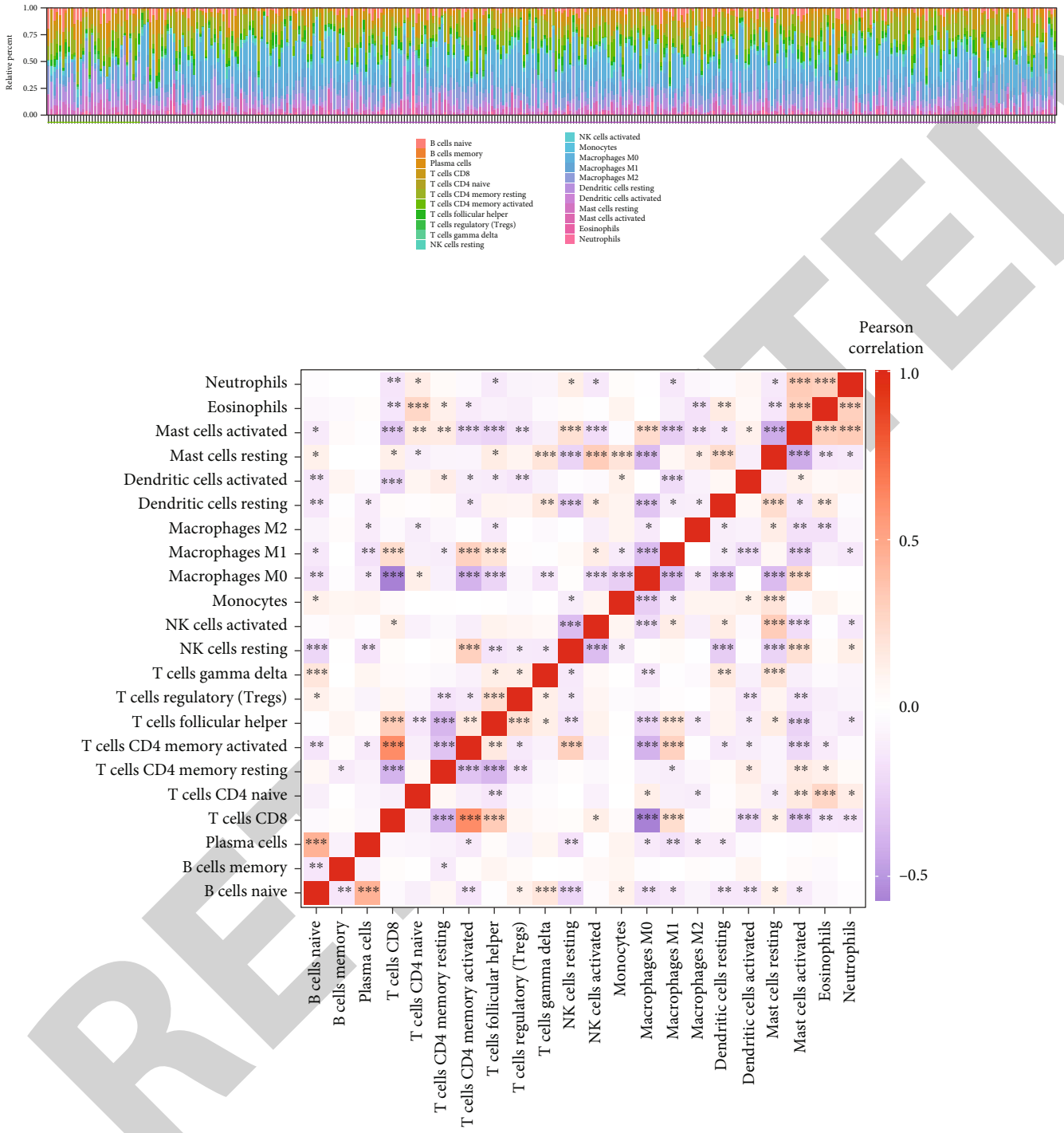

Figure 8: Percentage of immune cells in each patient and correlation of immune cells.

Spearman correlation analysis was performed for the amount of gene expression as well as the immune cell content. A $P < 0.05$ was required for statistical significance.

(3) GSEA Enrichment Analysis. The gene set enrichment analysis (http://www.broadinstitute.org/gsea) was performed on the expression profiles of OSCC patients, to identify genes that were differentially expressed between the high- and low-expression groups of patients. The gene set was filtered using the maximum and minimum gene set sizes of 500 and 15 genes, respectively. After 100 times of permutation, enriched gene sets were obtained based on P value <0.05 and a false discovery rate of 0.25.

(4) TISIDB Immunogene Correlation Analysis. TISIDB (http://cis.hku.hk/TISIDB/index.php) is an online database for tumor-immune system interactions, which integrates multiple types of heterogeneous data which are integrated into multiple categories of information of each gene. TISIDB fuses data information from multiple databases and is a

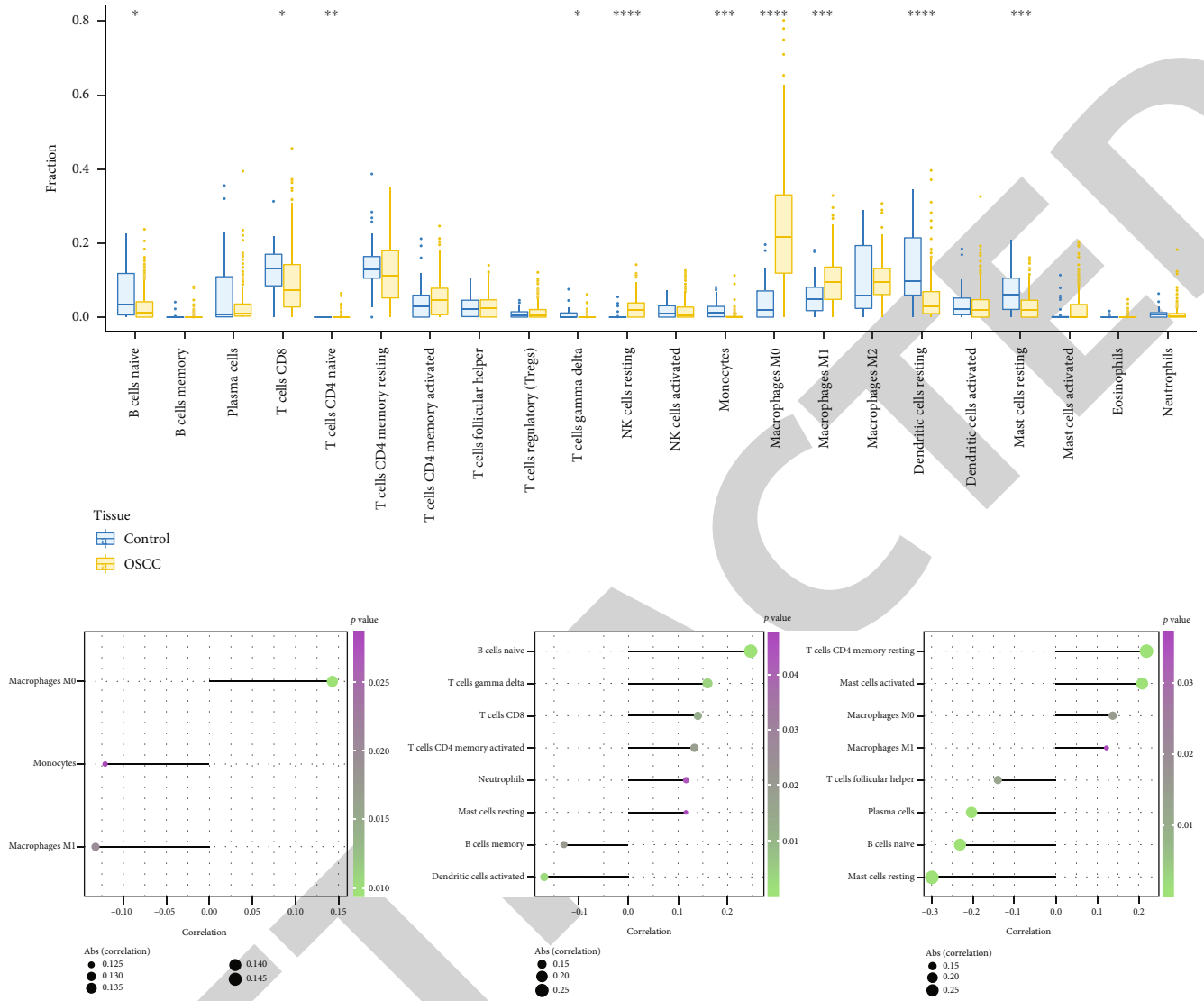

Figure 9: Correlation of key lncRNAs with immune cells.

valuable resource for cancer immunology research and treatment. The immune gene set used to investigate tumor-immune system interactions was derived from the TISIDB in the present study.

2.3. Statistical Analysis. The survival curves were generated by the Kaplan-Meier method and compared by log-rank. All statistical analyses were conducted in R language (version 3.6). All statistical tests were bilateral; a $P < 0.05$ suggested that the difference was statistically significant.

3. Results

3.1. Analysis of Abnormally Expressed lncRNA in OSCC Tissues. The lncRNA differentially expressed in OSCC tissues and associated with immune were screened and analyzed by bioinformatics, and a total of 3054 differentially expressed lncRNA were screened, and most of them were highly associated with immunogenes, as shown in Figure 1.

The differential analysis on differentially expressed lncRNA in OSCC tissues extracted above was performed using limma. The results showed that 76 immune-related lncRNA were differentially expressed between the tumor group and the normal group, as shown in Figure 2.

The analysis on cancer characteristics, phenotype, and subcellular localization for differentially expressed lncRNA was performed through the LncSEA database. The results showed that lncRNA could participate in solid tumor cell migration, proliferation, apoptosis, etc. and was enriched in several OSCC-related gene sets. The subcellular localization was mainly in the ribosome and cytoplasm, as shown in Figure 3.

3.2. Key lncRNA Acquisition and Survival Analysis. The abnormally expressed lncRNA obtained above was analyzed, and the feature selection was completed by SVM and random forest regression in machine learning; see Figures 4–6.

The 15 lncRNAs with the highest importance mentioned above were selected, to draw the Kaplan-Meier curve and to

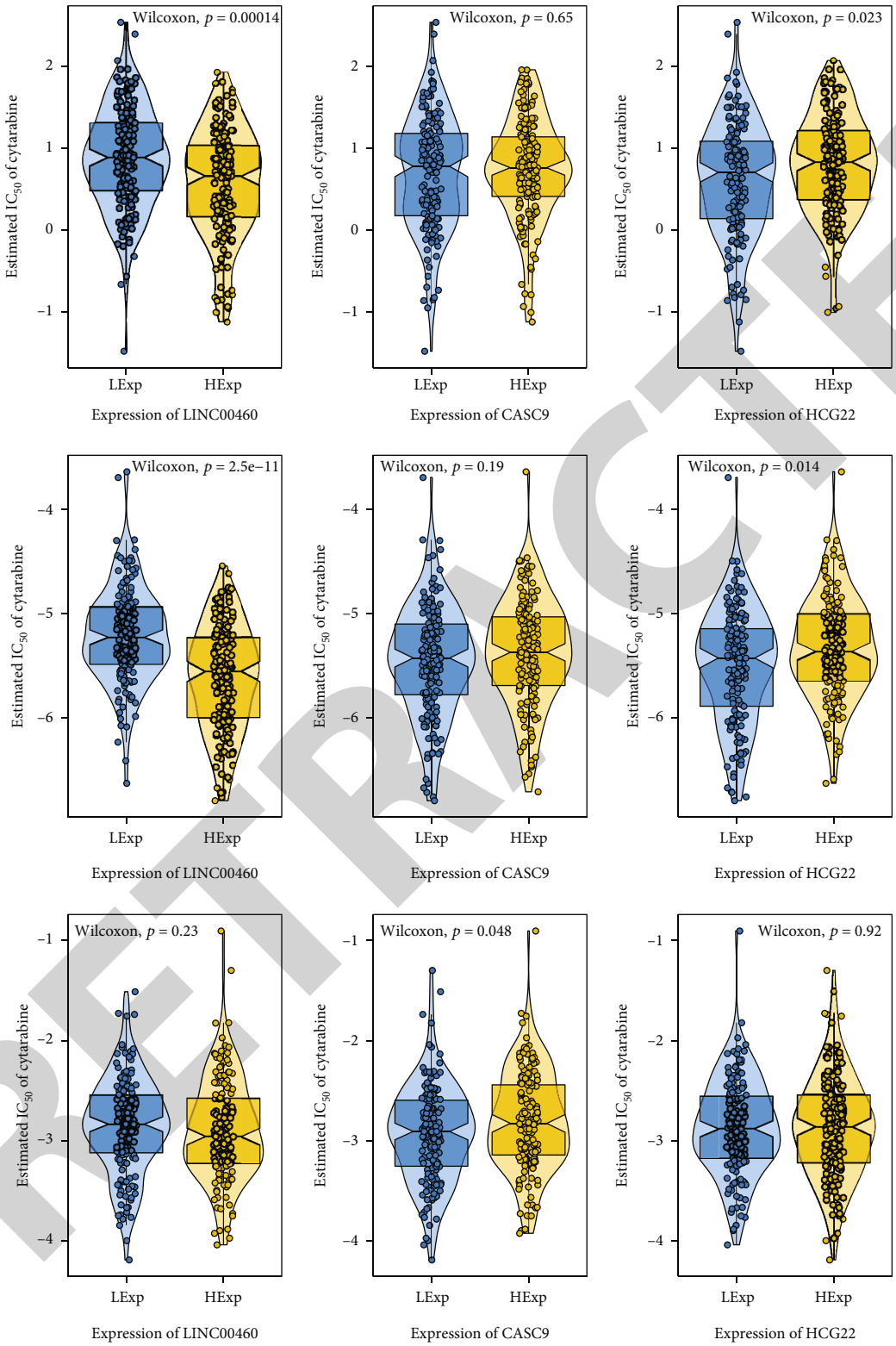

Figure 10: Abnormally expressed lncRNA can affect the sensitivity of cytarabine, docetaxel, and paclitaxel.

complete the survival curve analysis as well as the analysis and collation of relevant data. The results showed that the LINC00460, CASC9, and HCG22 were statistically significant and could be involved in regulating the prognosis of OSCC patients, as shown in Figure 7.

3.3. Clinical Predictive Value of Key lncRNA. The percentage of immune cells in each patient and the relationship between immune cells are shown in Figure 8.

In the present study, macrophages M0 and macrophages M1 were significantly higher in the OSCC group than in

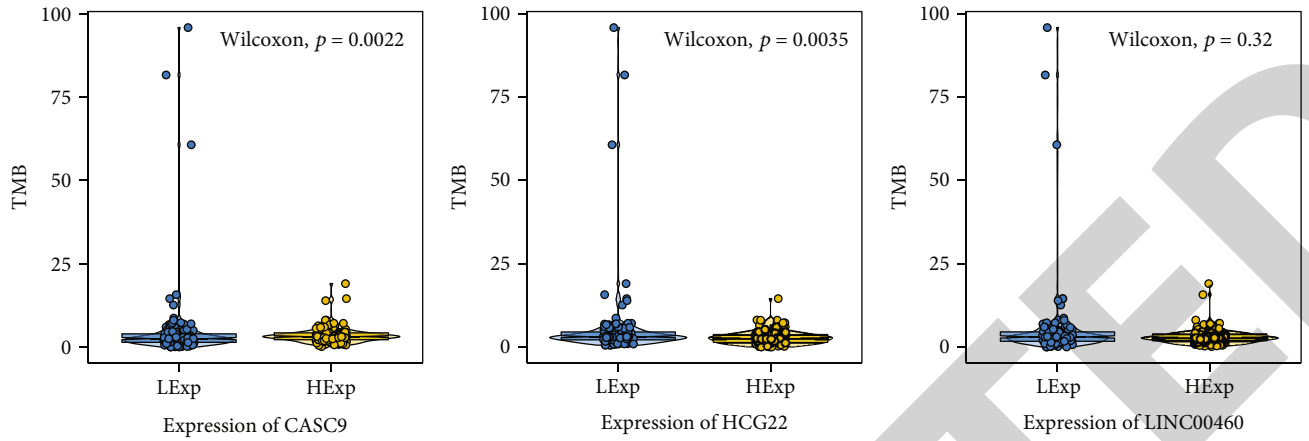

Figure 11: Effect of abnormally expressed lncRNA on TMB.

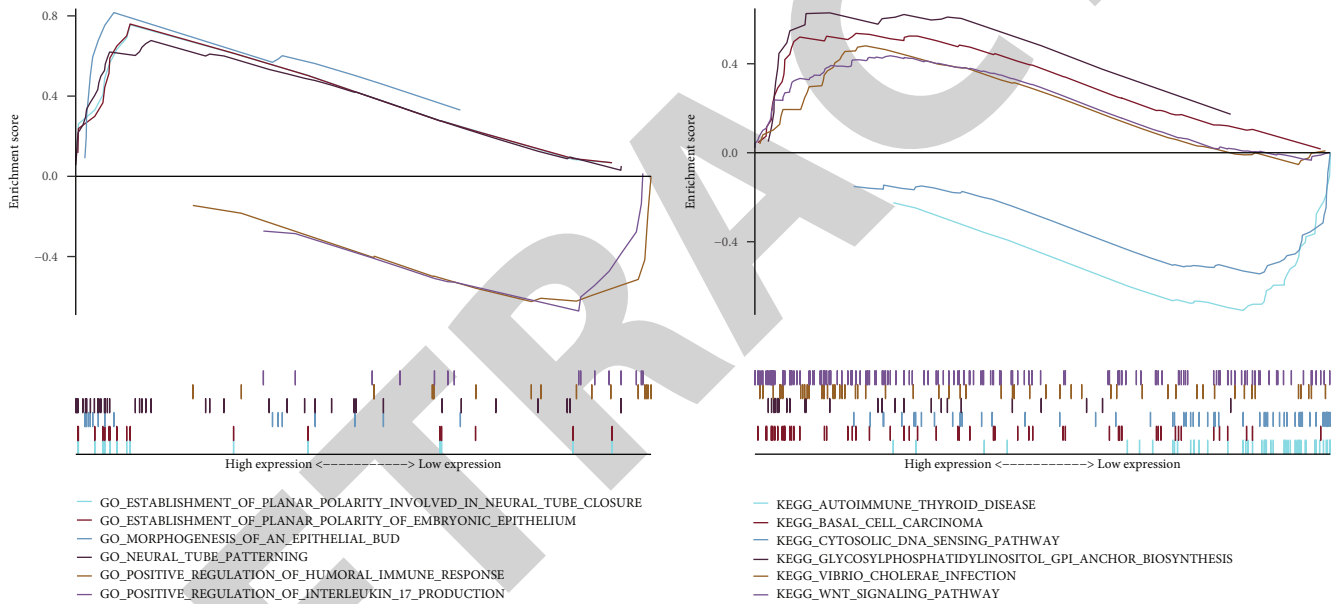

Figure 12: GO and KEGG enrichment results for the CASC9.

normal patients. LINC00460 and CASC9 were positively correlated with M0, while CASC9 was negatively correlated with M1, and LINC00460 was positively correlated with M1. HCG22 was positively correlated with mast cell resting; LINC00460 was negatively correlated with mast cell resting, as shown in Figure 9.

In the present study, we searched relevant databases and analyzed the sensitivity of different chemotherapeutic samples to chemotherapeutic drugs using the "pRRophetic" function. The results showed that the abnormally expressed lncRNA could affect the sensitivity of cytarabine, docetaxel, and paclitaxel, and TMB (tumor mutational burden) was significantly different in high- and low-expression groups of CASC9 and HCG22, as shown in Figures 10 and 11.

3.4. Analysis of Key lncRNA-Related Signaling Mechanisms. We analyzed and investigated the signaling pathways and biological processes involved by the three key lncRNAs obtained above, further explored the effects of candidate genes on signaling pathways and biological processes related to disease progression, and completed the analysis and collation of data. The results of GSEA analysis are shown : for the LINC00460, ammonium ion metabolic process and connective tissue replacement were observed in GO enrichment, while alpha linolenic acid metabolism and arachidonic acid metabolism were observed in KEGG enrichment; for the CASC9, morphogenesis of an epithelial bud and neural tube patterning were observed in GO enrichment, while autoimmune thyroid disease and basal cell carcinoma were observed in KEGG enrichment; for the HCG22, epidermal cell differentiation and cornification were observed in GO enrichment, while aminoacyl tRNA biosynthesis and alpha-linolenic acid metabolism were observed in KEGG enrichment, as shown in Figures 12–14.

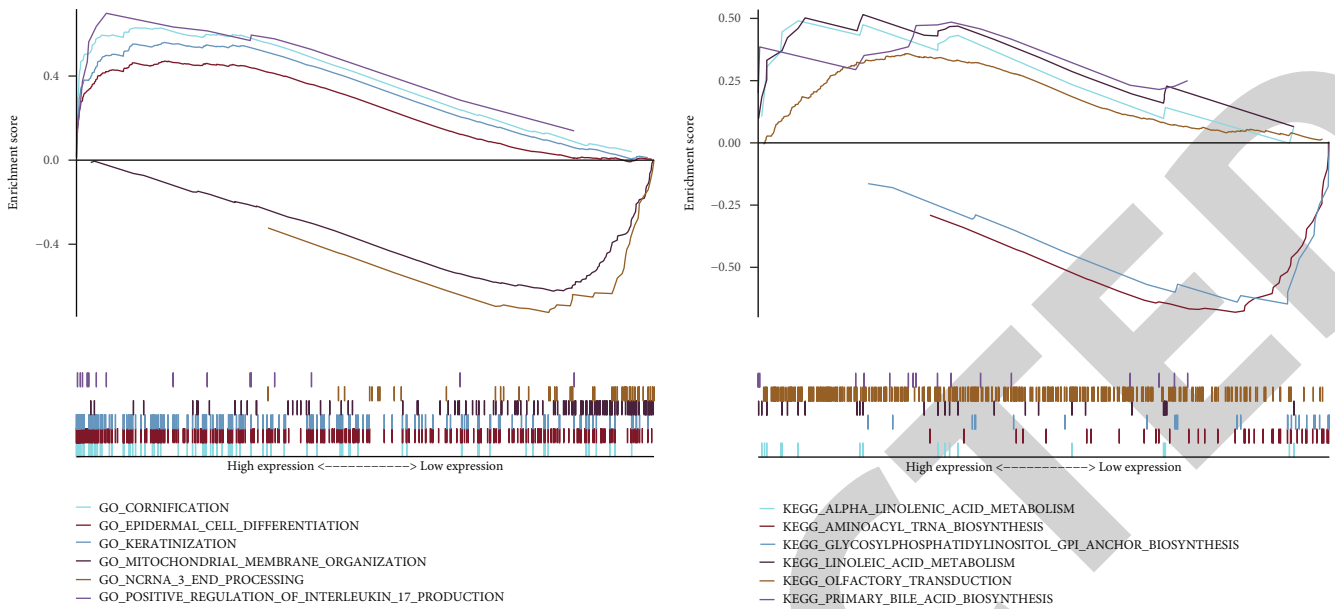

Figure 13: GO and KEGG enrichment results for the HCG22.

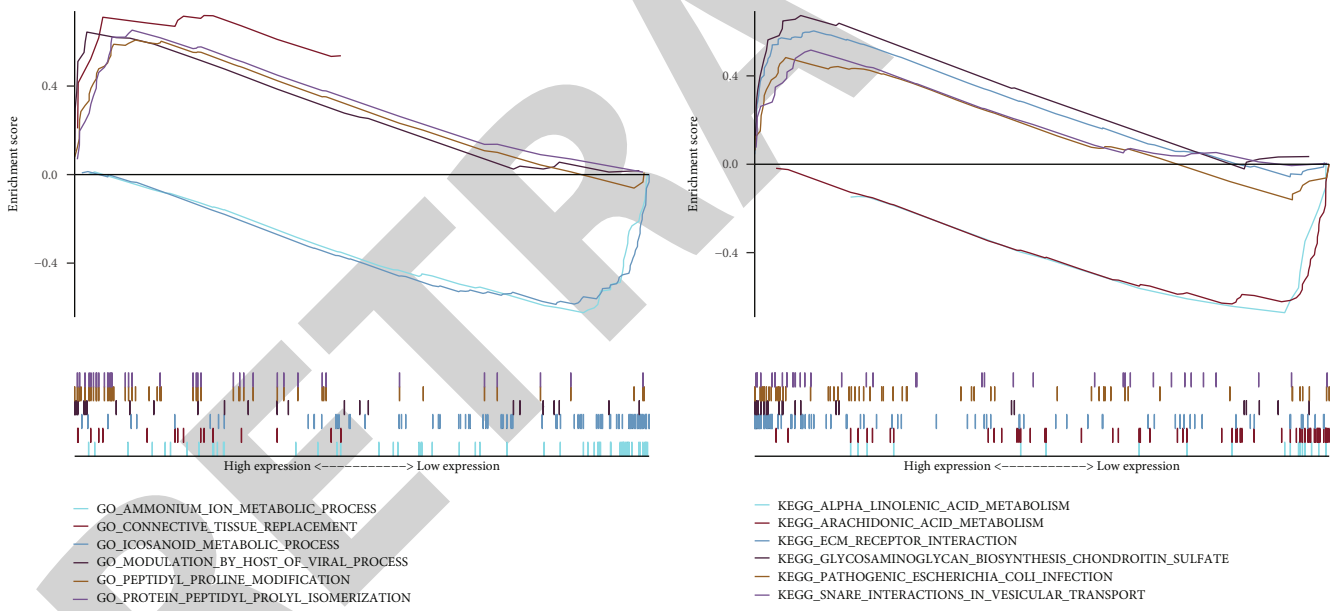

Figure 14: GO and KEGG enrichment results for the LINC00460.

3.5. Prediction of the OSCC Onset Risk and Clinical Correlation Analysis. In the present study, we further constructed the nomogram model to predict patient prognosis. The results of logistic regression analysis showed that different clinical indicators of OSCC and the expression of key lncRNAs contributed in varying degrees throughout the scoring. Meanwhile, the 3-year and 5-year OS (overall survival) was predicted. In addition, we further explored the relationship between key lncRNAs and clinical symptoms and found that significant intergroup differences in the expression levels of these key lncRNAs were observed for several clinical indicators. CASC9 and HCG22 were significantly correlated with the age and stage of OSCC patients, as shown in Figure 15.

3.6. Construction of Key lncRNA ceRNA Network and Relationship with Immune Regulation Related Genes. To further elucidate the bioinformatics analysis, functions, and molecular mechanisms of lncRNA differentially expressed in OSCC tissues, we constructed the ceRNA network for differentially expressed lncRNA, to provide a reference basis for the subsequent analysis of the regulatory mechanisms of key differentially expressed lncRNA. Therefore, a total of 2 key lncRNA and 79 miRNAs were extracted from the

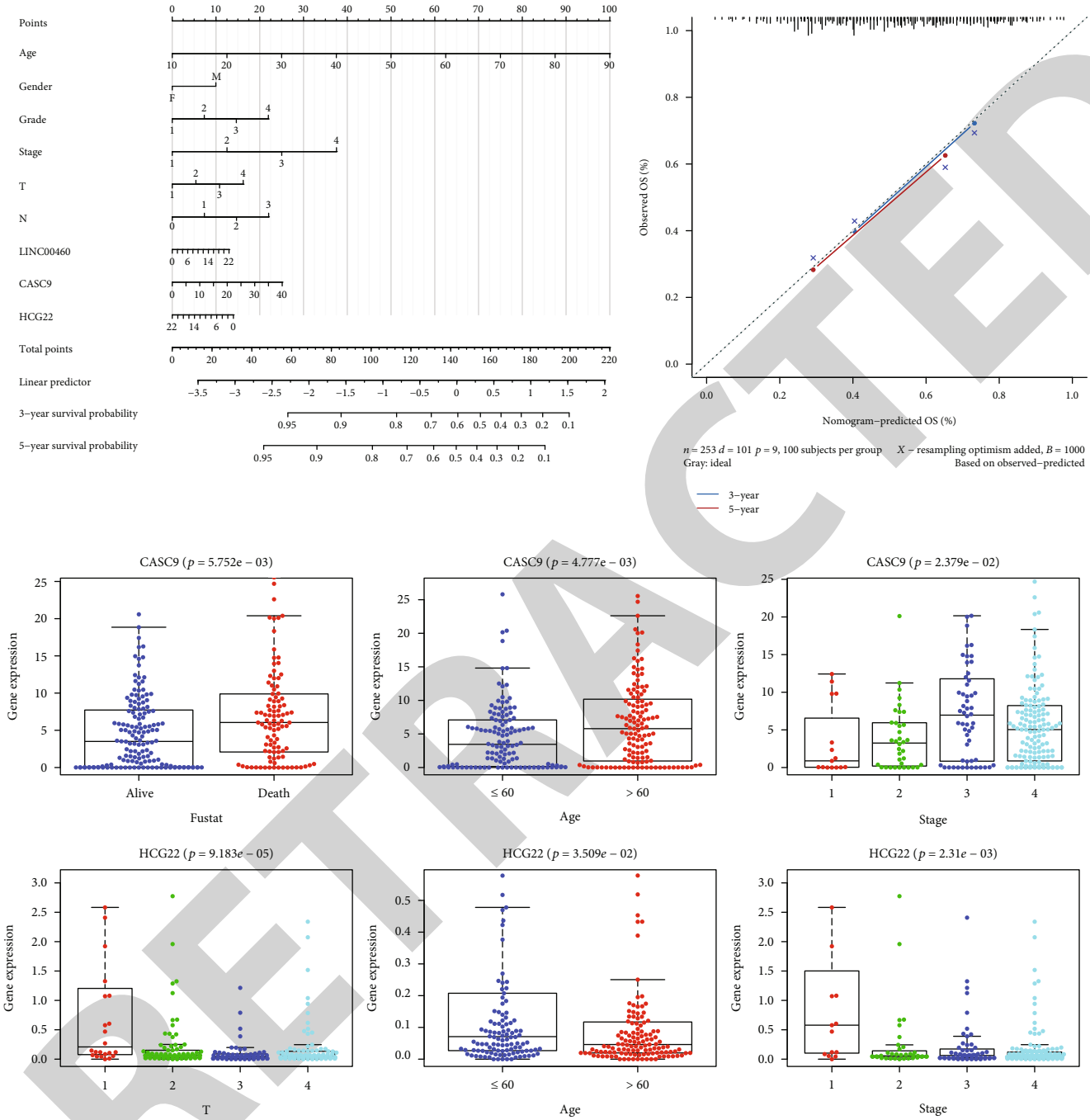

Figure 15: Prediction of the OSCC onset risk and clinical correlation analysis.

database, to complete 86 pairs of interactions; the target mRNAs were predicted based on the above miRNAs. A total of 631 pairs of interactions were predicted (including 21 miRNAs and 562 mRNAs), and the regulatory mechanism of key gene ceRNA network was constructed, as shown in Figure 16.

To further analyze the relationship between differentially expressed lncRNA and immunoregulation-related genes, different types of gene subsets, mostly involving immunomodulators, chemokines, and cell receptors, were obtained with the help of TISIDB. A strong correlation between immunomodulatory genes and the expression levels of key differentially expressed lncRNA were observed, including the following: HCG22 was negatively correlated with immunosuppressive factors and major histocompatibility complexes; CASC9 was negatively correlated with the immunosuppressive factor, MHC, and MHC receptor; and LINC00460 gene was positively correlated with MHC but negatively correlated with the MHC receptor, as shown in Figure 17.

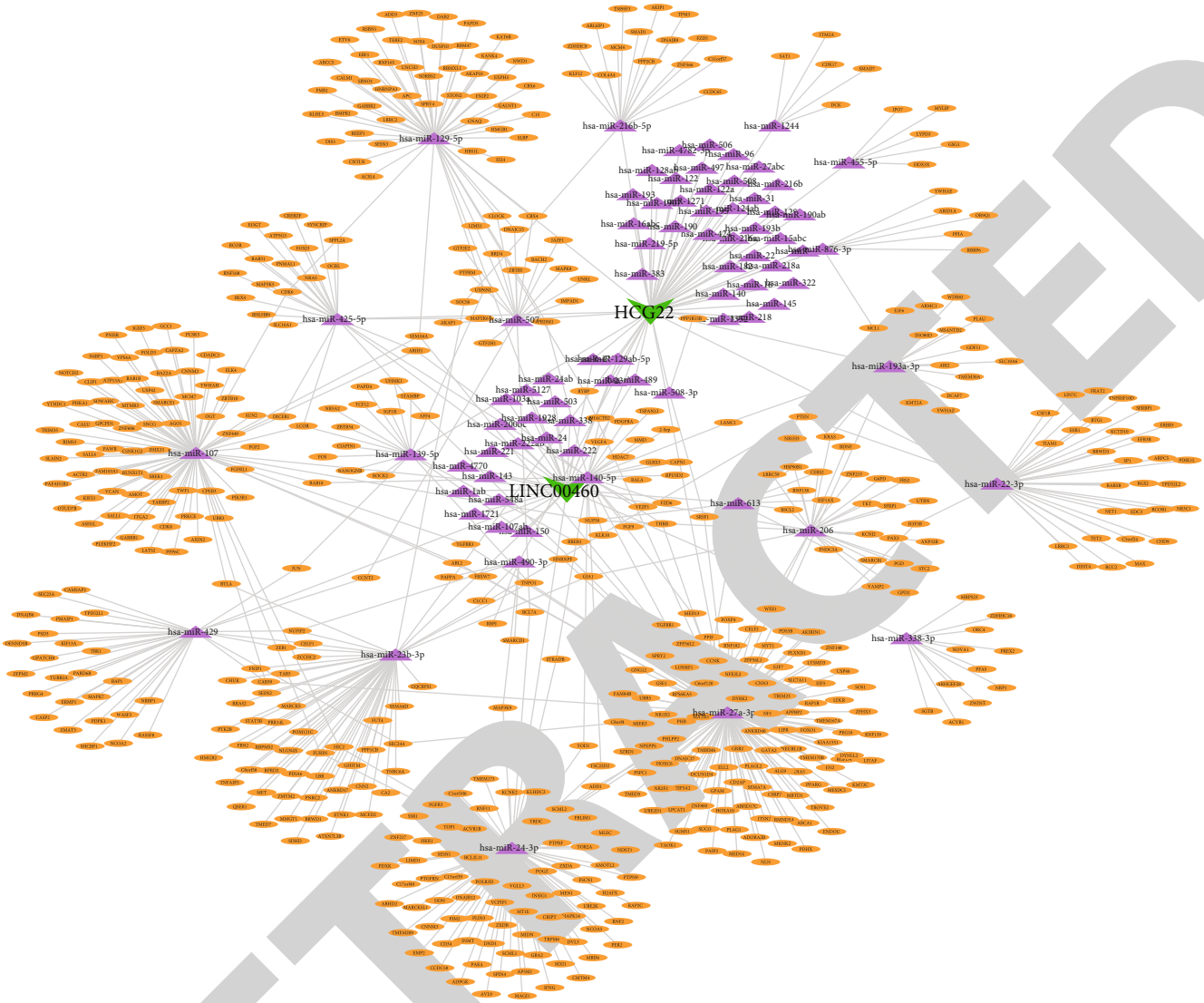

Figure 16: Construction of key lncRNA ceRNA network.

4. Discussion

OSCC is a malignant tumor with a high incidence and poor long-term outcome despite the increasing improvement of the combined (disciplinary) and sequential therapy for patients, hardly reaching the expected therapeutic goals [14]. However, early detection and radical treatment bring new ideas and methods to the treatment of tumor patients [15, 16]. In recent years, with the rise of gene expression profiling chips, strengthening the core method for analyzing the tumor gene structure of OSCC patients is essential for guiding clinical treatment [17]. Other scholars have found [18, 19] that the lncRNA-mediated complex network can regulate a large number of coding genes. At present, lncRNA and its target genes have become a hot topic in oncology research, and more and more studies have confirmed that differentially expressed lncRNA can be involved in the development and progression of OSCC [20]. In the present study, a total of 76 immune-related lncRNAs differed in tumor and paracarcinoma tissues, and Cancer Hallmark, Phenotype, and Subcellular Location analysis were completed. The results showed that lncRNA can participate in the invasion, metastasis, proliferation, and apoptosis process of tumor cells, which can provide new ideas and methods for the treatment of OSCC. In this study, we screened the differentially expressed genes of OSCC with the help of lncRNA expression profiling chip. The 15 lncRNAs with the highest importance mentioned above were selected, to draw the Kaplan-Meier curve, complete the survival curve analysis, and complete the analysis and collation of relevant data. The results showed that LINC00460, CASC9, and HCG22 were of statistical significance and could directly participate in and regulate the prognosis of OSCC patients. We completed GO and KEGG enrichment for the LINC00460, CASC9, and HCG22, further indicating that the screening results of this study were accurate and reliable.

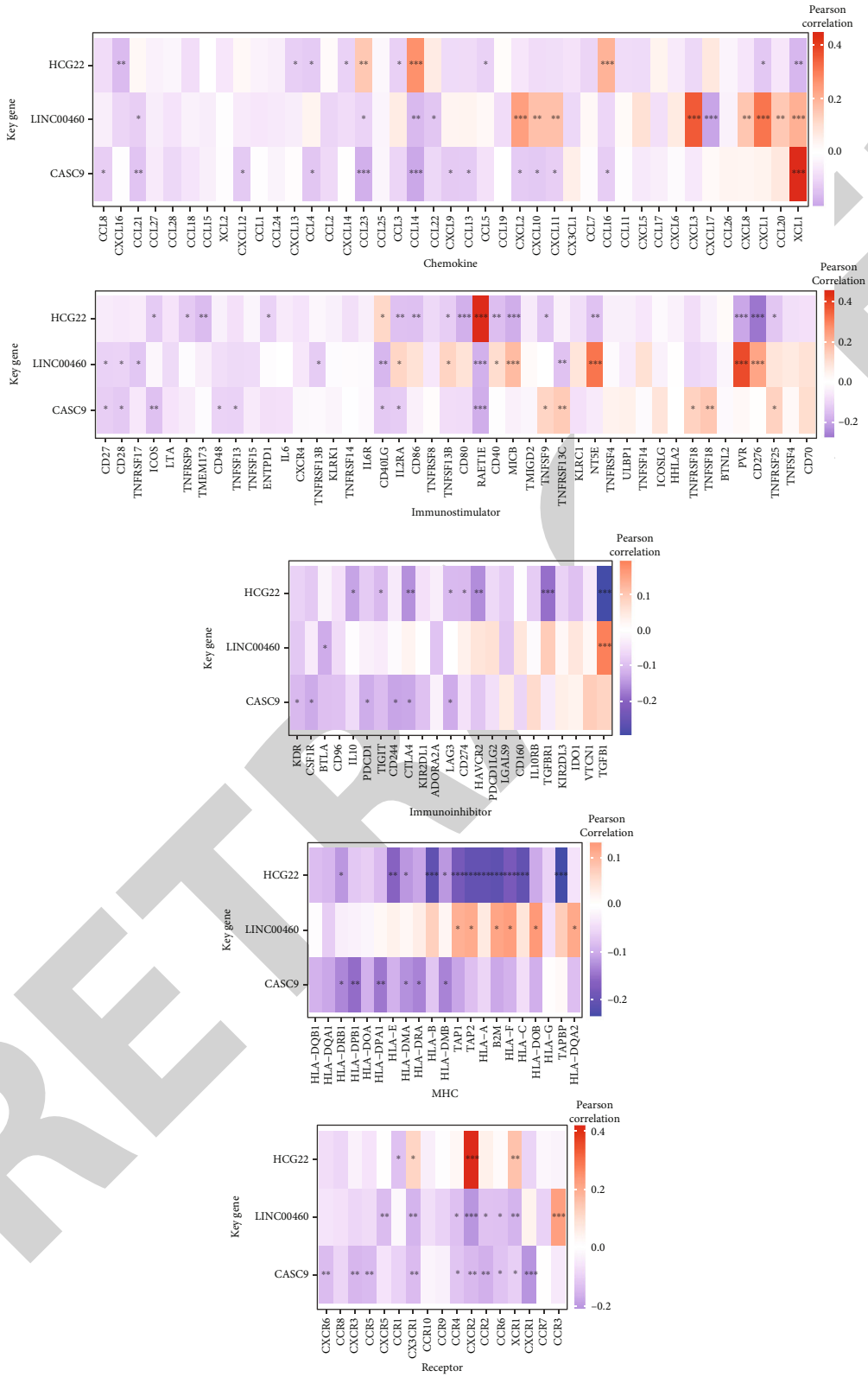

Figure 17: Relationship between differentially expressed lncRNA and immunoregulation-related genes.

Due to the complex transcription pattern of lncRNA and the ability of forming multiple secondary functional structures, it is difficult to predict its biological functions based on nucleotide sequences [21]. To address the existing drawbacks and shortcomings, we constructed a coexpression network of differentially expressed lncRNA and

mRNA, assigned the differential gene to the subnetwork related to phenotypic functions, and inferred the function of lncRNA involved in the formation of subnetworks, which contributed to the prediction of possible regulatory mechanisms and roles [22]. Based on the coexpression network, lncRNA LINC00460 and lncRNA HCG22 were found to have coexpression network node genes. Combined with the occurrence mechanism of OSCC, it can be inferred that key node genes of lncRNA LINC00460 and lncRNA HCG22 may directly participate in the occurrence and progression of OSCC. With uncontrollable invasiveness, OSCC is prone to cervical lymphatic metastasis which mostly moves along the cervical lymphatic chain, while the proportion of distant spread through blood is low. The lymphatic metastasis will reduce the quality of life of the patient. Therefore, an improved therapeutic schedule, particularly considering the possibility of cervical lymphatic metastasis and its treatment as well as the necessity of cervical lymph node dissection, is the key for treating OSCC [23]. The relationship between lncRNA LINC00460, lncRNA CASC9, lncRNA HCG22, and lymphatic metastasis of OSCC patients was investigated, and patient follow-up was completed. LINC00460 and CASC9 were positively correlated with M0. CASC9 was negatively correlated with M1, but LINC00460 was positively correlated with M1. HCG22 was positively correlated with Mast cells resting, but LINC00460 was negatively correlated with Mast cells resting. The abnormally expressed lncRNA could affect the sensitivity of cytarabine, docetaxel, and paclitaxel, and TMB was significantly different in both high- and low-expression groups of CASC9 and HCG22. In the present study, a strong correlation of LINC00460, CASC9, and HCG22 with immune-related genes can be observed in OSCC patients, which can provide new ideas and methods for the treatment of OSCC. Therefore, for patients with suspected OSCC, multiomics immune-related lncRNA analysis should be enhanced and lncRNA LINC00460, lncRNA CASC9, and lncRNA HCG22 determination should be completed, to provide new therapeutic targets for the treatment of OSCC.

In the present study, we screened and analyzed the differentially expressed and immune-related lncRNA in OSCC tissues by bioinformatics; analyzed the correlation between key lncRNAs and immunoregulation-related genes; performed LncSEA enrichment analysis, drug sensitivity analysis, immune cell infiltration, and GSEA enrichment analysis; explored the clinical prediction value of key lncRNAs and the specific signaling mechanisms; predicted the onset risk of OSCC; and performed the immune correlation analysis.

Data Availability

The datasets used and analyzed during the current study are all available from the corresponding author.

Conflicts of Interest

The authors declare that they have no conflicts of interest.

References

[1] H. Zeng, M. Luo, L. Chen, X. Ma, and X. Ma, "Machine learning analysis of DNA methylation in a hypoxia-immune model of oral squamous cell carcinoma," *International Immunopharmacology*, vol. 89, no. Part B, article 107098, 2020.

[2] H. Sung, J. Ferlay, R. L. Siegel et al., "Global cancer statistics 2020: GLOBOCAN estimates of incidence and mortality worldwide for 36 cancers in 185 countries," *CA: a Cancer Journal for Clinicians*, vol. 71, no. 3, pp. 209–249, 2021.

[3] L. Statello, C. J. Guo, L. L. Chen, and M. Huarte, "Gene regulation by long non-coding RNAs and its biological functions," *Nature Reviews Molecular Cell Biology*, vol. 22, no. 2, pp. 96–118, 2021.

[4] L. Ying, D. Su, Z. Chunliu et al., "Multiomics analysis reveals high-immune infiltration in tumor-adjacent lung tissues affects the prognosis of stage I NSCLC," *Journal of Clinical Oncology*, vol. 39, Supplement 15, pp. 8540–8540, 2021.

[5] M. Garofalo, G. Di Leva, G. Romano et al., "*miR-221 &222* regulate TRAIL resistance and enhance tumorigenicity through PTEN and TIMP3 downregulation," *Cancer Cell*, vol. 16, no. 6, pp. 498–509, 2009.

[6] Q. Duan, M. Xu, M. Wu, X. Zhang, M. Gan, and H. Jiang, "Long noncoding RNA UCA1 promotes cell growth, migration, and invasion by targeting miR-143-3p in oral squamous cell carcinoma," *Cancer Medicine*, vol. 9, no. 9, pp. 3115–3129, 2020.

[7] Y. Qu, Y. He, Y. Yang et al., "ALDH3A1 acts as a prognostic biomarker and inhibits the epithelial mesenchymal transition of oral squamous cell carcinoma through IL-6/STAT3 signaling pathway," *Journal of Cancer*, vol. 11, no. 9, pp. 2621–2631, 2020.

[8] A. P. Piantanida, L. E. Acosta, L. Brocardo, C. Capurro, C. A. Greer, and L. Rela, "Selective Cre-mediated gene deletion identifies connexin 43 as the main connexin channel supporting olfactory ensheathing cell networks," *Journal of Comparative Neurology*, vol. 527, no. 7, pp. 1278–1289, 2019.

[9] X. Wang, X. Chen, and H. Liu, "Expression and bioinformatics-based functional analysis of UAP1 in lung adenocarcinoma," *Cancer Management and Research*, vol. Volume 12, pp. 12111–12121, 2020.

[10] G. Z. Huang, Q. Q. Wu, Z. N. Zheng, T. R. Shao, and X. Z. Lv, "Identification of candidate biomarkers and analysis of prognostic values in oral squamous cell carcinoma," *Frontiers in Oncology*, vol. 9, p. 1054, 2019.

[11] H. T. Wu, W. T. Chen, W. J. Chen, C. L. Li, and J. Liu, "Bioinformatics analysis reveals that ANXA1 and SPINK5 are novel tumor suppressor genes in patients with oral squamous cell carcinoma," *Translational Cancer Research*, vol. 10, no. 4, pp. 1761–1772, 2021.

[12] Y. Liu, Z. Li, Y. Qi, X. Wen, and L. Zhang, "Metagenomic analysis reveals a changing microbiome associated with the depth of invasion of oral squamous cell carcinoma," *Frontiers in Microbiology*, vol. 13, article 795777, 2022.

[13] Y. Gong, H. T. Huang, Y. Liang, T. Trimarchi, I. Aifantis, and A. Tsirigos, "lncRNA-screen: an interactive platform for computationally screening long non-coding RNAs in large genomics datasets," *BMC Genomics*, vol. 18, no. 1, p. 434, 2017.

[14] S. B. Chinn and J. N. Myers, "Oral cavity carcinoma: current management, controversies, and future directions," *Journal of Clinical Oncology*, vol. 33, no. 29, pp. 3269–3276, 2015.

Hindawi
Disease Markers
Volume 2022, Article ID 5911408, 10 pages
https://doi.org/10.1155/2022/5911408

Review Article

Neutrophil to Lymphocyte Ratio and Platelet to Lymphocyte Ratio in Poststroke Depression: A Systematic Review and Meta-Analysis

Shirin Sarejloo,[1] Erfan Abadifard,[2] Zhian Jamal Othman,[3] Fatemeh Zafarani,[4] Monireh Khanzadeh,[4] Saeed Sadigh-Eteghad,[5] Fereshteh Farajdokht,[5] Asghar Mohammadpoorasl,[6] and Shokoufeh Khanzadeh[4]

[1]*Cardiovascular Research Center, Shiraz University of Medical Sciences, Shiraz, Iran*
[2]*Students' Scientific Research Center (SSRC), Tehran University of Medical Sciences, Tehran, Iran*
[3]*Department of Physical Education and Sport Sciences, Cihan University, Erbil, Iraq*
[4]*Student Research Committee, Tabriz University of Medical Sciences, Tabriz, Iran*
[5]*Neurosciences Research Center, Tabriz University of Medical Sciences, Tabriz, Iran*
[6]*Department of Statistics and Epidemiology, Faculty of Health, Tabriz University of Medical Sciences, Tabriz, Iran*

Correspondence should be addressed to Shokoufeh Khanzadeh; khshokufe7@gmail.com

Received 6 February 2022; Revised 24 March 2022; Accepted 14 July 2022; Published 8 August 2022

Academic Editor: Xianwei Zeng

Objectives. Evidence shows that stroke-induced inflammatory responses play an essential role in the development of poststroke depression (PSD). The goal of this systematic review and meta-analysis was to critically evaluate the literature regarding the use of the neutrophil to lymphocyte ratio (NLR) as a reliable means to detect early PSD development, to help clinicians institute early interventions and improve outcomes. *Methods*. Electronic databases, including Web of Science, PubMed, Google Scholar, and Scopus, were searched, and eight studies were included. We assessed the certainty of the associations with GRADE methods. *Results*. We found that patients with PSD had higher NLR than the stroke patients with no depression (SMD = 0.51; CI 95% = 0.29-0.73, $p < 0.001$). Also, we found a significantly higher PLR in the patients with PSD when compared to the stroke patients with no depression (SMD = 0.66; CI 95% = 0.19-1.13, $p < 0.001$). *Conclusion*. These findings indicated that NLR and PLR could be considered inexpensive biomarkers for the prediction of PSD.

1. Introduction

Poststroke depression (PSD) is the most common psychiatric sequela of stroke, affecting about one-third of stroke survivors during the first five years [1, 2]. The presence of depressive episode after stroke diagnosis by physical examination or neuroimaging is associated with a diagnosis of PSD [3]. PSD has been linked to a variety of adverse clinical outcomes, including extended hospital stays, serious functional disability, profound reductions in cognition and quality of life, and inadequate poststroke rehabilitation, and higher mortality [1, 2, 4–6], which all impose a heavy burden on caregivers, healthcare system, and society [7]. This emphasizes the need for early detection of PSD in stroke survivors and identifying people at risk of developing PSD [8].

The complexity of PSD pathophysiology and uncertainty about its predisposing risk factors and underlying biological mechanisms make its prevention, diagnosis, and treatment a complicated task. Thus, the discovery of specific biomarkers at the early stage of stroke is highly demanded because it may assist in predicting PSD [9] and unraveling the pathophysiological mechanisms of PSD, which could lead to the development of specialized targeted treatments [4, 10]. Emerging evidence shows that stroke, depression, and PSD are strongly associated with microglial and astrocyte

activation and high levels of proinflammatory cytokines [11]. However, this is critical to detect early as a lot of patients with stroke were previously healthy and nonsymptomatic.

The neutrophil to lymphocyte ratio (NLR) and platelet to lymphocyte ratio (PLR), derived from complete blood count (CBC) differential test, are promising noninvasive prognostic and diagnostic biomarkers in cardiovascular diseases [12–15], cancer [16–18], rheumatologic disease [19], and some neurologic diseases [20–27]. In addition, some previous studies reported significant association of NLR and PLR with PSD, but others did not find any relationship. Although the debate concerning the relationship between these hematological indices and PSD has raged unabated for over a decade, no systematic reviews or meta-analyses have been published. Hence, we performed a comprehensive review and meta-analysis to see if NLR and PLR are linked to PSD susceptibility in patients with stroke, to help clinicians institute early interventions and improve outcomes.

2. Methods

2.1. Search Strategy. In compliance with the Preferred Reporting Items for Systematic Review and Meta-Analyses (PRISMA) standards [28], we performed a systematic review and meta-analysis to collect all published papers (Figure 1). No registered review protocol exists.

Two reviewers, who were entirely blind to the author and journal details, separately conducted a systematic literature search in the online databases of PubMed, Web of Science, and Scopus, using the following key words: ((post-stroke depression) OR PSD OR (depression after stroke) OR (depression after cerebrovascular events)) AND ((neutrophil AND lymphocyte AND ratio) OR (neutrophil-to-lymphocyte) OR NLR). The most recent update to the search was on September 14, 2021. We did not limit our search to a specific language or year of release. To find possibly suitable studies, researchers combed through the reference lists of studies found. Additionally, the Prospero Register was combed for information on unpublished and continuing reviews. Because most of the recognized publications were conducted in China, we also conducted a rapid nonsystematic check through Google Scholar as a secondary resource in English and Chinese to uncover grey literature and more relevant studies.

2.2. Criteria for Inclusion and Exclusion. Prospective and retrospective cohort studies that evaluated the prognostic role of NLR and PLR in the development of PSD were included. The included articles were checked for adequate and informative data, including the number of subjects in both the PSD and non-PSD (NPSD) groups and mean and standard deviation (SD) of NLR and PLR in both groups. The studies that reported median and interquartile range (IQR) or/and range were also included, and statistical methods were used to estimate mean and SD.

Animal, cross-sectional, and case-control studies, letters to editors, case series, case reports, conference papers, studies with overlapping data, and duplicated studies were excluded.

2.3. Extraction of Data. Two authors independently investigated the titles/abstracts of the publications obtained. The full texts of relevant studies independently were checked for eligibility by the same two authors. A third independent author handled any disagreements between authors in both stages.

The following information was extracted: first author, year of publication, study location, study design, age (months), the duration of follow-up, depression scale type, type of stroke (ischemic or hemorrhagic), total sample size as well as number of PSD and NPSD cases, mean and SD of NLR and PLR levels, or any data for estimating the mean and SD (median and IQR or/and range).

2.4. Quality Assessment. Two authors independently assessed the quality of the included studies, using the Newcastle-Ottawa scale for cohort studies. The scale has three parts: selection (4 items), comparability (2 items), and outcome (3 items), with a cumulative score of 0 to 9. A leading expert finally settled any differences through arbitration. Studies with scores higher than 7 were considered high quality, those with scores between 5 and 7 were considered moderate quality, and those with scores lower than 7 were considered low quality.

2.5. Statistical Analysis. For the NLR and PLR levels, the standardized mean difference (SMD) was provided with a 95 percent confidence interval (CI). The methods introduced by Wan et al. were used to calculate the mean and SD from the median, sample size, range, or IQR [29].

The chi-squared (χ^2) test and the I^2 statistic were used to determine the degree of heterogeneity between study results. Significant heterogeneity of data was defined as $I^2 > 75\%$ and $p < 0.05$. In the case of significant heterogeneity, a random effects model was used for meta-analysis; otherwise, we utilized the fixed effects model. Subgroup analysis was performed in the analysis of differences in NLR levels between PSD and NPSD groups according to the duration of follow-up (acute/medium-term phase of stroke (≤1 month) vs. long-term phase (>1 month)), language (Chinese vs. English), and quality of studies (high quality (NOS score > 7) vs. moderate quality (NOS scores 5-7)). Egger's and Begg's tests and the Funnel plot were used to detect potential publication bias, and those with Egger's test $p < 0.05$ were considered significant publication bias. For statistical analysis, Stata 12.0 software (Stata Corporation, College Station, TX, USA) was used. Statistical significance was defined as a $p < 0.05$.

2.6. Certainty of Evidence. The certainty of evidence was determined using the GRADE (Grading of Recommendations Assessment, Development and Evaluation) approach by one author for the outcome investigated in meta-analysis (PSD). Finally, the assessments were confirmed by the senior author. According to GRADE, observational studies start at low certainty and may be upgraded for dose-response gradient or for large effect, if suspected biases work against the observed direction of effect, and may be

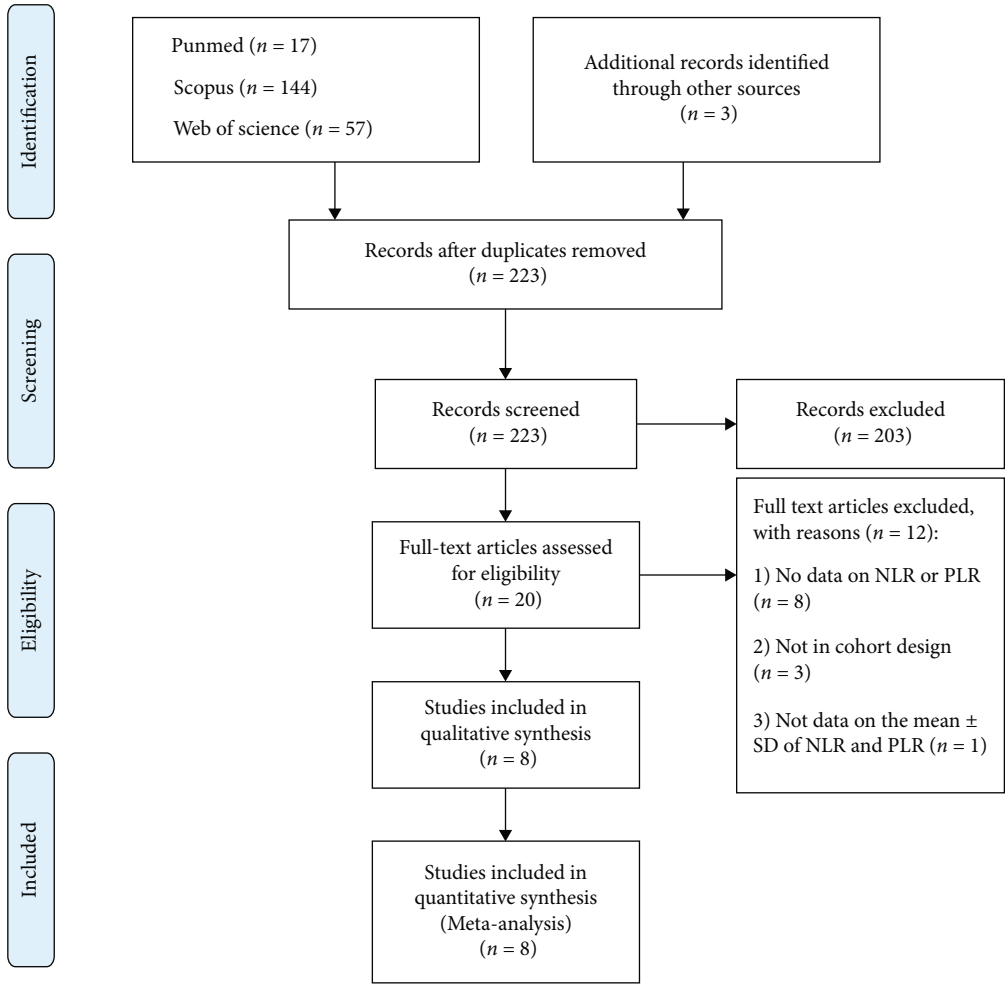

Figure 1: Flow chart of search and study selection.

downgraded for publication bias, imprecision, indirectness, inconsistency, and risk of bias.

3. Results

3.1. Literature Search and Selection. Figure 1 shows the process of identifying and selecting research articles in this systematic review. In addition to 218 studies found from the initial database search, three further studies were identified through reference lists of relevant articles. After removing duplicates, titles, and abstracts, the remaining studies were reviewed, and 20 studies were included for full-text review. Then, 12 studies were excluded (the reasons for exclusion are clarified in Figure 1), and finally, 8 studies were included in the meta-analysis.

3.2. Characteristics of the Included Studies. From studies that were included in this meta-analysis, seven studies were in English [20–26] and one in Chinese [27]. Overall, 2194 patients with stroke were enrolled in the selected studies, and 593 patients finally developed PSD. The general characteristics of the included studies are shown in Table 1. Also, the quality assessment of included studies was determined with the Newcastle-Ottawa scale (NOS) (Table 1). Overall, seven studies compared the NLR levels [20–23, 25–27], and three studies determined the PLR levels [20, 23, 24].

3.3. Difference in NLR Level in Patients with and without PSD. NLR levels in the PSD group were compared with those of the NPSD group in seven cohort studies [20–23, 25–27] with 1831 patients with stroke, of whom 516 were diagnosed with PSD at the end of the follow-up period. Compared with the NPSD group, NLR levels were significantly higher in the PSD group (SMD = 0.51; CI 95% = 0.29-0.73, $p < 0.001$). The included studies were statistically heterogeneous ($I^2 = 74.7\%$, $p = 0.001$); thus, the random effects model was used for the meta-analysis (Figure 2). However, the certainty of this summary estimate of effect was deemed to be very low using the GRADE approach (Table 2).

In the subgroup analysis according to the follow-up period, three studies assessed the PSD in the acute/medium-term phase of stroke (≤1 month) [21, 23, 26] including 883 patients with stroke of whom 252 developed PSD and four studies concerned the long-term phase and included 948 patients with stroke of whom 264 developed PSD [20, 22, 25, 27]. The NLR levels in patients of the

Table 1: Characteristics of studies included in the meta-analysis.

First author	Study year	Country	Age group (years)	Language	Stroke type	Follow-up period (month)	Depression assessment tool	Sample size		NLR		PLR		NOS score
								PSD	NPSD	PSD	NPSD	PSD	NPSD	
Chen et al.	2016	China	18-80	English	ND	1	HAMD	78	221	3.36 ± 1.13	2.56 ± 1.06	—	—	7
Stern et al.	2017	USA	≥18	English	ICH/ IVH	12	HDRS	13	76	6.25 ± 6.44	7.25 ± 5.49	—	—	7
Wang et al.	2017	China	18-80	English	ND	1	HAMD	45	107	2.11 ± 0.93	2.01 ± 0.83	—	—	8
Quiqian et al.	2019	China	ND	English	AIS	1	HAMD	77	286	—	—	131.83 ± 37.17	109.73 ± 30.62	8
Gong et al.	2020	China	≥18	English	ICH	3	HAMD	107	265	6.74 ± 4.24	3.95 ± 2.58	—	—	8
Hu et al.	2020	China	ND	English	AIS	6	HAMD	104	272	3.66 ± 1.61	2.97 ± 1.11	177.03 ± 91.43	115 ± 40.60	8
Xia et al.	2020	China	42-80	Chinese	AIS	3	HAMD	40	70	3.24 ± 1.38	2.38 ± 1.17	—	—	8
Hu et al.	2021	China	18-80	English	AIS	1	HAMD	129	303	2.65 ± 1.53	2.17 ± 0.92	125.01 ± 44.90	114.63 ± 37.19	6

PSD: poststroke depression; NPSD: nonpoststroke depression; NLR: neutrophil to lymphocyte ratio; PLR: platelet to lymphocyte ratio; ND: not declared; HAMD: Hamilton Depression Scale; HDRS: Hamilton Depression Rating Scale; HADS: the hospital anxiety and depression scale; AIS: acute ischemic stroke; ICH: hemorrhagic stroke; IVH: intraventricular hemorrhage; NOS: Newcastle-Ottawa scale.

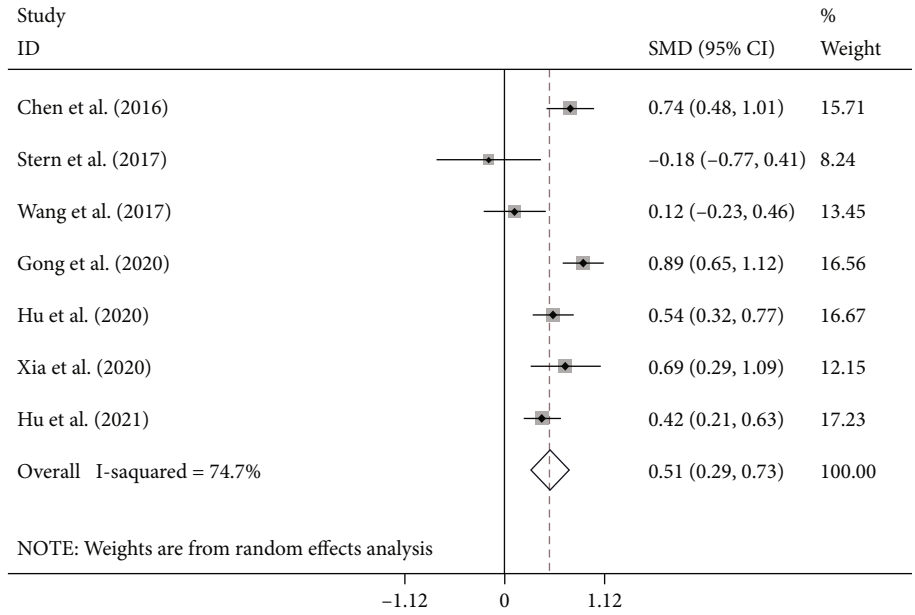

Figure 2: Meta-analysis of NLR levels in PSD and NPSD groups (fixed model).

PSD group were significantly more than those of the NPSD group in both the acute/medium-term and long-term phase (SMD = 0.44, CI 95% = 0.13-0.76, $p < 0.006$ and SMD = 0.56, CI 95% = 0.23-0.89, $p = 0.001$, respectively) (Figure 3).

In another subgroup analysis according to the quality of studies, there were four studies with high quality (NOS score > 7), including 1010 patients with stroke of whom 296 developed PSD, and three studies with moderate quality (NOS scores 5-7) included 821 patients with stroke of whom 220 developed PSD. There was no study with low quality. The NLR levels in patients of the PSD group were significantly more than those of the NPSD group in both study groups with high and moderate qualities (SMD = 0.51, CI 95% = 0.29-0.73, $p < 0.001$ and SMD = 0.41, CI 95% = 0.03-0.79, $p = 0.034$, respectively) (Figure 4).

In another subgroup analysis according to language, there were six studies written in English and one study in Chinese. The NLR levels in patients of the PSD group were significantly more than those of the NPSD group in studies written in either English or Chinese (SMD = 0.48, CI 95% = 0.24-0.73, $p < 0.001$ and SMD = 0.69, CI 95% = 0.29-1.09, $p = 0.001$, respectively) (Figure 5).

3.4. Differences in PLR Level in Patients with and without PSD. PLR levels in the PSD group were compared with those of the NPSD group in three cohort studies [20, 23, 24] with 1117 patients with stroke, of which 310 patients were diagnosed with PSD. Compared with the NPSD group, the PSD groups had higher NLR levels (SMD = 0.66, CI 95% = 0.19-1.13, $p < 0.001$). The included studies were statistically heterogeneous ($I^2 = 91.8\%$, $p < 0.001$). Thus, the random effects model was used for the meta-analysis (Figure 6). However, the certainty of this summary estimate of effect was deemed to be very low using the GRADE approach (Table 2). Because of limited studies on PLR, we could not perform any subgroup analysis in this context.

3.5. Publication Bias and Small Study Effect. Funnel plot and Egger's test were performed to test publication bias. As shown in Figure 7, the results of studies on the prognostic role of neither NLR nor PLR indicated publication bias (Egger's test $p = 0.06$ and 0.37 and Begg's test $p = 0.08$ and 0.54, respectively).

4. Discussion

To the best of our knowledge, this is the first time that the prognostic role of NLR and PLR in PSD has been reviewed systematically. Searching main electronic databases for relevant articles, we identified nine studies meeting our inclusion criteria and found two main findings.

We observed that the PSD group had higher NLR levels than the NPSD group (SMD = 0.51; CI 95% = 0.29-0.73, $p < 0.001$). In addition, the PSD group's NLR levels were significantly elevated compared to those of the NPSD group (SMD = 0.66; CI 95% = 0.19-1.13, $p < 0.001$).

Over the past decade, most research in stroke has emphasized the relationship between stroke and inflammation. Stroke, either hemorrhagic or ischemic, leads to a lack of glucose and oxygen, ATP depletion, neuronal death, and inflammation in the nervous system [4].

However, the knowledge about the link between PSD and stroke-induced inflammation is limited [4, 21]. Some researchers suggest that inflammatory mediators change the structure and function of hypothalamic orexin-releasing neurons and decrease the activity and production of monoamine neurotransmitters, such as serotonin, dopamine, and norepinephrine, which may contribute to symptoms of PSD [4, 30, 31]. NLR and PLR as novel inflammatory biomarkers are reported in a variety of neurological disorders. In this study, we found that patients with stroke who developed PSD had considerably higher levels of NLR and PLR than those who did not develop PSD.

Table 2: GRADE[1] evidence profile for cohort studies on the role of NLR and PLR in poststroke depression.

No. of studies	Study design	Certainty assessment					No. of patients		Certainty[7]	Importance
		Risk of bias[2]	Inconsistency[3]	Indirectness[4]	Imprecision[5]	Publication bias[6]	Participants, *n*	Cases, *n*		
NLR										
7	Observational studies	Not serious	Serious	Not serious	Not serious	None	1831	516	⨁◯◯◯ very low	Critical
PLR										
3	Observational studies	Not serious	Very serious	Not serious	Not serious	None	1117	310	⨁◯◯◯ very low	Critical

[1]Grading of Recommendations Assessment, Development and Evaluation. [2]Risk of bias based on the Newcastle-Ottawa scale. [3]When I^2 was <30%, inconsistency was considered not serious limitation; when $I^2 > 50$, it was considered serious limitation; and when I^2 was more than 75%, it was considered very serious limitation. [5]Serious limitations were considered when there were fewer than 400 participants for each outcome, and very serious limitations were considered when there were fewer than 300 participants for each outcome. [6]Funnel plot revealed no asymmetry; neither test of publication bias approached $p < 0.10$. [7]Data from cohort studies begin with a grade of "low." Downgraded for very serious inconsistency. [8]Data from cohort studies begin with a grade of "low." Downgraded for serious inconsistency.

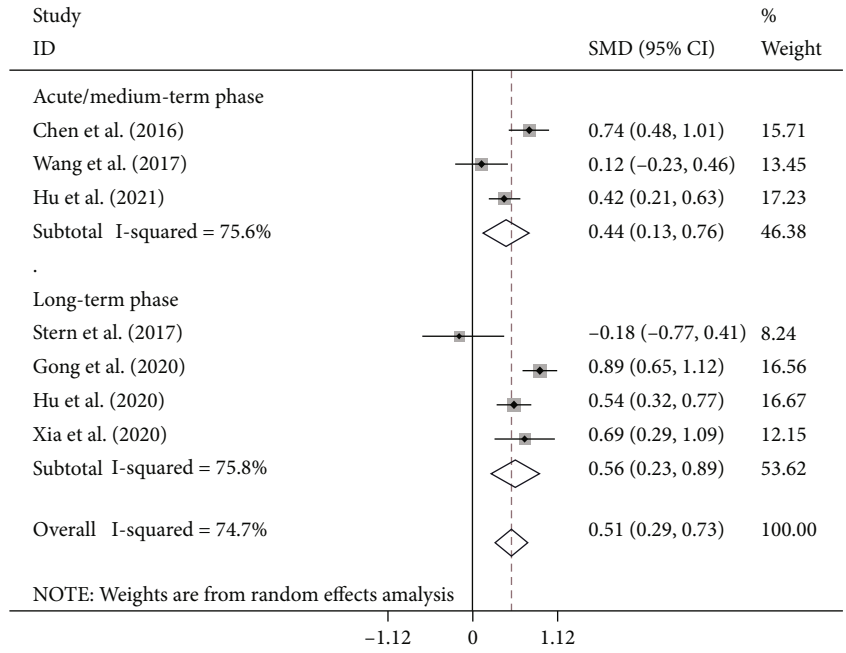

Figure 3: Subgroup meta-analysis of NLR levels in PSD and NPSD groups (random effects model) according to the follow-up period.

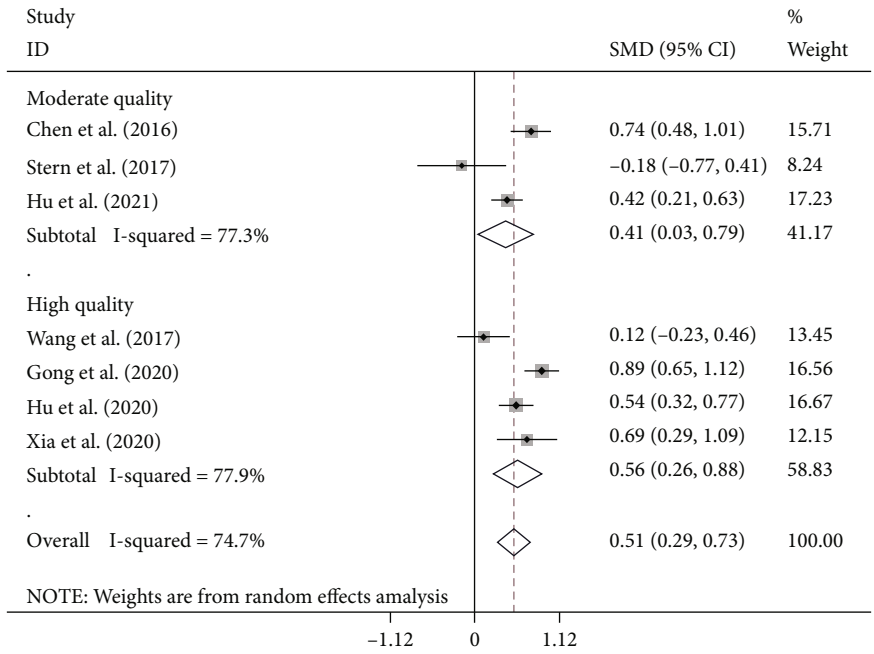

Figure 4: Subgroup meta-analysis of NLR levels in PSD and NPSD groups (random effects model) according to the quality of studies based on the NOS scoring system.

The NLR is a practical, low-cost, and easily accessible new inflammatory index [21]. Neutrophils are the earliest part of the immune system to enter the CNS after a stroke [21, 32]. Their activation and recruitment at the site of infarction always coincide with the maximum synthesis of proinflammatory mediators (such as TNF-α and IL-6) and associated biomarkers (such as CRP), which result in neuronal damage after stroke [20, 21].

Also, lymphocytes are a type of inflammatory cells with protective and regulatory roles. CD^{4+} T lymphocytes play a key role in preventing poststroke cell injury [21, 23, 32]. Their anti-inflammatory function is linked to the release of anti-inflammatory chemicals (such as TGF-β and IL-10). Therefore, high NLR shows high neutrophil and low lymphocyte counts and indicates a high level of systemic inflammation [20, 21, 32]. Since NLR is less likely to be influenced

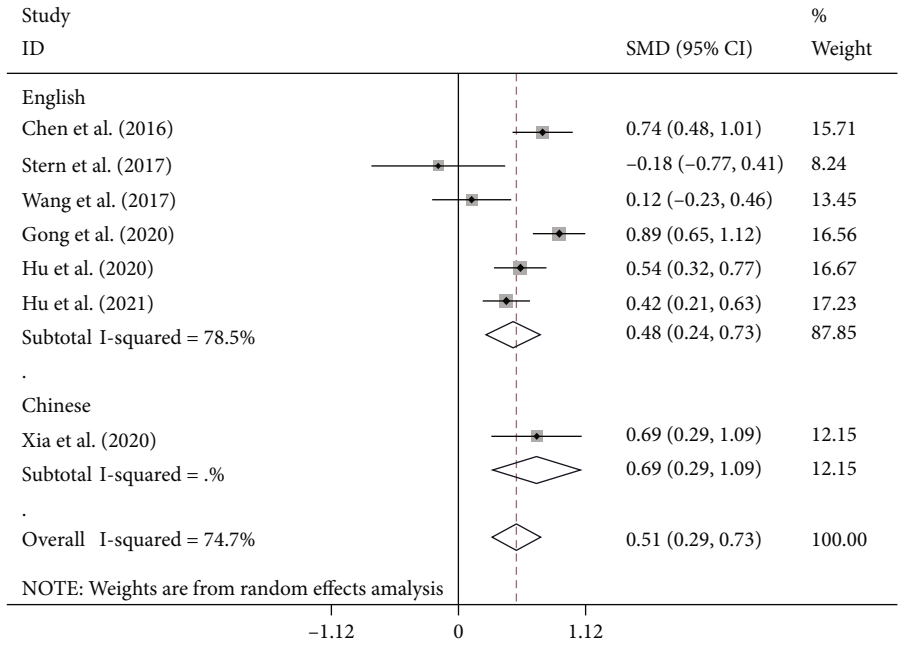

Figure 5: Subgroup meta-analysis of NLR levels in PSD and NPSD groups (random effects model) according to language.

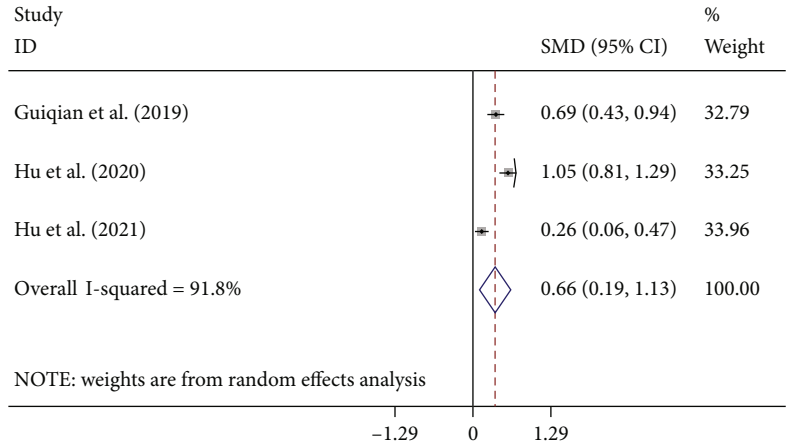

Figure 6: Meta-analysis of PLR levels in PSD and NPSD groups (random effects model).

by confounding factors, it may have more predictive value than each parameter on its own [30].

Another low-cost, repeatable, and easily measured index is the PLR. Platelets clump together at the site of injury during a stroke [20, 23, 24]. They are the first-line proinflammatory cells that control parameters like macrophage and neutrophil's recruitment and endothelial permeability [4, 30]. Platelets' dense granules also contain a lot of serotonin and glutamate, which is released as a part of the inflammatory process and could participate in the pathophysiology of PSD [4, 20, 23, 24, 30].

Because the elevated level of NLR and PLR in PSD patients compared to NPSD is solid evidence for the role of inflammation in PSD, anti-inflammatory drugs may be considered potential therapies for PSD [4]. A systematic review published recently found that anti-inflammatory medication, particularly celecoxib, can reduce depression symptoms [33]. In another recent study, a total of 161 individuals with acute ischemic stroke (AIS) were administered with natalizumab, an immunoglobulin against the leukocyte adhesion molecule 4 integrin. The results demonstrated that administration of natalizumab up to 9 h after a stroke contributes to functional and cognitive recovery [34].

4.1. Limitations. The findings of this report are subject to some limitations. First, the data extracted from the relevant articles did not permit assessing the relationship between ratios and symptom severity. Second, heterogeneity in studies was greater than expected due to various treatment regimens, duration of recorded stays, center protocols, different study populations, different times of blood tests from which NLR was calculated, and different study designs. Therefore,

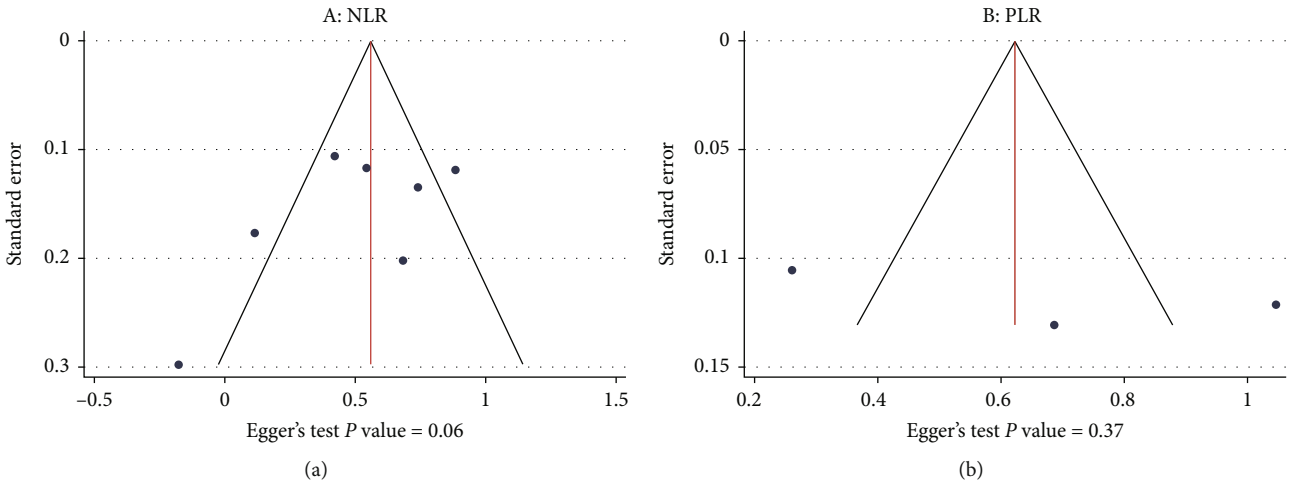

Figure 7: Egger's test and Funnel plot showing publication bias: (a) studies on NLR levels in the PSD and NPSD groups; (b) studies on PLR levels in the PSD and NPSD groups.

widespread validity is a concern, and future larger prospective studies are needed. Third, several of the studies are limited by bias whether selection or publication, which should be considered. Fourth, effect size for several of the tests was limited to a few studies. Thereby, widespread adoption and applicability are again a concern warranting further studies. In addition, the study protocol was not prospectively registered. Finally, other biomarker of immune function such as C-reactive protein and cytokines were not assessed; hence, it is impossible to say if elevated NLR and PLR represent an independent marker of immune system abnormalities in PSD patients. Finally, all of the included studies had relatively small sample sizes.

5. Conclusion

In conclusion, our meta-analysis provided additional evidence for the role of stroke-induced inflammation in PSD and concluded that NLR and PLR might be used as low-cost predictive biomarkers for PSD. These indicators can b5e extensively employed in the clinic. However, further large-scale and high-quality studies are needed to better understand the link between inflammation and PSD.

Data Availability

All data generated or analyzed during this study are included in this published article.

Conflicts of Interest

The authors declare that there is no conflict of interest regarding the publication of this article.

References

[1] F. Bartoli, C. di Brita, C. Crocamo, M. Clerici, and G. Carrà, "Early post-stroke depression and mortality: meta-analysis and meta-regression," *Frontiers in Psychiatry*, vol. 9, p. 530, 2018.

[2] W. Cai, C. Mueller, Y. J. Li, W. D. Shen, and R. Stewart, "Post stroke depression and risk of stroke recurrence and mortality: a systematic review and meta-analysis," *Ageing Research Reviews*, vol. 50, pp. 102–109, 2019.

[3] R. G. Robinson and R. E. Jorge, "Post-stroke depression: a review," *The American Journal of Psychiatry*, vol. 173, no. 3, pp. 221–231, 2016.

[4] H. Wen, K. B. Weymann, L. Wood, and Q. M. Wang, "Inflammatory signaling in post-stroke fatigue and depression," *European Neurology*, vol. 80, no. 3-4, pp. 138–148, 2019.

[5] C.-Y. Kwon, B. Lee, S. Y. Chung et al., "Efficacy and safety of Sihogayonggolmoryeo-tang (Saikokaryukotsuboreito, Chai-Hu-Jia-Long-Gu-Mu-Li-Tang) for post-stroke depression: a systematic review and meta-analysis," *Scientific Reports*, vol. 9, no. 1, pp. 1–20, 2019.

[6] C. I. Ezema, P. C. Akusoba, M. C. Nweke, C. U. Uchewoke, J. Agono, and G. Usoro, "Influence of post-stroke depression on functional independence in activities of daily living," *Ethiopian journal of health sciences*, vol. 29, no. 1, pp. 841–846, 2019.

[7] J.-W. Hung, Y. C. Huang, J. H. Chen et al., "Factors associated with strain in informal caregivers of stroke patients," *Chang Gung Medical Journal*, vol. 35, no. 5, pp. 392–401, 2012.

[8] K. Kowalska, P. Pasinska, E. Klimiec-Moskal et al., "C-reactive protein and post-stroke depressive symptoms," *Scientific Reports*, vol. 10, no. 1, pp. 1–7, 2020.

[9] H.-b. Liang, J.-r. He, X.-q. Tu et al., "MicroRNA-140-5p: a novel circulating biomarker for early warning of late-onset post-stroke depression," *Journal of Psychiatric Research*, vol. 115, pp. 129–141, 2019.

[10] H. Zhao, M. Mo, C. Miao et al., "Association of serum biomarker neurofilament light concentration with post-stroke depression: a preliminary study," *General Hospital Psychiatry*, vol. 64, pp. 17–25, 2020.

[11] R. F. Villa, F. Ferrari, and A. Moretti, "Post-stroke depression: mechanisms and pharmacological treatment," *Pharmacology & Therapeutics*, vol. 184, pp. 131–144, 2018.

[12] G. Lin, C. Dai, K. Xu, and M. Wu, "Predictive value of neutrophil to lymphocyte ratio and red cell distribution width on death for ST segment elevation myocardial infarction," *Scientific Reports*, vol. 11, no. 1, pp. 1–7, 2021.

[13] S. Li, J. Yang, J. Dong et al., "Neutrophil to lymphocyte ratio and fibrinogen values in predicting patients with type B aortic dissection," *Scientific Reports*, vol. 11, no. 1, pp. 1–7, 2021.

[14] W. Li, Q. Liu, and Y. Tang, "Platelet to lymphocyte ratio in the prediction of adverse outcomes after acute coronary syndrome: a meta-analysis," *Scientific Reports*, vol. 7, no. 1, pp. 1–9, 2017.

[15] M. A. Nematollahi, A. Askarinejad, A. Asadollahi et al., "Association and predictive capability of body composition and diabetes mellitus using artificial intelligence: a cohort study," 2022.

[16] A. Lauko, B. Thapa, M. Sharma et al., "Neutrophil to lymphocyte ratio influences impact of steroids on efficacy of immune checkpoint inhibitors in lung cancer brain metastases," *Scientific Reports*, vol. 11, no. 1, pp. 1–9, 2021.

[17] J. Zhu, D. Jiao, Y. Zhao et al., "Development of a predictive model utilizing the neutrophil to lymphocyte ratio to predict neoadjuvant chemotherapy efficacy in early breast cancer patients," *Scientific Reports*, vol. 11, no. 1, pp. 1–10, 2021.

[18] D.-Y. Li, X. Y. Hao, T. M. Ma, H. X. Dai, and Y. S. Song, "The prognostic value of platelet-to-lymphocyte ratio in urological cancers: a meta-analysis," *Scientific Reports*, vol. 7, no. 1, pp. 1–9, 2017.

[19] N. Moghimi, A. Faridfar, H. Jelodari Mamaghani et al., "Evaluation of the relationship between vitamin D levels and related serum markers as well as disease activity in patients with rheumatoid arthritis: a cross-sectional study," *Journal of Bioengineering Research*, vol. 3, no. 4, pp. 1–9, 2021.

[20] J. Hu, W. Zhou, Z. Zhou, J. Han, and W. Dong, "Elevated neutrophil-to-lymphocyte and platelet-to-lymphocyte ratios predict post-stroke depression with acute ischemic stroke," *Experimental and Therapeutic Medicine*, vol. 19, no. 4, pp. 2497–2504, 2020.

[21] H. Chen, X. Luan, K. Zhao et al., "The association between neutrophil-to-lymphocyte ratio and post-stroke depression," *Clinica Chimica Acta*, vol. 486, pp. 298–302, 2018.

[22] X. Gong, Z. Lu, X. Feng et al., "Elevated neutrophil-to-lymphocyte ratio predicts depression after intracerebral hemorrhage," *Neuropsychiatric Disease and Treatment*, vol. 16, pp. 2153–2159, 2020.

[23] J. Hu, L. Wang, K. Fan et al., "The association between systemic inflammatory markers and post-stroke depression: a prospective stroke cohort," *Clinical Interventions in Aging*, vol. 16, pp. 1231–1239, 2021.

[24] G. Huang, H. Chen, Q. Wang et al., "High platelet-to-lymphocyte ratio are associated with post-stroke depression," *Journal of Affective Disorders*, vol. 246, pp. 105–111, 2019.

[25] S. Stern-Nezer, I. Eyngorn, M. Mlynash et al., "Depression one year after hemorrhagic stroke is associated with late worsening of outcomes," *NeuroRehabilitation*, vol. 41, no. 1, pp. 179–187, 2017.

[26] Q. Wang, Z. Zhu, Y. Liu, X. Tu, and J. He, "Relationship between serum vitamin D levels and inflammatory markers in acute stroke patients," *Brain and Behavior: A Cognitive Neuroscience Perspective*, vol. 8, no. 2, article e00885, 2018.

[27] L. Xia, W. Houqing, X. Tie, W. Mengdi, and L. Xun, "The value of homocysteine combined with high-sensitivity C-reactive protein in predicting post-stroke depression," *Translational Medicine*, vol. 9, no. 5, pp. 280–283, 2020.

[28] K. Knobloch, U. Yoon, and P. M. Vogt, "Preferred reporting items for systematic reviews and meta-analyses (PRISMA) statement and publication bias," *Journal of Cranio-Maxillofacial Surgery*, vol. 39, no. 2, pp. 91-92, 2011.

[29] X. Wan, W. Wang, J. Liu, and T. Tong, "Estimating the sample mean and standard deviation from the sample size, median, range and/or interquartile range," *BMC Medical Research Methodology*, vol. 14, no. 1, pp. 1–13, 2014.

[30] M. G. Mazza, S. Lucchi, A. G. M. Tringali, A. Rossetti, E. R. Botti, and M. Clerici, "Neutrophil/lymphocyte ratio and platelet/lymphocyte ratio in mood disorders: a meta-analysis," *Progress in Neuro-Psychopharmacology & Biological Psychiatry*, vol. 84, pp. 229–236, 2018.

[31] Z. Wang, Y. Shi, F. Liu et al., "Diversiform etiologies for post-stroke depression," *Frontiers in Psychiatry*, vol. 9, p. 761, 2019.

[32] F. Zhang, Y. Ren, W. Fu et al., "Association between neutrophil to lymphocyte ratio and blood glucose level at admission in patients with spontaneous intracerebral hemorrhage," *Scientific Reports*, vol. 9, no. 1, pp. 1–9, 2019.

[33] O. Köhler, M. E. Benros, M. Nordentoft et al., "Effect of anti-inflammatory treatment on depression, depressive symptoms, and adverse effects," *JAMA psychiatry*, vol. 71, no. 12, pp. 1381–1391, 2014.

[34] J. Elkins, R. Veltkamp, J. Montaner et al., "Safety and efficacy of natalizumab in patients with acute ischaemic stroke (ACTION): a randomised, placebo-controlled, double-blind phase 2 trial," *Lancet Neurology*, vol. 16, no. 3, pp. 217–226, 2017.

Hindawi
Disease Markers
Volume 2022, Article ID 3380048, 6 pages
https://doi.org/10.1155/2022/3380048

Research Article

Effects of High-Frequency Chest Wall Oscillation Expectoration System on Pulmonary Rehabilitation and Cortisol Function in Patients with Severe AECOPD

Guohua Cheng, Jialing Wu, Zizi Hu, Yumie Xiao, Biyuan Zeng, and Yuqiong Zhou

Rehabilitation Department, Fourth Hospital of Changsha, Changsha 410005, China

Correspondence should be addressed to Guohua Cheng; shamocgh@126.com

Received 29 April 2022; Revised 18 June 2022; Accepted 8 July 2022; Published 22 July 2022

Academic Editor: Xianwei Zeng

Objective. To investigate the effect of high-frequency chest wall oscillatory expectoration system (HFCWO) on pulmonary rehabilitation and cortisol function in patients with severe acute exacerbation of chronic obstructive pulmonary disease (AECOPD). *Methods*. The 65 severe AECOPD patients admitted to our hospital from January 2019 to May 2020 were divided into group A with 33 cases and group B with 32 cases by random number table method. After 14 days of intervention, the improvement time of clinical symptoms in the two groups was recorded, and blood gas, lung function, inflammatory, and cortisol function-related indicators were evaluated before and after treatment. *Results*. The remission time of expectoration, pulmonary signs, and hospital stay in group A were significantly shorter than those in group B ($P < 0.05$). Compared with before treatment, blood oxygen partial pressure (PaO_2), forced vital capacity (FVC), forced expiratory volume at 1 s (EFV1), and EFV1/FVC increased significantly; blood carbon dioxide partial pressure ($PaCO_2$), C-reactive protein (CRP), interleukin-6 (IL-6), white blood cell count (WBC), plasma cortisol (COR), and adrenocorticotropic hormone (ACTH) levels were significantly decreased, and the above indicators in group A increased or decreased more significantly than those in group B ($P < 0.05$); there was no significant difference in tolerance and adverse reactions between the two groups ($P > 0.05$). *Conclusion*. HFCWO has good pulmonary rehabilitation effect in the treatment of severe AECOPD and can significantly improve the blood gas indexes, inflammation, and cortisol function of patients, which is safe and feasible.

1. Introduction

The chronic obstructive pulmonary disease (COPD) is manifested as symptoms of cough and asthma, etc., mainly due to airflow obstruction, and manifested as markedly abnormal lung function during acute exacerbations, which can be life-threatening in severe cases [1]. According to relevant reports, the mortality of the acute exacerbation of chronic obstructive pulmonary disease (AECOPD) is predicted to be among the top five worldwide, and the cause of death is associated with excessive phlegm and ineffective drainage [2, 3]. Therefore, pulmonary rehabilitation is crucial for patients with AECOPD, and physical therapies are the most widely used to improve respiratory symptoms and lung volumes and to shorten recovery time [4, 5]. As two commonly used pulmonary physiotherapies, both high-frequency chest wall oscillation (HFCWO) and expiration with the glottis open in the lateral posture (ELTGOL) can effectively improve the lung function and blood gas indicators of patients with AECOPD, and HFCWO is better as shown by some studies [6], but there are relatively few relevant reports in China. In addition, it was found that the abnormally increased plasma cortisol (COR) in patients with AECOPD is likely to cause adrenocortical dysfunction or aggravate the disease [7]; and adrenocortical function may be related to many factors such as inflammation and low oxygen [8]. In this regard, this study not only analyzed the effect of HFCWO on the pulmonary rehabilitation of patients with severe AECOPD from clinical symptoms, pulmonary function, and blood gas indicators but also explored

its feasibility from COR and inflammatory indicators, to provide a reference for the further application of HFCWO in clinical practice. The report is as follows.

2. Materials and Methods

2.1. Patient Information. Sixty-five patients with severe AECOPD, who were admitted to our hospital from January 2019 to May 2020, were used as subjects and divided into group A (33 cases) and group B (32 cases) using the table of random numbers. Group A consisted of 23 males and 10 females, with an age of 60-85 years, averaged at 67.36 ± 5.95, with COPD duration of 5-40 years, averaged at 11.67 ± 4.52 years, including 12 cases complicated with diabetes mellitus and 15 cases complicated with hypertension. Group B consisted of 21 males and 11 females, with an age of 63-89 years, averaged at 68.03 ± 4.76, with COPD duration of 7-35 years, averaged at 12.34 ± 3.06 years, including 13 cases complicated with diabetes mellitus and 13 cases complicated with hypertension. The baseline data of the two groups were matched ($P > 0.05$) and comparable. The study was approved by the ethics committee of the hospital.

2.2. Inclusion and Exclusion Criteria. Inclusion criteria were as follows: (1) consistent with AECOPD-related criteria [9], confirmed by clinical and imaging diagnosis; (2) age > 18 years; (3) clear consciousness and normal reading and writing; (4) able to cooperate with the treatment and examination of this study; (5) no more than 10 d of acute exacerbation; and (6) informed and signed the consent form.

Exclusion criteria were as follows: (1) organic lesions; (2) fractures; (3) large amounts of pus visible in the chest; (4) presence of primary suprarenal lesions or other endocrine symptoms; (5) confusing symptoms such as pulmonary embolism and bronchiectasis; and (6) malignancy, blood coagulation disorders, and dysimmunity.

2.3. Methods. Patients in the 2 groups received routine comprehensive treatment according to the *Chinese Expert Consensus on the Diagnosis and Treatment of AECOPD* (updated version in 2017) [9], such as oxygen therapy, respiratory support, relieving cough and asthma, anti-infection, or nutritional support. In addition, HFCWO intervention was given to group A: select the supine position or lateral position as the case may be, clear the airway, put the towel on the back and the forebreast, set the frequency to 10-12 Hz, pressure to about 5 kPa, and time to 15-20 min, and press the start button to start vibration after the above preparation is completed. The secretions during treatment, if any, were promptly aspirated and removed. After the treatment, secondary cleaning was performed to the patient's respiratory tract. ELTGOL was performed to patients in group B: select the lateral position, let the patient breathe normally, open the glottis through the throat and tongue when the residual volume is reached slowly to ease the airway compression, and press the abdomen when the patient slowly exhales, which is similar to the left chest wall compression in principle and was aimed at promoting air escape. The procedure was about 5 min a time, repeated once every 2 min, and repeated 3 times. The patient maintained the right lateral posture during rest. The 14 d intervention was performed for both groups. The therapeutic schedule was timely adjusted in case that the patient's condition worsened or the effects were not obvious.

2.4. Observational Indicators

2.4.1. Improvement of Symptoms. The remission time of expectoration and pulmonary signs and the length of stay (LOS) were recorded for patients in the 2 groups.

2.4.2. Blood Gas Indicators. The partial pressure of oxygen (PaO_2) and the partial pressure of carbon dioxide ($PaCO_2$) of the 2 groups were determined by the automatic blood gas analyzer.

2.4.3. Pulmonary Function. The forced vital capacity (FVC) and the forced expiratory volume in the first second (FEV1) of the 2 groups were measured by the pulmonary function tester, and FEV1/FVC was calculated.

2.4.4. Inflammatory Indicators. Fasting blood was collected in the morning. C-reactive protein (CRP) and interleukin-6 (IL-6) of the 2 groups were determined by the enzyme-linked immunosorbent assay (ELISA), and blood routine examination was performed to obtain the white blood cell count (WBC).

2.4.5. Cortisol Function. Fasting blood was collected in the morning. The plasma COR and adrenocorticotrophic hormone (ACTH) of the 2 groups were measured by chemiluminescence.

The above indicators were measured before treatment and after 14 d of treatment. In addition, the tolerance and adverse reactions during treatment were observed for the 2 groups.

2.5. Statistical Processing. SPSS 20.0 statistical software was used to process the data. Enumeration data were expressed as cases (%). Measurement data following the normal distribution were expressed as $\bar{x} \pm s$. The t test, with the size of test $\alpha = 0.05$, was adopted.

3. Results

3.1. Improvement of Symptoms. The remission time of expectoration and pulmonary signs and the length of stay (LOS) of patients in group A were significantly shorter than those of group B ($P < 0.05$). See Table 1.

3.2. Blood Gas Indicators. After treatment, significantly increased PaO_2 and significantly decreased $PaCO_2$ were observed for both groups. Moreover, after treatment, group A had significantly higher PaO_2 and lower $PaCO_2$ than group B. The differences were statistically significant ($P < 0.05$). See Table 2.

3.3. Pulmonary Function. After treatment, FVC, FEV1, and FEV1/FVC obviously increased in both groups and were

Table 1: Comparison of symptom improvement between the two groups ($\bar{x} \pm s$, d).

Group	Sputum relief time	Remission time of lung signs	The length of time
Group A ($n = 33$)	3.45 ± 1.20	4.42 ± 1.00	10.61 ± 2.50
Group B ($n = 32$)	4.34 ± 0.97	5.94 ± 1.61	15.56 ± 3.26
t	-3.276	-4.576	-6.889
P	0.002	<0.001	<0.001

significantly higher in group A than in group B ($P < 0.05$). See Table 3.

3.4. Inflammatory Indicators. WBC, CRP, and IL-6 decreased significantly in both groups after treatment compared with those before treatment and were significantly lower in group A than in group B after treatment ($P < 0.05$). See Table 4.

3.5. Cortisol Function. COR and ACTH decreased significantly in both groups after treatment compared with those before treatment and were significantly lower in group A than in group B after treatment ($P < 0.05$). See Table 5.

3.6. Safety Evaluation. In group A, 31 cases (93.94%) did not have any discomfort, and 2 cases (6.06%) experienced mild accelerated heart rhythm during treatment. In group B, 28 cases (87.50%) tolerated the treatment without any discomfort, and 4 cases received intermittent treatment due to unskillfulness but did not have any adverse reactions. There was no significant difference in tolerance and adverse reactions between the 2 groups ($P > 0.05$).

4. Discussion

It is reported that AECOPD is an important factor leading to reduced lung function and death of patients [10]. Most patients with AECOPD receive comprehensive treatment of oxygen inhalation, eliminating phlegm and anti-inflammation, which can effectively improve symptoms including cough and restore the patient's breathing. However, conventional interventions generally have long cycles and poor clinical outcomes [11–13].

In recent years, physical therapy, such as common means of HFCWO and ELTGOL, has been frequently used for treating AECOPD [14, 15]. Our study shows that shorter remission time of expectoration and lung signs and much more obvious improvement of blood gas indicators and lung function can be observed in patients treated by HFCWO in comparison with those treated by ELTGOL. The reason for this is as follows: with respect to HFCWO, the patient's chest wall is slowly compressed and released through inflation and deflation. The generated airflow in the lungs drives the sputum to the large airway, and the mucus is eliminated with the help of coughing or inspiration [16]. It can evenly act on the patient's chest wall, change the nature of secretions through the mechanics principle, debond secretions in the terminal bronchus, and drive them to the large airway in the middle [17, 18]. HFCWO can significantly improve the efficiency of sputum drainage, increase the effectiveness of atomization intervention, and better improve the clinical symptoms of patients with AECOPD [19]. Meanwhile, the system has biofeedback and other related configurations, which is conducive to enhancing the sputum excretion ability of the body and reducing the number of coughs. Moreover, the system determines lung resonance frequency and viscosity, etc., calculates the strongest resonance, promotes the excretion of mucous secretions as much as possible, and can maximize sputum excretion more comprehensively and objectively compared to ELTGOL. It is reported in the literature that patients with moderate to severe COPD had significantly decreased sputum excretion and significantly improved dyspnea after HFCWO intervention [20]. Chakravorty et al. [21] also found that HFCWO had apparent advantages in improving pulmonary function of patients with COPD and reducing the risk of acute exacerbations. The findings of the present study are consistent with the above, reconfirming the therapeutic value of HFCWO in patients with severe AECOPD.

AECOPD has a complex pathogenesis, mostly involving viral or bacterial infections [22]. Increased serum levels of WBCs and interleukins suggest the presence of lower airway bacterial colonization, and abnormal inflammatory factors aggravate the disease [23]. CRP, WBC, and IL-6 are common inflammatory indicators. The above indicators are frequently used to assess the AECOPD condition, but the specificity is relatively poor. Recently, some scholars point out that AECOPD is associated with inflammation and hormonal imbalance, which lead to persistent damage to the patient's airway, consequently aggravating the disease [24]. COR is closely related to the body's stress response and plays a certain role in the body's environmental balance and stabilization and blood pressure regulation [25]. In addition, COR content is related to the hypothalamic-pituitary-adrenal axis, belonging to glucocorticoids; ACTH, however, can regulate hormones and is positively correlated with the COR content [26]. Reduced lung function, more sputum, and strong inflammation in patients with AECOPD aggravate lung injury and involve the kidney, resulting in reduced renal output and slower COR degradation. In addition, the progression of the disease affects the suprarenal function, further affecting COR decomposition, but its secretion and synthesis increase. The imbalance leads to the increase of serum COR level of the patient [27]. Our study showed that serum inflammatory indicators and plasma COR and ACTH levels decreased significantly after 14 d of HFCWO and ELTGOL treatment and that the relative decrease of the former was more remarkable, suggesting that both HFCWO and ELTGOL can effectively reduce the inflammatory reaction and improve cortisol function in patients with AECOPD. Promoting lung deflation by opening the glottis, ELTGOL can effectively eliminate the airway inflammation of patients, relieve dyspnea, and suppress the disease [28]. However, HFCWO has an advantage over ELTGOL in reducing inflammatory reaction and regulating cortisol function. Retention of more viscous airway secretions in patients with

Table 2: Comparison of blood gas indexes between the two groups ($\bar{x} \pm s$, mmHg).

Group	PaO_2		$PaCO_2$	
	Before the treatment	After treatment	Before the treatment	After treatment
Group A ($n = 33$)	71.06 ± 9.85	89.30 ± 8.52*	61.85 ± 6.66	44.06 ± 5.81*
Group B ($n = 32$)	70.75 ± 10.70	82.94 ± 7.82*	61.56 ± 7.68	48.06 ± 5.98*
t	0.122	3.137	0.161	-2.735
P	0.903	0.003	0.873	0.008

Note: vs. before treatment, *$P < 0.05$; PaO_2: partial pressure of blood oxygen; $PaCO_2$: partial pressure of carbon dioxide.

Table 3: Comparison of pulmonary function changes between the two groups ($\bar{x} \pm s$, %).

Group	FVC		EFV1		EFV1/FVC	
	Before the treatment	After treatment	Before the treatment	After treatment	Before the treatment	After treatment
Group A ($n = 33$)	55.24 ± 6.93	64.55 ± 6.72*	37.88 ± 8.43	48.03 ± 7.04*	54.36 ± 4.71	87.36 ± 10.96*
Group B ($n = 32$)	55.25 ± 6.62	60.41 ± 5.99*	38.19 ± 6.58	43.81 ± 6.28*	55.28 ± 4.95	80.47 ± 7.86*
t	-0.005	2.618	-0.164	2.547	-0.766	2.907
P	0.996	0.011	0.870	0.013	0.446	0.005

Note: vs. before treatment, *$P < 0.05$; FVC: forced vital capacity; FEV1: forced expiratory volume in first second; FEV1/FVC: forced expiratory volume in first second/forced vital capacity.

Table 4: Comparison of changes in serum inflammatory indexes between the two groups ($\bar{x} \pm s$).

Group	WBC ($\times 10^9$/L)		CRP (mg/L)		IL-6 (pg/mL)	
	Before the treatment	After treatment	Before the treatment	After treatment	Before the treatment	After treatment
Group A ($n = 33$)	11.07 ± 2.28	6.42 ± 1.54*	21.33 ± 7.38	5.80 ± 1.36*	180.27 ± 30.05	89.62 ± 17.58*
Group B ($n = 32$)	11.78 ± 3.21	8.26 ± 1.66*	23.54 ± 6.89	10.11 ± 3.08*	180.80 ± 34.47	102.03 ± 14.19*
t	-1.034	-4.623	-1.247	-7.332	-0.066	-3.126
P	0.305	<0.001	0.217	<0.001	0.947	0.003

Note: vs. before treatment, *$P < 0.05$; WBC = white blood cell count; CRP = C-reactive protein; IL-6 = interleukin-6.

Table 5: Comparison of cortisol function-related indicators between the two groups ($\bar{x} \pm s$).

Group	COR (nmol/L)		ACTH (pg/mL)	
	Before the treatment	After treatment	Before the treatment	After treatment
Group A ($n = 33$)	435.15 ± 56.59	175.43 ± 39.39*	64.60 ± 7.93	39.62 ± 6.54*
Group B ($n = 32$)	437.93 ± 45.31	203.36 ± 40.19*	63.25 ± 9.65	44.12 ± 8.95*
t	-0.218	-2.830	0.617	-2.318
P	0.828	0.006	0.539	0.024

Note: vs. before treatment, *$P < 0.05$; COR = cortisol; ACTH = adrenocorticotrophic hormone.

AECOPD can result in bacterial reproduction and aggravate lung infection. With the above advantages, HFCWO can realize more complete sputum removal compared with ELTGOL. The cortisol function of patients with COPD is influenced by many factors such as inflammation and hormones [29, 30]. The impact of different physical therapies on cortisol function of AECOPD patients shall be further confirmed by large sample and multicenter studies in the future. In addition, good tolerance without any obvious adverse reaction was observed for both groups. However, contraindications of HFCWO, such as bleeding, pulmonary embolism, fracture, or empyema, shall be noted in the actual use. The clinical indications and contraindications should be strictly controlled.

In conclusion, compared with ELTGOL, HFCWO shows more evident improvement on clinical symptoms, blood gas, pulmonary function, and cortisol function-related indicators in patients with severe AECOPD, which can be further studied and applied.

Data Availability

The data used to support the findings of this study are available from the corresponding author (Dr. Cheng) upon request.

Conflicts of Interest

The authors declare that they have no conflicts of interest.

References

[1] W. W. Labaki and S. R. Rosenberg, "Chronic obstructive pulmonary disease," *Annals of Internal Medicine*, vol. 173, no. 3, pp. ITC17–ITC32, 2020.

[2] R. Balkissoon and Journal Club—COPD2020 Update, "Global Initiative for Chronic Obstructive Lung Disease 2020 Report and the journal of the COPD foundation special edition, moving to a new definition for COPD: "COPDGene 2019"," *Chronic Obstructive Pulmonary Disease*, vol. 6, no. 4, pp. 64–72, 2019.

[3] S. P. Duffy and G. J. Criner, "Chronic obstructive pulmonary disease: evaluation and management," *Medical Clinics of North America*, vol. 103, no. 3, pp. 453–461, 2019.

[4] R. Gloeckl, T. Schneeberger, I. Jarosch, and K. Kenn, "Pulmonary rehabilitation and exercise training in chronic obstructive pulmonary disease," *Deutsches Ärzteblatt International*, vol. 115, no. 8, pp. 117–123, 2018.

[5] E. F. Wouters, R. Posthuma, M. Koopman et al., "An update on pulmonary rehabilitation techniques for patients with chronic obstructive pulmonary disease," *Respiratory Medicine*, vol. 14, no. 2, pp. 149–161, 2020.

[6] G. Prieur, Y. Combret, and C. Medrinal, "High flow nasal therapy during early pulmonary rehabilitation in patients with acute severe exacerbation of COPD: beneficial or illusory?," *Respiratory Research*, vol. 21, no. 1, p. 897, 2020.

[7] P. Wei, Y. Li, L. Wu et al., "Serum cortisol levels and adrenal gland size in patients with chronic obstructive pulmonary disease," *Translational Research*, vol. 13, no. 7, pp. 8150–8157, 2021.

[8] L. F. Tung, S. Y. Shen, Y. T. Chen, H. H. Shih, J. D. Yan, and S. C. Ho, "Early pulmonary rehabilitation increases 6MWD and reduces CRP in hospitalized patients with severe AECOPD," *ERS International Congress 2020 Abstracts*, vol. 14, no. 3, pp. 734–736, 2020.

[9] C. Ta, D. D. Mülazimoğlu, D. Doğan, N. Öcal, and Y. Arslan, "Effect of pulmonary rehabilitation on patients with severe and very severe COPD and emphysema," *Medical Journal of Bakirkoy*, vol. 17, no. 2, pp. 121–124, 2021.

[10] C. M. Riley and F. C. Sciurba, "Diagnosis and outpatient management of chronic obstructive pulmonary disease," *JAMA*, vol. 321, no. 8, pp. 786–797, 2019.

[11] J. S. Jerng, C. H. Tang, R. W. Cheng, M. Y. H. Wang, and K. Y. Hung, "Healthcare utilization,medical costs and mortality associated with malnutrition in patients with chronic obstructive pulmonary disease: a matched cohort study," *Current Medical Research and Opinion*, vol. 35, no. 7, pp. 1265–1273, 2019.

[12] X. Jie, W. Xudong, and L. Zhihai, "AECOPD research in the past ten years: a bibliographic analysis based on Web of Science," *Annals of Palliative Medicine*, vol. 10, no. 10, pp. 10401–10413, 2021.

[13] A. G. Mathioudakis, W. Janssens, P. Sivapalan et al., "Acute exacerbations of chronic obstructive pulmonary disease: in search of diagnostic biomarkers and treatable traits," *Thorax*, vol. 75, no. 6, pp. 520–527, 2020.

[14] T. Goktalay, S. E. Akdemir, A. O. Alpaydin, A. S. Coskun, P. Celik, and A. Yorgancioglu, "Does high-frequency chest wall oscillation therapy have any impact on the infective exacerbations of chronic obstructive pulmonary disease? A randomized controlled single-blind study," *Clinical Rehabilitation*, vol. 27, no. 8, pp. 710–718, 2013.

[15] F. C. Lanza, C. S. Alves, R. L. dos Santos, A. A. de Camargo, and S. Dal Corso, "Expiratory reserve volume during slow expiration with glottis opened in infralateral decubitus position (ELTGOL) in chronic pulmonary disease: technique description and reproducibility," *Respiratory Care*, vol. 60, no. 3, pp. 406–411, 2015.

[16] A. Nicolini, B. Grecchi, M. Ferrari-Bravo, and C. Barlascini, "Safety and effectiveness of the high-frequency chest wall oscillation vs intrapulmonary percussive ventilation in patients with severe COPD," *International Journal of Chronic Obstructive Pulmonary Disease*, vol. 13, pp. 617–625, 2018.

[17] T. Liu, Y. Kang, Z. Xu, Y. Lyu, L. Jia, and Y. Gao, "A study of the value of high frequency chest wall oscillation in patients with acute exacerbation of chronic obstructive pulmonary disease," *Zhonghua Jie He He Hu Xi Za Zhi*, vol. 37, no. 4, pp. 255–259, 2014.

[18] A. M. Esquinas, B. Patel, and E. Pravinkumar, "High-frequency chest wall oscillation in infective exacerbation of COPD: is airway secretion clearance the cornerstone?," *Clinical Rehabilitation*, vol. 28, no. 2, pp. 206-207, 2014.

[19] G. D. Alvarenga, H. R. Gamba, L. E. Hellman, V. G. Ferrari, and R. M. de Macedo, "Physiotherapy intervention during level I of pulmonary rehabilitation on chronic obstructive pulmonary disease: a systematic review," *The Open Respiratory Medicine Journal*, vol. 10, no. 1, pp. 12–19, 2016.

[20] N. M. Allam and M. M. Badawy, "Does high-frequency chest wall oscillation have an impact on improving pulmonary function in patients with smoke inhalation injury?," *Journal of Burn Care & Research*, vol. 42, no. 2, pp. 300–304, 2021.

[21] I. Chakravorty, K. Chahal, and G. Austin, "A pilot study of the impact of high -frequency chest wall oscillation in chronic obstructive pulmonary disease patients with mucus hypersecretion," *International Journal of Chronic Obstructive Pulmonary Disease*, vol. 6, no. 1, pp. 693–699, 2011.

[22] M. L. Chuang, Y. L. Chou, C. Y. Lee, and S. F. Huang, "Instantaneous responses to high-frequency chest wall oscillation in patients with acute pneumonic respiratory failure receiving mechanical ventilation," *Medicine*, vol. 96, no. 9, article e5912, 2017.

[23] D. Halpin, G. J. Criner, A. Papi et al., "Global initiative for the diagnosis, management, and prevention of chronic obstructive lung Disease. the 2020 GOLD science committee report on COVID-19 and Chronic Obstructive Pulmonary Disease," *American Journal of Respiratory and Critical Care Medicine*, vol. 203, no. 1, pp. 24–36, 2021.

[24] M. Macleod, A. Papi, M. Contoli et al., "Chronic obstructive pulmonary disease exacerbation fundamentals: diagnosis, treatment, prevention and disease impact," *Respirology*, vol. 26, no. 6, pp. 532–551, 2021.

[25] A. Mbchb and J. A. Wedzicha, "Definition, causes, pathogenesis, and consequences of chronic obstructive pulmonary disease exacerbations," *Clinics in Chest Medicine*, vol. 41, no. 3, pp. 421–438, 2020.

[26] L. M. Glenk, O. D. Kothgassner, A. Felnhofer et al., "Salivary cortisol responses to acute stress vary between allergic and healthy individuals: the role of plasma oxytocin, emotion regulation strategies, reported stress and anxiety," *Stress*, vol. 23, no. 3, pp. 275–283, 2020.

[27] A. Riek, L. Schrader, F. Zerbe, and S. Petow, "Comparison of cortisol concentrations in plasma and saliva in dairy cattle following ACTH stimulation," *The Journal of Dairy Research*, vol. 86, no. 4, pp. 406–409, 2019.

[28] F. Yang, N. Liu, J. Y. Hu et al., "Pulmonary rehabilitation guidelines in the principle of 4S for patients infected with 2019 novel coronavirus (2019-nCoV)," *Zhonghua jie he he hu xi za zhi = Zhonghua jiehe he huxi zazhi = Chinese Journal of Tuberculosis And Respiratory Diseases*, vol. 55, no. 43, 2020.

[29] L. Y. Liu, M. Zeng, C. M. Xie et al., "Oxidative stress status in patients with chronic obstructive pulmonary disease and its relation to glucocorticoid receptor levels," *Nan Fang Yi Ke Da Xue Xue Bao*, vol. 28, no. 6, pp. 992–996, 2008.

[30] L. Su, Y. Qiao, J. Luo et al., "Characteristics of the sputum microbiome in COPD exacerbations and correlations between clinical indices," *Journal of Translational Medicine*, vol. 20, no. 1, p. 76, 2022.

Hindawi
Disease Markers
Volume 2022, Article ID 8602068, 14 pages
https://doi.org/10.1155/2022/8602068

Research Article

C1R, CCL2, and TNFRSF1A Genes in Coronavirus Disease-COVID-19 Pathway Serve as Novel Molecular Biomarkers of GBM Prognosis and Immune Infiltration

Xianggang Wang,[1] **Guohua Yang**,[2] **Qingqing Wang**,[1] **Yilong Zhao**,[1] **Kaixin Ding**,[1] **Can Ji**,[1] **Zongyuan Shi**,[1] **Huaying Li**,[1] **Ying Li**,[2] **and Shujing Li**[1]

[1]*School of Life Science, Bengbu Medical College, 233030 Bengbu City, Anhui Province, China*
[2]*Department of Medical Genetics, School of Basic Medical Science, Demonstration Center for Experimental Basic Medicine Education, Wuhan University, 430071 Wuhan City, Hubei Province, China*

Correspondence should be addressed to Shujing Li; lishujing1234@126.com

Xianggang Wang and Guohua Yang contributed equally to this work.

Received 6 May 2022; Accepted 1 June 2022; Published 18 June 2022

Academic Editor: Xianwei Zeng

Glioblastoma multiforme (GBM) is a prevalent intracranial brain tumor associated with a high rate of recurrence and treatment difficulty. The prediction of novel molecular biomarkers through bioinformatics analysis may provide new clues into early detection and eventual treatment of GBM. Here, we used data from the GTEx and TCGA databases to identify 1923 differentially expressed genes (DEGs). GO and KEGG analyses indicated that DEGs were significantly enriched in immune response and coronavirus disease-COVID-19 pathways. Survival analyses revealed a significant correlation between high expression of C1R, CCL2, and TNFRSF1A in the coronavirus disease-COVID-19 pathway and the poor survival in GBM patients. Cell experiments indicated that the mRNA expression levels of C1R, CCL2, and TNFRSF1A in GBM cells were very high. Immune infiltration analysis revealed a significant difference in the proportion of immune cells in tumor and normal tissue, and the expression levels of C1R, CCL2, and TNFRSF1A were associated with immune cell infiltration of GBM. Additionally, the protein-protein interaction networks of C1R, CCL2, and TNFRSF1A involved a total of 65 nodes and 615 edges. These results suggest that C1R, CCL2, and TNFRSF1A may be used as molecular biomarkers of prognosis and immune infiltration in GBM patients in the future.

1. Introduction

Glioblastoma multiforme is a prevalent intracranial brain tumor, accounting for about 40%-50% of all intracranial tumors. Not only is GBM common, but it is a cancer with all sorts of frightening features and intimidating labels. First of all, GBM patients have a higher mortality rate. There are 40,000 to 80,000 new cases of GBM in China every year, with up to 30,000 deaths per year. In particular, there has been an increase in cancer patients under the age of 34, whose five-year mortality rate is the third-highest among all cancers, after pancreatic and lung cancer. Secondly, the recurrence rate of GBM is very high. Since glioblastoma is an invasive growth and invades mainly around neurons or along white matter fibers with ill-defined borders, surgery is generally difficult to remove completely. However, unresected glioblastoma is particularly prone to relapse, and relapse is often accompanied by biological malignant progression, from low-grade GBM to high-grade GBM. Third, GBM surgery is complicated. Because glioblastoma is located in the most important and complex brain of the human body, it may lead

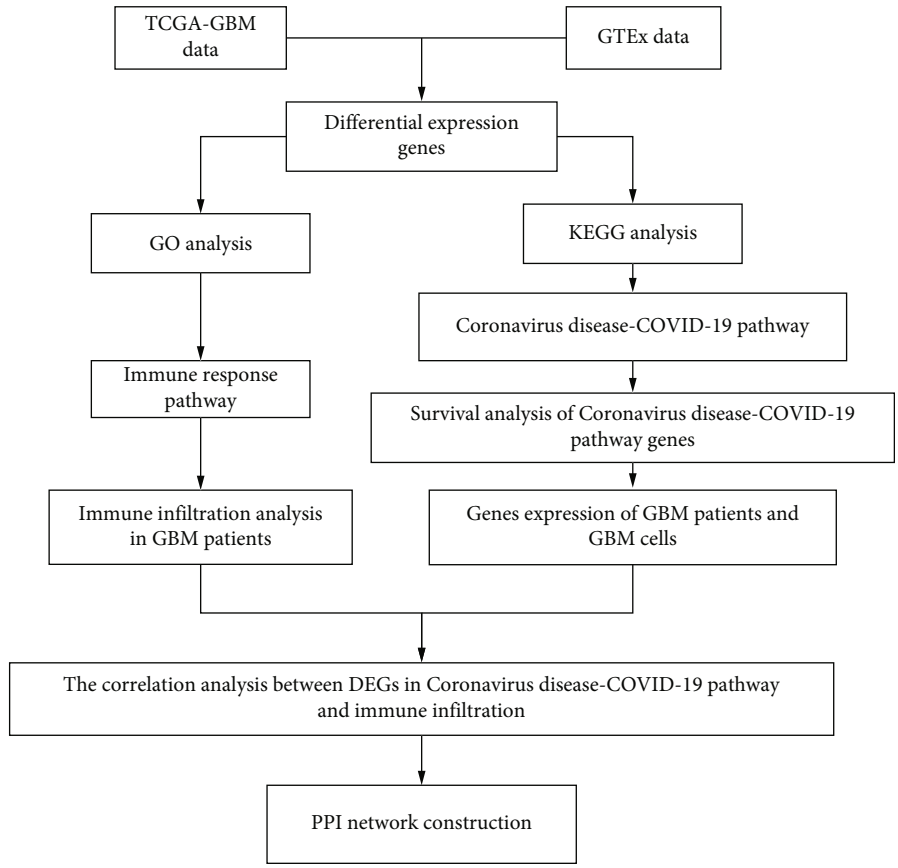

Figure 1: The flow diagram of this study.

to disability or death of the patient if it is accidentally damaged in the important tissues in the brain during surgery. The difficulty and risk of surgery are very high. Glioblastoma grows rapidly, with 70% to 80% of patients lasting 3-6 months and only 10% lasting more than 1 year [1, 2]. Generally, patients with glioblastoma after timely surgery can hardly live for more than two years.

With the rapid development of supercomputer technology and the continuous improvement of modern high-throughput sequencing technology, more and more large-scale gene transcriptomics and related clinical databases are freely available, and it has become an increasingly vital and effective method to explore the pathological mechanisms of diseases based on bioinformatics theory. The prediction of novel molecular biomarkers through bioinformatics analysis can provide new insights into early diagnosis, survival prediction, and eventual treatment. At present, new molecular biomarkers of liver hepatocellular carcinoma, breast cancer, lung carcinoma, and adrenocortical carcinoma have been successfully predicted using large-scale clinical databases and bioinformatics tools [3–7]. Compared with other pathological types of glioblastoma multiforme, the majority of GBM patients died from tumor recurrence, with a 5-year survival rate of less than 3%, resulting in insufficient data of patient samples in the TCGA database. Therefore, bioinformatics analysis of GBM patients has rarely been reported.

In this study, we aim to integrate information from the GTEx database and the TCGA database to identify DEGs through full-scale bioinformatics analysis. This may help to find the underlying molecular mechanisms of GBM development and may serve as biomarkers and molecular targets for the diagnosis and prognosis of GBM patients in the immediate future.

2. Results

2.1. Identification and Screening of 1923 DEGs. This study was conducted according to the flow chart (Figure 1). The GBM-GTEx and GBM-TCGA databases were used to identify a total of 1923 DEGs. Then, we screened 1118 upregulated DEGs and 805 downregulated DEGs in GBM samples compared with nontumor samples (Figure 2 and Supplementary Table S1).

2.2. GO Analysis of DEGs. To accurately study the function of 1923 DEGs in glioblastoma, we performed GO analysis using *R* software. The results showed that the most enriched BP terms were modulation of chemical synaptic transmission, neurotransmitter secretion, neutrophil activation involved in immune response, synapse organization, and so on. CCs analyses revealed that the DEGs were primarily enriched in transport vesicle and collagen-containing. MF analyses revealed that the DEGs were

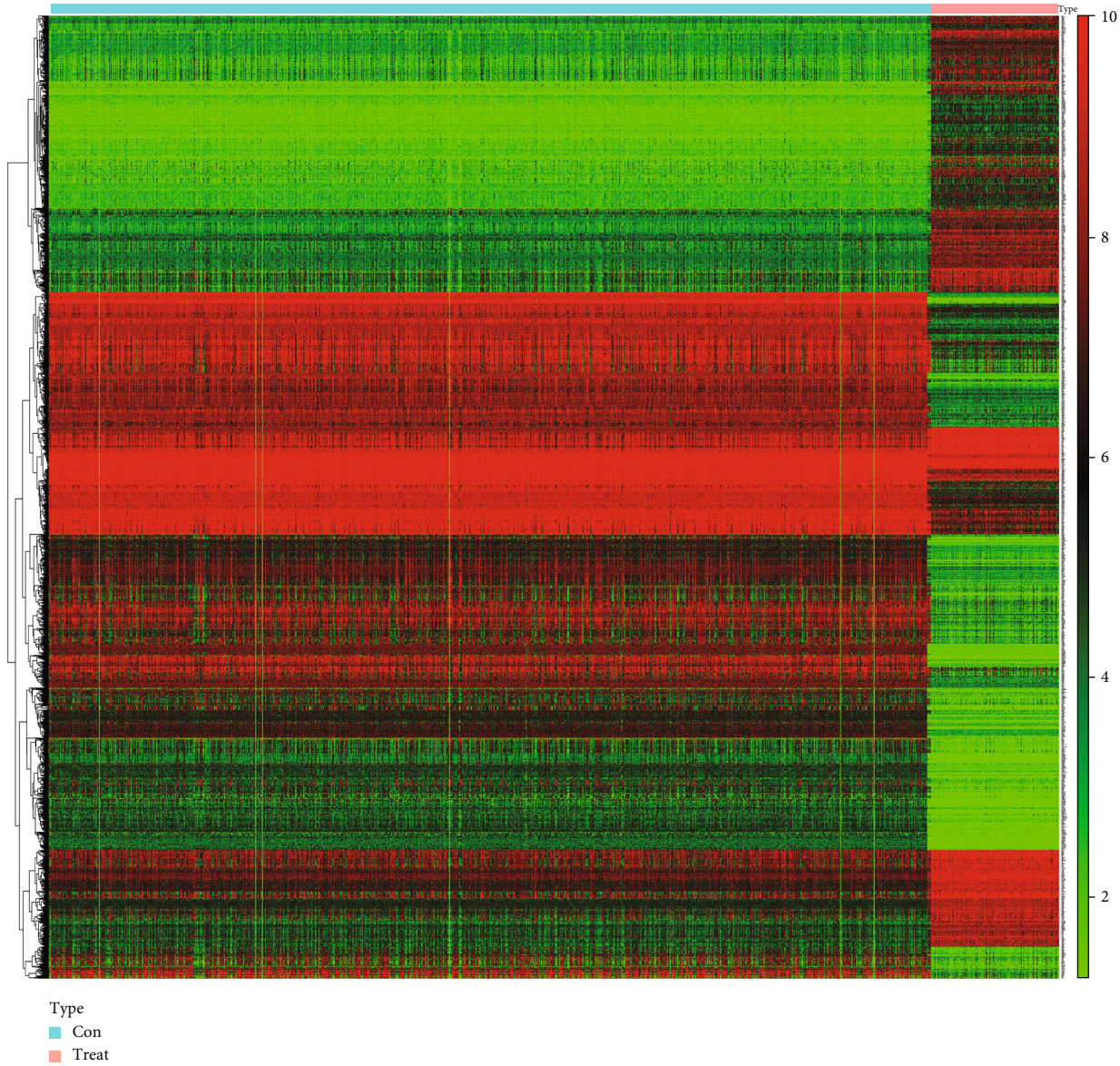

Figure 2: Heat map of DEGs. The red color and green color represented the upregulated and downregulated genes, respectively.

primarily enriched in phospholipid binding, gated channel activity, and so on (Figure 3(a)). Gene cluster analysis on BP modules with the top P value indicated that DEGs were significantly related to signal transduction processes and neutrophil activation involved in the immune response pathway (Figure 3(b)).

2.3. KEGG Pathway Analysis of DEGs. To elucidate the role of 1923 DEGs in glioblastoma, we used the KEGG pathway analysis. The results showed that the coronavirus disease-COVID-19, prion disease, Epstein-Barr virus infection, and phagosome pathways were significantly affected with $P < 0.001$ (Figure 4(a)). Cluster analysis showed that 44 DEGs were significantly enriched in the coronavirus disease-COVID-19 pathway (Figure 4(b)).

2.4. Survival Analysis of DEGs. To study the prognostic values of DEGs enriched in the pathways of coronavirus disease-COVID-19, we analyzed the overall survival of 169 GBM patients. We found that the high expression of C1R, CCL2, and TNFRSF1A genes was particularly associated with the low survival in GBM patients (Figure 5), while other 41 DEGs enriched in the pathway of coronavirus disease-COVID-19 were not significantly connected with the overall survival of GBM patients (Supplementary Table S1). The results suggested that C1R, CCL2, and TNFRSF1A genes might be potential prognostic factors.

2.5. Expression Analysis of DEGs in GBM Patients and Glioblastoma Cells. To detect the expression levels of C1R, CCL2, and TNFRSF1A in glioblastoma, we analyzed the

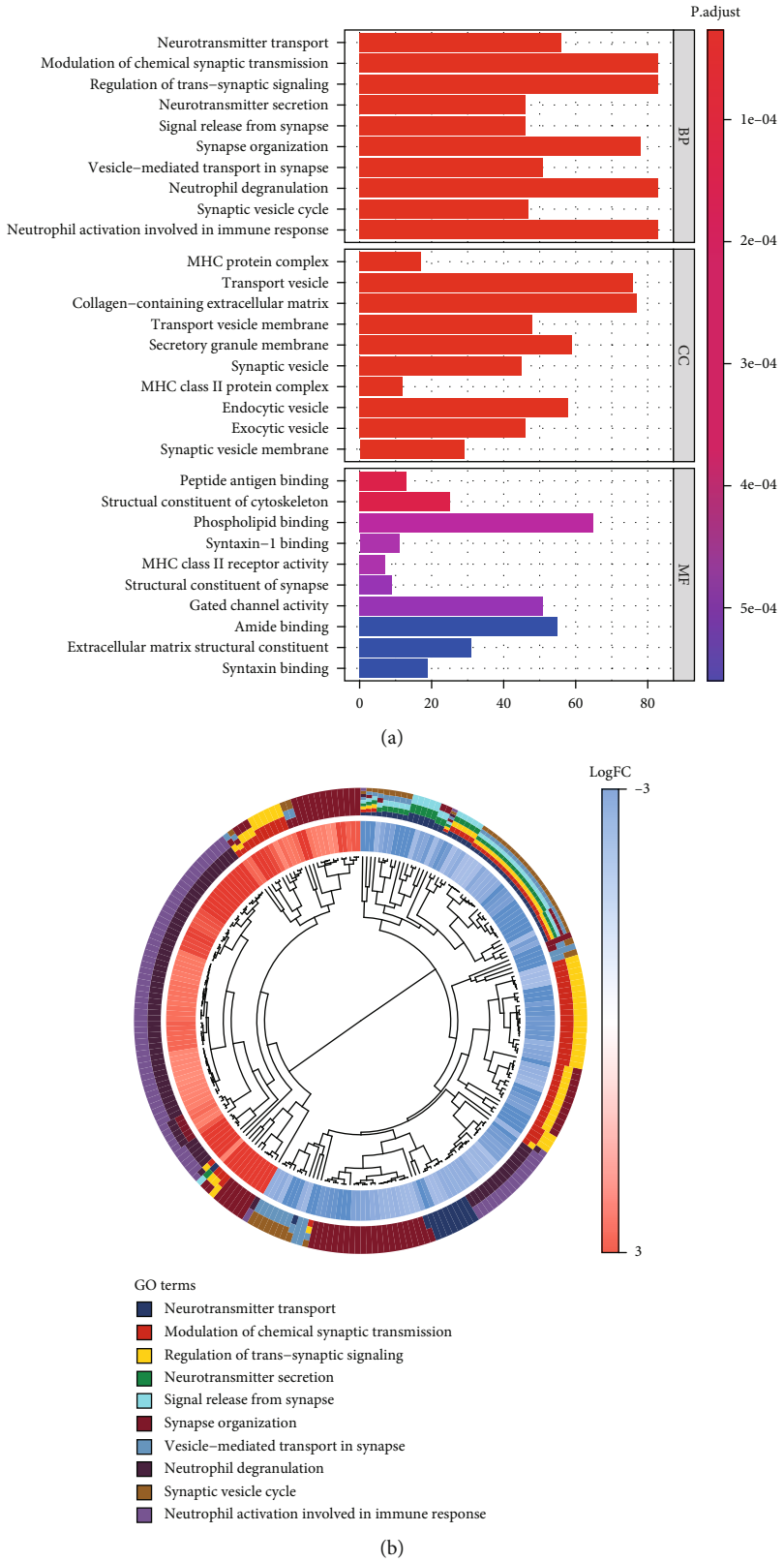

Figure 3: GO enrichment analysis of DEGs. (a) Biological process, cell components, and molecular function enrichment analyses of DEGs. (b) GO cluster analyses.

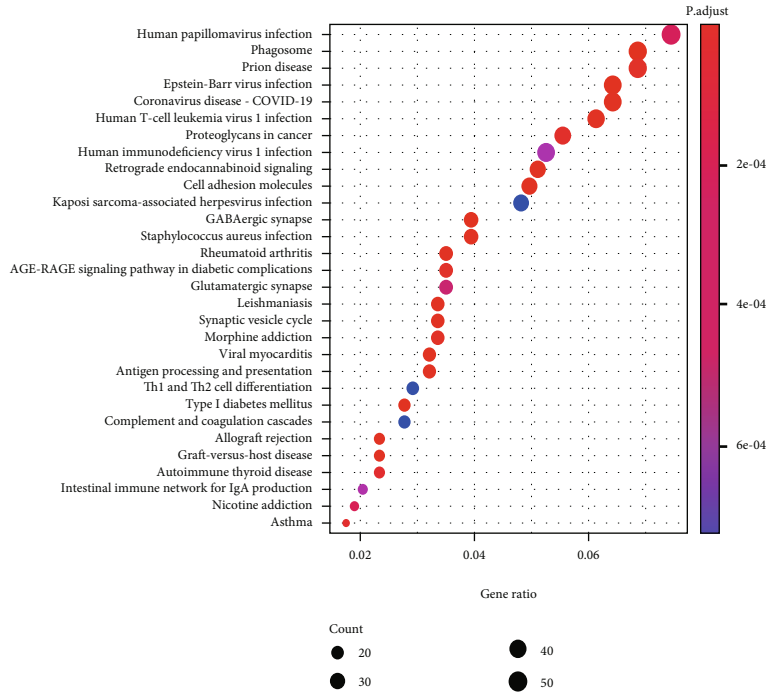

(a)

Figure 4: Continued.

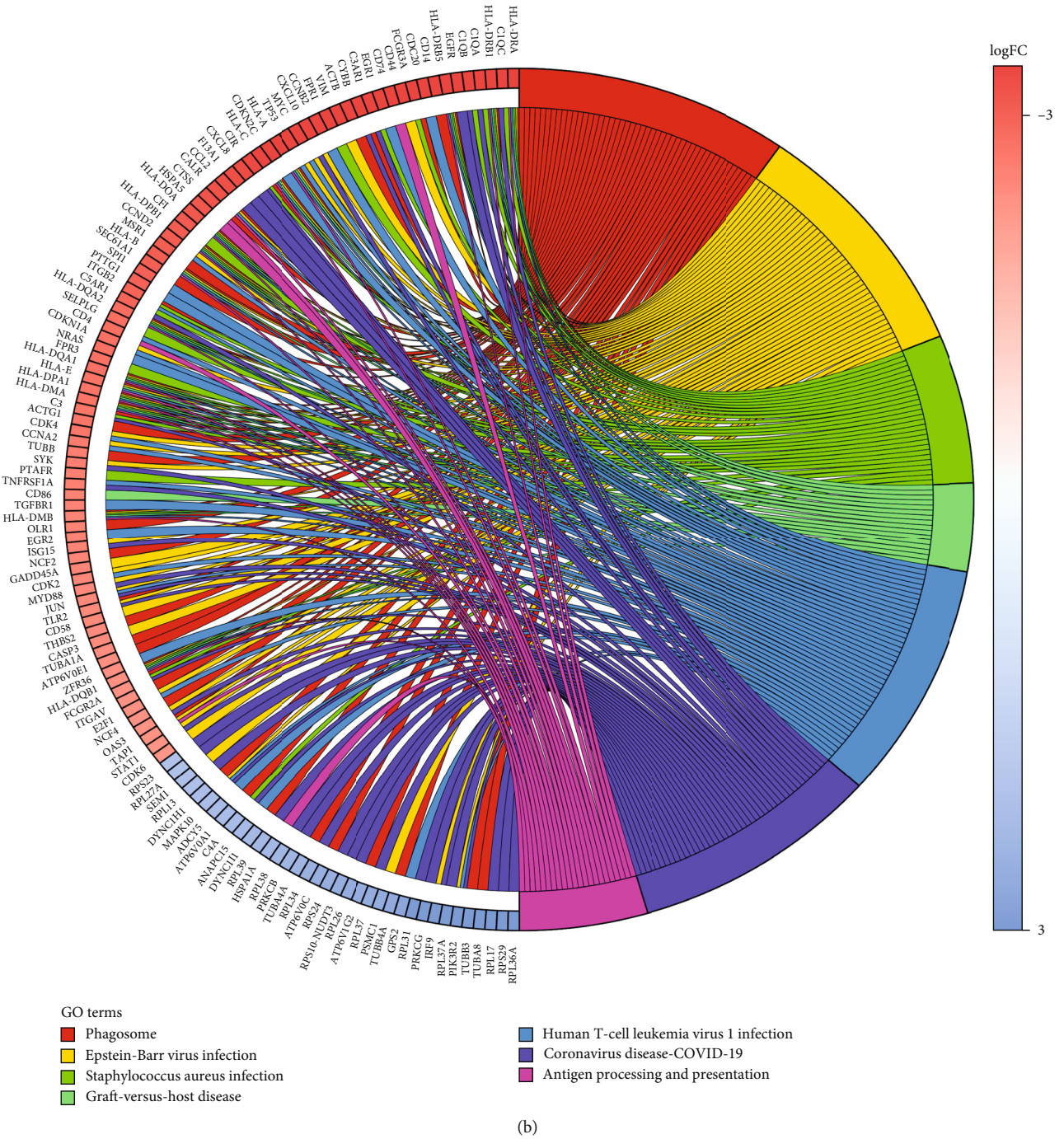

Figure 4: KEGG pathway enrichment analysis of DEGs. (a) KEGG pathway analysis of DEGs. (b) KEGG pathway cluster analyses.

mRNA levels of GBM patients and glioblastoma cells (Supplementary Table S2). C1R, CCL2, and TNFRSF1A mRNA levels were significantly higher in GBM samples than in normal samples (Figure 6(a) and Supplementary Table S3), which was verified by the GEPIA online tool (Supplementary Figure S1). Furthermore, the mRNA expression levels of these three genes were positively correlated (Supplementary Figure S2). We also performed experimental validation in the cell lines. Consistently, the mRNA levels of C1R, CCL2, and TNFRSF1A were strongly upregulated in U-87MG, U-251MG, and U-1118MG cells compared with those in HMC3 cells (Figure 6(b)). The results suggested that the expression of C1R, CCL2, and TNFRSF1A might promote the development of glioblastoma.

2.6. Immune Infiltration Analysis in GBM Patients. GO analysis suggested that DEGs were significantly associated with the immune response function. To determine which specific immune cells were responsible, we performed tumor cell immune infiltration analysis. The results indicated a significant difference in the proportion of immune cells in tumor

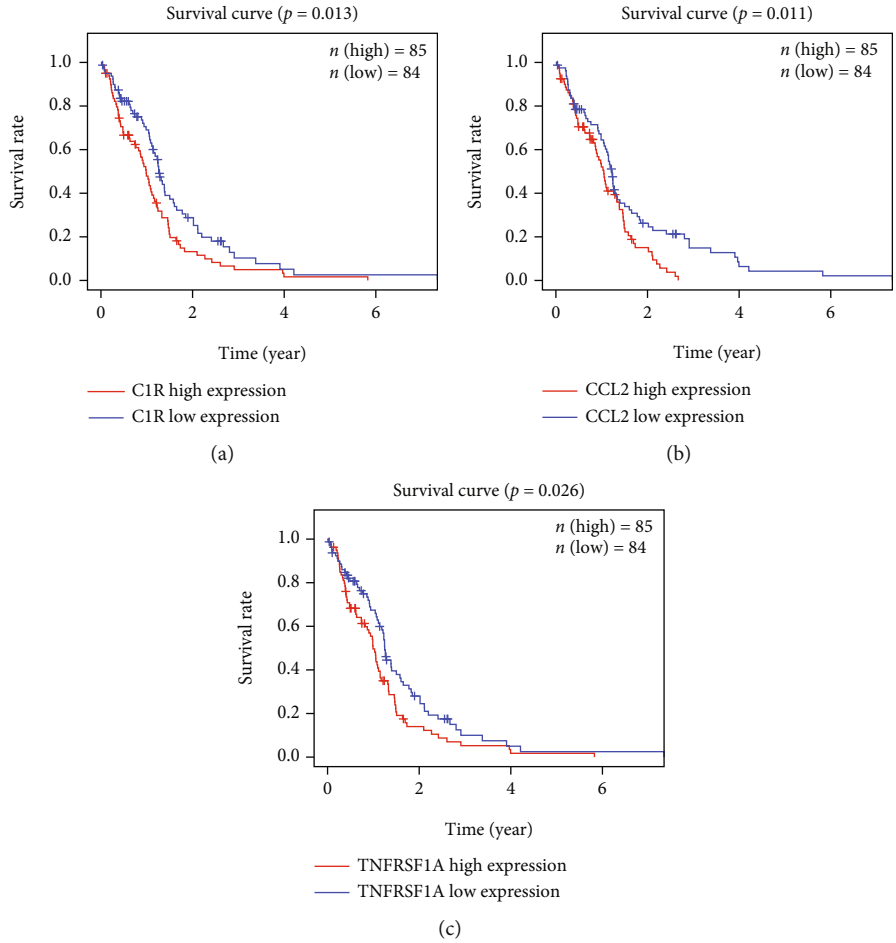

Figure 5: The correlation between the expression levels of three key DEGs and the survival rate of GBM patients: (a) C1R, (b) CCL2, and (c) TNFRSF1A.

and normal tissues. Compared with normal tumor tissues, GBM tissues contained more T cell CD4 memory resting, T cell gamma delta, NK cells activated, macrophage M0, macrophage M1, and macrophage M2, but it contained relative fewer B cell memory, T cell CD8, T cell CD4 naive, T cell follicular helper, and NK cell resting (Figures 7(a) and 7(b)). T cell follicular helper and NK cell resting were indicated a negative correlation with T cell CD4 memory resting (Pearson correlation = −0.50 and Pearson correlation = −0.52), while macrophage M1 and NK cells activated showed a moderate positive correlation (Pearson correlation = 0.52) (Figure 7(c)). In brief, these results suggested that the immune response to GBM was a complex network and was carried out in a rigorous manner.

2.7. C1R/CCL2/TNFRSF1A Genes Were Correlated with Immune Infiltration in GBM. To determine whether C1R, CCL2, and TNFRSF1A could be used as immunotherapy targets for GBM, we studied the correlation between the mRNA levels of C1R/CCL2/TNFRSF1A and GBM immune infiltration. The C1R expression was found to be negatively correlated with B cells, $CD8^+$ T cells, and neutrophil infiltration and positively associated with $CD4^+$ T cells, macrophages, and dendritic cell infiltration (Figure 8(a)). The expression of CCL2 was found to be negatively correlated with CD8+ T cells and macrophage infiltration and positively associated with B cells, $CD4^+$ T cells, neutrophil, and dendritic cell infiltration (Figure 8(b)). The TNFRSF1A expression was negatively correlated with $CD8^+$ T cell infiltration and positively associated with B cells, $CD4^+$ T cells, macrophages, neutrophil, and dendritic cell infiltration (Figure 8(c)). These data suggested that there might be a correlation between coronavirus disease-COVID-19 and immune infiltration of GBM.

2.8. PPI Network Analysis of C1R/CCL2/TNFRSF1A Genes. To determine the important genes and key gene modules, the PPI network of C1R, CCL2, and TNFRSF1A genes was constructed, containing 62 nodes and 615 edges. The interacted genes were A2M, ACKR3, AGT, C3, C3AR1, C5AR1, CALR, CASP3, CCR1, CD14, CD4, CD74, CD86, CSF1, CSF1R, CTGF, CX3CR1, CXCL10, CXCL16, CXCL8, CXCR4, CYBB, EGFR, F2R, FCGR3A, FGF13, GDF15, GFAP, GRN, HLA-A, HMOX1, HSPA1A, ISG15, ITGB2, JUN, LIF, MMP9, MSR1, NAMPT, OLR1, PLAU, PROCR, PTX3, RBP4, RHOA, S100A9, SAA1, SDC1, SOCS3, SPP1, STAT1, SYK, TAC1, TLR2, TNFRSF12A, TNFRSF1B, TNFRSF21, TNFRSF25, TNFRSF6B, TNFSF13B, TYROBP,

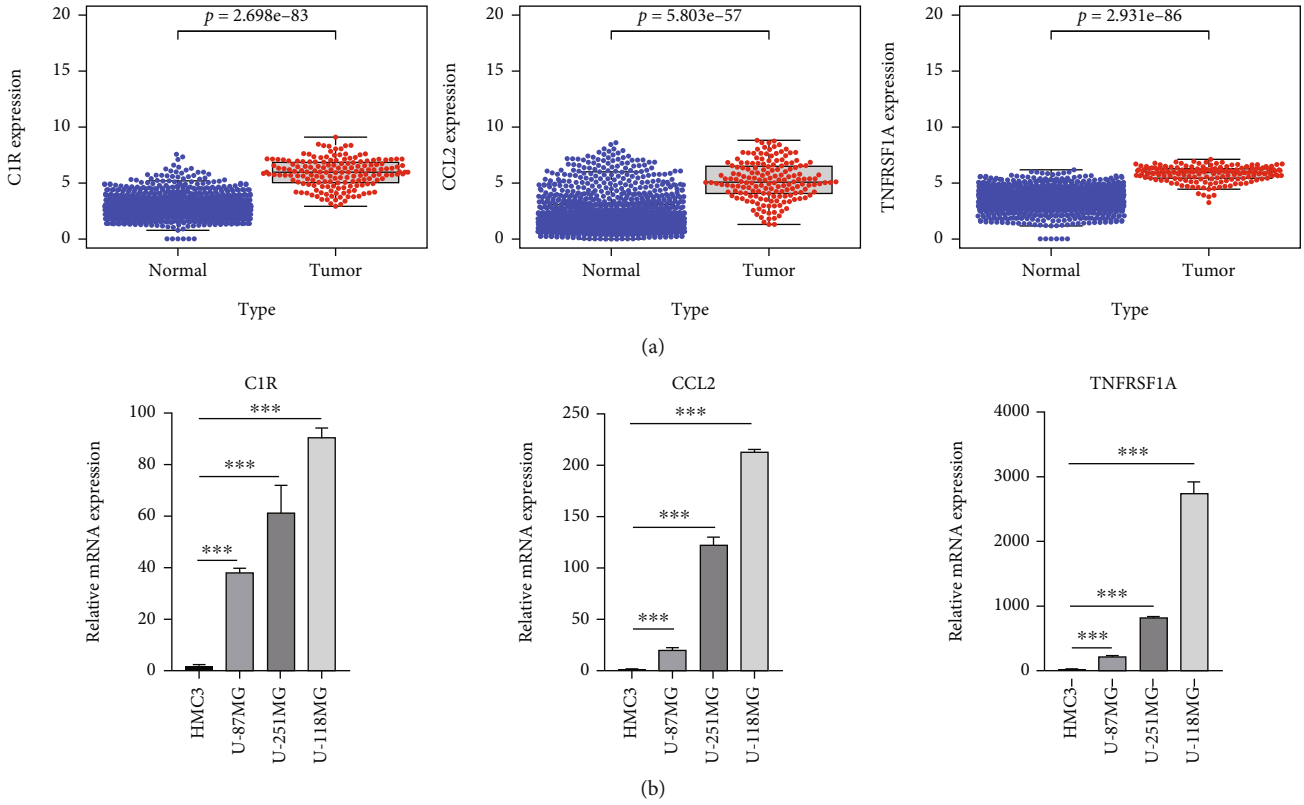

Figure 6: The expression levels of three key DEGs in GBM. (a) C1R, CCL2, and TNFRSF1A expression levels in the normal and GBM tissues. (b) The mRNA levels of C1R, CCL2, and TNFRSF1A in GBM cell lines. The experiments were performed independently three times. $^{*}P < 0.05$, $^{**}P < 0.01$, $^{***}P < 0.001$.

and VCAM1, which were mainly associated with the immune system (Figure 9 and Supplementary Table S4).

3. Discussion

Glioblastoma multiforme was one of the most deadly brain tumors. Surgical resection was the standard treatment for GBM, followed by chemotherapy with temozolomide (TMZ) and radiotherapy [8]. With the development of gene therapy, immunotherapy, and vaccine therapy, GBM treatment has been improved, but treatment options for controlling GBM recurrence were limited. GBM caused systemic immunosuppression and local immune dysfunction, leading to a more complex relationship between GBM and the peripheral tumor microenvironment (TME) [2, 9]. TME has been found to play a role in tumor genesis, development, and migration, as well as the development of malignancy and therapeutic resistance in a growing number of studies. TME cell composition and immune cell accessibility varied greatly between GBM subtypes and patients. These factors led to the immunosuppression of GBM, which further led to the failure of immunotherapy. The identification of immune genes and immune cell types that were actively involved in TME could help clarify the general mechanism of GBM immune suppression.

Moreover, in studies that have been reported, the onset of COVID-19 caused an activation of the immune system. SARS-COV-2 bound to the host ACE2 receptor through the viral spike protein receptor binding domain (RBD) and then invaded host cells to generate an immune cascade mechanism. Mucosal-associated invariant T (MAIT) cells and $\gamma\delta$T cells released inflammatory cytokines to respond to invasion [10]. Early response immune effector cells, including CTL and NK cells, were activated to fight the virus [11]. A number of studies have shown that the sign of COVID-19 was the cytokine storm with elevated levels of interleukin-6 (IL-6), IL-1β, complement C1r (C1R), tumor necrosis factor-alpha (TNF-α), chemokine (C-C-motif) ligand 2 (CCL2), and granulocyte-macrophage colony-stimulating factor (GM-CSF) [12].

In this study, enrichment pathway analysis indicated that DEGs in glioblastoma were strongly enriched in pathways of immune response and coronavirus disease-COVID-19 (Figures 3 and 4). The high expression levels of C1R, CCL2, and TNFRSF1A in coronavirus disease-COVID-19 pathway were significantly related to the low survival in GBM patients (Figure 5). Moreover, the mRNA expression levels of C1R, CCL2, and TNFRSF1A in glioblastoma cells or in GBM patients were found to be strongly upregulated (Figure 6 and Supplementary Figure S1), and the mRNA expression levels of these three genes were positively associated with each other (Supplementary Figure S2). The results indicated that the expression of C1R, CCL2, and TNFRSF1A might promote the development of glioblastoma and might be used as molecular biomarkers of prognosis and immune

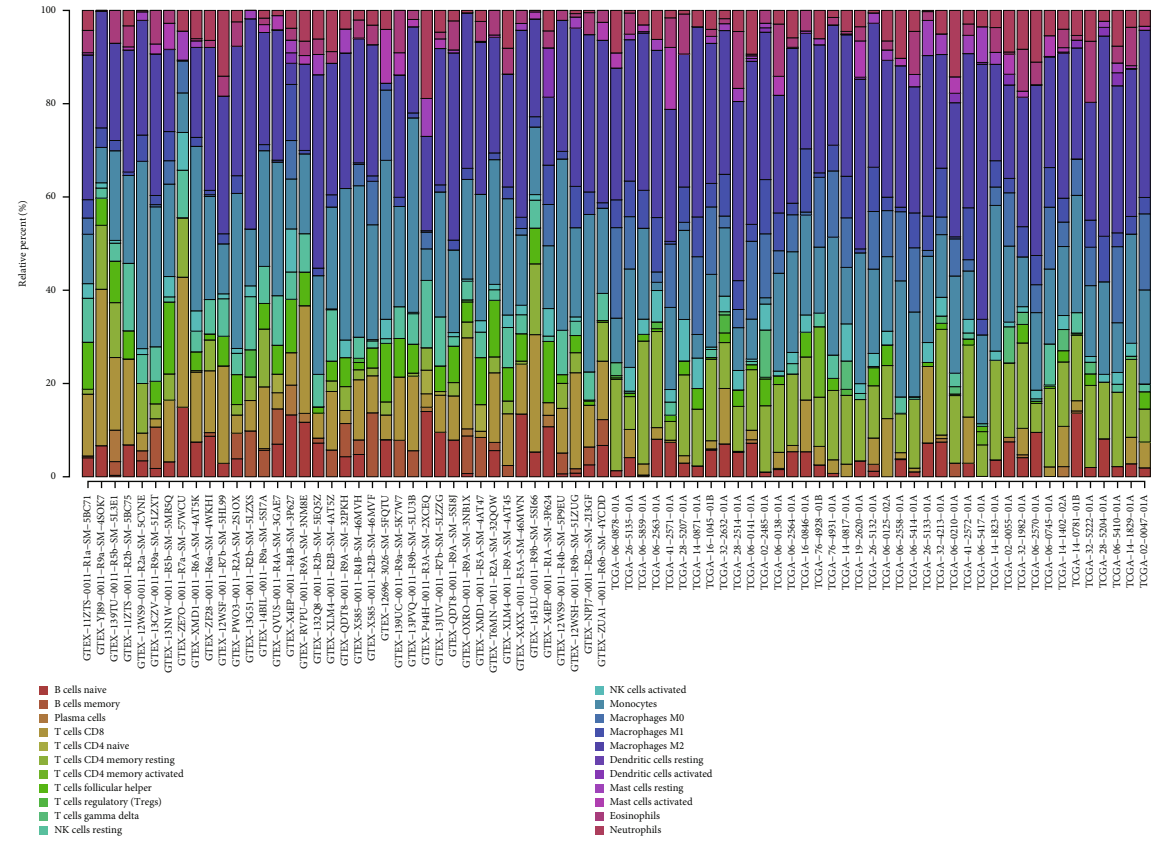

(a)

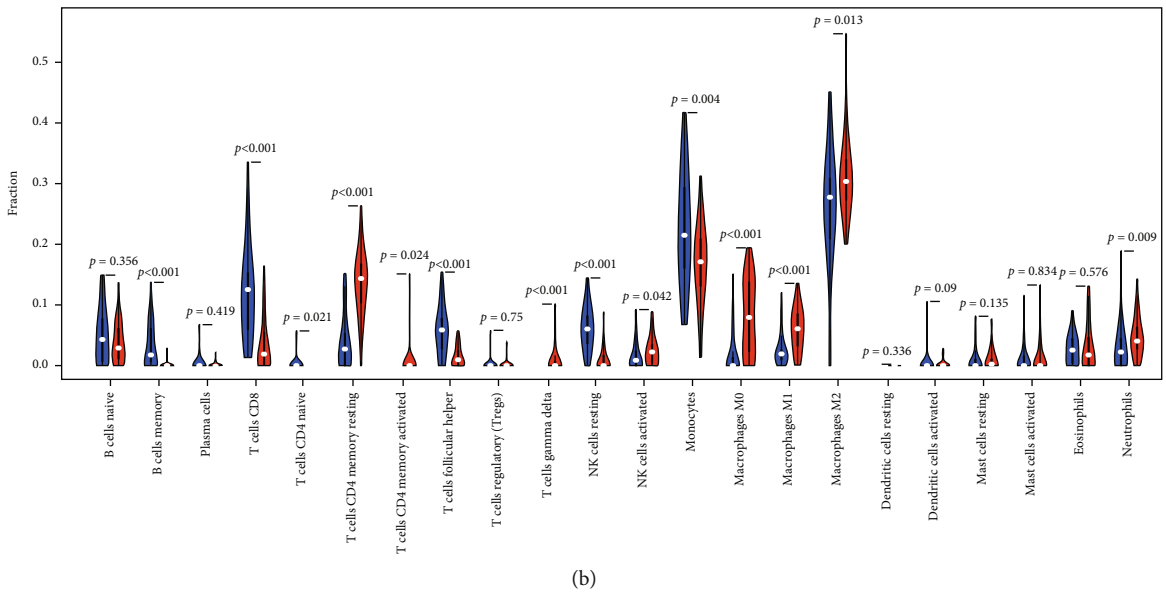

(b)

Figure 7: Continued.

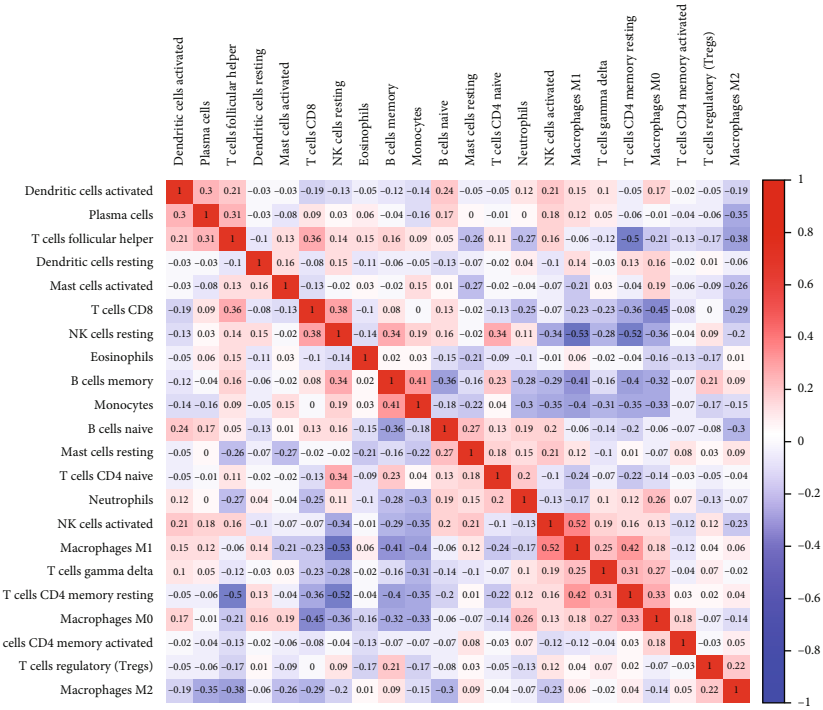

(c)

Figure 7: The proportion of immune cell abundance and correlation analysis of immune cells in GBM. (a) The landscape of immune infiltration in GBM and the difference of immune infiltration between tumor tissue and paired normal tissue. (b) Violin plot visualizing differentially infiltrated immune cells. The red color and green color represented normal tissue and tumor tissue, respectively. (c) Correlation heat map depicting correlations between infiltrating immune cells in GBM.

infiltration in GBM patients in the future. A recent study found the increase of CCL2 promoted carcinogenesis through esophageal mucosal inflammation [13]. Moreover, CCL2 could promote the survival and proliferation of THP-1, prostate cancer cell line PC3, renal cell carcinoma cell line 786-O and KAKI-1, and lung cancer cell line A549 [14, 15]. The growth of cutaneous squamous cell carcinoma and non-small-cell lung cancer was promoted by tumor-cell-derived complement components C1r and C1s [16]. However, there are few reports about the relationship between these three genes and glioblastoma and how C1R, CCL2, and TNFRSF1A promote the occurrence and development of GBM which requires further research in the future.

Our results also found that C1R, CCL2, and TNFRSF1A gene expression was significantly associated with GBM immune infiltration. The expression of C1R, CCL2, and TNFRSF1A was closely related to B cells, CD8+ T cells, CD4+ T cells, neutrophils, macrophages, and dendritic cell infiltration (Figure 8). Recent studies found that macrophages, monocytes, NK cells, and memory T lymphocytes were activated by the CCL2-CCR2 axis, thereby stimulating the release of proinflammatory cytokines such as tumor necrosis factor- (TNF-) α, interleukin-1, and interleukin-6 [17]. Moreover, macrophages were also activated by CCL2 to secrete tissue repair factors, such as transforming growth factor (TGF)–β, platelet-derived growth factor (PDGF), and vascular endothelial growth factor (VEGF) [18]. TNFRSF1A encoded a member of the TNF receptor superfamily of proteins. The encoded receptor was found in soluble and membrane-bound forms and interacted with soluble and membrane-bound forms, respectively, of its ligand, TNF-α [19, 20]. The binding of membrane-bound TNF-α to membrane-bound receptor induced receptor trimerization and activation, playing a function in cell survival, apoptosis, and inflammation. However, it needs further study how C1R, CCL2, and TNFRSF1A affect the immune infiltration of GBM cells.

The novel coronavirus disease outbreak of 2019 (COVID-19) has emerged as the world's most serious public health threat, infecting over 1.7 million people and killing over 100,000. Recent studies have shown that cancer patients are more likely to contract COVID-19 and have higher mortality rates [12]. The novel coronavirus SARS-CoV-2 binds to human angiotensin-converting enzyme II (ACE2) through its expressed S-protein and enters the cell, while ACE2 activates the expression of CCL2, and studies have also shown that the pathogenesis of COVID-19 is closely related to the excessive release of CCL2 [21–23]. Our results found that the expression levels of C1R, CCL2, and TNFRSF1A in GBM cells and patients were very high (Figure 6), and 35 gene biomarkers of immune cells were significantly correlated with C1R, CCL2, and TNFRSF1A (Supplementary Table S5). We believe that the C1R, CCL2, and TNFRSF1A genes in the

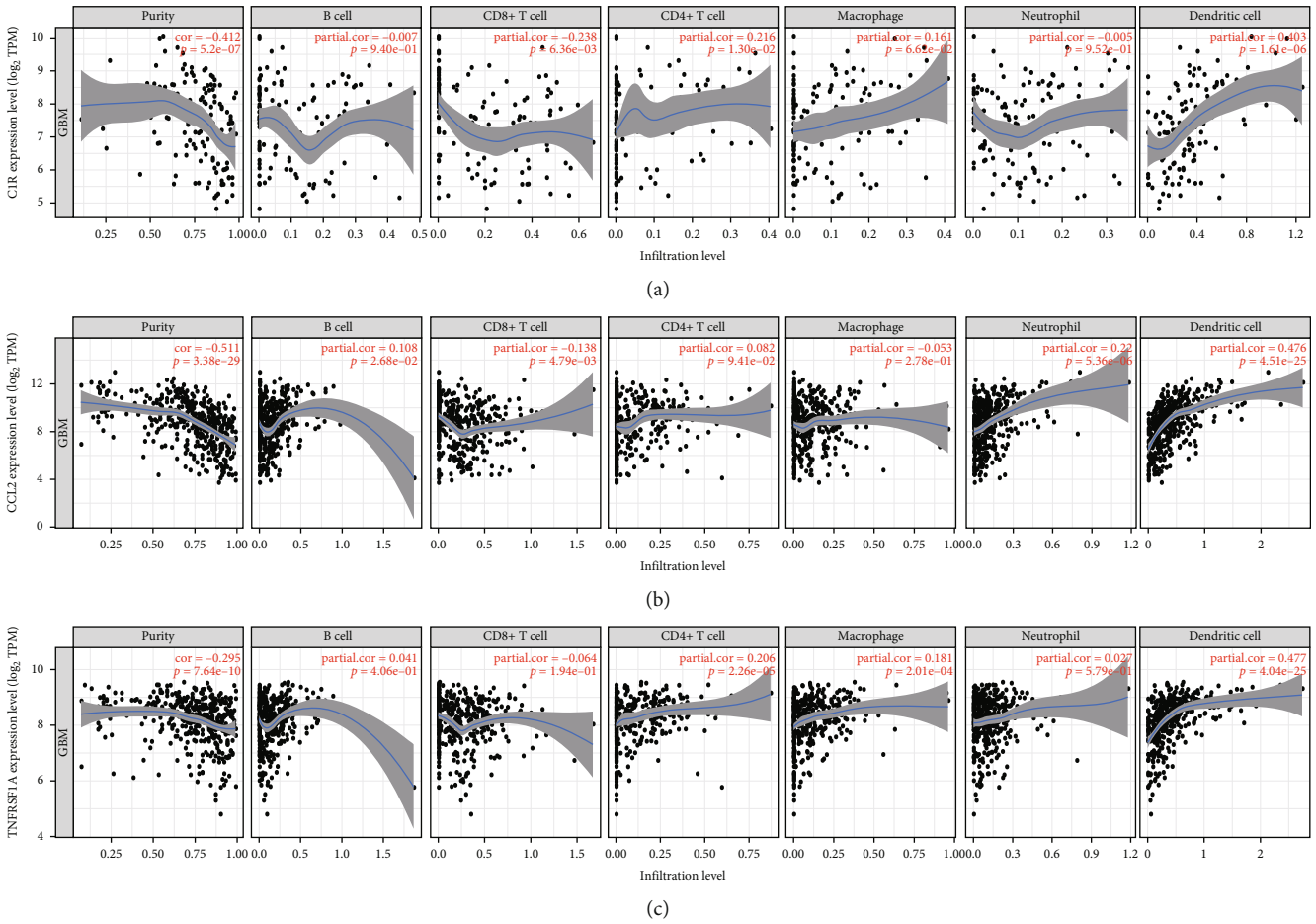

Figure 8: The correlation between three key DEGs and immune infiltration. Scatter plot showing the correlation of C1R (a), CCL2 (b), and TNFRSF1A (c) with immune cells, $^{*}P < 0.05$.

coronavirus-COVID-19 pathway may be activated in GBM patients, making GBM patients more susceptible to novel coronavirus infection. Some Chinese herbs such as quercetin and baicalin can bind to CCL2 receptor and thus act on immune response signaling pathway, tumor necrosis factor signaling pathway, and influenza A signaling pathway, which may play a dual role in anti-COVID-19 and GBM process.

4. Methods

4.1. Data Collection and DEG Screening. The GTEx (Gen Tissue Expression) database studied more than 7000 post-mortem samples from 449 previously healthy human donors, covering 44 tissues. We downloaded 1151 nontumor samples from the GTEx database to make up for the shortage of normal samples in the TCGA database and downloaded 169 GBM tumor samples and 5 nontumor samples from the TCGA database on the UCSC Xena (http://xena.ucsc.edu/) website. We used limma package of *R* software (version4.0.2) to identify DEGs between nontumor samples and GBM samples. The criteria for DEG screening were *P*.adjust <0.05.

4.2. GO and KEGG Pathway Analysis. GO analysis is a common method for functional enrichment studies on a large scale. KEGG is a database with a wide range of functions, storing rich data on biological pathways, genomes, drugs, and diseases. First, the official symbol of DEGs was converted through the org.hs.eg.db package based on *R* software (version 4.0.2). We used the Cluster Profiler package and the Go Plot package for GO and KEGG pathway analyses and cluster analyses, respectively. We used the limma package to identify the differential expression of mRNAs with $|\log($ foldchange$)| > 2$ thresholds and performed GO and KEGG analysis with the ggplot2 package in *R* software. *P*.adjust <0.05 was considered statistically significant.

4.3. Survival Analysis. According to the median value of the gene expression, we divided all samples into low and high expression groups. 169 TCGA tumor samples were evaluated for survival differences (Kaplan-Meier method) with *R* software. $P < 0.05$ was considered statistically significant.

4.4. Cell Experiments. U-87MG, U-251MG, U-118MG, and HMC3 cells (iCell Bioscience Inc., Procell Inc., Identified by STR) were cultured on DMEM medium (Gibco, Thermo Fisher Scientific, USA) supplemented with 10% fetal bovine

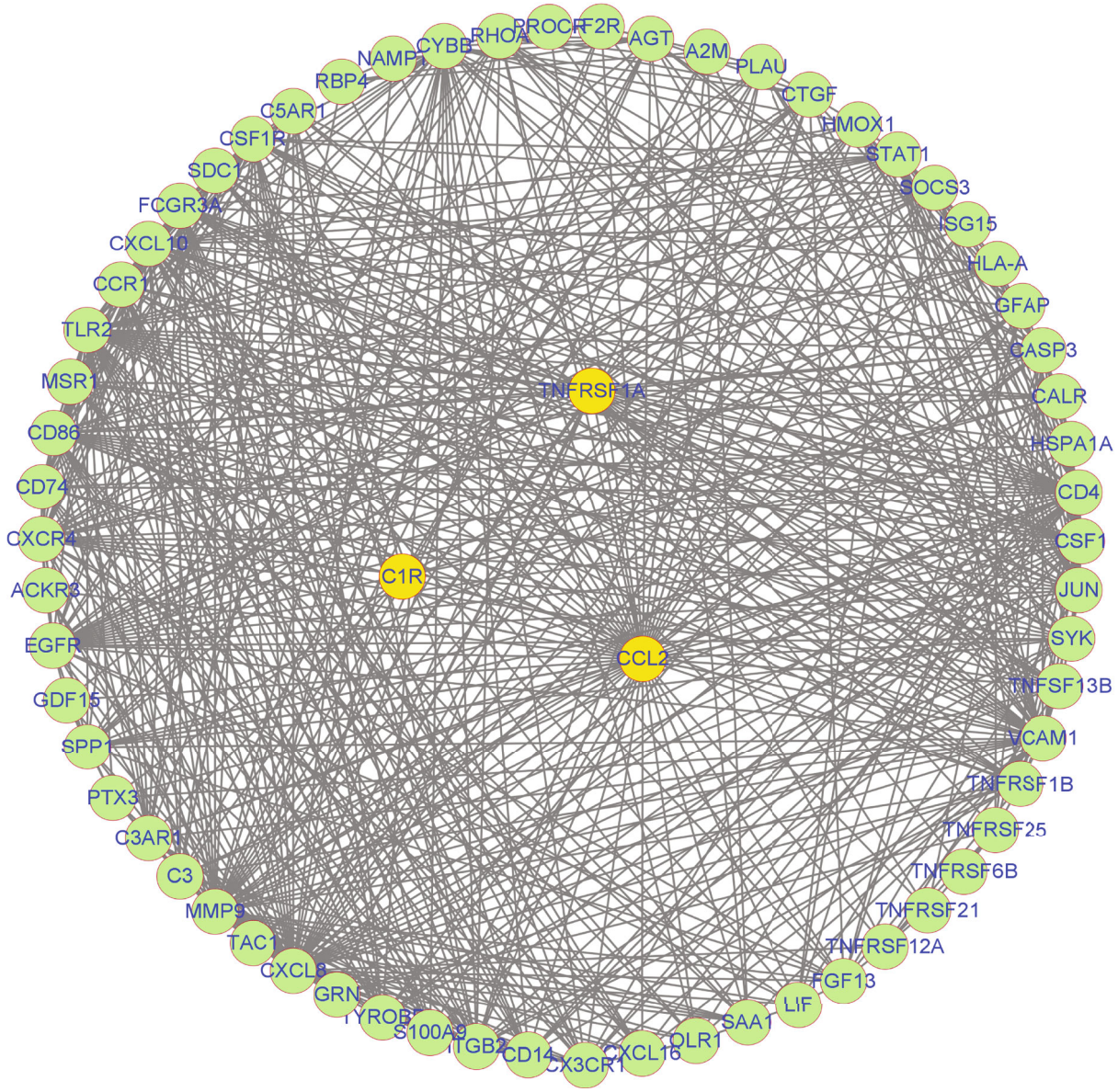

Figure 9: Construction of PPI network. Three key genes were marked with yellow circles. The interacted genes were marked with green circles.

serum (Life Technologies, USA) and 1% streptomycin and penicillin (100 μg/ml streptomycin and 100 U/ml penicillin, Life Technologies) at 37°C in 5% carbon dioxide chamber. Total RNA was extracted from cells for qRT-PCR analyses. The primers were as follows: C1R-fw: gctgcccacaccctgtatc. C1R-rv: gcccaggaacacatccaaagag. CCL2-fw: ctcgctcagccaggtaagg. CCL2-rv: actgtgggtaccacgtctgc. TNFRSF1A-fw: cctggacagaccgagtcc. TNFRSF1A-rv: ctttgtccctggtctcacc.

4.5. Immune Infiltration Analysis. The TIMER web server provides a rich resource for comprehensive analysis of immune infiltrations in different cancer types (https://cistrome.shinyapps.io/timer/). TIMER software was used to analyze the correlation between the abundance of 6 immune infiltrates and gene expression. Moreover, we used a two-sided Wilcoxon rank sum test to detect the effect of different somatic copy number changes on tumor invasion levels.

4.6. Protein–Protein Interaction Network Construction. STRING was a bioinformatics database that constructed the protein–protein interaction network (PPI) of DEGs based on the predicted and known PPIs. Subsequently, we analyzed the functional interactions among proteins and visualized the PPI network with Cytoscape software (version 3.7.2).

4.7. Statistical Analysis. All the data were processed and analyzed by the *R* software (version 4.0.2). Mann–Whitney test and *t*-test were used to compare the two groups of data and the optimal cut-off value generated by the *R* package "SURv Cutpoint" function for survival analyses. Moreover, we

divided the expression levels by dichotomy and evaluated the statistical significance of cell line experiments using the *t*-test in the GraphPad Prism version 8 software. $P < 0.05$ was considered statistically significant ($^{*}P < 0.05$, $^{**}P < 0.01$, $^{***}P < 0.001$).

Data Availability

Publicly available datasets were analyzed in this study, and these can be found in Genotype-Tissue Expression Program (https://commonfund.nih.gov/GTEx/) and The Cancer Genome Atlas Program (https://portal.gdc.cancer.gov). The authors confirm that the data supporting the findings of this study are available within the article and its Supplementary materials.

Conflicts of Interest

The authors declare no competing interests.

Authors' Contributions

Writing-original draft and bioinformatics analysis were contributed by X.W. Formal analysis and data curation were contributed by Q.W., C.J., Z.S., and Y.L. Cell experiments were contributed by Y.Z. and K.D. Supervision and project administration were contributed by G.Y. Conceptualization, writing-review and editing, and supervision were contributed by S.L. Xianggang Wang and Guohua Yang contributed equally to this work and share first authorship.

Acknowledgments

This work was supported by the National Natural Science Foundation of China (31800996), Excellent Young Talents Found Program of Higher Education Institutions of Anhui Province (gxyqZD2018061), and Anhui Province Innovation and Entrepreneurship Training Program for College Students (S202110367057).

Supplementary Materials

Supplementary Information. The online version contains supplementary material available at Supplementary Figure S1: C1R, CCL2, and TNFRSF1A expression levels in the GBM and normal issues with GEPIA online tool: (a) C1R, (b) CCL2, and (c) TNFRSF1A. Supplementary Figure S2: the correlation between C1R, CCL2, and TNFRSF1A with GEPIA online tool. (a) C1R and TNFRSF1A, (b) C1R and CCL2, (c) CCL2 and TNFRSF1A. Supplementary Table S1: the correlation between the expression level of other DEGs and the survival rate of glioma patients. Supplementary Table S2: the 1923 DEGs between GBM samples and nontumor samples. Supplementary Table S3: the C1R, CCL2, and TNFRSF1A expression levels with the normal and GBM tissues. Supplementary Table S4: the 62 nodes interacting with C1R, CCL2, and TNFRSF1A. Supplementary Table S5: the correlation between three key DEGs and gene biomarkers of immune cells in GBM. *(Supplementary Materials)*

References

[1] B. Campos, L. R. Olsen, T. Urup, and H. S. Poulsen, "A comprehensive profile of recurrent glioblastoma," *Oncogene*, vol. 35, no. 45, pp. 5819–5825, 2016.

[2] R. Batash, N. Asna, P. Schaffer, N. Francis, and M. Schaffer, "Glioblastoma multiforme, diagnosis and treatment; recent literature review," *Current Medicinal Chemistry*, vol. 24, no. 27, pp. 3002–3009, 2017.

[3] D. Tang, X. Zhao, L. Zhang, Z. Wang, and C. Wang, "Identification of hub genes to regulate breast cancer metastasis to brain by bioinformatics analyses," *Journal of Cellular Biochemistry*, vol. 120, no. 6, pp. 9522–9531, 2019.

[4] M. Gao, W. Kong, Z. Huang, and Z. Xie, "Identification of key genes related to lung squamous cell carcinoma using bioinformatics analysis," *International Journal of Molecular Sciences*, vol. 21, no. 8, p. 2994, 2020.

[5] S. Huang, Z. Song, T. Zhang et al., "Identification of immune cell infiltration and immune-related genes in the tumor microenvironment of glioblastomas," *Frontiers in Immunology*, vol. 11, article 585034, 2020.

[6] C. H. Jiang, X. Yuan, J. F. Li et al., "Bioinformatics-based screening of key genes for transformation of liver cirrhosis to hepatocellular carcinoma," *Journal of Translational Medicine*, vol. 18, no. 1, p. 40, 2020.

[7] H. Liu, Y. Gao, S. Hu, Z. Fan, X. Wang, and S. Li, "Bioinformatics analysis of differentially expressed rhythm genes in liver hepatocellular carcinoma," *Frontiers in Genetics*, vol. 12, article 680528, 2021.

[8] X. Li, Y. Gao, Z. Xu, Z. Zhang, Y. Zheng, and F. Qi, "Identification of prognostic genes in adrenocortical carcinoma microenvironment based on bioinformatic methods," *Cancer Medicine*, vol. 9, no. 3, pp. 1161–1172, 2020.

[9] M. M. Grabowski, E. W. Sankey, K. J. Ryan et al., "Immune suppression in gliomas," *Journal of Neuro-Oncology*, vol. 151, no. 1, pp. 3–12, 2021.

[10] S. Gangadevi, V. N. Badavath, A. Thakur et al., "Kobophenol a inhibits binding of host ACE2 receptor with spike RBD domain of SARS-CoV-2, a lead compound for blocking COVID-19," *Journal of Physical Chemistry Letters*, vol. 12, no. 7, pp. 1793–1802, 2021.

[11] A. Song, Y. Wu, W. Chu et al., "Involvement of miR-619-5p in resistance to cisplatin by regulating ATXN3 in oral squamous cell carcinoma," *International Journal of Biological Sciences*, vol. 17, no. 2, pp. 430–447, 2021.

[12] R. Gosain, Y. Abdou, A. Singh, N. Rana, I. Puzanov, and M. S. Ernstoff, "COVID-19 and cancer: a comprehensive review," *Current Oncology Reports*, vol. 22, no. 5, p. 53, 2020.

[13] H. Yang, Q. Zhang, M. Xu et al., "CCL2-CCR2 axis recruits tumor associated macrophages to induce immune evasion through PD-1 signaling in esophageal carcinogenesis," *Molecular Cancer*, vol. 19, no. 1, 2020.

[14] L. Fei, X. Ren, H. Yu, and Y. Zhan, "Targeting the CCL2/CCR2 axis in cancer immunotherapy: one stone, three birds?," *Frontiers in Immunology*, vol. 12, article 771210, 2021.

[15] S. Kadomoto, K. Izumi, and A. Mizokami, "Roles of CCL2-CCR2 axis in the tumor microenvironment," *International Journal of Molecular Sciences*, vol. 22, no. 16, p. 8530, 2021.

[16] C. Zhou, C. Li, S. Peng, L. Zhou, and H. Li, "Comprehensive analysis of the relationships between tumor mutation burden

with immune infiltrates in cervical cell carcinoma," *Frontiers in Molecular Biosciences*, vol. 7, article 582911, 2020.

[17] S. L. Deshmane, S. Kremlev, S. Amini, and B. E. Sawaya, "Monocyte chemoattractant protein-1 (MCP-1): an overview," *Journal of Interferon & Cytokine Research*, vol. 29, no. 6, pp. 313–326, 2009.

[18] S. Dommel and M. Bluher, "Does C-C motif chemokine ligand 2 (CCL2) link obesity to a pro-inflammatory state?," *International Journal of Molecular Sciences*, vol. 22, no. 3, p. 1500, 2021.

[19] R. Abdwani, E. Abdalla, S. Al Abrawi, and K. Al-Thihli, "TNFRSF1A gene causing tumor necrosis factor receptor-associated periodic syndrome in 2 siblings displaying variable disease severity and discordant heterozygosity for an MEFV E148Q variant," *The Journal of Rheumatology*, vol. 42, no. 8, pp. 1534-1535, 2015.

[20] S. P. Egusquiaguirre, J. E. Yeh, S. R. Walker, S. Liu, and D. A. Frank, "The STAT3 target gene TNFRSF1A modulates the NF-κB pathway in breast cancer cells," *Neoplasia*, vol. 20, no. 5, pp. 489–498, 2018.

[21] M. Hoffmann, H. Kleine-Weber, S. Schroeder, N. Krüger, and S. Phlmann, "SARS-CoV-2 cell entry depends on ACE2 and TMPRSS2 and is blocked by a clinically proven protease inhibitor," *Cell*, vol. 181, no. 2, pp. 271–280.e8, 2020.

[22] Y. Xiong, Y. Liu, L. Cao et al., "Transcriptomic characteristics of bronchoalveolar lavage fluid and peripheral blood mononuclear cells in COVID-19 patients," *Emerging Microbes and Infections*, vol. 9, pp. 761–770, 2020.

[23] I. Y. Chen, S. C. Chang, H. Y. Wu et al., "Upregulation of the chemokine (C-C motif) ligand 2 via a severe acute respiratory syndrome coronavirus spike-ACE2 signaling pathway," *Journal of Virology*, vol. 84, no. 15, pp. 7703–7712, 2010.

Hindawi
Disease Markers
Volume 2023, Article ID 9813418, 1 page
https://doi.org/10.1155/2023/9813418

Retraction

Retracted: Association between Mutation in SMARCAD1 and Basan Syndrome with Cutaneous Squamous Cell Carcinoma

Disease Markers

Received 20 June 2023; Accepted 20 June 2023; Published 21 June 2023

This article has been retracted by Hindawi following an investigation undertaken by the publisher [1]. This investigation has uncovered evidence of one or more of the following indicators of systematic manipulation of the publication process:

(1) Discrepancies in scope

(2) Discrepancies in the description of the research reported

(3) Discrepancies between the availability of data and the research described

(4) Inappropriate citations

(5) Incoherent, meaningless and/or irrelevant content included in the article

(6) Peer-review manipulation

The presence of these indicators undermines our confidence in the integrity of the article's content and we cannot, therefore, vouch for its reliability. Please note that this notice is intended solely to alert readers that the content of this article is unreliable. We have not investigated whether authors were aware of or involved in the systematic manipulation of the publication process.

In addition, our investigation has also shown that one or more of the following human-subject reporting requirements has not been met in this article: ethical approval by an Institutional Review Board (IRB) committee or equivalent, patient/participant consent to participate, and/or agreement to publish patient/participant details (where relevant).

Wiley and Hindawi regrets that the usual quality checks did not identify these issues before publication and have since put additional measures in place to safeguard research integrity.

We wish to credit our own Research Integrity and Research Publishing teams and anonymous and named external researchers and research integrity experts for contributing to this investigation.

The corresponding author, as the representative of all authors, has been given the opportunity to register their agreement or disagreement to this retraction. We have kept a record of any response received.

References

[1] Y. Xiong, T. Chen, J. Yu et al., "Association between Mutation in SMARCAD1 and Basan Syndrome with Cutaneous Squamous Cell Carcinoma," *Disease Markers*, vol. 2022, Article ID 7840710, 9 pages, 2022.

Hindawi
Disease Markers
Volume 2022, Article ID 7840710, 9 pages
https://doi.org/10.1155/2022/7840710

Research Article

Association between Mutation in SMARCAD1 and Basan Syndrome with Cutaneous Squamous Cell Carcinoma

Ying Xiong,[1] **Ting Chen**,[1] **Jia Yu**,[1] **He Zhou**,[2,3] **Baozhen Lu**,[1] **Lijie Chen**,[1] **Liwei Sun**,[1] **Can Wang**,[2,3] **Sujun Li**,[2,3,4] **and Bo Wu**[1]

[1]*Department of Dermatology, Affiliated Shenzhen Maternity & Child Healthcare Hospital, Southern Medical University, Shenzhen, Guangdong, China*
[2]*Shenzhen Mass Medical Co., Ltd., Shenzhen, Guangdong, China*
[3]*Shenzhen Dengding Biopharma Co., Ltd., Shenzhen, Guangdong, China*
[4]*Translational Medicine Institute of Jiangxi, The First Affiliated Hospital of Nanchang University, Nanchang, Jiangxi, China*

Correspondence should be addressed to Sujun Li; lisujun@gmail.com and Bo Wu; bowu2004@hotmail.com

Received 27 February 2022; Revised 5 April 2022; Accepted 20 April 2022; Published 10 May 2022

Academic Editor: Xianwei Zeng

Background. Basan syndrome is a rare autosomal-dominant ectodermal dysplasia with certain clinic-pathological features caused by mutations in the SMARCAD1 gene. Currently, no skin malignancy related to Basan syndrome has been reported. This study was aimed at identifying related gene mutations in a new Chinese pedigree with Basan syndrome and discovering the possible association between Basan syndrome and cutaneous squamous cell carcinoma (cSCC). *Methods.* We report a case of Basan syndrome from China with family history of cSCC. The pedigree contains 28 individuals. Among them, 12 members had Basan syndrome, while 4 affected members were diagnosed with cSCC in the 1st and 2nd generations. Whole exome sequencing (WES) and Sanger sequencing were performed for 7 available individuals. The specific gene mutation on pre-mRNA splicing was also analyzed using *in vitro* Minigene assay. In addition, sequencing data was analyzed with bioinformatics workflow, aiming to discover the gene associated with cSCC. *Results.* Gene sequencing results showed a heterozygous mutation, c.378+5G>A, in the SMARCAD1 gene in all tested individuals with Basan syndrome. Minigene result implicated the specific mutation may cause splicing variations by exon skipping occurring in the targeted exons. *Conclusion*. To the best of our knowledge, this is the first study reported Basan syndrome with family history of cSCC. Despite in this study we cannot draw any conclusion about the association between Basan syndrome and cSCC at the genetic level, this study encourages future works to substantiate this potential but important issue.

1. Introduction

Basan syndrome is a rare autosomal-dominant ectodermal dysplasia. After the individual is born, the major clinical manifestations of this disease include facial multiple eruptive milia, palmoplantar blisters and keratoderma, no sweat or fingerprint in the palmoplantar region, and onychodystrophy. The first pedigree with Basan syndrome, an Irish American family, was reported by Dr. Baird in 1964 [1]. As at 2021, only about 14 cases had been documented in literature [1–12].

Basan syndrome is caused by a mutation in the SMARCAD1 gene. By using the first-generation sequencing, Marks et al. detected a heterozygous mutation in the SMARCAD1 gene: c.378+3A>T. They believed this gene is likely to be the pathogenic gene of Basan syndrome [5]. In 2016, Dr. Li's team in China discovered a new gene site, c.378 +1G>T, in a Chinese family with Basan syndrome using

Figure 1: Clinical presentation of the proband and her father: (a) multiple eruptive milia appeared on the chin when the proband was born; (b) hyperkeratosis, skin atrophy, and mild pigmentation in the palmar region of the proband; (c) tapering of fingers and no fingerprint in the extremity of the proband's father; (d) longitudinal ridges of nails of the proband's father; and (e) obvious hyperkeratosis in the plantar region of the proband's father.

whole genome sequencing [6]. In 2017 and 2018, Chang et al. and Valentin et al. discovered mutations at new gene sites: c.378+5G>A and c.378+2T>G [2, 7]. It is worth noting that all 4 mutations mentioned above are at the same conservative splicing site in the SMARCAD1 gene. It is difficult to demonstrate any difference of those segregated mutations by simulating the real-world situation in vitro [5, 13]. However, less is known about the mechanism of splice site mutations of SMARCAD1 gene.

Now, we are reporting a new Chinese pedigree with Basan syndrome and family history of cutaneous squamous cell carcinoma (cSCC). To the best of our knowledge, no previous study has found the correlation between Basan syndrome and malignant cutaneous tumors. We aimed to identify pathogenic gene mutations in Basan syndrome and try to discover the possible association between Basan syndrome and cSCC.

2. Methods

The study was approved by the IRB of the Affiliated Shenzhen Maternity & Child Healthcare Hospital, Southern Medical University with case ID "Shenzhen Maternity & Child Healthcare Hospital Academic Review (2021) No. 43." Written consent forms were acquired from all participated family members.

2.1. Proband. The proband is a female aged 1 year and 4 months. At the time the proband was born, she exhibited facial multiple eruptive milia, mostly concentrating on the chin (Figure 1(a)). One week later, small (rice-sized) scattered blisters appeared at the end of hands and feet. The majority of blisters were in the palmoplantar region. A few small blisters also fused into larger ones. Later, blisters on hands and feet gradually ruptured and healed, while mild hyperpigmentation and skin atrophy gradually emerged. The proband exhibited no sweat or fingerprint on hands and feet. At the same time, hyperkeratosis, skin atrophy, and mild pigmentation in the palmar-plantar region can be observed (Figure 1(b)).

2.2. Pedigree Investigation. Several family members of the proband had the similar rash, including the father, grandfather, and great-grandfather. Figure 1 shows lack of fingerprint (Figure 1(c)), longitudinal ridges of nails (Figure 1(d)), and obvious hyperkeratosis in the plantar region of the proband's father (Figure 1(e)).

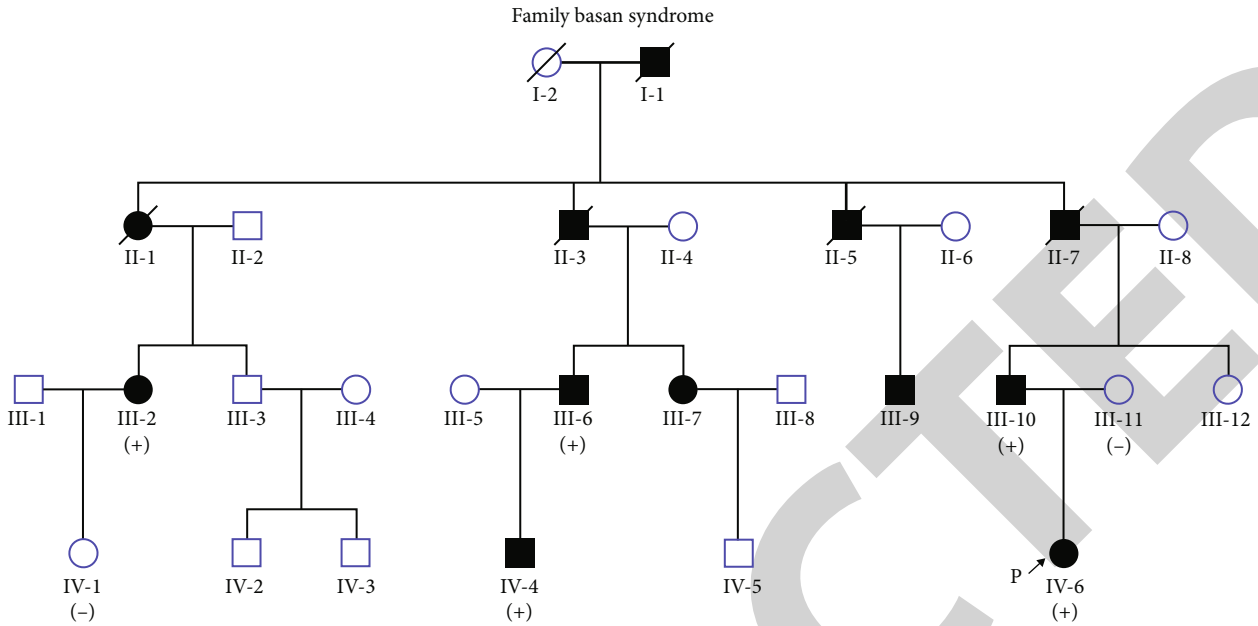

Figure 2: Pedigree chart. Individuals highlighted in black had Basan syndrome. (+) indicates the mutation in the SMARCAD1 gene had been confirmed by Sanger sequencing. (-) indicates no mutation in the SMARCAD1 gene was detected by Sanger sequencing.

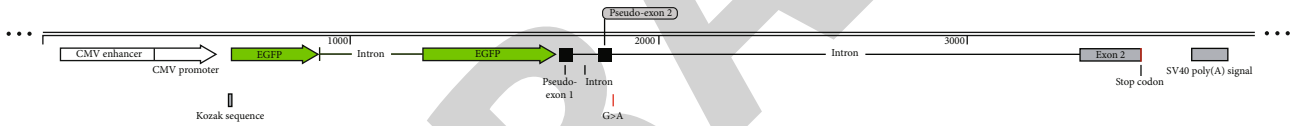

Figure 3: An illustration of plasmid construction. Pseudoexon 1 and pseudoexon 2 were introduced exogenously to construct the Minigene.

We investigated 4 generations in the proband's family. With the approval of the Institutional Review Board and consents of the proband's parents and other family members, we obtained 7 individuals' blood samples for genetic tests, including the proband, the parents, and 4 other family members (Figure 2, III-2, III-6, III-10, III-11, IV-1, IV-4, and IV-6).

2.3. Whole Exome Sequencing (WES) and Sanger Sequencing. Several previous studies have revealed the pathogenic gene of Basan syndrome: the SMARCAD1 gene [2, 5–7]. Therefore, in this study, we also targeted on this gene. We used the Berry Custom Design V2 to capture and enrich the target gene exons and adjacent splicing regions. We performed the sequencing on the NovaSeq 6000 platform. The raw data yielded 15.75 GB. The average depth of the target region was 117.77×. We designed specific primers for the exons where a mutation at the candidate pathogenic gene site is located. We also performed Sanger sequencing for the target gene. Chromas software was employed to analyze sequencing peaks.

2.4. Sequencing Analysis Workflow. We used the Trimmomatic software to filter the raw data. Then, we used the GRCh38 genome as the reference genome. BWA was employed to map the clean reads. The GATK was used for variant discovery. We performed the germline variant calling and variant filtering by germline short variant discovery in the GATK package. Finally, Founctator was employed for variants annotations.

2.5. Minigene

2.5.1. Plasmid Construction. In vitro Minigene splicing assay was carried out to verify the impact of the mutation on the splicing process. We used the genomic DNA of the proband or other normal family members as a template. Because the mutation is located after exon 1 of the SMARCAD1 gene and exon 1 does not encode, we directly used intron 1 and exon 2 in construction. In order to better simulate the real gene and ensure the constructed gene would not be misidentified, we added pseudoexon 1 and pseudoexon 2 in intron 1 (Figure 3).

The pseudoexon 1's sequence was ggagccaaaggtgaccgaggactgccagggccgcgaggcgagaag. The intron 1's sequence was gtgaggtgggttggccctggggcctgactactgagcagagaaggctcagtccagacacccctcacctgccattctgtgcag. The pseudoexon 2's sequence was ggtgaagctggccgtgcaggggagcccggagaccctggggaagat.

2.5.2. PCR Amplification. PCR amplification reaction was performed by the PrimeSTAR® with GXL DNA Polymerase reagent instruction and digested with vector XhoI/EcoRI.

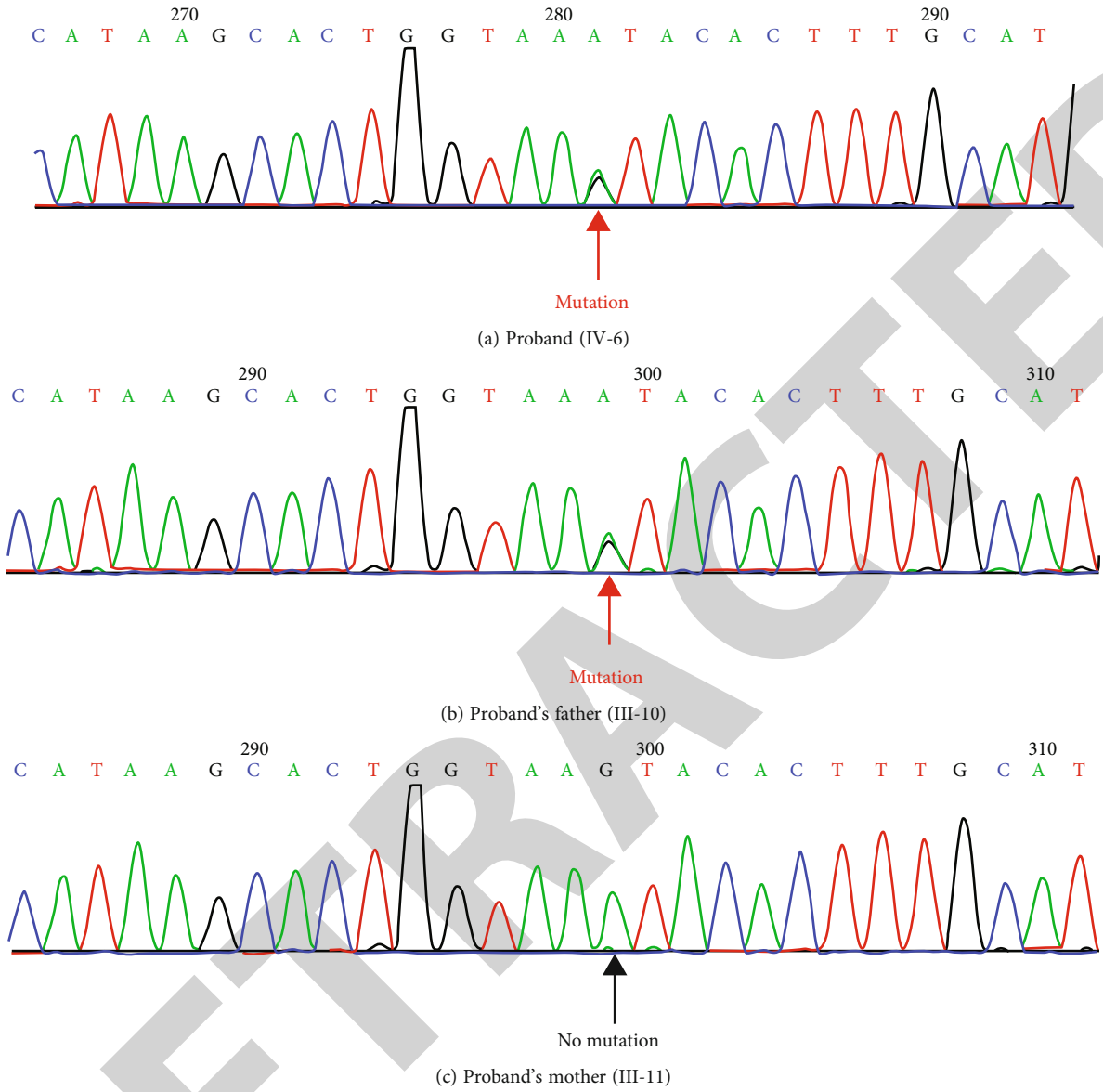

Figure 4: Sanger sequencing result of the pathogenic mutant gene of the (a) proband, (b) proband's father, and (c) proband's mother.

We performed the recombination reaction according to the Hieff Clone™ Plus One Step Cloning Kit. We delivered the bacteria solution, which contains recombinant cloned products, to the Shanghai Genassistant Biotechnology Company Ltd. for sequencing. We obtained the wild-type plasmid pMini-SMARCAD1-WT and the mutant plasmid pMini-SMARCAD1-MUT by selecting monoclonal colonies and performing plasmid extraction.

2.5.3. Cell Transfection and Transcript Sequencing. Empty vector plasmids as well as wild-type and mutant type SMARCAD1 plasmids were transfected into 293 T cells. Cell observation was made under fluorescence microscope in 48 hours. After the transfection succeed, the cells were collected. Twice rinses were performed with precooled PBS. We added lytic cells and, after 30 minutes, performed RNA extraction and reverse transcription. PCR and electrophoresis were performed. We performed sequencing on the wild-type and mutant PCR products and analyzed differences in splicing.

3. Results

3.1. Pedigree Investigation. Among 28 family members (4 generations), there were total 12 individuals exhibiting a consistent skin phenotype (Figure 1). All affected individuals in this pedigree presented multiple milia on face at birth, which disappeared within 6 months. The recurrent blisters in extremities started at first month, which self-healed within a week and finally disappeared within a year. But after that, palmoplantar hyperkeratosis appeared and became more and more obvious along with the increasing in age (Figure 1(e)). With time, tapering of fingers and longitudinal ridges of nails gradually appeared (Figures 1(c) and 1(d)). No fingerprint could be seen in extremities and all the

Table 1: Whole exome sequencing results.

	III-6	III-10	III-11	IV-1	IV-4	IV-6
Raw data base (GB)	14.98	18.48	13.13	16.31	14.76	12.88
Raw data reads	149,843,780	184,800,454	131,389,028	163,159,766	147,678,418	128,884,472
Clean data base (GB)	14.77	18.21	12.9	16.13	14.55	12.65
Clean data reads	148,997,060	183700867	130,066,438	162,540,046	146,819,461	127,529,011
Target reads	100,052,692	123,297,215	84,700,803	109,486,188	99062265	83,651,114
Fraction of target reads in mapped results	67.15%	67.12%	65.12%	67.36%	67.48%	65.59%
Average depth	160.22	193.60	136.44	176.87	157.72	136.29
Coverage (≥4x)	98.42%	98.43%	98.27%	98.24%	98.42%	98.24%
Coverage (≥10x)	98.29%	98.28%	98.09%	98.08%	98.23%	98.06%
Coverage (≥30x)	97.40%	97.23%	96.62%	96.95%	96.74%	96.45%
Coverage (≥100x)	80.17%	82.85%	70.65%	80.84%	77.43%	69.84%

Table 2: SMARCAD1 mapped reads.

	III-6	III-10	III-11	IV-1	IV-4	IV-6
SMARCAD1						
Ref-depth	92	90	132	135	70	50
Alt-depth	63	60	0	0	66	54
AF	0.406	0.400	0	0	0.485	0.519

affected individuals exhibited no or less sweat in hands and feet. Hairs and teeth were normal. Consanguineous marriage was denied.

According to the family history inquiry, among the 5 individuals who have passed away in the 1st and 2nd generation, only 1 individual (II-5) died of brain stroke with obesity, hypertension, and gout at the age of 54, while the remaining 4 individuals died of multiple metastases of finger cSCC. II-7 was a tailor. He had several years' history of dorsal digital skin ulcer but never sought for any medical treatment. He finally visited the hospital due to the severe deterioration of the ulcer (finger bone exposing). He took a skin biopsy and was diagnosed as cSCC. He was hospitalized for a finger amputation in Zhuhai People's Hospital in 2010. Although underwent standard chemotherapy, 2 years later, he died of multiple metastasis including lung metastasis and spinal metastasis at 51 years old. II-3, born in 1959, was a blue-collar worker. He was admitted to Tongji Hospital for a nonhealing ulcer of the dorsal finger in 2012. A pathological diagnosis of cSCC was made after the skin biopsy. Axillary metastasis emerged soon after surgical resection of the tumor. Finally, he died of uncontrollable bleeding from axillary metastatic tumor at 57 years old. Two other family members (I-1 and II-1, an accountant and a blue-collar worker) had similar experience and died due to massive bleeding of axillary metastatic tumor at the ages 36 and 45, respectively.

3.2. Mutation in the SMARCAD1 Gene. To identify the underlying pathological gene, we performed WES for the proband (IV-6). A heterozygous mutation in the SMARCAD1 gene NM_001254949.2: c.-10+5G>A (if counting from the beginning of the noncoding exon 1, this mutation would be named as c.378+5G>A) was identified. The WES result was further confirmed by Sanger sequencing (Figure 4(a)).

Sanger sequencing was also performed for III-2, III-6, III-10, III-11, IV-1, and IV-4. As shown in the pedigree chart (Figure 2), (+) indicates the mutation has been confirmed by Sanger sequencing. (-) indicates no mutation was detected by Sanger sequencing. III-2, III-6, III-10, and IV-4 were clinically diagnosed with Basan syndrome. They were also confirmed carrying the same mutation by Sanger sequencing. Figure 4(b) illustrates the mutation of the proband's father (III-10). III-11 and IV-1 did not carry this mutation, while no Basan syndrome was diagnosed. Figure 4(c) illustrates that the mutation was not discovered in the proband's mother (III-11). This revealed that the mutation cosegregated with Basan syndrome in this pedigree. Bioinformatics analysis showed that this mutation was not detected in the 1000 genome database, ExAC databases, or gnomAD database.

3.3. WES Results

3.3.1. Quality of the WES Data. One of the 7 collected blood samples (III-2) was contaminated due to misoperation before performing WES. Therefore, WES was performed for only 6 individuals. Table 1 summarizes the results. All of the 6 samples had a coverage higher than 98% at 4X. The average depth was 160.22 for III-6, 193.60 for III-10, 136.44 for III-11, 176.87 for IV-1, 157.72 for IV-4, and 136.29 for IV-6. In summary, the sequencing data had reached the required quality for next step analysis.

3.3.2. SMARCAD1 and Other Gene Mutation Analyses in WES. Based on the WES data, we performed target analysis for the SMARCAD1 gene to further confirm the association between SMARCAD1 and Basan syndrome. As shown in Table 2, all Basan syndrome patients carried the mutation SMARCAD1, chr4: 94253676G>A. Specifically, III-6 had 63 reads mapped to SMARCAD1 variant with a frequency of 0.406; III-10 had 60 reads mapped with a frequency of 0.400; IV-4 had 66 reads mapped with a frequency of

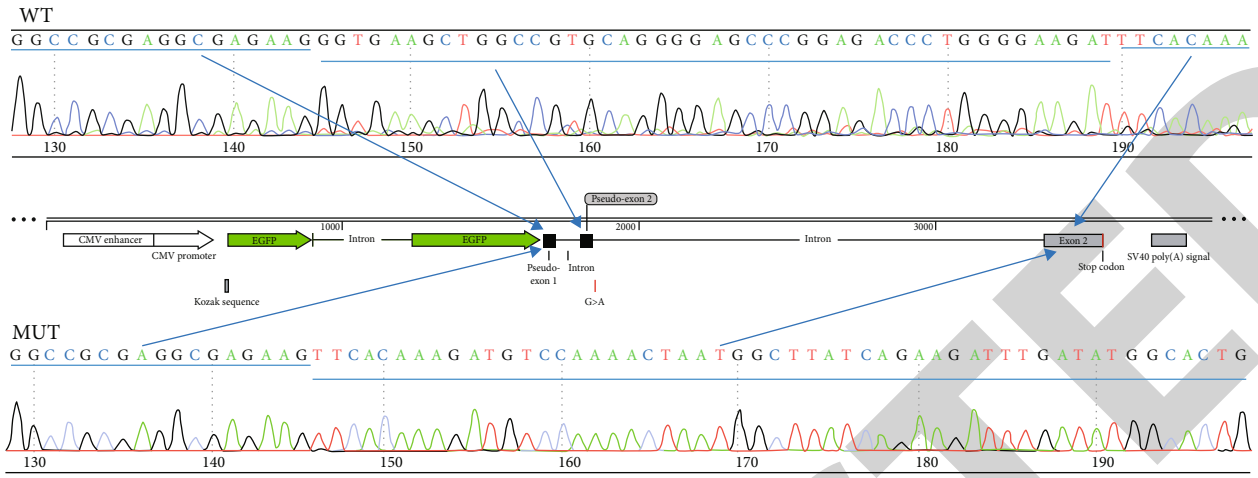

Figure 5: An illustration of Minigene analysis.

0.485; and IV-6 had 54 reads mapped with a frequency of 0.519. Other family member who was not diagnosed with Basan syndrome did not carry this mutation.

As described above, the family history revealed 4 affected members with cSCC in the 1st and 2nd generations. This family exhibited high cooccurrence rate between Basan syndrome and cSCC. To discover the potential highly related gene mutations, we further investigated WES results in the ClinVar database and COSMIC database, aiming for cancer-related gene mutations. Due to the limited samples available, we set out to apply strict filtering criteria for finding possible associated gene mutations. The criteria only kept mutations occurring in the four individuals with Basan syndrome (III-6, III-10, IV-4, and IV-6) but not in other two non-Basan individuals (III-11 and IV-1). The results from the filtering criteria retained 3434 mutations. Out of these 3434 mutations, only one mutation, rs751141, was mapped to the ClinVar database. The annotation of rs751141 shows that it is a risk factor related to "hypercholesterolemia, familial."

The above-mentioned 3434 mutations were then mapped in the COSMIC database. In order to find more significance related to the FAMILIAL cancer, we only retained the exonic area and presented as "nonsynonymous" or "frameshift." After filtering, three genetic variants appeared in individuals with Basan syndrome but not in non-Basan individuals: rs3085861 (SETBP1), rs663651 (SETBP1), and rs2454206 (TET2). Both SETBP1 gene and TET2 gene have been reported associating with skin cancers, including cSCC [14]. However, according to dbSNP, all of the three genetic variants observed in this study are common variants.

3.3.3. Functional Analysis. Minigene was preformed to further analyze the SMARCAD1 pre-mRNA splicing. We constructed a Minigene containing genomic sequence from intron 1, pseudoexon 1, pseudoexon 2, and exon 2. Our data indicated that the mutation in the SMARCAD1 gene site can lead to splicing variations: pseudoexon 1, pseudoexon 2, and exon 2 were all detected in the wild type, but pseudoexon 2 was skipped in the mutation type (Figure 5). This mutation was located in the intron 1. No other potential splicing site was found. The Minigene result demonstrated that this mutation in intron 1 may cause the gene-splicing variation. Contrarily, no mutation in the intron (wild-type) exhibited normal expression of pseudoexon 1, pseudoexon 2, or exon 2.

4. Discussion

In this study, we reported a new Chinese pedigree with Basan syndrome and family history of cSCC. We identified the pathogenic mutation site in the SMARCAD1 gene. To the best of our knowledge, this is the 15th Basan syndrome case reported in the world, and the first reported Basan syndrome pedigree with history of cSCC.

The mode of inheritance in the pedigree reported here is autosomal-dominant inheritance. Its clinical symptoms are in line with the typical clinical manifestations of Basan syndrome, which belongs to the supporting evidence (PP4). Its mutation site is c.378+5G>A in SMARCAD1, which is identical to the case of Basan syndrome reported in Chang [7]. This mutation site has not been reported in the public databases of human mutation, such as ExAC, 1000G, and gnomAD. It is a rare mutation and belongs to the moderate pathogenicity evidence (PM2). This mutation was detected in multiple patients in the family, which belongs to the supporting evidence (PP1-Moderate). With the verification by Minigene, we found that it may cause splicing variation, which belongs to the strong pathogenicity evidence (PS3-Moderate). According to the Genetic Variant Classification published by the American College of Medical Genetics and Genomics (ACMG), this mutation type should be classified as a potential pathogenicity to Basan syndrome.

SMARCAD1 is a member of the chromatin remodeling ATPase of SNF2 helicase superfamily, located at 4q22 [2]. It is widely expressed in 27 normal human tissues, including thyroid, testis, and skin [15]. It has been discovered that the SMARCAD1 gene has two isoforms with different transcription starting sites. The long isoform contains 24 exons expressed. It encodes 1028 amino acid proteins. It is widely

Table 3: Summary of phenotypes and mutation types related to mutations in the SMARCAD1 gene.

Reference	Adermatoglyphia			Basan syndrome			Huriez syndrome
	2011 Burger [22]	2014 Mark [5]	2018 Valentin [2]	2016 Li [6]	2018 Chang [7]	Pedigree reported in this study	2021 Loh [19]
Milia on the chin	—	+	+	+	++	+	—
Nonfingerprint	+	+	+	+	++	+	+
Finger flexion contracture	+	—	—	+	++	Mild	+
Blisters or erosions	—	+	+	+	++	+	—
Hyperkeratosis at the pressured palmoplantar area	+	—	+	2/8	—	+	+
Nail disease	—	—	—	Onychodystrophy 1/8	—	Longitudinal ridges	Longitudinal ridge and hypoplasia, thin fingers
Palmoplantar pigmentation spots	—	—	+	5/8	—	Mild	—
Less or no sweat	+	++	—	+	—	+	+
Other clinical manifestations	—	—	—	Knuckle pads 7/8	Bilateral syndactyly	Tapering of the fingers	Scleroatrophy of the hands, tapering of the fingers, and poikiloderma of the nose
Autosomal-dominant inheritance	+	+	No family history	+	++	+	+
Mutation types in the SMARCAD1 gene	c.378+1G>T [18] c.378+1G>A c.378+2T>C c.378+5G>C [16]	c.378 +3A>T	c.378 +2T>G	c.378+1G>T	45-kb heterozygous deletion (chr4:95,129,542-95,174,582), c.378 +5G>A	c.378+5G>A	NC_000004.12:g.94252297_94253585del [19] c.378+2T>C, c.378+2_3insT [25], c.363_378+2 del [25]

expressed at a low level. The short isoform, as known as the skin-specific isoform, is mostly expressed on skin fibroblasts and keratinocytes [7]. SMARCAD1 is a transcription factor. It participates in many biological processes. It may be involved in dermatoglyph and sweat gland development by regulating the expression of epidermal differentiation-associated genes [16]. In addition, it also plays an import role in repairing potentially lethal DNA double-strand breaks [13] and maintaining genome integrity by stabilizing active replication [17]. Multiple studies have demonstrated that break points and mutations of the gene are involved in several human diseases, such as genodermatosis [5, 18, 19], malignant peripheral nerve sheath tumors [20], breast cancer [17], and pancreatic cancer [21].

Besides Basan syndrome, there are two other phenotypes of genodermatosis related to the SMARCAD1 gene: adermatoglyphia and Huriez syndrome. Adermatoglyphia (OMIM: 136000) is clinically characterized by no fingerprint, mildly clubbed finger, and less or no sweat on the palmoplantar due to decreased number of sweat glands [22]. Mutations (c.378 +1G>T, c.378+2T>C, c.378+5G>C, and c.378+1G>A) in the SMARCAD1 gene were found to be associated with this disease [16, 18]. Huriez syndrome (OMIM: 181600) is another rare autosomal-dominant genodermatosis, which shows three serial clinical manifestations: congenital sclerosis and atrophy at the end of extremities, palmoplantar keratoderma, and nail dysplasia. One feature of this disease is the risk of 15% to develop aggressive cSCC in the affected skin region at age 30 to 50 [23]. The cSCC in Huriez syndrome seems to be more aggressive and more likely to develop metastases than usual cSCC [24]. Huriez syndrome was first recognized in 1963 by Huriez and coworkers. But the causative SMARCAD1 gene was only characterized for a few years due to the rarity of the disease [25]. Till now, related mutation sites, including c.378+2T>C, c.378+2_3insT, c.363_378+2del, and NC_000004.12:g.94252297_94253585del, were screened in the SMARCAD1 gene [19, 25].

From the perspective of clinical characteristics (listed in Table 3), adermatoglyphia, Basan syndrome, and Huriez syndrome have similarities: mild palmoplantar keratoderma, less or no sweat in the palmoplantar region, and finger flexion contracture. However, clinical manifestations of adermatoglyphia do not include blister or milia. Patients with adermatoglyphia have normal nails. For Basan syndrome, patients are vulnerable to milia and blisters. Patients with Huriez syndrome are more vulnerable to cSCC, skin heterochromia, hand sclerosis and atrophy, and thin fingers. As shown in Table 3, adermatoglyphia and Basan syndrome share the same mutation site in the SMARCAD1 gene: c.378+1G>T. Adermatoglyphia and Huriez syndrome share the same mutation site: c.378+2T>C. We suspect that adermatoglyphia, Basan syndrome, and Huriez syndrome belong to the same disease spectrum, while adermatoglyphia is the mildest and Huriez syndrome is the most severe. Some researchers hypothesize that the risk of cSCC would increase if a patient presents both adermatoglyphia and Basan syndrome [25]. However, there is no such reported case due to the rarity of these diseases.

Four of twelve members in the reported pedigree with Basan syndrome died due to hand cSCC metastasis. This demonstrates the potential association between cSCC and Basan syndrome, which is partially in line with Gunther's hypothesis [25]. In this study, we investigated gene mutations through WES aiming to verify the potential association between cSCC and Basan syndrome. We located three genetic variants shared by individuals with Basan syndrome but not by non-Basan individuals in the pedigree. The corresponding mutant genes have been reported associating with skin cancers, including cSCC [14]. However, these three genetic variants are common variants reported in dbSNP. Therefore, we currently cannot draw any conclusion about the association between cSCC and Basan syndrome. There are several reasons account for this issue. Foremost, even we succeeded in examining most available Basan patients in this pedigree, the number of cases is still small. In addition, due to the 4 cSCC patients had passed away for years, we failed to acquire their tissues from the local hospitals. These are main limitations in this study. Nevertheless, with the high incidence rate of cSCC in this Basan syndrome pedigree, we believe that this potential association is worth to be evaluated in future studies, especially roles and mechanisms of SMARCAD1 gene mutations in tumorigenesis and metastasis.

In conclusion, we discovered a new Chinese pedigree with Basan syndrome and family history of cSCC. We confirmed a gene mutation in the SMARCAD1 gene c.378 +5G>A and expanded the disease spectrum. Minigene results showed the mutation at the intron may cause splicing variations. We also intended to assess the potential association between Basan syndrome and cSCC. Despite currently we cannot draw any conclusion, this report encourages future works to substantiate this potential but important issue.

Data Availability

The data used in this research are available from the corresponding author upon reasonable request.

Conflicts of Interest

The authors declare that they have no conflicts of interest.

Authors' Contributions

Ying Xiong and Ting Chen contributed equally to this work.

Acknowledgments

We appreciate the pedigree for the support. We also show gratitude to participating staffs in the Dermatology and Central Laboratory for collecting clinical data and providing Sanger sequencing for free. We thank Professor Ming Li for valuable comments.

References

[1] H. W. Baird 3rd, "Kindred showing congenital absence of the dermal ridges (fingerprints) and associated anomalies," *The Journal of Pediatrics*, vol. 64, no. 5, pp. 621–631, 1964.

Hindawi
Disease Markers
Volume 2022, Article ID 6010504, 15 pages
https://doi.org/10.1155/2022/6010504

Research Article

Aerobic Exercise Improves Type 2 Diabetes Mellitus-Related Cognitive Impairment by Inhibiting JAK2/STAT3 and Enhancing AMPK/SIRT1 Pathways in Mice

Lili Lin,[1] **Yonghua Wang**,[2] **Wenli Xu**,[1] **Chaolu Huang**,[1] **Jinrong Hu**,[1] **Xixi Chen**,[3] **Xinhuang Lv**,[4] **Yuelin Qin**,[1] **Xiaoyong Zhao**,[3,5] **and Haiyan Li**[1]

[1]*Department of Recovery (Department of Rehabilitation Medicine and Physiotherapy), The First Affiliated Hospital of Wenzhou Medical University, Wenzhou 325000 Zhejiang Province, China*
[2]*Department of Physical Education, Wenzhou Medical University, Wenzhou 325800 Zhejiang Province, China*
[3]*Department of Anesthesiology, The First Affiliated Hospital of Wenzhou Medical University, Wenzhou, 325000 Zhejiang Province, China*
[4]*Department of Neurology, The First Affiliated Hospital of Wenzhou Medical University, Wenzhou 325000 Zhejiang Province, China*
[5]*Department of Anesthesiology, Affiliated Hospital of Weifang Medical University, Weifang 261000, China*

Correspondence should be addressed to Xiaoyong Zhao; zhaoxiaoyong@wfmc.edu.cn and Haiyan Li; lihaiyan@wmu.edu.cn

Received 21 February 2022; Revised 6 April 2022; Accepted 16 April 2022; Published 5 May 2022

Academic Editor: Xianwei Zeng

Type 2 diabetes mellitus (T2DM) is a prevalent risk factor for cognitive impairment. Aerobic exercise can improve T2DM-related cognitive impairment; however, the possible mechanisms remain elusive. Thus, we assessed db/m mice and leptin receptor-deficient (db/db) mice that did or did not perform aerobic exercise (8 m/min, 60 min/day, and 5 days/week for 12 weeks). In this study, cognitive function was significantly impaired in the T2DM mice; aerobic exercise improved cognitive impairment through activating the AMPK/SIRT1 signalling pathway and inhibiting the JAK2/STAT3 signalling pathway in T2DM mice. However, after the application of RO8191 (JAK2 activator) or Compound C (AMPK inhibitor), the positive improvement of the exercise was evidently suppressed. Taken together, our data indicated that long-term aerobic exercise improves type 2 diabetes mellitus-related cognitive impairment by inhibiting JAK2/STAT3 and enhancing AMPK/SIRT1 pathways in mice.

1. Introduction

Type 2 diabetes mellitus (T2DM) is becoming an epidemic worldwide, and due to diet or genetic predisposition, an estimated 6.28% of the population experiences this chronic disease [1]. As one of the most serious health problems, T2DM is associated with an increased risk of renal and cardiovascular diseases (CVDs) [2], as well as neurological complications in both the peripheral and central nervous systems [3]. Accumulating evidence demonstrates that T2DM presents significant challenges related to maintaining physical independence and cognitive ability in the context of an ageing population, particularly with regard to cognitive impairment [4]. Individuals with T2DM develop cognitive impairment early and are likely to experience Alzheimer's disease, characterised by cognitive dysfunction [5], which is expected to continue to increase in prevalence over time [1]. Therefore, it is important to alleviate the cognitive impairment caused by T2DM to improve patient independence and quality of life.

Aerobic exercise is increasingly suggested as an effective nonpharmacological strategy to combat cognitive decline in T2DM patients [6]. For instance, Choi et al. identified one of the main proposed mechanisms whereby exercise affects

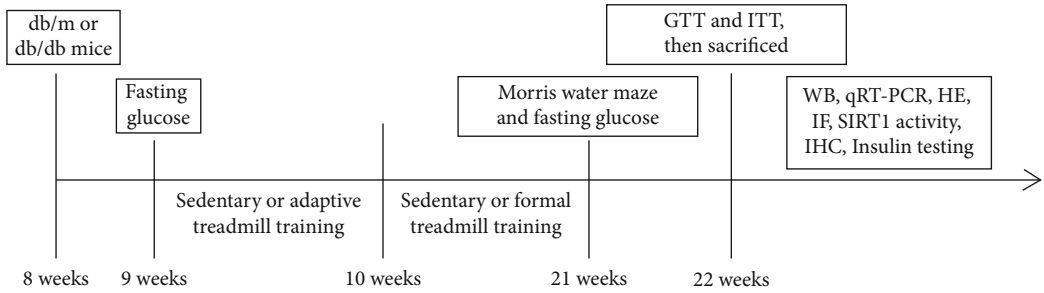

Figure 1: The time duration of animal study.

cognitive function by increasing the brain-derived neurotrophic factor (BDNF) [7]. Furthermore, aerobic exercise can also upregulate the expression of synaptic plasticity-associated proteins [8]. These findings imply that exercise may be an effective treatment for diabetes-related cognitive impairment. However, the molecular mechanism by which aerobic exercise improves cognitive function is poorly understood.

Janus kinase 2 (JAK2) is a vital component of nonreceptor tyrosine kinases [9]. Once activated, JAK2 phosphorylates and signal transducer and activator of transcription (STAT) established the downstream target [10]. Increasing evidence suggests that JAK2/STAT3 proteins have important functions in apoptosis and also participate in food intake under leptin-mediated control [11, 12]. Moreover, the JAK2/STAT3 pathway has been found to be related to memory dysfunction [13]. A recent study revealed that mice injected with the JAK inhibitor, AG490, exhibited spatial memory impairment [14]. Based on these data, we speculated that the JAK2/STAT3 pathway is involved in regulating cognitive impairment induced by T2DM; it is unclear whether exercise plays a role in regulating the JAK2/STAT3 pathway.

In addition, an increase in peripheral blood glucose concentration is a typical characteristic of T2DM, which leads to hippocampal energy metabolism disorder [15]. Adenosine monophosphate-activated protein kinase (AMPK), as well as sirtuin 1 (SIRT1), represent two enzymes involved in the regulation of energy metabolism [16]. AMPK, a regulator of body glucose and hippocampal energy balance [17], is widely administered to increase food intake [18] and forms one of the insulin receptor signalling pathways [19]. SIRT1 is one of the most important protective factors for metabolic syndrome. SIRT1 exhibits the ability to significantly extend cell lifespan and enhance neurogenesis by regulating various pathways [20], making it an exciting therapeutic target for neurodegenerative diseases. Thus, the essential role of AMPK/SIRT1 activity in energy metabolism led us to hypothesise that the AMPK/SIRT1 pathway may be related to the exercise-induced regulation in T2DM mice.

Therefore, in the present study, we explored the effect of aerobic exercise on cognitive impairment in T2DM mice and investigated whether the JAK2/STAT3 and AMPK/SIRT1 pathways are involved in the underlying mechanism.

2. Materials and Methods

2.1. Animals. Each animal experiment was carried out according to the recommendations of the ethics committee guidelines of Wenzhou Medical University (Protocol Number: wxdw 2016-0266). Specific pathogen-free (SPF) male leptin receptor-deficient db/db mice (C57BLKsJ/Nju, 8 weeks) and age-matched male db/m mice (C57BL/KsJNju) were obtained (Strain ID: T002407) from GemPharmatech Co., Ltd. All mice were maintained in conventional laboratory conditions (22°C–25°C, 50%–60% relative humidity), 12 : 12 h light-dark cycle. The time duration of animal study is shown in Figure 1.

2.2. Aerobic Exercise Training. At 8 weeks of age, we randomized db/m mice to the control (Con) or exercised (Con+Exe) groups. The db/db mice were randomly assigned to the sedentary (T2DM) and exercised (T2DM+Exe, T2DM+Exe+Vehicle, T2DM+Exe+RO8191, and T2DM+Exe+Compound C) groups. The exercised groups participated in adaptive treadmill training for 1 week (5 m/min, 30 min/day) and thereafter participated in 12 weeks (beginning at 10 weeks of age) of moderate-intensity treadmill training (5 days/week). In the first week of formal training, each animal ran at 8 m/min for 40 min/day; for the remaining weeks, the mice ran at 8 m/min for 1 h/day.

2.3. JAK2 Activator and AMPK Inhibitor. The application of JAK2 activator (RO8191) and AMPK inhibitor (Compound C) was conducted as previously reported [21, 22]. In brief, the mice were treated with RO8191 2 mg/kg/day for intraperitoneal injection. Compound C was injected intraperitoneally at 10 mg/kg/day. The T2DM+Exe+Vehicle mice were intraperitoneally inoculated with the solvents without the drug.

2.4. Glucose Tolerance Test (GTT) and Insulin Tolerance Test (ITT). GTT was performed after 12 h fasting by irrigating the stomach with glucose (20%, 2 mg/g body weight). ITT was performed after 6 h fasting by injecting insulin (0.75 mU/g body weight) into the intraperitoneal cavity. Levels of glucose were measured via tail blood before (0 time point) and after 15, 30, 60, and 120 min experiment using an Accu-Check glucometer (Roche, Mannheim, Germany).

2.5. Morris Water Maze (MWM) Test. The MWM test was conducted to evaluate the spatial learning and memory

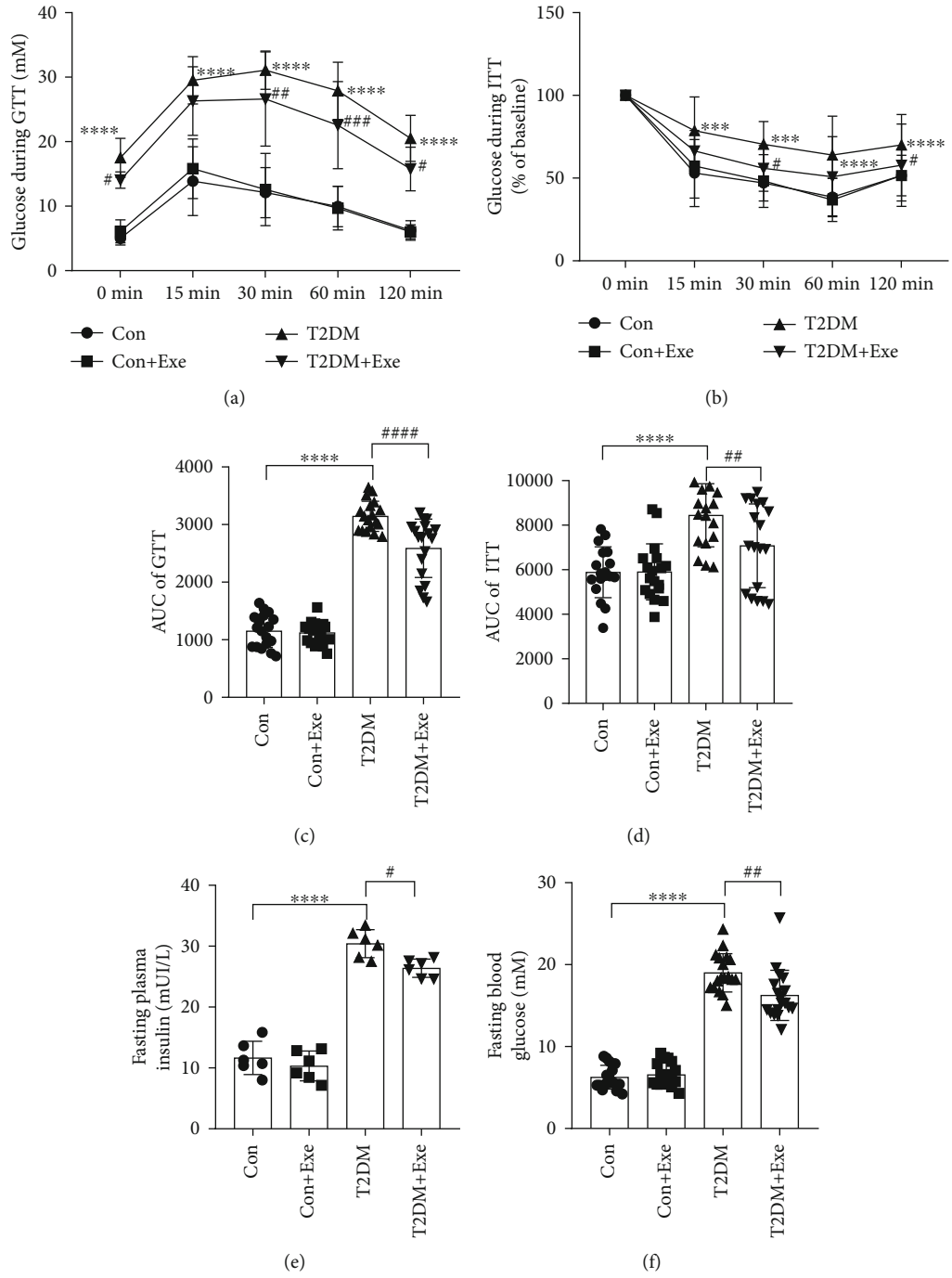

Figure 2: Effect of treadmill exercise in T2DM mice. (a) Glucose during glucose tolerance test (GTT) at age 22 weeks ($n = 18$). (b) Glucose during insulin tolerance test (ITT) (% of baseline) at age 22 weeks ($n = 18$). (c) Area under the curve (AUC) of the GTT ($n = 18$). (d) AUC of the ITT ($n = 18$). (e) Fasting plasma insulin ($n = 6$). (f) Fasting blood glucose (n =18). Data are expressed as mean ± SD. $^{*}P < 0.05$, significant difference compared with the Con group ($^{**}P < 0.01$, $^{***}P < 0.001$, $^{****}P < 0.001$). $^{\#}P < 0.05$, which is significantly different from the T2DM group ($^{\#\#}P < 0.01$, $^{\#\#\#}P < 0.001$, $^{\#\#\#\#}P < 0.001$).

abilities of experimental animals. In the 12th week of treadmill training, mice participated in the MWM test. Before starting the MWM test, the mice underwent one-day adaptive training in a circular water pot (height, 50 cm; diameter, 120 cm) containing 22°C white water. Then navigation training (5 consecutive days) and probe test (on day 6) were performed as described previously [23]. The order of the four start positions varied across testing days. A video tracking system (Shanghai Jiliang, China) was used to record.

2.6. Fasting Plasma Insulin Testing. The level of fasting plasma insulin was measured by the Mouse Insulin ELISA Kit (Abcam, UK, ab277390).

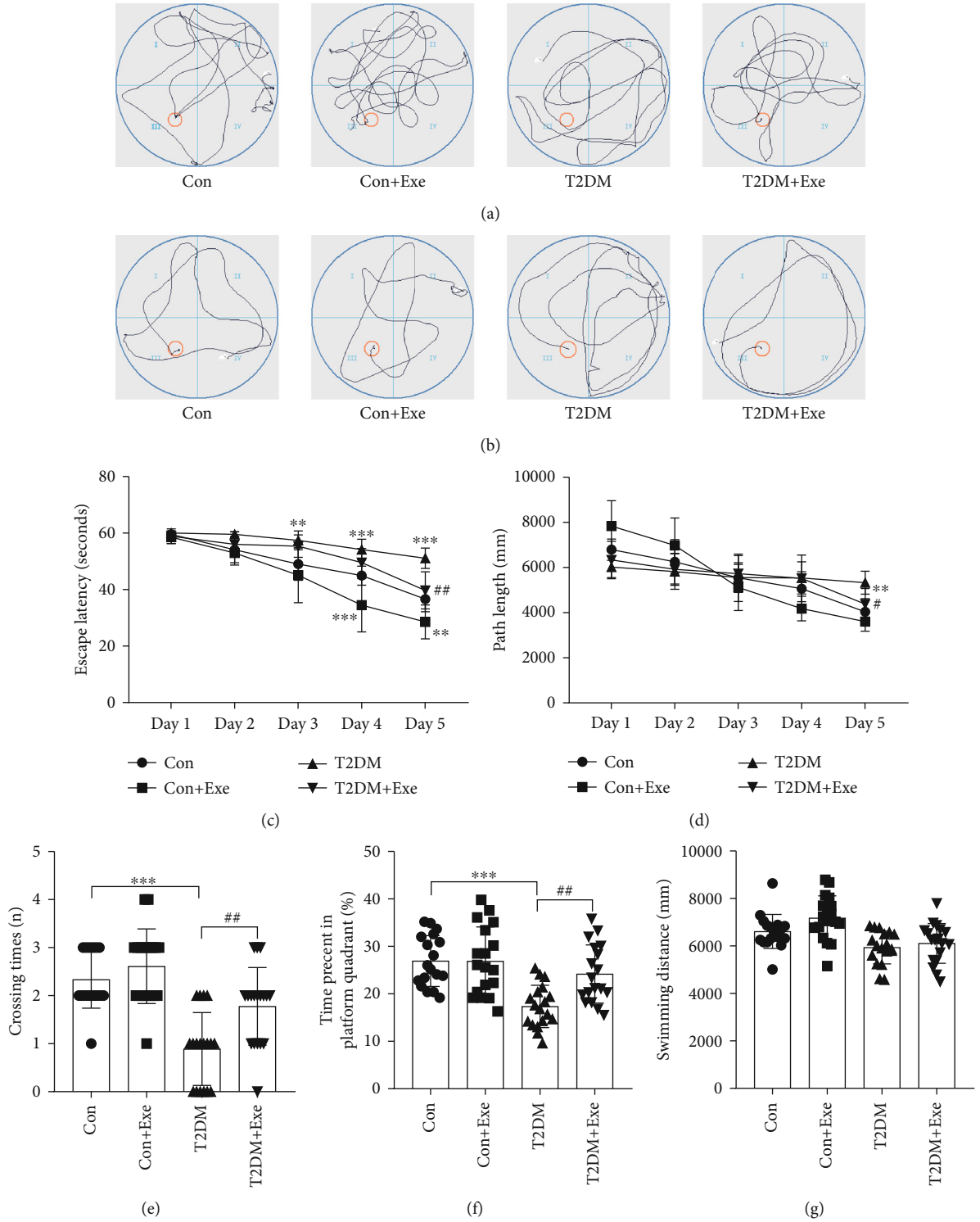

Figure 3: Effect of treadmill exercise on the acquisition of the MWM task. (a) Representative swimming trajectories of mice on the first trial day ($n = 18$). (b) Representative swimming trajectories of mice on the fifth trial day ($n = 18$). (c) Escape latency ($n = 18$). (d) Path length ($n = 18$). (e) Crossing times during the probe test ($n = 18$). (f) Percent of time spent in the platform quadrant during the probe test ($n = 18$). (g) Total swimming distance during the probe test ($n = 18$). Data are expressed as mean ± SD. $^{*}P < 0.05$, significant difference compared with the Con group ($^{**}P < 0.01$, $^{***}P < 0.001$). $^{\#}P < 0.05$, which is significantly different from the T2DM group ($^{\#\#}P < 0.01$).

2.7. Western Blotting (WB). Western blotting was conducted as described previously [6]. The specific information for antibodies and reagents is shown in Table S1. The experiment was repeated three times.

2.8. RNA Transcription and Quantitative Real-Time- (qRT-) PCR. Total RNA was isolated from the hippocampus using the RNA simple Total RNA kit (Tiangen, China,), and 0.1 μg RNA was used to prepare cDNA with PrimeScript

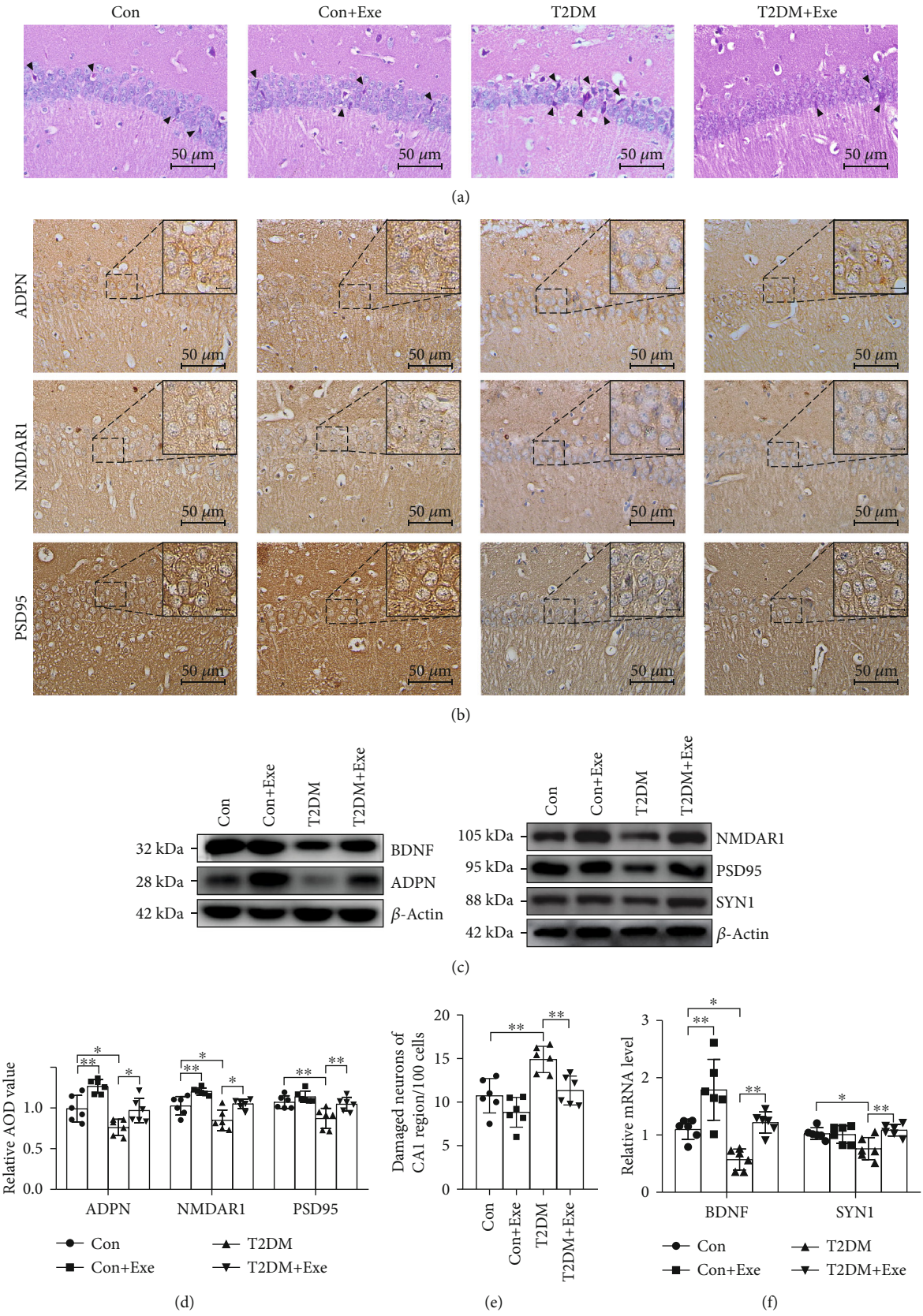

Figure 4: Continued.

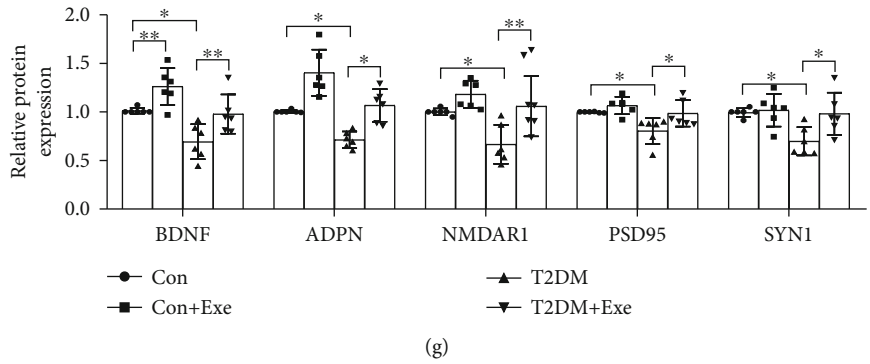

(g)

Figure 4: The damage of nerve cells and synaptic in the hippocampus caused by T2DM. (a) Cell histopathological changes in the CA1 region of the hippocampus by HE staining (arrowheads: the damaged neurons). Scale bar: 50 μm ($n = 6$). (b) Immunohistochemical staining in the CA1 region of the hippocampus. Scale bars: 50 μm ($n = 6$). (c) Western blotting ($n = 6$). (d) Immunohistochemical analysis ($n = 6$). (e) The histogram shows the number of damaged neurons of the CA1 region per 100 cells ($n = 6$). (f) The mRNA level ($n = 6$). (g) The histogram shows relative protein levels ($n = 6$). Data are expressed as mean ± SD. $^{*}P < 0.05$, significant difference ($^{**}P < 0.01$).

RT Master Mix (Takara, Dalian, China). For qRT-PCR, 0.3 μl of cDNA was added to 19.7 μl of total PCR reaction mixture, containing SYBR Premix Ex Taq (Roche Diagnostics, Basel, Switzerland). The melting curves of the primers were assessed before use. PCR amplification was performed in 96-well microtiter plates using a 7500 fast PCR machine (Applied Biosystems, Massachusetts, United States). The target gene and house-keeping gene, actin, were run on the same plate as per the protocol. By the $\Delta\Delta$Ct approach, we measured relative mRNA levels, in which ΔCt = actin Ct − target gene Ct. The qRT-PCR primers are shown in Table S2.

2.9. Immunohistochemical (IHC) and Immunofluorescence (IF) Staining. Immunohistochemical and immunofluorescence were performed as outlined previously [9]. Images of IHC were captured under a microscope (×400) and analysed using ImagePro Plus. A fluorescence microscope was used to obtain figures and capture pictures of IF at ×400 magnification. The analysis was conducted using ImageJ. Five digital images of each animal were selected for semi-quantitative analysis. The antibodies are shown in Table S1.

2.10. Hematoxylin-Eosin (HE) Staining. The HE was performed by using an HE staining kit (Solorbio, China, G1120). All images were captured at ×400 magnification under a microscope.

2.11. SIRT1 Activity. The activity of SIRT1 was measured by tissue Sirtuin 1 activity colorimetric quantitative detection kit (GMS50287.2, GENM2ED SCIENTIFICS INC. USA).

2.12. Statistical Analysis. Results are presented in the graphs of mean ± SD. GraphPad 8.0 was adopted for statistical analysis. A normal distribution test was performed using the Shapiro–Wilk test. Comparisons between the two groups were made by Student's t-test for statistical significance. Multiple groups were compared using two-way ANOVA or repeated-measures ANOVA and post hoc t-test with the Bonferroni correction. $P < 0.05$ represented for statistical significance. The information about degrees of freedom and F values is shown in Table S3.

3. Results

3.1. Aerobic Exercise Improved Blood Glucose and Insulin Level in T2DM Mice. After 12 weeks of treadmill intervention, T2DM+Exe mice displayed significantly improved in GTT and ITT compared to T2DM mice ($P < 0.05$, Figures 2(a)–2(d)). Compared to the Con group, the levels of plasma insulin and blood glucose were significantly higher in the T2DM group. Exercise improved the insulin and blood glucose levels ($P < 0.05$, Figures 2(e) and 2(f)).

3.2. Aerobic Exercise Improved T2DM-Related Cognitive Impairment. In this study, we performed the MWM test to investigate the influence of the treadmill on the spatial learning and memory functions of the T2DM mouse. From the representative swimming trajectories of the four groups of mice on the first day of navigation training and latency period, initial differences among the 4 groups were not significant (Figures 3(a) and 3(c)). After training, a significant delay was observed in the T2DM mice, which showed prolonged escape latency and path length compared with the Con mice on the fifth day. The escape latency and path length of the T2DM+Exe mice remarkably decreased compared with the T2DM mice ($P < 0.05$, Figures 3(c) and 3(d)). The representative trajectory of navigation training on the fifth day showed similar results (Figure 3(b)). During the probe test, the number of platform crossings and the time spent in the target quadrant of the T2DM group remarkably decreased in comparison with the Con group. Moreover, the T2DM+Exe mice displayed a higher crossing number and more time staying in the target quadrant compared with the T2DM group ($P < 0.05$, Figures 3(e) and 3(f)). The result of total swimming distances among the four groups was not significant ($P > 0.05$, Figure 3(g)).

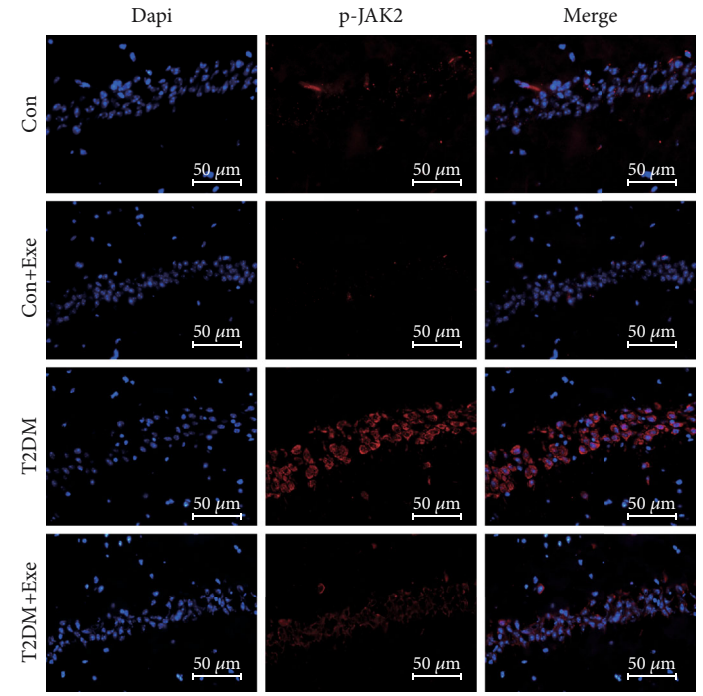

(a)

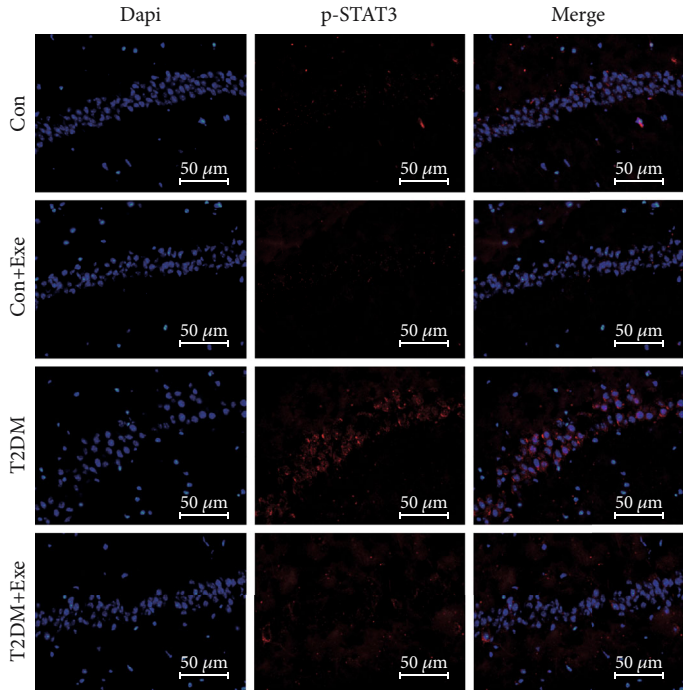

(b)

Figure 5: Continued.

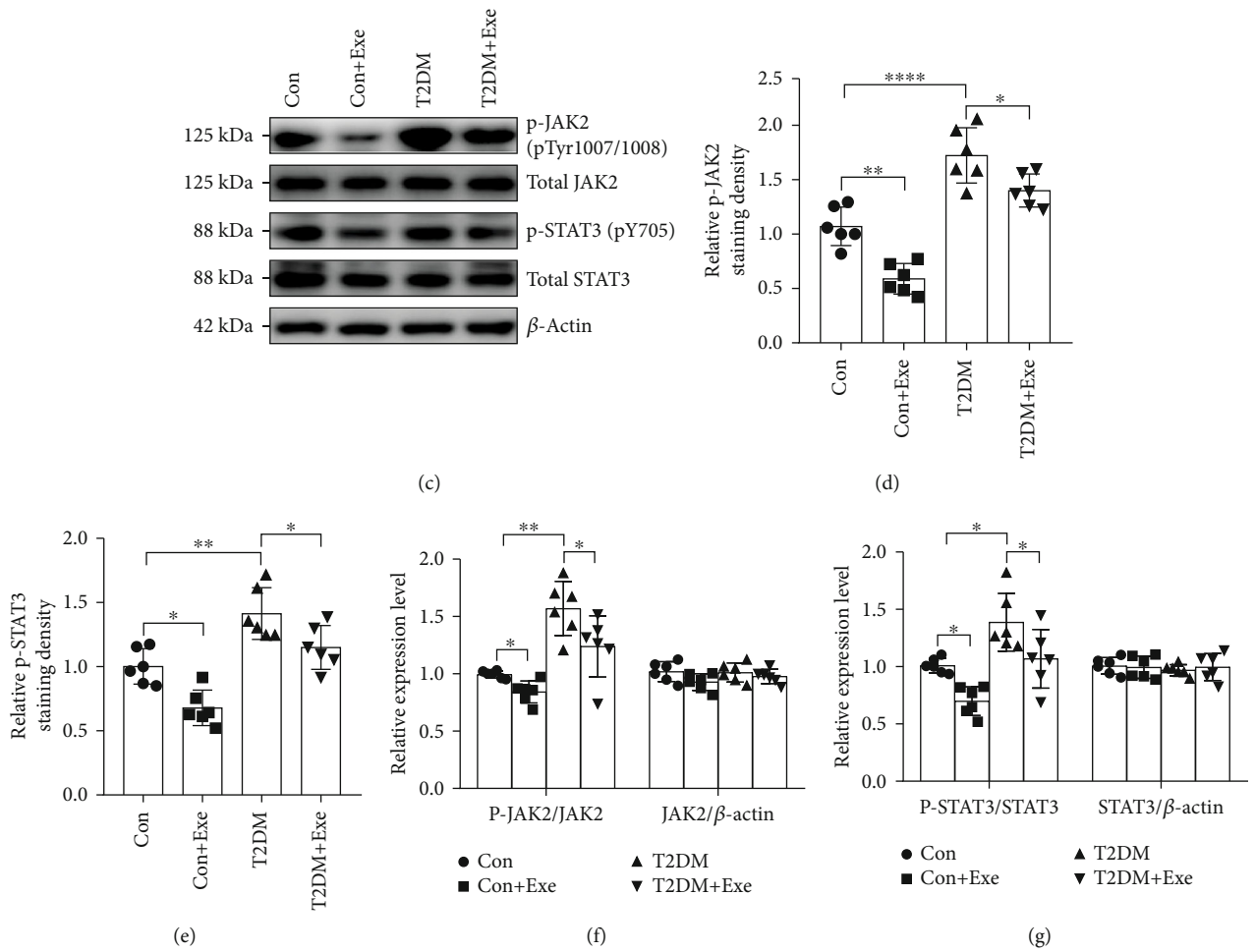

Figure 5: Effect of treadmill exercise on the JAK2/STAT3 signalling pathway in T2DM mice. (a, b) Representative images of p-JAK2 and p-STAT3 (red) in the CA1 region of the hippocampus. Scale bar: 50 μm ($n = 6$). (c) Western blotting ($n = 6$). (d, e) Immunofluorescence analysis ($n = 6$). (f, g) The histogram shows relative protein level ($n = 6$). Data are expressed as mean ± SD. $^{*}P < 0.05$, significant difference ($^{**}P < 0.01$, $^{***}P < 0.001$).

3.3. Aerobic Exercise Improved Nerve Cell Damage and Protected Synaptic Damage in the Hippocampus Caused by T2DM. To observe the damage of hippocampal nerve cells in diabetes, hematoxylin and eosin-stained paraffin sections were used to observe the hippocampal CA1 region. In the Con and Con+Exe groups, most of the neurons were arranged regularly and contained large, round nuclei. In the T2DM group, more nuclei had become pyknotic (contracted and dark, arrowheads in Figure 4(a)) and were surrounded by swollen and broken protrusions. In the T2DM+Exe group, the abnormal structure of the neurons was improved (Figure 4(a)). The number of damaged neurons significantly increased in the T2DM mice and markedly decreased after exercise intervention ($P < 0.05$, Figure 4(e)). In addition, immunohistochemical and Western blotting analyses showed that the positive expression of ADPN, PSD95, and NMDAR1 significantly declined within the T2DM group in comparison with the Con group. This improved in the exercise intervention group (Figures 4(b)–4(d) and 4(g)). Moreover, the protein expression and the mRNA levels of BDNF and SYN1 markedly decreased in the T2DM mice compared with the Con mice and evidently increased after training ($P < 0.05$, Figures 4(c), 4(f), and 4(g)).

3.4. Aerobic Exercise Attenuated the JAK2/STAT3 Pathway in T2DM Mice. We also observed that the hippocampal phospho-JAK2 and phospho-STAT3 levels in the T2DM group were significantly higher than those in the Con mice. With regard to the Con+Exe and T2DM+Exe mice, long-term treadmill significantly decreased phospho-JAK2 and phospho-STAT3 expression ($P < 0.05$, Figures 5(c), 5(f), and 5(g)). As depicted in the immunofluorescence of Figure 5, the same tendency of phospho-JAK2 and phospho-STAT3 levels was observed ($P < 0.05$, Figures 5(a), 5(b), 5(d), and 5(e)).

3.5. Aerobic Exercise Activated the AMPK/SIRT1 Pathway in T2DM Mice. To evaluate the effect of exercise on AMPK/SIRT1 pathway, we performed the western blotting. And the SIRT1 and phospho-AMPK expression evidently declined in the T2DM mice compared to the Con mice. In

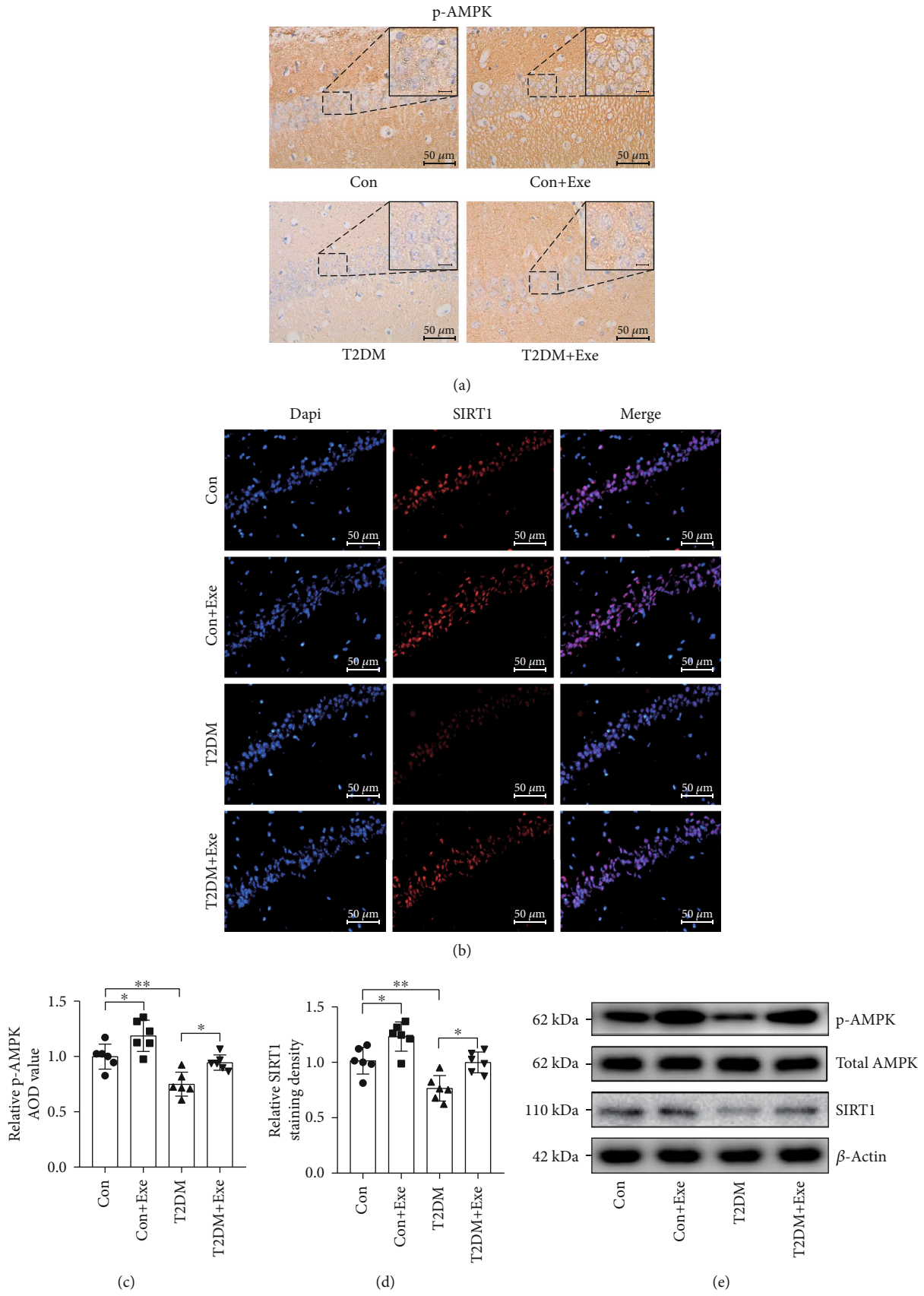

Figure 6: Continued.

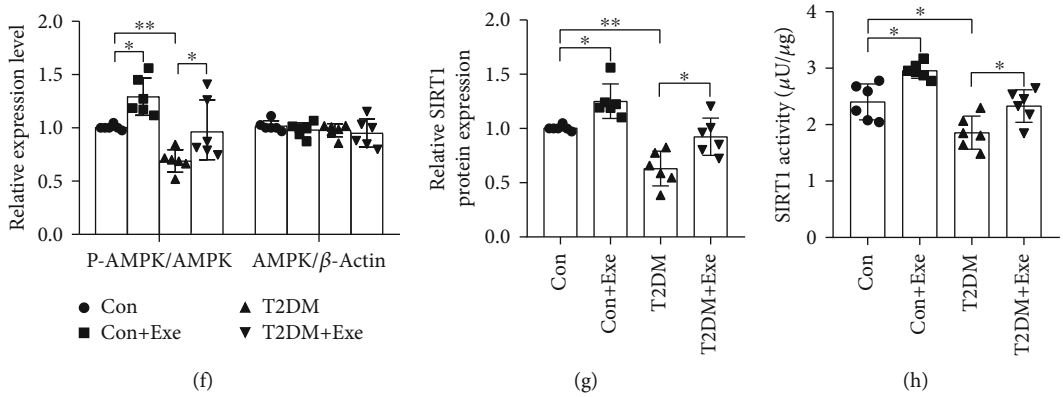

Figure 6: Effect of treadmill exercise on the AMPK/SIRT1 signalling pathway in T2DM mice. (a) Immunohistochemical staining of p-AMPK in the CA1 region of the hippocampus. Scale bars: 50 μm ($n = 6$). (b) Representative images of SIRT1 (red) in the CA1 region of the hippocampus. Scale bar: 50 μm ($n = 6$). (c) Immunohistochemical analysis ($n = 6$). (d) Immunofluorescence analysis ($n = 6$). (e) Western blotting ($n = 6$). (f, g) The histogram shows relative protein levels ($n = 6$). (h) SIRT1 activity ($n = 6$). Data are expressed as mean ± SD. $^{*}P < 0.05$, significant difference ($^{**}P < 0.01$, $^{***}P < 0.001$).

the Con+Exe and T2DM+Exe groups, exercise remarkably elevated SIRT1 and phospho-AMPK expression ($P < 0.05$, Figures 6(e)–6(g)). In addition, the same tendency of phospho-AMPK was observed in immunohistochemical staining, SIRT1 in immunofluorescence staining, and SIRT1 activity ($P < 0.05$, Figures 6(a)–6(d) and 6(h)).

3.6. Aerobic Exercise-Induced Improvement in the Learning and Memory Ability of T2DM Mice Was Dependent upon JAK2/STAT3 and AMPK/SIRT1. The JAK2 activator RO8191 was used to enhance the activation of JAK2/STAT3. The AMPK inhibitor Compound C was used to inhibit the activation of AMPK/SIRT1 (Supplementary Figure S1). From the representative swimming trajectories on the first day of navigation training and latency period, the difference among the three groups was insignificant (Figures 7(a) and 7(c)). However, escape latency and path length revealed an increase on the fifth day in the T2DM+Exe+RO8191 group compared to the T2DM+Exe+Vehicle group ($P < 0.05$, Figures 7(b)–7(d)). Compared to the T2DM+Exe group, the escape latency and path length of the T2DM+Exe+Compound C group remarkably increased ($P < 0.05$, Figures 7(b)–7(d)). During the probe test, the number of platform crossings and the time spent in the target quadrant of the T2DM+Exe+RO8191 group remarkably decreased in comparison with the T2DM+Exe+Vehicle group ($P < 0.05$, Figures 7(e) and 7(f)). And the T2DM+Exe+Compound C mice displayed a lower crossing number and less time staying in the target quadrant compared with the T2DM+Exe+Vehicle group ($P < 0.05$, Figures 7(e) and 7(f)). There was no significant difference among the three groups for total swimming distances ($P > 0.05$, Figure 7(g)).

3.7. Aerobic Exercise-Induced Improvement in Nerve Cell Damage and Protection in Synaptic Damage of T2DM Mice Was Dependent upon JAK2/STAT3 and AMPK/SIRT1. We observed the damage of hippocampal nerve cells in the CA1 region after the application of RO8191 or Compound C. The damaged nerve cells of RO8191-treated mice were significantly more than those of the vehicle mice ($P < 0.05$, Figures 8(a) and 8(e)). In the Compound C-treated mice, it was observed that more nuclei had become pyknotic (contracted and dark, arrowheads in Figure 8(a)) in comparison with the T2DM+Exe+Vehicle group ($P < 0.05$, Figures 8(a) and 8(h)). Further, the positive expression of ADPN, BDNF, SYN1, PSD95, and NMDAR1 significantly declined within the T2DM+Exe+RO8191 group in comparison with the T2DM+Exe+Vehicle group ($P < 0.05$, Figures 8(b), 8(c), 8(f), and 8(g)). Respectively, the positive expression of ADPN, BDNF, SYN1, PSD95, and NMDAR1 evidently decreased after the injection of Compound C ($P < 0.05$, Figures 8(b), 8(d), 8(i), and 8(j)).

4. Discussion

In the present study, we found that the 12 weeks of moderate-intensity treadmill training could improve the abnormal glycemia and insulin levels in db/db mice. Additionally, exercise remitted impaired glucose tolerance and insulin resistance. Emerging evidence has demonstrated that cognitive impairments occur in T2DM [24]. We found that cognitive dysfunction related to the function of the hippocampus existed in the T2DM mice, and we revealed that aerobic exercise improved it. In a subsequent investigation, we sought the possible mechanism responsible for the aforementioned phenomenon of recovery of cognitive function via exercise. We observed that phospho-JAK2 and phospho-STAT3 were increased, and the phospho-AMPK/SIRT1 was reduced in T2DM. However, aerobic exercise intervention over a long period improves this situation. Furthermore, JAK2 activator, RO8191, and AMPK inhibitor, Compound C, partly blocked the beneficial effects of aerobic exercise on cognitive function in T2DM mice. These results indicate that JAK2/STAT3 and AMPK/SIRT1 are potential

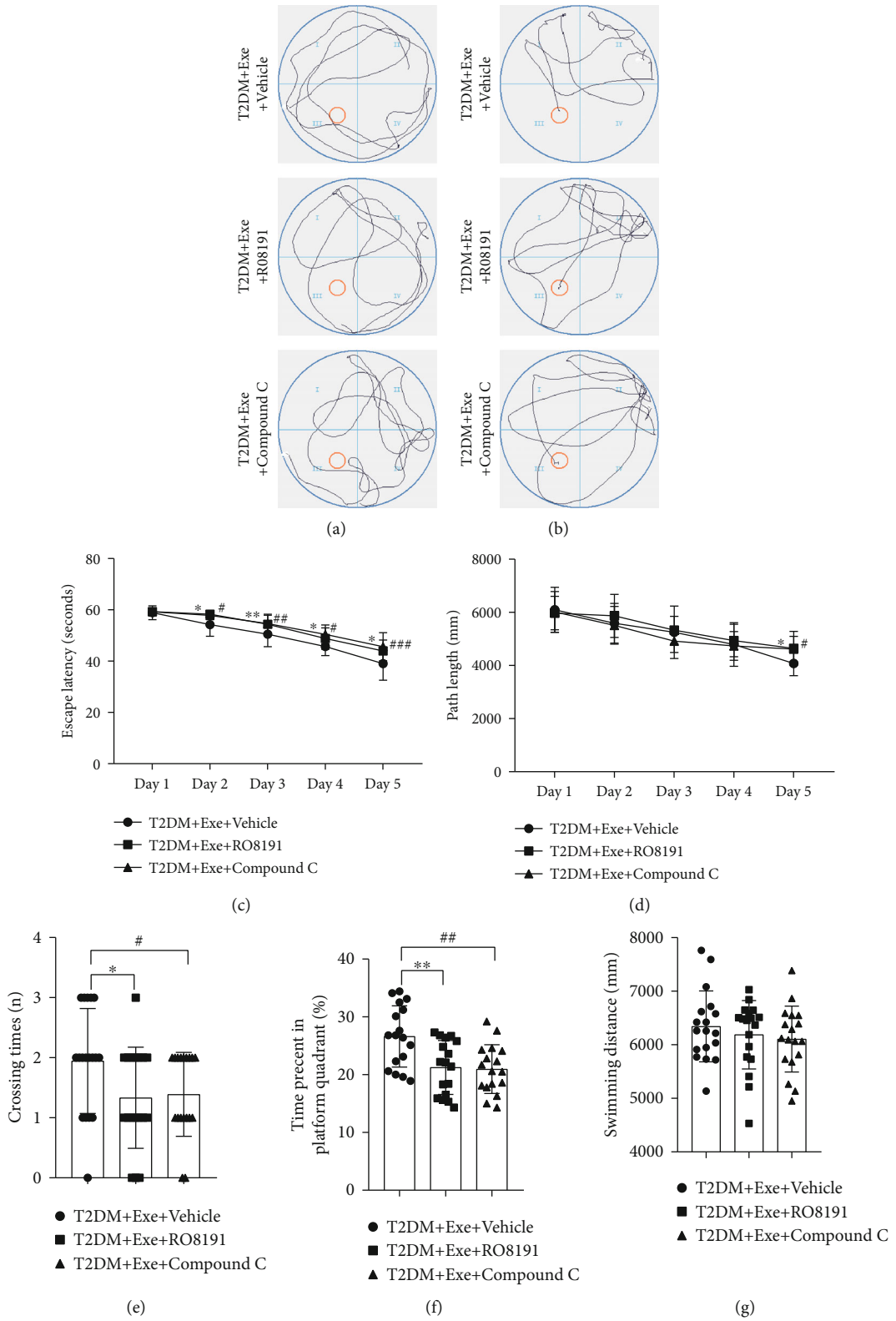

Figure 7: Effect of treadmill exercise on the acquisition of MWM task. (a) Representative swimming trajectories of mice on the first trial day ($n = 18$). (b) Representative swimming trajectories of mice on the fifth trial day ($n = 18$). (c) Escape latency ($n = 18$). (d) Path length ($n = 18$). (e) Crossing times during the probe test ($n = 18$). (f) Percent of time spent in the platform quadrant during the probe test ($n = 18$). (g) Total swimming distance during the probe test ($n = 18$). Data are expressed as mean ± SD. $^{*}P < 0.05$, significant difference between T2DM+Exe+RO8191 group and T2DM+Exe group ($^{**}P < 0.01$, $^{***}P < 0.001$). $^{\#}P < 0.05$, significant difference between T2DM+Exe+Compound C group and T2DM+Exe group ($^{\#\#}P < 0.01$, $^{\#\#\#}P < 0.001$).

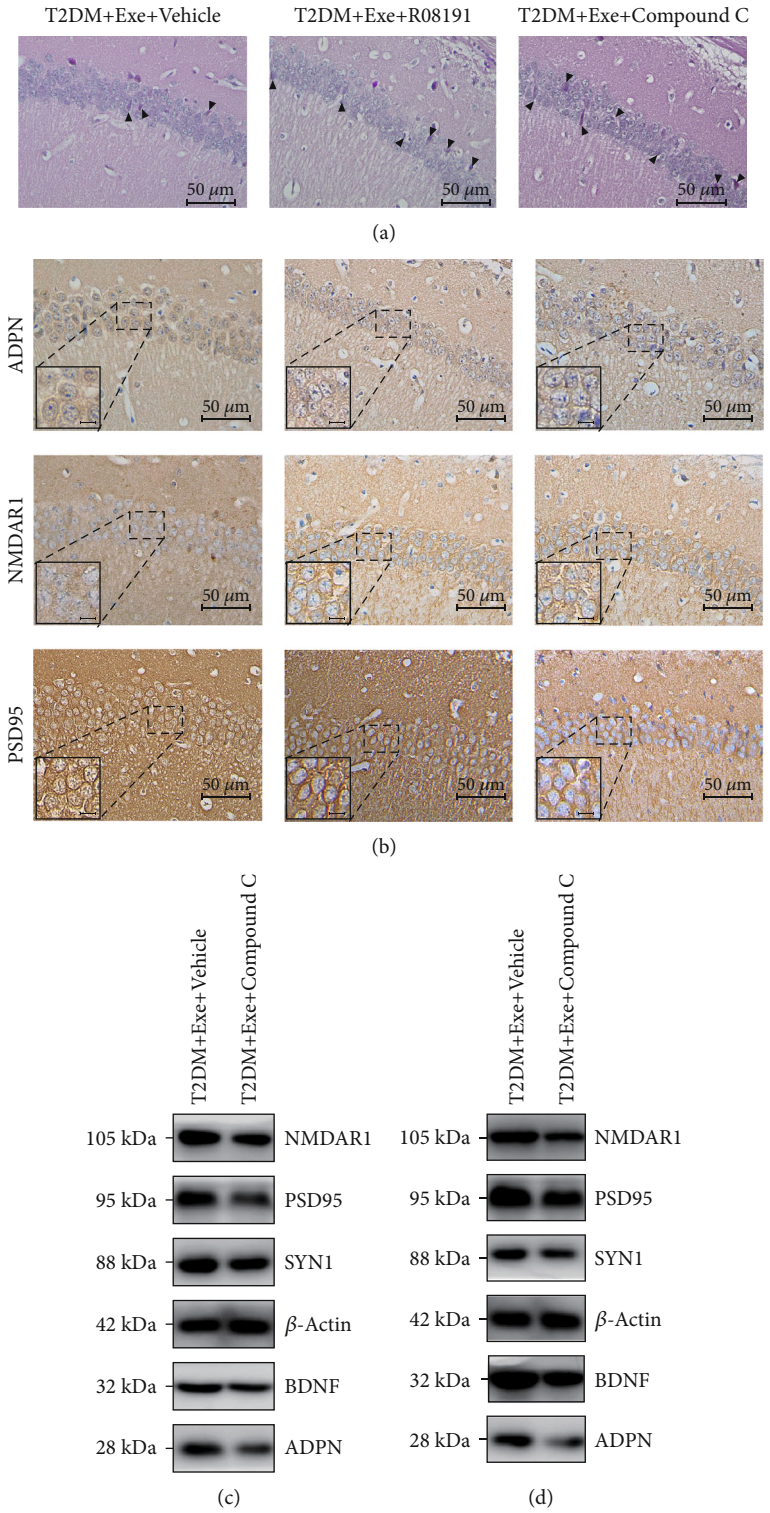

Figure 8: Continued.

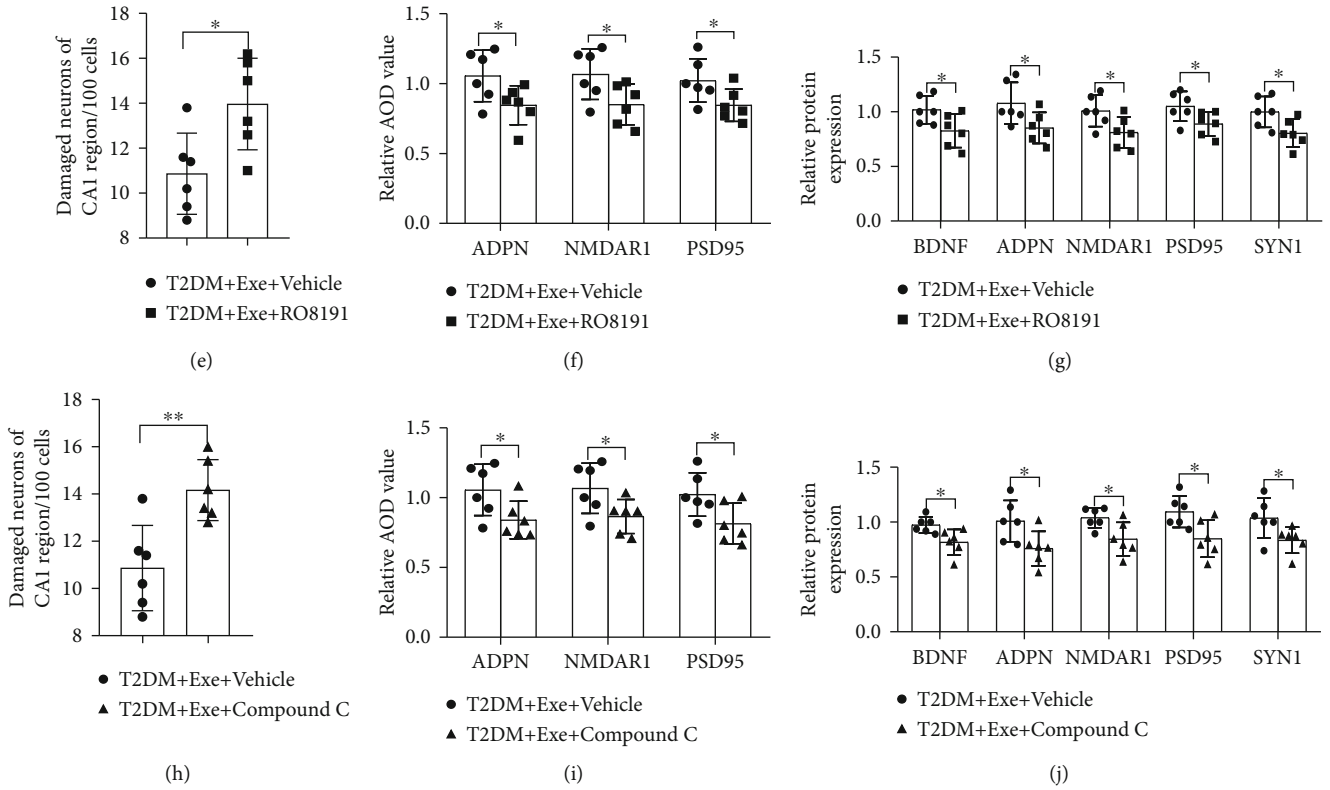

Figure 8: The damage of nerve cells and synaptic in the hippocampus. (a) Cell histopathological changes in the CA1 region of the hippocampus by HE staining (arrowheads: the damaged neurons). Scale bar: 50 μm ($n = 6$). (b) Immunohistochemical staining in the CA1 region of the hippocampus. Scale bars: 50 μm ($n = 6$). (c, d) Western blotting ($n = 6$). (e, h) The histogram shows the number of damaged neurons of the CA1 region per 100 cells ($n = 6$). (f, i) Immunohistochemical analysis ($n = 6$). (g, j) The histogram shows relative protein levels ($n = 6$). Data are expressed as mean ± SD. $^{*}P < 0.05$, significant difference ($^{**}P < 0.01$).

mechanisms by which aerobic exercise improves cognitive decline mediated by T2DM.

Cognitive impairment caused by diabetes can be explained by the loss of synapses caused by insulin resistance (IR). Synaptic dysfunction is the main pathophysiological sign of neurodegenerative diseases [25]. Further, previous studies have indicated that synaptic dysfunction is caused by IR in the brain [26], leading to cognitive decline. However, studies have shown that aerobic exercise could attenuate synaptic loss in models of neurodegenerative disorders, such as Alzheimer's disease [7]. In this study, aerobic exercise mitigated the changes in classical synaptic protein levels observed in T2DM. This is because exercise benefits glucose homeostasis in mice with IR. Glucose homeostasis affects the normal physiological activities of neurons and is able to induce synaptic proteins changes [27]. In this study, our data support that aerobic exercise efficiently improved the impaired cognition caused by diabetes. The expression of three classical synaptic proteins, PSD95, NMDAR1, and SYN1, decreased in the hippocampal CA1 area of diabetic mice, indicating that hippocampal synapse formation in diabetic mice was impaired. The aerobic exercise intervention enhanced hippocampal synaptic formation in T2DM mice. Additionally, we found more abnormal structure neurons in db/db mice, consistent with previous research results [23]. Aberrant insulin modulation in diabetic mice can cause abnormal nerve cell formation. Furthermore, our investigation suggested improvement of neuron shape within hippocampal CA1 region in db/db mice after exercise. Therefore, our research indicates that aerobic exercise has a protective effect on the synapses and neurons in diabetes.

We found that cognitive impairment in T2DM manifests as synaptic disorders and neuronal damage. Recent studies have shown that the JAK2/STAT3 pathway is related to synaptic disorders [28]. JAK2 has a negative impact on synapse formation [29] and insulin sensitivity in diabetes [30]. In addition, the activation of STAT3 has been shown to exacerbate neuronal damage [31]. However, to date, there is a lack of evidence to indicate that aerobic exercise can improve this situation through the JAK2/STAT3 pathway. In our experiments, our data confirmed that phospho-STAT3 and phospho-JAK2 levels were elevated in the mice model of T2DM. In contrast, prolonged aerobic exercise successfully reversed the increased signal of this pathway. Therefore, the data showed that the JAK2/STAT3 pathway is one of the potential mechanisms by which aerobic exercise reduces insulin resistance and protect synapse loss. To verify it, we used RO8191, an activator of JAK2, to activate JAK2/STAT3. We found that the positive effect of exercise on cognitive impairment is reversed after activating JAK2. This

indicated that exercise inhibited the JAK2/STAT3 pathway, which is likely one of the mechanisms by which aerobic exercise improves the symptoms of diabetes.

With regard to the AMPK/SIRT1 pathway, evidence has indicated that under pathological conditions, AMPK plays a crucial role in controlling synaptic plasticity and neuronal cell survival [32]. In hippocampal neurons of T2DM mice, the decrease in AMPK phosphorylation is related to the damaged of hippocampal neurons [33], and the activation of phospho-AMPK increases the expression of proteins involved in synaptic plasticity [34]. Moreover, SIRT1 has an important function in regulating neuronal injury [35]. In line with these results, we found that the phospho-AMPK in T2DM was significantly reduced. As confirmed in this study, aerobic exercise upregulated phospho-AMPK and SIRT1 in the hippocampus. Furthermore, we used Compound C, the AMPK inhibitor. Additionally, our data confirmed that the cognitive function improvement by exercise of T2DM mice was partly blocked after suppressing AMPK. Therefore, we believe that aerobic exercise may also prevent synapse formation disorders and improve symptoms of T2DM by activating the AMPK/SIRT1 pathway.

In summary, this study demonstrated that prolonged aerobic exercise can reverse the cognitive decline caused by T2DM, which may be related to the activity of AMPK/SIRT1 and the inhibition of JAK2/STAT3 signalling in T2DM mice. Aerobic exercise may also be used to prevent synapse formation disorders and cognitive decline through enhancing the AMPK/SIRT1 and inhibiting the JAK2/STAT3.

4.1. Limitations. Our study discusses the possible mechanism by which aerobic exercise improves T2DM-related cognitive impairment. However, in vitro, there is still no way to achieve aerobic exercise interventions, which are worth investigating in future studies. Meanwhile, we will concentrate on making it used in the clinic trail to verify it.

Data Availability

Data are available from the corresponding authors upon reasonable request.

Ethical Approval

This study was performed in line with the principles of the Declaration of Helsinki. Approval was granted by the Ethics Committee of Wenzhou Medical University (protocol number: wxdw 2016-0266).

Conflicts of Interest

The authors have no relevant financial or nonfinancial interests to disclose.

Authors' Contributions

All authors contributed to the study's conception and design. Material preparation, data collection, and the first draft of the manuscript were performed by Lili Lin and Yonghua Wang; analysis was performed by Xiaoyong Zhao and Wenli Xu; Jinrong Hu contributed to manuscript revision; Chaolu Huang and Xixi Chen contributed to the conception of the study; Xinhuang Lv helped perform the analysis with constructive discussions; Yuelin Qin contributed to manuscript preparation; Haiyan Li contributed significantly to experimental plan and revised the manuscript. All authors commented on previous versions of the manuscript. All authors read and approved the final manuscript. Lili Lin and Yonghua Wang contributed equally to the manuscript.

Acknowledgments

This work was supported by the National Natural Science Foundation of China (grant number 81501954), Wenzhou Municipal Science and Technology Bureau (grant number Y2020053), Weifang Science and Technology Bureau (grant number 2021YX028), and Shandong Provincial Project of Medical and Health Technology Development Program, China (grant number 2019WS605).

Supplementary Materials

Supplementary 1. The related pathways after application of inhibitors or activators. (A) (D) Western blotting ($n=6$). (B) (C) (E) (F) Histogram shows relative protein levels ($n=6$). Data are expressed as mean ± SD. * $P<0.05$, significant difference (** $P<0.01$).

Supplementary 2. Reagent and antibody.

Supplementary 3. Primers Information.

Supplementary 4. Statistical Information.

References

[1] M. Khan, M. J. Hashim, J. K. King, R. D. Govender, H. Mustafa, and J. al Kaabi, "Epidemiology of type 2 diabetes - global burden of disease and forecasted trends," *Journal of Epidemiology and Global Health*, vol. 10, no. 1, pp. 107–111, 2020.

[2] V. Jha, G. Garcia-Garcia, K. Iseki et al., "Chronic kidney disease: global dimension and perspectives," *Lancet*, vol. 382, no. 9888, pp. 260–272, 2013.

[3] P. O'Brien, L. M. Hinder, B. C. Callaghan, and E. L. Feldman, "Neurological consequences of obesity," *The Lancet. Neurology*, vol. 16, no. 6, pp. 465–477, 2017.

[4] P. Riederer, A. D. Korczyn, S. S. Ali et al., "The diabetic brain and cognition," *Journal of Neural Transmission*, vol. 124, no. 11, pp. 1431–1454, 2017.

[5] L. Jia, Y. du, L. Chu et al., "Prevalence, risk factors, and management of dementia and mild cognitive impairment in adults aged 60 years or older in China: a cross-sectional study," *Public Health*, vol. 5, no. 12, pp. e661–e671, 2020.

[6] J. Wang, Y. Niu, H. Tao, M. Xue, and C. Wan, "Knockdown of lncRNA TUG1 inhibits hippocampal neuronal apoptosis and participates in aerobic exercise-alleviated vascular cognitive impairment," *Biological Research*, vol. 53, no. 1, p. 53, 2020.

[7] S. H. Choi, E. Bylykbashi, Z. K. Chatila et al., "Combined adult neurogenesis and BDNF mimic exercise effects on cognition in an Alzheimer's mouse model," *Science*, vol. 361, no. 6406, p. - eaan8821, 2018.

[8] F. R. Rizzo, L. Guadalupi, K. Sanna et al., "Exercise protects from hippocampal inflammation and neurodegeneration in experimental autoimmune encephalomyelitis," *Brain, Behavior, and Immunity*, vol. 98, pp. 13–27, 2021.

[9] J. Milara, B. Ballester, A. Morell et al., "JAK2 mediates lung fibrosis, pulmonary vascular remodelling and hypertension in idiopathic pulmonary fibrosis: an experimental study," *Thorax*, vol. 73, no. 6, pp. 519–529, 2018.

[10] D. Schinnerl, K. Fortschegger, M. Kauer et al., "The role of the Janus-faced transcription factor PAX5-JAK2 in acute lymphoblastic leukemia," *Blood*, vol. 125, no. 8, pp. 1282–1291, 2015.

[11] Y. Sun, Y. Yang, Z. Qin et al., "The acute-phase protein orosomucoid regulates food intake and energy homeostasis via leptin receptor signaling pathway," *Diabetes*, vol. 65, no. 6, pp. 1630–1641, 2016.

[12] Z. Song, C. L. Jin, M. Ye, C. Q. Gao, H. C. Yan, and X. Q. Wang, "Lysine inhibits apoptosis in satellite cells to govern skeletal muscle growth via the JAK2-STAT3 pathway," *Food & Function*, vol. 11, no. 5, pp. 3941–3951, 2020.

[13] D. Dodington, H. Desai, and M. Woo, "JAK/STAT - emerging players in metabolism," *Trends in Endocrinology and Metabolism: TEM*, vol. 29, no. 1, pp. 55–65, 2018.

[14] T. Chiba, M. Yamada, J. Sasabe et al., "Amyloid-β causes memory impairment by disturbing the JAK2/STAT3 axis in hippocampal neurons," *Molecular Psychiatry*, vol. 14, no. 2, pp. 206–222, 2009.

[15] M. Foretz, B. Guigas, and B. Viollet, "Understanding the glucoregulatory mechanisms of metformin in type 2 diabetes mellitus," *Nature Reviews. Endocrinology*, vol. 15, no. 10, pp. 569–589, 2019.

[16] M. Packer, "Role of deranged energy deprivation signaling in the pathogenesis of cardiac and renal disease in states of perceived nutrient overabundance," *Circulation*, vol. 141, no. 25, pp. 2095–2105, 2020.

[17] S. Lin and D. Hardie, "AMPK: sensing glucose as well as cellular energy status," *Cell Metabolism*, vol. 27, no. 2, pp. 299–313, 2018.

[18] R. Fadó, R. Rodríguez-Rodríguez, and N. Casals, "The return of malonyl-CoA to the brain: cognition and other stories," *Progress in Lipid Research*, vol. 81, p. 101071, 2021.

[19] D. Steenberg, N. B. Jørgensen, J. B. Birk et al., "Exercise training reduces the insulin-sensitizing effect of a single bout of exercise in human skeletal muscle," *The Journal of Physiology*, vol. 597, no. 1, pp. 89–103, 2019.

[20] M. Ajami, H. Pazoki-Toroudi, H. Amani et al., "Therapeutic role of sirtuins in neurodegenerative disease and their modulation by polyphenols," *Neuroscience and Biobehavioral Reviews*, vol. 73, pp. 39–47, 2017.

[21] D. Ishibashi, T. Homma, T. Nakagaki et al., "Type I interferon protects neurons from prions in in vivo models," *Brain : a Journal of Neurology*, vol. 142, no. 4, pp. 1035–1050, 2019.

[22] F. Li, A. Sun, G. Cheng et al., "Compound C protects against cisplatin-induced nephrotoxicity through pleiotropic effects," *Frontiers in Physiology*, vol. 11, p. 614244, 2020.

[23] J. Xu, Z. Tang, Y. He et al., "Dl-3-n-butylphthalide ameliorates diabetic nephropathy by ameliorating excessive fibrosis and podocyte apoptosis," *Frontiers in Pharmacology*, vol. 12, p. 628950, 2021.

[24] G. Biessels and F. Despa, "Cognitive decline and dementia in diabetes mellitus: mechanisms and clinical implications," *Nature Reviews. Endocrinology*, vol. 14, no. 10, pp. 591–604, 2018.

[25] W. Chung, C. A. Welsh, B. A. Barres, and B. Stevens, "Do glia drive synaptic and cognitive impairment in disease?," *Nature Neuroscience*, vol. 18, no. 11, pp. 1539–1545, 2015.

[26] S. Fusco, M. Spinelli, S. Cocco et al., "Maternal insulin resistance multigenerationally impairs synaptic plasticity and memory via gametic mechanisms," *Nature Communications*, vol. 10, no. 1, p. 4799, 2019.

[27] E. Mäkinen, S. Lensu, M. Honkanen et al., "Rats bred for low intrinsic aerobic exercise capacity link obesity with brain inflammation and reduced structural plasticity of the hippocampus," *Brain, Behavior, and Immunity*, vol. 97, pp. 250–259, 2021.

[28] M. Yasuda, S. Nagappan-Chettiar, E. M. Johnson-Venkatesh, and H. Umemori, "An activity-dependent determinant of synapse elimination in the mammalian brain," *Neuron*, vol. 109, no. 8, pp. 1333–1349.e6, 2021.

[29] G. McGregor, A. Irving, and J. Harvey, "Canonical JAK-STAT signaling is pivotal for long-term depression at adult hippocampal temporoammonic-CA1 synapses," *FASEB Journal : Official Publication of the Federation of American Societies for Experimental Biology*, vol. 31, no. 8, pp. 3449–3466, 2017.

[30] Y. Zhang, B. Zhou, B. Deng et al., "Amyloid-β induces hepatic insulin resistance in vivo via JAK2," *Diabetes*, vol. 62, no. 4, pp. 1159–1166, 2013.

[31] D. Cui, T. Zeng, J. Ren et al., "KLF4 knockdown attenuates TBI-induced neuronal damage through p53 and JAK-STAT3 signaling," *CNS Neuroscience & Therapeutics*, vol. 23, no. 2, pp. 106–118, 2017.

[32] D. Kong, Y. Dagon, J. N. Campbell et al., "A postsynaptic AMPK→p21-activated kinase pathway drives fasting-induced synaptic plasticity in AgRP neurons," *Neuron*, vol. 91, no. 1, pp. 25–33, 2016.

[33] R. Ng, O. Y. Cheng, M. Jian et al., "Chronic adiponectin deficiency leads to Alzheimer's disease-like cognitive impairments and pathologies through AMPK inactivation and cerebral insulin resistance in aged mice," *Molecular Neurodegeneration*, vol. 11, no. 1, p. 71, 2016.

[34] W. Yang, X. Zhou, H. R. Zimmermann, and T. Ma, "Brain-specific suppression of AMPKα2 isoform impairs cognition and hippocampal LTP by PERK-mediated eIF2α phosphorylation," *Molecular Psychiatry*, vol. 26, no. 6, pp. 1880–1897, 2021.

[35] L. Bai, R. Liu, R. Wang et al., "Attenuation of Pb-induced Aβ generation and autophagic dysfunction via activation of SIRT1: neuroprotective properties of resveratrol," *Ecotoxicology and Environmental Safety*, vol. 222, p. 112511, 2021.

Hindawi
Disease Markers
Volume 2023, Article ID 9867801, 1 page
https://doi.org/10.1155/2023/9867801

Retraction

Retracted: Long Noncoding RNA TFAP2A-AS1 Suppressed Hepatitis B Virus Replication by Modulating miR-933/HDAC11

Disease Markers

Received 20 June 2023; Accepted 20 June 2023; Published 21 June 2023

This article has been retracted by Hindawi following an investigation undertaken by the publisher [1]. This investigation has uncovered evidence of one or more of the following indicators of systematic manipulation of the publication process:

(1) Discrepancies in scope

(2) Discrepancies in the description of the research reported

(3) Discrepancies between the availability of data and the research described

(4) Inappropriate citations

(5) Incoherent, meaningless and/or irrelevant content included in the article

(6) Peer-review manipulation

The presence of these indicators undermines our confidence in the integrity of the article's content and we cannot, therefore, vouch for its reliability. Please note that this notice is intended solely to alert readers that the content of this article is unreliable. We have not investigated whether authors were aware of or involved in the systematic manipulation of the publication process.

In addition, our investigation has also shown that one or more of the following human-subject reporting requirements has not been met in this article: ethical approval by an Institutional Review Board (IRB) committee or equivalent, patient/participant consent to participate, and/or agreement to publish patient/participant details (where relevant).

Wiley and Hindawi regrets that the usual quality checks did not identify these issues before publication and have since put additional measures in place to safeguard research integrity.

We wish to credit our own Research Integrity and Research Publishing teams and anonymous and named external researchers and research integrity experts for contributing to this investigation.

The corresponding author, as the representative of all authors, has been given the opportunity to register their agreement or disagreement to this retraction. We have kept a record of any response received.

References

[1] Y. Cheng, W. Shi, X. Cui et al., "Long Noncoding RNA TFAP2A-AS1 Suppressed Hepatitis B Virus Replication by Modulating miR-933/HDAC11," *Disease Markers*, vol. 2022, Article ID 7733390, 11 pages, 2022.

Hindawi
Disease Markers
Volume 2022, Article ID 7733390, 11 pages
https://doi.org/10.1155/2022/7733390

Research Article

Long Noncoding RNA TFAP2A-AS1 Suppressed Hepatitis B Virus Replication by Modulating miR-933/HDAC11

Yu Cheng,[1] Weiwu Shi,[2] Xudong Cui,[1] Lei Sun,[3] Yi Nan,[4] Hong Yao,[1] Jian Fan,[1] LiYing Zhu,[5] and Lei Yu[1]

[1]*Department of Infectious Disease, The Fourth Hospital of Harbin Medical University, Harbin, 150001 Heilongjiang, China*
[2]*Department of integrated internal medicine, Shanghai Donghai Senior Nursing Hospital, Shanghai, China*
[3]*Department of Ophthalmology, The Fourth Hospital of Harbin Medical University, Harbin, 150001 Heilongjiang, China*
[4]*Traditional Chinese Medicine College of Ningxia Medical University, Yinchuan 750004, China*
[5]*Department of Infectious Disease, The Second Hospital of Harbin Medical University, Harbin, 150000 Heilongjiang, China*

Correspondence should be addressed to LiYing Zhu; zlyhmu@163.com and Lei Yu; widedoor@sina.com

Received 8 December 2021; Accepted 29 January 2022; Published 18 April 2022

Academic Editor: XIANWEI ZENG

Objective. Studies have shown that long noncoding RNAs (lncRNAs) play crucial roles in multiple tumor types and regulate various biological processes. The present study tried to study lncRNA TFAP2A-AS1 in HBV infection hepatocellular carcinoma. *Methods.* The level of TFAP2A-AS1 and miR-933 in HCC cell and samples were detected by qRT-PCR assay. Luciferase reporter gene assay was carried out to study the mechanism of TFAP2A-AS1 and miR-933. Cell proliferation was measured by CCK-8 assay. HBV DNA replication was detected by RT-qPCR. *Results.* We firstly demonstrated that TFAP2A-AS1 was downregulated in HCC cell lines and HBV-infected HCC samples compared with nontumor tissues. However, miR-933 was upregulated in HCC cell lines and HBV-infected HCC samples compared with nontumor tissues, and miR-933 was negatively associated with the expression of TFAP2A-AS1 in HBV-correlated HCC samples. TFAP2A-AS1 and HDAC11 expression was decreased and miR-933 was upregulated in the HBV-infected cell HepG2.2.15. TFAP2A-AS1 acted as a sponge for miR-933 and HDAC11 was one direct target gene for miR-933. Overexpression of TFAP2A-AS1 suppressed cell growth, HBV DNA replication, HbeAg, and HbsAg expression, while knockdown of TFAP2A-AS1 enhanced cell proliferation, HBV DNA replication, HbeAg, and HbsAg expression in HepG2.2.15 cell. In addition, ectopic expression of miR-933 promoted cell growth, HBV DNA replication, HbeAg, and HbsAg expression in HepG2.2.15 cell. TFAP2A-AS1 suppressed HBV replication and infection through regulating HDAC11. *Conclusion.* These data demonstrated that TFAP2A-AS1 acted crucial roles in the modulation of HbeAg and HbsAg expression and HBV replication and may be one potential target for HBV infection treatment.

1. Introduction

HBV (hepatitis B virus) could cause acute or chronic infection of hepatitis B, which was supposed to be the most risk factor for hepatocellular carcinoma and chronic liver cirrhosis [1–4]. Epidemiological reports show that there are 400 million people with HBV infection worldwide and the number is still increasing. Importantly, more than 30% HBV infection cases were from China [5–7]. HBV can relax genome of rcDNA (circular DNA) in the nucleocapsid and then converted into cccDNA (covalently closed circular DNA), which acted important roles in viral persistence [8–10]. Thus, it is of great significance to investigate the mechanism of HCC development induced by HBV.

Long noncoding RNAs (lncRNAs) are one group of transcripts more than 200 nucleotides in length that have limited or no protein-coding capacity [11–16]. References revealed that lncRNAs were misregulated in a variety of tumors including bladder tumor, ovarian cancer, neuroblastoma, gallbladder cancer, and also HBV-induced hepatocellular carcinoma [17–21]. LncRNAs regulate diverse cell processes such as cell differentiation, development, apoptosis, metabolism, and protein synthesis [22–27]. Recently, TFAP2A-AS1 has been identified to be downregulated in

breast cancer cell and samples, and TFAP2A-AS1 overexpression suppressed cell invasion and proliferation and decreased tumor development in vivo [28]. However, its role in HBV infection and HBV-correlated HCC remains uncovered.

We manifested that TFAP2A-AS1 was downregulated in HCC cell lines and HBV-infected HCC samples and ectopic expression of TFAP2A-AS1 suppressed HBV replication and infection.

2. Materials and Methods

2.1. Clinical Samples. HBV-induced HCC specimens and nontumor tissues were collected from our hospital and were stored in liquid nitrogen until used. This research was agreed by the Clinical Ethics Committee of The Fourth Hospital of Harbin Medical University and informed consents were obtained.

2.2. Cell Transfection and Culture. HCC cells without HBV infection HepG2 and HepG2.2.15 (HCC cell with HBV infection) were purchased from ATCC and cultured in DMEM medium (Gibco, USA), supplemented by streptomycin, penicillin, and FBS. pcDNA-control, pcDNA-TFAP2A-AS1, si-control and si- TFAP2A-AS1, miR-scramble, and miR-933 mimic were synthesized from GenePharma (Shanghai, China). Cell transfection was performed by Lipofectamine2000 with the product's protocol.

2.3. Luciferase Reporter Gene Assay. Fragment from 3′UTR of TFAP2A-AS1 and mutant 3′UTR of TFAP2A-AS1 containing miR-933 binding sites were incloned into the psiCHECK2 plasmid (Promega, WI, USA). Scramble or miR-933 mimic and HDAC11 wt-3′UTR and HDAC11 mut-3′UTR and luciferase reporter vector were transfected to cells and the luciferase activity was evaluated with Luciferase Reporter kit (Promega).

2.4. RT-qPCR. RNA was extracted from specimen or cell using the TRIzol kit (Invitrogen, CA, USA) with the product's instructions. RT-qPCR (Quantitative RT-PCR) was employed to measure mRNA, miRNA, and lncRNA expression with TaKaRa SYBR Green (Dalian, China) on 7500 ABI system (Applied Biosystems, CA, USA). The method of $2^{-\Delta\Delta Ct}$ was utilized to calculate relative fold change. Primers are shown as follows: GAPDH: F, 5′-TGTTCG TCATGG GTGTGA AC-3′, 5′-ATGGCA TGGACT GTGGTC AT-3′; miR-933: F, 5′-ATTATA TGTGCG CAGGGA GACC-3′, R, 5′-GCGAGC ACAGAA TTAATA CGACTC ACTATA GG-3′; TFAP2A-AS1: F, 5′-CTTGAC AGCTCC AGGGGT TA-3′, R, 5′-TCTAGA CTTGCA GGCACA CA-3′.

2.5. HBV Replication and Gene Expression Analysis. The DNA of HBV from cell supernatants was extracted by the Viral Column DNA out reagent (TIANDZ, China) following to the product's information and measured with RT-qPCR method. The HBsAg (hepatitis B surface antigen) and HBeAg (hepatitis B e antigen) expression in supernatants of HCC cell was determined with the ELISA reagent (Biotech, Shanghai).

2.6. Statistical Analysis. Data were analyzed with SPSS-19.0 (Chicago, USA) and showed as the mean ± SD (standard deviation). Student's *t*-test was applied to measure comparison difference between two groups. p data of <0.05 was represented as significant.

3. Results

3.1. TFAP2A-AS1 Level in HBV-Associated HCC Samples. RT-qPCR assay was carried out to determine TFAP2A-AS1 in HCC cell, HBV-infected HCC samples, and nontumor tissues. As indicated in Figure 1(a), TFAP2A-AS1 was downregulated in HCC cell lines compared with HL-7702. TFAP2A-AS1 level was lower in HBV-infected HCC samples compared with nontumor tissues (Figure 1(b)). Moreover, TFAP2A-AS1 was downregulated in 31 cases (77.5%) compared to nontumor tissues (Figure 1(c)).

3.2. miR-933 Level in HBV-Associated HCC Samples. RT-qPCR analysis was carried out to detect miR-933 expression in HCC cell, HBV-infected HCC samples, and nontumor tissues. As indicated in Figure 2(a), miR-933 was upregulated in HCC cell lines compared to HL-7702. MiR-933 level was higher in HBV-infected HCC samples compared to nontumor tissues (Figure 2(b)). Moreover, miR-933 was upregulated in 27 cases (67.5%) compared to nontumor tissues (Figure 2(c)). MiR-933 expression was negatively associated with TFAP2A-AS1 expression in HBV-correlated HCC samples (Figure 2(d)).

3.3. TFAP2A-AS1 Sponged miR-933 in HCC Cell. MiR-933 was significantly upregulated in HepG2.2.15 cell after transfected with miR-933 mimic (Figure 3(a)). Based on the bioinformatics Starbase forecast (http://starbase.sysu.edu.cn/index.php), TFAP2A-AS1 potentially bind to miR-933 (Figure 3(b)). Elevated expression of miR-933 decreased luciferase activity of TFAP2A-AS1-Wt but not TFAP2A-AS1-Mut (Figure 3(c)). RT-qPCR assay showed that TFAP2A-AS1 was overexpressed in HepG2.2.15 cell after transfected with pcDNA-TFAP2A-AS1 (Figure 3(d)). Overexpression of TFAP2A-AS1 repressed miR-933 expression in HepG2.2.15 cell (Figure 3(e)).

3.4. miR-933 Targeted HDAC11 in HCC Cell. Based on the bioinformatics TargetScan system (http://www.targetscan.org/vert_72/), HDAC11 potentially bind to miR-933 (Figure 4(a)). Overexpression of miR-933 suppressed luciferase activity of HDAC11-Wt but not HDAC11-Mut (Figure 4(b)). RT-qPCR assay was performed and indicated that elevated expression of miR-933 suppressed HDAC11 in HepG2.2.15 cell (Figure 4(c)). Overexpression of HDAC11 promoted HDAC11 expression in HepG2.2.15 cell (Figure 4(d)).

3.5. TFAP2A-AS1 and miR-933 Level in HBV-Infected Cell. The levels of TFAP2A-AS1, miR-933, and HDAC11 were detected by qRT-PCR analysis in HBV-infected HepG2 (HepG2.2.15) cell and HepG2 cell. TFAP2A-AS1 expression was downregulated in HepG2.2.15 cell compared to HepG2 cell (Figure 5(a)). MiR-933 level was overexpressed in

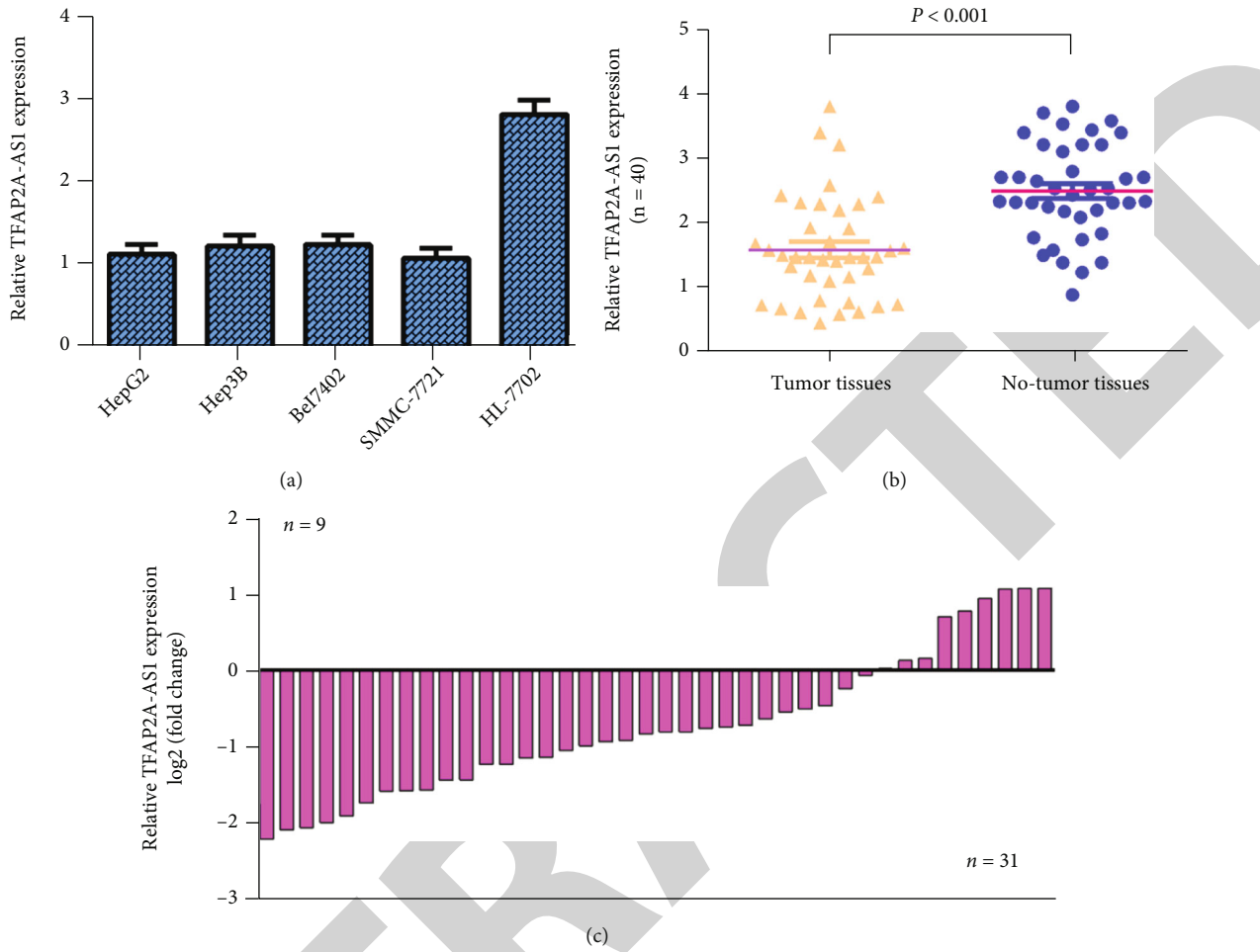

Figure 1: TFAP2A-AS1 level in HBV-associated HCC samples. (a) TFAP2A-AS1 expression was detected by RT-qPCR assay in HCC cell lines and HL-7702. (b) TFAP2A-AS1 in HBV-infected HCC samples and no-tumor tissues was measured by RT-qPCR analysis. (c) TFAP2A-AS1 was downregulated in 31 cases (77.5%) compared to no-tumor tissues.

HepG2.2.15 cell compared to HepG2 cell (Figure 5(b)). Moreover, HDAC11 expression was decreased in HepG2.2.15 cell compared to HepG2 cell (Figure 5(c)).

3.6. TFAP2A-AS1 Inhibited HBV Replication and Infection. To identify whether TFAP2A-AS1 regulated HBV replication and expression, cell was treated with pcDNA-control, pcDNA-TFAP2A-AS1, si-control, and si-TFAP2A-AS1, respectively. RT-qPCR assay was carried out to indicate that TFAP2A-AS1 was downregulated in HepG2.2.15 cell after transfected with si-TFAP2A-AS1 (Figure 6(e)). Ectopic expression of TFAP2A-AS1 suppressed cell growth (Figure 6(a)), while TFAP2A-AS1 knockdown enhanced cell proliferation in HepG2.2.15 cell using CCK-8 assays (Figure 6(f)). HbsAg and HbeAg levels were determined with ELISA, and DNA replication of HBV was detected by RT-qPCR. Elevated expression of TFAP2A-AS1 suppressed DNA replication of HBV (Figure 6(b)), while knockdown of TFAP2A-AS1 increased HBV DNA replication (Figure 6(g)). Moreover, TFAP2A-AS1 overexpression inhibited expression of HbsAg (Figure 6(c)) and HbeAg (Figure 6(d)), while TFAP2A-AS1 knockdown enhanced their expression (Figures 6(h) and 6(i)).

3.7. miR-933 Increased HBV Replication and Infection. To learn whether miR-933 modulate HBV replication and expression, cell was treated with scramble and miR-933 mimic, respectively. Ectopic expression of miR-933 promoted cell growth in HepG2.2.15 cell using CCK-8 assays (Figure 7(a)). Elevated expression of miR-933 promoted DNA replication of HBV (Figure 7(b)). Ectopic expression of miR-933 enhanced the expression of HbsAg (Figure 7(c)) and HbeAg (Figure 7(d)).

3.8. TFAP2A-AS1 Suppressed HBV Replication and Infection through Modulating HDAC11. To study whether TFAP2A-AS1 suppressed HBV replication and infection through regulating HDAC11, cells were transfected with si-TFAP2A-AS1 and cotransfected pcDNA-HDAC11 or its pcDNA-control. The results indicated that knockdown of TFAP2A-AS1 enhanced HBV DNA replication, while cotransfection with pcDNA-HDAC11 inhibited HBV DNA replication (Figure 8(a)). Ectopic expression of HDAC11 suppressed the expression of HbeAg (Figure 8(b)) and HbsAg (Figure 8(c)) in TFAP2A-AS1 knockdown-HepG2.2.15 cells.

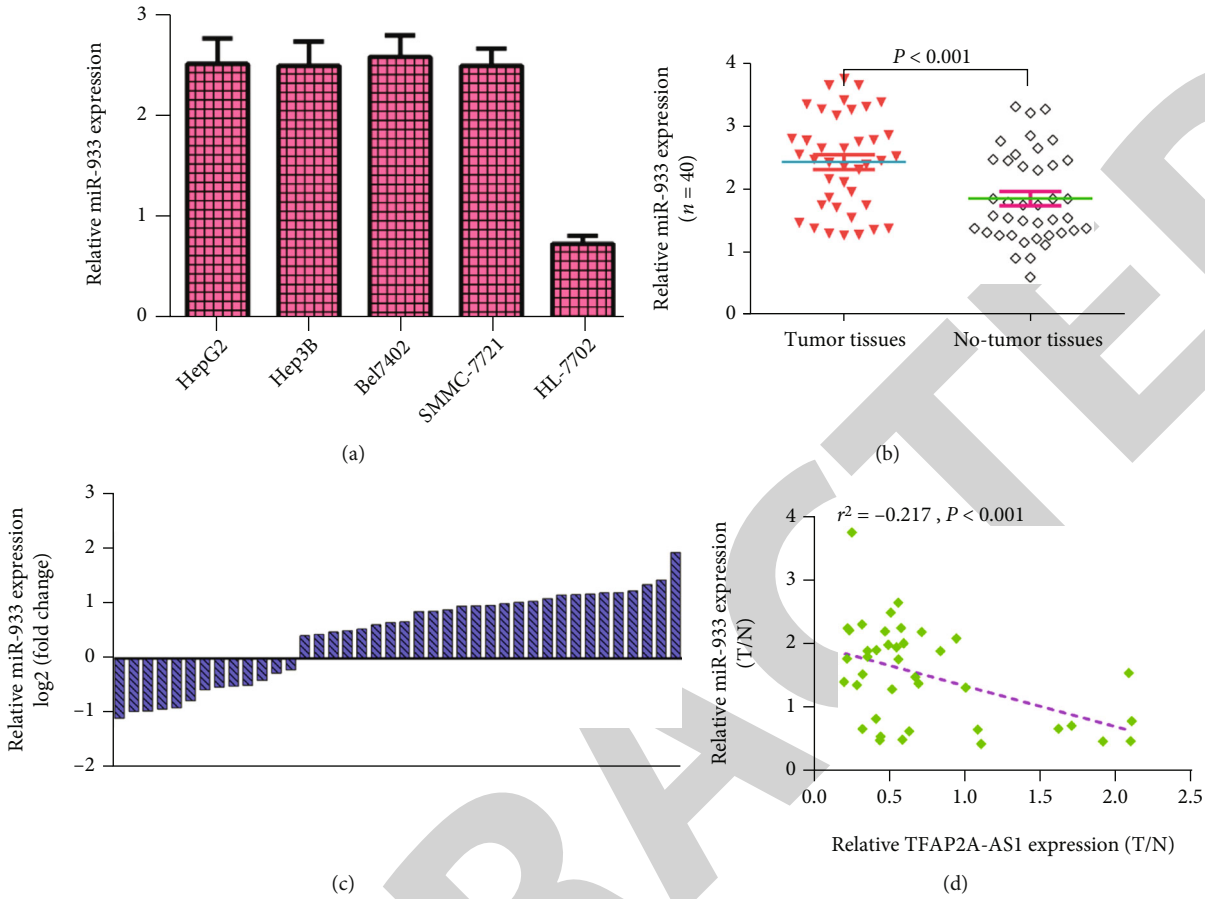

Figure 2: miR-933 level in HBV-associated HCC samples. (a) miR-933 expression was detected by RT-qPCR assay in HCC cell lines and HL-7702. (b) miR-933 in HBV-infected HCC samples and no-tumor tissues was measured by RT-qPCR analysis. (c) miR-933 was upregulated in 27 cases (67.5%) compared to no-tumor tissues. (d) miR-933 was negatively associated with expression of TFAP2A-AS1 in HBV-correlated HCC samples.

4. Discussion

To improve the treatment of HBV infection and associated HCC, new therapies must be explored. We firstly showed that TFAP2A-AS1 was downregulated in HCC cell lines and HBV-infected HCC samples compared to nontumor tissues. However, miR-933 was upregulated in HCC cell lines and HBV-infected HCC samples compared to nontumor tissues, and miR-933 was negatively associated with the expression of TFAP2A-AS1 in HBV-correlated HCC samples. The expression of TFAP2A-AS1 and HDAC11 was decreased while miR-933 was overexpressed in HBV-infected cell HepG2.2.15. TFAP2A-AS1 acted as one sponge for miR-933 and HDAC11 was one direct target gene for miR-933. Ectopic expression of TFAP2A-AS1 suppressed cell growth, HBV DNA replication, HbeAg, and HbsAg expression, while knockdown of TFAP2A-AS1 enhanced cell proliferation, HBV DNA replication, HbeAg, and HbsAg expression in HepG2.2.15 cell. In addition, ectopic expression of miR-933 promoted cell growth, HBV DNA replication, HbeAg, and HbsAg expression in HepG2.2.15 cell. TFAP2A-AS1 suppressed HBV replication and infection through modulating HDAC11. These data illustrated that TFAP2A-AS1 acted crucial roles in the modulation of HBV replication and may be one potential therapeutic target for HBV infection.

Studies have shown that lncRNAs exerted crucial roles in multiple tumor types and modulated various biological processes [29–31]. For instance, Deng et al. [32] showed that lncRNA F11-AS1 suppressed HBV-associated HCC development through modulating miR-211-5p/NR1I3. Feng et al. indicated that PCNA and lncRNA PCNAP1 was upregulated in HBV-infectious chimeric mice and PCNAP1 promoted HBV replication via regulating PCNA/miR-154/HBV signaling [33]. LncRNA H19 was proved to induce HBV-related HCC development by modulating miR-22 [34]. Recently, TFAP2A-AS1 was identified to be downregulated in breast cancer cell and samples and TFAP2A-AS1 overexpression suppressed cell invasion and proliferation and decreased tumor development in vivo [28]. We also found that TFAP2A-AS1 was downregulated in HCC cell lines and HBV-infected HCC samples. Ectopic expression of TFAP2A-AS1 suppressed cell growth, HBV DNA replication, HbeAg, and HbsAg expression, while knockdown of TFAP2A-AS1 enhanced cell proliferation, HBV DNA replication, HbeAg, and HbsAg expression in HepG2.2.15 cell.

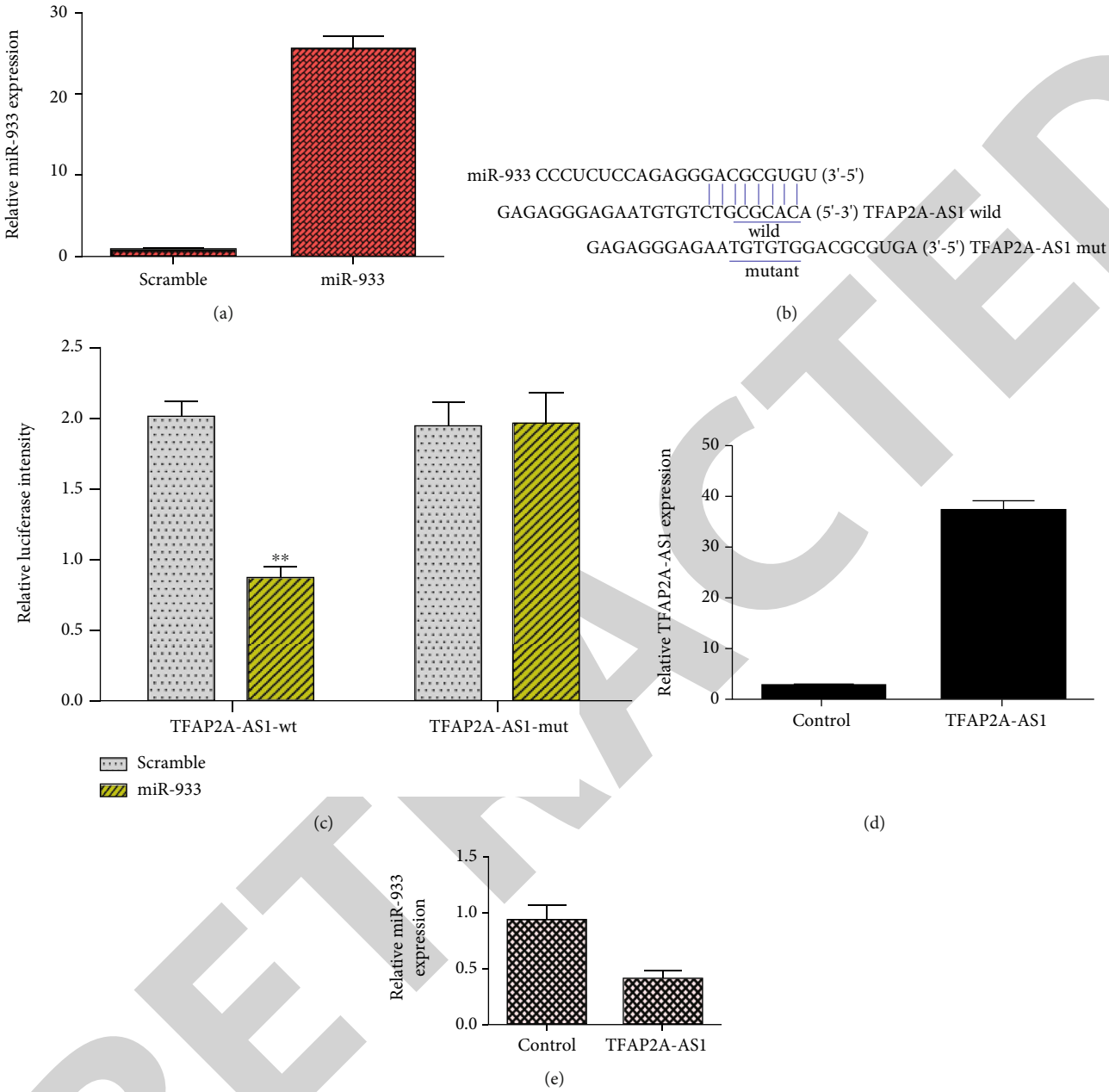

Figure 3: TFAP2A-AS1 sponged miR-933 in HCC cell. (a) The miR-933 expression was detected by RT-qPCR assay. (b) Based on bioinformatics Starbase forecast (http://starbase.sysu.edu.cn/index.php), TFAP2A-AS1 potentially binded to miR-933. (c) Elevated expression of miR-933 decreased luciferase activity of TFAP2A-AS1-Wt but not TFAP2A-AS1-Mut. (d) RT-qPCR assay was carried out to show that TFAP2A-AS1 was overexpressed in HepG2.2.15 cell after transfected with pcDNA-TFAP2A-AS1. (e) Overexpression of TFAP2A-AS1 repressed miR-933 in HepG2.2.15 cell. $^{**}p < 0.01$.

Multiple studies have shown that lncRNA participated in tumor progression and occurrence by acting as one sponge for miRNAs and their correlated genes [35–37]. Zhao et al. [38] found that lncRNA TINCR inhibited HCC invasion and growth through sponging miR-218-5p/DDX5. Wu et al. [39] showed that lncRNA SUMO1P3 induced HCC development by promoting Wnt/β-catenin pathway via sponging miR-320a. Dai et al. [40] demonstrated that lncRNA TUG1 enhanced HCC progression through modulating DLX2/miR-216b-5p axis. Zheng et al. [41] demonstrated that linc00467 promoted HCC development through sponging NEDD9/miR-18a-5p. A recent study showed that TFAP2A-AS1 suppressed breast cancer progression through sponging miR-933 [28]. Based on the bioinformatics TargetScan system, HDAC11 can potentially bind to miR-933. Overexpression of miR-933 suppressed luciferase activity of HDAC11-Wt but not HDAC11-Mut. Overexpression of TFAP2A-AS1 repressed miR-933 in HepG2.2.15 cell. MiR-933 expression level was higher in HBV-infected HCC samples compared to nontumor tissues.

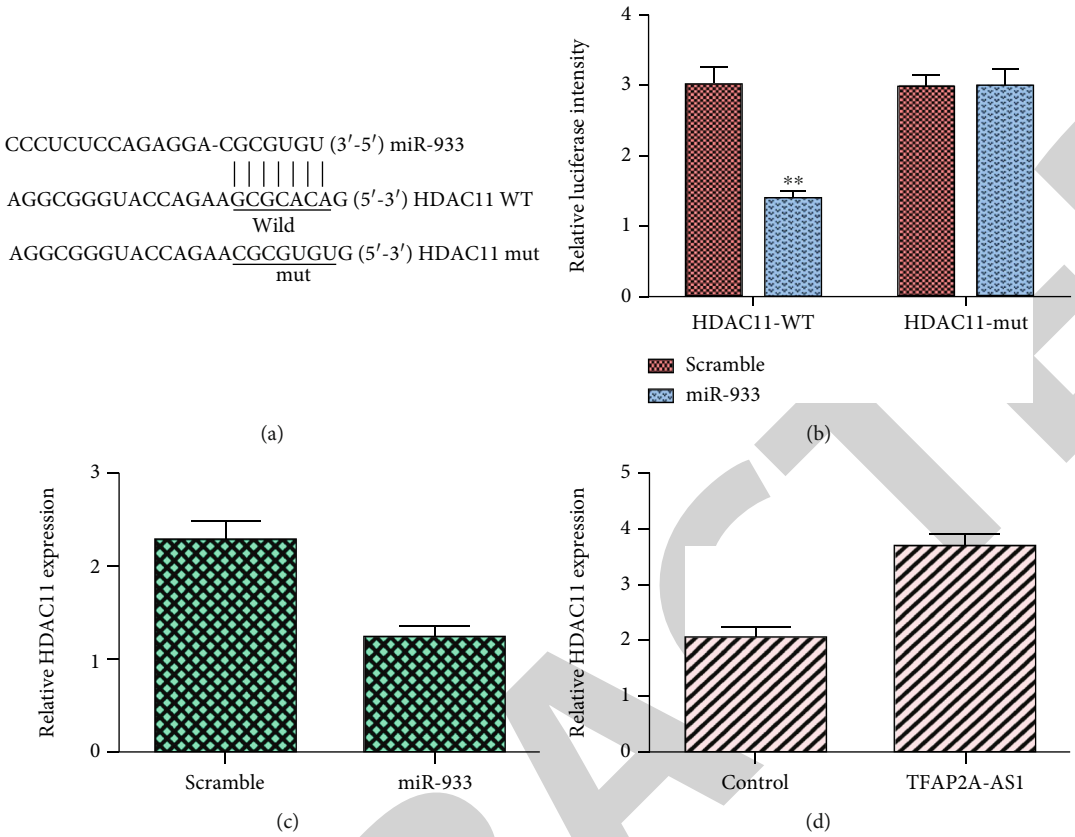

Figure 4: miR-933 targeted HDAC11 in HCC cell. (a) Based on bioinformatics TargetScan system (http://www.targetscan.org/vert_72/), HDAC11 potentially binded to miR-933. (b) Overexpression of miR-933 suppressed luciferase activity of HDAC11-Wt but not HDAC11-Mut. (c) RT-qPCR assay was performed to indicate that elevated expression of miR-933 suppressed HDAC11 in HepG2.2.15 cell. (d) Overexpression of HDAC11 promoted HDAC11 level in HepG2.2.15 cell. $^{**}p < 0.01$.

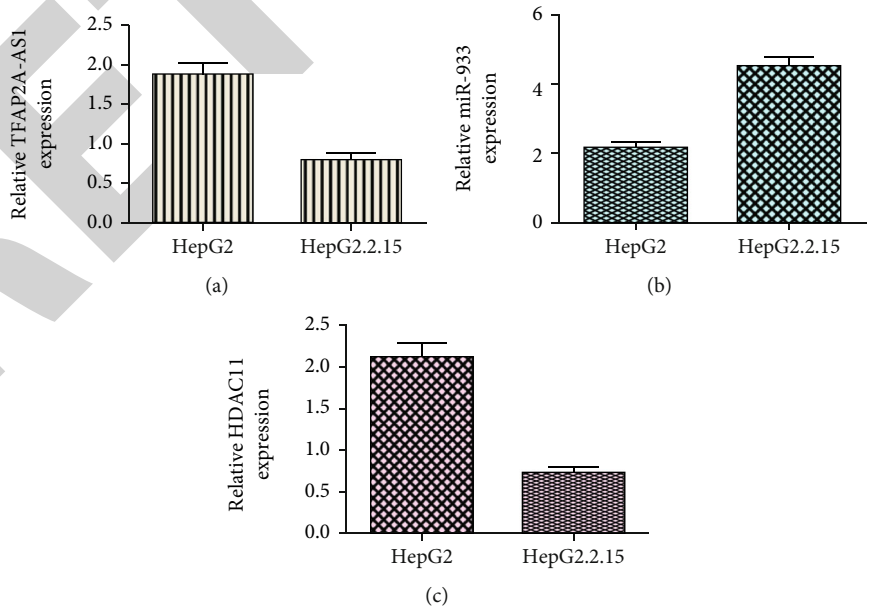

Figure 5: TFAP2A-AS1 and miR-933 level in HBV-infected cell. (a) TFAP2A-AS1 was downregulated in HepG2.2.15 cell compared to HepG2 cell. (b) The miR-933 level was measured by RT-qPCR assay. (c) The miR-933 HDAC11 was measured by RT-qPCR assay.

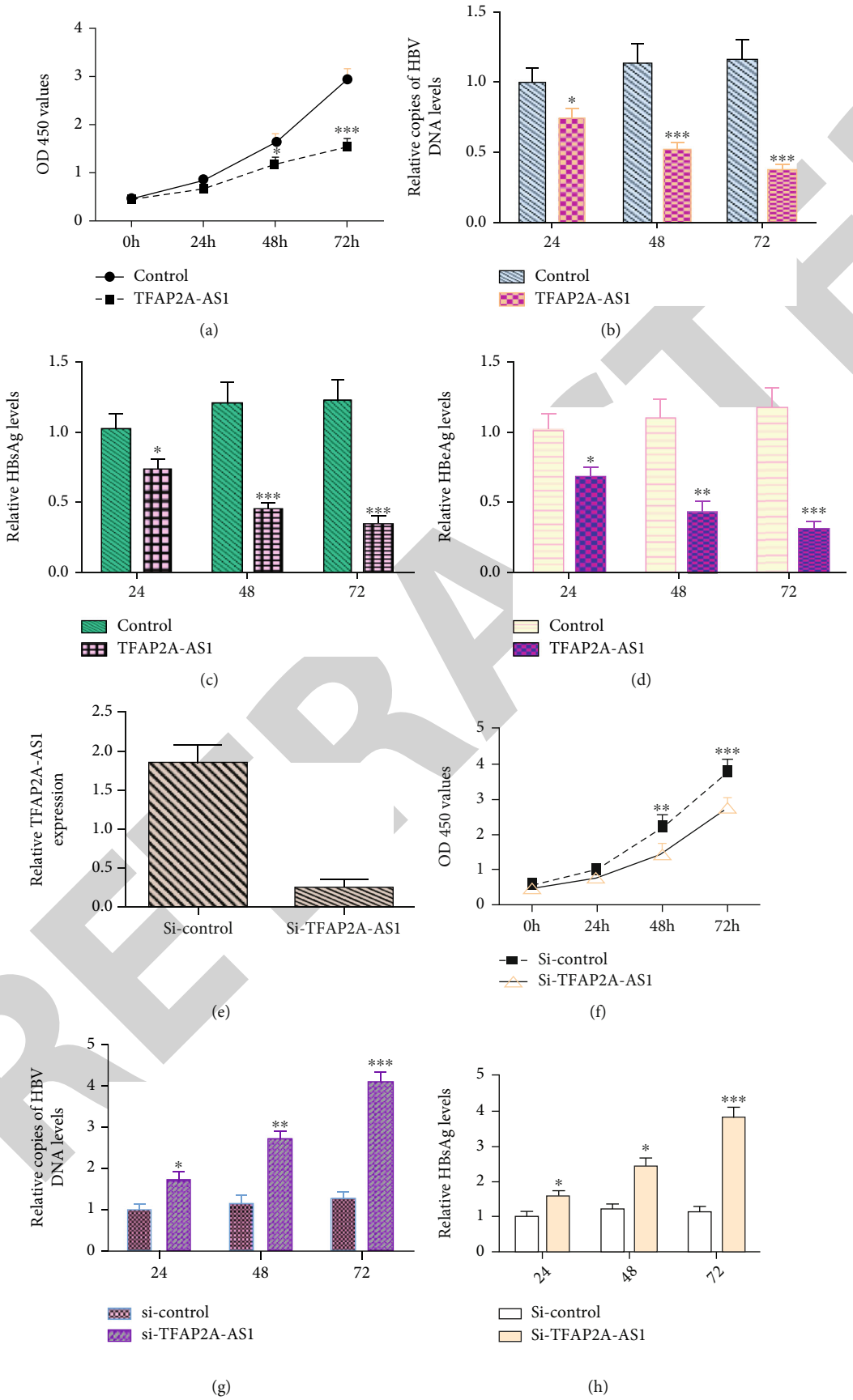

Figure 6: Continued.

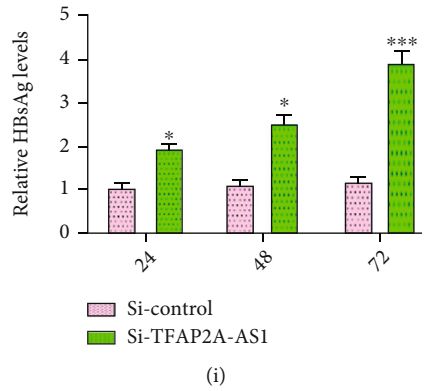

Figure 6: TFAP2A-AS1 inhibited HBV replication and infection. (a) Ectopic expression of TFAP2A-AS1 suppressed cell growth in HepG2.2.15 cell. (b) Elevated expression of TFAP2A-AS1 suppressed DNA replication of HBV. (c) TFAP2A-AS1 overexpression inhibited HbsAg expression in HepG2.2.15 cell. (d) Elevated expression of TFAP2A-AS1 HbeAg expression in HepG2.2.15 cell. (e) The expression of TFAP2A-AS1 was detected by RT-qPCR assay. (f) TFAP2A-AS1 knockdown enhanced cell proliferation in HepG2.2.15 cell using CCK-8 assays. (g) Knockdown of TFAP2A-AS1 increased HBV DNA replication. (h) TFAP2A-AS1 knockdown enhanced HbsAg expression. (i) HbeAg level was determined with ELISA. $^{*}p < 0.05$, $^{**}p < 0.01$, and $^{***}p < 0.001$.

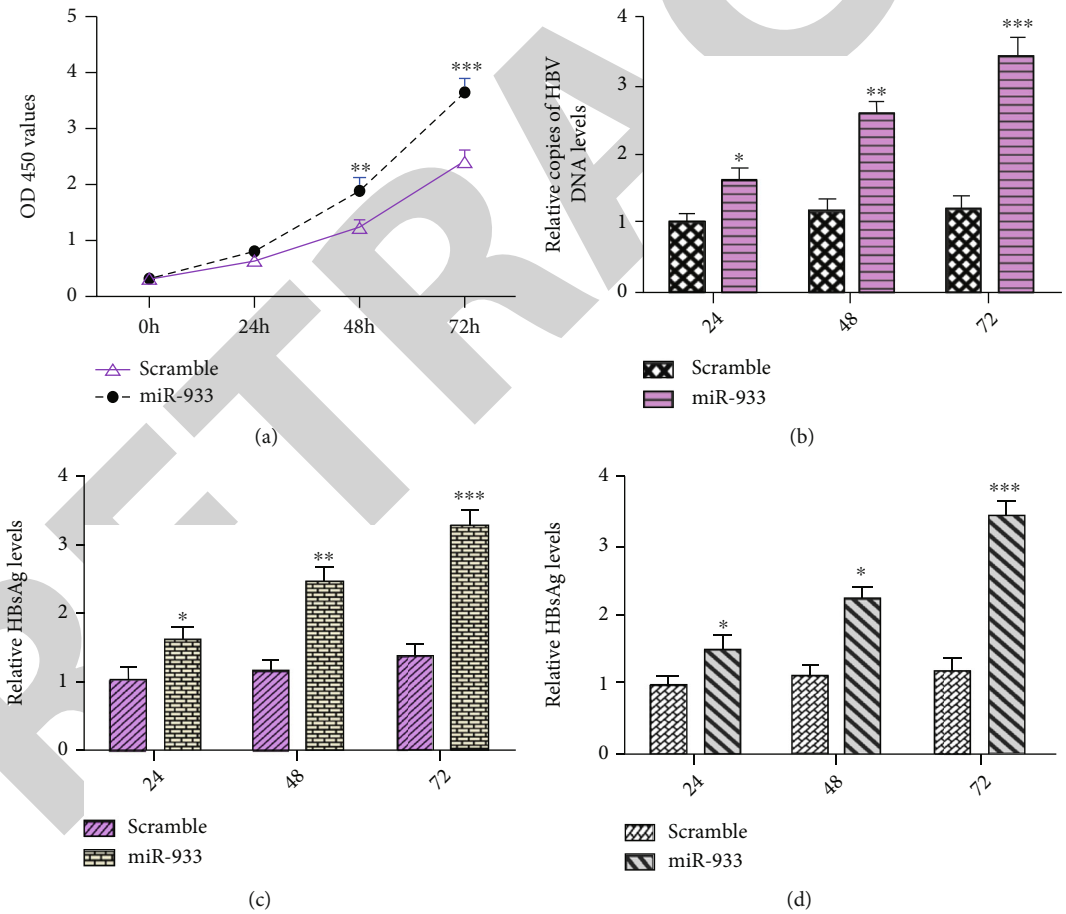

Figure 7: miR-933 increased HBV replication and infection. (a) Ectopic expression of miR-933 promoted cell growth in HepG2.2.15 cell using CCK-8 assays. (b) Elevated expression of miR-933 promoted DNA replication of HBV. (c) Ectopic expression of miR-933 enhanced HbsAg expression. (d) HbeAg level was determined with ELISA. $^{*}p < 0.05$, $^{**}p < 0.01$, and $^{***}p < 0.001$.

miR-933 expression was negatively associated with the expression of TFAP2A-AS1 in HBV-correlated HCC samples. Moreover, HDAC11 suppressed HBV replication via epigenetic inhibition of cDNA transcription [42]. Furthermore, we showed that TFAP2A-AS1 suppressed HBV replication and infection through modulating HDAC11.

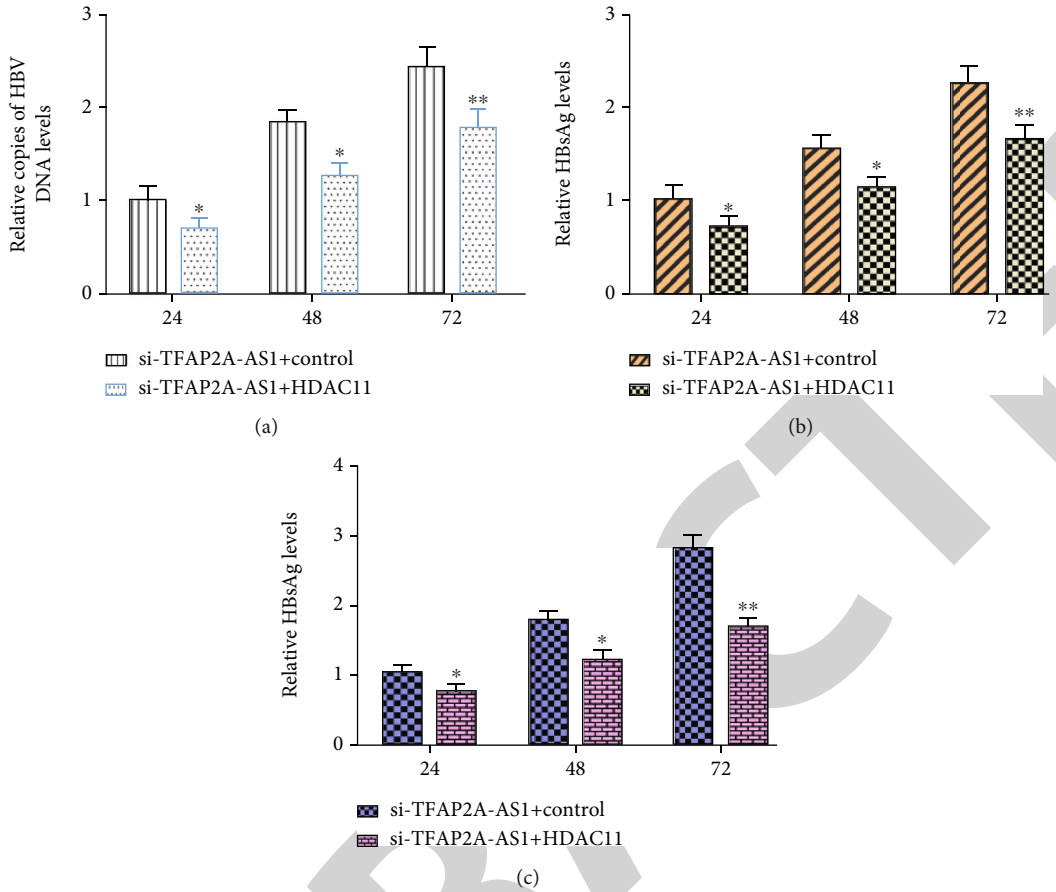

Figure 8: TFAP2A-AS1 suppressed HBV replication and infection through modulating HDAC11. (a) Knockdown of TFAP2A-AS1 enhanced HBV DNA replication, while cotransfection with pcDNA-HDAC11 inhibited HBV DNA replication. (b) HbeAg level was determined with ELISA. (c) HbsAg level was determined with ELISA. $^{*}p < 0.05$ and $^{**}p < 0.01$.

Our manuscript has some limitations. The sample size is small and more samples are needed to study the expression of TFAP2A-AS1. Secondly, the function of TFAP2A-AS1 needs to be verified in vivo.

5. Conclusion

Collectively, our data showed that TFAP2A-AS1 was down-regulated in HCC cell lines and HBV-infected HCC samples, and ectopic expression of TFAP2A-AS1 suppressed HBV replication and infection through modulating miR-933/HDAC11. These data suggested that TFAP2A-AS1 may be a potential therapeutic target for HBV infection.

Abbreviations

HBV: Hepatitis B virus
HCC: Hepatocellular carcinoma
lncRNAs: Long noncoding RNAs
ncRNAs: Noncoding RNAs
miR-933: microRNA-933
ATCC: American Type Culture Collection
FBS: Fetal bovine serum
cDNAs: Complementary DNAs.

Data Availability

The authors can make data available on request through an email to the corresponding author, Lei Yu, Email: wide-door@sina.com and Liying Zhu, Email: zlyhmu@163.com

Ethical Approval

This study was performed with the approval of the Clinical Ethics Committee of the Four Affiliated Hospital of Harbi Medical University. Each patient has written an informed consent.

Consent

No consent was necessary.

Conflicts of Interest

We declare that they have no conflicts of interest.

Authors' Contributions

Y C, NN F, XD C, LY Z, L S, Y N, H Y, J F, and L Y have all contributed to designing and writing the manuscript. Yu Cheng, Weiwu Shi and Xudong Cui are co-first authors.

Acknowledgments

This work was supported by the Postdoctoral Scientific Research Developmental Fund of Heilongjiang Province (No. LBH-Q14115) and sponsored by the National Science and Technology Major Project (2014ZX10002002), Natural Science Foundation of Heilongjiang Province (ZD2015019), and Special Fund of the Fourth Affiliated Hospital of Harbin Medical University (HYDSYTB202206).

References

[1] J. Jin, S. Tang, L. Xia et al., "MicroRNA-501 promotes HBV replication by targeting HBXIP," *Biochemical and Biophysical Research Communications*, vol. 430, no. 4, pp. 1228–1233, 2013.

[2] R. Lamontagne, J. Casciano, and M. Bouchard, "A broad investigation of the HBV-mediated changes to primary hepatocyte physiology reveals HBV significantly alters metabolic pathways," *Metabolism, Clinical and Experimental*, vol. 83, pp. 50–59, 2018.

[3] M. Ohno, M. Otsuka, T. Kishikawa et al., "Specific delivery of microRNA93 into HBV-replicating hepatocytes downregulates protein expression of liver cancer susceptible gene MICA," *Oncotarget*, vol. 5, no. 14, pp. 5581–5590, 2014.

[4] H. Pan, D. D. Niu, H. Feng, L. F. P. Ng, E. C. Ren, and W. N. Chen, "Cellular transcription modulator SMARCE1 binds to HBV core promoter containing naturally occurring deletions and represses viral replication," *Biochimica et Biophysica Acta (BBA)-Molecular Basis of Disease*, vol. 1772, no. 9, pp. 1075–1084, 2007.

[5] E. M. Janahi, Z. Ilyas, S. Al-Othman et al., "Hepatitis B Virus Genotypes in the Kingdom of Bahrain: Prevalence, Gender Distribution and Impact on Hepatic Biomarkers," *Medicina*, vol. 55, no. 10, 2019.

[6] Y. Jin, N. Geng, L. Zhao et al., "The prevalence of HBV infection: a retrospective study of 13-years in a public hospital of Northeast China," *Viral Immunology*, vol. 33, 2019.

[7] A. Schweitzer, J. Horn, R. T. Mikolajczyk, G. Krause, and J. J. Ott, "Estimations of worldwide prevalence of chronic hepatitis B virus infection: a systematic review of data published between 1965 and 2013," *The Lancet*, vol. 386, no. 10003, pp. 1546–1555, 2015.

[8] Q. Ou, J. Guo, Y. Zeng, and H. Chen, "Insights for clinical diagnostic indicators of virus and host in chronic hepatitis B infection," *Journal of Viral Hepatitis*, vol. 27, 2020.

[9] M. S. Farag, M. J. van Campenhout, M. Pfefferkorn et al., "Hepatitis B virus RNA as early predictor for response to PEGylated interferon alfa in HBeAg negative chronic hepatitis B," *Clinical Infectious Diseases*, vol. 72, 2020.

[10] N. Lin, A. Ye, J. Lin et al., "Diagnostic value of detection of Pregenomic RNA in sera of hepatitis B virus-infected patients with different clinical outcomes," *Journal of Clinical Microbiology*, vol. 58, no. 2, 2020.

[11] Z. Li, X. Li, X. Chen et al., "Emerging roles of long non-coding RNAs in neuropathic pain," *Cell Proliferation*, vol. 52, no. 1, 2019.

[12] Y. F. Zou, Y. Zhong, J. Wu et al., "Long non-coding PANDAR as a novel biomarker in human cancer: a systematic review," *Cell Proliferation*, vol. 51, no. 1, 2018.

[13] S. B. Zhu, W. Fu, L. Zhang et al., "LINC00473 antagonizes the tumour suppressor miR-195 to mediate the pathogenesis of Wilms tumour via IKKα," *Cell Proliferation*, vol. 51, no. 1, 2018.

[14] J. Zhao, C. Zhang, Z. Gao, H. Wu, R. Gu, and R. Jiang, "Retracted: Long non-coding RNA ASBEL promotes osteosarcoma cell proliferation, migration, and invasion by regulating microRNA-21," *Journal of Cellular Biochemistry*, vol. 119, no. 8, pp. 6461–6469, 2018.

[15] W. C. Xiong, N. Han, N. Wu et al., "Interplay between long noncoding RNA ZEB1-AS1 and miR-101/ZEB1 axis regulates proliferation and migration of colorectal cancer cells," *American Journal of Translational Research*, vol. 10, no. 2, pp. 605–617, 2018.

[16] Q. Chen, X. Huang, and R. Li, "lncRNA MALAT1/miR-205-5p axis regulates MPP-induced cell apoptosis in MN9D cells by directly targeting LRRK2," *American Journal of Translational Research*, vol. 10, no. 2, pp. 563–572, 2018.

[17] A. He, Y. Liu, Z. Chen et al., "Over-expression of long noncoding RNA BANCR inhibits malignant phenotypes of human bladder cancer," *Journal of Experimental & Clinical Cancer Research*, vol. 35, no. 1, 2016.

[18] X. Fu, L. Zhang, L. Dan, K. Wang, and Y. Xu, "LncRNA EWSAT1 promotes ovarian cancer progression through targeting miR-330-5p expression," *American Journal of Translational Research*, vol. 9, no. 9, pp. 4094–4103, 2017.

[19] N. Malyshok, O. Mankovska, and V. Kashuba, "Prediction of ANRIL long non-coding RNA sponge activity in neuroblastoma and Alzheimer disease," *FEBS Journal*, vol. 283, pp. 282–282, 2016.

[20] M. Z. Ma, B. F. Chu, Y. Zhang et al., "Long non-coding RNA CCAT1 promotes gallbladder cancer development via negative modulation of miRNA-218-5p," *Cell Death & Disease*, vol. 6, no. 1, 2015.

[21] B. He, F. Peng, W. Li, and Y. Jiang, "Interaction of lncRNA-MALAT1 and miR-124 regulates HBx-induced cancer stem cell properties in HepG2 through PI3K/Akt signaling," *Journal of Cellular Biochemistry*, vol. 120, no. 3, pp. 2908–2918, 2019.

[22] Z. Li, X. Li, C. Chen et al., "Long non-coding RNAs in nucleus pulposus cell function and intervertebral disc degeneration," *Cell Proliferation*, vol. 51, no. 5, 2018.

[23] L. Meng, P. Ma, R. Cai, Q. Guan, M. Wang, and B. Jin, "Long noncoding RNA ZEB1-AS1 promotes the tumorigenesis of glioma cancer cells by modulating the miR-200c/141-ZEB1 axis," *American Journal of Translational Research*, vol. 10, no. 11, pp. 3395–3412, 2018.

[24] G. Ping, W. Xiong, L. Zhang, Y. Li, Y. Zhang, and Y. Zhao, "Silencing long noncoding RNA PVT1 inhibits tumorigenesis and cisplatin resistance of colorectal cancer," *American Journal of Translational Research*, vol. 10, no. 1, pp. 138–149, 2018.

[25] C. Zhang, C. Su, Q. Song, F. Dong, S. Yu, and J. Huo, "LncRNA PICART1 suppressed non-small cell lung cancer cells proliferation and invasion by targeting AKT1 signaling pathway," *American Journal of Translational Research*, vol. 10, no. 12, pp. 4193–4201, 2018.

Hindawi
Disease Markers
Volume 2022, Article ID 8255018, 8 pages
https://doi.org/10.1155/2022/8255018

Research Article

Infarction Patterns and Recurrent Adverse Cerebrovascular Events in Moyamoya Disease

Shao-Chen Yu,[1,2] **Zi-Han Yin**,[1,2] **Chao-Fan Zeng**,[1,2] **Fa Lin**,[1,2] **Long Ma**,[1,2] **Yan Zhang**,[1,2] **Dong Zhang**,[1,2] **and Ji-Zong Zhao**[1,2,3,4,5]

[1]*Department of Neurosurgery, Beijing Tiantan Hospital, Capital Medical University, Beijing, China*
[2]*China National Clinical Research Center for Neurological Diseases, Beijing, China*
[3]*Savaid Medical School, University of Chinese Academy of Sciences, Beijing 100049, China*
[4]*Center of Stroke, Beijing Institute for Brain Disorders, Beijing, China*
[5]*Beijing Key Laboratory of Translational Medicine for Cerebrovascular Disease, Beijing, China*

Correspondence should be addressed to Ji-Zong Zhao; zhaojizong@bjtth.org

Received 11 January 2022; Accepted 17 March 2022; Published 29 March 2022

Academic Editor: Liangqun Rong

For moyamoya disease (MMD) patients who suffered an acute ischemic attack, the infarction patterns on DWI and its association with recurrent adverse cerebrovascular events (ACEs) after bypass surgery remain unknown. 327 patients who suffered an acute ischemic attack and received following revascularization surgery were retrospectively reviewed and were divided into three patterns according to the lesion number and distribution on DWI that obtained within 7 days of onset: no acute infarction (NAI), single acute infarction (SAI), and multiple acute infarctions (MAIs). We used Cox proportional hazard models to estimate hazard ratios (HR) for associations of infarction patterns and the risk of recurrent ACEs and strokes. Over a median follow-up of 41 months (IQR 26-60), there were 61 ACEs and 27 strokes. Compared to the NAI cohort, patients with SAI (HR, 2.92; 95% CI, 1.41-6.05; $p = 0.004$) and MAIs (HR, 4.44; 95% CI, 2.10-9.41; $p < 0.001$) were associated with higher risk of ACEs recurrences. In analysis adjusted for age and surgery modalities, the corresponding HR was 2.90 (95% CI: 1.41-5.98) for SAI and 4.10 (95% CI: 1.95-8.63) for MAIs, and this effect remained persistent on further adjustment for several potential confounders. Similar but less precise association was found in separate analysis that only takes into account stroke recurrences. Thus, different infarction patterns on DWI imply different risks of recurrent ACEs, and more attention should be paid to prevent ACEs in MMD patients with MAIs.

1. Introduction

Moyamoya disease (MMD) is a rare cerebrovascular disorder characterized by bilateral, progressive stenosis in the terminal portions of the internal carotid arteries, with the formation of an abnormal vascular network of basal collaterals. [1] It is a nonnegligible cause of stroke in patients younger than 50 years old, especially in Asia. Majority of MMD patients may manifest as ischemic symptoms, including TIA and cerebral infarctions. [2–4] Without timely and effective treatment, many patients will sooner or later progress into devastating consequences. [5–7] At present, restore perfusion through revascularization surgery remains the most definite therapeutic strategy for preventing future strokes and TIAs, which were adverse cerebrovascular events (ACEs) we concerned most. [8–10] However, there are still many patients experienced recurrent ACEs after revascularization surgery. Hence, discovering simple and feasible imaging parameters that can efficiently define those patients in the early stage is imperative in respect to optimize therapeutic strategy and decrease mortality.

As the most sensitive tool to detect acute cerebral infarctions, diffusion-weighted imaging (DWI) is pivotal in stroke research. [11, 12] Infarction patterns on DWI and their associations with stroke etiologies and long-term prognosis have been well defined. In general stroke patients, it has been testified that, compared to those with no acute infarction (NAI) and single acute infarction (SAI), patients with

multiple acute infarctions (MAIs) convey a significantly higher risk of recurrent ACEs. [13, 14] However, it is unclear whether this rule still holds true in MMD patients. So far, rare studies have focused on the infarction patterns in MMD, [15, 16] and none of them studied their underlying prognostic differences.

In this retrospective cohort study, we sought to clarify the infarction patterns and the unequal properties of ACEs recurrences between different infarction patterns among MMD patients who suffered an acute ischemic attack and received revascularization surgery.

2. Materials and Methods

2.1. Design and Populations. We prepared this manuscript according to the Strengthening the Reporting of Observational Studies in Epidemiology (STROBE) statements.

This is a subset of a multicenter retrospective cohort study with prospective follow-up and ongoing online data accrual (electronic data capture system) designed to facilitate longitudinal assessment of patients with moyamoya phenomenon and received revascularization surgery. We screened more than two thousand consecutive patients who underwent revascularization surgery for moyamoya disease at Beijing Tiantan Hospital from January 2008 to January 2020 (Figure 1). Patients that suffered an acute ischemic attack that was confirmed by DWI within 7days of symptom onset were considered as eligible. Asymptomatic patients, patients with hemorrhagic manifestation or with unilateral angiopathy, and those lost to follow-up were excluded. Those combined with other diseases that clearly related to stroke and patients with chronic or recurrent infarctions before surgery were also excluded to achieve higher homogeneity.

2.2. Data Collections. Demographic, clinical, and treatment data were extracted from the EDC system. All image data other than DWI were previously provided by the imaging department and were inputted into the EDC system after rechecked by expert neurosurgeons. Specifically, the following data were collected: (1) baseline characteristics (age, sex, comorbidities (hypertension, diabetes mellitus, and hyperlipidemia), and medical history (previous TIA and family history of MMD)), (2) index event characteristics (onset-to-DWI duration and preventive treatment (antiplatelet, anticoagulant, or statin treatment) and presentation), (3) imaging characteristics (perfusion status and cerebrovascular traits (SUZUKI stage, presence of aneurysm, and posterior circulation involvement)), and (4) surgery characteristics (mRS at admission, DWI-to-surgery duration, and surgery modalities). Decrease in regional cerebral blood flow compared to the contralateral hemisphere or cerebellum was considered as perfusion impairment. The Suzuki stages were determined by the anteroposterior and lateral views of the bilateral internal carotid arteries on DSA. If the Suzuki stage on both sides was inconsistent, the higher side shall prevail. Patients with obvious posterior-cerebral-artery stenosis or moyamoya vessel formation on DSA were identified as posterior circulation involvement. Patients who underwent combined revascularization surgery were classified into the direct surgery modality group due to the similarity in surgical procedures and treatment outcomes. Omissions and mistakes were supplemented and corrected by thorough review of the medical records and visual inspection of source brain images as much as possible.

2.3. Stroke Patterns Interpretation. All DWI images were centrally assessed by a certified and trained neurosurgeon and a neuroradiologist in random order either through the PACS (picture archiving and communication system) or scanned digital format (patients referred to our center). Discrepant cases were adjudicated by consensus among three or more readers.

Using published templates, [17] patients were grouped into 3 categories (NAI, SAI, and MAIs) according to the lesion number on DWI. Any hyperintense lesions on DWI with corresponding presentation were deemed to be acute infarctions. Uninterrupted lesions visible in contiguous territories were defined as SAI, while MAIs refers to multiple noncontiguous hyperintense lesions that were topographically distinct. SAI were further classified into small perforator artery infarct (diameter < 2 cm), large perforator artery infarct (diameter ≥ 2 cm), pial infarct, large territorial infarct, and border-zone infarct. MAIs were further classified into infarcts in unilateral anterior circulation, infarcts in bilateral anterior circulation, infarcts in posterior circulation, infarcts in both anterior and posterior circulation, and infarcts in multiple border-zone areas, similar as previous studies. [18, 19]

2.4. Follow-Up and Outcomes. Discharged patients are advised to visit the clinic regularly, usually at 3 months, 6 months, and every year thereafter. Those did not show up on time are followed up via phone interviews (patients or their next of kin) by participating investigator who was masked to clinical and imaging characteristics. Detailed description of the follow-up events and neurological status were recorded. Follow-up was complete through October 2021. Primary end point was recurrent ACEs with subsidiary analyses focused only on recurrent strokes. We define ACEs as any stroke or TIA of cerebrovascular origin that developed beyond 30 days after surgery. Stroke was defined as a rapid onset of focal retinal or cerebral deficit lasting > 24 hours. TIA was defined as a new retinal or cerebral dysfunction sustained < 24 hours with no new lesion on CT or MRI.

2.5. Statistical Analysis. Continuous and categorical variables were presented as median (IQR) and n (%), respectively. Kruskal-Wallis test, χ^2 test, or Fisher's exact test were taken to compare differences between different infarction patterns where appropriate. Kaplan-Meier curves with a log-rank test were constructed to describe and examine the recurrences of ACEs over time between different infarction patterns. Hazard ratios (HRs) along with 95% confidence intervals (CIs) for recurrent ACEs were calculated using Cox proportional hazard models and were adjusted for (1) established confounders (age and surgery modalities) (model 1), (2) model 1 plus potential confounders in the present study

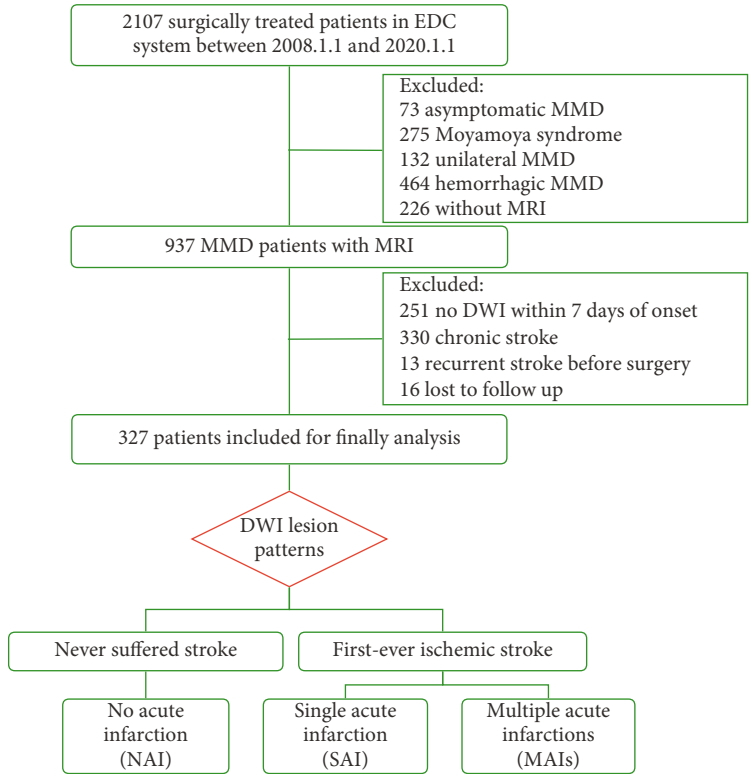

Figure 1: Flow chart for patient enrollment. Abbreviation: EDC: electronic data capture; MMD: moyamoya disease; DWI: diffusion-weighted imaging.

(age, surgery modalities, and posterior circulation involvement) (model 2), and (3) model 2 plus potential confounders previously reported (age, surgery modalities, posterior circulation involvement, and previous TIA) (model 3), respectively. Subsidiary analyses focused only on recurrent strokes were then conducted to examine the similar association. Additional sensitivity analyses restricted to patients exempted from repeated revascularization were applied to verify the robustness of the results. The Bonferroni method was used to avoid bias caused by multiple comparisons when necessary. Age is included in the COX regression model as a binary variable (≤18 vs >18 years old), and missing data were not imputed. A two-sided $\alpha < 0 \cdot 05$ was considered statistically significant. Statistical analyses were done using R, version 3.6.3 (R Foundation, Vienna, Austria) and SPSS, version 24 (IBM Corporation, Armonk, NY).

3. Results

3.1. Baseline Characteristics. From January 2008 to January 2020, a total of 2107 patients with moyamoya phenomenon in the EDC system were screened. After stepwise exclusion, 327 patients who suffered an acute ischemic attack and received revascularization surgery were included for final analysis (flowchart for enrollment was shown in Figure 1). Among them, 122 (37.3%) patients had NAI, 126 (38.5%) patients had SAI, and 79 (24.2%) patients had MAIs on DWI. Table 1 shows the summary of patient characteristics (52% women, median age 35 [range 3–63]), stratified by infarction patterns. Baseline characteristics were well balanced among the three cohorts, except patients with MAIs were more likely to be bilateral perfusion impaired, patients with SAI tended to receive revascularization surgery within 3 months after symptom onset, and patients with NAI were more likely to have a history of TIA but a lower admission mRS.

3.2. Infarction Patterns. 122 patients did not show any infarction on DWI, and the rest 205 (62.7%) patients showed at least one infarction, consisting of 126 (61.5%) SAI and 79 (38.5%) MAIs. Regarding patients with SAI, large territorial infarction was the most common pattern, observed in 47 patients (37.3%), followed by border-zone infarction in 34 (27.0%), small perforator artery infarction (diameter<2 cm) in 20 (15.9%), pial infarction in 18 (14.3%), and large perforator artery infarction (diameter ≥2 cm) in 7 (5.6%). While for patients with MAIs, infarcts exhibit in unilateral anterior circulation was the most common, observed in 36 patients (45.6%), followed by multiple border-zone in 18 (22.8%), bilateral anterior circulation in 13 (16.5%), anterior and posterior circulation in 11 (13.9%), and only 1 (1.3%) patient developed MAIs in posterior circulation.

3.3. Stroke Patterns and Risk of Recurrent ACEs and Strokes. Over a median follow-up of 41 months (IQR 26-60, total 14162 months at risk), there were 61 ACEs and 27 strokes, and majority of them were developed in the first 2 years (50/61 for ACEs and 22/27 for stroke). Among those

Table 1: Baseline characteristics of patients.

Characteristics	Overall ($n = 327$), n (%)	Infarction patterns, n (%)			p value
		NAI ($n = 122$)	SAI ($n = 126$)	MAIs ($n = 79$)	
Age, y, (IQR)	35 (14-45)	32 (12-45)	34 (16-44)	39 (24-46)	0.166
≤18	91 (27.8)	40 (32.8)	32 (25.4)	19 (24.1)	0.297
>18	236 (72.2)	82 (67.25)	94 (74.6)	60 (75.9)	
Female	170 (52)	64 (52.5)	64 (50.8)	42 (53.2)	0.939
Current or previous smoking	64 (19.6)	19 (15.6)	35 (23.8)	10 (19.0)	0.26
Alcohol consumption	78 (23.9)	21 (17.2)	35 (27.8)	22 (27.8)	0.094
Comorbidity					
Any	113 (34.6)	39 (32.0)	44 (34.9)	30 (38.0)	0.678
Hypertension	96 (29.4)	33 (27.0)	37 (29.4)	26 (32.9)	0.672
Diabetes	31 (9.5)	6 (4.9)	14 (11.1)	11 (13.9)	0.075
Hyperlipidemia	25 (7.6)	9 (7.4)	12 (9.5)	4 (5.1)	0.50
Family history of MMD	16 (4.9)	4 (3.3)	10 (7.9)	2 (2.5)	0.139
Previous TIA	107 (32.7)	48 (39.3)	36 (28.6)	23 (29.1)	0.143
Time since last TIA> 3 months	42 (12.8)	20 (16.4)	14 (11.1)	8 (10.1)	0.328
mRS at admission					
0-2	307 (93.9)	122 (100)	112 (88.9)	73 (92.4)	0.001
3-5	20 (6.1)	0 (0)	14 (11.1)	6 (7.6)	
Antithrombotic agents	122 (37.3)	37 (30.3)	54 (42.9)	31 (39.2)	0.115
Statin	92 (28.1)	27 (22.1)	39 (31.0)	26 (32.9)	0.169
Onset to DWI duration, d, (IQR)	2 (1-2)	2 (1-2)	2 (1-2)	2 (1-2)	0.851
SUZUKI stage*					
1-2	90 (29.4)	37 (33.3)	26 (21.8)	27 (35.5)	0.094
3-4	155 (50.7)	58 (52.3)	63 (52.9)	34 (44.7)	
5-6	61 (19.9)	16 (14.4)	30 (25.2)	15 (19.7)	
Bilateral CBF decrease †	232 (71.4)	77 (63.1)	94 (75.8)	61 (77.2)	0.037
Present of aneurysms ‡	11 (3.4)	6 (4.9)	3 (2.4)	2 (2.5)	0.484
PCA involvement ‡	107 (32.7)	34 (27.9)	48 (38.1)	25 (31.6)	0.223
Onset to surgery duration, m					
≤ 3	238 (72.8)	95 (77.9)	81 (64.3)	62 (78.5)	0.024
> 3	89 (27.2)	27 (22.1)	45 (35.7)	17 (21.5)	
Surgery modality					
Indirect	195 (59.6)	79 (64.8)	73 (57.9)	43 (54.4)	0.306
Direct	132 (40.4)	43 (35.2)	53 (42.1)	36 (45.6)	
Repeated revascularization	82 (25.1)	28 (34.1)	35 (42.7)	19 (23.2)	0.661
Duration between surgeries, m, (IQR)	8 (6-12)	8 (5-12)	8 (6-11)	9 (6-12)	0.681

*21 patients without digital subtraction angiography before surgery. †2 missing data, 308 patients were assessed via computed tomography perfusion, 5 via arterial spin labeling MR perfusion, 4 via perfusion weighted imaging, and 8 via single-photon emission computerized tomography. ‡310 patients were evaluated by digital subtraction angiography (DSA), and 17 patients were evaluated either by computed tomography angiography (CTA) or magnetic resonance angiography (MRA). Abbreviations: MMD: moyamoya disease; TIA: transient ischemic attack; DWI: diffusion-weighted imaging; CBF: cerebral blood flow; PCA: posterior cerebral artery; IQR: interquartile range.

without ACEs, 94% were followed-up for over 2 years. Recurrent ACEs rates per 100 person-year of follow-up across the 3 stroke patterns (NAI, SAI, and MAIs) were 2.3, 6.0, and 8.8, respectively. Kaplan-Meier curves in Figure 2 show cumulative rate of ACEs and stroke among different infarction patterns. Comparing to the NAI cohort, patients with SAI (HR, 2.92; 95% CI, 1.41-6.05; $p = 0.004$) and MAIs (HR, 4.44; 95% CI, 2.10-9.41; $p < 0.001$) were associated with higher risk of ACEs recurrence. In analysis adjusted for previously documented confounders (age and surgery modalities), the HR of recurrent ACEs for patients with MAIs was 4.10 (95% CI: 1.95-8.63, $p < 0.001$). This effect persisted (HR 4.55, 95% CI 2.01-8.96, $p < 0.001$) when further adjusted for confounders in the present study (posterior circulation involvement). After additional adjustment for previously reported potential confounder (history of TIA), this association remain unchanged (HR 4.41, 95% CI 2.10-9.32, $p < 0.001$). A similar but less precise association

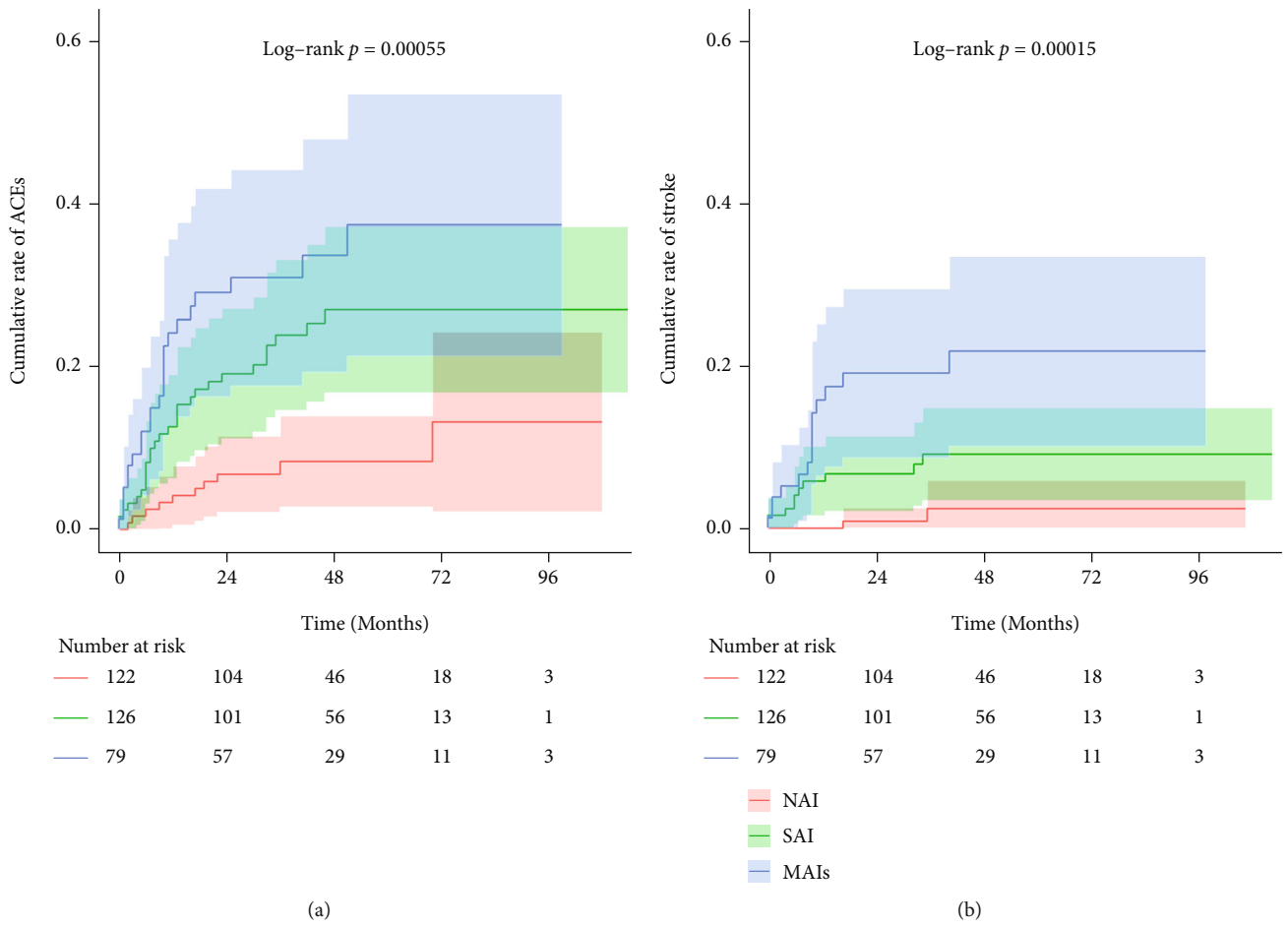

Figure 2: Cumulative Kaplan-Meier curves for recurrent ACEs (a) and strokes (b) during follow-up according to infarction patterns.

was observed in a separate analysis that only considered stroke recurrence ($n = 27$, including 23 ischemic and 4 hemorrhagic strokes) (Table 2). Sensitivity analyses restricted to patients received single revascularization surgery that yielded consistent results as shown in supplemental materials (available here).

4. Discussions

In this research, we clearly depicted the infarction patterns of MMD patients who suffered an acute ischemic attack and found a significant association between infarction patterns and recurrent ACEs after revascularization. This effect was not affected by established or potential clinically relevant confounding factors. Subsidiary analyses revealed a similar but less precise association with recurrent strokes due to the extremely low event of stroke in patients with NAI ($n = 2$). In addition, these positive associations were further confirmed by serial sensitivity analyses.

Due to the rarity of disease and dilemma in rapid access to MRI scan, the infarction patterns of MMD patients remain largely unknown. Here, we found that, among MMD patients who suffered an acute ischemic attack, approximately 60% had positive lesions on DWI, and nearly 40% of them may present as MAIs, which is in the range of previous reported 16%-50% for stroke patients in general. [19–23] Different infarction patterns may occur as a consequence of obstruction of major arteries, thrombosis, or collapse of moyamoya vessels and collateral failure, alone or at the same time. Recently, Dong et al. [15] found that embolism (83.7%) was the most likely mechanism in MMD patients who suffered an acute ischemic stroke, and majority of them showed good collateral status (86%). In our data, infarctions caused by hemodynamic damage alone account for only 15.9% (52/327), suggesting mechanism other than collateral failure should be considered. Besides, Ji et al. [16] indicated that age-specific infarction patterns exist in MMD; on the contrary, we denoted no significant differences in infarction patterns between child-onset (< 18 years old) and adult-onset patients when dichotomized it into SAI and MAIs ($p = 0.828$, data not shown), suggesting a disease-specific infarct mechanism to explain this phenomenon instead of age.

Most importantly, our study demonstrates that among MMD patients who suffered an acute attack, the increase in the number of acute infarctions was positively (p value for trend = 0.001) and independently associated with higher risk of recurrent ACEs after revascularization surgery, which is in line with previous studies confine to patients with specific TOAST subtypes. [14] The worldwide TIAregistry.org

Table 2: Hazard ratios of ACEs and stroke according to infarction patterns.

Stroke patterns	Unadjusted, HR (95% CI)	p value	Model 1, HR (95% CI)	p value	Model 2, HR (95% CI)	p value	Model 3, HR (95% CI)	p value
ACEs								
NAI	Ref		Ref		Ref		Ref	
SAI	2.92 (1.41-6.05)	0.004	2.90 (1.41-5.98)	0.004	2.81 (1.36-5.80)	0.005	2.93 (1.42-6.07)	0.004
MAIs	4.44 (2.10-9.45)	0.000	4.10 (1.95-8.63)	0.000	4.25 (2.01-8.96)	0.000	4.41 (2.09-9.33)	0.000
p value for trend		0.001		0.001		0.001		0.001
Stroke								
NAI	Ref		Ref		Ref		Ref	
SAI	4.97 (1.09-22.68)	0.039	4.90 (1.07-22.40)	0.04	4.55 (0.99-20.84)	0.051	4.75 (1.03-21.82)	0.045
MAIs	11.92 (2.71-52.46)	0.001	11.79 (2.67-51.97)	0.001	11.70 (2.65-51.67)	0.001	12.10 (2.73-53.59)	0.001
p value for trend		0.002		0.002		0.001		0.001

Model 1, adjusted for age and surgery modality; model 2, model 1 plus posterior circulation involvement; model 3, model 2 plus previous TIA. Abbreviation: CI: confidence interval; ACEs: adverse cerebrovascular events.

project, which focused on the one-year risk of major cardiovascular events in patients with TIA or minor stroke (including all the five TOAST subtypes), had shown that patients with MAIs had over two folds higher risk than those with NAI. [24] Apart from this, the subgroup analysis of the CHANCE trial recruited 1089 patients with TIA or minor stroke (excluded patients with cardioembolism and with other determined pathogenesis) and demonstrated that patients with MAIs had nearly 6 times the risk of recurrent stroke compared to those with NAI. Meanwhile, MAIs put the patient at a constant high risk of stroke although it benefited the most from dual antiplatelet treatment [18]. Tomohisa et al. [22] followed up 272 cryptogenic stroke patients for more than 3 years and found that MAIs were independently associated with recurrent stroke and all-cause mortality. In the current study that restricted to MMD, patients with MAIs had hazard ratios for recurrent ACEs and stroke nearly 4 and 10 times more than the hazard ratios in the reference category of NAI. All these along with our findings support that, in spite of disparities in stroke etiology, patients with MAIs share common unstable sources of recurring ACEs.

However, we currently have no credible explanation for such a distinct association. We speculate that brain tissue vulnerable to ischemic attacks are broader in patients with MAIs, and it is unlikely to correct established hypoperfusion with focal revascularization, let alone to reverse the natural history of MMD [25]. In addition to hemodynamic compromise, there are increasing evidence that supports the causality between thromboembolic mechanisms and MMD relevant infarctions [15, 26–28]. Microembolic singles are frequently detected by transcranial Doppler before and after surgery in MMD patients, and their association with previous ischemic events and predictive value of future cerebral events has been verified in several TOAST subtypes [26, 29–31]. Unless back to normal, the extensive moyamoya network may constantly serve as a fountain of emboli thereby contribute to subsequent ACEs. Interestingly, Caplan et al. support the hypothesis that infarction in MMD is resulted from the combination of hypoperfusion and embolism [32]. Taken together, we suggest that mechanism by which MAIs increase the risk of recurrent ACEs is heterogeneous, and the one-size-fits-all strategy (revascularization) alone is insufficient to eliminate the high risk of recurrent ACEs for patients with MAIs. The CARESS trial [33] and the CLAIR trial [34] have shown the superiority of dual antiplatelet therapy in reducing embolic signals. Given the potential causality between embolic singles and higher risk of ACEs in patients with MAIs, we thus wonder whether the combination of revascularization surgery and antithrombotic agents would bring extra benefits to certain MMD patients, such as those with MAIs. However, this is beyond the scope of our study and further researches are warranted to address this conundrum.

Our study highlighted the value of baseline DWI in risk stratification of long-term ACEs recurrences, and we thought our findings may potentially contribute to better and more individualized treatment strategies. Considering that most of the ACEs (82%) and strokes (81.5%) occurred within two years after surgery, we strongly recommend that patients with MMD suffering from acute ischemia, especially those with MAIs, should be followed up regularly within two years after surgery. Further clinical trials are warranted to address whether dual antiplatelet therapy can provide additional benefits in patients with MAIs that show embolic pattern.

As strength, our cohort study demonstrated a strong association between baseline imaging parameter (stroke patterns) and long-term prognosis after surgery through a relatively large sample size. However, our study is subject to certain limitations. First, selection bias is inevitable due to its retrospective nature, although we have tried our best to cover all the eligible patients admitted to one of the largest stroke centers in China. Second, this study only included patients who suffered an acute ischemic attack followed by surgical treatment; therefore, neither the infarct patterns of conservatively treated patients nor the difference in the surgical benefits could be assessed. Third, due to the high prevalence of variations and diversiform changes in the vascular network, the arterial territory in MMD patients

may be distinct from others. Thus, detailed infarction patterns determined by normal template may lead to errors. However, these errors were minimized when divided patients into three cohorts according to the number of infarcts. In addition, the length of time from onset to DWI varies; therefore, some of the MAIs may be caused by recurring infarcts during the acute phase, leading to a overestimated ratio of MAIs [35]. Finally, 89.9% (294/327) patients in our study were younger than 50; a full set of vascular examinations were not mandatory; therefore, some of them may harbor other covert source of embolism.

5. Conclusion

Overall, our study demonstrated that, for MMD patients who suffered an ischemic attack and received subsequent revascularization surgery, infarction patterns on baseline DWI were significantly associated with the risk of recurrent ACEs thereby could be used as effective tool to define patients remain at high risk of future ACEs. Patients with MAIs should be carefully followed up for at least 2 years, and further studies are warranted to test whether additional antithrombotic agents can provide better curative effect for those patients.

Abbreviations

MMD: Moyamoya disease
ACEs: Adverse cerebrovascular events
TIA: Transient ischemic attack
DWI: Diffusion-weighted imaging
NAI: No acute infarction
SAI: Single acute infarction
MAIs: Multiple acute infarctions
EDC: Electronic data capture
CRESS: Clopidogrel and aspirin for reduction of emboli in symptomatic carotid stenosis
CLAIR: Clopidogrel plus aspirin versus aspirin alone for reducing embolization.

Data Availability

Data supporting the findings of this study are available from the corresponding author upon reasonable request.

Ethical Approval

This study was designed abide by the Declaration of Helsinki and approved by the ethics committee of Beijing Tiantan Hospital (KY2016-048-01).

Consent

Informed consents were collected from all included patients or their guardians.

Conflicts of Interest

The authors declare that there is no conflict of interest regarding the publication of this article.

Authors' Contributions

Shao-Chen Yu designed the study, drafted the manuscript, and analyzed the data. Zi-Han Yin, Chao-Fan Zeng, Lin Fa, and Long Ma contributed to the discussion and revised the manuscript. Yan Zhang and Dong Zhang made contribution to the interpretation of data. Ji-Zong Zhao designed the study and revised it critically for important intellectual content.

Acknowledgments

This work was supported by the "13th Five-Year Plan" National Science and Technology Supporting Plan (Grant Number: 2015BAI12B04) and the program of Beijing Municipal Commission of Education (Grant Number: KM201910025014). We are very grateful to Mi Shen (M.D., Department of Radiology, Beijing Tiantan Hospital, Capital Medical University, China National Clinical Research Center for Neurological Diseases, Center of Stroke, Beijing Institute for Brain Disorders) for his valuable suggestions in the interpretation of image data.

Supplementary Materials

Supplemental materials consist of (1) a table showing detailed infarction patterns and infarction patterns according to surgery modality and age, and (2) a table and a figure showing results of the sensitivity analyses, that are, Hazard Ratios and cumulative Kaplan-Meier curves for recurrent ACEs and strokes during follow-up according to infarction patterns, including patients received single revascularization surgery and (3) an additional checklist of STROBE Statement. *(Supplementary Materials)*

References

[1] S. Kuroda and K. Houkin, "Moyamoya disease: current concepts and future perspectives," *Lancet Neurology*, vol. 7, no. 11, pp. 1056–1066, 2008.

[2] L. Duan, X. Y. Bao, W. Z. Yang et al., "Moyamoya disease in China: its clinical features and outcomes," *Stroke*, vol. 43, no. 1, pp. 56–60, 2012.

[3] J. S. Kim, "Moyamoya disease: epidemiology, clinical features, and diagnosis," *Journal of stroke*, vol. 18, no. 1, pp. 2–11, 2016.

[4] S. Wu, B. Wu, M. Liu et al., "Stroke in China: advances and challenges in epidemiology, prevention, and management," *Lancet Neurology*, vol. 18, no. 4, pp. 394–405, 2019.

[5] C. L. Hallemeier, K. M. Rich, R. L. Grubb et al., "Clinical features and outcome in North American adults with moyamoya phenomenon," *Stroke*, vol. 37, no. 6, pp. 1490–1496, 2006.

[6] S. Kuroda, T. Ishikawa, K. Houkin, R. Nanba, M. Hokari, and Y. Iwasaki, "Incidence and clinical features of disease progression in adult moyamoya disease," *Stroke*, vol. 36, no. 10, pp. 2148–2153, 2005.

[7] E. W. Church, T. E. Bell-Stephens, M. G. Bigder, S. Gummidipundi, S. S. Han, and G. K. Steinberg, "Clinical course of unilateral moyamoya disease," *Neurosurgery*, vol. 87, no. 6, pp. 1262–1268, 2020.

[8] J. P. Jeon, J. E. Kim, W. S. Cho, J. S. Bang, Y. J. Son, and C. W. Oh, "Meta-analysis of the surgical outcomes of symptomatic

moyamoya disease in adults," *Journal of Neurosurgery*, vol. 128, no. 3, pp. 793–799, 2018.

[9] E. J. Ha, K. H. Kim, K. C. Wang et al., "Long-term outcomes of indirect bypass for 629 children with Moyamoya disease: longitudinal and cross-sectional analysis," *Stroke*, vol. 50, no. 11, pp. 3177–3183, 2019.

[10] T. Kim, C. W. Oh, O. K. Kwon et al., "Stroke prevention by direct revascularization for patients with adult-onset moyamoya disease presenting with ischemia," *Journal of Neurosurgery*, vol. 124, no. 6, pp. 1788–1793, 2016.

[11] C. Z. Simonsen, M. H. Madsen, M. L. Schmitz, I. K. Mikkelsen, M. Fisher, and G. Andersen, "Sensitivity of diffusion-and perfusion-weighted imaging for diagnosing acute ischemic stroke is 97.5%," *Stroke*, vol. 46, pp. 98–101, 2015.

[12] J. A. Chalela, C. S. Kidwell, L. M. Nentwich et al., "Magnetic resonance imaging and computed tomography in emergency assessment of patients with suspected acute stroke: a prospective comparison," *The Lancet*, vol. 369, no. 9558, pp. 293–298, 2007.

[13] C. Zhang, X. Zhao, C. Wang et al., "Prediction factors of recurrent ischemic events in one year after minor stroke," *PLoS One*, vol. 10, no. 3, pp. 1–12, 2015.

[14] J. M. Jung, D. W. Kang, K. H. Yu et al., "Predictors of recurrent stroke in patients with symptomatic intracranial arterial stenosis," *Stroke*, vol. 43, no. 10, pp. 2785–2787, 2012.

[15] D. Y. Kim, J. P. Son, J. Y. Yeon et al., "Infarct pattern and collateral status in adult moyamoya disease," *Stroke*, vol. 48, no. 1, pp. 111–116, 2017.

[16] H. J. Cho, Y. H. Jung, Y. D. Kim, H. S. Nam, D. S. Kim, and J. H. Heo, "The different infarct patterns between adulthood-onset and childhood-onset moyamoya disease," *Journal of Neurology, Neurosurgery, and Psychiatry*, vol. 82, no. 1, pp. 38–40, 2011.

[17] L. Tatu, T. Moulin, J. Bogousslavsky, and H. Duvernoy, "Arterial territories of the human brain cerebral hemispheres," *Neurology*, vol. 50, no. 6, pp. 1699–1708, 1998.

[18] J. Jing, X. Meng, X. Zhao et al., "Dual antiplatelet therapy in transient ischemic attack and minor stroke with different infarction patterns subgroup analysis of the CHANCE randomized clinical trial," *JAMA Neurology*, vol. 75, no. 6, pp. 711–719, 2018.

[19] D. K. Lee, J. S. Kim, S. U. Kwon, S. H. Yoo, and D. W. Kang, "Lesion patterns and stroke mechanism in atherosclerotic middle cerebral artery disease: early diffusion-weighted imaging study," *Stroke*, vol. 36, no. 12, pp. 2583–2588, 2005.

[20] D. W. Kang, J. A. Chalela, M. A. Ezzeddine, and S. Warach, "Association of ischemic lesion patterns on early diffusion-weighted imaging with TOAST stroke subtypes," *Archives of Neurology*, vol. 60, no. 12, pp. 1730–1734, 2003.

[21] A. E. Baird, K. O. Lövblad, G. Schlaug, R. R. Edelman, and S. Warach, "Multiple acute stroke syndrome: marker of embolic disease?," *Neurology*, vol. 54, no. 3, pp. 674–678, 2000.

[22] T. Nezu, T. Mukai, J. Uemura et al., "Multiple infarcts are associated with long-term stroke recurrence and all-cause mortality in cryptogenic stroke patients," *Stroke*, vol. 47, no. 9, pp. 2209–2215, 2016.

[23] H. M. Wen, W. W. M. Lam, T. Rainer et al., "Multiple acute cerebral infarcts on diffusion-weighted imaging and risk of recurrent stroke," *Neurology*, vol. 63, no. 7, pp. 1317–1319, 2004.

[24] P. Amarenco, P. C. Lavallée, J. Labreuche et al., "One-year risk of stroke after transient ischemic attack or minor stroke," *The New England Journal of Medicine*, vol. 374, no. 16, pp. 1533–1542, 2016.

[25] S. C. Tho-Calvi, D. Thompson, D. Saunders et al., "Clinical features, course, and outcomes of a UK cohort of pediatric moyamoya," *Neurology*, vol. 90, no. 9, pp. E763–E770, 2018.

[26] C. Jeon, J. Y. Yeon, K. I. Jo, S. C. Hong, and J. S. Kim, "Clinical role of microembolic signals in adult moyamoya disease with ischemic stroke," *Stroke*, vol. 50, no. 5, pp. 1130–1135, 2019.

[27] Y. Iguchi, K. Kimura, Y. Tateishi, K. Shibazaki, T. Iwanaga, and T. Inoue, "Microembolic signals are associated with progression of arterial lesion in moyamoya disease: a case report," *Journal of the Neurological Sciences*, vol. 260, no. 1-2, pp. 253–255, 2007.

[28] J. G. Shulman, S. Snider, H. Vaitkevicius, V. L. Babikian, and N. J. Patel, "Direct visualization of arterial emboli in moyamoya syndrome," *Frontiers in Neurology*, vol. 8, pp. 1–5, 2017.

[29] J. Chen, L. Duan, W. H. Xu, Y. Q. Han, L. Y. Cui, and S. Gao, "Microembolic signals predict cerebral ischaemic events in patients with moyamoya disease," *European Journal of Neurology*, vol. 21, no. 5, pp. 785–790, 2014.

[30] S. Gao, S. W. Ka, T. Hansberg, W. W. M. Lam, D. W. Droste, and E. B. Ringelstein, "Microembolic signal predicts recurrent cerebral ischemic events in acute stroke patients with middle cerebral artery stenosis," *Stroke*, vol. 35, no. 12, pp. 2832–2836, 2004.

[31] A. S. Das, R. W. Regenhardt, S. LaRose et al., "Microembolic signals detected by transcranial Doppler predict future stroke and poor outcomes," *Journal of Neuroimaging*, vol. 30, no. 6, pp. 882–889, 2020.

[32] L. R. Caplan and M. Hennerici, "Impaired clearance of emboli (washout) is an important link between hypoperfusion, embolism, and ischemic stroke," *Archives of Neurology*, vol. 55, no. 11, pp. 1475–1482, 1998.

[33] H. S. Markus, D. W. Droste, M. Kaps et al., "Dual antiplatelet therapy with clopidogrel and aspirin in symptomatic carotid stenosis evaluated using Doppler embolic signal detection: the clopidogrel and aspirin for reduction of emboli in symptomatic carotid stenosis (CARESS) trial," *Circulation*, vol. 111, no. 17, pp. 2233–2240, 2005.

[34] K. S. L. Wong, C. Chen, J. Fu et al., "Clopidogrel plus aspirin versus aspirin alone for reducing embolisation in patients with acute symptomatic cerebral or carotid artery stenosis (CLAIR study): a randomised, open-label, blinded-endpoint trial," *The Lancet Neurology*, vol. 9, no. 5, pp. 489–497, 2010.

[35] D. W. Kang, L. L. Latour, J. A. Chalela, J. Dambrosia, and S. Warach, "Early ischemic lesion recurrence within a week after acute ischemic stroke," *Annals of Neurology*, vol. 54, no. 1, pp. 66–74, 2003.

Hindawi
Disease Markers
Volume 2022, Article ID 1983455, 14 pages
https://doi.org/10.1155/2022/1983455

Review Article

The Neutrophil to Lymphocyte Ratio in Poststroke Infection: A Systematic Review and Meta-Analysis

Shokoufeh Khanzadeh,[1] **Brandon Lucke-Wold**,[2] **Fatemeh Eshghyar**,[3] **Katayoun Rezaei**,[4] **and Alec Clark**[5]

[1]*Student Research Committee, Tabriz University of Medical Sciences, Tabriz, Iran*
[2]*University of Florida, Department of Neurosurgery, Gainesville, USA*
[3]*Tehran University of Medical Sciences, School of Medicine, Tehran, Iran*
[4]*Student Research Committee, University of Kharazmi, Karaj, Iran*
[5]*University of Central Florida, School of Medicine, Orlando, USA*

Correspondence should be addressed to Shokoufeh Khanzadeh; khshokufe7@gmail.com

Received 22 December 2021; Revised 21 January 2022; Accepted 11 February 2022; Published 11 March 2022

Academic Editor: XIANWEI ZENG

Ischemic and hemorrhagic strokes have multiple downstream consequences for patients. One of the most critical is poststroke infection (PSI). The goal of this systematic review and meta-analysis was to critically evaluate the literature regarding the use of the neutrophil to lymphocyte ratio (NLR) as a reliable means to detect early PSI development, particularly poststroke pneumonia (PSP) development to help clinicians institute early interventions and improve outcomes. The following were the inclusion criteria: (1) cross-sectional, case-control, and cohort studies; (2) studies comparing NLR data from PSI or PSP patients to controls; and (3) studies with a control group of stroke patients without infection. There was not any language or publication preference. The Newcastle-Ottawa Scale was used by two writers to assess the quality of the included studies. We assessed the certainty of the associations with GRADE methods. Web of Science, PubMed, and Scopus were searched, and 25 studies were included in the qualitative review. Among them, 15 studies were included in the meta-analysis. Standardized mean difference (SMD) was reported with a 95% confidence interval (CI) for the NLR levels. Patients with PSI had significantly higher NLR levels than stroke patients without infection (SMD = 1.08; CI 95% = 0.78-1.39, P value < 0.001). In addition, the NLR levels of the stroke patients with pneumonia were significantly higher than those without pneumonia (SMD = 0.98; CI 95% = 0.81-1.14, P value < 0.001). However, data extracted from the qualitative review suggested that NLR could not predict urinary tract infection, sepsis, or ventriculitis in stroke patients. Our study indicated that NLR could be recommended as an inexpensive biomarker for predicting infection, particularly pneumonia, in stroke patients. It can help clinicians institute early interventions that can reduce PSI and improve outcomes.

1. Introduction

It has been well documented in the cardiovascular literature that the neutrophil to lymphocyte ratio (NLR) is an important marker for clinical outcome [1]. Emerging data from the stroke literature has also highlighted the importance of this ratio as a key marker for outcome [2]. Lux and colleagues found that a high NLR at 24 hours poststroke was associated with poor overall outcomes following ischemic stroke [3]. Kakhki and colleagues similarly linked a high NLR to poor poststroke outcomes [4]. There is a growing body of evidence to support the utility of the NLR as a predictive biomarker for the development of several poststroke complications, including infection, delirium, depression, hemorrhagic transformation, and early neurological deterioration [5, 6]. Of these, infection is both the most common poststroke complication and the best predictor of mortality in stroke patients [7]. Thus, the development of infection is one of the most crucial complications to diagnose early in the poststroke setting. This is critical to detect early as a lot

of patients with stroke were previously health and nonsymptomatic. Although poststroke infection (PSI) includes several types of infections, such as urinary tract infection (UTI) and sepsis, poststroke pneumonia (PSP) carries the highest mortality rate in these patients [8]. In recent years, a considerable amount of literature has been published on the predictive role of the NLR in PSI, particularly PSP [4, 9–32]. In fact, the elevated NLR has been postulated to signal an aberrant inflammatory state predisposing to further complications [33]. As studies continue to emerge regarding this important topic, the need for a systematic review to guide clinical decision making is apparent. The key is to understand what an elevated ratio might mean for a patient poststroke to help clinicians institute early interventions and improve outcomes. Some previous studies reported significant association between NLR and several types of PSI, but others did not find any relationship. However, to the best of our knowledge, there was not any systematic review of the available literature performed regarding these important topics. The goal of this systematic review and meta-analysis was to consolidate the available data on the role of the NLR in predicting PSI, particularly PSP, to help guide further clinical management utilizing the predictive capabilities of the NLR.

2. Methods

The PRISMA (Preferred Reporting Items for Systematic Reviews and Meta-analysis) guidelines were used to conduct this systematic review and meta-analysis. No registered review protocol exists. Two independent investigators conducted a systematic evaluation of peer-reviewed papers by searching PubMed, Web of Science, and Scopus databases regardless of funding source to find relevant articles published until October 2021. The search was conducted using following keywords: (infection OR bacteraemia OR sepsis OR pneumonia) AND (stroke OR cerebral infarction OR brain infarction OR cerebral hemorrhage OR intracranial hemorrhage) AND (neutrophil-to-lymphocyte ratio OR neutrophil to lymphocyte ratio OR NLR). We did not limit our searching to a specific language or release year. Furthermore, to identify grey literature and further relevant studies, we also conducted a quick nonsystematic search in Google Scholar as a secondary database in English and Chinese, because the majority of identified articles were conducted in China. The Prospero Register was also searched for information on unreleased and ongoing investigations.

2.1. Criteria for Inclusion and Exclusion. We identify eligible studies according to the PICOS (population, intervention, control, outcomes, and study design) principle in order to ensure the systematic search of available literature. The inclusion criteria were presented below:

(a) *Population*: *Patients with PSI*. PSI was defined as sepsis, PSP, UTI, and other types of infection. If a study reported only PSP among stroke patients, it would be excluded from the analysis of differences in NLR level between PSI and controls; then, we would include it in the separate analysis concerning PSP cases solely. This action was taken to increase the homogeneity between studies.

(b) *Intervention*. NLR

(c) *Control*. Stroke patients without PSI

(d) *Outcomes*. The prognostic performance of NLR in PSI and PSP

(e) *Study Design*. Cross-sectional, case-control, and cohort studies

The criteria for exclusion were as follows: (1) reviews, letters to the editor, animal studies, case series, and case reports; (2) studies using overlapping data; and (3) data in the absence of a control group.

2.2. Data Extraction. One investigator extracted the data, which was then double-checked by another. The first author, year of publication, language, study location, study design, age group (adult or children), mean age, male %, total sample size, number of cases and controls individually, and NLR level data in cases and controls were all extracted. A third author was consulted to establish a consensus when there were disputes.

2.3. Quality Assessment of Included Studies. The Newcastle-Ottawa Scale (NOS), which includes three sections: selection (4 items), comparability (2 items), and outcome (3 items), and a total score of 0 to 9, was used by two writers to assess the quality of the studies included. Any disagreements were finally resolved through arbitration by a third author.

2.4. Statistical Analysis. Standard mean differences (SMDs) were used to accommodate the differences in NLR measurement techniques across various studies. In our study, SMDs with a 95% confidence interval (CI) were used to assess NLR differences between PSI or PSP patients and controls. The mean and SD from the median, range, or IQR were calculated using the methodology provided by Wan et al. [34]. The Cochrane Q-test and I^2 index were employed to estimate the between-study heterogeneity. It should be emphasized that for Cochrane's Q-test, a P value of less than 0.1 was considered statistically significant, and I^2 indexes of 0.75, 0.50, and 0.25, respectively, indicated high, moderate, and low levels of heterogeneity. Also, a random effect model was adopted for meta-analysis of heterogeneous results. Otherwise, we used the fixed-effect model. We performed subgroup analysis according to study design and region to identify the source of heterogeneity. In addition, we assessed publication bias by using the funnel plot and Egger's test, which measures the funnel plot's asymmetry. STATA 12.0 was used to perform statistical analyses of the NLR differences between cases and controls (Stata Corporation, College Station, TX, USA). Except where mentioned, we judged P value < 0.05 to be statistically significant.

2.5. Certainty of Evidence. The certainty of evidence was determined using the GRADE (Grading of Recommendations Assessment, Development and Evaluation) approach

by one author for two outcomes investigated in meta-analysis (PSI and PSP). Finally, the assessments were confirmed by the senior author. According to GRADE, observational studies start at low certainty and may be upgraded for dose–response gradient or for large effect, if suspected biases work against the observed direction of effect, and may be downgraded for publication bias, imprecision, indirectness, inconsistency, and risk of bias.

2.6. Role of the Funding Source. This review received no external funding or other support.

3. Results

3.1. Search and Selection of Literature. In this systematic review, the process of discovering and selecting articles is depicted in Figure 1. The first search yielded 59 PubMed records, 140 Web of Science records, and 737 Scopus records. Also, one study was identified through other sources. When 58 duplicate articles were omitted, and a review of the titles and abstracts of the 879 remaining records were conducted, 40 papers were chosen for full-text review. After reading the complete text, 15 of the 40 studies were eliminated due to a lack of data on NLR ($n = 10$), single case ($n = 1$), and review reports ($n = 4$). As a result, the quantitative analysis covered a total of 25 studies [4, 9–32]. Of them, 15 studies comprising 6,410 patients with stroke, 876 of whom developed PSI and 615 of whom developed PSP, were included in the meta-analysis [10, 11, 13, 14, 20, 22, 24–32].

3.2. Characteristics of the Included Studies. This systematic review included 25 studies, of which 12 were retrospective [10, 12, 14, 18, 22–25, 28, 30–32] and 13 were prospective [4, 9, 11, 13, 15–17, 19–21, 26, 27, 29]. Among 25 studies, 15 were included in the meta-analysis; nine were retrospective [10, 14, 22, 24, 25, 28, 30–32], and six were prospective [11, 13, 20, 26, 27, 29]. In terms of document language, all of the documents were written in the English language.

Table 1 shows the characteristics of the studies that were included in the meta-analysis, and Table 2 shows characteristics of those that were included only in the qualitative review. In addition, the scale named NOS was used to assess the quality of the included research (Tables 1 and 2). In total, six studies compared NLR levels in PSI patients and controls [11, 20, 22, 24, 27, 31], and nine studies reported NLR levels in the PSP group against controls [10, 13, 14, 25, 26, 28–30, 32].

However, the certainty of this summary estimate of effect was deemed to be very low using the GRADE approach (Table 3).

3.3. Difference in NLR Level in Patients with and without PSI. In 6 cohort studies [11, 20, 22, 24, 27, 31] with 2,416 patients with stroke, NLR levels in the PSI group were compared to those in the nonpoststroke infection (NPSI) group, with 876 patients diagnosed with PSI after the follow-up period. Because the included studies were statistically heterogeneous ($I^2 = 89.7\%$, P value < 0.001), the analysis was conducted using the random effect model (Figure 2). The PSI groups had significantly higher NLR levels than the NPSI group (SMD = 1.08; CI 95% = 0.78-1.39, P value < 0.001). However, the certainty of evidence was downgraded to very low for this outcome (Table 3).

In the subgroup analysis, according to study design, three were retrospective studies [22, 24, 31] with 779 patients with stroke, 164 of whom developed PSI. Three were prospective studies [11, 20, 27] with 1,637 patients with stroke, 712 of whom developed PSI. In both retrospective and prospective studies, the NLR levels in patients in the PSI group were significantly higher than those in the NPSI group (SMD = 1.26, CI 95% = 0.91-1.60, P value <0 .001 and SMD = 0.93, CI 95% = 0.45-1.40, P value < 0.001, respectively) (Figure 3).

3.4. Differences in NLR Level in Patients with and without PSP. In 9 studies [10, 13, 14, 25, 26, 28–30, 32] with 3,994 stroke patients, of whom 615 were eventually diagnosed with PSP, NLR levels in the PSP group were compared to those in the nonpoststroke pneumonia (NPSP) group. The NLR levels of the PSP groups were significantly higher than those of the NPSP group (SMD = 0.98; CI 95% = 0.81-1.14, P value < 0.001). Because the included studies were statistically heterogeneous ($I^2 = 65.4\%$, P value = 0.003), the meta-analysis was conducted using the random effect model (Figure 4).

In subgroup analysis according to study design, there were six retrospective studies [10, 14, 25, 28, 30, 32] with 3,263 patients with stroke, 458 of whom got PSP, and three prospective studies [13, 26, 29] with 731 patients with stroke, 157 of whom got PSP. In both retrospective and prospective studies, the NLR levels in the PSP group were substantially higher than those in the NPSP group (SMD = 0.94, CI 95% = 0.75-1.13, P value < 0.001 and SMD = 1.07, CI 95% = 0.74-1.39, P value < 0.001, respectively) (Figure 5).

In another subgroup analysis according to study region, there were seven studies [10, 13, 25, 28–30, 32] in East Asia including 3,385 patients with stroke, of whom 509 had PSP, and two studies [14, 26] in Europe including 609 patients with stroke, of whom 106 developed PSP. In the studies in both East Asia and Europe, the NLR levels in patients with PSP were significantly higher than those in patients with NPSP (SMD = 1.02, CI 95% = 0.84-1.20, P value < 0.001 and SMD = 0.77, CI 95% = 0.48-1.07, P value < 0.001, respectively) (Figure 6).

3.5. Publication Bias Assessment. The funnel plot and Egger's test were used to assess the publication bias. As demonstrated in Figure 7, there was no evidence of publication bias in research on the role of NLR in PSI or PSP (Egger's test P value = 0.36 and 0.28, respectively).

4. Discussion

Our study had two main findings. First, the NLR level was significantly elevated in PSI patients. Second, patients with PSP had a higher level of NLR compared to the NPSP group. It is important to note the dynamic roles of neutrophils and lymphocytes in the setting of a stroke to understand the

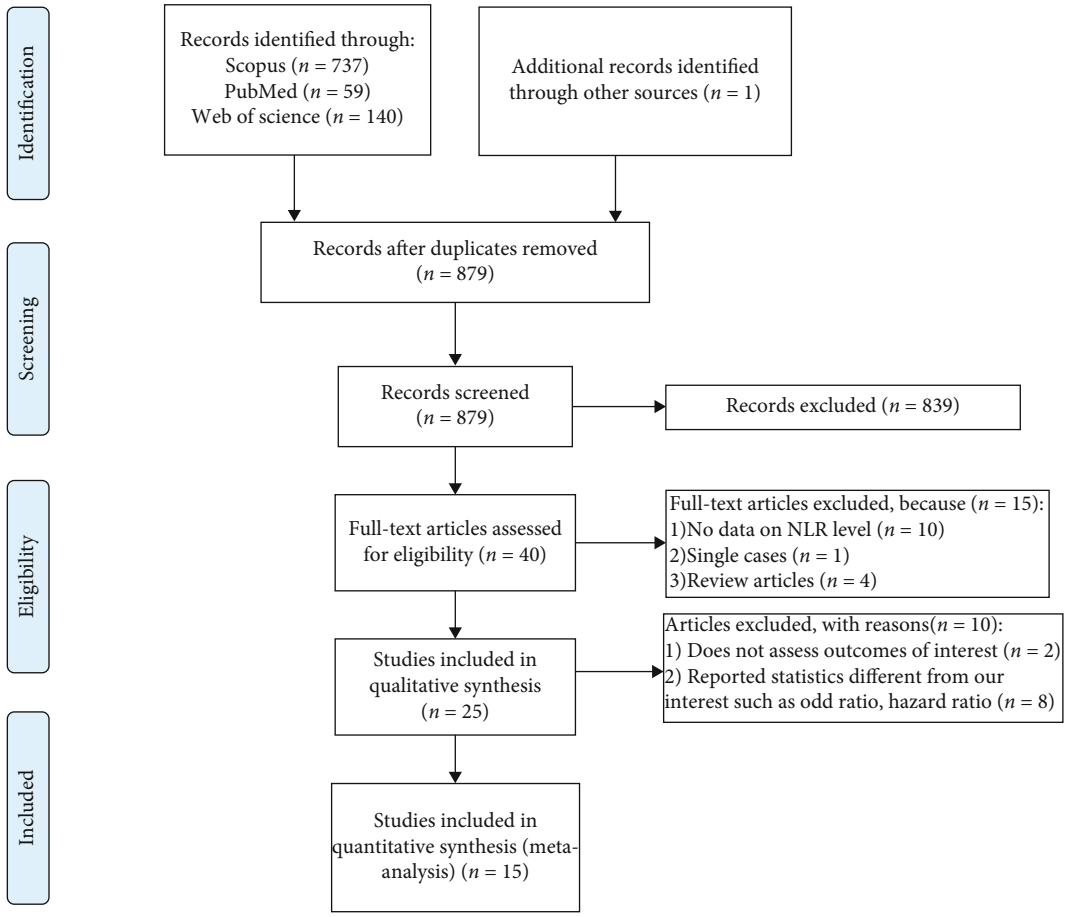

Figure 1: Flow chart of search and study selection.

importance of their relative proportion in the clinical context. It is well-known that levels of neutrophils measured in patients who have strokes are significantly higher than in nonstroke controls [35]. Further, it has been demonstrated that relative levels of neutrophils are predictive of stroke severity, with higher neutrophil counts predictive of more severe strokes [36]. Further work is needed to address role in predicting hemorrhagic conversion [37]. Other groups have found predictive benefit for acute intracerebral hemorrhage [38]. There are several mechanisms by which neutrophil counts may increase in these conditions, but the exact interplay of mechanisms is not currently well established [39]. It is known that neutrophils play a central role in eliminating infarcted neural tissue in the early poststroke period [40]. In the immediate poststroke period, neutrophils migrate to areas of insufficient blood flow via extravasation from nearby blood vessels [41]. Once there, neutrophils target neurovascular units and become activated after the length of ischemia is sufficiently prolonged, releasing mediators such as enzymes through the formation of extracellular traps (NETs) [42]. Pathways involving gene expression appear to be related to the elevation of neutrophil levels as well, including kynurenine pathway upregulation leading to increased tryptophan oxidation and upregulation of arginase 1 [43]. Although the absolute number of neutrophils is increased in stroke patients, their activity related to bacterial killing, like NETosis and oxidative burst, is significantly impaired [44, 45]. This impairment is one of the important mechanisms of stroke-induced immunosuppression and subsequent infection [45].

In addition to neutrophilia, lymphopenia seen in stroke patients exacerbates the elevation in the NLR, adding to its potential diagnostic utility for these patients [46]. Lymphopenia reflects immune depression in this context [47]. There are several mechanisms that may be at play in mediating the development of lymphopenia, but these interactions are similarly not well established. Possible mechanisms at play include a response to physiological stress under the influence of cortisol and a reduction of available regulatory T cells [48]. Additionally, lymphopenia may still be present up to 14 days following a stroke [49]. This, in turn, may make these patients more vulnerable to infections such as pneumonia [50]. This is especially true for patients that have failed recanalization, and the systemic inflammatory response index may be of adjuvant utility [51].

Outlining the relevance of elevated NLR in stroke patients forms the basis for understanding its potential diagnostic and prognostic value in the clinical setting. Recent evidence demonstrates that elevated NLR is associated with poor outcomes in stroke patients, including in-hospital mortality rates [52]. Petrone et al. also found that NLR was significantly higher in stroke patients with poor outcomes

Table 1: General characteristics of included studies in meta-analysis.

First author	Year of publication	Location	Design	Type of stroke	Mean age	Male (%)	Time of blood test	Time of monitoring presence of infection	NLR in PSI						NLR in PSP						NOS score
									PSI group			NPSI group			PSP group			NPSP group			
									Sample size	Mean	SD	Sample size	Mean	SD	Sample size	Mean	SD	Sample size	Mean	SD	
Freng, H.	2018	East Asia	P	Ischemic	69.32	60.52	Within 24 h of admission	Not declared	—	—	—	—	—	—	50	6.30	2.37	254	4.60	1.96	7
Nam, K.W.	2018	East Asia	R	Ischemic	67.00	60.00	Within 24 h of admission	Within 7 days of admission	—	—	—	—	—	—	112	4.20	3.43	1205	2.58	1.64	8
Deng, Q.W.	2020	East Asia	P	Ischemic	72.33	63.10	Within 24 h of admission	Within 7 days of admission	219	10.16	7.26	114	6.72	3.88	—	—	—	—	—	—	7
Gemmeren, T.V.	2020	Europe	P	Ischemic	74.33	60.00	Within 24 h of admission	Within 7 days of admission	—	—	—	—	—	—	27	6.11	4.77	68	3.48	0.87	9
He, L.	2020	East Asia	P	Ischemic	66.72	48.84	Within 24 h of admission	Within 7 days of admission	194	6.74	2.52	412	4.54	2.62	—	—	—	—	—	—	8
Lan, Y.	2020	East Asia	R	Ischemic	59.34	73.55	Within 24 h of admission	Within 7 days of admission	59	3.99	2.24	198	2.49	1.20	—	—	—	—	—	—	8
Wang, L.	2020	East Asia	P	Ischemic	66.94	48.37	At 36 hours after	Within hospitalization	299	8.65	5.34	499	3.49	2.37	—	—	—	—	—	—	7
Zhu, Y.	2020	East Asia	R	Ischemic	62.00	67.90	Not declared	Within 7 days of admission	—	—	—	—	—	—	31	16.33	13.83	81	6.23	4.22	7
Cheng, W.	2021	East Asia	R	Ischemic	63.94	47.94	Within 24 h of admission	Within 7 days of admission	—	—	—	—	—	—	52	3.83	2.84	682	2.20	1.07	7
Gens, R.	2021	Europe	R	Ischemic	75.03	53.89	Within 24 h of admission	Within 7 days of admission	—	—	—	—	—	—	79	4.10	2.10	435	2.80	1.90	6
Kashiwasaki, D.	2021	East Asia	R	Hemorrhagic	68.10	54.50	Within 8 h of admission	Within hospitalization	54	6.21	1.37	89	4.51	0.77	—	—	—	—	—	—	7
Wang, Q.	2021	East Asia	R	Both types	67.05	73.50	Within 24 h of admission	Within 7 days of admission	—	—	—	—	—	—	64	7.32	4.59	264	3.55	3.53	7
Xia, G.H.	2021	East Asia	P	Ischemic	60.07	70.48	At admission	Within 7 days of admission	—	—	—	—	—	—	80	6.05	4.30	252	2.79	1.49	8

Table 1: Continued.

First author	Year of publication	Location	Design	Type of stroke	Mean age	Male (%)	Time of blood test	Time of monitoring presence of infection	NLR in PSI						NLR in PSP						NOS score
									PSI group			NPSI group			PSP group			NPSP group			
									Sample size	Mean	SD	Sample size	Mean	SD	Sample size	Mean	SD	Sample size	Mean	SD	
Zhang, H.	2021	East Asia	R	Ischemic	68.00	64.00	Within 24 h of admission	Within 7 days of admission	51	4.28	2.46	328	2.64	1.13	—	—	—	—	—	—	6
Zhang, B.	2021	East Asia	R	Ischemic	63.33	65.50	Within 24 h of admission	Within 7 days of admission	—	—	—	—	—	—	120	10.50	6.90	138	6.53	3.82	6

P: prospective; R: retrospective; NLR: neutrophil to lymphocyte ratio; PSI: poststroke infection; NPSI: nonpoststroke infection; PSP: poststroke pneumonia; NPSP: nonpoststroke pneumonia; SD: standard deviation; h: hours.

Table 2: General characteristic of studies included only in qualitative review.

First author	Year of publication	Location	Design	Type of stroke	Mean age	Male (%)	Time of blood test	Time of monitoring presence of infection	Main findings	NOS score
Giede-Jeppe, A.	2017	Europe	P	Hemorrhagic	70.74	46.54	At admission	Within 7 days of admission	The NLR > 4.6 is a good predictor of PSP (P value < 0.01) and sepsis (P value < 0.01), but not UTI (P value = 0.13).	8
Duan, Zh.	2018	East Asia	R	Ischemic	65.66	39.45	Within 4.5 h of admission	Not declared	The NLR > 7.0 is a good predictor of PSP (P value < 0.01).	9
Almufti, F.	2019	USA	P	Hemorrhagic	⊠	31	Within 24 h of admission	Not declared	The NLR ≥ 5.9 is a good predictor of PSP (P value < 0.001) and fever (P value = 0.02) but not sepsis (P value = 0.07).	7
Giede-Jeppe, A.	2019	Europe	P	Hemorrhagic	53	30.73	At admission	Within 7 days of admission	The NLR ≥ 7.05 is a good predictor of PSP (P value = 0.01). However, it could not predict either ventriculitis or sepsis (P value = 0.87 and P value = 0.45, respectively).	7
Giede-Jeppe, A.	2019	Europe	P	Ischemic	72.66	52.8	At admission	Within hospitalization	NLR is independently associated with PSP (risk ratio [95% CI]: 1.083[1.019–1.151] per 1 point increment; $P = 0.01$).	5
Guo, R.	2019	East Asia	R	Hemorrhagic	46.09	57.93	Within 24 h of admission	Within 7 days of admission	The NLR ≥ 8.25 is a good predictor of PSP (P value < 0.02).	6
Kakhki, R.D.	2020	Iran	P	Both types	66.96	47.77	At admission	Not declared	The NLR > 5.0 is a good predictor of PSI in patients with ischemic (P value = 0.01) stroke but not hemorrhagic (P value = 0.11) stroke (overall P value < 0.01). Also, it could predict PSP in ischemic (P value = 0.03) stroke but not hemorrhagic (P value = 0.11) stroke (overall P value < 0.01). However, it could not predict UTI and sepsis in either ischemic (P value = 0.22 and P value = 0.19, respectively) or hemorrhagic (P value = 0.1 and P value = 0.97, respectively) stroke (P value = 0.94 and P value =0.34, respectively).	5
Gusdon, A.	2021	USA	P	Hemorrhagic	54	35	Within 5 days of admission	Not declared	The NLR ≥ 8.25 is a good predictor of PSI (P value < 0.01).	6
Hou, D.	2021	East Asia	P	Both types	81.29	51.79	At admission	Within hospitalization	The NLR > 5.0 is a good predictor of PSP (P value < 0.01) but not UTI (P value = 1).	6

Table 2: Continued.

First author	Year of publication	Location	Design	Type of stroke	Mean age	Male (%)	Time of blood test	Time of monitoring presence of infection	Main findings	NOS score
Kim, T.J.	2021	East Asia	R	Ischemic	97.7	59.7	At admission	Within hospitalization	The NLR is a good predictor of PSP (P value = 0.01) and sepsis (P value < 0.01).	5

P: prospective; R: retrospective; NLR: neutrophil to lymphocyte ratio; PSI: poststroke infection; PSP: poststroke pneumonia; UTI: urinary tract infection.

Table 3: GRADE evidence profile for cohort studies of the neutrophil to lymphocyte ratio in poststroke infection.

Certainty assessment							No. of patients			
No. of studies	Study design	Risk of bias[2]	Inconsistency[3]	Indirectness	Imprecision[5]	Publication bias[6]	Participants, n	Cases, n	Certainty[7]	Importance
Poststroke infection										
6	Observational studies	Not serious	Very serious	Not serious	Not serious	None	2416	876	⨁◯◯◯ very low	Critical
Poststroke pneumonia										
9	Observational studies	Not serious	Serious	Not serious	Not serious	None	3994	615	⨁◯◯◯ very low	Critical

[1]Grading of Recommendations Assessment, Development and Evaluation. [2]Risk of bias based on Newcastle-Ottawa Scale. [3]When I^2 was <30% inconsistency considered as not serious limitation, >50 considered as serious, and more than 75% considered as very serious limitation. [5]Serious limitations when there was fewer than 4000 participants for each outcome and very serious limitations when there was fewer than 300 participants for each outcome. [6]Funnel plot revealed no asymmetry; neither test of publication bias approached $P < 0.10$. [7]Data from cohort studies begin with a grade of "low." Downgraded for very serious inconsistency. [8]Data from cohort studies begin with a grade of "low." Downgraded for serious inconsistency.

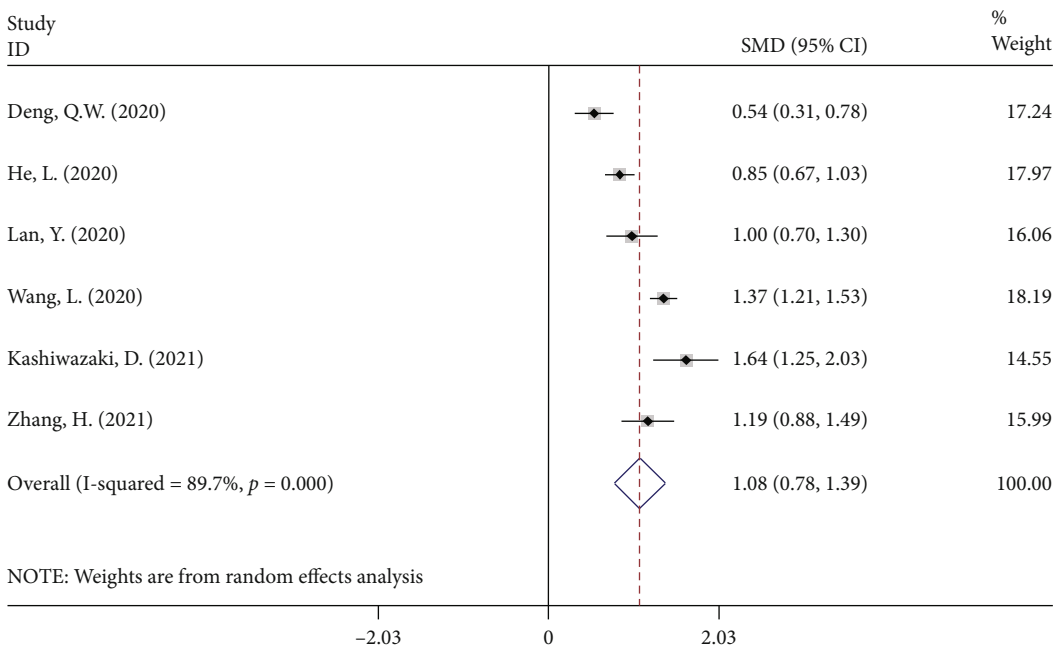

Figure 2: Meta-analysis of differences in NLR level between PSI and NPSI patients.

compared to those with favorable outcomes, and in fact, asserted that high NLR should be considered a predictor for poor prognosis after stroke [53]. The addition of mean platelet volume might even improve accuracy of the NLR results. Such easily obtainable and not expensive laboratory biomarkers can have a great role in everyday clinical practice and management of stroke patients [54]. Recent studies have demonstrated a variable degree of evidence supporting the diagnostic utility of NLR in predicting PSI rates, particularly rates of PSP development [4, 9–32]. A retrospective study by Nam et al. demonstrated that the predictive potential of NLR further increased when combined with the Pneumonia

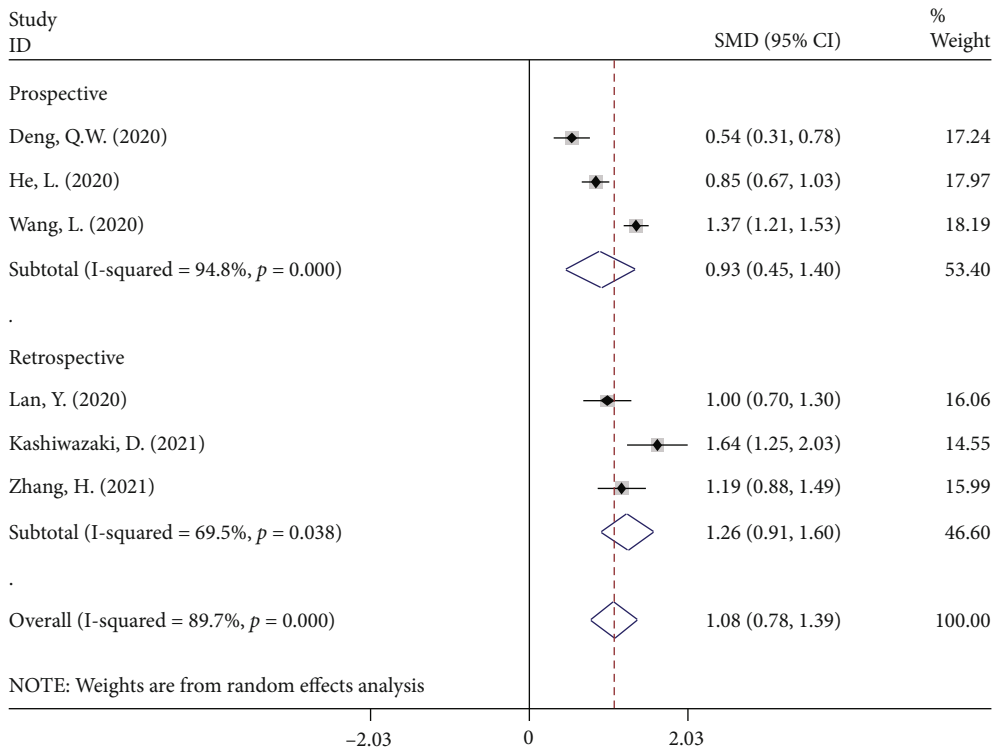

Figure 3: Subgroup analysis of differences in NLR level between PSI and NPSI according to study design.

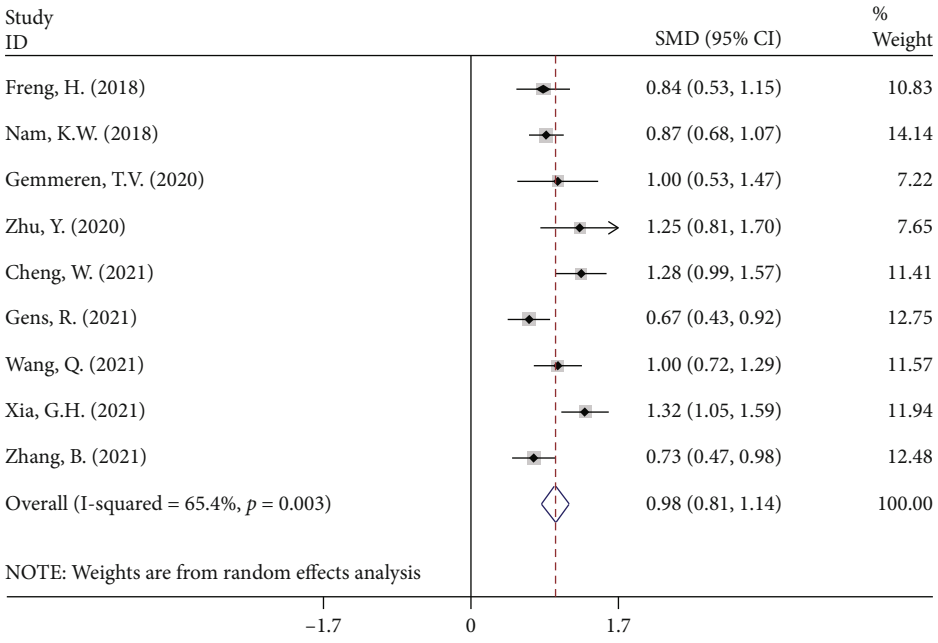

Figure 4: Meta-analysis of differences in NLR level between PSP and NPSP patients.

Severity Index ($P < 0.001$) [25]. In another study, researchers suggested that the NLR by itself was a weak predictor of pneumonia development and was much stronger when used in conjunction with a prediction model that considered other factors such as age, gender, and dysphagia [55]. As such, it appears that although the NLR ratio has demonstrated utility in predicting pneumonia outcomes in stroke patients on its own, using this marker in conjunction with other models and diagnostic tools, such as the Pneumonia Severity Index, may greatly increase its predictive ability [11].

In this context, it appears that prospective and retrospective studies also demonstrate varying degrees of support for the diagnostic utility of the NLR in predicting PSP and other

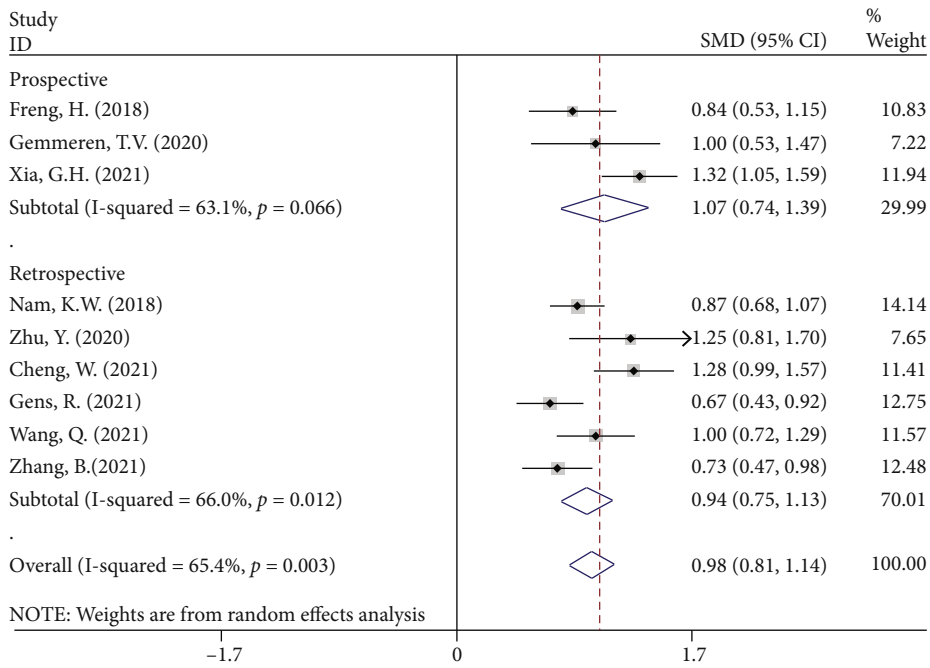

Figure 5: Subgroup analysis of differences in NLR level between PSP and NPSP according to study design.

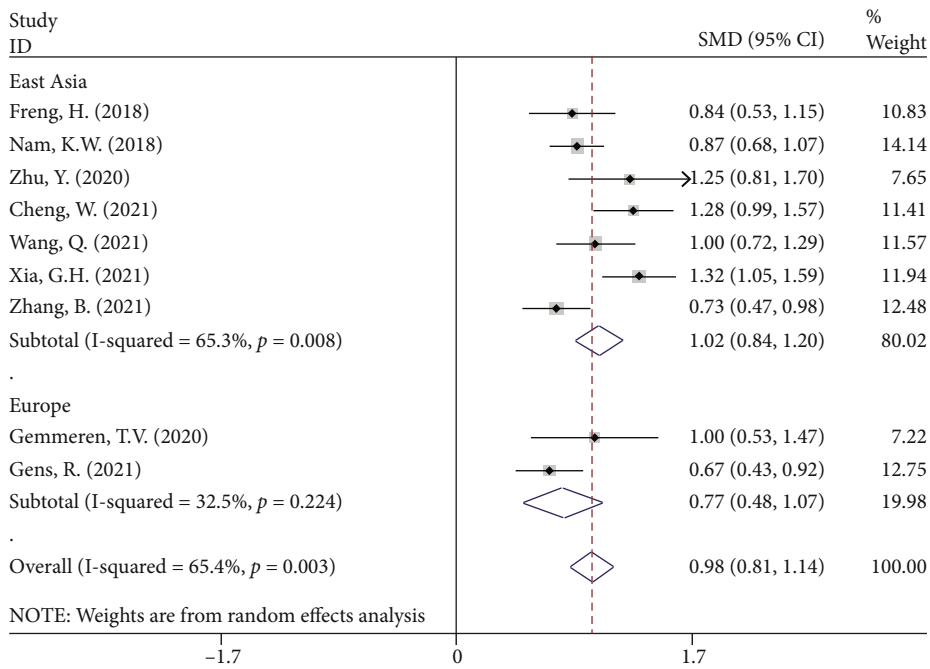

Figure 6: Subgroup analysis of differences in NLR level between PSP and NPSP according to study location.

infection rates. In general, retrospective studies currently indicate more support for the diagnostic utility of NLR as a predictor of PSP and other infection development. However, both types of studies have demonstrated statistical significance on this front.

In addition, some studies were included solely in the qualitative review [4, 9, 12, 15–19, 21, 23]. The majority of them assessed the relationship between NLR and PSP [4, 9, 12, 15–18, 21, 23] and reported that NLR could predict pneumonia after stroke, similar to our findings. UTI is another type of PSP whose relationship with NLR was investigated in included studies. Gens et al. showed that NLR within 24 h after stroke onset was not statistically different among patients developing UTI than those without UTI (P value = 0.074) [14]. This finding is in agreement with findings reported by Kashiwazaki et al. (P value = 0.948) [22],

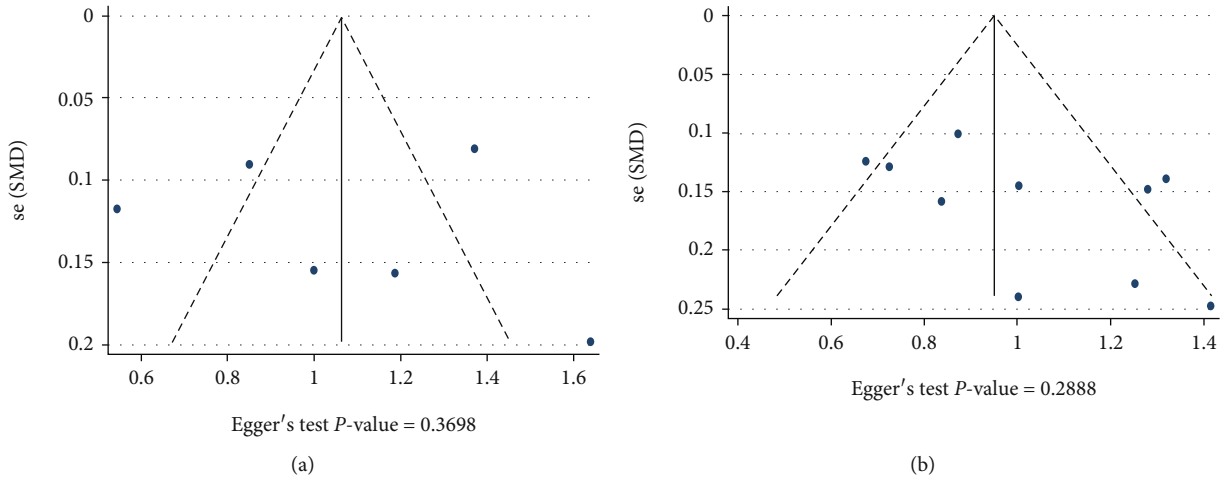

Figure 7: (a) Publication bias assessment based on Funnel plot and Egger's test in data of PSI. (b) Publication bias in data of PSP.

Hou et al. (P value = 1) [21], Giede-Jeppe et al. (P value = 0.13) [15], and Wang et al. (P value = 0.10) [27]. In accordance with these studies, it seems that NLR cannot predict UTI after stroke.

Also, a number of researchers have sought to determine the relationship between NLR and sepsis after stroke. Kashiwazaki et al. found that there was not any association between NLR and sepsis after either ischemic (P value = 0.19) or hemorrhagic (P value = 0.97) stroke (overall P value = 0.34) [22]. Their results agree with the findings of Al-Mufti et al., which showed that admission NLR could not predict the development of sepsis after stroke (P value = 0.29) [9]. However, in their study, NLR showed a good predictive value for fever > 101.5°F (P value = 0.04) after stroke [9]. In accordance with their results, Giede-Jeppe et al. revealed that NLR could predict the occurrence of neither sepsis nor ventriculitis in patients with stroke due to aneurysmal subarachnoid hemorrhage (P value = 0.45; P value = 0.87) [17]. These results match those observed in another study by the same researchers on ischemic stroke patients [16]. However, in another study, the same authors revealed that NLR could predict sepsis (P value < 0.001) in stroke patients with intracranial hemorrhage [15]. Also, Kim et al. reported that NLR had a predictive role in poststroke sepsis (P value < 0.01) [23]. In light of the findings of these studies, we can say that the role of NLR in poststroke sepsis remains controversial.

4.1. Strengths and Limitations. This study has several strengths. First, studies were obtained through a systematic search of the literature, augmented with manual searches of reference lists of retrieved papers and systematic reviews. Second, we assessed certainty in the estimates with GRADE, highlighting the remaining uncertainty regarding causal relationships between NLR and PSI or PSP. However, some limitations of our study do exist. Heterogeneity in studies was greater than expected due to various treatment regimens, duration of recorded stays, center protocols, different study populations, different times of blood tests from which NLR was calculated, and different study designs. Therefore, widespread validity is a concern, and future larger prospective studies are needed. Furthermore, several of the studies are limited by bias whether selection or publication, which should be considered. In addition, geographic variability is essential to consider in the context of these results. The majority of current studies on this topic were performed in East Asia and Europe. Given that disparities in both stroke rates and stroke outcomes have been shown between different geological locations, such as Asian and North American countries, it is important to note that the results from the studies on this topic to date may not be as applicable to stroke patients located in different geographical regions [56]. Thus, similar prospective and retrospective studies are warranted in wider geographic locations to characterize any potential differences between these populations. Finally, effect size for several of the tests was limited to a few studies. Thereby widespread adoption and applicability are again a concern warranting further studies. In addition, most studies on the relationship between NLR and PSI have only focused on pneumonia because it is the most common PSI. Researchers have not treated PSI in many details. Searching the databases, we found limited data on the predictive role of admission NLR in sepsis, ventriculitis, and UTI after stroke. Therefore, we could not use the meta-analytic method; however, we reported their findings. Further studies, which take these types of PSI into account, are therefore recommended.

5. Conclusion

In conclusion, there has been a recent interest in determining the utility of the NLR as a diagnostic marker for predicting the development of PSP and other infections after stroke. As it currently stands, data collected from prospective and retrospective studies demonstrate a variable degree of support for the predictive potential of the NLR in this context. However, in general, data suggests that the NLR has significant predictive potential for developing PSP and other infections. This predictive potential increases even further when combined with other diagnostic tools such as the Pneumonia Severity Index. Along with administering a larger study to

further validate this relationship, additional studies including populations outside of East Asia and Europe are warranted to assess this relationship in a broader context.

Data Availability

The datasets generated during and/or analyzed during the current study are available from the corresponding author on reasonable request.

Ethical Approval

This study adhered to international ethical standards.

Conflicts of Interest

The authors declare that they have no conflicts of interest.

Authors' Contributions

SK and BL contributed to conceptualization and data organization; KR and FE contributed to data analysis; AC contributed to writing and clinical analysis.

References

[1] T. Angkananard, T. Anothaisintawee, M. McEvoy, J. Attia, and A. Thakkinstian, "Neutrophil lymphocyte ratio and cardiovascular disease risk: a systematic review and meta-analysis," *BioMed Research International*, vol. 2018, Article ID 2703518, 11 pages, 2018.

[2] S. A. Jamali, M. T. Turnbull, T. Kanekiyo et al., "Elevated neutrophil-lymphocyte ratio is predictive of poor outcomes following aneurysmal subarachnoid hemorrhage," *Journal of Stroke and Cerebrovascular Diseases*, vol. 29, no. 4, p. 104631, 2020.

[3] D. Lux, V. Alakbarzade, L. Bridge et al., "The association of neutrophil-lymphocyte ratio and lymphocyte-monocyte ratio with 3-month clinical outcome after mechanical thrombectomy following stroke," *Journal of Neuroinflammation*, vol. 17, no. 1, p. 60, 2020.

[4] R. D. Kakhki, M. Dehghanei, R. ArefNezhad, and H. Motedayyen, "The predicting role of neutrophil- lymphocyte ratio in patients with acute ischemic and hemorrhagic stroke," *Journal of Stroke and Cerebrovascular Diseases*, vol. 29, no. 11, p. 105233, 2020.

[5] K. Guldolf, F. Vandervorst, R. Gens, A. Ourtani, T. Scheinok, and S. De Raedt, "Neutrophil-to-lymphocyte ratio predicts delirium after stroke," *Age and Ageing*, vol. 50, no. 5, pp. 1626–1632, 2021.

[6] P. Gong, Y. Liu, Y. Gong et al., "The association of neutrophil to lymphocyte ratio, platelet to lymphocyte ratio, and lymphocyte to monocyte ratio with post-thrombolysis early neurological outcomes in patients with acute ischemic stroke," *Journal of Neuroinflammation*, vol. 18, no. 1, p. 51, 2021.

[7] M. H. Rashid, A. Kabir, M. U. Waris, U. Salman, and S. Zain, "Role of prophylactic antibiotics in critical care of stroke patients - a preventive approach to post-stroke infections?," *Cureus*, vol. 12, no. 3, article e7158, 2020.

[8] N. Leangpanich, Y. Chuphanitsakun, K. Pakaranodom, K. Kerdjarern, and W. Poonual, "Scoring of post stroke pneumonia in Uttaradit Hospital," *Journal of Multidisciplinary Healthcare*, vol. Volume 12, pp. 917–923, 2019.

[9] F. Al-Mufti, K. Amuluru, N. Damodara et al., "Admission neutrophil–lymphocyte ratio predicts delayed cerebral ischemia following aneurysmal subarachnoid hemorrhage," *Journal of Neurointerventional Surgery*, vol. 11, no. 11, pp. 1135–1140, 2019.

[10] W. Cheng, L. Chen, H. Yu, D. Lu, R. Yu, and J. Chen, "Value of combining of the NLR and the fibrinogen level for predicting stroke-associated pneumonia," *Neuropsychiatric Disease and Treatment*, vol. Volume 17, pp. 1697–1705, 2021.

[11] Q.-W. Deng, P.-Y. Gong, X.-L. Chen et al., "Admission blood cell counts are predictive of stroke-associated infection in acute ischemic stroke patients treated with endovascular therapy," *Neurological Sciences*, vol. 42, no. 6, pp. 2397–2409, 2021.

[12] Z. Duan, H. Wang, Z. Wang et al., "Neutrophil-lymphocyte ratio predicts functional and safety outcomes after endovascular treatment for acute ischemic stroke," *Cerebrovascular Diseases*, vol. 45, no. 5-6, pp. 221–227, 2018.

[13] H.-X. Feng, Y. Cheng, W. Zhu et al., "T-lymphocyte subsets as a predictive biomarker for stroke-associated pneumonia," *American Journal of Translational Research*, vol. 10, no. 12, pp. 4367–4375, 2018.

[14] R. Gens, A. Ourtani, A. De Vos, J. De Keyser, and S. De Raedt, "Usefulness of the neutrophil-to-lymphocyte ratio as a predictor of pneumonia and urinary tract infection within the first week after acute ischemic stroke," *Frontiers in Neurology*, vol. 12, p. 747, 2021.

[15] A. Giede-Jeppe, T. Bobinger, S. T. Gerner et al., "Neutrophil-to-lymphocyte ratio is an independent predictor for in-hospital mortality in spontaneous intracerebral hemorrhage," *Cerebrovascular Diseases*, vol. 44, no. 1-2, pp. 26–34, 2017.

[16] A. Giede-Jeppe, D. Madžar, J. A. Sembill et al., "Increased neutrophil-to-lymphocyte ratio is associated with unfavorable functional outcome in acute ischemic stroke," *Neurocritical care*, vol. 33, no. 1, pp. 97–104, 2020.

[17] A. Giede-Jeppe, J. Reichl, M. I. Sprügel et al., "Neutrophil-to-lymphocyte ratio as an independent predictor for unfavorable functional outcome in aneurysmal subarachnoid hemorrhage," *Journal of Neurosurgery*, vol. 132, no. 2, pp. 400–407, 2019.

[18] R. Guo, Y. Wu, R. Chen et al., "Clinical value of neutrophil-to-lymphocyte ratio in primary intraventricular hemorrhage," *World Neurosurgery*, vol. 127, pp. e1051–e1056, 2019.

[19] A. M. Gusdon, J. P. Savarraj, E. Shihabeddin et al., "Time course of peripheral leukocytosis and clinical outcomes after aneurysmal subarachnoid hemorrhage," *Frontiers in Neurology*, vol. 12, 2021.

[20] L. He, J. Wang, F. Wang, L. Zhang, L. Zhang, and W. Zhao, "Increased neutrophil-to-lymphocyte ratio predicts the development of post-stroke infections in patients with acute ischemic stroke," *BMC Neurology*, vol. 20, no. 1, pp. 1–7, 2020.

[21] D. Hou, C. Wang, X. Ye, P. Zhong, and D. Wu, "Persistent inflammation worsens short-term outcomes in massive stroke patients," *BMC Neurology*, vol. 21, no. 1, pp. 1–8, 2021.

[22] D. Kashiwazaki, T. Tomita, T. Shibata et al., "Impact of perihematomal edema on infectious complications after spontaneous intracerebral hemorrhage," *Journal of Stroke and Cerebrovascular Diseases*, vol. 30, no. 7, p. 105827, 2021.

[23] T. J. Kim, C.-H. Lee, H. Mo, H.-Y. Jeong, S.-B. Ko, and B.-W. Yoon, "Abstract WP315: neutrophil-to-lymphocyte ratio

is a useful predictor of aspiration pneumonia in patients with acute ischemic stroke," *Stroke*, vol. 49, no. 1, p. WP315, 2018.

[24] Y. Lan, W. Sun, Y. Chen et al., "Nomogram including neutrophil-to-lymphocyte ratio for the prediction of stroke-associated infections," *Frontiers in Neurology*, vol. 11, 2020.

[25] K.-W. Nam, T. J. Kim, J. S. Lee et al., "High neutrophil-to-lymphocyte ratio predicts stroke-associated pneumonia," *Stroke*, vol. 49, no. 8, pp. 1886–1892, 2018.

[26] T. van Gemmeren, R. Schuppner, G. M. Grosse et al., "Early post-stroke infections are associated with an impaired function of neutrophil granulocytes," *Journal of Clinical Medicine*, vol. 9, no. 3, p. 872, 2020.

[27] L. Wang, W. Guo, C. Wang et al., "Dynamic change of neutrophil to lymphocyte ratios and infection in patients with acute ischemic stroke," *Current Neurovascular Research*, vol. 17, no. 3, pp. 294–303, 2020.

[28] Q. Wang, Y. Liu, L. Han et al., "Risk factors for acute stroke-associated pneumonia and prediction of neutrophil-to-lymphocyte ratios," *The American Journal of Emergency Medicine*, vol. 41, pp. 55–59, 2021.

[29] G.-H. Xia, M.-S. Zhang, Q.-H. Wu et al., "Dysbiosis of gut microbiota is an independent risk factor of stroke-associated pneumonia: a Chinese pilot study," *Frontiers in Cellular and Infection Microbiology*, vol. 11, 2021.

[30] B. Zhang, W. Zhao, C. Wu et al., "SDL index predicts stroke-associated pneumonia in patients after endovascular therapy," *Frontiers in Neurology*, vol. 12, p. 149, 2021.

[31] H. Zhang, T. Wu, X. Tian, P. Lyu, J. Wang, and Y. Cao, "High neutrophil percentage-to-albumin ratio can predict occurrence of stroke-associated infection," *Frontiers in Neurology*, vol. 12, 2021.

[32] Y. Zhu, J. Gao, Q. Lv, Q. Yin, and D. Yang, "Risk factors and outcomes of stroke-associated pneumonia in patients with stroke and acute large artery occlusion treated with endovascular thrombectomy," *Journal of Stroke and Cerebrovascular Diseases*, vol. 29, no. 11, p. 105223, 2020.

[33] S. V. Okar, M. A. Topcuoglu, M. Yemisci, C. Cakir Aktas, K. K. Oguz, and E. M. Arsava, "Post-stroke inflammatory response is linked to volume loss in the contralateral hemisphere," *Journal of Neuroimmunology*, vol. 344, article 577247, 2020.

[34] X. Wan, W. Wang, J. Liu, and T. Tong, "Estimating the sample mean and standard deviation from the sample size, median, range and/or interquartile range," *BMC Medical Research Methodology*, vol. 14, no. 1, pp. 1–13, 2014.

[35] G. C. O'Connell and J. H. C. Chang, "Analysis of early stroke-induced changes in circulating leukocyte counts using transcriptomic deconvolution," *Translational Neuroscience*, vol. 9, pp. 161–166, 2018.

[36] Y. N. Fang, M. S. Tong, P. H. Sung et al., "Higher neutrophil counts and neutrophil-to-lymphocyte ratio predict prognostic outcomes in patients after non-atrial fibrillation-caused ischemic stroke," *Biomedical Journal*, vol. 40, no. 3, pp. 154–162, 2017.

[37] M. Switonska, N. Piekus-Slomka, A. Slomka, P. Sokal, E. Zekanowska, and S. Lattanzi, "Neutrophil-to-lymphocyte ratio and symptomatic hemorrhagic transformation in ischemic stroke patients undergoing revascularization," *Brain Sciences*, vol. 10, no. 11, p. 771, 2020.

[38] S. Lattanzi, C. Cagnetti, C. Rinaldi, S. Angelocola, L. Provinciali, and M. Silvestrini, "Neutrophil-to-lymphocyte ratio improves outcome prediction of acute intracerebral hemorrhage," *Journal of the Neurological Sciences*, vol. 387, pp. 98–102, 2018.

[39] A. B. Petrone, G. C. O'Connell, M. D. Regier, P. D. Chantler, J. W. Simpkins, and T. L. Barr, "The role of arginase 1 in post-stroke immunosuppression and ischemic stroke severity," *Translational Stroke Research*, vol. 7, no. 2, pp. 103–110, 2016.

[40] D. M. Hermann, C. Kleinschnitz, and M. Gunzer, "Role of polymorphonuclear neutrophils in the reperfused ischemic brain: insights from cell-type-specific immunodepletion and fluorescence microscopy studies," *Therapeutic Advances in Neurological Disorders*, vol. 11, p. 175628641879860, 2018.

[41] E. Kolaczkowska and P. Kubes, "Neutrophil recruitment and function in health and inflammation," *Nature Reviews. Immunology*, vol. 13, no. 3, pp. 159–175, 2013.

[42] I. Perez-de-Puig, F. Miró-Mur, M. Ferrer-Ferrer et al., "Neutrophil recruitment to the brain in mouse and human ischemic stroke," *Acta Neuropathologica*, vol. 129, no. 2, pp. 239–257, 2015.

[43] R. Brouns, R. Verkerk, T. Aerts et al., "The role of tryptophan catabolism along the kynurenine pathway in acute ischemic stroke," *Neurochemical Research*, vol. 35, no. 9, pp. 1315–1322, 2010.

[44] M. Y. Pektezel, E. Yilmaz, E. M. Arsava, and M. A. Topcuoglu, "Neutrophil-to-lymphocyte ratio and response to intravenous thrombolysis in patients with acute ischemic stroke," *Journal of Stroke and Cerebrovascular Diseases*, vol. 28, no. 7, pp. 1853–1859, 2019.

[45] J. Faura, A. Bustamante, F. Miró-Mur, and J. Montaner, "Stroke-induced immunosuppression: implications for the prevention and prediction of post-stroke infections," *Journal of Neuroinflammation*, vol. 18, no. 1, pp. 1–14, 2021.

[46] Z. Guo, S. Yu, L. Xiao et al., "Dynamic change of neutrophil to lymphocyte ratio and hemorrhagic transformation after thrombolysis in stroke," *Journal of Neuroinflammation*, vol. 13, no. 1, p. 199, 2016.

[47] A. Semerano, D. Strambo, G. Martino et al., "Leukocyte counts and ratios are predictive of stroke outcome and hemorrhagic complications independently of infections," *Frontiers in Neurology*, vol. 11, p. 201, 2020.

[48] J. Hu, W. Zhou, Z. Zhou, J. Han, and W. Dong, "Elevated neutrophil-to-lymphocyte and platelet-to-lymphocyte ratios predict post-stroke depression with acute ischemic stroke," *Experimental and Therapeutic Medicine*, vol. 19, no. 4, pp. 2497–2504, 2020.

[49] A. Vogelgesang, U. Grunwald, S. Langner et al., "Analysis of lymphocyte subsets in patients with stroke and their influence on infection after stroke," *Stroke*, vol. 39, no. 1, pp. 237–241, 2008.

[50] D. Sharma, K. J. Spring, and S. M. M. Bhaskar, "Neutrophil-lymphocyte ratio in acute ischemic stroke: immunopathology, management, and prognosis," *Acta Neurologica Scandinavica*, vol. 144, no. 5, pp. 486–499, 2021.

[51] S. Lattanzi, D. Norata, A. A. Divani et al., "Systemic inflammatory response index and futile recanalization in patients with ischemic stroke undergoing endovascular treatment," *Brain Sciences*, vol. 11, no. 9, p. 1164, 2021.

[52] W. Li, M. Hou, Z. Ding, X. Liu, Y. Shao, and X. Li, "Prognostic value of neutrophil-to-lymphocyte ratio in stroke: a systematic review and meta-analysis," *Frontiers in Neurology*, vol. 12, p. 686983, 2021.

[53] A. B. Petrone, R. D. Eisenman, K. N. Steele, L. T. Mosmiller, O. Urhie, and M. J. Zdilla, "Temporal dynamics of peripheral neutrophil and lymphocytes following acute ischemic stroke," *Neurological Sciences*, vol. 40, no. 9, pp. 1877–1885, 2019.

[54] M. Zheng, S. Chen, Y. Zhu, and X. Gu, "Mean platelet volume: a new predictor of ischaemic stroke risk in patients with non-valvular atrial fibrillation," *BMC Cardiovascular Disorders*, vol. 20, no. 1, p. 241, 2020.

[55] H. Chen, X. Luan, K. Zhao et al., "The association between neutrophil-to-lymphocyte ratio and post-stroke depression," *Clinica Chimica Acta*, vol. 486, pp. 298–302, 2018.

[56] A. de Havenon, K. Sheth, K. C. Johnston et al., "Acute ischemic stroke interventions in the United States and racial, socioeconomic, and geographic disparities," *Neurology*, vol. 97, no. 23, pp. e2292–e2303, 2021.

Hindawi
Disease Markers
Volume 2022, Article ID 2559004, 9 pages
https://doi.org/10.1155/2022/2559004

Research Article

Multimodality Treatment of Brain Arteriovenous Malformations with One-Staged Hybrid Operation: Clinical Characteristics and Long-Term Prognosis

Yuanfeng Jiang,[1] Chaofan Zeng,[2] Yiqun Zhang,[3] Xiaobo Xu,[4] Hancheng Qiu,[2] and Weijian Jiang[5]

[1]*Medical College of Soochow University, Suzhou, China*
[2]*Department of Neurosurgery, Beijing Tiantan Hospital, Capital Medical University, Beijing, China*
[3]*Department of Critical Care Medicine, New Era Stroke Care and Research Institute, The PLA Rocket Force Characteristic Medical Center, Beijing, China*
[4]*Department of Neurology, New Era Stroke Care and Research Institute, The PLA Rocket Force Characteristic Medical Center, Beijing, China*
[5]*Department of Vascular Neurosurgery, New Era Stroke Care and Research Institute, The PLA Rocket Force Characteristic Medical Center, Beijing, China*

Correspondence should be addressed to Weijian Jiang; jiangweijian2018@163.com

Received 20 December 2021; Revised 19 January 2022; Accepted 4 February 2022; Published 27 February 2022

Academic Editor: Liangqun Rong

Objective. We aimed to evaluate the clinical characteristics and long-term prognosis of brain arteriovenous malformations (bAVMs) treated with multimodality management of one-staged hybrid operation. *Methods*. We identified bAVM patients treated with one-staged hybrid operation from a multicenter prospective cohort study (NCT03774017) between January 2016 and June 2020. Patients were divided into unruptured and ruptured groups by the hemorrhagic presentation. Long-term (>12 months) neurological disability, postoperative complications of stroke, and nidus obliteration were evaluated and compared between groups. Prognostic predictors associated with outcomes were analyzed. *Results*. A total of 130 patients were identified in the study receiving one-staged hybrid operations, including 61 unruptured cases and 69 ruptured cases. Mean age was 29.1 years old, with 78 (60.0%) being male. Patients included in the study were followed up for a mean period of 37.4 (11.07) months. The annual hemorrhagic risk was 4.2% per year. Thirteen postoperative stroke events were detected in 11 patients (8.5%). Long-term disability occurred in 6.9% of cases, and 86.2% of patients experienced an unchanged or improved neurological status at the last follow-up. All patients achieved complete obliteration on follow-up angiographies. Increased AVM volume was associated with a higher risk of postoperative stroke (odds ratio (OR) 1.021, 95% confidence interval (CI) 1.006-1.037, and $P = 0.006$). Poor neurological status (OR 6.461, 95% CI 1.309-31.889, and $P = 0.022$) and infratentorial location (OR 5.618, 95% CI 1.158-27.246, and $P = 0.032$) were independent predictors for long-term disability. *Conclusions*. One-staged hybrid operation of embolization combined microsurgical resection can be performed as a safe and effective strategy for bAVM treatments. Long-term prognosis of complete obliteration with low rates of morbidity and mortality can be achieved. Unruptured and ruptured bAVMs acquired similar favorable outcomes after the multimodality treatment.

1. Introduction

Brain arteriovenous malformations (bAVMs) are congenital anomalies of dilated arteries and veins without capillary networks, allowing high-flow arterial blood to shunt directly into the venous system [1, 2]. Intracranial hemorrhage is the most common primary manifestation with an annual bleeding rate of 2%-4%, which leads to a high risk of

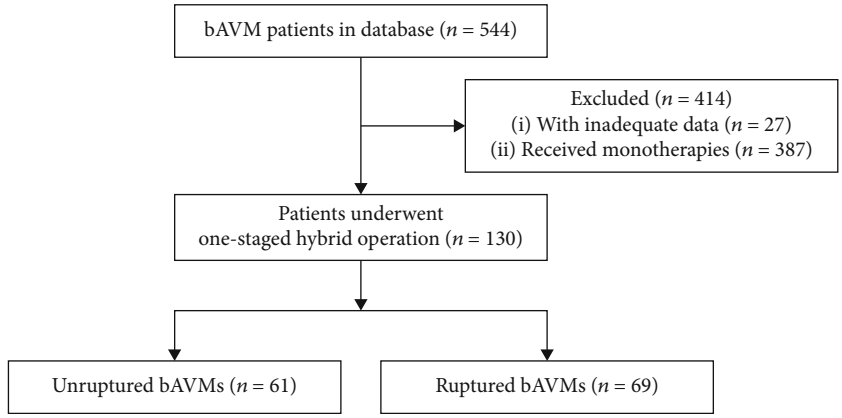

Figure 1: Flow diagram of the study participants. bAVMs: brain arteriovenous malformations.

neurological morbidity and mortality [3]. Thus, appropriate managements of completely obliterating the lesions are necessary.

Modern treatments are available for bAVMs, including endovascular embolization, microsurgical resection, stereotactic radiosurgery alone, or in combination [4]. The integrated strategy of endovascular embolization and microsurgical resection is commonly utilized in the treatment of bAVMs as novel multimodality management in many institutions [5–8]. Endovascular embolization facilitates the subsequent microsurgery by reducing blood flows and volume for surgical safety, formatting clear resecting planes for less injury, and potentially protecting eloquent areas [9–13]. Intraoperative digital subtraction angiography (DSA) is applied to detect any residual lesions during operation [14]. Besides, the interval risks and gradient hemodynamic changes were diminished as compared with multistaged treatments. However, few studies have assessed the applicable population, preoperative embolization strategy, and the long-term outcomes of the one-staged hybrid operation for bAVM treatment. We presumed that the multimodality management can be performed as a safe and effective strategy for bAVM treatments, with low rate of morbidity and residual lesions in the long term. Therefore, we aimed to describe the clinical experience and evaluate the long-term safety and benefits of bAVMs treated with hybrid operations in this study.

2. Materials and Methods

2.1. Study Design and Participants. BAVM patients were reviewed from the database of a multicenter prospective cohort study (NCT03774017) between January 2016 and June 2020. Patients who underwent endovascular embolization combined microsurgical resection in one-staged hybrid operation were included in the study. Patients with inadequate clinical data or receiving monotherapies of embolization or microsurgery were excluded. The clinical outcomes between unruptured and ruptured bAVMs were compared. The study was approved by the Institutional Review Board (IRB) of Beijing Tiantan Hospital (KY2016-034-02). Written informed consents were obtained from all participants.

2.2. Data Collection. Data of demographics, personal and operation history, clinical features, and radiographic presentations were obtained. The operation history included endovascular embolization and radiosurgery. Different primary symptoms were summarized into four categories: hemorrhage, seizure, neurological dysfunction, and headache. Radiographic presentations included morphology of bAVMs, eloquent location, and angioarchitecture of lesions. The bAVMs were classified by the Spetzler-Martin (SM) grading scale, and the bAVM volume was calculated by $(\text{width} \times \text{height} \times \text{length})/2$ [15]. The clinical outcomes and bVMs obliteration were acquired from the evaluation of discharge and follow-up. Two experienced neurosurgeons (Y.J. and C.Z.) independently evaluated the radiographic findings.

2.3. Treatment. The multimodality treatment of microsurgery and endovascular embolization was decided by a multidisciplinary team with neurosurgeons and neurointerventionalists involved. Preoperative embolization was conducted as an adjunctive therapy. The subsequent microsurgical resection was performed immediately in the hybrid operating room, with the assistance of neuronavigation and indocyanine fluorescence angiography (ICG). Intraoperative DSA was applied during microsurgery to confirm the complete elimination of bAVMs. The hybrid management followed the study protocol across the multicenters [16].

2.4. Outcome Evaluation and Follow-Up. The clinical status was assessed by the modified Rankin Scale (mRS) on admission, at discharge and in follow-up. The primary outcome was defined as the neurological disability (mRS score > 2). Postoperative stroke, defined as intracranial hemorrhage or cerebral infarction, was considered as the secondary outcome [16]. Besides, all-cause mortality and obliteration of bAVM lesions were collected. Patients were followed up in the 3^{rd}, 6^{th}, 12^{th} months, and annually after the operation. The short-term outcomes were obtained at discharge, and long-term outcomes were evaluated at the last follow-up.

2.5. Statistical Analysis. SPSS (version 26.0, IBM, NY, USA) was used for statistical analyses in the study. The categorical variables were reported as frequencies, and continuous

Table 1: Baseline characteristics of unruptured and ruptured bAVM patients.

Variables	Total ($n = 130$)	Unruptured ($n = 61$)	Ruptured ($n = 69$)	P value
Age (mean (SD)), y	29.1 (13.24)	29.9 (12.29)	28.3 (14.08)	0.507[†]
Sex, male (%)	78 (60.0)	40 (65.6)	38 (55.1)	0.223[‡]
Prior treatments (%)				
Embolization	12 (9.2)	2 (3.3)	10 (14.5)	0.057[‡]
Primary symptom (%)				
Hemorrhage	69 (53.1)	0 (0)	69 (100.0)	<0.001*[§]
Seizure	42 (32.3)	38 (62.3)	4 (5.8)	<0.001*[‡]
Neurological dysfunction	29 (22.3)	9 (14.8)	20 (29.0)	0.052[‡]
Headache	10 (7.7)	5 (8.2)	5 (7.2)	>0.999[‡]
Admission mRS score (%)				
Mean (SD)	1.3 (1.04)	1.1 (0.66)	1.5 (1.26)	0.012*[†]
Good (0-2)	120 (92.3)	61 (100.0)	59 (85.5)	0.006*[§]
Poor (3–5)	10 (7.7)	0 (0)	10 (14.5)	
Spetzler-Martin grade (%)				0.537[‖]
I	10 (7.7)	3 (4.9)	7 (10.1)	
II	39 (30.0)	21 (34.4)	18 (26.1)	
III	51 (39.2)	26 (42.6)	25 (36.2)	
IV	25 (19.2)	9 (14.8)	16 (23.2)	
V	5 (3.8)	2 (3.3)	3 (4.3)	
AVM morphology and angioarchitecture (%)				
Maximum diameter (median (IQR)), cm	3.9 (1.73)	4.0 (1.40)	3.7 (2.00)	0.278[‖]
Volume (median (IQR)), cm^3	15.1 (26.27)	19.5 (24.05)	10.9 (28.25)	0.124[‖]
AVM location				
Supratentorial	119 (91.5)	56 (91.8)	63 (91.3)	0.919[‡]
Infratentorial	11 (8.5)	5 (8.2)	6 (8.7)	
Eloquence	75 (57.7)	30 (49.2)	45 (65.2)	0.065[‡]
Anterior circulation involvement	86 (66.2)	41 (67.2)	45 (65.2)	0.810[‡]
Deep perforator supply	19 (14.6)	8 (13.1)	11 (15.9)	0.649[‡]
Deep venous drainage	36 (27.7)	14 (23.0)	22 (31.9)	0.256[‡]
Follow-up (mean (SD)), month	37.4 (11.07)	36.6 (11.51)	38.1 (10.70)	0.458[†]

SD: standard deviation; SRS: stereotactic radiosurgery; mRS: modified Rankin Scale; AVM: arteriovenous malformation; IQR: interquartile range. [†]Student's t-test. [‡]Pearson Chi-square test. [§]Fisher's exact test. [‖]Mann-Whitney U test. *$P < 0.05$, significant difference.

Table 2: Comparison of clinical outcomes between unruptured and ruptured bAVM patients.

Variables	Total ($n = 130$)	Unruptured ($n = 61$)	Ruptured ($n = 69$)	P value
Duration of microsurgery (mean (SD)), h	5.9 (3.80)	5.7 (3.56)	6.1 (4.03)	0.646[†]
Length of stay (mean (SD)), d	21.1 (10.48)	20.9 (10.19)	21.3 (10.80)	0.824[†]
Postoperative stroke (%)	11 (8.5)			
Intracranial hemorrhage	8 (6.2)	2 (3.3)	6 (8.7)	0.359[‡]
Cerebral infarction	5 (3.8)	2 (3.3)	3 (4.3)	>0.999[‡]
Short-term outcomes (%)				
mRS score (mean (SD))	1.5 (1.58)	1.2 (1.41)	1.8 (1.73)	0.019*[†]
Neurological disability	31 (23.8)	10 (16.4)	21 (30.4)	0.061[‡]
Long-term outcomes (%)				
mRS score (mean (SD))	0.8 (1.17)	0.6 (1.10)	0.9 (1.21)	0.113[†]
Neurological disability	9 (6.9)	3 (4.9)	6 (8.7)	0.617[‡]
Mortality	2 (1.5)	1 (1.6)	1 (1.4)	>0.999[§]
Obliteration	130 (100.0)	61 (100.0)	69 (100.0)	>0.999[‡]

SD: standard deviation; bAVM: brain arteriovenous malformation. [†]Student's t-test. [‡]Pearson Chi-square test. [§]Fisher's exact test. *$P < 0.05$, significant difference.

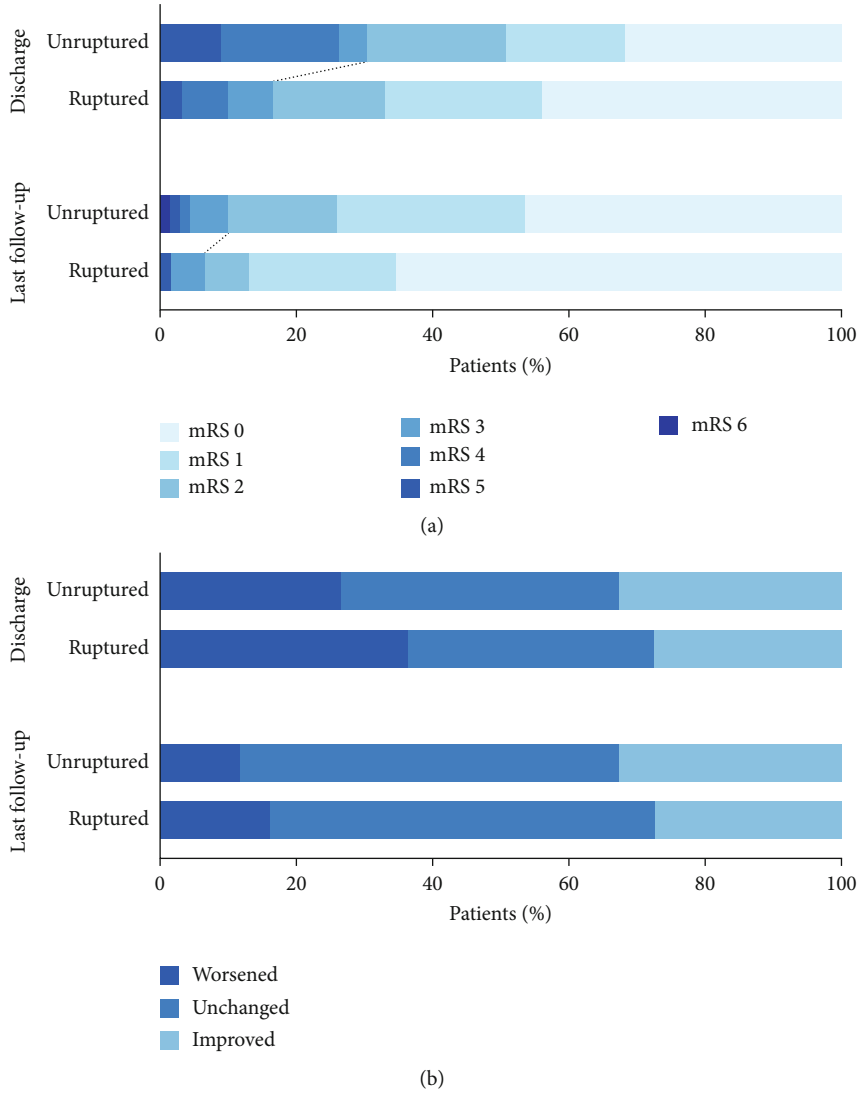

Figure 2: Comparison of neurological outcomes between unruptured and ruptured groups. (a) The proportions of patients with mRS scores ranging from 0 to 6 are shown for patients at discharge and last follow-up. (b) There was no significant difference in the variation of mRS score at discharge and last follow-up between groups, and worsened status occurred in 31.5% of patients at discharge and 13.8% of patients at last follow-up. mRS: modified Rankin Scale.

variables were presented as mean (standard deviation (SD)) and median (interquartile range (IQR)). The Pearson Chi-square test or Fisher's exact test was used to compare categorical variables between groups. Student's t-test or Mann-Whitney U test was performed to compare continuous variables. Univariate and multivariate logistic regression analyses were conducted to identify the predictors for postoperative stroke and long-term neurological disability. Variables that achieved $P < 0.10$ in univariate analyses were included in multivariate analyses. Age and sex were adjusted in the multivariate analyses. Statistical significance was defined as P value < 0.05.

3. Results

Five hundred and forty-four patients were involved in the prospective multicentered cohort study. After excluding 414 patients with incomplete data or cured by monotherapies, a total of 130 bAVM patients (unruptured : ruptured $= 61 : 69$) receiving one-staged hybrid operation were enrolled in the study (Figure 1).

3.1. Baseline Characteristics. Demographic, clinical, and radiographic characteristics of unruptured and ruptured bAVM patients are summarized in Table 1. The mean age on admission was 29.1 years (range, 5-64). Sixteen cases (12.3%) had received prior interventions, including endovascular embolization in 12 (9.2%) and radiosurgery in 4 (3.1%). Hemorrhage (53.1%) manifested as the most common onset symptom, followed by seizure (32.3%), neurological dysfunction (22.3%), and headache (7.7%). Poor neurological status (mRS > 2) accounts for 7.7% of cases ($n = 10$) on admission. Thirty cases (23.1%) were high grade (IV-V). The mean size and volume of bAVM lesions were

3.9 (1.73) cm and 15.1 (26.27) cm^3. Infratentorial locations were involved in 11 cases (8.5%), and eloquent areas were detected in 57.7% of cases ($n = 75$). Supplies of the anterior cerebral circulation and perforating arteries were identified in 86 (66.2%) and 19 cases (14.6%), respectively. 27.7% of cases ($n = 36$) had deep venous drainage. The follow-up duration was 37.4 months on average (range, 8-53). Compared with the unruptured group, patients with ruptured bAVMs tended to present poor neurological status and were less likely to exhibit seizure ($P < 0.05$ for both).

3.2. Clinical Outcomes. Treatment features and clinical outcomes between unruptured and ruptured bAVM patients are presented in Table 2. The annualized hemorrhagic risk for the bAVMs was 4.2% per year. On average, the duration of microsurgical resection in the hybrid operation was 5.9 hours (unruptured vs.ruptured = 5.7 (3.56) h vs.6.1 (4.03) h, $P = 0.646$). Seven (5.4%) bAVM remnants were detected by intraoperative DSA and subsequently resected. All residual lesions were confirmed as complete elimination during the third angiographies. In the postoperative period, thirteen stroke events occurred in 11 patients (8.5%), including eight intracranial hemorrhages and five cerebral infractions. Two cases experienced both types of stroke, which contributed to unfavorable outcomes. The length of stay averaged 21.1 days, with no significant intergroup difference (unruptured vs. ruptured = 20.9 (10.19) days vs.21.3 (10.80) days, $P = 0.824$). The short-term mRS score was 1.5 (1.58) on average. Though the ruptured group possessed a significantly higher mRS score at discharge ($P = 0.019$), the long-term outcomes were similar between groups ($P > 0.05$ for all). Eleven patients were disabled (6.9%) or dead (1.5%), while 119 patients (91.5%) achieved neurological deficit-free (mRS ≤ 2) at last follow-up (Figure 2(a)). In regard to the variation of mRS scores (Figure 2(b)), most patients experienced an unchanged or improved neurological status by the time of discharge (68.5%, $n = 89$) and last follow-up (86.2%, $n = 112$). The long-term mRS score was significantly lower than that on admission and in the short term. ($P < 0.0001$; $P < 0.001$, respectively) (Figure 3). In terms of the obliteration of bAVMs, there were no residual lesions detected in the follow-up angiographies.

3.3. Predictors for Postoperative Stroke and Long-Term Neurological Disability. In the analyses of the predictors related to clinical outcomes, the univariate analysis demonstrated that age at diagnosis, AVM maximum diameter, AVM volume, and duration of microsurgery were associated with the occurrence of postoperative stroke. After adjusting for male sex in the multivariate analysis, AVM volume (OR 1.021, 95% CI 1.006-1.037, and $P = 0.006$) remained an independent risk factor for postoperative stroke (Table 3).

Predictors for long-term neurological disability were analyzed. Univariate analysis showed that onset neurological dysfunction, poor neurological status, and infratentorial location were associated with long-term neurological disability. Poor neurological status (OR 6.461, 95% CI 1.309-31.889, and $P = 0.022$) and infratentorial location (OR 5.618, 95% CI 1.158-27.246, and $P = 0.032$) were confirmed as significant risk factors for long-term neurological disability in the age and sex adjusted multivariate logistic regression analysis (Table 4).

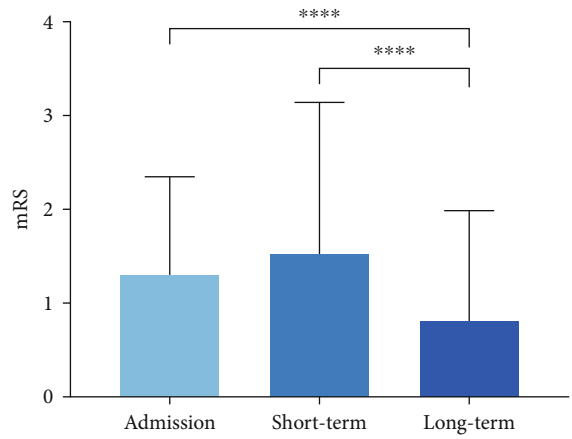

Figure 3: Comparison of the neurological status in different timepoints of bAVM patients. The mRS score of patients in the long-term follow-up was significantly lower than that on admission and in the short-term follow-up (****$P < 0.0001$; ***$P < 0.001$, respectively). mRS: modified Rankin Scale.

4. Discussion

One-staged hybrid operation incorporates the advantages of endovascular embolization and microsurgical resection, but the long-term prognosis has not been described. In this study, we identified the long-term safety and efficacy of bAVM patients who underwent the hybrid operation. The multimodality management can be performed as a safe and effective strategy for treating bAVMs, by achieving a low morbidity rate of 6.9% and a mortality rate of 1.5%, with complete obliteration in the follow-up. Postoperative stroke was observed in 8.5% of patients during hospitalization. Furthermore, we found that increased AVM volume was associated with a higher risk of postoperative stroke; poor neurological status and infratentorial location were correlated with a higher risk of long-term disability. The safety and efficacy of the management for the complex bAVMs has been confirmed by previous studies [5–8]. Recently, our team has also demonstrated that the suite was an efficient treatment for SM grade III-V bAVMs [17]. The preoperative embolization was capable of minimizing the surgical difficulties, and the hybrid operation had obvious shorter resection compared with the monotherapy of microsurgery. The advantages are vital for neurosurgeons with insufficient surgical experience in the operations of high-grade bAVMs or under emergency circumstances.

In the current study, the majority of patients reached long-term neurological deficit-free. The low rate of morbidity was proposed to be associated with the therapeutic preoperative embolization [10, 18]. The modalities of endovascular embolization and microsurgical resection have been used as single or combined approaches for curing bAVMs. Typically, microsurgical resection is favored as the approach to achieve a superior rate of complete obliteration

Table 3: Logistic regression analysis for postoperative stroke.

Variables	Univariate analysis			Multivariate analysis†		
	OR	95% CI	*P* value	OR	95% CI	*P* value
Age	1.047	0.999-1.097	0.055	1.049	0.994-1.107	0.081
Male sex	2.878	0.798-10.383	0.106	0.236	0.055-1.010	0.052
Onset symptom						
Hemorrhage	1.609	0.447-5.787	0.467			
Seizure	0.439	0.091-2.128	0.307			
Neurological dysfunction	2.149	0.582-7.925	0.251			
Poor neurological status	3.083	0.568-16.741	0.192			
AVM location						
Supratentorial	Ref	Ref	Ref			
Infratentorial	1.090	0.126-9.407	0.938			
AVM maximum diameter	1.723	1.106-2.685	0.016	1.452	0.899-2.346	0.884
AVM volume	1.021	1.006-1.037	0.006	1.021	1.006-1.037	0.006*
Eloquence	2.070	0.523-8.189	0.300			
Deep venous drainage	2.366	0.674-8.302	0.179			
Duration of microsurgery	1.119	1.003-1.247	0.043	1.084	0.945-1.243	0.356

OR: odds ratio; CI: confidence interval; AVM: arteriovenous malformation. †The multivariate model was adjusted for male sex. *$P < 0.05$, significant difference.

with an acceptable incidence of morbidity and complications [4]. Endovascular embolization reaches a low rate of unfavorable outcomes as curative or adjuvant therapies [19]. The strategy facilitates the surgical resection by occluding the feeding arteries and degrading the bAVMs or embolizing the deep perforators that are inaccessible for microsurgeries [20–22]. Grüter et al. confirmed the safety of the combined treatment in a retrospective study of 18 bAVM patients, with a complication rate of 11% [5]. Kocer et al. performed single-stage combined treatments on 31 bAVMs with SM grades III-V [23], in which the long-term disability and mortality rate was 6.4%. It is suggested that high-grade bAVMs can be eliminated by reducing the rate of morbidity and mortality by the hybrid operation.

Although the accumulation of treatment-related risks of the combined operation has been concerned, the complications of one-staged multimodality management were comparable with single approaches. In the present study, the postoperative complications occurred in 8.5% of patients, which conformed to the previous studies with a rate of 7.2%-12.5% [8, 24]. A recent meta-analysis of treatment for bAVMs demonstrated that complications were observed in 7.4% after microsurgery and in 6.6% after embolization [20]. Brown et al. conducted the hybrid treatment in 19 bAVM cases, in which neurological outcomes were similar with staged managements without hemorrhagic events after microsurgery or embolization [6]. In our study, the clinical outcomes were similar between one-staged hybrid operation and multistaged operations ($P = 0.269$ for both). However, the stage of preoperative embolization varied across different institutions. The multistaged strategy was adopted to minimize the risk of normal perfusion pressure breakthrough (NPPB) by progressively reducing the blood flow and normalize the hemodynamics of large or high-flow bAVMs [25–27]. Nevertheless, the stepwise modality carried potential risks of hemorrhage in-between the interventions, which ranged from 5.9% to 20% [28–30]. The unfavorable outcomes may correlate with the recanalization of the nidus and the recruitment of new collateral circulation from adjacent feeding arteries after embolization [19]. Conversely, the management of one-staged hybrid operation diminished the additional treatment risks by prompt resection followed preoperative embolization [5].

The primary goal of bAVM treatment is to completely obliterate the lesions, thereby eliminating the bleeding risk and reducing morbidity or mortality. In the study by Blauwblomme et al., the recurrence occurred in 4.35% of patients following the combined embolization and surgery [31]. Other series reported the occlusion rates that vary from 95.5% to 100% after hybrid treatment [23, 32]. Similarly, the one-staged hybrid management resulted in the total eradication of lesions in our study. By routine intraoperative DSA checking, remnant lesions can be detected and resected subsequently before closure. Importantly, the complete obliteration of high-grade bAVMs highlighted the advantage of hybrid operation. Nevertheless, there may remain false-negative examination findings owing to the arterial spasm or temporary thrombosis. Thus, the delayed angiographies at 1-3 years after treatment are necessary [33].

Radiographic characteristics of bAVMs result in subtypes with different operative risks. In the present study, the AVM volume was significantly associated with postoperative complications of stroke. Previous report has revealed that the AVM size was a predictor for complications following microsurgery [24]. The larger size indicated more difficulties during surgery and higher treatment risks after the procedure. Reduction in blood flow and volume of bAVMs facilitates surgical resection. Therefore, preoperative occlusion of the volume is significantly required. The poor neurological status and infratentorial location were identified as

Table 4: Logistic regression analysis for long-term neurological disability.

Variables	Univariate analysis			Multivariate analysis†		
	OR	95% CI	*P* value	OR	95% CI	*P* value
Age	1.001	0.955-1.049	0.972	1.004	0.956-1.053	0.883
Male sex	1.277	0.369-4.422	0.700	0.890	0.234-3.379	0.864
Onset symptom						
Hemorrhage	1.609	0.447-5.787	0.467			
Seizure	0.769	0.193-3.061	0.710			
Neurological dysfunction	3.299	0.928-11.728	0.065	1.928	0.447-8.316	0.375
Poor neurological status	6.000	1.298-27.735	0.022	6.461	1.309-31.889	0.022*
AVM location						
Supratentorial	Ref	Ref	Ref	Ref	Ref	Ref
Infratentorial	5.203	1.151-23.517	0.032	5.618	1.158-27.246	0.032*
Maximum diameter	1.270	0.814-1.980	0.292			
AVM volume	1.012	0.998-1.027	0.103			
Eloquence	2.070	0.523-8.189	0.300			
Deep venous drainage	0.977	0.244-3.909	0.974			
Duration of microsurgery	1.018	0.878-1.181	0.814			

OR: odds ratio; CI: confidence interval; AVM: arteriovenous malformation. †The multivariate model was adjusted for age and male sex. *$P < 0.05$, significant difference.

risk factors for long-term disability. van Swieten et al. proposed that the preoperative status determined the neurological outcomes [34]. Infratentorial bAVMs were proved to carry a higher risk of worse outcomes [12, 35]. In addition, the correlation between prior hemorrhage and neurological outcomes remained controversial. Ellis et al. reported that the hemorrhagic presentation was associated with morbidity and mortality [35]. However, other studies suggested that nonhemorrhage was correlated with neurological complications [24, 36]. In our series, although more poor neurological conditions were identified in ruptured bAVMs on admission, these patients achieved equivalent long-term outcomes after hybrid operations.

There are several limitations in our study. First, it is a nonrandomized prospective study with a relatively small sample size. Second, variables including concomitant aneurysms and diffusiveness of AVM nidus were not enrolled in the study, which might result in potential bias of baseline characteristics. Third, parts of patients were followed up with magnetic resonance angiography (MRA), which might lead to false-negative detection of residual lesions. Fourth, a longer-term angiographic follow-up was needed to detect the recurrent and residual bAVMs.

5. Conclusions

One-staged hybrid operation of combined embolization and microsurgery can be performed as a safe and effective strategy for treating bAVMs. Long-term prognosis of complete obliteration with low rates of morbidity and mortality can be achieved by multimodality management. Unruptured and ruptured bAVMs acquired similar favorable outcomes after treatments. Increased AVM volume was associated with a higher risk of postoperative stroke. Poor neurological status and infratentorial location were independent predictors for long-term disability.

Data Availability

The data used to support the findings of this study are available from the corresponding author upon request.

Conflicts of Interest

The authors declare that they have no conflicts of interest.

Authors' Contributions

Yuanfeng Jiang and Chaofan Zeng contributed equally to this work.

Acknowledgments

This study was supported by the Science Foundation for Post Doctorate Research of the Beijing (No. 2017-ZZ-123).

References

[1] R. M. Friedlander, "Arteriovenous malformations of the brain," *The New England Journal of Medicine*, vol. 356, no. 26, pp. 2704–2712, 2007.

[2] S. I. Nikolaev, S. Vetiska, X. Bonilla et al., "Somatic activating KRAS mutations in arteriovenous malformations of the brain," *The New England Journal of Medicine*, vol. 378, no. 3, pp. 250–261, 2018.

[3] H. Kim, R. Al-Shahi Salman, C. E. McCulloch, C. Stapf, and W. L. Young, "Untreated brain arteriovenous malformation: patient-level meta-analysis of hemorrhage predictors," *Neurology*, vol. 83, no. 7, pp. 590–597, 2014.

[4] M. T. Lawton, W. C. Rutledge, H. Kim et al., "Brain arteriovenous malformations," *Nature Reviews. Disease Primers*, vol. 1, no. 1, article 15008, 2015.

[5] B. E. Gruter, I. Mendelowitsch, M. Diepers, L. Remonda, J. Fandino, and S. Marbacher, "Combined endovascular and microsurgical treatment of arteriovenous malformations in the hybrid operating room," *World Neurosurgery*, vol. 117, pp. e204–e214, 2018.

[6] D. Brown, C. Graham, A. Smith et al., "Same day embolisation followed by microsurgical resection of brain arteriovenous malformations: a single centre early experience," *British Journal of Neurosurgery*, vol. 35, pp. 80–83, 2021.

[7] Y. Murayama, H. Arakawa, T. Ishibashi et al., "Combined surgical and endovascular treatment of complex cerebrovascular diseases in the hybrid operating room," *Journal of Neurointerventional Surgery*, vol. 5, no. 5, pp. 489–493, 2013.

[8] M. Santin, J. Todeschi, R. Pop et al., "A combined single-stage procedure to treat brain AVM," *Neuro-Chirurgie*, vol. 66, no. 5, pp. 349–358, 2020.

[9] R. F. Spetzler, N. A. Martin, L. P. Carter, R. A. Flom, P. A. Raudzens, and E. Wilkinson, "Surgical management of large AVM's by staged embolization and operative excision," *Journal of Neurosurgery*, vol. 67, no. 1, pp. 17–28, 1987.

[10] G. Rodríguez-Boto, R. Gutiérrez-González, A. Gil, C. Serna, and L. López-Ibor, "Combined staged therapy of complex arteriovenous malformations: initial experience," *Acta Neurologica Scandinavica*, vol. 127, no. 4, pp. 260–267, 2013.

[11] B. C. Flores, D. R. Klinger, K. L. Rickert et al., "Management of intracranial aneurysms associated with arteriovenous malformations," *Neurosurgical Focus*, vol. 37, no. 3, p. E11, 2014.

[12] C. P. Derdeyn, G. J. Zipfel, F. C. Albuquerque et al., "Management of brain arteriovenous malformations: a scientific statement for healthcare professionals from the American Heart Association/American Stroke Association," *Stroke*, vol. 48, no. 8, pp. e200–e224, 2017.

[13] T. Iwama, K. Yoshimura, E. Keller et al., "Emergency craniotomy for intraparenchymal massive hematoma after embolization of supratentorial arteriovenous malformations," *Neurosurgery*, vol. 53, no. 6, pp. 1251–1260, 2003, discussion 8-60.

[14] Y. Murayama, K. Irie, T. Saguchi et al., "Robotic digital subtraction angiography systems within the hybrid operating room," *Neurosurgery*, vol. 68, no. 5, pp. 1427–1433, 2011, discussion 33.

[15] C. S. Ogilvy, P. E. Stieg, I. Awad et al., "Recommendations for the management of intracranial arteriovenous malformations: a statement for healthcare professionals from a special writing group of the Stroke Council, American Stroke Association," *Circulation*, vol. 103, no. 21, pp. 2644–2657, 2001.

[16] M. Wang, Y. Jiao, Y. Cao, S. Wang, and J. Zhao, "Surgical management of complex brain arteriovenous malformations with hybrid operating technique: study protocol of a prospective registry and a pragmatic clinical trial," *BMC Neurology*, vol. 19, no. 1, p. 75, 2019.

[17] Y. Chen, R. Li, L. Ma et al., "Single-stage combined embolization and resection for Spetzler-Martin grade III/IV/V arteriovenous malformations: a single-center experience and literature review," *Frontiers in Neurology*, vol. 11, article 570198, 2020.

[18] D. H. Sahlein, P. Mora, T. Becske, and P. K. Nelson, "Nidal embolization of brain arteriovenous malformations: rates of cure, partial embolization, and clinical outcome," *Journal of Neurosurgery*, vol. 117, no. 1, pp. 65–77, 2012.

[19] M. G. Zaki Ghali, P. Kan, and G. W. Britz, "Curative embolization of arteriovenous malformations," *World Neurosurgery*, vol. 129, pp. 467–486, 2019.

[20] J. van Beijnum, H. B. van der Worp, D. R. Buis et al., "Treatment of brain arteriovenous malformations: a systematic review and meta-analysis," *Journal of the American Medical Association*, vol. 306, no. 18, pp. 2011–2019, 2011.

[21] A. Wang, G. K. Mandigo, N. A. Feldstein et al., "Curative treatment for low-grade arteriovenous malformations," *Journal of NeuroInterventional Surgery*, vol. 12, no. 1, 2019.

[22] S. Natarajan, B. Ghodke, G. Britz, D. Born, and L. Sekhar, "Multimodality treatment of brain arteriovenous malformations with microsurgery after embolization with onyx: single-center experience and technical nuances," *Neurosurgery*, vol. 62, no. 6, pp. 1213–1226, 2008.

[23] N. Kocer, S. G. Kandemirli, R. Dashti et al., "Single-stage planning for total cure of grade III-V brain arteriovenous malformations by embolization alone or in combination with microsurgical resection," *Neuroradiology*, vol. 61, no. 2, pp. 195–205, 2019.

[24] T. Theofanis, N. Chalouhi, R. Dalyai et al., "Microsurgery for cerebral arteriovenous malformations: postoperative outcomes and predictors of complications in 264 cases," *Neurosurgical Focus*, vol. 37, no. 3, p. E10, 2014.

[25] W. L. Young, A. Kader, E. Ornstein et al., "Cerebral hyperemia after arteriovenous malformation resection is related to "breakthrough" complications but not to feeding artery pressure," *The Columbia University Arteriovenous Malformation Study Project. Neurosurgery*, vol. 38, no. 6, 1996.

[26] V. Katsaridis, C. Papagiannaki, and E. Aimar, "Curative embolization of cerebral arteriovenous malformations (AVMs) with Onyx in 101 patients," *Neuroradiology*, vol. 50, no. 7, pp. 589–597, 2008.

[27] M. B. Potts, D. W. Zumofen, E. Raz, P. K. Nelson, and H. A. Riina, "Curing arteriovenous malformations using embolization," *Neurosurgical focus.*, vol. 37, no. 3, p. E19, 2014.

[28] X. Lv, Z. Wu, Y. Li, X. Yang, and C. Jiang, "Hemorrhage risk after partial endovascular NBCA and ONYX embolization for brain arteriovenous malformation," *Neurological Research*, vol. 34, no. 6, pp. 552–556, 2012.

[29] A. Hartmann, H. Mast, J. P. Mohr et al., "Determinants of staged endovascular and surgical treatment outcome of brain arteriovenous malformations," *Stroke*, vol. 36, no. 11, pp. 2431–2435, 2005.

[30] J. J. Jafar, A. J. Davis, A. Berenstein, I. S. Choi, and M. J. Kupersmith, "The effect of embolization with N-butyl cyanoacrylate prior to surgical resection of cerebral arteriovenous malformations," *Journal of Neurosurgery*, vol. 78, no. 1, pp. 60–69, 1993.

[31] T. Blauwblomme, M. Bourgeois, P. Meyer et al., "Long-term outcome of 106 consecutive pediatric ruptured brain arteriovenous malformations after combined treatment," *Stroke*, vol. 45, no. 6, pp. 1664–1671, 2014.

[32] M. Kotowski, A. Sarrafzadeh, B. Schatlo et al., "Intraoperative angiography reloaded: a new hybrid operating theater for combined endovascular and surgical treatment of cerebral arteriovenous malformations: a pilot study on 25 patients," *Acta Neurochirurgica*, vol. 155, no. 11, pp. 2071–2078, 2013.

[33] A. A. Ivanov, A. Alaraj, F. T. Charbel, V. Aletich, and S. Amin-Hanjani, "Recurrence of cerebral arteriovenous malformations

following resection in adults: does preoperative embolization increase the risk?," *Neurosurgery*, vol. 78, no. 4, pp. 562–571, 2016.

[34] J. C. van Swieten, P. J. Koudstaal, M. C. Visser, H. J. Schouten, and J. van Gijn, "Interobserver agreement for the assessment of handicap in stroke patients," *Stroke*, vol. 19, no. 5, pp. 604–607, 1988.

[35] M. J. Ellis, D. Armstrong, S. Vachhrajani et al., "Angioarchitectural features associated with hemorrhagic presentation in pediatric cerebral arteriovenous malformations," *Journal of NeuroInterventional Surgery*, vol. 5, no. 3, pp. 191–195, 2013.

[36] M. T. Lawton, H. Kim, C. E. McCulloch, B. Mikhak, and W. L. Young, "A supplementary grading scale for selecting patients with brain arteriovenous malformations for surgery," *Neurosurgery*, vol. 66, no. 4, pp. 702–713, 2010.

Hindawi
Disease Markers
Volume 2022, Article ID 3229888, 14 pages
https://doi.org/10.1155/2022/3229888

Research Article

Shufeiya Recipe Improves Monocrotaline-Induced Pulmonary Hypertension in Rats by Regulating SIRT3/FOXO3a and Its Downstream Signaling Pathways

Zhuangzhuang Jia,[1,2] **Haifeng Yan**,[3] **Shuai Wang**,[1] **Lin Wang**,[1,2] **Yawen Cao**,[1,2] **Shanshan Lin**,[1,2] **Zeyu Zhang**,[1,2] **Ci Wang**,[1,2] **Xianliang Wang**,[1] **and Jingyuan Mao**[1]

[1]*Department of Cardiovascular Diseases, First Teaching Hospital of Tianjin University of Traditional Chinese Medicine, National Clinical Research Center for Chinese Medicine Acupuncture and Moxibustion, Tianjin 300381, China*
[2]*Tianjin University of Traditional Chinese Medicine, Tianjin 301617, China*
[3]*Department of Cardiovascular Diseases, The First Affiliated Hospital of Henan University of Traditional Chinese Medicine, Zhengzhou, Henan 450000, China*

Correspondence should be addressed to Xianliang Wang; xlwang1981@126.com and Jingyuan Mao; jymao@126.com

Received 13 December 2021; Revised 21 January 2022; Accepted 25 January 2022; Published 18 February 2022

Academic Editor: XIANWEI ZENG

Pulmonary hypertension (PH) is a chronic and progressive disease caused by obstructions and functional changes of small pulmonary arteries. Current treatment options of PH are costly with patients needing long-term taking medicine. The traditional Chinese medicine (TCM) compound "Shufeiya Recipe" was used to intervene in monocrotaline- (MCT-) induced pulmonary hypertension in rats. The rats were randomly divided into the control group, model group, positive drug (Sildenafil) group, and Shufeiya Recipe low-, moderate-, and high-dose groups. The improvement effect of the Shufeiya Recipe on the mean pulmonary artery pressure (mPAP) was assessed in PH rats, and pathological staining was used to observe the pathological changes of lung tissue. The impact of the Shufeiya Recipe on oxidative stress damage in rats with pulmonary hypertension and the regulation of SIRT3/FOXO3a and its downstream signaling pathways were determined. The results showed that Shufeiya Recipe could significantly downregulate mPAP and improve lung histopathological changes; downregulate serum levels of reactive oxygen species (ROS); upregulate the concentrations of COX-1 and COX-2 and the activity of Mn-SOD; inhibit oxidative response damage; promote the protein expression of SIRT3, FOXO3a, p-PI3K, p-AKT, and p-eNOS; increase the level of expression of NO, sGC, cGMP, and PKG; and downregulate the level of protein expression of Ras, p-MEK1/2, p-ERK1/2 and c-fos. These results indicate that Shufeiya Recipe can improve MCT-induced pulmonary hypertension in rats by regulating SIRT3/FOXO3a and its downstream PI3K/AKT/eNOS and Ras/ERK signaling pathways.

1. Introduction

Pulmonary hypertension (PH) is a chronic and progressive disease caused by obstruction of small pulmonary arteries. It is characterized by pulmonary vascular remodeling, increased pulmonary circulation resistance, and elevated pulmonary artery pressure (with an average pulmonary artery pressure at rest of ≥25 mmHg), ultimately leading to right heart failure and even death [1]. As many as 1% of patients are affected by pulmonary hypertension globally, with a prevalence of around 10% for people over 65 years old [2]. It is estimated that the 1-year mortality rate of patients with pulmonary hypertension is about 15%, while the 3-years mortality rate is approximately 30% [3]. Currently, most therapeutic drugs work by relaxing the blood vessels and inhibiting the proliferation of pulmonary artery smooth muscle cells [4]. These drugs are quite expensive, and PH patients often require intensive clinical care [5]. Therefore, it is of great significance to seek more effective prevention and control measures.

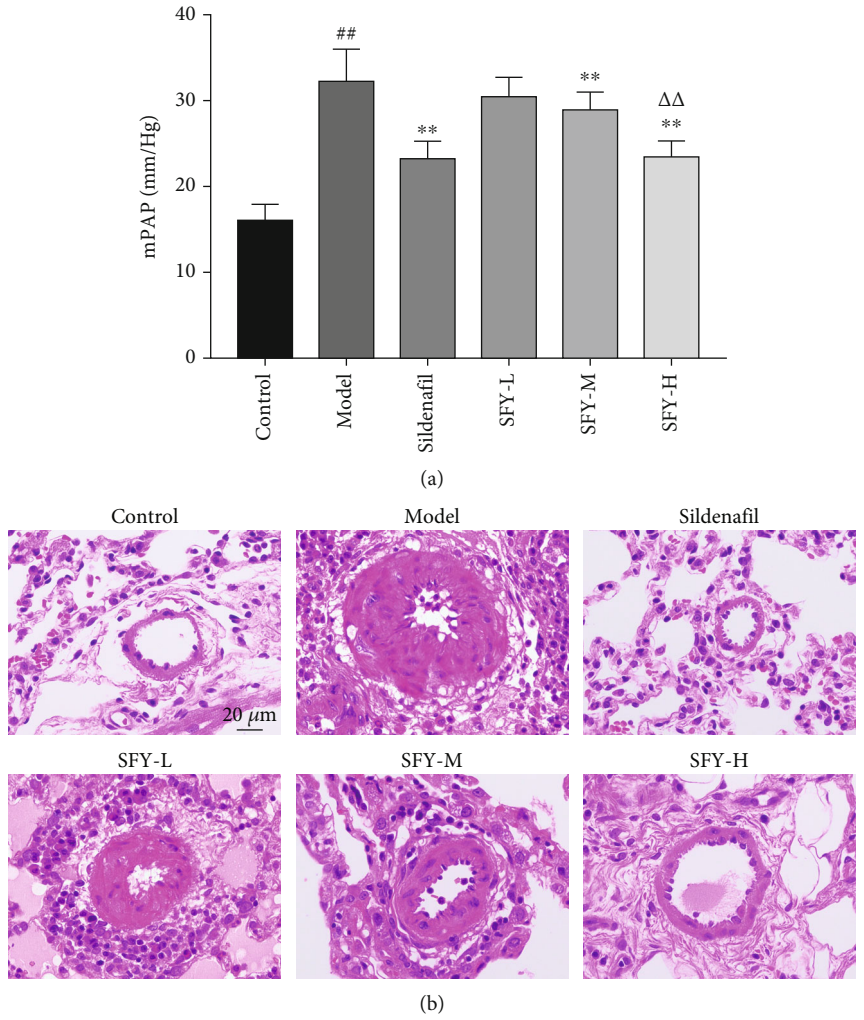

Figure 1: Shufeiya Recipe significantly relieved mPAP and pathological changes of lung tissue of PH rats. (a) Moderate and high doses of Shufeiya Recipe significantly decreased mPAP of PH rats. (b) Shufeiya Recipe relieved pathological changes of lung tissue of PH rats. $n = 10$; $^{\#\#}P < 0.01$ vs. the control group, $^{**}P < 0.01$ vs. the model group, and $^{\Delta\Delta}P < 0.01$ vs. the moderate-dose group of Shufeiya Recipe.

The occurrence and development of pulmonary hypertension involve many factors, such as hypoxia, inflammation, oxidative stress, and endothelial dysfunction, to name a few [6, 7]. Among them, oxidative stress is an important precursor to PH development [8]. An imbalance between the generation and removal of oxygen free radicals in the body and the excessive accumulation of ROS could promote the proliferation, vasoconstriction, and reconstruction of smooth muscle cells [9]. Mitochondria are the primary site of ROS generation. When mitochondrial dysfunction occurs, this can lead to oxidative stress damage [10, 11]. Under normal circumstances, cells can inhibit the overproduction of ROS and maintain its normal function by increasing the activity of antioxidant enzymes, such as catalase (CAT), manganese superoxide dismutase (Mn-SOD), and glutathione peroxidase (GSH-Px). [12]. Previous studies have shown that silent information regulator3 (SIRT3) could increase the expression level of forkhead box O3 (FOXO3a) and enhance the activity of MnSOD [13, 14]. The increase in the activity of Mn-SOD and CAT could reduce ROS generation, inhibiting the expression of Ras protein and promoting the activation of the PI3K/AKT signaling pathway. On the other hand, excessive ROS could activate the Ras protein, promoting the expression of downstream substrates MEK1/2 and ERK1 protein, which in turn mediate the increase in c-fos promoter activity, inducing cell proliferation and differentiation, and facilitating pulmonary hypertension [15, 16]. However, the activated upstream PI3K could trigger AKT, activating the phosphorylation sites of eNOS Ser1177 and Thr495 to promote NO synthesis [17–19]. Subsequently, the soluble guanylate cyclase (sGC) in the vascular smooth muscle cells could be activated, converting guanosine triphosphate (GTP) into cyclic guanosine monophosphate (cGMP), thereby activating cGMP-dependent protein kinases G (PKG), leading to vasodilation and limiting pulmonary hypertension [20–22].

Traditional Chinese medicine has the advantages of being a multi-component, multi-target, and multi-mechanistic treatment modality, which is gradually gaining recognition in the clinical treatment of PH. The traditional Chinese medicine compound "Shufeiya Recipe" comprises four Chinese herbs: *Radix Salviae*, *Carthami Flos*, *Cornus Officinalis Sieb.*

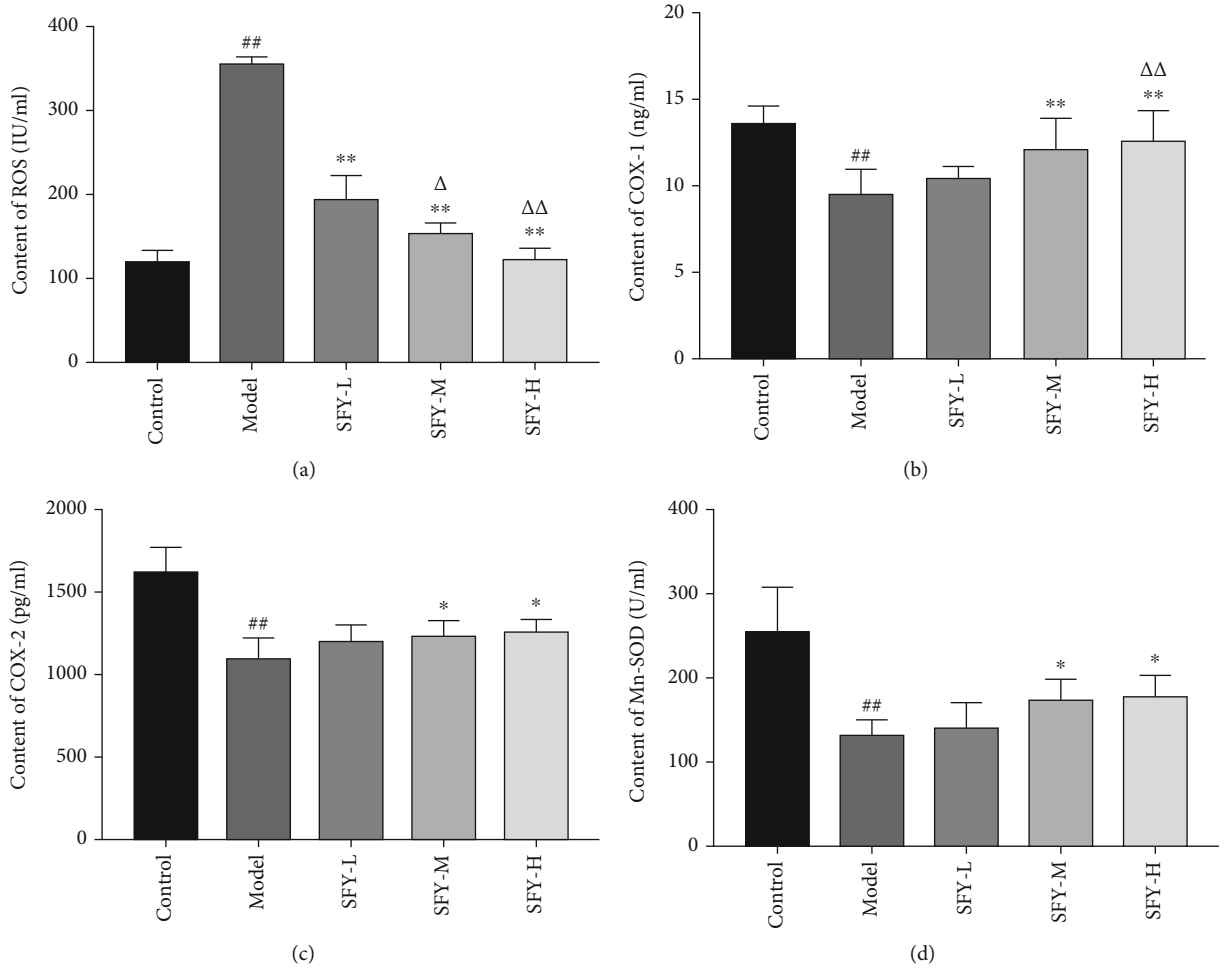

Figure 2: Shufeiya Recipe significantly inhibited the oxidative stress level of PH rats. (a) Shufeiya Recipe significantly downregulated the level of ROS accumulation of PH rats, $n = 3$. (b–d) Shufeiya Recipe increased COX-1, COX-2, and Mn-SOD contents of PH rats, $n = 6$. $^{\#\#}P < 0.01$ vs. the control group; $^{**}P < 0.01$ vs. the model group; and $^{\Delta}P < 0.05$, $^{\Delta\Delta}P < 0.01$ vs. the low-dose group of Shufeiya Recipe.

Et Zucc., and *Platycodon Grandiforus*. *Radix Salviae* and *Carthami Flos* were shown to promote blood circulation while inhibiting blood stasis, inflammation and oxidation [23, 24]. *Cornus Officinalis Sieb. Et Zucc.* was shown to protect the heart and the brain and act as an antioxidant as well as an immune regulator, etc. [25], while *Platycodon Grandiforus* could regulate pulmonary inflammation, inhibit cell apoptosis, and protect the heart [26–28]. In this study, Shufeiya Recipe was used as an intervention in MCT-induced pulmonary hypertension in rats to observe its effect in improving PH and regulating SIRT3/FOXO3a and its downstream PI3K/AKT/eNOS and Ras/ERK signaling pathways.

2. Materials and Methods

2.1. Animal. Specific pathogen-free (SPF) adult male Sprague-Dawley (SD) rats weighing 230~250 g were purchased from SiPeiFu Laboratory Animal Technology (Beijing, China) with laboratory animal license number: SCXK (Beijing) 2019-0010. All rats were housed in an air-conditioned room at 22 ± 2°C with a 12/12 hour light/dark cycle, in which the rats had free access to food and water.

2.2. Experimental Drugs. Shufeiya Recipe is composed of 20 g *Platycodon Grandiforus*, 15 g *Radix Salviae*, 15 g *Carthami Flos*, and 15 g *Cornus Officinalis Sieb. Et Zucc.* According to the human to rat dose conversion method, the dosage was adjusted to a low dose (crude drug concentration of 0.2925 g/ml), moderate dose (crude drug concentration of 0.5850 g/ml), and high dose (crude drug concentration of 1.1700 g/ml). The positive control drug used was sildenafil (Yuanye Bio-Technology Co., Ltd., China), the specification is 1 g, the batch number is X23A8Y42189, and a concentration of 2.5 mg/ml was prepared by dissolving in distilled water.

2.3. Modeling and Grouping Methods. 60 SD rats were randomly divided into 6 groups: control group, model group, sildenafil group, and Shufeiya Recipe low- (SFY-L), moderate- (SFY-M), and high-dose (SFY-H) groups, with 10 rats in each group. A single intraperitoneal injection of MCT (60 mg/kg) was used to establish the PH rat model. The rats in the control group and the model group were given 1 ml/100 g distilled water by gavage, the sildenafil group was given sildenafil solution 25 mg/kg by gavage, and the low-, moderate-, and high-

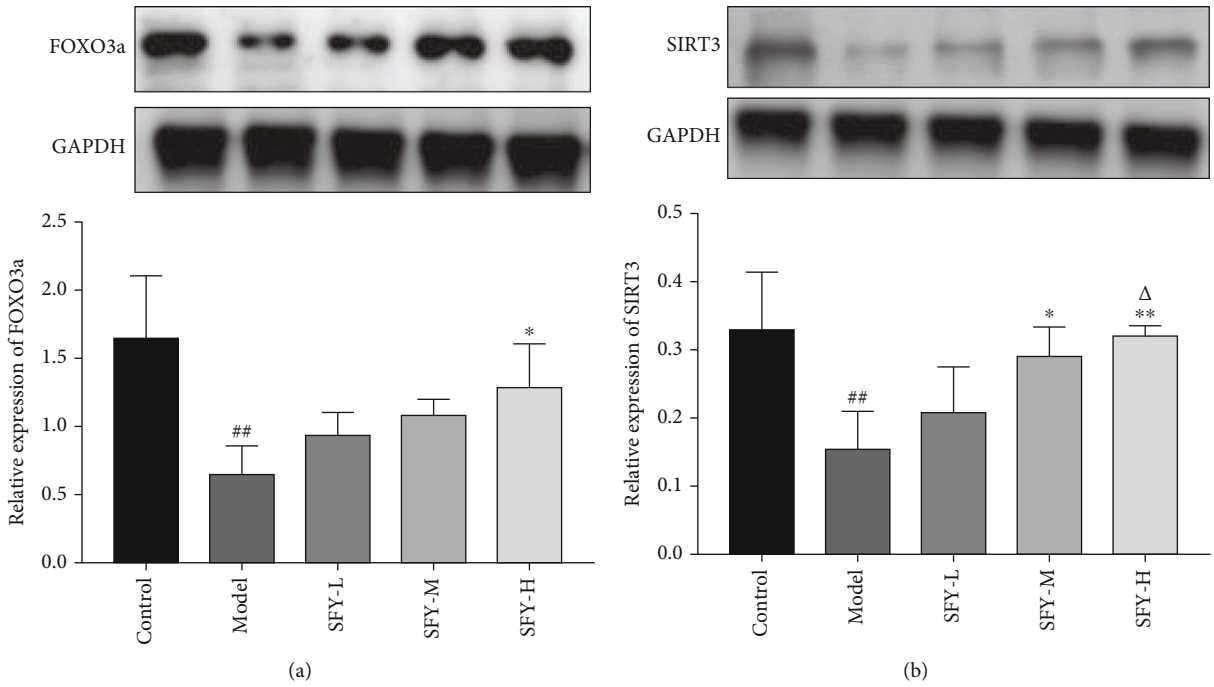

Figure 3: Shufeiya Recipe activated the SIRT3/FOXO3a signaling pathway of PH rats. (a) The high-dose group of Shufeiya Recipe stimulated the expression of FOXO3a. (b) The moderate- and high-dose groups of Shufeiya Recipe upregulated the expression level of SIRT3, and the most marked improvement was obtained by the high-dose treatment of Shufeiya Recipe. $n = 3$; $^{\#\#}P < 0.01$ vs. the control group; $^{*}P < 0.05$, $^{**}P < 0.01$ vs. the model group; and $^{\triangle}P < 0.05$ vs. the low-dose group of Shufeiya Recipe.

dose groups of Shufeiya Recipe were given a concentration of 0.2925 g/ml, 0.5850 g/ml, an d1.1700 g/ml of Shufeiya Recipe solution 1 ml/100 g by gavage, respectively, and each intervention was given by intragastric administration once daily for 14 consecutive days.

2.4. Determination of mPAP in Rats with Pulmonary Hypertension. After 14 days of the administration, the rats were anesthetized with 1.5% tribromoethanol (0.8 ml/100 g). Stripping the external jugular vein and ligating the distal end, then a 2 ~ 3 mm V-shaped opening was made at the proximal end of the external jugular vein. Next, a catheter was inserted into the V-shaped opening and was gently advanced. The changes of mPAP in rats were determined according to the waveform shown by the Hemodynamic Recording System.

2.5. Morphological Changes of Lung Tissues. The animals were anesthetized by intraperitoneal injection of tribromoethanol solution and the middle and upper lobes of the left lung of the rats were taken, rinsed with physiological saline, and fixed in 4% paraformaldehyde for 72 h. The specimens were made into paraffin-embedded sections with a thickness of 5 μm along the hilum, and the slices were stained with conventional HE and mounted with neutral gum. The pathomorphological changes of the lung tissues of the rats in each group were observed under a microscope.

2.6. Detection of Oxidative Stress Levels. Enzyme-linked immunosorbent assay (ELISA) was used to detect ROS (JL21051, Jianglaibio Co. Ltd., China), cyclooxygenase-1 (COX-1) (RA21050, Bioswamp Co. Ltd., China), and cyclooxygenase-2 (COX-2) (RA20086, Bioswamp Co. Ltd., China) in the serum of rats with pulmonary hypertension. The hydroxylamine method was used to detect manganese superoxide dismutase (Mn-SOD) (A001-2, Jiancheng Bioengineering Institute, China). The specific steps were carried out in accordance with the manufacturer's requirements.

2.7. Detection of the Expression Levels of NO, sGC, and cGMP. The middle and upper lobe tissues of the left lung of rats were taken for homogenization. The microwell plate method was used to evaluate the nitric oxide (NO) content (JL13431, Jianglaibio Co. Ltd., China), and the ELISA was used to detect the soluble guanylyl cyclase (sGC) (JL46177, Jianglaibio Co. Ltd., China) content and cyclic guanosine monophosphate (cGMP) (JL11179, Jiangglaibio Co. Ltd., China) content. The specific steps were carried out in accordance with the manufacturer's requirements.

2.8. Western Blotting. The total protein of rat lung tissues in each group was extracted, and the protein concentration was measured using the bicinchoninic acid (BCA) method. The extracted proteins were then separated by sodium dodecyl sulfate-polyacrylamide gel electrophoresis (SDS-PAGE), and the proteins were then transferred onto the polyvinylidene fluoride (PVDF) membrane. After blocking with 5% skimmed milk powder for 2 h, primary antibodies SIRT3 (ab246522, 1 : 1000), FOXO3a (ab109629, 1 : 1000), p-PI3K (AF3242, 1 : 1000), AKT (CSB-PA008118, 1 : 1000), p-eNOS (CSB-PA000659, 1 : 1000), PKG (DF7018, 1 : 1000), Ras (ab52939, 1: 2000), p-MEK1/2 (AF8035, 1 : 1000), p-

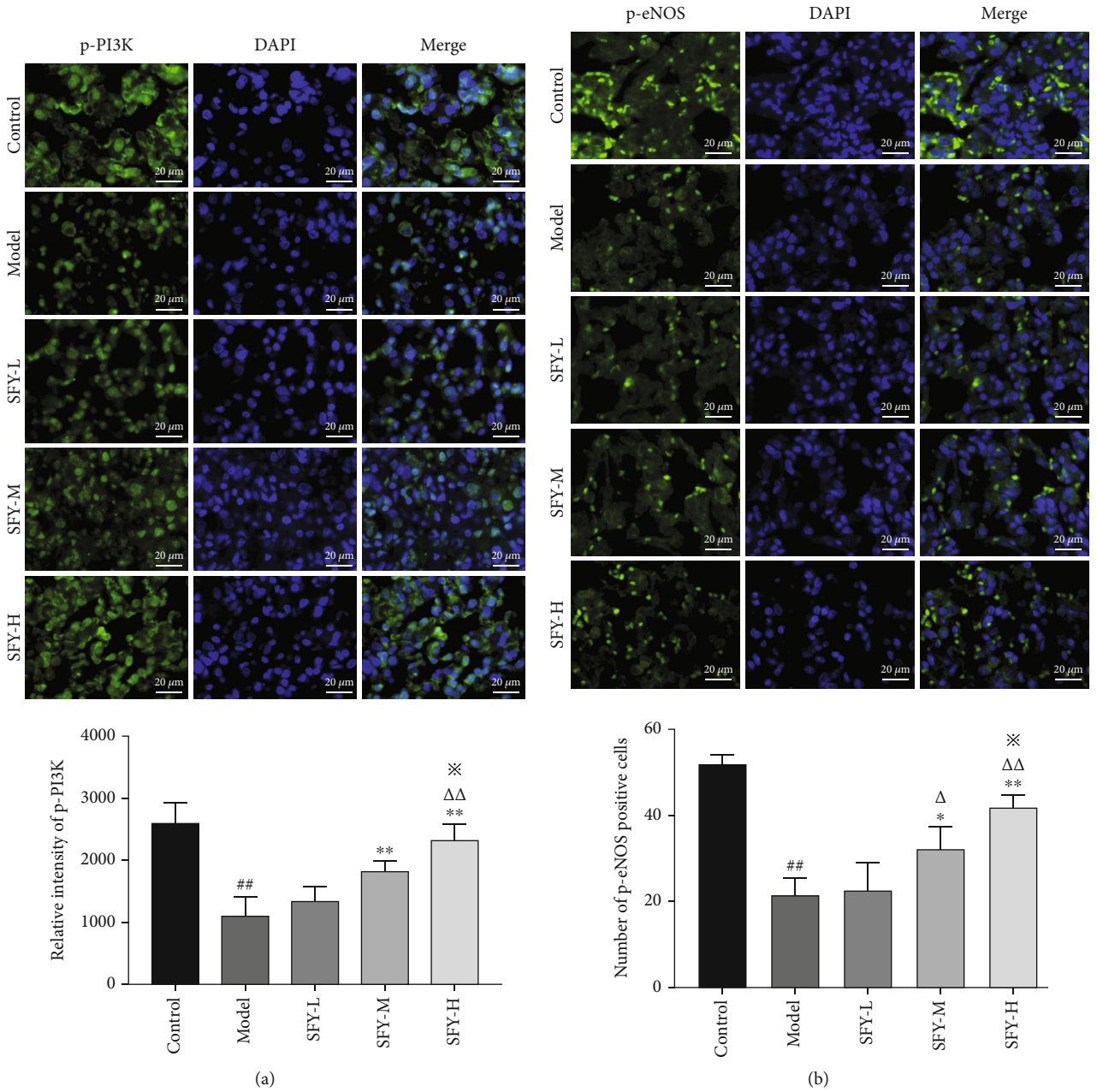

Figure 4: Continued.

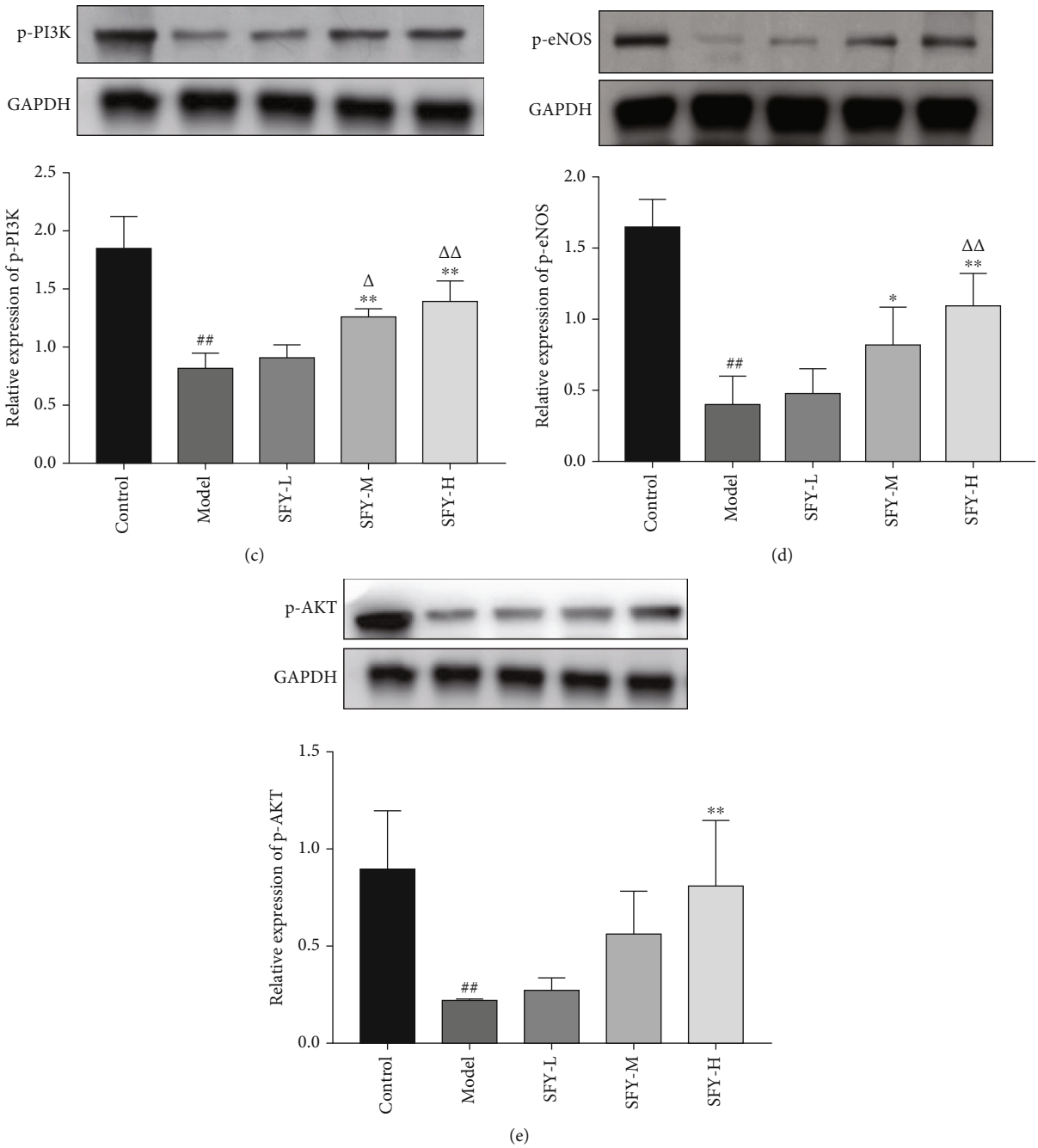

Figure 4: Shufeiya Recipe activated the PI3K/AKT/eNOS signaling pathway of PH rats. (a, b) Moderate and high groups of Shufeiya Recipe upregulated the relative immunofluorescence intensity of p-PI3K and p-eNOS. (c–e) Different doses of Shufeiya Recipe upregulated the protein expression level of p-PI3K, p-AKT, and p-eNOS. $n = 3$, $^{\#\#}P < 0.01$ vs. the control group; $^{*}P < 0.05$, $^{**}P < 0.01$ vs. the model group; $^{\triangle}P < 0.05$, $^{\triangle\triangle}P < 0.01$ vs. the low-dose group of Shufeiya Recipe; $^{\divideontimes}P < 0.05$ vs. the moderate-dose group of Shufeiya Recipe.

ERK1/2 (ab201015, 1 : 1000), and c-fos (ab134122, 1 : 2000) were added separately and incubated at 4°C overnight. The next day, after 1 h incubation with HRP-labeled secondary antibodies at room temperature, the target bands were exposed with an ultrasensitive multifunction imager, and the expression intensity of each target protein/β-actin was analyzed using ImageJ software 1.8.0.

2.9. Immunofluorescence Analysis. Paraffin sections of the lung tissue of rats were prepared. After deparaffinization and hydration, these sections were immersed in boiling sodium citrate solution for antigen retrieval and then blocked with normal goat serum for 30 min. The primary antibodies p-PI3K (AF3242, 1 : 1000), p-eNOS (CSB-PA000659, 1 : 200), and p-ERK1/2 (ab201015, 1 : 200) were added on the sections separately, which were placed in a humid box and incubated overnight at 4°C. The next day, FITC-labeled fluorescent secondary antibodies were incubated at 37°C in the dark. After staining the nucleus with DAPI solution, the high-power field of view was randomly selected and photographed using an

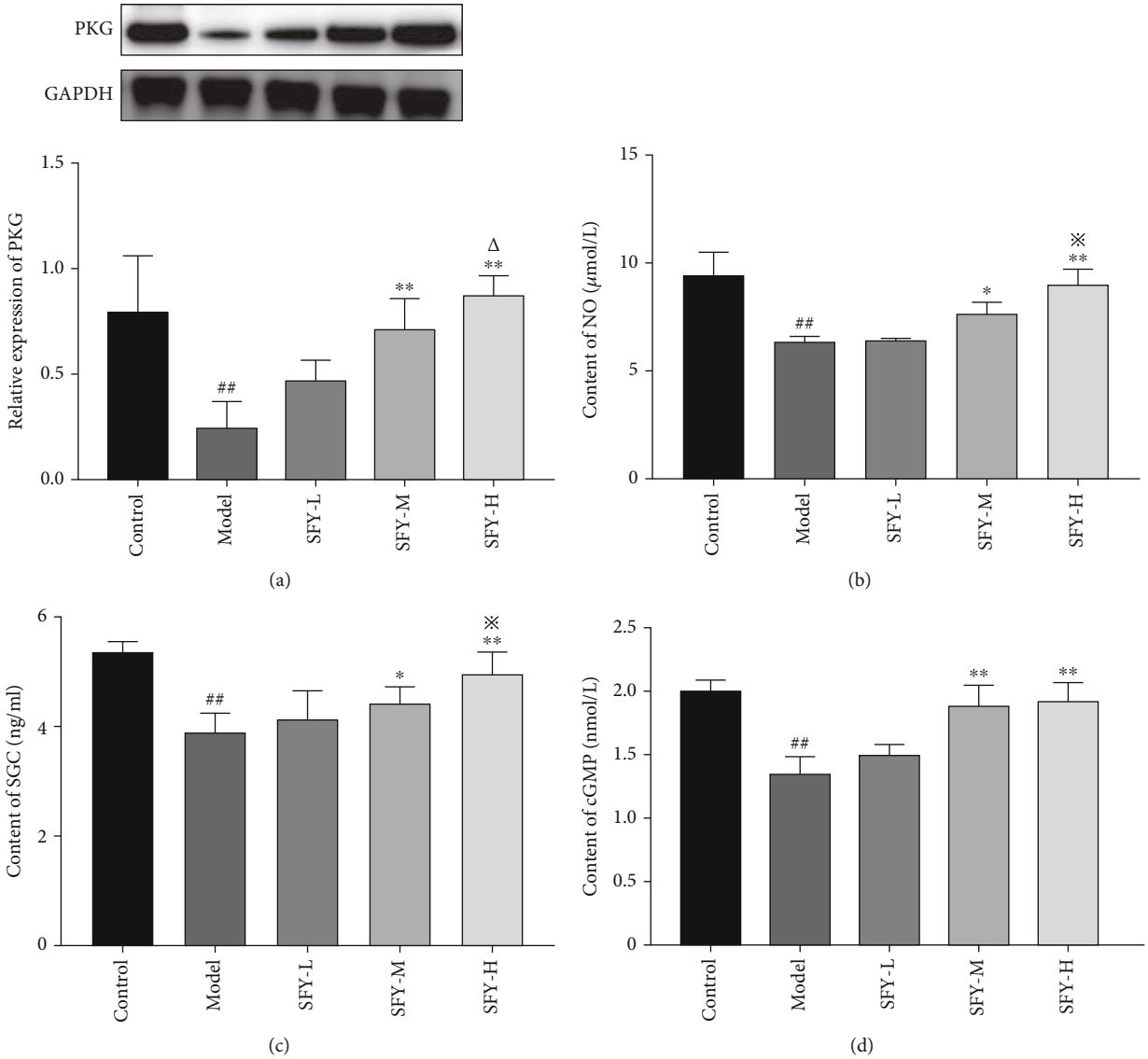

Figure 5: Shufeiya Recipe upregulated concentration of NO, sGC, and cGMP and the protein expression level of PKG in PH rats. (a) Moderate and high groups of Shufeiya Recipe upregulated the protein expression level of PKG, $n = 3$. (b) Moderate and high groups of Shufeiya Recipe upregulated the concentration of NO, $n = 3$. (c, d) Moderate and high groups of Shufeiya Recipe upregulated the concentration of sGC and cGMP, $n = 6$. $^{\#\#}P < 0.01$ vs. the control group; $^{*}P < 0.05$, $^{**}P < 0.01$ vs. the model group; $^{\triangle}P < 0.05$ vs. the low-dose group of Shufeiya Recipe; and $^{※}P < 0.05$ vs. the moderate-dose group of Shufeiya Recipe.

Olympus inverted fluorescence microscope, and the statistical analysis was performed.

2.10. Statistical Analysis. All data were expressed as the mean ± standard deviation. The intergroup differences in the data were evaluated by one-way analysis of variance (ANOVA) with the least significant difference (LSD) or Tamhane's T2 post hoc analysis using SPSS 20.0. $P < 0.05$ was considered statistically significant.

3. Results

3.1. Effects on mPAP and Pathological Changes of Lung Tissue. Compared with the control group, mPAP in the model group was significantly increased ($P < 0.01$). In contrast with the model group, mPAP in the sildenafil group and moderate- and high-dose groups of Shufeiya Recipe were significantly decreased ($P < 0.01$). The pulmonary tissue structure of rats in the control group was normal, showing intact, smooth, and neatly arranged intima of the pulmonary artery, and smooth muscle was not thickened. However, in the model group, the continuity of the pulmonary artery endothelium was damaged with irregular, intermittent hypertrophy of pulmonary arterioles, partially narrowed lumen, and significantly reduced effective area. In contrast with the model group, the pulmonary artery wall thickness and lumen stenosis of the sildenafil group and the Shufeiya Recipe groups showed significant improvement. Furthermore, the most marked improvement was obtained by the high-dose treatment of Shufeiya Recipe (Figure 1).

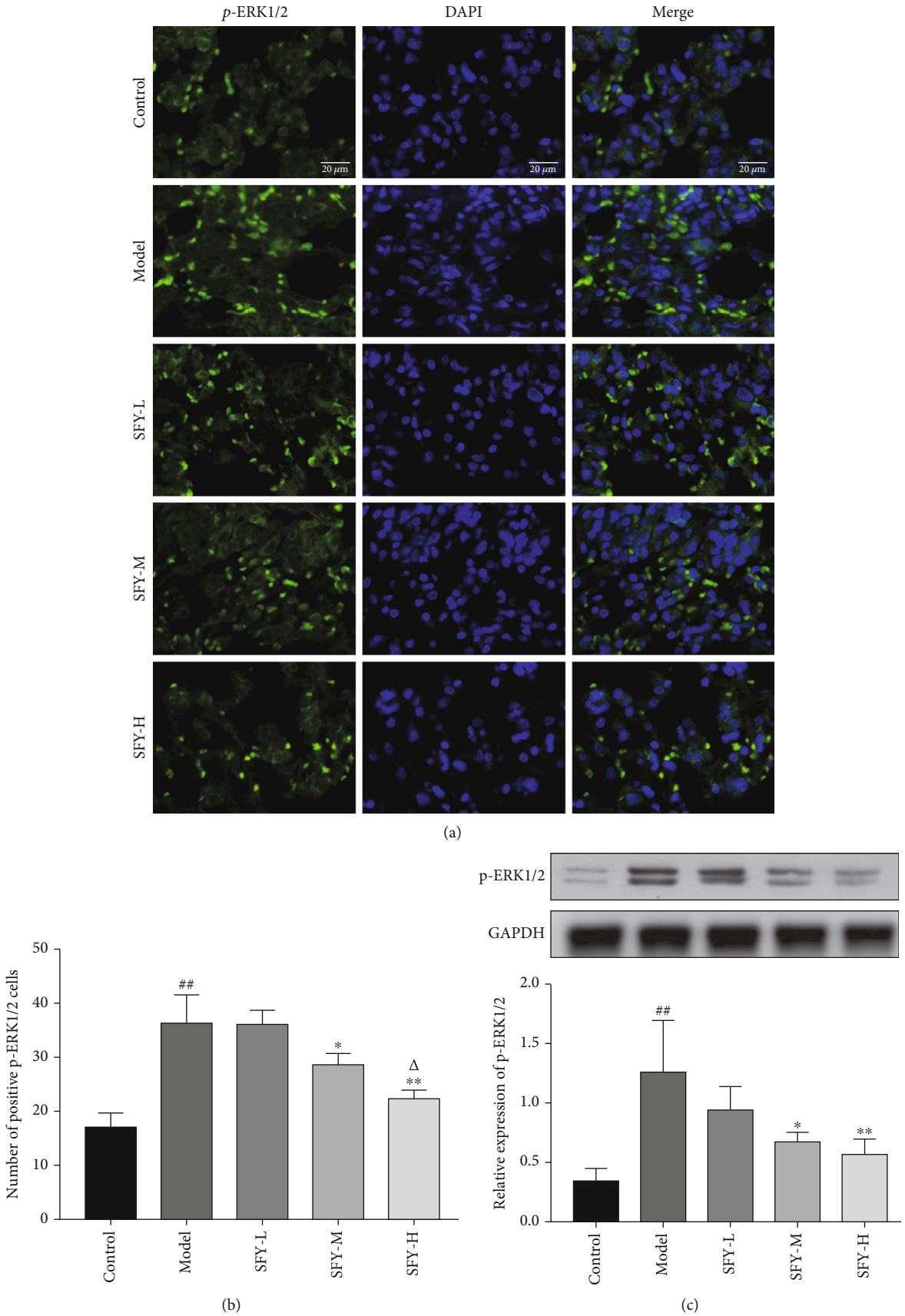

Figure 6: Continued.

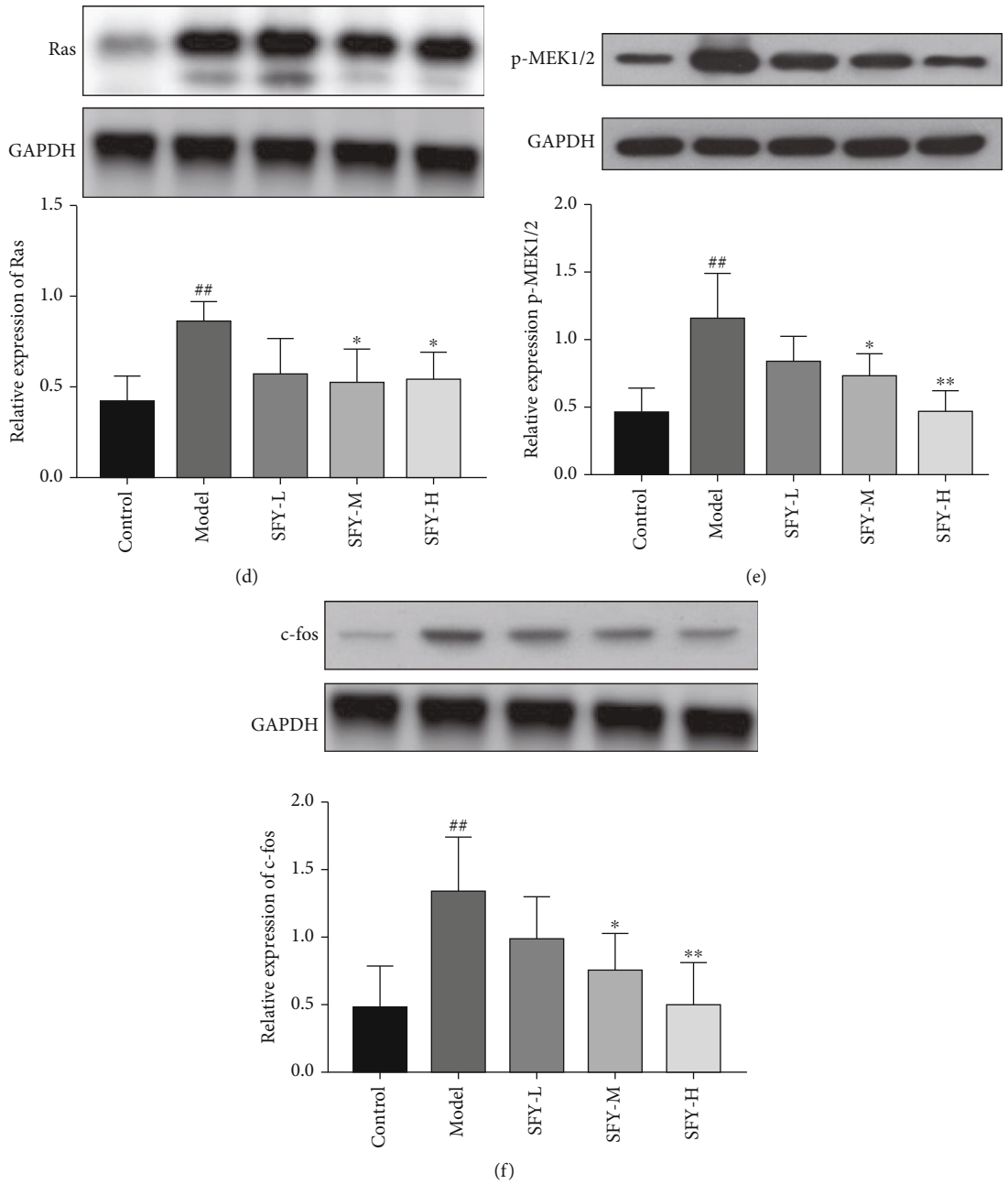

Figure 6: Shufeiya Recipe inhibited the Ras/ERK signaling pathway of PH rats. (a, b) Moderate and high groups of Shufeiya Recipe downregulated the relative immunofluorescence intensity of p-ERK1/2. (c–e) Different doses of Shufeiya Recipe downregulated the protein expression level of Ras, p-MEK1/2, p-ERK1/2, and c-fos. $n = 3$; $^{\#\#}P < 0.01$ vs. the control group; $^{*}P < 0.05$, $^{**}P < 0.01$ vs. the model group; $^{\triangle}P < 0.05$ vs. the moderate-dose group of Shufeiya Recipe.

3.2. Effects on Oxidative Stress Levels. Compared with the control group, the serum ROS content of the model group was significantly increased ($P < 0.01$), while the COX-1, COX-2, and Mn-SOD contents were significantly decreased ($P < 0.01$). As opposed to the model group, after the intervention of the high and moderate doses of Shufeiya Recipe, the oxidative stress level of PH rats was significantly inhibited, while the COX-1, COX-2, and Mn-SOD contents were significantly increased ($P < 0.05$, $P < 0.01$), and the level of ROS accumulation was significantly downregulated under each dose of Shufeiya Recipe treatment ($P < 0.01$) (Figure 2).

3.3. Effects on the SIRT3/FOXO3a Signaling Pathway. Contrasting with the control group, the protein expression level of SIRT3 and FOXO3a in the model group was visibly reduced ($P < 0.01$). On the other hand, compared with the model group, the expression level of SIRT3 protein in the Shufeiya Recipe high-dose group was dramatically increased ($P < 0.05$). In addition, the expression level of SIRT3 protein

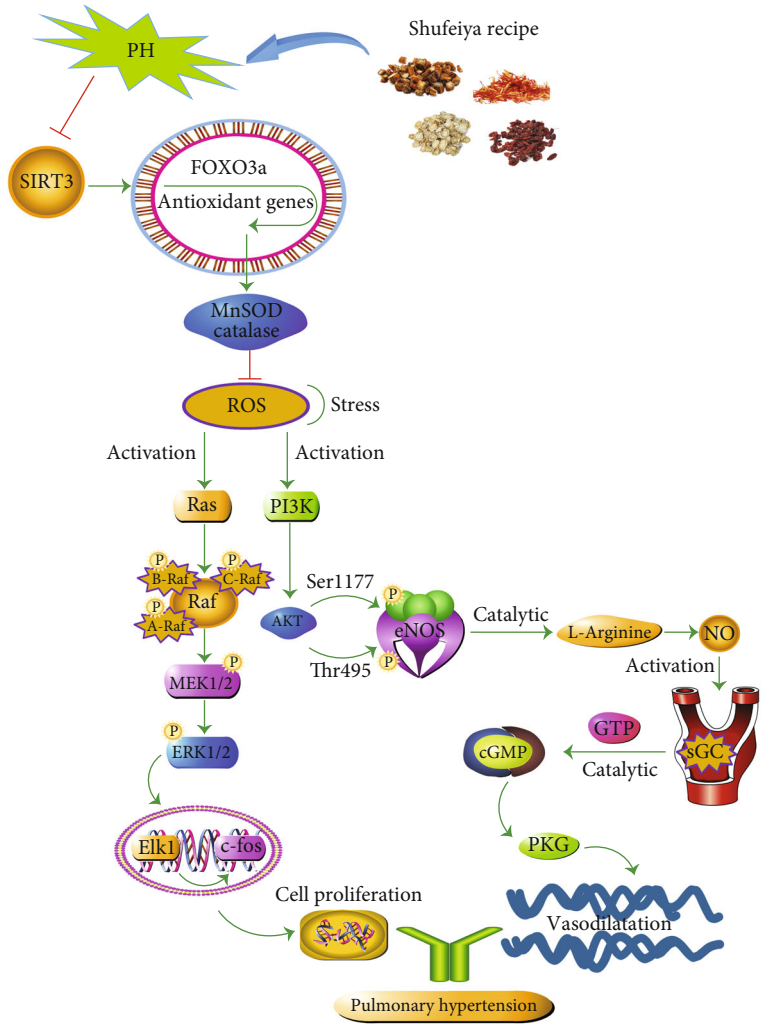

Figure 7: The protective mechanism of Shufeiya Recipe regulated PH

in the Shufeiya Recipe moderate-dose group and that of FOXO3a protein in the Shufeiya Recipe high-dose group were distinctively improved ($P < 0.05$) (Figure 3).

3.4. Effects on the PI3K/AKT/eNOS Signaling Pathway. The expression levels of p-PI3K, p-AKT, and p-eNOS in the model group were significantly reduced compared with the control group ($P < 0.01$). As opposed to the model group, the protein expression levels of p-PI3K in the moderate- and high-dose groups of Shufeiya Recipe were significantly increased ($P < 0.01$). Moreover, a high dose of Shufeiya Recipe also accelerated the expression of p-AKT($P < 0.01$). Furthermore, the protein expression levels of p-eNOS in both the Shufeiya Recipe moderate- and high-dose groups were significantly elevated ($P < 0.05$, $P < 0.01$). The most marked improvement was obtained by the high-dose treatment of Shufeiya Recipe (Figure 4).

3.5. Effects on the Expression of NO, sGC, cGMP, and PKG. In contrast with the control group, the concentration of NO, sGC, and cGMP and the protein expression level of PKG in the model rats were considerably reduced ($P < 0.01$). Compared to the model group, moderate and high doses of Shufeiya Recipe could significantly upregulate the concentration of NO, sGC, and cGMP and the protein expression level of PKG ($P < 0.05$, $P < 0.01$) (Figure 5).

3.6. Effects on the Ras/ERK Signaling Pathway. The protein expression levels of Ras, p-MEK1/2, p-ERK1/2, and c-fos in the model rats were dramatically higher than those in the control group ($P < 0.01$). However, in contrast to the model group, administering moderate and high doses of Shufeiya Recipe could induce an obvious reduction in the protein expression of Ras, p-MEK1/2, and p-ERK1/2 in PH rats ($P < 0.05$, $P < 0.01$). Interestingly, only the Shufeiya Recipe high-dose group showed decreased c-fos protein expression level in PH rats ($P < 0.01$) (Figure 6).

4. Discussion

The development and progression of pulmonary hypertension are closely associated with the abnormal function and/or structure of pulmonary arterioles and pulmonary vessels. If not controlled well, it will eventually lead to right

ventricular failure and even death in severe cases [29]. Pulmonary hypertension is preliminarily caused by long-term hypoxia or other factors that damage the structure and function of endothelial cells, causing imbalances of vasoactive substances such as NO and dysfunction of ion channels, resulting in abnormal endothelial cell barrier function and imbalance of secreted active factors, eventually leading to abnormal pulmonary vasoconstriction [30–32]. The pathological manifestations of PH are characterized by pulmonary artery intima injury and proliferation, hypertrophy and continuous contraction of the middle membrane layer, adventitia fibrosis, extracellular matrix remodeling, and inflammatory infiltration, to name a few. Besides, vasodilatation and in situ thrombosis can often be seen at the distal end of the lesion, leading to progressive stenosis and occlusion of the pulmonary artery lumen.

Oxidative stress is a key precursor to pulmonary hypertension. The imbalance between the generation and removal of oxygen free radicals leads to excessive ROS accumulation. ROS is directly related to pathological changes such as pulmonary artery smooth muscle cell proliferation, endothelial dysfunction, in situ thrombosis, inflammation, and vascular remodeling [33]. As a rate-limiting enzyme in the process of prostaglandin synthesis, COX-2 and its derivative metabolites have antioxidant properties [34]. It has been shown that knocking out the mouse COX-2 gene could increase the level of oxidative stress and the proliferation level of smooth muscle cells in mice with pulmonary hypertension [35]. COX-1 is a membrane penetrating protein complex, and changes in its level could cause a large amount of ROS to be released, while excessive ROS could affect the unsaturated fatty acids in the biofilm and cause lipid peroxidation [36].

As an important deacetylase in the mechanism of oxidative stress, SIRT3 has a regulatory effect on mitochondrial function. When mitochondrial dysfunction occurs, oxidative stress damage might follow [37]. Normally, cells can eliminate excess ROS through antioxidant enzymes such as Mn-SOD and CAT to maintain normal cell function. SIRT3 can not only directly regulate the activity of Mn-SOD and improve the function of ROS clearance [38] but also can deacetylate the forkhead transcription factor (FOXO3a), activate FOXO3a-dependent Mn-SOD and CAT, upregulate the expression of Mn-SOD, and inhibit excessive ROS generation. Excessive ROS can activate the Ras/ERK signaling pathway, and the activated Ras can cause the phosphorylation of its downstream substrate Raf kinase, upregulate the protein expression levels of its downstream substrates MEK1/2 and ERK1. Elk1 can, in turn, positively regulate the activity of the c-fos promoter, which induces the proliferation and differentiation of pulmonary artery smooth muscle cells and promotes the process of pulmonary hypertension [16].

In addition, the functional imbalance between ROS and the antioxidant system is one of the main causes of endothelial dysfunction [39]. Excessive ROS can inhibit the activation of the PI3K/AKT signaling pathway, resulting in a decrease in NO production. NO is produced by the enzymatic catalysis of endothelial nitric oxide synthase (eNOS), and previous studies in the pulmonary hypertension rat model have verified the involvement of NO in regulating eNOS phosphorylation and PI3K/AKT/eNOS and cGMP-PKG signaling pathways [40, 41]. Activated PI3K can phosphorylate lipids on the cell membrane and activate AKT, which can mediate downstream signals [42], which in turn causes conformational changes in the phosphorylation sites of Ser1177 and Thr495 of the eNOS amino acid residues to increase the activity of eNOS activity to promote the production of NO. Meanwhile, NO could activate sGC in vascular smooth muscle cells, and the activated sGC could catalyze the conversion of GTP into cGMP to activate cGMP-dependent protein kinase (PKG) [43], leading to vasodilation, thereby improving pulmonary hypertension.

Because traditional Chinese medicine has the advantages of being a multicomponent, multitarget, and multimechanistic treatment strategy, it has gradually received much attention in pulmonary hypertension therapy. Herein, we showed that Shufeiya Recipe, an empirical recipe for clinical treatment of pulmonary hypertension, has a good therapeutic potential. The *Radix Salviae* in Shufeiya Recipe mainly includes diterpenoids and phenolic acids, such as danshenol A, salvianolic acid A, and tanshinone IIA. These compounds have good pharmacological activities; for instance, the inhibition rate of the secretion of TNF-α, IL-1β, and IL-8 by danshenol A are 56.3%, 67.6%, and 51.7%, respectively [44]. Oxidative stress is an important mechanism in the occurrence and development of pulmonary hypertension, and salvianolic acid A and salvianolic acid B are famous for their strong antioxidant activities [45]. In addition, tanshinone IIA has been proved to inhibit myocardial remodeling, myocardial ischemia-reperfusion injury, and ischemic stroke and prevent liver cirrhosis by maintaining its antioxidant effect [46–48]. Studies have shown that tanshinone IIA has the pharmacological effects of activating the PI3K/AKT/mTOR signaling pathway, reducing oxidative stress, reducing expression of high-mobility group box B1 protein (HMGB1), and inhibiting inflammation [49–51]. In addition, Danshensu has shown a cardioprotective effect on isolated rat hearts by activating the AKT/ERK1/2/Nrf2 signaling pathway [52].

In addition, the main ingredients of *Carthami Flos* in the Shufeiya Recipe include safflower yellow and hydroxysafflor yellow A, which are often used to treat cardiovascular and cerebrovascular diseases [53]. They could also upregulate SOD activity and inhibit malondialdehyde (MDA) and ROS accumulation [54–56]. In particular, the flavonoids in *Carthami Flos* have a good regulatory effect on oxidative stress response [57] and could inhibit NO production and inflammatory response by decreasing the protein expression of iNOS and COX-2 genes [58]. *Cornus Officinalis Sieb. Et Zucc.* can increase the activities of SOD, CAT, and GPX [59], and the crude extract of *Cornus Officinalis Sieb. Et Zucc.* can regulate the protein expression levels of PI3K, Ras, and p-ERK1/2 [60]. Morroniside is an important active ingredient of *Cornus officinalis Sieb. Et Zucc.*, which can inhibit the expression of iNOS and COX-2 by regulating the NF-κB signaling pathway [61]. *Platycodon Grandiforus* mainly contains triterpenoid saponins and platycosides, which can suppress chronic airway inflammation and

oxidative stress damage by regulating the ROS/ERK signaling pathway [62] as well as reducing the thickness of alveolar septa [63]. Network pharmacology studies have shown that *Platycodon Grandiforus* could also improve a variety of pathological changes in the heart and lungs by regulating the PI3K/AKT signaling pathway [64]. These above studies provide a theoretical basis for Shufeiya Recipe in treating pulmonary hypertension. This study drew a conclusion that Shufeiya Recipe could differentially downregulate mPAP in PH rats and improve lung histopathological changes. Besides, it could downregulate ROS levels, upregulate the concentrations of COX-1 and COX-2 and the activity of Mn-SOD, and inhibit oxidative stress damage. Additionally, it could upregulate the protein expression levels of SIRT3 and FOXO3a; promote the protein expressions of p-PI3K, p-AKT, and p-eNOS; and increase the expression levels of NO, sGC, cGMP, and PKG. Moreover, it could downregulate the protein expression levels of Ras, p-MEK1/2, p-ERK1/2, and c-fos (Figure 7).

5. Conclusion

In summary, our results indicate that Shufeiya Recipe can improve MCT-induced pulmonary hypertension in rats by regulating SIRT3/FOXO3a and its downstream PI3K/AKT/eNOS and Ras/ERK signaling pathways.

Data Availability

The data used and/or analyzed during the current study are available upon direct request to the corresponding author.

Conflicts of Interest

The authors declared no conflict of interest regarding this article.

Authors' Contributions

Zhuangzhuang Jia and Haifen Yan contributed equally to this work. Jingyuan Mao was the corresponding author, and Xianliang Wang was the cocorresponding author in this article.

Acknowledgments

This research project was supported by the Ministry of Education of the People's Republic of China "Program for Innovative Research Team in University" (No. IRT_16254) and Traditional Chinese Medicine & Integrated Traditional Chinese and Western Medicine Project of Tianjin health commission and administration of TCM (No. 2021048).

References

[1] R. Zolty, "Pulmonary arterial hypertension specific therapy: the old and the new," *Pharmacology & Therapeutics*, vol. 214, 2020.

[2] M. M. Hoeper, M. Humbert, R. Souza et al., "A global view of pulmonary hypertension," *The Lancet Respiratory Medicine*, vol. 4, no. 4, pp. 306–322, 2016.

[3] E. Spiekerkoetter, S. M. Kawut, and V. A. de Jesus Perez, "New and emerging therapies for pulmonary arterial hypertension," *Annual Review of Medicine*, vol. 70, no. 1, pp. 45–59, 2019.

[4] J. Zhang, J. Dong, M. Martin et al., "AMP-activated protein kinase phosphorylation of angiotensin-converting enzyme 2 in endothelium mitigates pulmonary hypertension," *American Journal of Respiratory and Critical Care Medicine*, vol. 198, no. 4, pp. 509–520, 2018.

[5] S. L. Archer, E. K. Weir, and M. R. Wilkins, "Basic science of pulmonary arterial hypertension for clinicians: new concepts and experimental therapies," *Circulation*, vol. 121, no. 18, pp. 2045–2066, 2010.

[6] Q. Li, Y. Qiu, M. Mao et al., "Antioxidant mechanism of Rutin on hypoxia-induced pulmonary arterial cell proliferation," *Molecules*, vol. 19, no. 11, pp. 19036–19049, 2014.

[7] F. Veit, O. Pak, R. P. Brandes, and N. Weissmann, "Hypoxia-dependent reactive oxygen species signaling in the pulmonary circulation: focus on ion channels," *Antioxidants & Redox Signaling*, vol. 22, no. 6, pp. 537–552, 2015.

[8] A. C. Racanelli, S. A. Kikkers, A. M. K. Choi, and S. M. Cloonan, "Autophagy and inflammation in chronic respiratory disease," *Autophagy*, vol. 14, no. 2, pp. 221–232, 2018.

[9] K. G. Birukov, "Cyclic stretch, reactive oxygen species, and vascular remodeling," *Antioxidants & Redox Signaling*, vol. 11, no. 7, pp. 1651–1667, 2009.

[10] J. Baeza, M. J. Smallegan, and J. M. Denu, "Mechanisms and dynamics of protein acetylation in mitochondria," *Trends in Biochemical Sciences*, vol. 41, no. 3, pp. 231–244, 2016.

[11] C. Koentges, C. Bode, and H. Bugger, "SIRT3 in cardiac physiology and disease," *Frontiers in Cardiovascular Medicine*, vol. 3, p. 38, 2016.

[12] M. Zhai, B. Li, W. Duan et al., "Melatonin ameliorates myocardial ischemia reperfusion injury through SIRT3-dependent regulation of oxidative stress and apoptosis," *Journal of Pineal Research*, vol. 63, no. 2, 2017.

[13] D. B. Zorov, M. Juhaszova, and S. J. Sollott, "Mitochondrial reactive oxygen species (ROS) and ROS-induced ROS release," *Physiological Reviews*, vol. 94, no. 3, pp. 909–950, 2014.

[14] K. Y. Cheng, F. Guo, J. Q. Lu et al., "MnTM-4-PyP modulates endogenous antioxidant responses and protects primary cortical neurons against oxidative stress," *CNS Neuroscience & Therapeutics*, vol. 21, no. 5, pp. 435–445, 2015.

[15] G. Chang, Y. Chen, H. Zhang, and W. Zhou, "Trans sodium crocetinate alleviates ischemia/reperfusion-induced myocardial oxidative stress and apoptosis *via* the SIRT3/FOXO3a/SOD2 signaling pathway," *International Immunopharmacology*, vol. 71, pp. 361–371, 2019.

[16] M. Patel, D. Predescu, R. Tandon et al., "A Novel p38 Mitogen-activated Protein Kinase/Elk-1 Transcription Factor- dependent Molecular Mechanism Underlying Abnormal Endothelial Cell Proliferation in Plexogenic Pulmonary Arterial Hypertension∗," *Journal of Biological Chemistry*, vol. 288, no. 36, pp. 25701–25716, 2013.

[17] C. Zhou, Y. Chen, W. Kang et al., "Mir-455-3p-1 represses FGF7 expression to inhibit pulmonary arterial hypertension through inhibiting the RAS/ERK signaling pathway," *Journal of Molecular and Cellular Cardiology*, vol. 130, pp. 23–35, 2019.

[18] P. Abeyrathna and Y. Su, "The critical role of Akt in cardiovascular function," *Vascular Pharmacology*, vol. 74, pp. 38–48, 2015.

[19] J. Karar and A. Maity, "PI3K/AKT/mTOR pathway in angiogenesis," *Frontiers in Molecular Neuroscience*, vol. 4, p. 51, 2011.

[20] S. P. Cary, J. A. Winger, and M. A. Marletta, "Tonic and acute nitric oxide signaling through soluble guanylate cyclase is mediated by nonheme nitric oxide, ATP, and GTP," *Proceedings of the National Academy of Sciences of the United States of America*, vol. 102, no. 37, pp. 13064–13069, 2005.

[21] P. R. Evora, P. M. Evora, A. C. Celotto, A. J. Rodrigues, and E. E. Joviliano, "Cardiovascular therapeutics targets on the NO-sGC-cGMP signaling pathway: a critical overview," *Current Drug Targets*, vol. 13, no. 9, pp. 1207–1214, 2012.

[22] A. C. Swaminathan, H. Zhu, V. Tapson et al., "Treatment-related biomarkers in pulmonary hypertension patients on oral therapies," *Respiratory Research*, vol. 21, no. 1, p. 304, 2020.

[23] M. E. I. XD, C. Yan-Feng, C. Yan-Yun et al., "Danshen: a phytochemical and pharmacological overview," *Chinese Journal of Natural Medicines*, vol. 17, no. 1, pp. 59–80, 2019.

[24] H. Wan, Y. Yang, Z. Li et al., "Compatibility of ingredients of Danshen (RadixSalviaeMiltiorrhizae) and Honghua (Flos Carthami) and their protective effects on cerebral ischemia-reperfusion injury in rats," *Experimental and Therapeutic Medicine*, vol. 22, no. 2, p. 849, 2021.

[25] J. Huang, Y. Zhang, L. Dong et al., "Ethnopharmacology, phytochemistry, and pharmacology of *Cornus officinalis* Sieb. et Zucc," *Journal of Ethnopharmacology*, vol. 213, pp. 280–301, 2018.

[26] W. Hao, Y. Shi, Y. Qin et al., "Platycodon grandiflorumProtects against anthracycline-induced cardiotoxicity in early breast cancer patients," *Integrative Cancer Therapies*, vol. 19, 2020.

[27] E. M. Noh, J. M. Kim, H. Y. Lee et al., "Immuno-enhancement effects of Platycodon grandiflorum extracts in splenocytes and a cyclophosphamide-induced immunosuppressed rat model," *BMC Complementary and Alternative Medicine*, vol. 19, no. 1, p. 322, 2019.

[28] J. H. Sun, F. Sun, B. Yan, J. Y. Li, and L. Xin, "Data mining and systematic pharmacology to reveal the mechanisms of traditional Chinese medicine in *Mycoplasma pneumoniae* pneumonia treatment," *Biomedicine & Pharmacotherapy*, vol. 125, 2020.

[29] M. M. Hoeper, H. A. Ghofrani, E. Grünig, H. Klose, H. Olschewski, and S. Rosenkranz, "Pulmonary hypertension," *Deutsches Ärzteblatt International*, vol. 114, no. 5, pp. 73–84, 2017.

[30] T. Hashimoto-Kataoka, N. Hosen, T. Sonobe et al., "Interleukin-6/interleukin-21 signaling axis is critical in the pathogenesis of pulmonary arterial hypertension," *Proceedings of the National Academy of Sciences of the United States of America*, vol. 112, no. 20, pp. E2677–E2686, 2015.

[31] J. R. Klinger, S. H. Abman, and M. T. Gladwin, "Nitric oxide deficiency and endothelial dysfunction in pulmonary arterial hypertension," *American Journal of Respiratory and Critical Care Medicine*, vol. 188, no. 6, pp. 639–646, 2013.

[32] L. D. Maston, D. T. Jones, W. Giermakowska et al., "Central role of T helper 17 cells in chronic hypoxia-induced pulmonary hypertension," *The American Journal of Physiology-Lung Cellular and Molecular Physiology*, vol. 312, no. 5, pp. L609–l624, 2017.

[33] C. M. Wong, G. Bansal, L. Pavlickova, L. Marcocci, and Y. J. Suzuki, "Reactive oxygen species and antioxidants in pulmonary hypertension," *Antioxidants & Redox Signaling*, vol. 18, no. 14, pp. 1789–1796, 2013.

[34] J. A. Mitchell and N. S. Kirkby, "Eicosanoids, prostacyclin and cyclooxygenase in the cardiovascular system," *British Journal of Pharmacology*, vol. 176, no. 8, pp. 1038–1050, 2019.

[35] L. E. Fredenburgh, J. Ma, and M. A. Perrella, "Cyclooxygenase-2 inhibition and hypoxia-induced pulmonary hypertension: effects on pulmonary vascular remodeling and contractility," *Trends in Cardiovascular Medicine*, vol. 19, no. 2, pp. 31–37, 2009.

[36] N. K. Somanna, P. M. Wörner, S. N. Murthy et al., "Intratracheal administration of cyclooxygenase-1-transduced adipose tissue-derived stem cells ameliorates monocrotaline-induced pulmonary hypertension in rats," *American Journal of Physiology-Heart and Circulatory Physiology*, vol. 307, no. 8, pp. H1187–H1195, 2014.

[37] X. He, H. Zeng, and J. X. Chen, "Emerging role of SIRT3 in endothelial metabolism, angiogenesis, and cardiovascular disease," *Journal of Cellular Physiology*, vol. 234, no. 3, pp. 2252–2265, 2019.

[38] J. Lu, H. Zhang, X. Chen et al., "A small molecule activator of SIRT3 promotes deacetylation and activation of manganese superoxide dismutase," *Free Radical Biology and Medicine*, vol. 112, pp. 287–297, 2017.

[39] W. Zhang, Q. Huang, Z. Zeng, J. Wu, Y. Zhang, and Z. Chen, "Sirt1 inhibits oxidative stress in vascular endothelial cells," *Oxidative Medicine and Cellular Longevity*, vol. 2017, Article ID 7543973, 8 pages, 2017.

[40] Z. Zheng, S. Yu, W. Zhang et al., "Genistein attenuates monocrotaline-induced pulmonary arterial hypertension in rats by activating PI3K/Akt/eNOS signaling," *Histology & Histopathology*, vol. 32, no. 1, pp. 35–41, 2017.

[41] J. Wang, K. Yang, L. Xu et al., "Sildenafil inhibits hypoxia-induced transient receptor potential canonical protein expression in pulmonary arterial smooth muscle via cGMP-PKG-PPARγ axis," *American Journal of Respiratory Cell and Molecular Biology*, vol. 49, no. 2, pp. 231–240, 2013.

[42] Y. Yang, L. Yin, M. Zhu et al., "Protective effects of dioscin on vascular remodeling in pulmonary arterial hypertension *via* adjusting GRB2/ERK/PI3K-AKT signal," *Biomedicine & Pharmacotherapy*, vol. 133, article ???, 2021.

[43] M. Y. Lee, K. B. Tsai, J. H. Hsu, S. J. Shin, J. R. Wu, and J. L. Yeh, "Liraglutide prevents and reverses monocrotaline-induced pulmonary arterial hypertension by suppressing ET-1 and enhancing eNOS/sGC/PKG pathways," *Scientific Reports*, vol. 6, no. 1, 2016.

[44] S. Ma, D. Zhang, H. Lou, L. Sun, and J. Ji, "Evaluation of the anti-inflammatory activities of tanshinones isolated from *Salvia miltiorrhiza* var. *alba* roots in THP-1 macrophages," *Journal of Ethnopharmacology*, vol. 188, pp. 193–199, 2016.

[45] J. H. Ho and C. Y. Hong, "Salvianolic acids: small compounds with multiple mechanisms for cardiovascular protection," *Journal of Biomedical Science*, vol. 18, no. 1, p. 30, 2011.

[46] M. Cai, Y. Guo, S. Wang et al., "Tanshinone IIA elicits neuroprotective effect through activating the nuclear factor erythroid 2-related factor-dependent antioxidant response," *Rejuvenation Research*, vol. 20, no. 4, pp. 286–297, 2017.

[47] J. Feng, S. Li, and H. Chen, "Tanshinone IIA inhibits myocardial remodeling induced by pressure overload via suppressing oxidative stress and inflammation: possible role of silent information regulator 1," *European Journal of Pharmacology*, vol. 791, pp. 632–639, 2016.

[48] M. Shu, X. R. Hu, Z. A. Hung, D. D. Huang, and S. Zhang, "Effects of tanshinone IIA on fibrosis in a rat model of cirrhosis through heme oxygenase-1, inflammation, oxidative stress and apoptosis," *Molecular Medicine Reports*, vol. 13, no. 4, pp. 3036–3042, 2016.

[49] H. Hu, C. Zhai, G. Qian et al., "Protective effects of tanshinone IIA on myocardial ischemia reperfusion injury by reducing oxidative stress, HMGB1 expression, and inflammatory reaction," *Pharmaceutical Biology*, vol. 53, no. 12, pp. 1752–1758, 2015.

[50] Q. Li, L. Shen, Z. Wang, H. P. Jiang, and L. X. Liu, "Tanshinone IIA protects against myocardial ischemia reperfusion injury by activating the PI3K/Akt/mTOR signaling pathway," *Biomedicine & Pharmacotherapy*, vol. 84, pp. 106–114, 2016.

[51] W. Wei, Y. Liu, Q. Zhang, Y. Wang, X. Zhang, and H. Zhang, "Danshen-enhanced cardioprotective effect of cardioplegia on ischemia reperfusion injury in a human-induced pluripotent stem cell-derived cardiomyocytes model," *Artificial Organs*, vol. 41, no. 5, pp. 452–460, 2017.

[52] J. Yu, L. Wang, M. Akinyi et al., "Danshensu protects isolated heart against ischemia reperfusion injury through activation of Akt/ERK1/2/Nrf2 signaling," *International Journal of Clinical and Experimental Medicine*, vol. 8, no. 9, pp. 14793–14804, 2015.

[53] L. L. Zhang, K. Tian, Z. H. Tang et al., "Phytochemistry and pharmacology ofCarthamus tinctoriusL," *The American Journal of Chinese Medicine*, vol. 44, no. 2, pp. 197–226, 2016.

[54] E. M. Choi, G. H. Kim, and Y. S. Lee, "Carthamus tinctorius flower extract prevents H2O2-induced dysfunction and oxidative damage in osteoblastic MC3T3-E1 cells," *Phytotherapy Research*, vol. 24, no. 7, pp. 1037–1041, 2010.

[55] Y. He, H. Wan, Y. Du et al., "Protective effect of Danhong injection on cerebral ischemia-reperfusion injury in rats," *Journal of Ethnopharmacology*, vol. 144, no. 2, pp. 387–394, 2012.

[56] H. Liao, L. Banbury, H. Liang et al., "Effect of Honghua (*Flos Carthami*) on nitric oxide production in RAW 264.7 cells and α-glucosidase activity," *Journal of Traditional Chinese Medical Sciences*, vol. 34, no. 3, pp. 362–368, 2014.

[57] K. C. Li, Y. L. Ho, G. J. Huang, and Y. S. Chang, "Anti-oxidative and anti-inflammatory effects ofLobelia chinensis in VitroandIn vivo," *The American Journal of Chinese Medicine*, vol. 43, no. 2, pp. 269–287, 2015.

[58] C. C. Wang, C. S. Choy, Y. H. Liu et al., "Protective effect of dried safflower petal aqueous extract and its main constituent, carthamus yellow, against lipopolysaccharide-induced inflammation in RAW264.7 macrophages," *Journal of the Science of Food and Agriculture*, vol. 91, no. 2, pp. 218–225, 2011.

[59] D. Gao, Q. Li, Z. Gao, and L. Wang, "Antidiabetic effects of Corni Fructus extract in streptozotocin-induced diabetic rats," *Yonsei Medical Journal*, vol. 53, no. 4, pp. 691–700, 2012.

[60] C. L. Liao, J. H. Lin, J. C. Lien et al., "The crude extract of Corni Fructus inhibits the migration and invasion of U-2 OS human osteosarcoma cells through the inhibition of matrix metalloproteinase-2/-9 by MAPK signaling," *Environmental Toxicology*, vol. 30, no. 1, pp. 53–63, 2015.

[61] C. H. Park, J. S. Noh, J. H. Kim et al., "Evaluation of morroniside, iridoid glycoside from Corni Fructus, on diabetes-induced alterations such as oxidative stress, inflammation, and apoptosis in the liver of type 2 diabetic db/db mice," *Biological and Pharmaceutical Bulletin*, vol. 34, no. 10, pp. 1559–1565, 2011.

[62] J. H. Choi, Y. P. Hwang, E. H. Han et al., "Inhibition of acrolein-stimulated MUC5AC expression by *Platycodon grandiflorum* root-derived saponin in A549 cells," *Food and Chemical Toxicology*, vol. 49, no. 9, pp. 2157–2166, 2011.

[63] S. Lee, E. H. Han, M. K. Lim et al., "FermentedPlatycodon grandiflorumExtracts relieve airway inflammation and cough reflex SensitivityIn vivo," *Journal of Medicinal Food*, vol. 23, no. 10, pp. 1060–1069, 2020.

[64] M. Park, S. Y. Park, H. J. Lee, and C. E. Kim, "A systems-level analysis of mechanisms of Platycodon grandiflorum based on a network pharmacological approach," *Molecules*, vol. 23, no. 11, p. 2841, 2018.

Hindawi
Disease Markers
Volume 2022, Article ID 6517266, 11 pages
https://doi.org/10.1155/2022/6517266

Research Article

Urolithin B, a Gut Microbiota Metabolite, Reduced Susceptibility to Myocardial Arrhythmic Predisposition after Hypoxia

Xin Huang,[1,2] Hong Gao,[2] Xiaojie Jiang,[2] and Zeqi Zheng[1]

[1]*Department of Cardiology, The First Affiliated Hospital of Nanchang University, Nanchang 330008, China*
[2]*Department of Cardiology, The First Hospital of Nanchang, The Third Affiliated Hospital of Nanchang University, Affiliated Hospital of Sun Yat-sen University, Nanchang 330008, China*

Correspondence should be addressed to Zeqi Zheng; zeqizheng@126.com

Received 3 December 2021; Revised 13 January 2022; Accepted 20 January 2022; Published 8 February 2022

Academic Editor: XIANWEI ZENG

Cardiomyocyte apoptosis, neural remodeling, and gap junction channel change play critical roles in ventricular arrhythmia (VA) after acute myocardial infarction (AMI). Urolithin B (UB), one of the gut metabolites of ellagitannins, a class of antioxidant polyphenols, has various biological activities, but its direct role in cardiomyocyte apoptosis, neural remodeling, and gap junction channel change after AMI remains elusive. We investigated whether urolithin B reduced susceptibility of myocardial arrhythmic after myocardial infarction (MI). In vitro, the cardiomyocytes were subjected to hypoxia (94% N_2/5% CO_2/1% O_2) for 3 hours. Cardiomyocyte apoptosis was assessed by TUNEL staining and western blotting. Urolithin B was found to decrease the number of apoptotic cells after hypoxia. Moreover, there was a substantial decrease in the expression of neural remodeling markers in the urolithin B treatment group. Urolithin B significantly increased the expression level of gap junction channel protein. Mechanistically, urolithin B inhibited cardiomyocyte apoptosis by activating Akt/the mammalian target of rapamycin (mTOR) pathway, and the protection of urolithin B against cardiomyocyte apoptosis was compromised with Akt gene silencing. Furthermore, urolithin B suppressed nuclear translocation of nuclear factor-kB (NF-κB) to facilitate nerve remodeling. Taken together, our findings suggested that UB reduced the occurrence of myocardial arrhythmias after hypoxia via regulation of the Akt/mTOR pathway and NF-κB nuclear translocation, which highlights the potential of UB as a novel therapy for ischemic heart disease.

1. Introduction

Acute myocardial infarction (AMI), the leading cause of death worldwide, imposes immense health and economic burden [1, 2]. Arrhythmia, especially ventricular arrhythmia, is the major cause of sudden death in AMI patients [3]. Sympathetic neural remodeling [4, 5], gap junction remodeling [3], and cardiomyocyte apoptosis [6] contribute to fatal ventricular arrhythmia. In patients with AMI, timely and effective myocardial reperfusion using either thrombolytic therapy or primary percutaneous coronary intervention is one of the main treatment options against ventricular arrhythmia [2]. However, increasing numbers of evidence indicate that pharmacological interventions targeting neural remodeling, gap junction channel remodeling, and cardiomyocyte apoptosis reduce the incidence of arrhythmia, improving long-term prognosis. As a result, the regulation of neural remodeling, gap junction channels, and cardiomyocyte apoptosis via medications may be an essential therapeutic strategy for attenuating MI-induced arrhythmia.

Ellagitannins (ETs) are a class of polyphenols enriched in pomegranates, walnuts, and berries [2]. ETs are hydrolyzed by the gut microbiota to ellagic acid (EA), which is further hydrolyzed into urolithins [7]. Urolithin A (UA) and urolithin B (UB) are the main components of urolithin detected in various tissues [8]. Previous research demonstrated that UB protected the apoptosis [2], inflammation [9], and neural remodeling of myocardial tissues and inhibited gap junction channel expression, which were the key factors that cause arrhythmia [10, 11].

However, the mechanism of urolithin B in reducing the occurrence of arrhythmia through cardiomyocyte apoptosis, neural remodeling, and inhibited gap junction channels is unclear to date.

In this study, we investigated the relationship between the role of urolithin B and cardiomyocyte apoptosis, neural remodeling, and gap junction channels.

2. Investigations and Results

2.1. Ischemia Stimulates Cell Apoptosis and Alters Gap Junction and Neural Remodeling Levels of Cardiomyocyte In Vivo. To investigate the impact of ischemia on apoptosis, neural remodeling, and gap junction change in acute myocardial infarction tissues, we first examined the expression of apoptosis protein, neural remodeling protein, and gap junction protein in mouse myocardial infarction and normal heart samples. Western blotting results revealed that the expression of the apoptosis markers, bax and caspase-3, was substantially increased in myocardial infarction tissues compared with control tissues. By contrast, bcl2, an antiapoptotic marker, was lower than that in control tissues (Figures 1(a) and 1(b)). In addition, the suppressed gap junction protein connexin 43 (Cx43) was found in myocardial infarction tissues. Meanwhile, growth-associated protein-43 (GAP-43), a marker of nerve sprouting, and tyrosine hydroxylase (TH), a marker of the sympathetic nerve, were significantly elevated in myocardial infarction mice (Figures 1(c) and 1(d)). Taken together, these results showed that ischemia increased apoptosis and neural remodeling and downregulated gap junction of the cardiomyocyte in the myocardial infarction mice.

2.2. Hypoxia Stimulates Cardiomyocyte Apoptosis and Alters Gap Junction and Neural Remodeling Levels In Vitro. We further confirmed the effect of hypoxia on apoptosis protein, neural remodeling protein, and gap junction protein expression in cardiomyocytes. The TUNEL assay showed that hypoxia upregulated the apoptotic rate of cardiomyocytes compared with the control group (Figures 2(a) and 2(b)). Furthermore, the qRT-PCR and western blotting results suggested that the mRNA and protein expression of Bax, caspase-3, IL-6, TH, and GAP43 was increased in the hypoxia group, while the expression of bcl2 and CX43 was downregulated in the hypoxia group, compared with the control group (Figures 2(c)–2(o)).

2.3. Urolithin B Reduced Myocardial Apoptosis and Regulated Neural Remodeling and Gap Junction Channels. Previous work has demonstrated that urolithin B prevented cardiomyocytes from apoptosis caused by hypoxia [2]. We detected alterations in bcl2, bax, and caspase-3 and apoptotic rate of cardiomyocytes between the hypoxia group and the hypoxia+urolithin B group. The mRNA expression of bcl2 was markedly increased in the cardiomyocyte in the hypoxia+urolithin B group, while the expression of bax and caspase-3 was decreased in the hypoxia+urolithin B group (Figures 3(a)–3(c)). The protein expression patterns of bcl2, bax, and caspase-3 identified by western blotting were concordant with those of the qRT-PCR assay (Figures 3(d) and 3(e)). TUNEL staining suggested that the apoptotic rate of cardiomyocytes was dramatically downregulated in the urolithin B treatment group (Figures 3(f) and 3(g)). Previous research indicated that urolithin B retards the expression of the inflammatory cytokine IL-6 [9], which influences the expression of the gap junction protein Cx43 and neural remodeling proteins GAP-43 and TH [10, 11]. Therefore, we explored whether urolithin B regulates cardiomyocyte Cx43, GAP-43, and TH via IL-6. We determined the expression level of IL-6, Cx43, GAP-43, and TH by qRT-PCR. As expected, there was a substantial decrease in the mRNA expression of IL-6, GAP-43, and TH in the hypoxia+urolithin B group compared with the hypoxia group, while urolithin B significantly increased the level of Cx43 (Figures 3(h)–3(k)). Western blotting revealed that the expression trend of bcl2, bax, and caspase-3 proteins was consistent with qRT-PCR results. Based on these results, urolithin B reduced susceptibility of myocardial arrhythmia after hypoxia via suppressing cardiomyocyte apoptosis, inhibiting neural remodeling, and promoting gap junction channel expression.

2.4. Urolithin B Activates the Akt/mTOR Pathway to Inhibit Hypoxia-Induced Cardiomyocyte Apoptosis and Suppresses Nuclear Translocation of NF-κB to Facilitate Nerve Remodeling. To elucidate the underlying mechanisms of urolithin B on cardiomyocytes, we investigated the changes of the components of the apoptosis pathway by the western blotting assay. Zheng et al. identified that urolithin B attenuated cardiomyocyte apoptosis through the Akt/mTOR pathway under hypoxic conditions [2]. We found that urolithin B stimulation significantly increased the phosphorylation of Akt (S473) and mTOR (S2448) (Figures 4(a)–4(c)). Furthermore, urolithin B attenuated the expression of bax and caspase-3 proteins on cardiomyocytes, which was also blocked by an Akt inhibitor (Figures 4(d)–4(f)). Thus, our data suggested that urolithin B prevents cardiomyocyte apoptosis by regulating the Akt/mTOR pathway. Wang et al. revealed the nuclear factor-κB- (NF-κB-) dependent signal pathway involved in cardiac nerve remodeling after MI [12]. MI activated the NF-κB pathway and accelerated cardiac sympathetic hyperinnervation by GAP43 and TH [13]. The western blotting assay indicated that nuclear NF-κB was downregulated with urolithin B treatment. Moreover, nuclear IkBa levels were upregulated, which suggests that urolithin B suppressed nuclear translocation of NF-κB in an IkBa-dependent manner (Figures 4(g)–4(i)). The above results collectively suggest that urolithin B suppressed nuclear translocation of NF-κB to facilitate nerve remodeling and reduced susceptibility to myocardial arrhythmic predisposition.

3. Discussion

Our study demonstrated that urolithin B reduced susceptibility to myocardial arrhythmic predisposition after hypoxia, at least in part, via reduction of apoptosis, promotion of nerve remodeling, and inhibition of gap junction channels. In vitro studies showed that urolithin B treatment ameliorates myocardial hypoxia injury. Urolithin B alleviated cardiomyocyte apoptosis via activation of the Akt/mTOR pathway. Moreover, we further revealed that urolithin B suppressed nuclear translocation of NF-κB to facilitate nerve remodeling. Collectively, these findings suggested that urolithin B is a potential therapeutic for

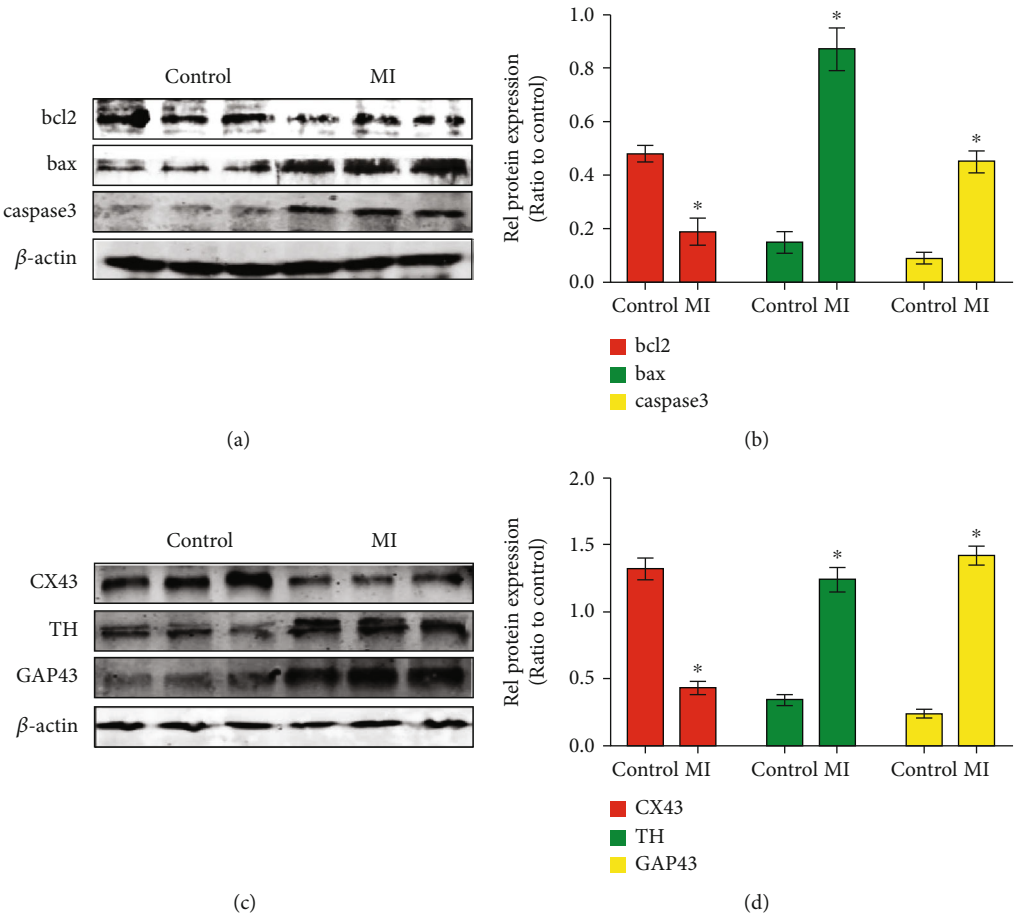

FIGURE 1: Ischemia stimulates cell apoptosis and alters gap junction and neural remodeling levels in vivo. (a, b) Western blotting and densitometric analysis of the protein levels of bcl2, bax, and caspase-3 in myocardial infarction tissues compared with control tissues. $^*p < 0.05$; $n = 5$ per group (Student's t-test). (c, d) Western blotting and densitometric analysis of the protein levels of CX43, TH, and GAP43 in myocardial infarction tissues compared with control tissues. $^*p < 0.05$; $n = 5$ per group (Student's t-test).

cardiac dysfunction and ventricular tachyarrhythmia following ischemic heart disease.

Myocardial apoptosis might be participating in the occurrence of tachyarrhythmia. In fact, Aime-Sempe et al. observed 50 right atrial myocardial specimens from patients with atrial fibrillation and found that most of the specimens had cardiomyocyte apoptosis [6]. Pathologically, apoptosis may cause arrhythmia in the following ways. Firstly, apoptosis contributed to the remodeling of cardiomyocytes, and the changes in the electrophysiological characteristics of the myocardial muscle triggered the frequent recurrence of the tachyarrhythmia. Secondly, in the process of apoptosis, the excitement of cardiomyocytes may increase and even form automatic rhythm points. When agitation reaches that point, anisotropic conduction occurs, which provides the basis for the anatomy of reentrant arrhythmia. The previous study indicated that urolithin B improved the cardiac function by preventing against cardiomyocyte apoptosis [2]. According to our study, we also confirmed that urolithin B inhibited cardiomyocyte apoptosis after hypoxia. Thus, urolithin B can effectively inhibit the formation of arrhythmias.

Cx43 is the predominant ventricular gap junction protein with the function of rapidly spreading and coordinating excitation signals for an effective heart contraction [14, 15]. Thus, it is critical for maintaining normal cardiac electrical conduction [16]. After MI, the reduced expression of Cx43 acts synergistically on conduction abnormalities and reentrant arrhythmias [17–19]. Roell et al. [20] reported that engraftment of Cx43-expressing cells can prevent postinfarct arrhythmia. On the contrary, Lerner et al. [21] demonstrated that in Cx43-defcient mice, the incidence of VAs increased markedly when the coronary artery was occluded. Sympathetic neural remodeling also accounts for the occurrence of arrhythmias after MI. It has been demonstrated that excessive sympathetic activity in the heart can directly lead to arrhythmias in both post-MI patients and animal models [22]. We verified that urolithin B retarded the secretion of inflammatory cytokine, such as IL-6 and TNF-α in our previous research [9]. The previous studies found that IL-6 might promote neural remodeling and inhibit gap junction channel expression [10, 11]. As expected, we observed that urolithin B promoted the expression of Cx43 and inhibited the expression

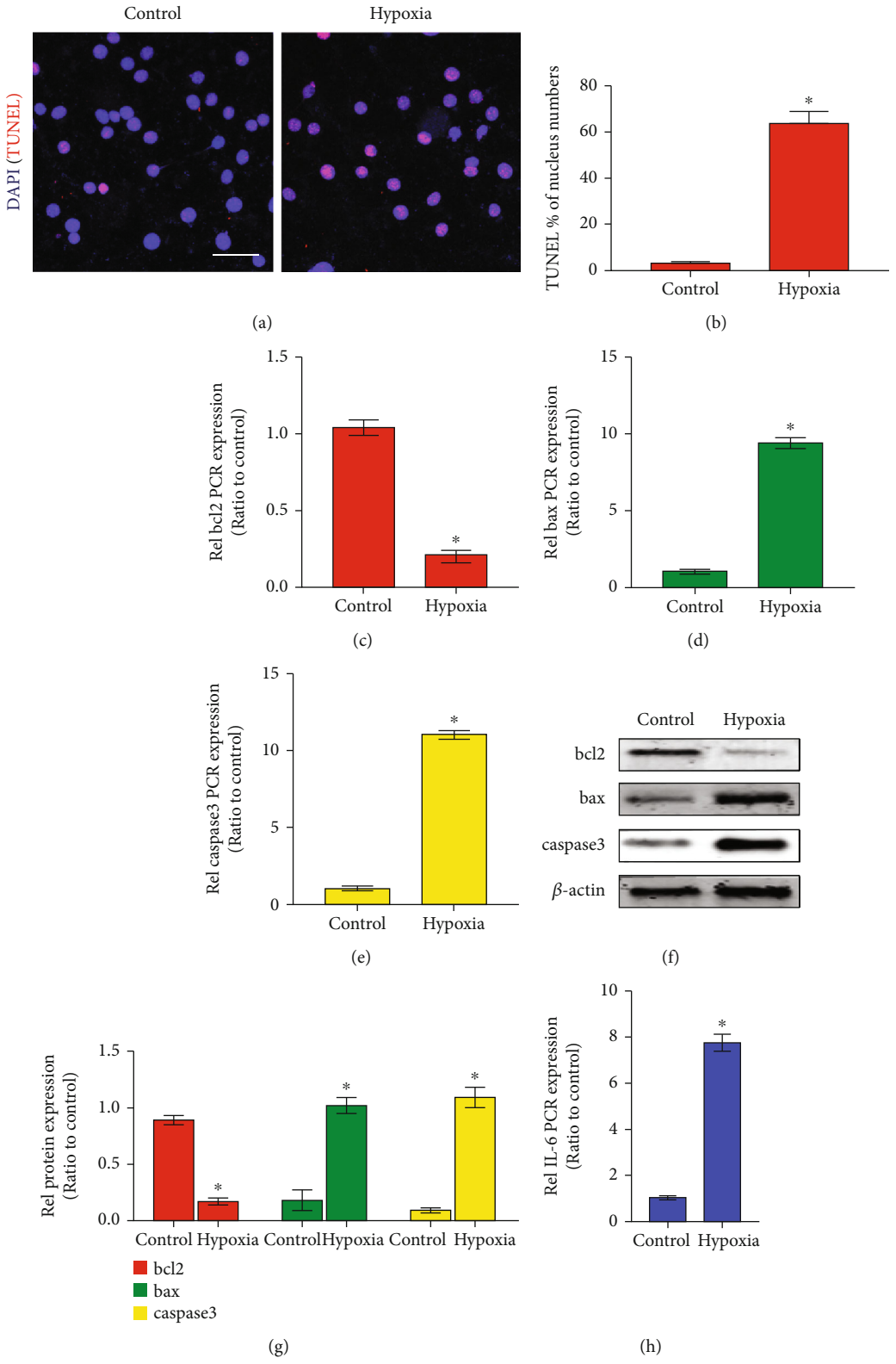

Figure 2: Continued.

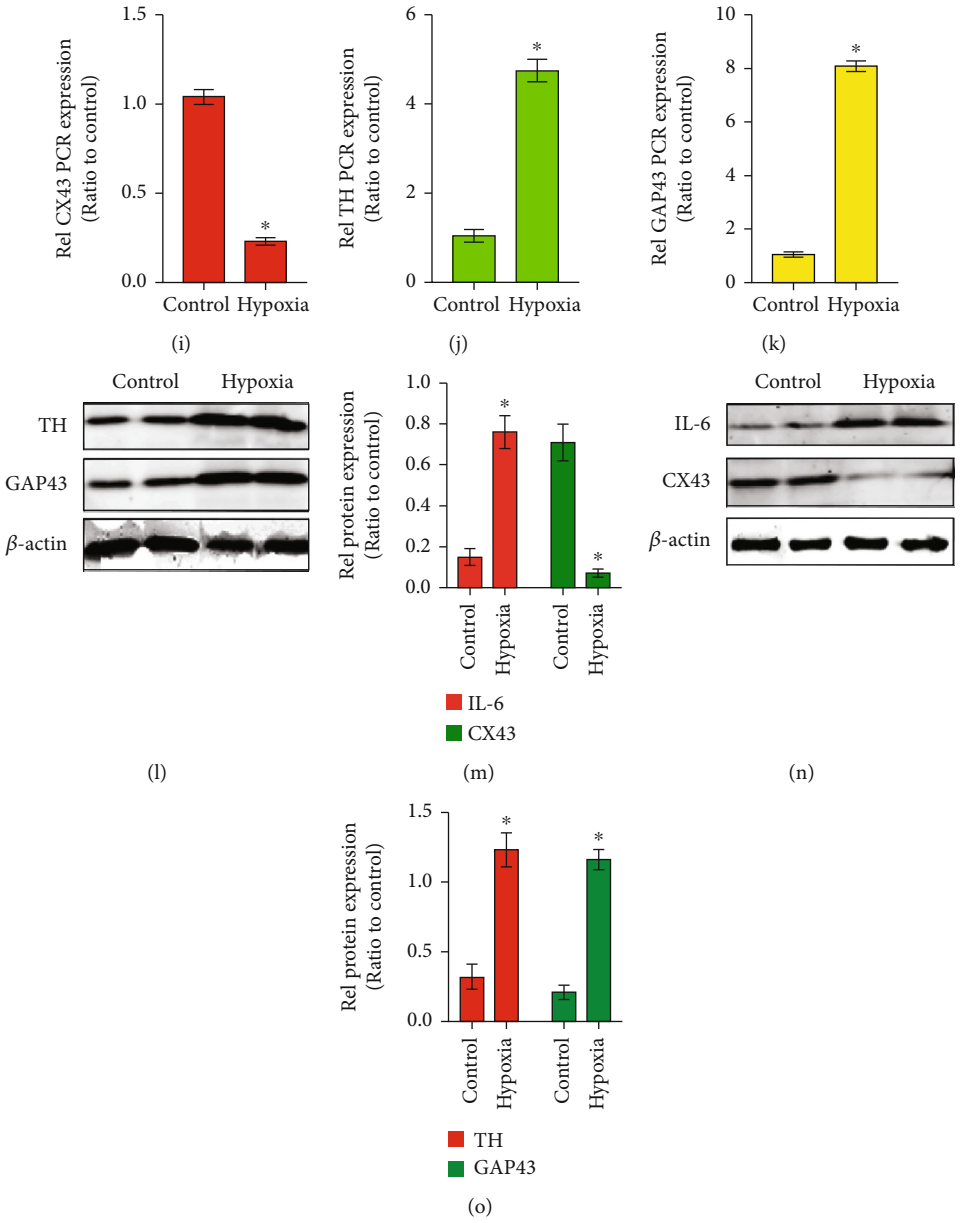

Figure 2: Hypoxia stimulates cardiomyocyte apoptosis and alters gap junction and neural remodeling levels in vitro. (a) TUNEL immunofluorescence staining in cardiomyocytes in the hypoxia group and control group (bar = 50 μm). (b) Quantification of the percentage of TUNEL-positive cardiomyocytes in the hypoxia group and control group. $^*p < 0.05$; $n = 5$ per group (Student's t-test). (c–e) Q-PCR assay detecting the expression levels of bcl2, bax, and caspase-3 in the hypoxia group and control group. (f) WB assay detecting the expression levels of bcl2, bax, and caspase-3 in the hypoxia group and control group. (g) Quantification of bcl2, bax, and caspase-3 protein levels. $^*p < 0.05$; $n = 5$ per group (Student's t-test). (h–k) Q-PCR assay detecting the expression levels of IL-6, CX43, TH, and GAP43 in the hypoxia group and control group. (l–o) Western blotting and densitometric analysis of the protein levels of IL-6, CX43, TH, and GAP43 in the hypoxia group and control group. $^*p < 0.05$; $n = 5$ per group (Student's t-test).

of GAP-43 and TH, markers of nerve remodeling. Therefore, inhibited cardiomyocyte apoptosis, deregulated nerve remodeling, and upregulated gap junction protein may be the primary reasons for UB to reduce susceptibility of arrhythmic predisposition post-MI.

The activated PI3K/Akt pathway, which is a major apoptosis signaling pathway, is involved in MI-induced cardiac dysfunction via affecting cardiomyocyte apoptosis. Cell apoptosis caused by activation of Akt was found in other disease models, including abdominal aortic aneurysm, atherosclerosis, and cardiac hypertrophy. Zheng et al. described that urolithin B protected cardiomyocytes against apoptosis [2]. In the present study, we verified that urolithin B reduced the apoptosis rate of cardiomyocytes, which agrees with other findings. NF-κB is considered to be the upstream of the inflammatory cascade and is involved in the inflammatory

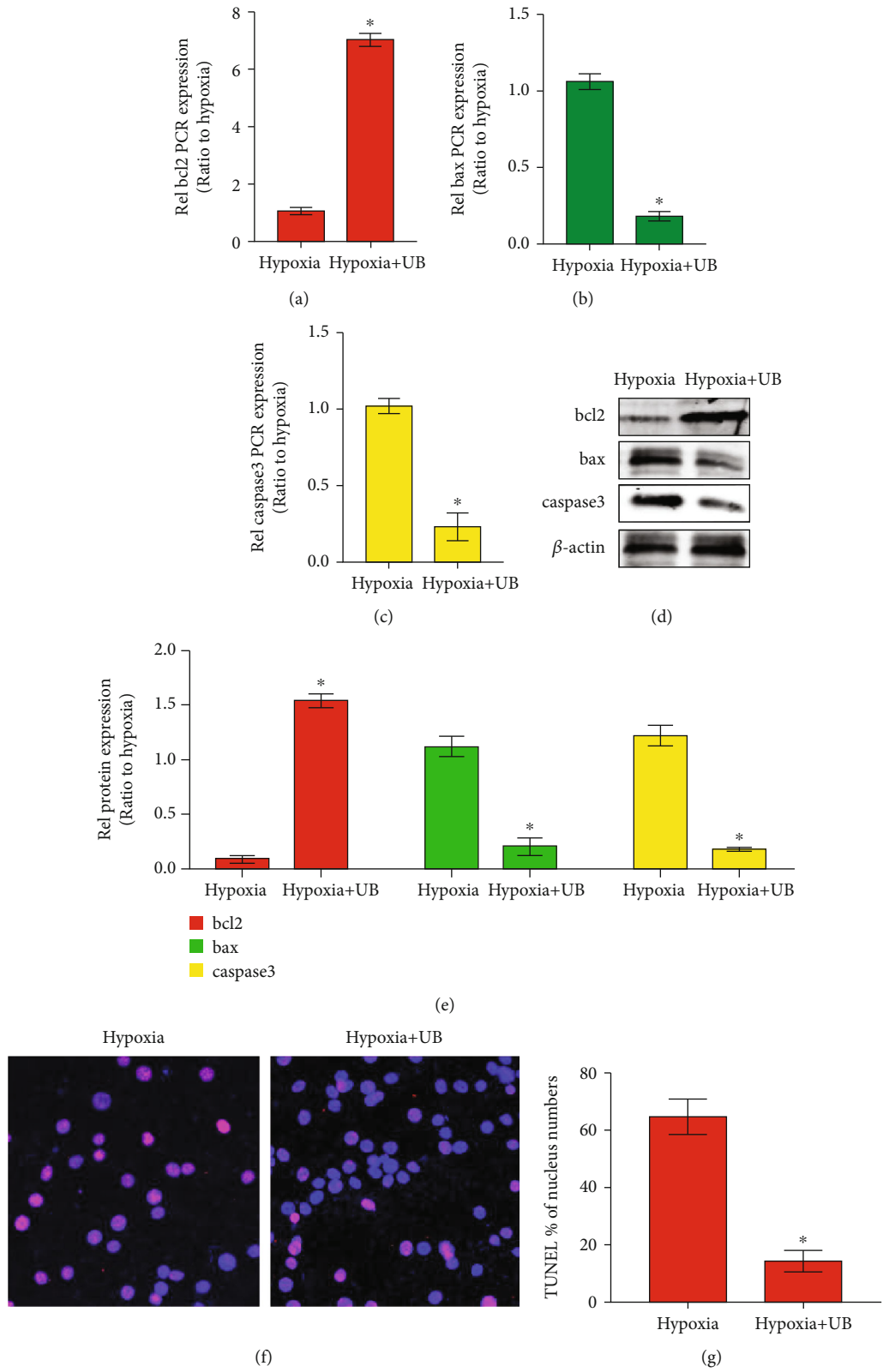

Figure 3: Continued.

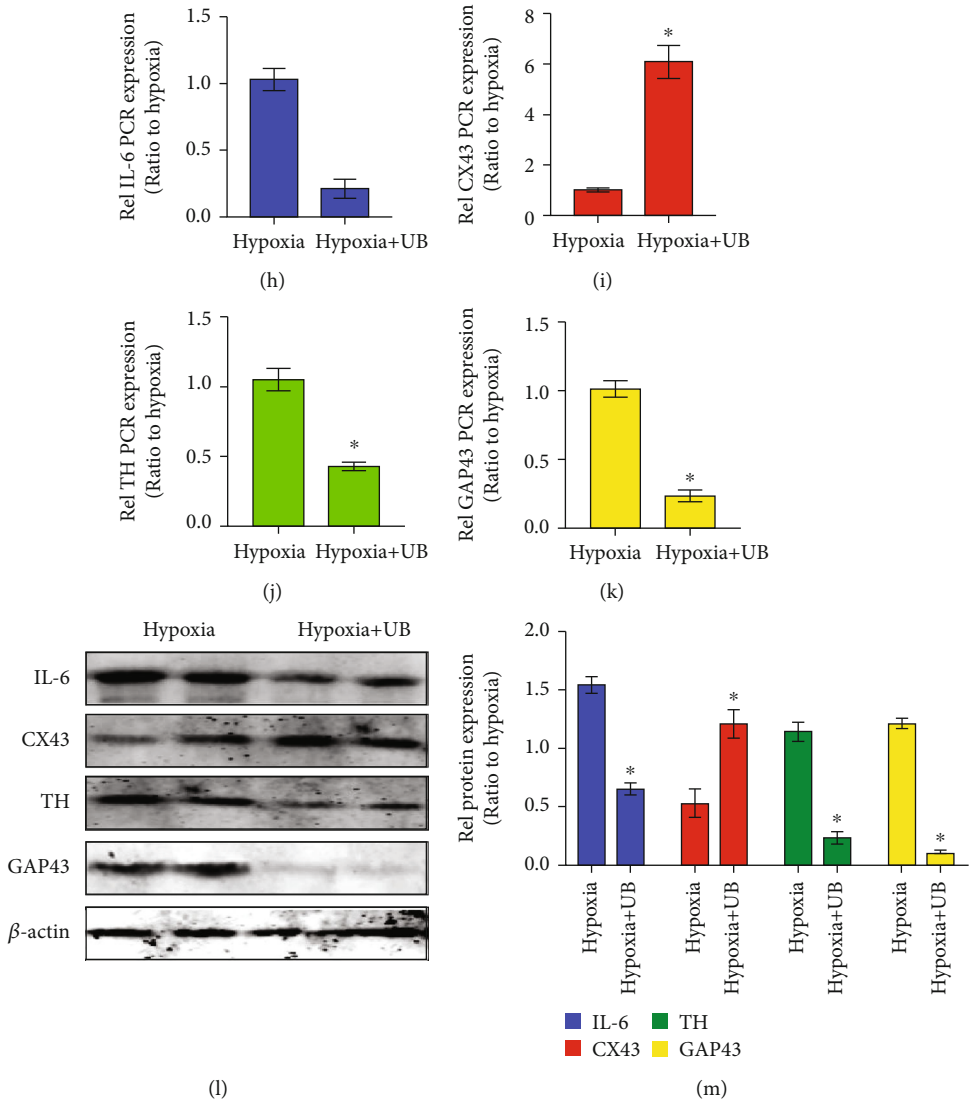

Figure 3: Urolithin B reduced myocardial apoptosis and regulated neural remodeling and gap junction channels. (a–c) Q-PCR assay detecting the expression levels of bcl2, bax, and caspase-3 in the hypoxia group and the hypoxia+urolithin B group. (d, e) WB assay detecting the expression levels of bcl2, bax, and caspase-3 in the hypoxia group and the hypoxia+urolithin B group. (f) TUNEL immunofluorescence staining in cardiomyocytes in the hypoxia group and the hypoxia+urolithin B group (bar = 50 μm). (g) Quantification of the percentage of TUNEL-positive cardiomyocytes in the hypoxia group and the hypoxia+urolithin B group. $^*p < 0.05$; $n = 5$ per group (Student's t-test). (h–k) Q-PCR assay detecting the expression levels of IL-6, CX43, TH, and GAP43 in the hypoxia group and the hypoxia+urolithin B group. (l, m) Western blotting and densitometric analysis of the protein levels of IL-6, CX43, TH, and GAP43 in the hypoxia group and control group. $^*p < 0.05$; $n = 5$ per group (Student's t-test).

response in various cardiac diseases, including MI [12]. Excess inflammatory response is responsible for cardiac nerve sprouting [12]. Previous studies revealed the nuclear NF-κB signal pathway involved in cardiac nerve remodeling after MI [12]. We preliminarily demonstrated that urolithin B treatment induced the downregulation of proinflammatory cytokine, such as TNF-α and IL-6, at mRNA and protein levels [9]. Thus, the treatment of urolithin B was closely associated with MI-induced sympathetic nerve sprouting.

We achieved the primary goal of our study; nevertheless, there are still some limitations of our study. Firstly, we did not assess the role of urolithin B in vivo, which may hinder further research on the specific mechanism of urolithin B or limit its application. Secondly, we previously reported that urolithin B suppressed myocardial fibrosis and retarded ventricular tachyarrhythmia, but we are not studying the relationship between ventricular gap junction channel and myocardial fibrosis. Thirdly, cell necrosis, necroptosis, and other potential types of cell death may be more related to arrhythmia after myocardial infarction, which was ruled out from the scenario.

To sum up, our results revealed that urolithin B suppresses cardiomyocyte apoptosis and alters gap junction and neural remodeling levels with MI. Mechanistically, the Akt/mTOR pathway and nuclear translocation of NF-κB were investigated

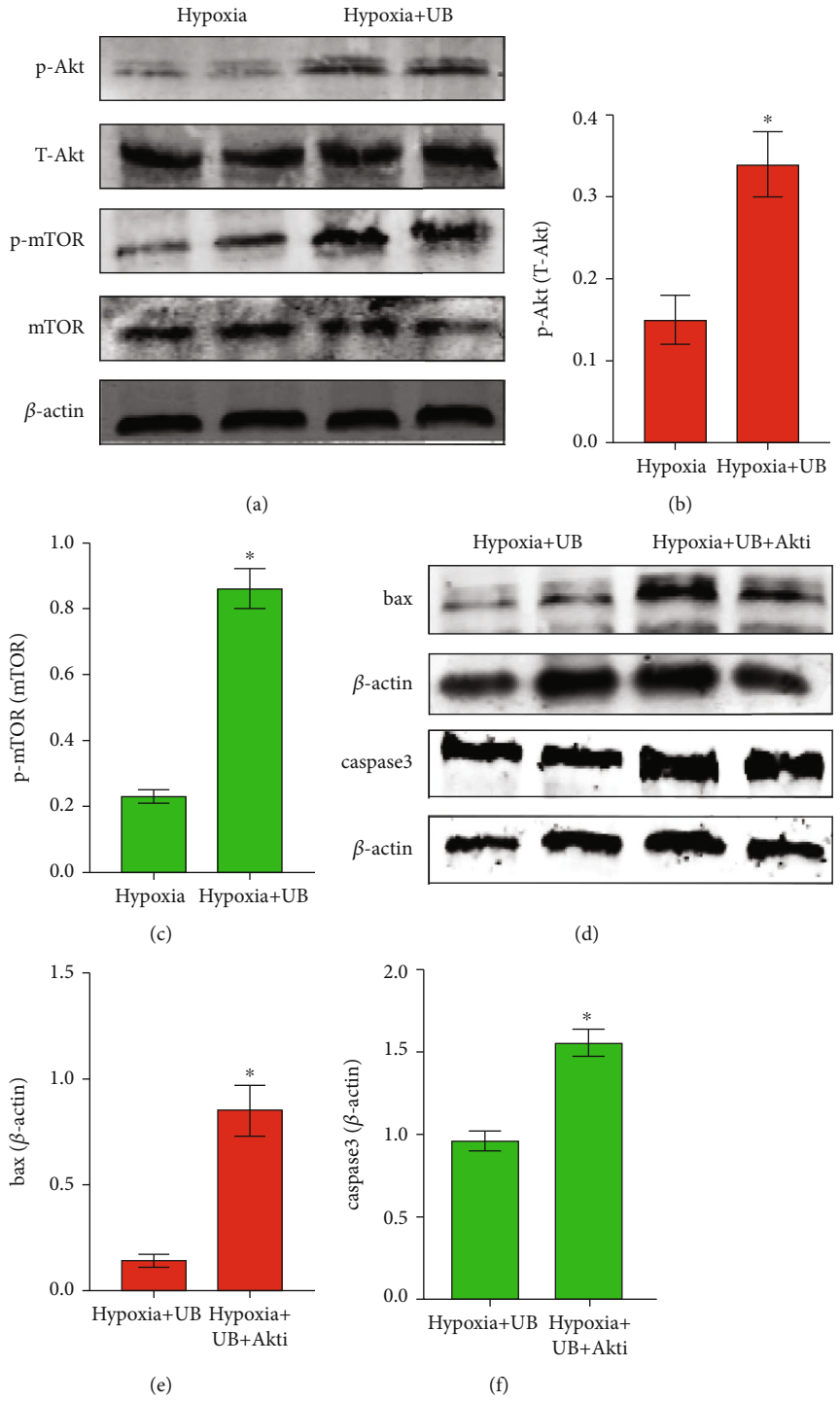

Figure 4: Continued.

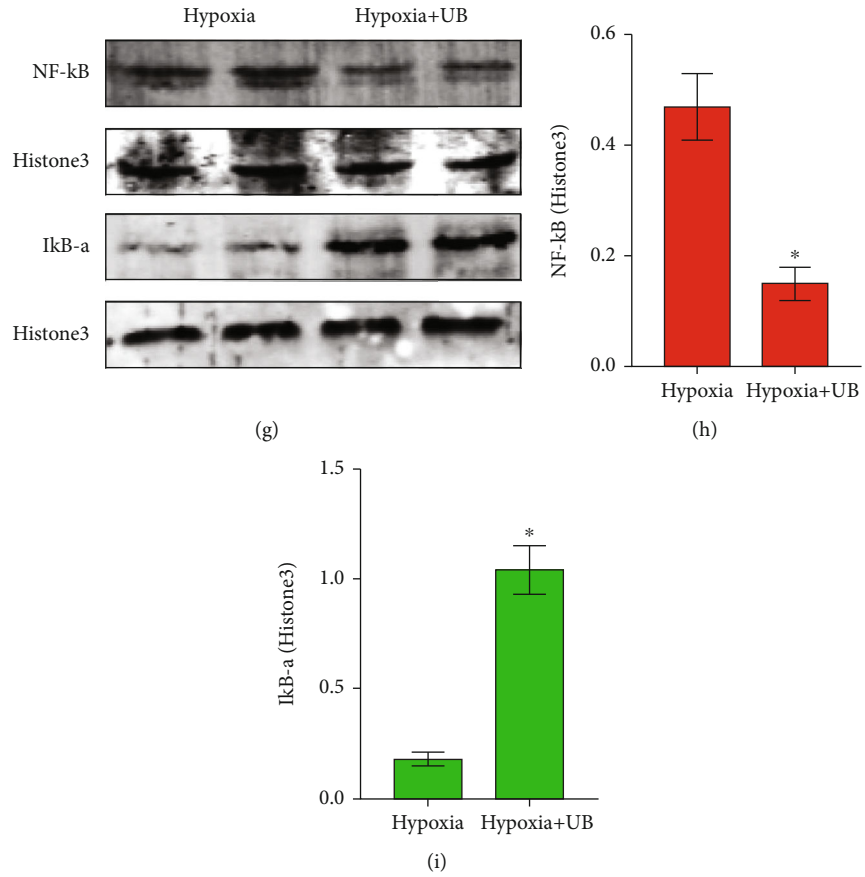

Figure 4: Urolithin B activates the PI3K/Akt pathway to inhibit hypoxia-induced cardiomyocyte apoptosis and suppressed nuclear translocation of NF-κB to facilitate nerve remodeling. (a–c) Western blotting results and densitometric analysis of p-Akt, T-Akt, p-mTOR, and T-mTOR protein levels in the hypoxia group and the hypoxia+urolithin B group. $^*p < 0.05$; $n = 5$ per group (Student's t-test). (d–f) Western blotting results and densitometric analysis of bax and caspase-3 protein levels in the hypoxia+urolithin B and hypoxia+urolithin B+Akti group. $^*p < 0.05$; $n = 5$ per group (Student's t-test). (g–i) Western blotting results and densitometric analysis of NF-κB and IkBa protein levels in the hypoxia group and the hypoxia+urolithin B group. $^*p < 0.05$; $n = 5$ per group (Student's t-test).

to contribute to the protective effect of urolithin B against cardiomyocyte hypoxia. These results highlight the potential of urolithin B to be used as adjuvant therapy for myocardial infarction.

4. Materials and Methods

4.1. Myocardial Infarction Model Establishment. C57BL/6 mice were obtained from the Laboratory Animal Center of Nanchang University. All animal experiments were approved by the Animal Research Committee of Nanchang University and performed in accordance with the National Institutes of Health Guide for the Care and Use of Laboratory Animals (no. 2016-0074). Briefly, adult male mice (56-70 days old) were anesthetized by an intraperitoneal injection of 3% pentobarbital sodium (40 mg/kg). The left anterior descending (LAD) coronary artery was ligated with a silk suture, 1 mm from the ascending aorta. In sham-operated animals, an analogous surgical operation was performed without occlusion of the LAD. All mice were sacrificed by cervical dislocation at the indicated time points [13].

4.2. Cell Culture, Hypoxia Model, and Chemical Treatment. Cardiomyocytes for the in vitro experiments were isolated from D1 C57BL/6 mice. Neonatal mice were anesthetized using 2% inhaled isoflurane. Isolation and culture of ventricular cardiomyocytes were performed as previously described [13]. Cells were cultured in serum-free, glucose-free, and sodium pyruvate-free Dulbecco's modified Eagle's medium (Invitrogen, Carlsbad, CA) and cultured in an anoxia chamber (In Vivo 500; Ruskinn Life Science) under hypoxia (94% N_2/5% CO_2/1% O_2) for 3 h. Pretreatment with urolithin B (Sigma, US) was performed as described previously [2].

4.3. Quantitative Real-Time Reverse Transcription PCR (qRT-PCR). The TRIzol reagent (Invitrogen) was used to extract total RNA, and complementary DNAs (cDNAs) were synthesized using the PrimeScript RT Reagent Kit (Takara, Otsu, Japan). RT-PCR was performed in a 20 μl reaction system and analyzed by using a SYBR Green RT-PCR Kit (Takara Biotechnology) with the LightCycler 480 II system (Roche Diagnostics, Basel, Switzerland). Glyceraldehyde-3-phosphate-dehydrogenase (GAPDH) mRNA was used as controls. The following primer sequences were used (5′-3′): bcl2 forward: 5′-CTTCGCCGA

GATGTCCAG-3′ and reverse: 5′-GGCTCAGATAGGCA CCC-A-3′; bax forward: 5′-CCCACCAGCTCTGAACAGT TC-3′ and reverse: 5′-CCAGCCACAAAGATGGTCAC-3′; caspase-3 forward: 5′-CTGAAGGCTCCTGG-TTTA-3′ and reverse: 5′-TGCCACTCTGCGATTTAC-3′; IL-6 forward: 5′-ACTCCATCTGCCCTTCA-3′ and reverse: 5′-ACTCCATCT GCCCTTCA-3′; CX43 forward: 5′-GAGTTTGCCTAAGG CGCT-C-3′ and reverse: 5′-AGGAGTTCA-ATCACTTGG CG-3′; TH forward: 5′-GCGATCAGGCCCAAGATGTA-3′ and reverse: 5′-AATGTATCGAGCCAGGTC-3′; GAP43 forward: 5′-AACGGAGACTG-CAGAAAGC-3′ and reverse: 5′-CCTTAGGTTTGGCTTCGTCT-3′; and GAPDH forward: 5′-TTCAATGGCACAGTCAAGGC-3′ and reverse: 5′-TCAC CCCATTT-GATGTTAGCG-3′. Primers were designed using Primer Express® software (Thermo Fisher Scientific, Frankfurter, Germany) with nucleotide sequences obtained from the GenBank database.

4.4. Western Blot Analysis. Protein was extracted from cardiomyocytes using lysis buffer containing protease inhibitors and a protein phosphatase inhibitor. Protein concentrations were determined with a bicinchoninic acid (BCA) protein assay kit (Pierce; Rockford, IL, USA). Protein was denatured at 100°C for 10 min. Equal quantities of protein extracts (50 μg) were separated using 10% SDS-PAGE gel and transferred onto a nitrocellulose membrane. Membranes were further probed with primary antibodies against phosphorylated (p)-Akt (1 : 1000; CST #4060), total (t)-Akt (1 : 1000; CST #9272), phosphorylated (p)-mTOR (1 : 1000; CST #5536), total (t)-mTOR (1 : 1000; CST #2972), bcl2 (1 : 1000; CST #3498), bax (1 : 1000; CST #5023), caspase-3 (1 : 1000; CST #14220), Cx43 (1 : 1000; CST #3512), GAP-43 (1 : 1000; CST #8945), TH (1 : 1000; CST #2792), IL-6 (1 : 1000; Abcam #ab233706)), NF-κB (1 : 1000; CST #8242), IkBa (1 : 1000, CST #4812), and β-actin (1 : 1000, CST #4970) at 4°C overnight. Then, membranes were incubated with an HRP-labeled secondary antibody in blocking buffer. Bands were detected using an enhanced electrochemiluminescence (ECL) detection kit. Finally, the density of proteins was analyzed using ImageJ software and normalized to β-actin.

4.5. TUNEL Immunofluorescence Staining. Cardiomyocytes were stimulated with hypoxia or stimulated with hypoxia followed by urolithin B. Then, the cells were fixed with formalin for 1 hour, and apoptotic cells were labeled with a TUNEL kit. Nuclei were stained with DAPI (Millipore, Beverly, MA, USA). The rate of apoptotic cells (positive TUNEL staining cells/DAPI staining cells) in the hypoxia+urolithin B group was compared with that in the hypoxia group. Images were captured under Leica TCS SP8 fluorescence confocal microscopy for further analysis.

4.6. Statistical Analysis. All data were analyzed with the statistical software GraphPad Prism 5.0 (GraphPad Software Inc.) and expressed as means ± SEM. The normal distribution was confirmed by the Shapiro-Wilk test ($p > 0.1$) with SPSS 17.0. The differences between each group were analyzed using one-way ANOVA. $p < 0.05$ was considered statistically significant. Further, the Tukey post hoc analysis ($\alpha = 0.05$) was done to confirm where the differences occurred between groups.

Data Availability

We have not used any publicly archived datasets.

Conflicts of Interest

The authors declare that there are no conflicts of interest regarding this study.

Authors' Contributions

Xin Huang conducted the experiments. Hong Gao and Zeqi Zheng wrote the manuscript. Xiaojie Jiang was responsible for the experimental design and data acquisition. All the authors take full responsibility for the work.

References

[1] G. A. Roth, C. Johnson, A. Abajobir et al., "Global, regional, and national burden of cardiovascular diseases for 10 causes, 1990 to 2015," *Journal of the American College of Cardiology*, vol. 70, pp. 1–25, 2017.

[2] D. Zheng, Z. Liu, Y. Zhou et al., "Urolithin B, a gut microbiota metabolite, protects against myocardial ischemia/reperfusion injury _via_ p62/Keap1/Nrf2 signaling pathway," *Pharmacological Research*, vol. 153, article 104655, 2020.

[3] W. Jiang, C. Chen, J. Huo et al., "Comparison between renal denervation and metoprolol on the susceptibility of ventricular arrhythmias in rats with myocardial infarction," *Scientific Reports*, vol. 8, p. 10206, 2018.

[4] K. Fukuda, H. Kanazawa, Y. Aizawa, J. L. Ardell, and K. Shivkumar, "Cardiac innervation and sudden cardiac death," *Circulation Research*, vol. 116, pp. 2005–2019, 2015.

[5] X. Liu, L. Sun, J. Chen et al., "Effects of local cardiac denervation on cardiac innervation and ventricular arrhythmia after chronic myocardial infarction," *PLoS One*, vol. 12, article e0181322, 2017.

[6] C. Aime-Sempe, T. Folliguet, C. Rucker-Martin et al., "Myocardial cell death in fibrillating and dilated human right atria," *Journal of the American College of Cardiology*, vol. 34, no. 5, pp. 1577–1586, 1999.

[7] P. Dey, "Gut microbiota in phytopharmacology: a comprehensive overview of concepts, reciprocal interactions, biotransformations and mode of actions," *Pharmacological Research*, vol. 147, article ???, 2019.

[8] F. A. Tomas-Barberan, A. Gonzalez-Sarrias, R. Garcia-Villalba et al., "Urolithins, the rescue of "old" metabolites to understand a "new" concept: metabotypes as a nexus among phenolic metabolism, microbiota dysbiosis, and host health status," *Molecular nutrition & food research*, vol. 61, 2017.

[9] H. Gao, X. Huang, Y. Tong, and X. Jiang, "Urolithin B improves cardiac function and reduces susceptibility to ventricular arrhythmias in rats after myocardial infarction," *European Journal of Pharmacology*, vol. 871, article ???, 2020.

[10] D. Hakkoum, L. Stoppini, and D. Muller, "Interleukin-6 promotes sprouting and functional recovery in lesioned organotypic hippocampal slice cultures," *Journal of Neurochemistry*, vol. 100, pp. 747–757, 2007.

[11] P. E. Lazzerini, F. Laghi-Pasini, M. Acampa et al., "Systemic inflammation rapidly induces reversible atrial electrical remodeling: the role of interleukin-6-mediated changes in connexin expression," *Journal of the American Heart Association*, vol. 8, no. 16, article e011006, 2019.

[12] Y. Wang, F. Suo, J. Liu et al., "Myocardial infarction induces sympathetic hyperinnervation via a nuclear factor-κB-dependent pathway in rabbit hearts," *Neuroscience Letters*, vol. 535, pp. 128–133, 2013.

[13] X. Si, H. Zheng, G. Wei et al., "circRNA Hipk3 induces cardiac regeneration after myocardial infarction in mice by binding to Notch1 and miR-133a," *Molecular Therapy–Nucleic Acids*, vol. 21, pp. 636–655, 2020.

[14] D. Garcia-Dorado, A. Rodriguez-Sinovas, and M. Ruiz-Meana, "Gap junction-mediated spread of cell injury and death during myocardial ischemia-reperfusion," *Cardiovascular Research*, vol. 61, no. 3, pp. 386–401, 2004.

[15] W. H. Litchenberg, L. W. Norman, A. K. Holwell, K. L. Martin, K. W. Hewett, and R. G. Gourdie, "The rate and anisotropy of impulse propagation in the postnatal terminal crest are correlated with remodeling of Cx43 gap junction pattern," *Cardiovascular Research*, vol. 45, no. 2, pp. 379–387, 2000.

[16] M. Menk, L. Giebelhauser, G. Vorderwulbecke et al., "Nucleated red blood cells as predictors of mortality in patients with acute respiratory distress syndrome (ARDS): an observational study," *Annals of Intensive Care*, vol. 8, p. 42, 2018.

[17] D. Adesse, R. C. Goldenberg, F. S. Fortes et al., "Gap junctions and Chagas disease," *Advances in Parasitology*, vol. 76, pp. 63–81, 2011.

[18] J. Gomes, M. Finlay, A. K. Ahmed et al., "Electrophysiological abnormalities precede overt structural changes in arrhythmogenic right ventricular cardiomyopathy due to mutations in desmoplakin-A combined murine and human study," *European Heart Journal*, vol. 33, pp. 1942–1953, 2012.

[19] E. Pervolaraki, J. Dachtler, R. A. Anderson, and A. V. Holden, "Ventricular myocardium development and the role of connexins in the human fetal heart," *Scientific Reports*, vol. 7, p. 12272, 2017.

[20] W. Roell, T. Lewalter, P. Sasse et al., "Engraftment of connexin 43-expressing cells prevents post-infarct arrhythmia," *Nature*, vol. 450, pp. 819–824, 2007.

[21] D. L. Lerner, K. A. Yamada, R. B. Schuessler, and J. E. Saffitz, "Accelerated onset and increased incidence of ventricular arrhythmias induced by ischemia in Cx43-deficient mice," *Circulation*, vol. 101, pp. 547–552, 2000.

[22] H. Jiang, X. Hu, Z. Lu et al., "Effects of sympathetic nerve stimulation on ischemia-induced ventricular arrhythmias by modulating connexin43 in rats," *Archives of Medical Research*, vol. 39, pp. 647–654, 2008.

Hindawi
Disease Markers
Volume 2022, Article ID 9309444, 12 pages
https://doi.org/10.1155/2022/9309444

Research Article

Changes of Electrocardiogram and Myocardial Enzymes in Patients with Intracerebral Hemorrhage

Guannan Qin,[1,2] Chuanyang Dai,[2] Shuang Feng,[3] and Guofeng Wu[2]

[1]*Guizhou Medical University, Guian New Area University Town, Guizhou Province 550025, China*
[2]*Emergency Department, Guizhou Province, The Affiliated Hospital of Guizhou Medical University, No. 28, Guiyijie Road, Liuguangmen, Guiyang City 550004, China*
[3]*Emergency Department, Shandong Province, Zibo Central Hospital, No. 54, Gongqingtuan West Road, Zhangdian District, Zibo City 255020, China*

Correspondence should be addressed to Guofeng Wu; wuguofeng3013@sina.com

Received 22 December 2021; Revised 17 January 2022; Accepted 18 January 2022; Published 1 February 2022

Academic Editor: XIANWEI ZENG

Purpose. Cardiac complications are common in patients with spontaneous intracerebral hemorrhage (ICH). The present study is aimed at observing the incidence of cardiac complications after ICH, so as at improving the understanding of the relationship between cardiac complications and ICH. *Methods*. This is a retrospective study on analyzing electrocardiogram (ECG) and serum myocardial enzyme of 208 patients with ICH admitted to a tertiary hospital from 2018 to 2019. For each patient, demographics, medical history, clinical presentation, ECG, serum myocardial enzyme, and head CT on admission were reviewed. Mortality was noted. *Results*. Among the 208 patients, 145 (69.71%) had one or more ECG abnormalities. The top three abnormalities were corrected QT interval (QTc) prolongation 52 (25%), ST depression 48 (23.08%), and T wave inversion 38 (18.27%). One hundred and thirty-nine patients (66.83%) had increased serum levels of at least one kind of myocardial enzyme, which were high-sensitive cardiac troponin T (hs-cTnT) 79 (37.98%), lactic dehydrogenase (LDH) 80 (38.46%), creatine kinase (CK) 57 (27.40%), and creatine kinase-myocardial subfraction (CKMB) 57 (27.40%). The logistic regression analysis showed the following: secondary intraventricular hemorrhage (SIVH) (odds ratio (OR) 5.32; 95% confidence interval (CI) 2.55–11.08; $p < 0.001$) and hematoma volume > 30 ml (OR 3.81; 95% CI 1.86–7.81; $p < 0.001$) were independent predictive factors of QTc prolongation; thalamus location (OR 5.79; 95% CI 1.94–17.28; $p < 0.05$), hematoma volume > 30 ml (OR 24.187; 95% CI 3.14-186.33; $p < 0.05$), insular involvement (OR 19.08; 95% CI 5.77-63.07; $p < 0.001$), and SIVH (OR 2.62; 95% CI 1.69-5.86; $p < 0.05$) were independent predictive factors of ST depression; insular involvement (OR 2.90; 95% CI 1.12–7.50; $p < 0.05$) and hematoma volume > 30 ml (OR 1.98; 95% CI 1.06–3.70; $p < 0.05$) were independent predictive factors of increase of CK; Glasgow Coma Scale (GCS) (OR 0.86; 95% CI 0.78–0.98; $p < 0.05$) and insular involvement (OR 5.56; 95% CI 1.98–15.62; $p < 0.05$) were independent predictive factors of increase of CKMB; SIVH (OR 2.05; 95% CI 1.07–3.92; $p < 0.05$) was independent predictive factor of increase of LDH; age (OR 1.03; 95% CI 1.01–1.06; $p < 0.05$), blood glucose on admission (OR 1.10; 95% CI 1.01–1.20; $p < 0.05$), and history of antiplatelet drug use (OR 3.50; 95% CI 1.01–12.12; $p < 0.05$) were independent predictive factors of hs-cTnT. All the injury indexes were not related to in-hospital mortality. *Conclusion*. The study suggests that insular involvement, hematoma volume > 30 ml, and SIVH are the strongest risk factors for ECG abnormalities and elevated myocardial enzymes after ICH followed which are the risk factors such as GCS, age, admission blood glucose, and ICH location in the thalamus.

1. Introduction

Despite advances in stroke care management, spontaneous intracerebral hemorrhage (ICH) is still a kind of serious stroke with high morbidity and mortality [1]. Secondary systemic complications are common and largely affect the outcomes of patients with ICH [2]. It is extremely important to identify and manage complications associated with clinical outcomes after ICH.

In fact, cardiac complications are frequently found in patients with acute stroke. Relevant studies mainly focused on ischemic stroke and subarachnoid hemorrhage, but few studies are on ICH [3, 4]. A study has shown that cardiac complications may occur in 1% to 4% of patients with ICH [5]. Markers of myocardial injury in the complications, such as myocardial markers and electrocardiogram (ECG), are associated with prognosis in patients with ICH [6, 7]. It is reported that ECG abnormalities after ICH are very common (56%-81%) [8, 9], which includes prolonged corrected QT (QTc) interval, ST-T changes, arrhythmias, and atrioventricular nodal blocks [10]. The most common cardiac biomarker in patients with ICH is troponin I [11]. The 2015 American Heart Association/American Stroke Association ICH guidelines recommend cardiac workup of patients with spontaneous ICH, including both ECG and cardiac troponin, to assess active coronary ischemia and concomitant myocardial injury [12].

However, little is known about the relationship between these markers and various characteristics of ICH [13]. Therefore, we investigated the prevalence of myocardial injury in patients with ICH and the possible associations with clinical and radiological findings. Our study aimed at improving the understanding of the possible association between myocardial injury and clinical characteristics in patients with ICH. Furthermore, it could be also helpful to identify high-risk patients and predict possible adverse events.

2. Materials and Methods

2.1. Patients. Ethics approval was obtained from the local institutional review board (NO. S2017-02). Because it was a retrospective study, no written informed consent was required. Between 2018 and 2019, 274 patients with spontaneous ICH were admitted to the Emergency Neurology Department, Guizhou Medical University. General inclusion criteria contained spontaneous ICH confirmed by computed tomography (CT) scan, with the age being older than 18 years. Exclusion criteria were CT angiography (CTA) or magnetic resonance angiography (MRA) diagnosis of ICH due to brain tumor or vascular abnormalities, insufficient clinical data, ECG recordings, and serum myocardial enzyme on admission. Sixty-six patients were excluded due to brain tumor ($N = 4$), vascular abnormalities ($N = 8$), insufficient clinical data ($N = 22$), and lack of ECG recordings or serum myocardial enzyme ($N = 32$). Therefore, the subjects of the study included 208 patients in total (Figure 1).

2.2. Data Collection. The data were retrospectively analyzed to determine such clinical characteristics of the patients as age, sex, medical history, time of onset at admission, Glasgow Coma Scale (GCS), location of hematoma, side of hematoma, presence of insular involvement, secondary intraventricular hemorrhage (SIVH), hematoma volume, blood tests (hemoglobin, platelet, white cell, and coagulation level), ECG findings, and level of serum myocardial enzyme. The location of hematoma was classified into basal ganglia, lobar, thalamus, cerebellum, brain stem, and primary intraventricular hemorrhage (PIVH). Hematoma volume was measured through the ABC/2 method. Within 1 hour after admission, laboratory tests (blood tests, ECG, etc.) were performed for all involved patients. Mortality during hospitalization was reviewed.

2.3. ECG Analyses. ECG (12-lead) recordings were collected on admission before treatment at a paper speed of 25 millimeters per second, with an amplitude calibration of 10 millimeters per millivolt, and were analyzed by the same attending cardiologist, who did not know the details of the patients. Abnormalities of ECG are judged by the following criteria [6]: (a) rhythm: sinus rhythm, atrial fibrillation, or ectopic beats; (b) heart rate: sinus bradycardia (<60 beats/minute) and sinus tachycardia (>100 beats/min); (c) PR interval: short <0.12 seconds and prolonged >0.2 seconds; (d) QRS complex width: prolonged >0.12 seconds; (e) corrected QT interval (QTc) (using the Bazett formula): prolonged at >0.45 seconds in females and >0.44 seconds in males; (f) ST segment depression: downsloping or horizontal > 0.05 millivolts; (g) ST segment elevation: convexity of the ST segment upward > 0.1 millivolts; and (h) T wave inversion: negative T wave of ≥1 millimeters in depth in two or more contiguous leads, with exclusion of leads aVR, III, and V1.

2.4. The Analysis of Serum Myocardial Enzyme. The elevation standard of myocardial enzyme is judged according to the reference range of our hospital's laboratory: (a) high creatine kinase (CK) value: >198 U/l; (b) high creatine kinase-myocardial subfraction (CKMB) value: >25 U/l; (c) high lactic dehydrogenase (LDH) value: >250 U/l; and (d) high-sensitive cardiac troponin T (hs-cTnT) value: >0.014 ng/ml.

2.5. Other Blood Tests. The standards for these tests also followed the hospital's laboratory criteria: (a) leukocytosis: white blood cell count $> 10 \times 10^9$/l; (b) low platelet count: platelet count $< 100 \times 10^9$/l; (c) abnormal hemoglobin level: hemoglobin levels up or down; and (d) coagulation abnormalities: one or more of the terms of prothrombin time (PT), activated partial thromboplastin time (APTT), international normalized ratio (INR), and D-dimer and fibrinogen up or down.

2.6. Statistical Analysis. The descriptive statistics are expressed as the mean ± standard deviation (SD) or medians with interquartile ranges (IQR) for the continuous variables, while the categorical variables are expressed as percentages, as appropriate. Univariate analysis was used to determine the possible relationships between each ECG abnormality and clinical features, as well as each elevated serum myocardial enzyme and clinical features, by means of either the chi-square test or Fisher's exact test. If an ECG abnormality was observed in more than 10% of patients, it was analyzed.

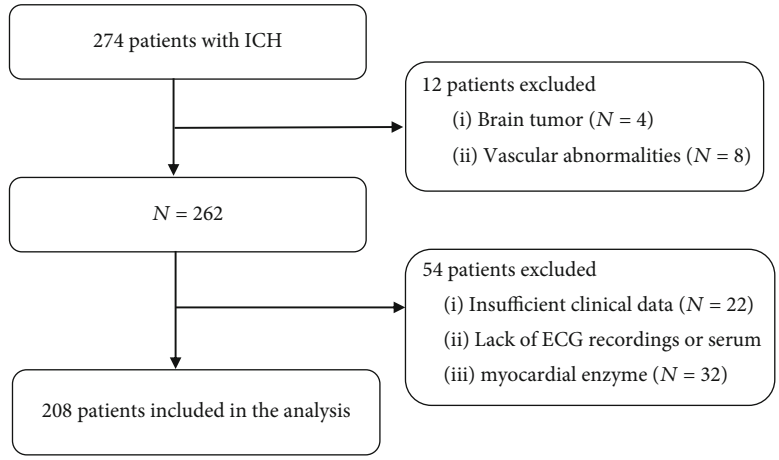

Figure 1: Research flow chart.

The relationship between in-hospital mortality and markers of cardiac injury, including ECG abnormalities observed in more than 10% of patients and serum myocardial enzymes, was also analyzed using the methods mentioned above.

The analysis of multivariate logistic regression was used to determine the independent correlation factors with ECG abnormalities and elevated serum myocardial enzymes and mortality. The variables with a significant level of $p < 0.05$ in the univariate analysis were included as independent variables in the logistic regression analyses. Only those variables with $p < 0.05$ in two-tailed tests were retained within the model. Odds ratios (OR) and 95% confidence intervals (CI) were reported. A value of $p < 0.05$ was regarded as statistical significance. All statistical analysis was conducted by virtue of SPSS (version 22.0; IBM Corporation, Armonk, NY, USA).

3. Results

The results of the clinical information, level of myocardial enzyme, and imaging findings of 208 patients with ICH are summarized in Table 1. There were 136 males (65.38%) and 72 females, with a mean age of 61.23 years (range: 29-93). The GCS was ≤8 in 60 cases (28.85%). Past history included hypertension in 140 cases (67.31%), type 2 diabetes in 16 (7.69%), cerebrovascular diseases in 32 (15.38%), coronary heart disease in 11 (5.29%), smoking history in 76 (36.54%), drinking history in 45 (21.63%), history of antiplatelet drug use in 14 (6.73%), and anticoagulant drug use in 1 (0.48%). The mean time of onset on admission was 6 hours (3, 24). The mean blood glucose was 7.43 mmol/l (5.93, 9.97) on admission. Hematoma was located in the basal ganglia in 100 cases (48.08%), lobar region in 62 (29.81%), thalamus in 28 (13.46%), cerebellum in 11 (5.29%), brain stem in 4 (1.92%), and primary intraventricular hemorrhage in 1 (0.48%). Hematoma involved the insular lobe in 20 cases (9.62%) and secondary intraventricular hemorrhage (26.92%) in 56 cases. 96 cases (46.15%) had hematoma on the right side. The hematoma was >30 ml in 87 cases (41.83%), and the mean volume was 27 ml (10, 50). The blood routine tests showed leukocytosis in 8 cases (3.85%), low platelet count in 2 cases (0.96%), abnormal hemoglobin level in 3 cases (1.44%), and coagulation abnormalities in 2 cases (0.96%). One or more ECG abnormalities were observed in 145 cases (69.71%). The most common ECG abnormality was QTc prolongation (25.00%), followed by ST segment depression (23.08%) and T wave inversion (18.27%). Elevated levels of one more kind of abnormal myocardial enzymes were observed in 139 patients (66.83%). The most common type was LDH (38.4%), followed by hs-cTnT (37.9%), CK 57 (27.40%), and CKMB 57 (27.40%). Relevant ECG abnormalities that reached at least 10% of prevalence in the cohort were included in a univariate analysis and are illustrated in Tables 2 and 3. Relevant elevated myocardial enzymes were included in a univariate analysis and are illustrated in Tables 2 and 4.

3.1. Analysis of QTc Prolongation. The univariate analysis presented that QTc prolongation was associated with location of the cerebellum ($p = 0.049$), SIVH ($p < 0.001$), and hematoma volume > 30 ml ($p < 0.001$). The logistic regression analysis showed that SIVH (OR 5.32; 95% CI 2.55–11.08; $p < 0.001$) and hematoma volume > 30 ml (OR 3.81; 95% CI 1.86–7.81; $p < 0.001$) were independent predictive factors of QTc prolongation.

3.2. Analysis of ST Depression. The univariate analysis showed that ST depression was associated with GCS ≤ 8 ($p = 0.009$), location of the thalamus ($p = 0.029$), insular involvement ($p < 0.001$), SIVH ($p = 0.009$), and hematoma volume > 30 ml ($p = 0.008$). The logistic regression analysis depicts that location of the thalamus (OR 5.79; 95% CI 1.94–17.28; $p < 0.05$), hematoma volume > 30 ml (OR 3.68; 95% CI 1.40–9.67; $p < 0.05$), insular involvement (OR 19.08; 95% CI 5.77–63.07; $p < 0.001$), and SIVH (OR 2.62; 95% CI 1.17–5.86; $p < 0.05$) were independent predictive factors of ST depression.

3.3. Analysis of Inverted T Wave. The univariate analysis showed that inverted T wave was associated with age ($p = 0.006$), history of cerebrovascular diseases ($p = 0.01$), history of antiplatelet drug use ($p = 0.001$), location of basal ganglia ($p < 0.001$), lobar ($p < 0.001$), and thalamus ($p < 0.001$). The logistic regression analysis showed that there was no independent predictive factor of inverted T wave.

Table 1: Baseline characteristics of 208 patients with ICH.

Characteristics	Patient data
Age	
Years (SD)	61.23 (13.64)
≤60 years, *n* (%)	110 (52.88)
Male, *n* (%)	136 (65.38)
History, *n* (%)	
History of hypertension	140 (67.31)
History of type 2 diabetes	16 (7.69)
History of cerebrovascular diseases	32 (15.38)
History of coronary heart disease	11 (5.29)
History of smoking	76 (36.54)
History of drinking	45 (21.63)
Antiplatelet drugs	14 (6.73)
Anticoagulant drugs	1 (0.48)
Time, h (IQR)	6 (21)
GCS ≤ 8, *n* (%)	60 (28.85)
Blood glucose, mmol/l (IQR)	7.43 (4.04)
Location of hematoma, *n* (%)	
Basal ganglia	100 (48.08)
Lobar	62 (29.81)
Thalamus	28 (13.46)
Cerebellum	11 (5.29)
Brain stem	4 (1.92)
Primary intraventricular hemorrhage	1 (0.48)
Right-sided hematoma, *n* (%)	96 (46.15)
Insular involvement, *n* (%)	20 (9.62)
Secondary intraventricular hemorrhage, *n* (%)	56 (26.92)
Hematoma volume	
Median, ml (IQR)	27 (40)
>30 ml, *n* (%)	87 (41.83)
Other blood tests, *n* (%)	
Leukocytosis	8 (3.85)
Low platelet count	2 (0.96)
Abnormal hemoglobin level	3 (1.44)
Coagulation abnormalities	2 (0.96)
ECG abnormalities, *n* (%)	
QTc prolongation	52 (25.00)
ST depression	48 (23.08)
Inverted T wave	38 (18.27)
LBBB	11 (5.29)
PVC	8 (3.85)
RBBB	3 (1.44)
Atrial fibrillation	2 (0.96)
Myocardial enzymes values (IQR)	
CK, U/l	122.25 (129.05)
CKMB, U/l	19.4 (12.14)
LDH, U/l	233 (84.5)
hs-cTnT, ng/ml	0.012 (0.011)
Elevated myocardial enzymes, *n* (%)	
CK	57 (27.4)
CKMB	57 (27.4)
LDH	80 (38.46)
hs-cTnT	79 (37.98)
Mortality, *n* (%)	17 (8.17)

ICH: intracerebral hemorrhage; SD: standard deviation; Time: time of onset on admission; GCS: Glasgow Coma Scale; ECG: electrocardiogram; QTc: corrected QT interval; LBBB: left bundle branch block; PVC: premature ventricular contraction; RBBB: right bundle branch block; CK: creatine kinase; CKMB: creatine kinase-myocardial subfraction; LDH: lactic dehydrogenase; hs-cTnT: high-sensitive cardiac troponin T.

3.4. Analysis of LBBB. The univariate analysis showed that LBBB was associated with GCS ($p = 0.003$), primary intraventricular hemorrhage ($p = 0.046$), hematoma volume > 30 ml ($p = 0.001$), and abnormal hemoglobin level ($p < 0.001$). The logistic regression analysis showed that there was no independent predictive factor of LBBB.

3.5. Analysis of Increase in CK. The univariate analysis showed that the increase in CK was associated with insular involvement ($p = 0.017$) and hematoma volume > 30 ml ($p = 0.024$). The logistic regression analysis showed that insular involvement (OR 2.9; 95% CI 1.12–7.50; $p < 0.05$) and hematoma volume > 30 ml (OR 1.98; 95% CI 1.06–3.70; $p < 0.05$) were independent predictive factors of the increase in CK.

3.6. Analysis of Increase in CKMB. The univariate analysis showed that the increase in CKMB was associated with time of onset at admission ($p = 0.039$), GCS ($p < 0.001$), blood glucose ($p = 0.02$), and insular involvement ($p < 0.001$). The logistic regression analysis showed that GCS (OR 0.87; 95% CI 0.79–0.95; $p < 0.05$) and insular involvement (OR 5.57; 95% CI 1.98–15.64; $p = 0.001$) were independent predictive factors of the increase in CKMB.

3.7. Analysis of Increase in LDH. The univariate analysis showed that the increase in LDH was associated with GCS ($p = 0.013$), blood glucose ($p = 0.008$), SIVH ($p = 0.007$), and hematoma volume > 30 ml ($p = 0.006$). The logistic regression analysis showed that SIVH (OR 2.05; 95% CI 1.071–3.92; $p < 0.05$) was an independent predictive factor of the increase in LDH.

3.8. Analysis of Increase in hs-cTnT. The univariate analysis showed that the increase in hs-cTnT was associated with age ($p = 0.003$), history of T2D (type 2 diabetes) ($p = 0.008$), history of antiplatelet drug use ($p = 0.007$), blood glucose ($p = 0.024$), location of basal ganglia ($p = 0.046$), and leukocytosis ($p = 0.025$). The analysis of logistic regression showed that age (OR 1.03; 95% CI 1.01-1.06; $p < 0.05$), blood glucose (OR 1.10; 95% CI 1.01-1.20; $p < 0.05$), and history of antiplatelet drug use (OR 3.504; 95% CI 1.01-12.12; $p < 0.05$) were independent predictive factors of the increase in hs-cTnT.

Table 2: Univariate analysis of significant ECG changes and elevated myocardial enzymes in ICH. Significant values ($p < 0.05$) are in bold.

Variable	QTc prolongation ($n = 52$)	ST depression ($n = 48$)	Inverted T wave ($n = 38$)	LBBB ($n = 11$)	Elevated CK ($n = 57$)	Elevated CKMB ($n = 57$)	Elevated LDH ($n = 80$)	Elevated hs-cTnT ($n = 79$)
Age (SD)	60.37 (13.49)	61.79 (12.38)	**66.92 (13.50)***	60.18 (11.80)	60.58 (13.63)	58.42 (13.57)	59.66 (14.20)	**64.91 (14.81)***
Male (%)	34 (65.38)	33 (68.75)	20 (52.63)	8 (72.73)	42 (73.68)	43 (75.44)	49 (61.25)	51 (64.56)
History of hypertension (%)	37 (71.15)	33 (68.75)	28 (73.68)	9 (81.82)	39 (68.42)	39 (68.42)	54 (67.50)	57 (72.15)
History of type 2 diabetes (%)	6 (11.54)	4 (8.33)	2 (5.26)	1 (9.09)	5 (8.77)	4 (7.02)	4 (5.00)	**11 (13.92)***
History of cerebrovascular diseases (%)	9 (17.31)	10 (20.83)	**11 (28.95)***	1 (9.09)	12 (21.05)	10 (17.54)	10 (12.50)	14 (17.72)
History of coronary heart disease (%)	2 (3.85)	2 (4.17)	4 (10.53)	2 (18.18)	3 (5.26)	4 (7.02)	5 (6.25)	7 (8.86)
History of smoking (%)	19 (36.54)	19 (39.58)	11 (28.95)	3 (27.27)	22 (38.60)	25 (43.86)	28 (35.00)	28 (35.44)
History of drinking (%)	11 (21.15)	11 (22.92)	4 (10.53)	2 (18.18)	10 (17.54)	13 (22.81)	15 (18.75)	16 (20.25)
History of antiplatelet drugs (%)	5 (9.62)	5 (10.42)	**7 (18.42)***	0 (0.00)	7 (12.28)	7 (12.28)	7 (8.75)	**10 (12.82)***
History of anticoagulant drugs (%)	0 (0.00)	1 (2.08)	1 (2.63)	0 (0.00)	0 (0.00)	0 (0.00)	0 (0.00)	0 (0.00)
Time (IQR)	5.00 (18.25)	6.50 (17.50)	6 (21)	5 (5)	7 (21)	**5 (6)***	5 (11)	6 (21)
GCS ≤ 8 (%)	32 (61.54)	**27 (56.25)***	24 (63.16)	**3 (27.27)***	37 (64.91)	**30 (52.63)***	**49 (61.25)***	51 (64.56)
Blood glucose (IQR)	7.93 (4.01)	7.94 (5.43)	7.065 (3.60)	10.39 (5.34)	7.91 (3.43)	**8.03 (4.09)***	**7.97 (4.55)***	**7.91 (4.61)***
Basal ganglia (%)	26 (50.00)	21 (43.75)	**8 (21.05)***	8 (72.73)	27 (47.37)	26 (45.61)	42 (52.50)	**31 (39.24)***
Lobar (%)	18 (34.62)	16 (33.33)	**2 (5.26)***	1 (9.09)	20 (35.09)	18 (31.58)	23 (28.75)	28 (35.44)
Thalamus (%)	7 (13.46)	**11 (22.92)***	**28 (73.68)***	0 (0.00)	6 (10.53)	10 (17.54)	11 (13.75)	14 (17.72)
Cerebellum (%)	**0 (0.00)***	0 (0.00)	0 (0.00)	1 (9.09)	3 (5.26)	1 (1.75)	4 (5.00)	3 (3.80)
Brain stem (%)	0 (0.00)	0 (0.00)	0 (0.00)	0 (0.00)	0 (0.00)	2 (3.51)	0 (0.00)	1 (1.27)
PIVH (%)	0 (0.00)	0 (0.00)	0 (0.00)	**1 (9.09)***	0 (0.00)	0 (0.00)	0 (0.00)	1 (1.27)
Right-sided hematoma (%)	24 (46.15)	23 (47.92)	17 (44.74)	2 (18.18)	27 (47.37)	27 (47.37)	33 (41.25)	36 (45.57)
Insular involvement (%)	8 (15.38)	**14 (29.17)***	2 (5.26)	0 (0.00)	**10 (17.54)***	**13 (22.81)***	9 (11.25)	6 (7.59)
SIVH (%)	**27 (51.92)***	**20 (41.67)***	14 (36.84)	2 (18.18)	16 (28.07)	18 (31.58)	**30 (37.50)***	22 (27.85)
Hematoma volume > 30 ml (%)	**35 (67.31)***	**28 (58.33)***	12 (31.58)	**11 (90.91)***	**31 (54.38)***	30 (52.63)	**43 (53.75)***	36 (45.57)
Leukocytosis (%)	3 (5.77)	2 (4.17)	0 (0.00)	0 (0.00)	0 (0.00)	3 (5.26)	3 (3.75)	**0 (0.00)***
Low platelet count (%)	0 (0.00)	1 (2.08)	1 (2.63)	0 (0.00)	1 (1.75)	1 (1.75)	1 (1.25)	0 (0.00)

Table 2: Continued.

Variable	QTc prolongation ($n = 52$)	ST depression ($n = 48$)	Inverted T wave ($n = 38$)	LBBB ($n = 11$)	Elevated CK ($n = 57$)	Elevated CKMB ($n = 57$)	Elevated LDH ($n = 80$)	Elevated hs-cTnT ($n = 79$)
Abnormal hemoglobin level (%)	1 (1.92)	1 (2.08)	0 (0.00)	**2 (18.18)***	1 (1.75)	1 (1.75)	2 (2.50)	1 (1.28)
Coagulation abnormalities (%)	0 (0.00)	0 (0.00)	0 (0.00)	0 (0.00)	0 (0.00)	0 (0.00)	0 (0.00)	1 (1.28)
Mortality (%)	3 (5.77)	5 (10.42)	3 (7.89)	4 (36.36)	6 (10.53)	8 (14.04)	8 (10.00)	10 (12.66)

ECG: electrocardiogram; ICH: intracerebral hemorrhage; SD: standard deviation; Time: time of onset on admission; GCS: Glasgow Coma Scale; PIVH: primary intraventricular hemorrhage; SIVH: secondary intraventricular hemorrhage; QTc: corrected QT interval; LBBB: left bundle branch block; CK: creatine kinase; CKMB: creatine kinase-myocardial subfraction; LDH: lactic dehydrogenase; hs-cTnT: high-sensitive cardiac troponin T.

Table 3: Univariate analysis of significant ECG changes in ICH. Significant values ($p < 0.05$) are in bold.

Variable	Entire cohort ($n = 208$)	QTc prolongation ($n = 52$)	p value	ST depression ($n = 48$)	p value	Inverted T wave ($n = 38$)	p value	LBBB ($n = 11$)	p value
Age (SD)	61.23 (13.64)	60.37 (13.49)	0.601	61.79 (12.38)	0.576	66.92 (13.50)	**0.006***	60.18 (11.80)	0.77
Male	136 (65.38)	34 (65.38)	1.000	33 (68.75)	0.808	20 (52.63)	0.068	8 (72.73)	0.876
History of hypertension	140 (67.31)	37 (71.15)	0.495	33 (68.75)	0.849	28 (73.68)	0.127	9 (81.82)	0.644
History of type 2 diabetes	16 (7.69)	6 (11.54)	0.229	4 (8.33)	0.233	2 (5.26)	0.776	1 (9.09)	1
History of cerebrovascular diseases	32 (15.38)	9 (17.31)	0.657	10 (20.83)	0.692	11 (28.95)	**0.01***	1 (9.09)	0.858
History of coronary heart disease	11 (5.29)	2 (3.85)	0.592	2 (4.17)	0.617	4 (10.53)	0.232	2 (18.18)	0.208
History of smoking	76 (36.54)	19 (36.54)	1.000	19 (39.58)	0.806	11 (28.95)	0.282	3 (27.27)	0.72
History of drinking	45 (21.63)	11 (21.15)	0.923	11 (22.92)	0.576	4 (10.53)	0.066	2 (18.18)	1
History of antiplatelet drugs	14 (6.73)	5 (9.62)	0.338	5 (10.42)	0.245	7 (18.42)	**0.001***	0 (0.00)	0.360
History of anticoagulant drugs	1 (0.48)	0 (0.00)	0.563	1 (2.08)	0.067	1 (2.63)	0.410	0 (0.00)	0.813
Time (IQR)	6 (21)	5.00 (18.25)	0.205	6.50 (17.50)	0.810	6 (21)	0.255	5 (5)	0.2
GCS ≤ 8	60 (28.85)	32 (61.54)	0.077	27 (56.25)	**0.009***	24 (63.16)	0.229	3 (27.27)	**0.003***
Blood glucose (IQR)	7.43 (4.04)	7.93 (4.01)	0.129	7.94 (5.43)	0.061	7.065 (3.60)	0.902	10.39 (5.34)	0.104
Basal ganglia	100 (48.08)	26 (50.00)	0.749	21 (43.75)	0.494	8 (21.05)	**<0.001***	8 (72.73)	0.099
Lobar	62 (29.81)	18 (34.62)	0.381	16 (33.33)	0.543	2 (5.26)	**<0.001***	1 (9.09)	0.221
Thalamus	28 (13.46)	7 (13.46)	1.000	11 (22.92)	**0.029***	28 (73.68)	**<0.001***	0 (0.00)	0.368
Cerebellum	11 (5.29)	0 (0.00)	**0.049***	0 (0.00)	0.062	0 (0.00)	0.226	1 (9.09)	1
Brain stem	4 (1.92)	0 (0.00)	0.244	0 (0.00)	0.269	0 (0.00)	0.763	0 (0.00)	1
PIVH	1 (0.48)	0 (0.00)	0.563	0 (0.00)	0.583	0 (0.00)	1	1 (9.09)	**0.046***
Right-sided hematoma	96 (46.15)	24 (46.15)	1.000	23 (47.92)	0.780	17 (44.74)	0.846	2 (18.18)	0.052
Insular involvement	20 (9.62)	8 (15.38)	0.103	14 (29.17)	**<0.001***	2 (5.26)	0.482	0 (0.00)	0.552
SIVH	56 (26.92)	27 (51.92)	**<0.001***	20 (41.67)	**0.009***	14 (36.84)	0.127	2 (18.18)	0.733
Hematoma volume > 30 ml	87 (41.83)	35 (67.31)	**<0.001***	28 (58.33)	**0.008***	12 (31.58)	0.157	11 (90.91)	**0.001***
Leukocytosis	8 (3.85)	3 (5.77)	0.405	2 (4.17)	0.895	0 (0.00)	0.173	0 (0.00)	0.495
Low platelet count	2 (0.96)	0 (0.00)	0.412	1 (2.08)	0.364	1 (2.63)	0.243	0 (0.00)	0.737
Abnormal hemoglobin level	3 (1.44)	1 (1.92)	0.737	1 (2.08)	0.671	0 (0.00)	0.409	2 (18.18)	**<0.001***
Coagulation abnormalities	2 (0.96)	0 (0.00)	0.412	0 (0.00)	0.436	0 (0.00)	0.502	0 (0.00)	0.737
Mortality	17 (8.17)	3 (5.77)	0.465	5 (10.42)	0.518	3 (7.89)	0.945	4 (36.36)	0.052

ECG: electrocardiogram; ICH: intracerebral hemorrhage; SD: standard deviation; Time: time of onset on admission; GCS: Glasgow Coma Scale; PIVH: primary intraventricular hemorrhage; SIVH: secondary intraventricular hemorrhage; QTc: corrected QT interval; LBBB: left bundle branch block.

Table 4: Univariate analysis of elevated myocardial enzymes in ICH. Significant values ($p < 0.05$) are in bold.

Variable	Entire cohort ($n = 208$)	Elevated CK ($n = 57$)	p value	Elevated CKMB ($n = 57$)	p value	Elevated LDH ($n = 80$)	p value	Elevated hs-cTnT ($n = 79$)	p value
Age (SD)	61.23 (13.64)	60.58 (13.63)	0.675	58.42 (13.57)	0.070	59.66 (14.20)	0.200	64.91 (14.81)	**0.003***
Male (%)	136 (65.38)	42 (73.68)	0.122	43 (75.44)	0.061	49 (61.25)	0.322	51 (64.56)	0.844
History of hypertension	140 (67.31)	39 (68.42)	0.833	39 (68.42)	0.833	54 (67.50)	0.963	57 (72.15)	0.244
History of type 2 diabetes	16 (7.69)	5 (8.77)	0.720	4 (7.02)	0.822	4 (5.00)	0.249	11 (13.92)	**0.008***
History of cerebrovascular diseases	32 (15.38)	12 (21.05)	0.164	10 (17.54)	0.596	10 (12.50)	0.362	14 (17.72)	0.465
History of coronary heart disease	11 (5.29)	3 (5.26)	0.992	4 (7.02)	0.494	5 (6.25)	0.624	7 (8.86)	0.072
History of smoking	76 (36.54)	22 (38.60)	0.705	25 (43.86)	0.178	28 (35.00)	0.716	28 (35.44)	0.797
History of drinking	45 (21.63)	10 (17.54)	0.379	13 (22.81)	0.801	15 (18.75)	0.424	16 (20.25)	0.705
History of antiplatelet drugs	14 (6.73)	7 (12.28)	0.050	7 (12.28)	0.050	7 (8.75)	0.358	10 (12.82)	**0.007***
History of anticoagulant drugs	1 (0.48)	0 (0.00)	0.538	0 (0.00)	0.538	0 (0.00)	0.428	0 (0.00)	0.437
Time (IQR)	6 (21)	7 (21)	0.287	5 (6)	**0.039***	5 (11)	0.167	6 (21)	0.452
GCS ≤ 8	60 (28.85)	37 (64.91)	0.222	30 (52.63)	**<0.001***	49 (61.25)	**0.013***	51 (64.56)	0.100
Blood glucose (IQR)	7.43 (4.04)	7.91 (3.43)	0.346	8.03 (4.09)	**0.02***	7.97 (4.55)	**0.008***	7.91 (4.61)	**0.024***
Basal ganglia	100 (48.08)	27 (47.37)	0.900	26 (45.61)	0.662	42 (52.50)	0.313	31 (39.24)	**0.046***
Lobar	62 (29.81)	20 (35.09)	0.306	18 (31.58)	0.732	23 (28.75)	0.792	28 (35.44)	0.164
Thalamus	28 (13.46)	6 (10.53)	0.446	10 (17.54)	0.289	11 (13.75)	0.923	14 (17.72)	0.159
Cerebellum	11 (5.29)	3 (5.26)	0.992	1 (1.75)	0.162	4 (5.00)	0.883	3 (3.80)	0.452
Brain stem	4 (1.92)	0 (0.00)	0.215	2 (3.51)	0.306	0 (0.00)	0.110	1 (1.27)	0.589
PIVH	1 (0.48)	0 (0.00)	0.538	0 (0.00)	0.538	0 (0.00)	0.428	1 (1.27)	0.200
Right-sided hematoma	96 (46.15)	27 (47.37)	0.829	27 (47.37)	0.829	33 (41.25)	0.262	36 (45.57)	0.895
Insular involvement	20 (9.62)	10 (17.54)	**0.017***	13 (22.81)	**<0.001***	9 (11.25)	0.527	6 (7.59)	0.439
SIVH	56 (26.92)	16 (28.07)	0.819	18 (31.58)	0.352	30 (37.50)	**0.007***	22 (27.85)	0.814
Hematoma volume > 30 ml	87 (41.83)	31 (54.38)	**0.024***	30 (52.63)	0.052	43 (53.75)	**0.006***	36 (45.57)	0.392
Leukocytosis	8 (3.85)	0 (0.00)	0.076	3 (5.26)	0.514	3 (3.75)	0.955	0 (0.00)	**0.025***
Low platelet count	2 (0.96)	1 (1.75)	0.472	1 (1.75)	0.472	1 (1.25)	0.736	0 (0.00)	0.271
Abnormal hemoglobin level	3 (1.44)	1 (1.75)	0.817	1 (1.75)	0.817	2 (2.50)	0.312	1 (1.28)	0.881
Coagulation abnormalities	2 (0.96)	0 (0.00)	0.383	0 (0.00)	0.383	0 (0.00)	0.261	1 (1.28)	0.714
Mortality	17 (8.17)	6 (10.53)	0.447	8 (14.03)	0.058	8 (10.00)	0.447	10 (12.65)	0.058

ICH: intracerebral hemorrhage; SD: standard deviation; Time: time of onset on admission; GCS: Glasgow Coma Scale; PIVH: primary intraventricular hemorrhage; SIVH: secondary intraventricular hemorrhage; CK: creatine kinase; CKMB: creatine kinase-myocardial subfraction; LDH: lactic dehydrogenase; hs-cTnT: high-sensitive cardiac troponin T.

3.9. Impact of Cardiac Injury Markers on Mortality. In a univariate analysis, there was no ECG abnormality observed in more than 10% of patients and elevated serum myocardial enzyme associated with in-hospital mortality.

4. Discussion

Many researchers have observed the changes of ECG and myocardial enzymes in ICH patients. However, their studies only attach the importance to one or two markers of ECG and myocardial enzymes, the analysis on both of which is less researched in the same group of patients. Therefore, it is impossible to fully discover what factors affect the heart after ICH. In this study, ECG and myocardial enzymes of 208 patients with ICH were analyzed together so as to further clarify the relationship between different characteristics of ICH and cardiac complications. The result showed that insular involvement, hematoma volume > 30 ml, and SIVH were the strongest risk factors triggering the abnormalities of ECG and myocardial enzyme after ICH, followed by GCS, age, admission blood glucose, and location of the thalamus.

ECG abnormalities (69.71%) were common in patients with ICH in our study, which was basically consistent with the incidence reported in literature [8, 9]. The most common ECG abnormalities were prolonged QTC, ST segment depression, and inverted T wave. Some researchers have also found that these abnormalities were often observed during the acute phase of ICH [14]. Then, we examined the factors associated with ECG abnormalities. We found that hematoma volume and SIVH were the two strongest determinants of ECG abnormalities, which is consistent with the previous reports [15].

In the study, elevated myocardial enzymes (74.52%) were also found in the plasma of patients with ICH, among which, LDH was the most common one, followed by hs-cTnT. Studies have shown that LDH levels are increased in patients with central nervous system diseases such as cerebral infarction and hypoxic-ischemic encephalopathy [16, 17], as well as ICH [18]. The proportion of increased troponin in this study (37.98%) is higher than that in other studies (27.4%) [6] and (22%) [19]. It seems to have to do with the inconsistent types of cardiac troponin in the two studies. hs-cTnT was studied in this study while cTnI or cTnT in others. We examined the risk factors associated with the four myocardial enzymes observed. Insular involvement was the main determinant of myocardial enzyme elevation, related to two kinds. In addition, GCS, hematoma volume, SIVH, age, and blood glucose levels were also associated with one item, respectively. This is consistent with many studies, in which myocardial enzyme correlated with markers of disease severity such as hematoma volume, NIHSS score, and intraventricular hemorrhage [20–22].

Insula is important to cardiac sympathetic output maintenance. ICH patients whose insula was involved had an increased risk of cardiac complications [23], which is consistent with our findings. It also showed that the risk was elevated when the right hemisphere was involved. Although there is evidence that insular cortex-mediated sympathetic control is hemispheric dominant [24], the experimental results are still inconsistent [25]. However, our results did not show a difference in ECG or serum myocardial enzyme effects between left and right hemisphere hematoma. The reason may be that our study was a clinical retrospective study, and the results were derived from animal experiments. Therefore, the hematoma location identified in our study is not as accurate as in animal studies, which seems to influence judgments of hemispheric laterality.

Hematoma extension to the third and fourth ventricles may trigger destruction of the baroreflex receptors around the area [26], because of the abundant network structures controlling autonomic nerve function around the third and fourth ventricles, involving the paraventricular nucleus of the hypothalamus, periaqueductal gray matter, brain stem, and so on. Expansion of the intraventricular hematoma may lead to acute autonomic nervous system disorders and elevated circulating catecholamine levels, which could lead to cardiac complications [27]. In addition, the central control of the autonomic nervous system was thought to be located in the insular cortex, cingulate gyrus, amygdala, and hypothalamus [28]. Cardiovascular autonomic centers may also involve the extrainsular regions and their interconnecting fibers [29]. Therefore, the larger the hematoma, the more severe the pressure on the central control area, and the more severe the damage to the contact fibers. This also increases the risk of heart complications and explains why both hematoma volume > 30 ml and SIVH were independent risk factors for ECG and myocardial enzyme abnormities.

Our study found that lower GCS was closely related to the increase of CKMB after ICH and also an independent predictor. However, in patients with traumatic brain injury (TBI), researchers did not find association between GCS and the development of cardiac dysfunction [29]. An explanation for the difference could be that the damage of hematoma in ICH to the brain tissue is limited, while it is diffused in TBI. This kind of diffuse lesion may mask the effect of the autonomic nerve center on the heart. The study confirmed that cardiac complications were more frequent with increasing grading of diffuse brain injury [30]. In addition, GCS reflects the functional integrity of the brain stem. And the brain stem, especially the caudal autonomic centers, is very important for the nervous influences to the heart. One study observed the heart rate variability (HRV) in patients in coma due to different diseases. HRV was found a progressive trend associated with deepening of coma, assessed by the GCS [31]. This is consistent with our findings, asserting that GCS could predict the occurrence of cardiac complications in central nervous system diseases.

We demonstrated that location of the thalamus is an independent risk factor for ST depression. This is related to the fact that the thalamus is a relay station for autonomous afferent impulses to the insular cortex [32] and is also involved in the autonomic nervous system pathway [33]. Racho et al. had also noted the importance of the thalamus in the regulation of the ANS, through the observation of Takotsubo cardiomyopathy after a thalamic stroke [34].

Elevated troponin is frequently detected in patients with stroke [6, 35]. In this study, admission blood glucose level, age, and history of antiplatelet drug use were found to be risk factors for elevated troponin. Type 2 diabetes has been proven

to have a significant association with elevated hs-cTnT levels in community-dwelling population; fasting blood glucose played a crucial role in this association [36]. Sharain et al. studied 830 patients and found that older age was also associated with elevated hs-cTnT [37]. We believe that admission blood glucose and age also affect the increase of troponin after ICH. The main reason why blood glucose and age affect the increase of troponin after ICH may be that hyperglycemia and old age reduce the cardiac tolerance of patients and are also prone to cardiac complications such as myocardial ischemia or necrosis after ICH.

History of antiplatelet drug use means those patients suffered from severe atherosclerosis, such as coronary artery occlusion. Scheitz et al. [38] believed that troponin may be chronically elevated or acutely elevated in patients with stroke, which needs to be determined by further evaluation. Thus, in our study, troponin may be chronically elevated in the patients with a history of antiplatelet drugs. The cause may be the coronary factors.

The relationship between injury markers and in-hospital mortality was further investigated. Compared to the published literature, alteration of the injury markers in patients with ICH was not found to be associated with in-hospital mortality. The previous reports showed an association between ECG abnormalities and outcome. However, it is arguable which abnormality can predict the prognosis. Some studies have shown that QT interval could predict the mortality of ICH patients [7, 39]. But other researchers disagreed with this hypothesis. In their study, inversion of T waves was the only ECG aberrancy that is related to the clinical outcome [9]. The same situation also occurs in the relationship between myocardial enzymes and clinical prognosis. Some argued that elevation in cardiac troponin levels has been associated with in-hospital mortality [11, 40, 41], but other studies suggested the opposite case [42]. The possible reason for the inconsistency of the results is that multiple factors independent from ICH could affect ECG and myocardial enzymes, such as medicine, medical history, and structural cardiac pathologies. As these variables could not be controlled completely in all the current researches, any conclusions drawn from this topic are not fully convincing and precise. Our research is no exception. Therefore, it is still uncertain what injury markers could accurately predict the prognosis until a better research method is designed. Another reason of our failure in discovering the correlation between cardiac injury markers and prognosis may be the choice of endpoint observed in this study. The purpose of this study was to determine factors for ECG and increased myocardial enzyme after ICH, so we only analyzed in-hospital mortality. If we were able to include outcomes at 3-6 months, we might have a different finding.

This study had important clinical implications. The ECG and myocardial enzymes of the same group of ICH patients at admission were observed. The possible independent predictors of the early cardiac injury markers were analyzed, albeit this study did not find the relationship between these markers and in-hospital mortality. Our findings are still conducive for clinicians to early identify those patients with ICH who are at high risk of secondary heart injury and intervene in advance. This may improve the prognosis of the patients, but further research is needed.

4.1. Limitations. The study is limited in respect of retrospective feature. The single-center study reflected the cardiac complications associated with ICH in the specific patients of Guiyang. Therefore, the results may not be promoted in different groups of patients. It also had a small sample size, which reduced the statistical power and increased the chance of type 2 errors. Additionally, the dynamic changes of ECG and cardiac enzymes were not included as parameter into our study, resulting in a lack of data on whether these changes were transient or permanent. Due to the lack of complete outcome measures for the patients such as mortality at 3 to 6 months and scores from the Glasgow Outcome Scale or Modified Rankin Scale, this resulted in possibly ambiguous associations between cardiac injury markers and prognosis. Despite the limitations, our findings allow for some useful clinical speculations.

5. Conclusion

We studied ECG abnormalities and changes of serum myocardial enzymes and the relationship between these markers of cardiac damage and the detailed characteristics of ICH in a series of patients and demonstrated that insular involvement, hematoma volume > 30 ml, and SIVH were the strongest risk factors for ECG and myocardial enzyme abnormalities after ICH. The risk factors are as follows: GCS, age, admission blood glucose, and location of the thalamus. Further prospective studies are needed to corroborate our findings.

Data Availability

Data are available to researchers on request for purposes of reproducing the results or replicating the procedure by directly contacting the corresponding author.

Disclosure

The funding body did not take part in the design of the study and collection, analysis, and interpretation of data and in writing the manuscript.

Conflicts of Interest

The authors report no potential conflicts of interest.

Acknowledgments

This research was supported by the Natural Science Foundation of China (81971126/H0906) and Guizhou Science and Technology Foundation (qiankehe zhicheng (2017) 2881).

References

[1] B. A. Gross, B. T. Jankowitz, and R. M. Friedlander, "Cerebral intraparenchymal Hemorrhage," *JAMA The Journal of the American Medical Association*, vol. 321, no. 13, pp. 1295–1303, 2019.

[2] M. Stein, G. F. Hamann, B. Misselwitz, E. Uhl, M. Kolodziej, and M. H. Reinges, "In-hospital mortality and complication rates in surgically and conservatively treated patients with spontaneous intracerebral hemorrhage," *World Neurosurgery*, vol. 88, pp. 306–310, 2016.

[3] Y. W. Kuo, M. Lee, Y. C. Huang, and J. D. Lee, "Initial in-hospital heart rate is associated with three-month functional outcomes after acute ischemic stroke," *BMC Neurology*, vol. 21, no. 1, p. 222, 2021.

[4] A. Kerro, T. Woods, and J. J. Chang, "Neurogenic stunned myocardium in subarachnoid hemorrhage," *Journal of Critical Care*, vol. 38, pp. 27–34, 2017.

[5] R. J. Koivunen, E. Haapaniemi, J. Satopää, M. Niemelä, T. Tatlisumak, and J. Putaala, "Medical acute complications of intracerebral hemorrhage in young adults," *Stroke Research and Treatment*, vol. 2015, Article ID 357696, 7 pages, 2015.

[6] Y. He, Q. Liu, J. Wang, D. W. Wang, H. Ding, and W. Wang, "Prognostic value of elevated cardiac troponin I in patients with intracerebral hemorrhage," *Clinical Cardiology*, vol. 43, no. 4, pp. 338–345, 2020.

[7] S. M. Z. Ziabari, N. Akhundzadeh, M. Shakiba, and P. Keshavarz, "The relationship between QT interval and intra-hospital mortality in patients with spontaneous intracranial hemorrhage," *Advanced Journal of Emergency Medicine*, vol. 4, no. 2, p. e25, 2020.

[8] S. Takeuchi, K. Nagatani, N. Otani, K. Wada, and K. Mori, "Electrocardiograph abnormalities in intracerebral hemorrhage," *Journal of Clinical Neuroscience*, vol. 22, no. 12, pp. 1959–1962, 2015.

[9] M. Bree, Y. Roos, I. Bilt et al., "Prevalence and characterization of ECG abnormalities after intracerebral hemorrhage," *Neurocritical Care*, vol. 12, no. 1, pp. 50–55, 2009.

[10] C. D'Amore, M. Paciaroni, G. Silvestrelli et al., "Severity of acute intracerebral haemorrhage, elderly age and atrial fibrillation: independent predictors of poor outcome at three months," *European Journal of Internal Medicine*, vol. 24, no. 4, pp. 310–313, 2013.

[11] M. C. Garrett, R. J. Komotar, R. M. Starke, D. Doshi, M. L. Otten, and E. S. Connolly, "Elevated troponin levels are predictive of mortality in surgical intracerebral hemorrhage patients," *Neurocritical Care*, vol. 12, no. 2, pp. 199–203, 2010.

[12] L. B. Morgenstern, J. H. Rd, C. Anderson et al., "Guidelines for the management of spontaneous intracerebral hemorrhage: a guideline for healthcare professionals from the American Heart Association/American Stroke Association," *Stroke*, vol. 46, no. 7, p. 2032, 2015.

[13] A. Lele, V. Lakireddy, S. Gorbachov, N. Chaikittisilpa, V. Krishnamoorthy, and M. S. Vavilala, "A narrative review of cardiovascular abnormalities after spontaneous intracerebral hemorrhage," *Journal of Neurosurgical Anesthesiology*, vol. 31, no. 2, pp. 199–211, 2019.

[14] Z. Chen, P. Venkat, D. Seyfried, M. Chopp, T. Yan, and J. Chen, "Brain-heart interaction cardiac complications after stroke," *Circulation Research*, vol. 121, no. 4, pp. 451–468, 2017.

[15] A. Loggini, A. Mansour, F. E. Ammar et al., "Inversion of T waves on admission is associated with mortality in spontaneous intracerebral hemorrhage," *Journal of Stroke and Cerebrovascular Diseases*, vol. 30, no. 6, article 105776, 2021.

[16] Y. Lampl, Y. Paniri, Y. Eshel, and I. Sarova-Pinhas, "Cerebrospinal fluid lactate dehydrogenase levels in early stroke and transient ischemic attacks," *Stroke*, vol. 21, no. 6, pp. 854–857, 1990.

[17] M. Thoresen, X. Liu, S. Jary et al., "Lactate dehydrogenase in hypothermia-treated newborn infants with hypoxic-ischaemic encephalopathy," *Acta Paediatrica*, vol. 101, no. 10, pp. 1038–1044, 2012.

[18] H. Chu, C. Huang, J. Dong et al., "Lactate dehydrogenase predicts early hematoma expansion and poor outcomes in intracerebral hemorrhage patients," *Translational Stroke Research*, vol. 10, no. 6, pp. 620–629, 2019.

[19] L. Hansheng, C. Yuan, and X. Zongyi, "Relationship between serum cardiac troponin T level and outcome in insular lobe hemorrhage patients," *Chinese Journal of Geriatric Heart Brain and Vessel Diseases*, vol. 21, no. 3, pp. 286–289, 2019.

[20] K. Shibazaki, K. Kimura, K. Sakai, J. Aoki, and Y. Sakamoto, "Plasma brain natriuretic peptide is elevated in the acute phase of intracerebral hemorrhage," *Journal of Clinical Neuroscience*, vol. 21, no. 2, pp. 221–224, 2014.

[21] M. L. James, R. Blessing, B. G. Phillips-Bute, E. Bennett, and D. T. Laskowitz, "S100b and BNP predict functional neurological outcome after intracerebral hemorrhage," *Biomarkers*, vol. 14, no. 6, pp. 388–394, 2009.

[22] Y. Goya, K. Shibazaki, K. Sakai et al., "Brain natriuretic peptide upon admission as a biological marker of short-term mortality after intracerebral hemorrhage," *European Neurology*, vol. 71, no. 3-4, pp. 203–207, 2014.

[23] F. R. Marins, M. Limboro-Filho, B. F. D'Abreu et al., "Autonomic and cardiovascular consequences resulting from experimental hemorrhagic stroke in the left or right intermediate insular cortex in rats," *Autonomic Neuroscience*, vol. 227, article 102695, 2020.

[24] S. Oppenheimer and D. Cechetto, "The insular cortex and the regulation of cardiac function," *Comprehensive Physiology*, vol. 6, no. 2, pp. 1081–1133, 2016.

[25] F. R. Marins, M. Limborço-Filho, C. H. Xavier et al., "Functional topography of cardiovascular regulation along the rostrocaudal axis of the rat posterior insular cortex," *Clinical and Experimental Pharmacology & Physiology*, vol. 43, no. 4, pp. 484–493, 2016.

[26] M. Sykora, T. Steiner, S. Poli, A. Rocco, P. Turcani, and J. Diedler, "Autonomic effects of intraventricular extension in intracerebral hemorrhage," *Neurocritical Care*, vol. 16, no. 1, pp. 102–108, 2012.

[27] C.-H. Chen, S.-C. Tang, D.-Y. Lee et al., "Impact of supratentorial cerebral hemorrhage on the complexity of heart rate variability in acute stroke," *Scientific Reports*, vol. 8, no. 1, p. 11473, 2018.

[28] S. De Raedt, A. De Vos, and J. De Keyser, "Autonomic dysfunction in acute ischemic stroke: an underexplored therapeutic area?," *Journal of the Neurological Sciences*, vol. 348, no. 1-2, pp. 24–34, 2015.

[29] M. Dutsch, M. Burger, C. Dorfler, S. Schwab, and M. J. Hilz, "Cardiovascular autonomic function in poststroke patients," *Neurology*, vol. 69, no. 24, pp. 2249–2255, 2007.

[30] V. Chakradhar and J. Kasal, "Cardiac dysfunction in adult patients with traumatic brain injury: a prospective cohort study," *Clinical Medicine & Research*, vol. 16, no. 3-4, pp. 57–65, 2018.

[31] M. Estévez-Báez, C. Machado, B. García-Sánchez et al., "Autonomic impairment of patients in coma with different Glasgow

Coma Scale (GCS) assessed with heart rate variability," *Brain Injury*, vol. 33, no. 4, pp. 496–516, 2019.

[32] F. C. David, "Cortical control of the autonomic nervous system," *Experimental Physiology*, vol. 2, no. 99, pp. 326–331, 2014.

[33] N. Kuriyama, T. Mizuno, F. Niwa, Y. Watanabe, and M. Nakagawa, "Autonomic nervous dysfunction during acute cerebral infarction," *Neurological Research*, vol. 32, no. 8, pp. 821–827, 2010.

[34] A. Racho, A. Briosa, L. Pereira, M. Rodrigues, and T. Geraldes, "Thalamic role in the autonomic nervous system: the evidence of a case of Takotsubo cardiomyopathy following thalamic ischemic stroke," *Clinical Neurology and Neurosurgery*, vol. 200, article 106378, 2021.

[35] N. Grassl, S. Baumann, M. Kruska et al., "Acute ischemic stroke and elevated troponin: Diagnostic work-up and therapeutic consequences," *Deutsche Medizinische Wochenschrift*, vol. 146, no. 8, pp. 534–541, 2021.

[36] S. Fu, R. Jin, L. Luo, and P. Ye, "Baseline type 2 diabetes had a significant association with elevated high sensitivity cardiac troponin T levels in Chinese community-dwelling population: a 5-year prospective analysis," *Nutrition & Metabolism*, vol. 14, no. 1, p. 73, 2017.

[37] K. Sharain, V. C. Vasile, Y. Sandoval et al., "The elevated high-sensitivity cardiac troponin T pilot: diagnoses and outcomes," *Mayo Clinic Proceedings*, vol. 96, no. 9, pp. 2366–2375, 2021.

[38] J. F. Scheitz, C. H. Nolte, U. Laufs, and M. Endres, "Application and interpretation of high-sensitivity cardiac troponin assays in patients with acute ischemic stroke," *Stroke*, vol. 46, no. 4, pp. 1132–1140, 2015.

[39] C. H. Huang, W. J. Chen, W. T. Chang, P. K. Yip, and Y. T. Lee, "QTc dispersion as a prognostic factor in intracerebral hemorrhage," *American Journal of Emergency Medicine*, vol. 22, no. 3, pp. 141–144, 2004.

[40] A. Hays and M. N. Diringer, "Elevated troponin levels are associated with higher mortality following intracerebral hemorrhage," *Neurology*, vol. 66, no. 9, pp. 1330–1334, 2006.

[41] R. Sandhu, W. S. Aronow, A. Rajdev et al., "Relation of cardiac troponin I levels with in-hospital mortality in patients with ischemic stroke, intracerebral hemorrhage, and subarachnoid hemorrhage," *American Journal of Cardiology*, vol. 102, no. 5, pp. 632–634, 2008.

[42] B. V. Maramattom, E. M. Manno, J. R. Fulgham, A. S. Jaffe, and E. F. Wijdicks, "Clinical importance of cardiac troponin release and cardiac abnormalities in patients with supratentorial cerebral hemorrhages," *Mayo Clinic Proceedings*, vol. 81, no. 2, pp. 192–196, 2006.